DECEMBER 1955

A.I.Ch.E. JOURNAL

Published by the American Institute of Chemical Engineers

CONTENTS

Transient Behavior of Single-phase Natural-circulation Loop Systems
C. D. ALSTAD, H. S. ISBIN, N. R. AMUNDSON, AND J. P. SILVERS

Dispersed-phase Holdup in Packed, Countercurrent Liquid-liquid Extraction Columns
C. E. WICKS AND R. B. BECKMANN

Flow of Non-Newtonian Fluids—Correlation for the Laminar, Transition, and Turbulent Flow Regions
A. B. METZNER AND J. C. REED

Capacity Factors in the Performance of Perforated-plate Columns
C. D'A. HUNT, D. N. HANSON, AND C. R. WILKE

Benedict Equation of State: Application to Vapor-liquid Equilibria
E. J. CULLEN AND K. A. KOBE

Gas Absorption Accompanied by Chemical Reaction
P. V. DANCKWERTS

Forced-convection Heat Transfer in Cylindrical Pipes with Temperature-dependent Volume Heat Sources Within the Fluid
LEONARD TOPPER

Continuous Reactions in Distillation Equipment
L. H. BELCK

Kinetics of the Methane-steam Reaction
W. W. AKERS AND D. P. CAMP

Graphical Solutions on Dimensionless-number Plots
BRYANT FITCH

Continuous Stirred Tank Reactors: A New Graphical Method for Complex Reactions and Reflux Designs
E. L. PIRET AND OLEGH BILOUS

Kinetics of the Liquid-phase Oxidation of Ethanol
JOHN KLASSEN AND R. S. KIRK

Activity Coefficients at Infinite Dilution
M. F. GAUTREAUX, JR., AND JESSE COATES

Heat Transfer to Water in an Annulus
PHILIP MILER, J. J. BYRNES, AND D. M. BENFORADO

Numerical Solution of Two-dimensional Heat-flow Problems
JIM DOUGLAS, JR., AND D. W. PEACEMAN

Chemical Reactor Stability and Sensitivity: Part I
OLEGH BILOUS AND N. R. AMUNDSON

Ion Diffusion in Mass Transfer Between Phases
T. K. SHERWOOD AND J. C. WEI

Equivalent Isothermal Temperatures for Nonisothermal Reactors
J. B. MALLOY AND H. S. SEELIG

Dynamics of Vapor Bubbles and Boiling Heat Transfer
H. K. FORSTER AND N. ZUBER

Plant Performance of a 13-ft.-diameter Extractive-distillation Column
J. A. GERSTER, TOKURO MIZUSHINA, T. N. MARLES, AND A. W. CATANACH

Pipe-line Design for Non-Newtonian Fluids
E. B. CHRISTIANSEN, N. W. RYAN, AND W. E. STEVENS

Entrainment Removal by a Wire-mesh Separator
C. L. CARPENTER AND D. F. OTHMER

PUBLIC LIBRARY
JAN 19 1956
DETROIT

Foote
LITHIUM HYDROXIDE

The basic lithium salt for industrial use, Foote lithium hydroxide provides chemically unique properties which are being applied to a host of products ranging from ceramic formulations to multi-purpose grease manufacture and welding rod coatings. Many other industrial uses of lithium are in the development stage.

Foote's integrated lithium facilities—raw material, production, research—are your assurance of an abundant supply of lithium for you and all industry.

We invite you to investigate and apply the unusual properties of lithium hydroxide and its derivatives in your products or processes.

Write for technical data sheets.

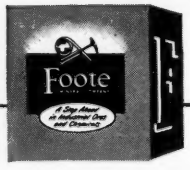

LITHIUM HYDROXIDE FOR INDUSTRY

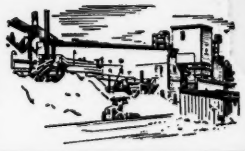

Kings Mountain, N.C. . . . where Foote is mining large deposits of spodumene.

Sunbright, Va. . . . the world's largest lithium chemical plant.

FOOTE MINERAL COMPANY

448 Eighteen West Chelten Building, Philadelphia 44, Pa.

RESEARCH LABORATORIES: Berwyn, Pa. • PLANTS: Exton, Pa.; Kings Mountain, N.C.; Sunbright, Va.

DECEMBER 1955

A.I.Ch.E. JOURNAL

Vol. 1
No. 4

ADVISORY BOARD

C. M. Cooper, O. E. Dwyer,
W. C. Edmister, E. R. Gilliland,
A. N. Hixson, W. R. Marshall, Jr.,
R. H. Newton, R. L. Pigford,
J. M. Smith, Theodore Vermeulen,
R. R. White, R. H. Wilhelm

PUBLISHER

F. J. Van Antwerpen

EDITOR

Harding Bliss

The A.I.Ch. E. Journal, an official publication of the American Institute of Chemical Engineers, is devoted in the main to theoretical developments and research in chemical engineering and allied branches of engineering and science. Manuscripts should be submitted to the New York office.

The Year One 413

Books 415

Transient Behavior of Single-phase Natural-circulation Loop Systems ..... C. D. Alstad, H. S. Isbin, N. R. Amundson, and J. P. Silvers 417

Dispersed-phase Holdup in Packed, Countercurrent Liquid-liquid Extraction Columns. ... . C. E. Wicks and R. B. Beckmann 426

Flow of Non-Newtonian Fluids—Correlation for the Laminar, Transition, and Turbulent Flow Regions ..... A. B. Metzner and J. C. Reed 434

Capacity Factors in the Performance of Perforated-plate Columns ..... C. D'a. Hunt, D. N. Hanson, and C. R. Wilke 441

Benedict Equation of State: Application to Vapor-liquid Equilibria .... E. J. Cullen and K. A. Kobe 452

Gas Absorption Accompanied by Chemical Reaction ..... P. V. Danckwerts 456

Forced-convection Heat Transfer in Cylindrical Pipes with Temperature-dependent Volume Heat Sources Within the Fluid ..... Leonard Topper 463

Continuous Reactions in Distillation Equipment ..... L. H. Belck 467

Kinetics of the Methane-steam Reaction ..... W. W. Akers and D. P. Camp 471

Graphical Solutions on Dimensionless-number Plots ..... Bryant Fitch 475

Continuous Stirred Tank Reactors: A New Graphical Method for Complex Reactions and Reflux Designs ..... E. L. Piret and Olegh Bilous 480

Kinetics of the Liquid-phase Oxidation of Ethanol ..... John Klassen and R. S. Kirk 488

Activity Coefficients at Infinite Dilution ..... M. F. Gautreaux, Jr., and Jesse Coates 496

Heat Transfer to Water in an Annulus ..... Philip Miller, J. J. Byrnes, and D. M. Benforado 501

Numerical Solution of Two-dimensional Heat-flow Problems. Jim Douglas, Jr., and D. W. Peaceman 505

Errata 506

Chemical Reactor Stability and Sensitivity: Part I ..... Olegh Bilous and N. R. Amundson 513

Ion Diffusion in Mass Transfer Between Phases ..... T. K. Sherwood and J. C. Wei 522

Equivalent Isothermal Temperatures for Nonisothermal Reactors .... J. B. Malloy and H. S. Seelig 528

Dynamics of Vapor Bubbles and Boiling Heat Transfer ..... H. K. Forster and N. Zuber 531

Plant Performance of a 13-ft.-diameter Extractive-distillation Column ..... J. A. Gerster, Tokuro Mizushina, T. N. Marks, and A. W. Catanach 536

Pipe-line Design for Non-Newtonian Fluids ..... E. B. Christiansen, N. W. Ryan, and W. E. Stevens 544

Entrainment Removal by a Wire-mesh Separator ..... C. L. Carpenter and D. F. Othmer 549

Communications to the Editor 558

Index 564

Publication Office, Orange, Connecticut. Published quarterly in March, June, September, and December by the American Institute of Chemical Engineers, 25 West 45 Street, New York 36 New York. Manuscripts and other communications should be sent to the New York office. Correspondence with the editor may be addressed to him at Yale University, 225 Prospect Street, New Haven 11, Connecticut. Statements and opinions in the *A.I.Ch.E. Journal* are those of the contributors, and the American Institute of Chemical Engineers assumes no responsibility for them. Subscriptions: one year, member $4.50, nonmember $9.00; two years, member $7.50, nonmember $16.00; additional yearly postage, Canada 50 cents, Pan American Union $1.50, other foreign $2.00 (foreign subscriptions payable in advance). Single copies: $3.00. Second-class mail privileges authorized at Orange, Connecticut. Copyright 1955 by the American Institute of Chemical Engineers.

LIQUID HYDROGEN

for nuclear physics-rocket research-solid state studies

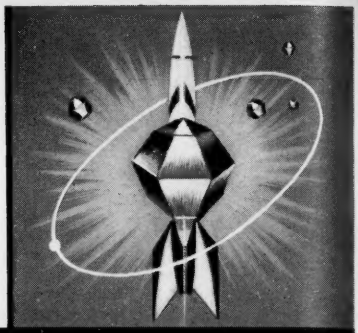

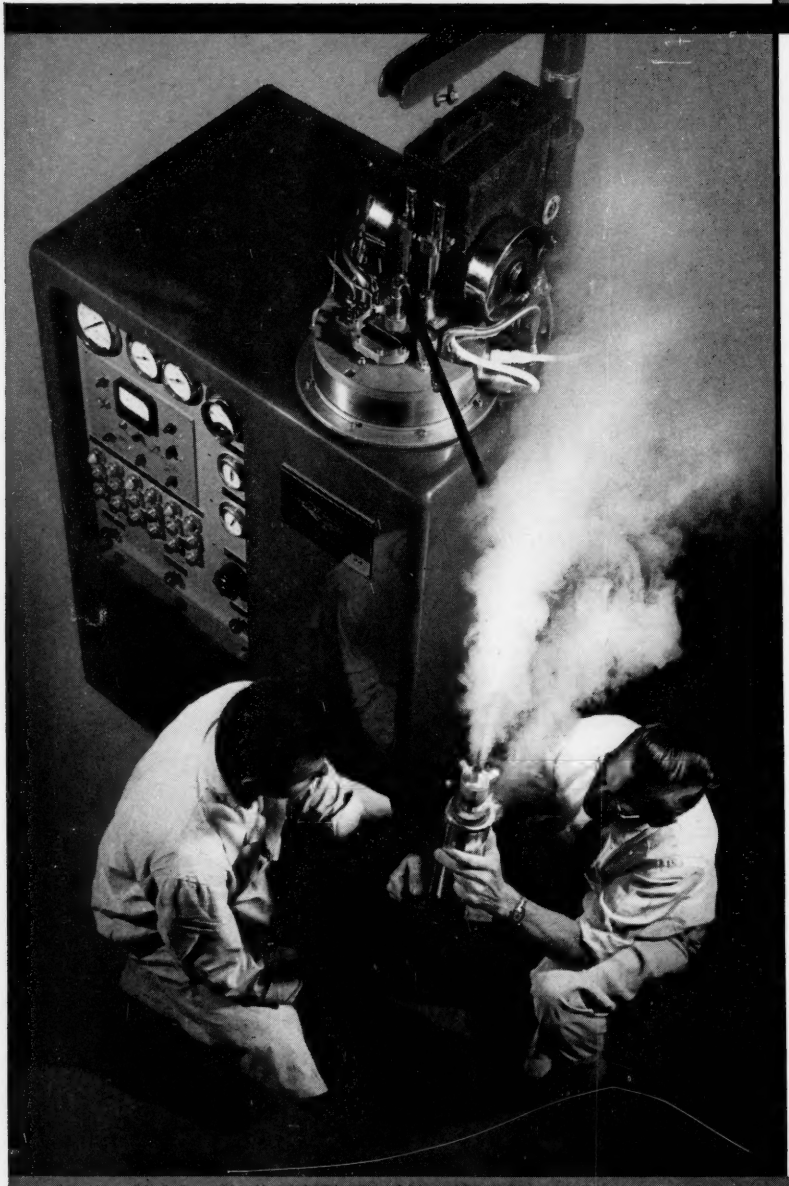

Announcing

a new, simplified method for liquefying hydrogen in quantity to help expedite your research projects.

The ADL Collins Helium Cryostat, without the use of an auxiliary coil, can now produce liquid hydrogen at the rate of from 8 to 10 liters per hour. It can easily be operated by a trained technician and has an internal storage space of 10 liters.

Of primary importance to you are the safety advantages inherent in this low pressure system — at no point does the pressure in the hydrogen circuit exceed 15 PSIG. Further, the basic apparatus has been thoroughly proved through more than eight years of field operation.

Should your research also require liquid helium, a changeover from hydrogen liquefaction to helium liquefaction or vice versa can be made in less than 30 minutes without shutting down the machine and without loss of efficiency.

For further information on this new cryogenic development, write for Bulletin H-1.

Arthur D. Little, Inc. 30 Memorial Drive Cambridge 42, Mass.

An *Air Products* OXYGEN PLANT

belongs in this picture

Is your Company one of the many concerns in the process industries that are contemplating expansion requiring the use of tonnage or high purity oxygen?

If so, the specialized experience of Air Products in this field (based on more than 700 successful installations) can be of substantial help in formulating your plans. An Air Products Oxygen Plant engineered specifically for your particular requirements can be a real money-maker.

We are equipped to design and build:

Large Capacity Tonnage Generators, regardless of size, purity, high or low pressure cycle, with liquid oxygen pumps, if your oxygen should be under pressure

or

"Packaged" High Purity Generators, producing high purity oxygen and nitrogen simultaneously —oxygen delivered safely under pressure by Air Products patented liquid oxygen pumps.

Send us information regarding your requirements.

Specialists in Low-Temperature Processing

Air Products
INCORPORATED
Dept. M, Box 538 Allentown, Pa.

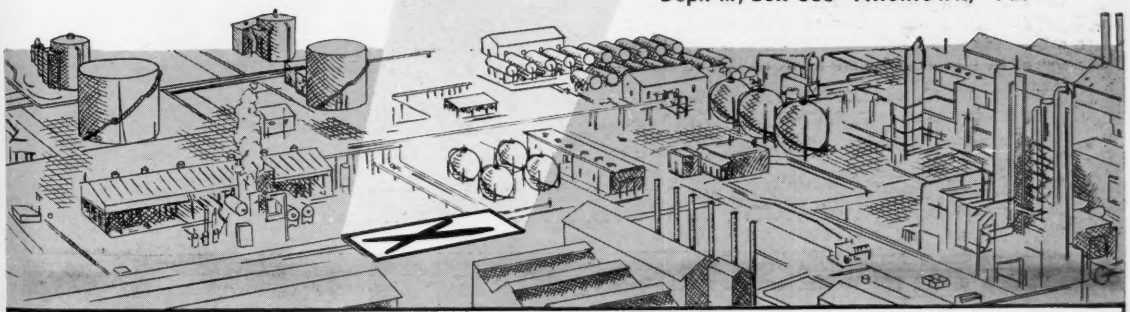

Cost Analyses • Process Design • Apparatus Design • Apparatus Manufacture

CEC increases the scope of

industrial mass spectrometry

through two great instruments for process monitoring and control

Consolidated's Model 21-610 mass-spectrometer and its companion, the new Model 21-620, far excel all other instruments of comparable price in performance capabilities and reliability in industrial environment. The extreme sensitivity of the 21-610—accurate to a few parts per million—qualify it for highly critical purity studies as well as process monitoring and control applications. Fitted with an accessory hand-held probe, either model serves as a leak detector for any gas within its mass-range. The 21-620's resolving power up to mass 150 further extends the applicability of an industrial mass-spectrometer to research laboratories and medical centers, as well as to plants of chemical, petro-chemical, petroleum and gas industries. Nearly identical in appearance, the 21-610 features the Diatron ion analyzer and the 21-620, a new cycloidal focusing analyzer.

21-620 Except for slightly less sensitivity, the 21-620 has all the capabilities of the 21-610 plus many others. Where the task is to analyze "heavy" gases or liquids, either in plant locations or in the laboratory, the 21-620 process monitor mass-spectrometer is the ideal control instrument.

21-610 The 21-610 is completely self-contained, needing only 110 volts and a small quantity of cooling water for operation. Moderately priced, easily movable, and economical to operate, the 21-610 is industry's ideal instrument for chemical research, process control and leak detection.

CEC Service Engineers quick change of ion analyzers (right) adds flexibility to Consolidated's two process monitoring mass-spectrometers. A cycloidal focusing analyzer assembly of the 21-620 type is being mounted in the vacuum rack in place of the Diatron analyzer of the 21-610.

The basic instrument can be augmented by many available accessories, thus broadening its application scope. At the far right, are a gas or light-liquid sample inlet system and chart recorder.

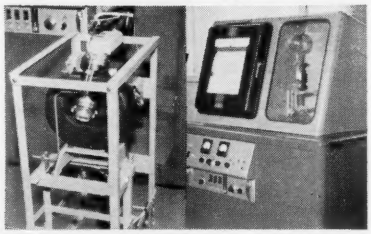

Consolidated Engineering
CORPORATION
300 North Sierra Madre Villa, Pasadena 15, California

Sales and Service through **CEC INSTRUMENTS, INC.,** *a subsidiary with offices in: Pasadena, Atlanta, Chicago, Dallas, Detroit, New York, Philadelphia, Washington, D. C.*

ANALYTICAL INSTRUMENTS FOR SCIENCE AND INDUSTRY

Investigate the application of industrial mass-spectrometry to your business. For full details about CEC's two companion process monitoring mass-spectrometers, send for Bulletin CEC 1824A-X23.

THE YEAR ONE

With this December issue of the *A.I.Ch.E. Journal* we complete our first year of publication. The infant has been, on the whole, well behaved and it is hoped that the officers and directors of the Institute, who should claim the honor of parenthood, will feel some pride in it. The editor, who may be said to stand in the position of godfather, feels that the youngster is at least holding his own. All difficulties which have been experienced are certainly minor when compared with the abundant help freely given by all concerned.

It is a great pleasure to be able to report that our circulation has grown rapidly, in particular that it has been increased by 25% since the first issue. This increase, we hope, indicates general satisfaction with our efforts, but it also implies that there was a very great need for a publication of this sort and that the officers and directors decided wisely in setting forth on this venture.

It was realized at the outset that this journal would have its principal appeal to chemical engineers in research and development, whether they were pursuing these interests in academic life or in industry. There was some fear, on the editor's part at least, that the contributions of the academicians might far outweigh those of industrialists. It is, therefore, particularly gratifying to see that about one third of the papers of the September and December issues originated in industry. It is still our great hope that this proportion will rise, as the research and development engineers in industry have much to tell their academic colleagues. The opposite is also true, of course, but the flow of information in this direction has always been fairly abundant. There has been in academic circles a quite justifiable tendency to simplify the problem, to delimit the system in such a manner that an answer could be found. Industrialists, on the other hand, are more often concerned with problems for which the answer must be found. The interplay of these two approaches can be enormously fruitful for all of us: the industrialist will find new ideas in the universities to help with his solutions and the university people will learn what directions are interesting and, perhaps, what simplifying assumptions are or are not justified. We hope that the *A.I.Ch.E. Journal* will bring together as many different ideas and approaches as possible. Examples of what we may expect in this regard are found in two papers scheduled for early next year in which entrainment behavior and plate efficiencies in large commercial towers are reported on and compared with theoretical work in simplified and idealized systems carried out in university laboratories.

The subject matter covered in this first year has been satisfactorily broad. The unit operations, thermodynamics, and kinetics, on which the science of chemical engineering is based, have been represented in many papers. The powerful assistance of advanced mathematics has been called into play in many instances, and it is hoped that this will please the already well versed and stimulate the rest to a new appreciation and respect for such assistance and a new zeal to review and refresh their comprehension of mathematics.

In our ensuing years we hope to expand our coverage of research in chemical engineering, and the editor will welcome suggestions as to how this aim may be best accomplished and how the *Journal* may, in general, be improved.

This review of our first year can best be concluded with a broad acknowledgment of the gratitude due to many people who have given invaluable assistance: the authors and reviewers of our papers, the officers and directors of the Institute, and particularly the Publisher, the Advisory Board, various members who have volunteered many fine ideas and criticisms, and the staff assistants.

H. B.

write for your free copy

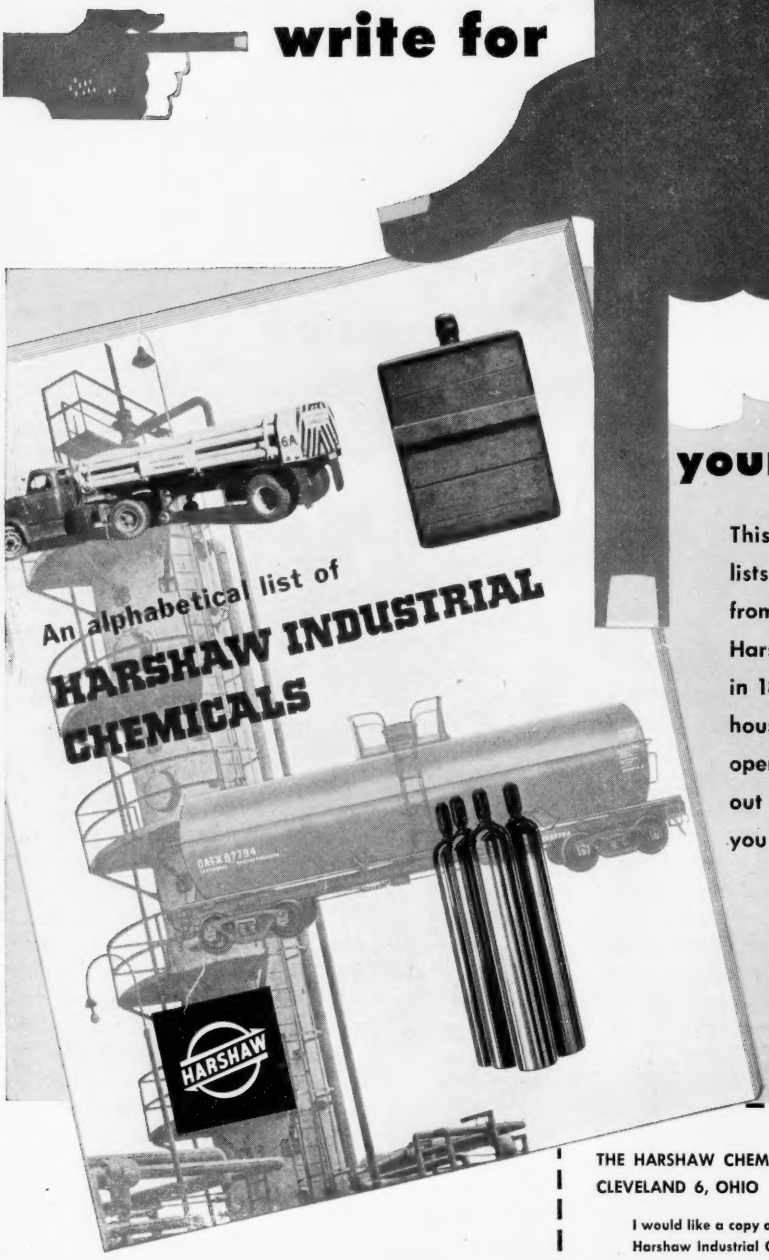

This 24-page booklet alphabetically lists the many chemicals available from Harshaw. Read the story about Harshaw's growth since its beginning in 1897. Pictures of plants, warehouses, research and manufacturing operations are scattered throughout the book. We will gladly send you a copy if you write.

THE HARSHAW CHEMICAL CO.

CLEVELAND 6, OHIO

Chicago • Cincinnati • Cleveland • Detroit • Houston • Los Angeles
New York • Philadelphia • Pittsburgh

THE HARSHAW CHEMICAL CO.
CLEVELAND 6, OHIO

I would like a copy of your free booklet "An Alphabetical List of Harshaw Industrial Chemicals."

MY NAME _____

COMPANY NAME _____

ADDRESS _____

CITY _____ ZONE ____ STATE _____

BOOKS

Process Engineering Economics. Herbert E. Schweyer. McGraw-Hill Book Company, Inc., New York (1955). 409 pages. $7.50.

The first five chapters of the text, covering economic principles and elementary accounting procedures, are intended to provide a background for the application of economic principles to engineering problems, which constitutes the subject of the remaining seven chapters.

After a short introductory chapter the time value of money is discussed as a function of its use, and some basic equations frequently used in process engineering economics are derived. The principle of the equivalence of different methods of paying back capital with interest is considered and illustrated. The subject of amortization is then examined, thus furnishing an application of the principle of equivalence to a practical, recurrent case. Depreciation and depletion are presented along with various ways for including them in the accounting system.

Capital requirements for process plants are considered in relation to the nature of the operation, the size of the plant, and the prevailing economic conditions. Cost indexes, equipment costs, and sources of capital are concisely reviewed. The balance sheet is introduced and explained. The author then goes on to explore the costs of plant operation and the selling of the product to the consumer. The relations among profits, sales, cost of sales, plant production, and selling price are graphically illustrated.

The remainder of the text is devoted to applications of economic principles in the process industries. The selection of alternates is treated as an economic problem and is amply illustrated, four different methods of comparison being discussed. Rate of return and payout time are then introduced as guides for the valuation of proposals. The economics of replacement of existing facilities is discussed, "irreducible factors" receiving brief attention. The economic balance first is introduced as a general problem and then is applied to problems concerning insulation, evaporation, reactor vessels, fluid flow, heat transfer, and mass transfer. Economic balance with two (or more) independent variables is treated, and combined operations are considered from the economic-balance viewpoint. Cyclic operations and yield and recovery each receive special treatment in a separate chapter, as does inventory as an economic problem in the process industries. Economic analysis of a complete process is the subject of the summarized discussion of the last chapter.

Professor Schweyer has apparently intended his book to be primarily a text for engineering students. In addition, it is designed to be of use to the practicing engineer. A great instruction advantage is gained by means of the seventy illustrative problems that are worked out in detail in the text. Also a total of 189 problem statements are given at the ends of chapters, enabling the student to apply the subject matter to concrete examples.

"Process Engineering Economics" provides the essentials of economics and accounting as applied in the process industries and, in addition, supplies a thorough grounding in the principles and applications of the economic balance.

ROBERT M. SECOR

Principles of Industrial Waste Treatment. C. Fred Gurnham. John Wiley and Sons, Inc., New York (1955). 392 pages. $9.50.

Professor Gurnham's basic idea in writing this book is an excellent one. It is his feeling that closer cooperation and understanding between chemical engineers and sanitary engineers would be to the advantage of both groups and should lead to fruitful results in the cause of industrial waste disposal. A unique feature of the book is the presentation of the subject matter of industrial waste disposal in the framework of the chemical engineer's unit operations and unit processes.

The first few chapters are devoted to a discussion of the waste picture in terms of the effects of pollution on streams and sewerage systems. There follows a presentation of the unit operation of sedimentation, filtration, and heat transfer and of the unit processes of *p*H adjustment, oxidation and reduction, coagulation, ion exchange, and biological treatments. To the sanitary engineer the book should be of importance because of the interesting and logical organization of subject matter which results. The chemical engineer will be interested in seeing his familiar classification applied in this case and extended to include biological treatments.

The book has been written for use primarily as a text for students in either chemical engineering or sanitary engineering. The subject matter is largely qualitative in nature and should be readily grasped by students in either group. The engineer practicing in the field of waste disposal will be interested in the book not as a reference source but as a basis for orienting his thinking on problems. The engineer practicing in other fields will find it most useful in developing an appreciation of the complexity of waste disposal problems in terms of their effects on streams and sewer systems and their bearing on the design and operation of industrial plants. The exposition is in general clear and logical. The discussion could have been simplified in several places by more effective use of flow sheets and diagrams.

C. A. WALKER

The Chemistry of the Petroleum Hydrocarbons. Volumes 2 and 3. Edited by Benjamin T. Brooks, Cecil E. Boord, Stewart S. Kurtz, and Louis Schmerling. Reinhold Publishing Corporation, New York (1955). Volume 2, 448 pages, $13.50. Volume 3, 690 pages, $18.00.

Like the first volume in this series, these volumes help to fill the need for reference books containing the scientific fundamentals that are applied in the hydrocarbon industry. These volumes are a compilation of information written by outstanding contributors in the field of hydrocarbon chemistry.

Most of the articles include a discussion of the relevant reactions and operational techniques involving the hydrocarbons; derivatives of the hydrocarbons have been excluded for the sake of brevity. Much emphasis is placed on theoretical considerations, such as probable mechanisms of reactions; kinetics of reactions; role of catalysts; thermodynamic equilibria of reactions; and structural, physical, and chemical comparisons of reactants and products. Other applied problems are considered: the uses of hydrocarbon products, special reactions of hydrocarbons, commercial operation, and many others. Again because of the limited space many problems of this type have been omitted, such as problems of apparatus design, process engineering, and analytical testing methods.

The volumes are lucidly written and necessary information is neatly condensed in the form of tables and graphs. Mention should be made of the badly drawn graphs in Chapter 45, "Vinyl Polymerisation." Such figures are out of place in this article.

FRANK BARR-DAVID

The Roger Adams Symposium: Papers Presented at a Symposium in Honor of Roger Adams at the University of Illinois, September 3-4, 1954. W. R. Brode, T. R. Johnson, S. M. McElvain, R. L. Shriner. W. M. Stanley, and E. H. Volwiler. John Wiley and Sons, Inc., New York (1955). 140 pages. $3.75.

This book is a collection of papers presented at a symposium honoring Roger Adams on the occasion of his retirement from the chairmanship of the Chemistry Department at the University of Illinois on September

(*Continued on page* 568)

WILMAD TUBING...

Product of Pride and Precision

• PRECISION BORE TUBING

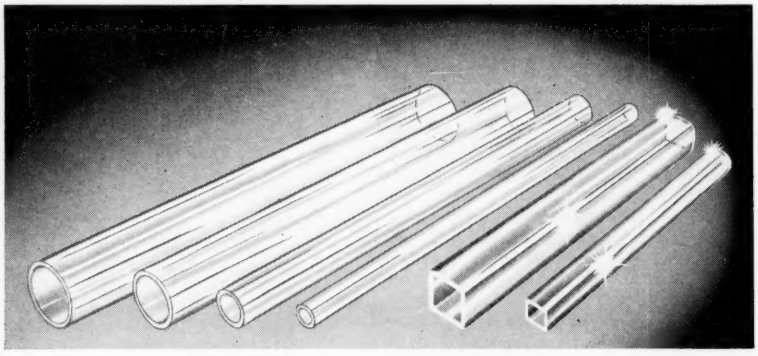

Many industrial and electronic engineers who need extreme accuracy in glass tubing use Wilmad Precision Bore Tubing exclusively. Ideal for use in barometers, bearings, dashpots, manometers, voltage regulators, capacitors, rotameter tubes, burettes, viscosimeters, wave guide tubes, UHF tuners and cavities, and hundreds of other applications.

Made in various shapes and sizes . . . square, rectangular, hexagonal, and tapered up to 7" ID. Fluted and other special shapes can be made to meet individual requirements. Available in Pyrex Brand, Vycor Brand and most of the electronic glasses.

• PRECISION BORE CAPILLARY TUBING

Our claim of consistently achieving an accuracy and uniformity hitherto considered impossible is no idle boast. In a size range that runs from .004" ID to .100" ID, our tolerance limits are set at ±.0002".

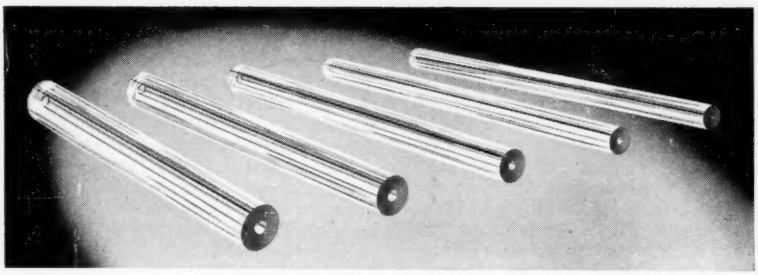

Send for this free catalog TODAY

We welcome the opportunity of discussing with your Engineering Department any particularly difficult problems they might have in the precision glass field. We will be glad to help you find a solution.

WILMAD GLASS COMPANY, INC.

DEPT. A

LANDISVILLE • NEW JERSEY

SPECIALISTS IN RESEARCH LABORATORY GLASSWARE

CHEMICAL · LABORATORY W GLASSWARE

Transient Behavior of Single-phase Natural-circulation Loop Systems

C. D. ALSTAD, H. S. ISBIN, N. R. AMUNDSON
University of Minnesota, Minneapolis
and
J. P. SILVERS
Argonne National Laboratory, Chicago, Illinois

A useful method is reported for calculating temperatures and rates of flow in the unsteady-state operation of natural-circulation loops in single phase. A one-dimensional mathematical model is used with the assumptions that (1) at any instant the volumetric rate of flow is constant around the loop and (2) steady-state friction factors can be applied in transient operations. The loop, consisting of a heat source, heat sink, hot leg, cold leg, and connecting piping, is divided into a number of finite increments. The transient behavior is calculated by the iterative application of the finite-difference momentum and energy balances. Numerical computations made for several cases of transient operations were carried out with the aid of the Standard Eastern Automatic Computer (SEAC).

Comparisons of predicted with actual performances were checked by use of two experimental loops employing water and found satisfactory.

A number of practical problems arising in boiler and nuclear-reactor-coolant designs have demonstrated the desirability of establishing a method for the prediction of temperatures and rates of flow in the transient operation of natural-circulation loops. To the authors' knowledge, this paper presents the first published comparisons of calculated and experimental transient behavior of a natural-circulation loop involving liquid water as the circulating fluid. The principal objective of this study was to determine the reliability of the calculations based upon numerical solutions of finite-difference energy and flow equations. Solutions were obtained through the use of the Standard Eastern Automatic Computer (SEAC).

Figures 1 and 2 illustrate the natural-circulation loops, and Table 1 lists the conditions for the transient operation of the loops for several problems computed. Details of the loops and the conditions of operation are given in later sections, along with an illustration of the complete system of equations used for one problem. The complexities of the physical problems were appreciated at the outset, and thus it was desirable to start with a simplified mathematical model and to introduce only needed refinements. For the numerical transient evaluations, it was necessary to calculate and experimentally to verify the loop parameters for steady-state flow. The refinement of the loop parameters on the transient calculations is presented, for example, as revisions of computer problem 3. (*See* Table 2.)

PREVIOUS INVESTIGATIONS

Of the extensive literature on transient flow, it is of interest to note that Jenny(*9*), among others, pre-

C. D. Alstad is at present with Dow Chemical Company, Midland, Michigan, and J. P. Silvers is with Avco Manufacturing Corporation, Stratford, Connecticut.

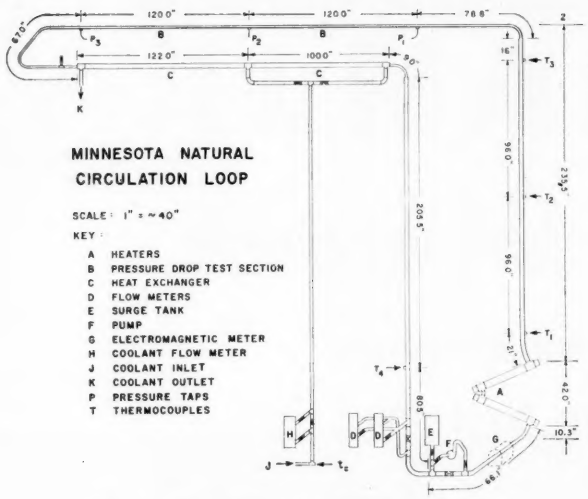

Fig. 1. Minnesota natural-circulation loop.

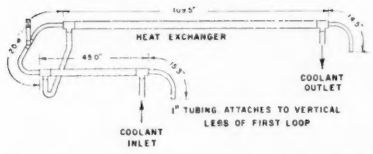

Fig. 2. Top section of second natural-circulation loop.

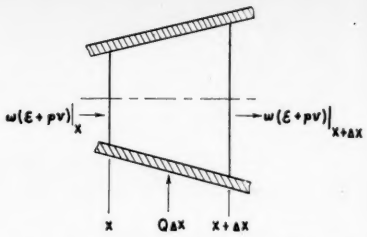

Fig. 3. Volume element of fluid for energy.

sented the derivation of the equation of motion for the unsteady turbulent flow of fluid in a horizontal tube. Accelerated flow may occur in a steady, nonuniform flow, such as at the entrance to a tube, from a reservoir wherein the boundary layer grows along the tube. Among those who have studied this problem is Langhaar(*11*). Grace(*6*) considered the oscillatory motion of a fluid in a pipe, and Valensi(*21*) was concerned with the oscillatory viscous flow in a U tube. Schonfeld(*20*), considering isothermal transient viscous flow in pipes for the case where a finite pressure differential is applied to a fluid initially at rest, found that the flow of fluid approached steady-state conditions asymptotically. He also studied forced oscillation in round tubes and natural oscillation in U tubes. The mixing-length theory of Prandtl and Von Karmen was used to study fully developed turbulent flow in round tubes and wide-open canals. Daily and Deemer(*4*) reported that steady-state friction factors were applicable to the transient flow of fluid and found that the total pressure drop across a given section could be calculated from the sum of the instantaneous frictional pressure drop and acceleration head. DeJuhasz(*5*) presented a graphical method for determining the response of a system to unbalances. Velocity and pressure may be determined as functions of time and position for isothermal systems subjected to known disturbances. Binnie

TABLE 1.—FLOW CONDITIONS FOR COMPUTER PROBLEMS

Computer problem	Initial volumetric rate of flow	Initial temp., °F.	Nature of step change	Coolant temp., °F.	Comments
1*	0	Uniform around loop 80.5	Abrupt heat input 4 heaters, 25.08 kw.	40	First loop
2	0	Uniform around loop 122.0	Abrupt heat input 4 heaters, 24.75 kw.	37.5	First loop
3	0.00137 cu. ft./sec.	144.0 in riser 77.5 in downcomer	Bottom heater, 6.30 kw. Abrupt heat input 3 heaters, 18.58 kw.	36.5	First loop
4	0	Uniform around loop 109.0	Abrupt heat input Top three heaters, 19.17 kw.	40	Second loop

*Not reported in this paper.
Revisions to computor problems pertain to changes in loop parameters and number of subdivisions. (*See* Table 2.)

TABLE 2—NATURE OF REVISIONS FOR COMPUTER PROBLEM 3

	Comments	Heat transfer coefficient		Loop resistance	Heater lag	Heat transfer to heater walls	Heater volume, cu ft.
		Cooler (Over-all)	Vertical riser (Film)				
Initial problem		$U = 35.1V$	$h = 43V$	$R_l = 10^6 V^{1.65}$	Not taken into account	Not taken into account	0.176 (calc'd.)
First revision	Error in heat capacity of tubing walls corrected. Simple heater lag taken into account.	Same	Same	Same	$Q' = q'(1 - 0.189e^{-18.3V\tau})$	Same	Same
Second revision	Film heat transfer coefficient revised. Cooler coefficient revised to take into account cooler subdivisions. Loop resistance evaluated on basis of 10 gal./min. for coolant flow. Improved heater lag equation used. Heater volume measured.	$U = 41.5V$	$h = 58.7V$	$R_l = 690{,}000V^{1.58}$	$Q' = q'(1 - 0.173e^{-18.3V\tau} - 0.827e^{-197V\tau})$	Same	0.184 (measured)
Third revision	Heat transfer to heater walls taken into account.	Same	Same	Same	Same	Taken into account	Same
Fourth revision	Size of subdivisions nearly doubled.	Equation corrected to take into account subdivisions.	Same	Same	Same	Same	Same

NOTE.—*Same* designates condition of previous revision not changed.

(*2*) treated a somewhat similar problem but obtained an analytical solution. He was able to calculate the pressure surges which occur in long pipe lines because of the closure of a valve. Allowance was made for the effect of friction, which was assumed proportional to velocity. For cases where the friction was not directly proportional to velocity, the method gives an approximate value. Hall(*7*) considered pulsating flows and their effect on orifice and flow coefficients. The calculated accelerations of fluids in an isothermal U loop were experimentally verified by Leppert(*14*).

EXPERIMENTAL LOOPS

Two experimental loops were designed, erected, and instrumented. A schematic drawing of the first convection loop is given in Figure 1. To obtain faster accelerations, the top horizontal section of the first loop was replaced by a much shorter, larger-diameter section as illustrated in Figure 2, and this arrangement with its new method of measuring flow constituted the second circulation loop. The flowmeter for the first experimental loop was a differential pressure transmitter and recorder which measured the pressure drop across the horizontal pressure-drop test section. Though this method of evaluating the transient flow from the pressure-drop readings was cumbersome, it was found to be satisfactory for the relatively slow transient in the first circulation loop. An electromagnetic flowmeter was used to measure the instantaneous volumetric rate of flow in the second loop.

The heater consisted of four 7.5-kw. Chromalox immersion heaters arranged in a V shape as noted in Figure 1. Bare platinum–platinum-rhodium thermocouples (24 gauge) were directly exposed to the fluid to obtain maximum response. The fluid temperatures T_1 to T_4 were determined at locations noted in Figure 1 and were recorded on a Leeds and Northrup Speedomax recorder. Concentric tube heat exchangers were used to cool the flow. The general arrangements for the two loops are shown in Figures 1 and 2.

The vertical riser and downcomer sections were made of 1-in. O.D. hard-brass tubing (0.872 in. avg. I.D.), giving the loop an over-all height of about 24 ft. As shown in Figure 1, the system of valving in the bottom horizontal return section permitted runs also to be made with forced circulation by use of the pump and rotameters. Compressed air was introduced to a small surge tank (4-in.-diam. brass pipe, 11½ in. long) to regulate the pressures over a range of about 40 to 80 lb./sq.in. A minimum liquid level was maintained in the surge tank to reduce pressure fluctuations during the transient operations.

Steady-state–flow runs were made to determine the physical parameters

TABLE 3.—LOOP PARAMETERS FOR SECOND EXPERIMENTAL LOOP

Heat Transfer Coefficients	
Over-all coefficients for heat exchanger (cooler)	$U-16.1V$
3/4-in. tubing	$h_{3/4}=56.7V$
1-in. tubing	$h_1=31.7V$
Heater section	$h_h=16.0V$
Loop Resistances	
Turbulent flow	$R_l=332{,}000V^{1.64}$
Viscous flow	$R_l=2{,}500\mu V$
Dimensions and Other Values	
$D_o=1.000$ in., $D_n=0.872$ in., $\delta=0.00573$ ft., $\rho_w c_w=53.0$ B.t.u./(cu. ft.) (°F.) for 1-in. tubing	
$a_l=\frac{\rho}{g}\int\frac{dx}{A}=(\rho/g)\sum_{n-1}^{N}\frac{x_n}{A_n}=16{,}990\ \rho/g=32{,}200$ lb. sec.^{2}/ft.^{5}	
1-in. tubing	$\frac{L}{A}=14{,}530$ ft.$^{-1}$
3/4-in. tubing	$\frac{L}{A}=1{,}880$
1-in. pipe	$\frac{L}{A}=280$
Heater	$\frac{L}{A}=290$
$\rho c=60.9$ B.t.u./(cu. ft.) (°F.)	Average density used

TABLE 4.—FINITE DIFFERENCE EQUATIONS FOR COMPUTER PROBLEM 4

Subdivision	
Hot leg 1-15	$T'_n=(1-197.1\ V\triangle\tau)\ T_n+168.5\ V\triangle\tau\ T_{n-1}+28.6\ V\triangle\tau\ t_n$ $t'_n=(1-105\ V\triangle\tau)\ t_n+105\ V\triangle\tau\ T_n$
Cooler 16-24	$T'_n=(1-183.1\ V\triangle\tau)\ T_n+168.5\ V\triangle\tau\ T_{n-1}+14.6\ V\triangle\tau\ t_c$
Cold leg 25-44	$T'_n=(1-192.8\ V\triangle\tau)\ T_n+164.2\ V\triangle\tau\ T_{n-1}+28.6\ V\triangle\tau\ t_n$ $t'_n=(1-105V\triangle\tau)\ t_n+105\ V\triangle\tau\ T_n$
Heater 45-48	$T'_n=(1-27.7\ V\triangle\tau)\ T_n+21.7\ V\triangle\tau\ T_{n-1}+6.0\ V\triangle\tau\ t_n$ $+0.338\ (Q_{KW})_n\ \triangle\tau\ (1-0.173\ e^{-18.3V\tau}-0.827\ e^{-0.1\tau})$ $t'_n=(1-16.5\ V\triangle\tau)\ t_n+16.5\ V\triangle\tau\ T_n$
Flow equations	$V'=V+\triangle\tau(0.0000311\ H'_l-0.0481V)$ for $V<0.00085$ $V'=V+\triangle\tau(0.0000311\ H'_l-10.32V^{1.64})$ for $V>0.00085$ $H_l=\sum_{n=1}^{48}\rho_n Z_n$
Conditions of restraint	$Z_1=-1.3475$; $Z_{2-13}=-1.4308$; $Z_{14}=-1.1075$; $Z_{15-24}=0$; $Z_{25}=0.3640$; $Z_{26-41}=1.4687$; $Z_{42}=0.1156$; $Z_{43}=0$; $Z_{44}=-0.8542$; $Z_{45-48}=-0.8750$
	$\rho_n=62.404+0.4556\left(\frac{T_n}{100}\right)-0.9605\left(\frac{T_n}{100}\right)^2+0.08164\left(\frac{T_n}{100}\right)^3$ $n_{49}=n_1$
Operating conditions	$V=0$, $\tau=0$; $t_c=40.0$, $(Q_{KW})_{45}=0$; $(Q_{KW})_{46-49}=6.39$; $(T_{1-48})_{\tau=0}=109.0$; $(T_n)_{\tau=0}=(t_n)_{\tau=0}$

of the experimental loops. These parameters include the friction factors, over-all heat transfer coefficients for the coolers, fluid film heat transfer coefficients, total loop resistance, and heater lag. It was possible to demonstrate that simplified relations could be used for some of the parameters; for example, the correlations used for the over-all heat transfer coefficient in the cooler, the film heat transfer coefficient in the vertical riser, and the loop resistance are given in Table 2. These correlations are discussed in reference *1*, including the manner in which the number of subdivisions in the cooler affects the over-all heat transfer coefficient.

All the transient runs reported in this paper involve a sudden increase in the heat input to the loop. It was recognized that a step change in heater switch settings would not introduce instantaneously the corresponding power change to the fluid. Consequently, it was deemed desirable to introduce into the finite-difference-method calculations heater-lag equations of various degrees of complexity. The initial calculations made for all runs on the first circulation loop involved no corrections for the heater lag, and, as illustrated in Table 2, heater-lag provisions, along with other refinements in loop parameters, were then introduced into the succeeding revisions. The determination of the heater-lag time was approached from both a theoretical and an experimental point of view, and the details are given in reference *1*. It is to be noted that all refinements introduced for the heater lag were made independently of the transient operation of the natural-circulation loops and were based only on the performance of steady-state–flow runs.

TRANSIENT ANALYSIS

The transient analysis is restricted to the one-dimensional, nonsteady, rectilinear flow of real fluids. The assumption of one-dimensional flow is strictly applicable to cases where the velocity of the fluid is uniform over the entire cross section of flow. The analysis is therefore valid only for an ideal case, but in practice an average velocity may be used for a variety of velocity profiles and the problem considered ideal. It is assumed that the fluid is continuous, no sources or sinks therefore existing, and that no heat is generated or lost within the body, for instance by chemical reaction. The effects due to the conduction of heat along the longitudinal axis are assumed to be negligible.

The continuity equation may be written as

$$\frac{\partial\rho}{\partial\tau}+\frac{1}{A}\frac{\partial(\rho uA)}{\partial x}=0 \qquad (1)$$

In a system consisting of the volume element of fluid shown in Figure 3, where it is assumed that there is no shaft work, the heat input, Q, is defined as net heat added to the system per foot per second, and the symbol ϵ represents the total energy per pound of fluid, $E+(u^2/2\alpha g_c)+(g/g_c)z$. The energy balance is

$$\frac{-\partial[w(\epsilon+pv)]}{\partial x}+Q=A\frac{\partial(\rho\epsilon)}{\partial\tau} \quad (2)$$

Introduction of the continuity equation leads to

$$u\frac{\partial}{\partial x}\left(E+\frac{u^2}{2\alpha g_c}+\frac{g}{g_c}z\right)+\frac{\partial}{\partial\tau}\left(E+\frac{u^2}{2\alpha g_c}+\frac{g}{g_c}z\right)+\frac{1}{\rho A}\frac{\partial}{\partial x}(puA)=\frac{Q}{\rho A} \quad (3)$$

which may be written as

$$\frac{D\epsilon}{D\tau}\times\frac{1}{\rho A}\frac{\partial(puA)}{\partial x}=\frac{Q}{\rho A} \quad (4)$$

An alternate form is

$$\frac{D}{D\tau}\left(H+\frac{u^2}{2\alpha g_c}+\frac{g}{g_c}z\right)-\frac{1}{\rho}\frac{\partial p}{\partial\tau}=\frac{Q}{\rho A} \quad (5)$$

The equation for motion for flow in a uniform pipe is

$$\frac{1}{g_c}\left(\frac{\partial u}{\partial\tau}+u\frac{\partial u}{\partial x}\right)+\frac{1}{\rho}\frac{\partial p}{\partial x}+\overline{F}+\frac{g}{g_c}\frac{\partial z}{\partial x}=0 \quad (6)$$

The pipe friction, F, has not yet been given an explicit definition. The general equation of motion must, however, reduce to the simple mechanical energy balance for steady-state conditions. It is therefore assumed that

$$\overline{F}=\frac{f_\tau u^2}{2g_cD} \quad (7)$$

The resultant equation of motion is

$$\frac{1}{g_c}\left(\frac{\partial u}{\partial\tau}+u\frac{\partial u}{\partial x}\right)+\frac{1}{\rho}\frac{\partial p}{\partial x}+\frac{g}{g_c}\frac{\partial z}{\partial x}+\frac{f_\tau u^2}{2g_cD}=0 \quad (8)$$

It is not necessarily true that f_τ will correspond to the Moody friction factor, as the form of the frictional losses has been only assumed and may itself be in error. Recent experiments (*4*), however, have shown the validity of Equation (8) at least for isothermal flow. These results indicate that f_τ corresponds to the Moody friction factor of steady state when transient velocities from 15 to 75 ft./sec. and accelerations from 0 to 35 ft./sec.^{2} are used. It was reported that the total observed pressure drops could be calculated from steady-state velocity losses and acceleration heads except during periods of initial impulse.

The method of approach in applying the unsteady-state partial-differential equations to loop systems is to reduce the equations of motion and the energy balance to simplified finite-difference equations. Coasting, or isothermal transients, has been considered in reference *1*, and in this section the nonisothermal transient behavior is considered.

The equation of motion, Equation (8), is applied to the schematic loop shown in Figure 4. For this application, F represents the frictional losses which are given by the ordinary steady-state correlations. For the transient case, the thermal loads of the two heat exchangers generally will not be equal and will fluctuate with time. The nonisothermal operation of the convective loop for an all-liquid system would require the addition of a surge tank as shown in dotted lines in Figure 4. It is assumed that the presence of the surge tank will not affect the loop flow except to minimize the pressure fluctuations. The additional assumption made is that the volumetric rate of flow is uniform around the loop at any instant (independent of position). An estimate of the differences in volumetric flow rates in the hot and cold legs is given in reference *1*, and an alternate method based upon the use of an instantaneous constant weight rate of flow also is noted.

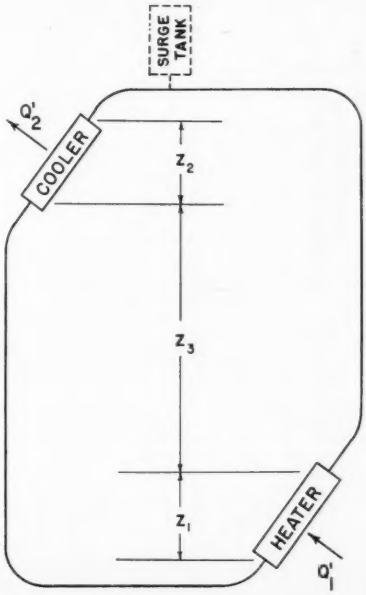

Fig. 4. Natural-circulation loop (schematic).

With the assumption that $\partial V/\partial x=0$ and $\partial V/\partial\tau$ is independent of x, the equation of motion can be simplified to

$$\frac{dV}{d\tau}=\frac{-\int_o\rho dz-\int_o\rho\overline{F}dx}{\int_o\frac{\rho}{g_c}\frac{dx}{A}} \quad (9)$$

Equation (9) may be symbolized as follows:

$$\frac{dV}{d\tau}=\frac{H_l-R_l}{a_l} \quad (10)$$

This equation expresses the volumetric acceleration in terms of the net driving force, which is the difference between the loop hydraulic head and total loop resistance and the loop geometry. The total loop resistance to flow, R_l, is identical with the steady-state values for similar temperatures and rates of flow. H_l corresponds to the loop hydraulic head, and a_l to the loop constant. In order to solve this equation simultaneously with the energy equation, it will be necessary to replace the derivative by its finite-difference approximation. This gives

$$V'=V+\Delta\tau\left[\frac{H'_l-R_l}{a_l}\right] \quad (11)$$

where the prime denotes a forward extrapolation in time. The time interval should be small enough that H_l, R_l, and a_l may be evaluated at either end of the time interval without appreciable effect on the solution. The energy equation, as noted below, permits the evaluation of H_l.

It can be readily ascertained that a suitable form of the energy equation is simply a heat balance.

$$\frac{DH}{D\tau}=C_p\left(\frac{\partial T}{\partial\tau}+u\frac{\partial T}{\partial x}\right)=\frac{Q}{\rho A} \quad (12)$$

Heat conduction along the axis of flow and the mechanical energy terms can be neglected. Replacing

the partial derivatives by their approximate finite differences results in

$$\frac{T'_{x+\Delta x}-T_{x+\Delta x}}{\Delta\tau}+\frac{V}{A\,\Delta x}\left(T_{x+\Delta x}-T_x\right)=\frac{Q}{\rho C_p A} \quad (13)$$

or

$$T'_{x+\Delta x}=\left(1-\frac{V\Delta\tau}{A\,\Delta x}\right)T_{x+\Delta x}+\frac{V\Delta\tau}{A\,\Delta x}T_x+\frac{Q\Delta\tau}{\rho C_p A} \quad (14)$$

This equation determines the change of temperature with time over a volume element of fluid subject to given conditions of rate of flow and of feed input.

The analysis would begin by subdividing the loop into a number, say N, of finite elements. Equation (14) would then be applied to each subdivision with the appropriate value of Q, ϱ, A, and Δx to give N equations of the form

$$T'_n=\left(1-\frac{V\Delta\tau}{\overline{V}_n}\right)T_n+\frac{V\Delta\tau}{\overline{V}_n}T_{n-1}+\frac{Q_n\Delta\tau}{\rho_n C_p A_n} \quad (15)$$

where $\overline{V}_n = A_n\,\Delta x_n$, the volume of the subdivision. For a particular value of the time increment, the right side of this equation is known from initial conditions and method of subdivision. The temperature distribution and therefore the hydraulic head, H'_l, may then be evaluated at the new instant. With the aid of Equation (11) the rate of flow may also be determined at the new instant. Repeated applications of these two equations will produce a record of temperature and rates of flow.

The heat added from the surroundings, Q, will in general be composed of both direct heat addition, such as by an immersion heater, and heat gained through the walls; for example,

$$Q = q + U\pi D\,(t - T)$$

where q = direct heat input (immersion heater, etc.), U = local over-all or film heat transfer coefficient, and t = local external temperature (wall temperature). Equation (15) may be generalized as

$$T_{n,\,m+1}=\left(1-\beta_n\Delta\tau-\frac{V\Delta\tau}{\overline{V}_n}\right)T_{n,\,m}+\frac{V\Delta\tau}{\overline{V}_n}T_{n-1,\,m}+\beta_n\,\Delta\tau\,t_{n,\,m}+\frac{q_n\,\Delta\tau}{\rho_n C_p A_n} \quad (16)$$

where $\beta_n=\dfrac{U_n\,\pi D}{\rho_n C_p A_n}$ and $\tau = m\Delta\tau$

for m an integer.

The interchange of heat between the fluid and the confining piping needs to be taken into account if the heat capacity of the metal walls is relatively large or if there are significant heat losses from the loop system. For the experimental loop reported in this paper, sufficient insulation was provided so that only the raising and lowering of the pipe-wall temperature needed to be taken into account. A simple heat balance (no longitudinal conduction, no external heat losses, and no radial temperature distributions) for the confining walls of the subdivision yields

$$\frac{dt_n}{d\tau}=\frac{h}{\dfrac{(D_o^{\,2}-D_n^{\,2})}{4D_n}\,\rho_w C_w}\,(t_n-T_n) \quad (17)$$

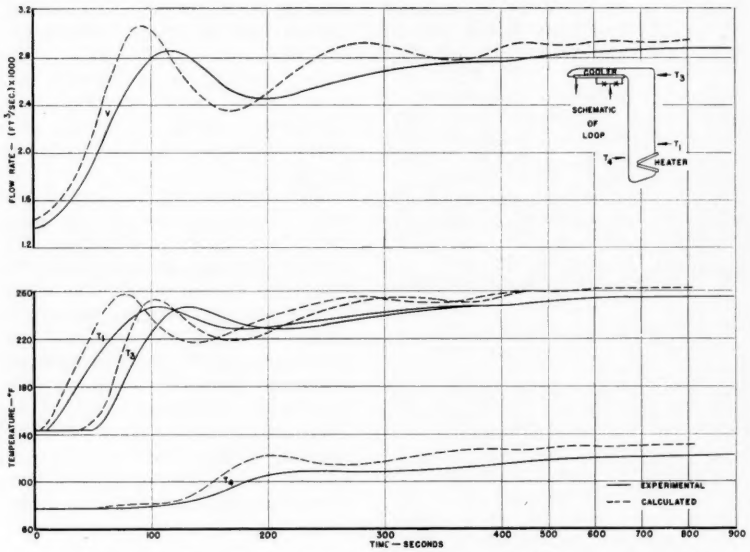

Fig. 5. Comparisons of calculated and experimental transient operations, computer problem 3, first revision.

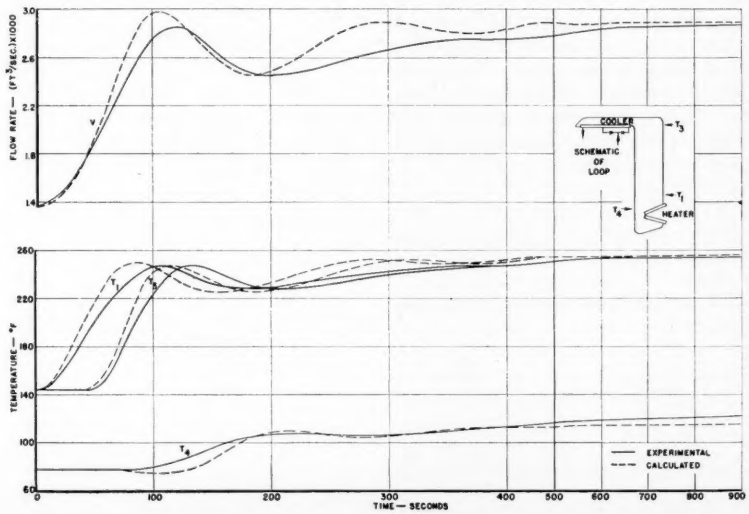

Fig. 6. Comparisons of calculated and experimental transient operations, computer problem 3, second revision.

In finite-difference form Equation (17) is written as

$$t'_n = \left(1 - \frac{h\Delta\tau}{\delta\rho_w c_w}\right) t_n + \frac{h\Delta\tau}{\delta\rho_w c_w} T_n \tag{18}$$

where $\delta = (D_o^2 - D_n^2)/4D_n$ (in feet) approximates the wall thickness.

STABILITY AND CONVERGENCE OF FINITE-DIFFERENCE EQUATIONS

In cases where it is impossible to obtain an exact solution of a partial-differential equation, an approximate solution may be obtained from a corresponding finite-difference equation. The merit of such a numerical solution will then depend upon the convergence of the finite-difference solution to the exact solution. The magnitude of the increments used affects not only the convergence of the numerical solution but also the stability of the solution. Errors may be compounded in the computation and result in instability. The general problem of stability and convergence of numerical solutions has been discussed in detail in the literature (*3, 8, 12, 13, 15, 16, 18, 19*, among others), primarily for the wave and heat-conduction equations. Though the flow equation (11) would be difficult to analyze formally for convergence and stability, a relatively simple means of curbing an error in time and distance for the heat balance leads to the following criteria for stability (*1*):

$$\text{For } b = \frac{V\Delta\tau}{\overline{V}_n} = \text{mesh ratio}$$

$$a = 1 - \beta_n \Delta\tau - b$$

$$|a| \leqslant 1, \quad |b| \leqslant 1, \quad |a+b| \leqslant 1$$

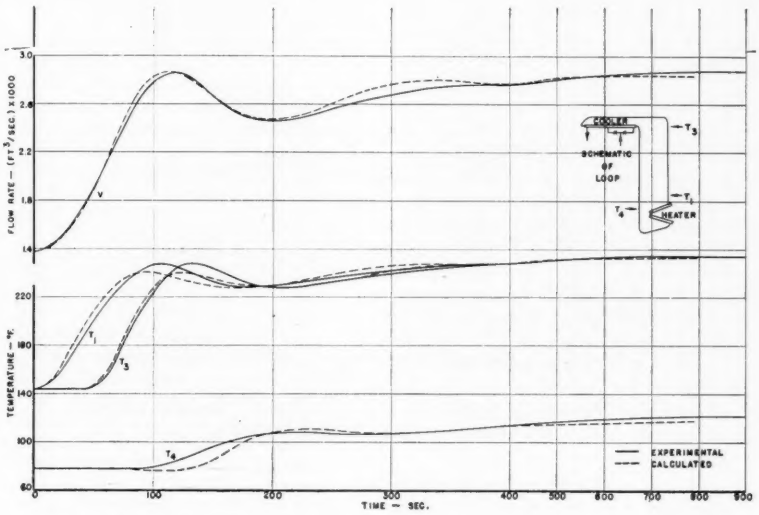

Fig. 7. Comparisons of calculated and experimental transient operations, computer problem 3, third revision.

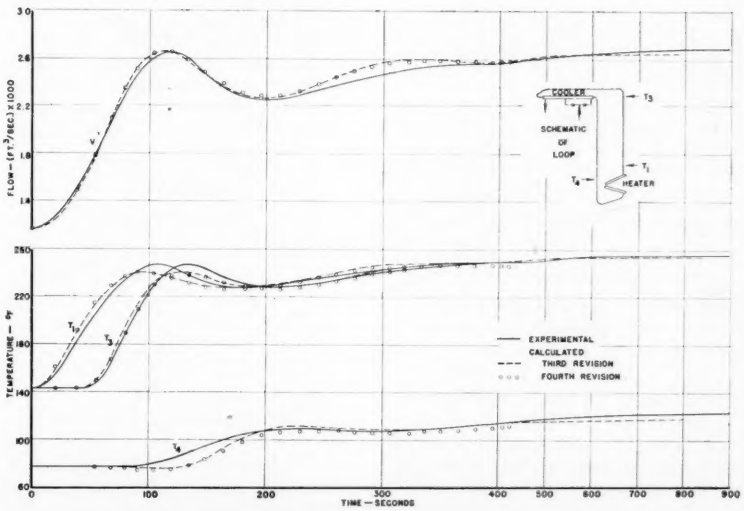

Fig. 8. Comparisons of calculated and experimental transient operations, computer problem 3, fourth revision.

ILLUSTRATION OF FINITE DIFFERENCE EQUATIONS FOR COMPUTER EVALUATIONS

The method of loop subdivision and the evaluations of the constants in the finite-difference equations are illustrated for computer problem 4. This problem concerns the response of the second experimental loop to an abrupt input of heat starting with the fluid at uniform temperature and at rest. The operating conditions are summarized in Table 1. Table 3 summarizes the loop parameters used in the calculations.

Temperatures of the fluid and wall for each subdivision are evaluated through the use of Equations (16) and (18), respectively. A summary of the actual equations employed is given in Table 4. Equation (11) is used to determine the flow. The approximation used for the computation of the hydraulic head, H'_l, is

$$H'_l = \int_o \rho' \, dx = \sum_{n=1}^{N} \rho' Z_n$$

where Z_n represents the vertical projection of the subdivision. A negative value is used if the flow is upward in the subdivision, and a positive value for downward flow. The total number of subdivisions is N. The densities are computed from the fluid temperature and the relation

$$\rho_n = 62.404 + 0.4556\left(\frac{T_n}{100}\right) - 0.9605\left(\frac{T_n}{100}\right)^2 + 0.08164\left(\frac{T_n}{100}\right)^3 \tag{19}$$

This density equation was obtained by applying the method of least squares to the tabulated densities of water given in McAdams (*17*) and in the International Critical Tables. The equation is valid for temperatures up to 300°F. and is accurate to 0.01% for low pressures. The evaluation of the loop constant, a_p, is given in Table 3, and the flow equations for viscous and turbulent flow are given in Table 4.

COMPARISON OF EXPERIMENTAL AND CALCULATED TRANSIENT LOOP RUNS

A total of sixty-four transient natural-circulation runs was made on the first loop. These runs served to demonstrate the reproducibility of the tests and to characterize the response to abrupt additions and release of heat to the fluid under various initial conditions. Attention is focused on only two runs on the first loop for purposes of comparing the experimental results with the numerical solution of the finite-difference equations. The conditions of the two runs for computer problems 2 and 3 are listed in Table 1. The progressive refinement of the relations for the loop parameters including a reduction in the number of subdivisions and the effects on the numerical evaluations of computer problem 3 are summarized in Table 2 and illustrated in Figures 5 to 10. The comparisons of calculated and experimental values of flow and temperatures given in Figure 6 indicate that the transient operation of the natural-circulation loop can be predicted with a fair degree of assurance. Several points of departure may be summarized as follows:

1. Difference between the initial maximum values of T_1 and T_3 indicates that the film heat transfer coefficient should be increased.
2. Lag between experimental and calculated temperatures indicates the importance of the heater lag.
3. Difference between initial flow rates indicates more precision required in specifying loop resistance.
4. Difference between steady-state temperatures indicates the need for an improved cooler equation.

The successive improvement of the loop parameters for revisions 2 and 3 and the approach of the calculated values to the experimental values are revealed in Figures 6 and 7. The fourth revision of computer problem 3, given by Figure 8, shows little or no departure from the third revision even though the number of subdivisions in the loop was nearly halved.

Computer problem 2 represents a more exacting test of the analytical equations for the volumetric flow starts at zero. The same finite-difference equations that were successful for the third revision of computer problem 3 were applied in the second revision of computer problem 2. The calculated and experimental results are shown in Figure 9, and, in general, the agreement is satisfying. Further improvement could be achieved by correcting the heat transfer coefficient and refining the viscous-flow loop resistance.

The second loop, with its faster response, provided a relatively severe test of the analytical approach. Computer problem 4 was calculated for operating conditions corresponding to transient run 65, which was made on the second loop. The finite volume subdivisions used were of the same order of magnitude as those employed in the third revision of computer problem 3, and the details of the equations have been previously noted. The comparisons of the calculated and experimental results are shown in Figure 10. The agreement between experimental and predicted values is generally very good. Had the heat transfer coefficient for the cooler been corrected for the num-

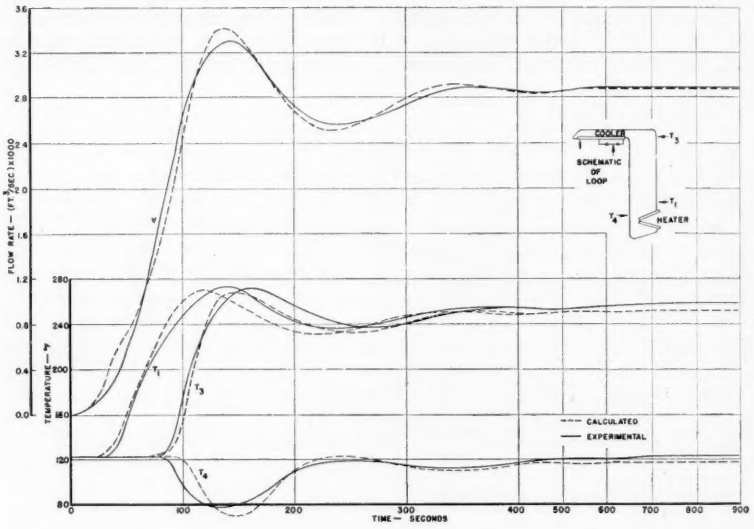

Fig. 9. Comparisons of calculated and experimental transient operations, computer problem 2, first revision.

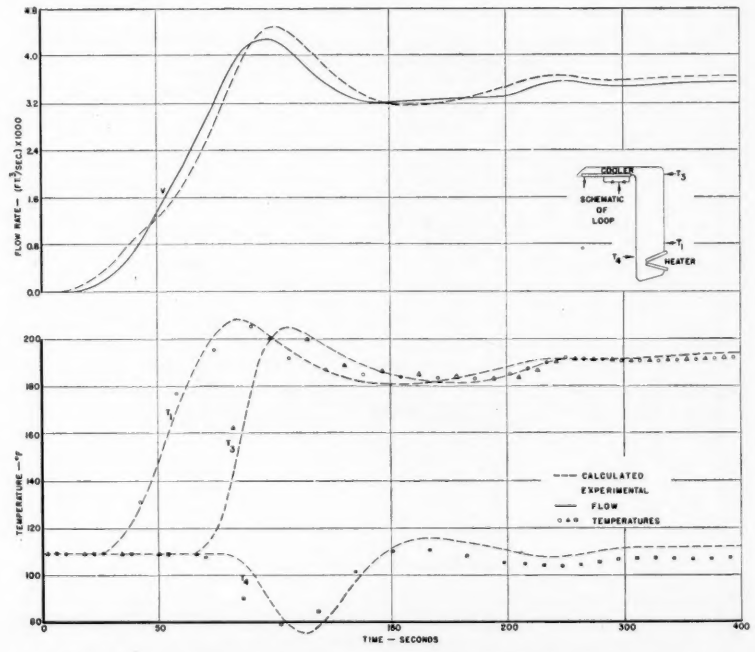

Fig. 10. Comparisons of calculated and experimental transient operations, computer problem 4.

ber of subdivisions, better agreement of steady-state values would have been attained.

SUMMARY

A method for predicting the transient behavior of a single-phase, natural-circulation loop was demonstrated. The method employs the iterative solution of the finite-difference energy and momentum balances and has the following points of interest:

1. The one-dimensional analysis appears to be sufficient for engineering purposes.
2. The assumption of uniform average volumetric flow around the loop at a given instant is sufficiently valid for most expected conditions.
3. The finite-difference equations may be simplified considerably by the use of an average fluid density in the flow equation except for the hydraulic-head term.
4. The degree of reliability of the mathematical model will depend upon the accuracy with which the physical parameters are known or can be estimated; for example, two main factors are loop resistance and heat transferred to the fluid.
5. Relatively large subdivisions may be employed in the finite-difference equations if the proper mesh ratio is chosen.

ACKNOWLEDGMENT

The work described in this paper was made possible by contract AT(11-1)211 between the Atomic Energy Commission and the Chemical Engineering Department of the University of Minnesota. It is a pleasure to acknowledge the encouragement and assistance of J. C. Boyce, Associate Director of the Argonne National Laboratory, in formulating an effective liaison between A.N.L. and the university. Further, the cooperation and assistance of P. C. Ostergaard of the Westinghouse Atomic Power Division is appreciated. The coding of the problem by, and the general assistance of, the National Bureau of Standards are gratefully acknowledged.

NOTATION

a = temperature coefficient = $1-\beta\Delta\tau$-b, lb.mass/sec.^{2}/ft.^{5}

a_l = loop constant = $\int_o \rho/g\, dx/A$

A = cross-sectional area, sq.ft.

b = mesh ratio = $V\Delta\tau/V_n$

$C_p = c$ = specific heat of fluid, B.t.u./(lb.mass) (°F.)

D = diameter, ft.

E = internal energy, B.t.u./lb.mass

ε = total energy = $E + u^2/2\alpha g_o + (g/g_c)z$, B.t.u./lb.mass

f = Moody friction factor

f' = Fanning friction factor

$f\tau$ = friction factor for transient flow (in this paper $f\tau = f$)

F = frictional loss, total, ft.(lb. force)/lb.mass

$\overline{F}$ = frictional loss per unit length, ft.(lb.force)/ft.(lb.mass)

g = local acceleration of gravity, ft./sec.^{2}

g_c = conversion factor in Newton's law of motion, 32.2(lb.mass) ft./(lb.force)sec.^{2}

G = mass rate of flow, lb.mass/(sq.ft.)(sec.)

GPM = coolant rate of flow gal./min.

h = film heat transfer coefficient, B.t.u./(sec.)(sq.ft.)(°F.)

h' = film heat transfer coefficient, B.t.u./(hr.)(sq.ft.)(°F.)

H = enthalpy, B.t.u./lb.mass

H_l = loop hydraulic head = $\int_o \rho dz$, lb.mass/sq.ft.

k = thermal conductivity, B.t.u./(sec.)(sq.ft.)(°F./ft.)

L = length, ft.

m = integer, denoting time position

n = integer, denoting space position

N = number of subdivisions in loop

p = pressure, lb.force/sq.ft.

q = linear rate of heat input to heater element, B.t.u./(ft.)(sec.)

q' = rate of heat input to heater element, B.t.u./sec.

Q_{kw} = rate of heat input to heater element, kw.

Q = linear rate of heat input to fluid, B.t.u./(ft.)(sec.)

Q' = rate of heat input to fluid, B.t.u./sec.

r = pipe radius, ft.

Re = Reynolds' number = $Du\rho/\mu$

R_l = total loop resistance = $\int_o \rho F dx$, lb.mass/sq.ft.

T = fluid temperature, °F.

t = external temperature, wall or coolant, °F.

u = linear velocity, ft./sec.

U = over-all heat transfer coefficient, B.t.u./(sec.)(sq.ft.)(°F.)

v = specific volume = $1/\rho$, cu.ft./lb.mass

V = volumetric rate of flow, cu.ft./sec.

$\overline{V}_n$ = volume of subdivision = $A_n\Delta x_n$, cu.ft.

$\overline{V}_c$ = total cooler volume, cu.ft.

$\overline{V}_e$ = heater element volume, cu.ft.

$V\Delta\tau/V_n$ = mesh ratio

w = mass rate of flow, lb.mass/sec.

x = distance along streamline, ft.

x_n = length of subdivision, ft.

z = vertical projection, ft.

Z_n = vertical projection of subdivision, ft.

α = coefficient in kinetic energy term = ½ for viscous flow = 1 for turbulent flow

$\delta = (D_o^2 - D_n^2)/4D_n \cong$ wall thickness, ft.

μ = viscosity, lb./ft.sec.

μ_{cp} = viscosity, centipoises

ρ = density, lb./cu.ft.

ρc = volumetric heat capacity of fluid = ρc_p, B.t.u./(cu.ft.)(°F.)

$\rho_e c_e$ = volumetric heat capacity of heater element, B.t.u./(cu.ft.)(°F.)

$\rho_w c_w$ = volumetric heat capacity of walls, B.t.u./(cu.ft.)(°F.)

τ = time, sec.

$\int_o$ = integration around closed loop

LITERATURE CITED

1. Alstad, C. D., H. S. Isbin, N. R. Amundson, J. P. Silvers, A.N.L. 5409 (in preparation for distrition to A.E.C. depository libraries).
2. Binnie, A. M., *Quart. J. Mech. & Applied Math.*, 4, 330 (1951).
3. Crank, J., and P. Nicolson, *Proc. Cambridge Phil. Soc.*, 43, 50 (1947).
4. Daily, J. W., and K. C. Deemer, *Trans. Am. Soc. Mech. Engrs.*, 76, 87 (1954).
5. DeJuhasz, K. J., *J. Franklin Inst.*, 223, 463 (1937).
6. Grace, S. F., *Phil. Mag.*, 5, 933 (1928).
7. Hall, N. A., *Trans. Am. Soc. Mech. Engrs.* 74, 925 (1952).
8. Hildebrand, F. B., *J. Math. and Phys.*, 31, 35 (1952).
9. Jenny, E., "Berechungen und Modelversuche uber Druckwellen Grossen Amplituden in Auspuff Leitungen," E.T.H. Promationarbeit Basel, Zurich (1949).
10. Jordan, Karoly, "Calculus of Finite Differences," 2 ed., Chelsea Publishing Co., New York (1947).
11. Langhaar, H. L., *J. Appl. Mechanics*, 9, No. 2, p. 55 (1942).
12. Leppert, George, *J. Am. Soc. Naval Engrs.*, 64, No. 3 (August, 1952).
13. Leppert, George, *Mech. Eng.*, 75, 1017 (1953).
14. Leppert, George, "Derivation and Experimental Verification of a Transient Flow Equation," *Argonne Natl. Laboratory Memo.* (May 29, 1952).
15. Leutert, Werner, *J. Math. and Phys.* 30, 245 (1951).
16. ———, and George G. O'Brien, *J. Math. and Phys.*, 30, 252 (1951).
17. McAdams, W. H., "Heat Transmission," McGraw-Hill Book Company, Inc., New York (1950).
18. O'Brien, George G., Morton A. Hyman, and Sidney Kaplan, *J. Math. and Phys.* 29, 223 (1950).
19. Richter, H., *Forschungsarb. Gebiete Ingenieurw.*, 338, (1930).
20. Schonfeld, J. C., *Appl. Sci. Research*, A1, 169 (1948).
21. Valensi, J., *Compt. rend.*, 224, 446 (1947).

(Presented at A.I.Ch.E. New York meeting)

Dispersed-phase Holdup in Packed, Countercurrent Liquid-liquid Extraction Columns

C. E. Wicks and R. B. Beckmann

Carnegie Institute of Technology, Pittsburgh, Pennsylvania

This investigation is a study of the effect of flow rates and packing size and column diameter upon the holdup of a toluene dispersed phase, flowing countercurrent to a continuous water phase in packed liquid-liquid extraction columns. Six different packings were used: ¼-, ⅜-, ½-, ⅝-, ¾-, and 1-in. nonporous, unglazed-porcelain Raschig rings. Three extraction columns, 3, 4, and 6 in. I. D., were used in the experimental work.

Three types of dispersed-phase holdup, free, operational, and total, have been investigated. An empirical correlation is presented for the total holdup data below the loading point. A correlation of the effect of packing size on the exponential term r and the coefficient A_1 is developed for packing sizes ½ in. or larger when the column-diameter-to-packing-size ratio is at least 8 to 1. The term $A_1(V_D)^r$ in the equation accounts for at least 90% of the total holdup. The small magnitude of the residual term $B_1(V_D)(V_C)^s$ did not permit a definite correlation of the coefficient B_1 or the exponent s.

Observation of the dispersed-phase holdup during column operation revealed a transitional behavior of the ⅜-in. rings as compared with that of the ¼- and ½-in. or larger packing. Two, and sometimes three, regimes of flow occur in packed extraction columns. The increase in holdup with increasing continuous-phase flow rate differed for each zone. In the two zones below the loading zone the holdup was found to increase linearly with the dispersed-phase flow rate for a constant continuous-phase flow rate. A new method of randomly packing an extraction column has been found to give reproducible holdup data.

During recent years the widespread use of packed, dispersed-solvent, extraction columns as a means of separating the components of solutions has made apparent the need of fundamental information on the extraction mechanism of the column in order to improve the operational efficiency. A consideration of the problem of predicting the height of packing required for any given separation suggests the following five basic factors which need to be taken into consideration: (1) the resistance to diffusion in the continuous phase adjacent to the interface, (2) the resistance to transfer across the interface, (3) the resistance to transfer in or out of the body of the droplet, (4) the interfacial area of contact of the phases, and (5) the limitations on flow rates for a given packing. It was realized at the outset that in order to provide this fundamental information each of these factors will probably require individual investigations. This paper is concerned with the effect of flow rates and the effect of packing size and column diameter upon the dispersed-phase holdup within a randomly packed extraction column. Holdup information, along with drop-size information, for a given system and packing provides a means for calculating the interfacial contact area when it is below the loading rates.

Very little information has appeared in the literature on the determination of holdup* in packed extraction columns. In general, the available holdup data can be classified into two principal categories, depending upon the manner in which the data were obtained: (1) holdup data in which the volume of holdup was measured by draining the column and separating the desired phase and (2) holdup data obtained by simultaneously closing all streams to and from the column and then measuring the volume of continuous phase needed to restore the altered two-phase interface to its initial position. The relationship, if any, existing between these two forms of holdup has not yet been clarified.

Row, Koffolt, and Withrow (*10*) obtained holdup data during study of the rate of mass transfer of benzoic acid from water to toluene by use of an 8.75-in. I. D. packed column. The tower was packed with ½-in. unglazed Berl saddles, ½-in. unglazed Raschig rings, and knitted copper cloth packing. The hold-

C. E. Wicks is at present at Oregon State College, Corvallis, Oregon.

Complete tabular material has been deposited as Document 4747 with the American Documentation Institute, Auxiliary Publications Service, Library of Congress, Washington 25, D.C., and may be obtained for $5.00 for photoprints or $2.25 for microfilm.

*When liquid-liquid extraction columns are dealt with, the term *holdup* will be used to designate the fractional holdup of the dispersed phase in that portion of the total column volume which may be occupied by liquid.

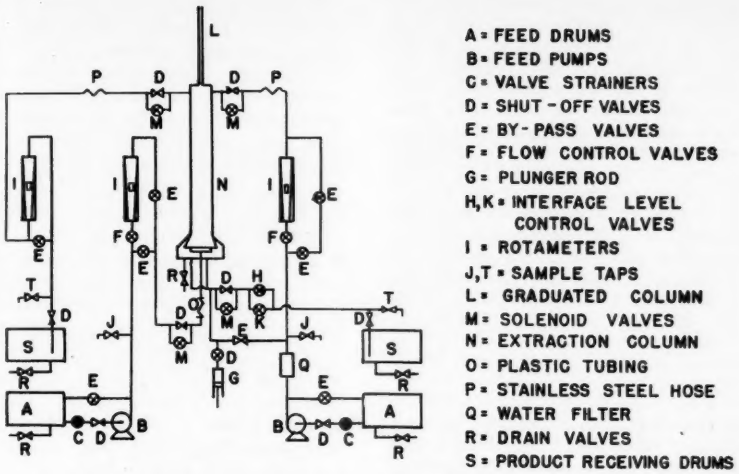
A = FEED DRUMS
B = FEED PUMPS
C = VALVE STRAINERS
D = SHUT-OFF VALVES
E = BY-PASS VALVES
F = FLOW CONTROL VALVES
G = PLUNGER ROD
H,K = INTERFACE LEVEL CONTROL VALVES
I = ROTAMETERS
J,T = SAMPLE TAPS
L = GRADUATED COLUMN
M = SOLENOID VALVES
N = EXTRACTION COLUMN
O = PLASTIC TUBING
P = STAINLESS STEEL HOSE
Q = WATER FILTER
R = DRAIN VALVES
S = PRODUCT RECEIVING DRUMS

Fig. 1. Schematic flow diagram of extraction equipment.

up data, measured by correcting the interfacial level, indicated a sharp increase in the liquid holdup as flooding was approached. There also appeared to be more or less rough correlation between holdup values and capacity coefficients Ka. Allerton, Strom and Treybal(*1*) measured holdup in a 3.56-in. I. D. column packed with ½-in. carbon rings with benzoic acid as the solute in the kerosene-water system. Their results indicated an increase in holdup with increasing rates of both phases. Gier and Hougen(*6*) reported similar results in their holdup measurements made in a 6.0-in. I. D. column packed with ½- and ⅜-in. unglazed Raschig rings. The holdup data which they obtained by determining the volume alteration in the interfacial level lowering were found to be a linear function of the dispersed-phase rate when the continuous-phase rate was constant.

Gayler and Pratt(*4*) and Gayler, Roberts, and Pratt(*5*) conducted an extensive study of dispersed-phase holdup using 3-, 6-, and 12-in. I. D. columns with a packed height of 10 ft. The packing used was ¼-, ⅜-, ½-, ¾-, 1-, and 1½-in. ceramic Raschig rings and ¼-, ½-, and 1-in. ceramic Berl saddles. The continuous phase in each of the systems studied was water; methyl isobutyl ketone, butyl acetate, dibutyl carbitol, benzene, and isooctane were each used as the dispersed phase. The normal holdup data used by the authors in developing their conclusions were obtained by determining the volume alteration in the interfacial level lowering. During the course of the investigation it was found that an additional volume of the dispersed phase was always present in the column. This was presumably present in the form of droplets which were trapped in the packing. The quantity of permanent holdup present was determined by draining the column after removing the normal holdup from the column. The authors concluded that only the normal holdup was involved in the mass transfer operation; consequently, the normal holdup data were correlated by means of the following equation:

$$V_D + \frac{X}{1-X} V_C = F\bar{v}_o X (1 - X) \qquad (1)$$

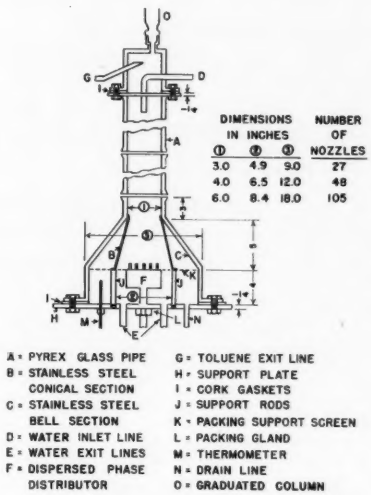
DIMENSIONS IN INCHES
NUMBER OF NOZZLES
① ② ③
3.0 4.9 9.0 27
4.0 6.5 12.0 48
6.0 8.4 18.0 105
A = PYREX GLASS PIPE
B = STAINLESS STEEL CONICAL SECTION
C = STAINLESS STEEL BELL SECTION
D = WATER INLET LINE
E = WATER EXIT LINES
F = DISPERSED PHASE DISTRIBUTOR
G = TOLUENE EXIT LINE
H = SUPPORT PLATE
I = CORK GASKETS
J = SUPPORT RODS
K = PACKING SUPPORT SCREEN
L = PACKING GLAND
M = THERMOMETER
N = DRAIN LINE
O = GRADUATED COLUMN

Fig. 2. Extraction-column details.

where V_D and V_C are superficial velocity of the dispersed phase and the continuous phase respectively, X is the fractional holdup, F is the fractional voidage of packing, and $\bar{v}_o$ is a velocity, characteristic of a given packing. A plot of $V_D + (X/1-X)V_C$ against $X(1-X)$ for a given packing should produce a straight line through the origin. However, the present authors have found that the data for the 3-in. I. D. column and for the majority of the 6-in. I. D. column require separate lines for each different continuous-phase flow rate. Gayler and Pratt(*4*) also presented the following equation for normal holdup at flooding:

$$X_{flood} = 0.62 \frac{V_D^{\,2} a_p}{gF^3} \qquad (2)$$

which must be in error, for a substitution of the proper values for the variables into the equation resulted in values of X_{flood} greater than one, which is an impossibility.

APPARATUS

A schematic flow diagram of the extraction equipment is presented in Figure 1. The material of construction for all lines, valves, valve strainers, and column parts (unless otherwise stated) was type-304 stainless steel. All lines were ½-in. N.P.S. pipe with the exception of short sections of ¼-in. N.P.S. pipe on the rotameter control panels in the line to the plunger rod, and in the drain lines. The feed drums and the receiver drums were standard 55-gal. drums, black iron for toluene and galvanized iron for water. The feed pumps were Eastern, type 2-J, three-stage centrifugal pumps.

Flow rates in the system were regulated by ¼-in. needle valves with 40 threads to the inch. The flow of the water entering, and the toluene entering and leaving, the column was measured by rotameters covering a flow range of 0.01 to 0.89 gal. of water/min. Two 3-ft. lengths of stainless steel hose were employed to provide flexibility in the elevation of the lines at the top of the column. This arrangement permitted a variation in the column height without changing the flow system. The level of the two-phase interface was regulated by means of two parallel valves in the water exit line, a ½-in. globe valve for coarse adjustments, and a ¼-in. needle valve for fine control.

The extraction column is shown in detail in Figure 2. Three extraction columns, 3, 4, and 6 in. I. D., were used in the experimental work. The structural features of each of the columns used were identical. Pertinent dimensions are given in Figure 2. The extraction column consisted of

two 2-ft. flanged sections of Pyrex-glass pipe supported on a 20-gauge stainless steel bell section. A ¼-in.-thick stainless steel top section was fitted with an aqueous feed line, an extract exiting line, and a ½-in. pipe, threaded into the top of the section, which connected a small graduated column to the extraction column.

The aqueous phase entered the column through a ½-in. pipe which ends 1½ in. below the two-phase interface. The aqueous raffinate was removed from the column through two ½-in. pipes threaded into the base flange of the column. Toluene entered the column through the dispersed-phase distributor and was dispersed by a number of sharp-edged nozzles (0.106 in. I. D., 0.014 in. wall thickness and 1¼ in. long) made from stainless steel hypodermic tubing. These nozzles were spaced in concentric circles with a minimum circumferential distance of ½ in. between nozzles. The number of nozzles used on each of the dispersed-phase distributors for the various sizes of the columns was maintained approximately proportional to the column cross-sectional area. The number of nozzles per distributor for each column is given in Figure 2. The distributor was flush with the bottom of the packing with the nozzles embedded 1¼ in. into the packing. Thus the cross-sectional area of the annular space between the dispersed-phase distributor and the stainless steel cone at this point was equal to the cross-sectional area of the column, as recommended by Blanding and Elgin (*2*). The drops of toluene rose through the column packing into the separating section where they coalesced at the interface, forming a layer of toluene above the two-phase interface. The toluene extract overflowed the column through ½-in. pipe welded into the top section.

The support screen for the column packing is a type-304 stainless steel screen, 3¾ mesh with 0.054-in. wire and openings 0.213 in. square. This screen was held in place by the dispersed-phase distributor and by four ½-in. stainless steel rods, which were threaded into the base flange of the column. This bottom flange was bolted firmly to the structural steel support through Dravo Elasto-rib, vibration-insulating material.

All gaskets used between glass sections of the column were fabricated from ⅛-in. Johns Manville 84-S asbestos sheet. The gasket material used between the glass section of the column and the top or bottom sections was ¼-in. hard-cork sheet.

COLUMN PACKING

Six different packings were used: ¼-, ⅜-, ½-, ⅝-, ¾-, and 1-in. nonporous unglazed porcelain Raschig rings. The actual dimensions of these packings are summarized in Table 2. The column was packed by slowly dropping several rings at a time into the empty column filled with water. Initially no attempt was made to obtain the densest possible arrangement of the packing, thus following general procedure used in extraction investigations. After repeated attempts to obtain reproducible data, however, it was decided that a new, more satisfactory means of packing was needed. Only when the random-packed column was settled by passing an air stream up through the column at a rate high enough to flood the column, i.e., by using the method generally accepted for a packed absorption column, was reproducible data obtained. The procedure adopted for the measurement of the superficial area a_p and the void fraction was as follows. The number of pieces of packing dumped into the column was carefully counted and the volume of the column to be packed was accurately measured. Since the surface area and the volume per piece of packing were known, the superficial area a_p and the dry void fraction F of the packing can be calculated. These are reported in Table 3.

LIQUID-LIQUID SYSTEM

The binary solvent system of nitration-grade toluene - distilled water was studied. Prior to this investigation mass transfer in the toluene water-diethylamine system had been studied by Leibson and Beckmann (*7*), using similar equipment. Accurate values for the equilibrium distribution constant for the toluene-water-diethylamine system as a function of temperature and solute concentration were available from the work of Morello and Beckmann (*9*) and Wehn and Franke (*11*). From the mutual-solubility data of Wehn and Franke, it is evident that at 0 wt. % concentrations of diethylamine for either the water or the toluene phase, the solubility of one phase in the other is negligible. This validates the simplifying assumption that the volumetric flow rate of each phase throughout the column is constant.

EXPERIMENTAL PROCEDURE

The holdup of the dispersed-solvent phase, toluene, passing countercurrent to the continuous aqueous phase, was investigated. Before operation was started, the liquids in the feed drums were mutually saturated with the opposite solvent. During operation the two-phase interface was located at an established mark, 3 in.

Table 1.—Coefficients and Exponents for Correlation of Total Holdup Data

$$X_T = A_1 (V_D)^r + B_1 (V_D)(V_C)^s$$

Column diameter I. D., in.	Packing size, in.	A^1	r	B_1	s
3	¼	35.2	0.0556	4.40×10^{-3}	1.850
	⅜	19.6	0.304	4.25×10^{-3}	2.003
	½	6.5	0.428	4.00×10^{-3}	1.318
	¾	2.18	0.482	7.15×10^{-8}	3.252
	Spray	0.175	0.635	8.15×10^{-8}	2.266
4	⅜	26.3	0.250	5.30×10^{-4}	2.142
	½	16.0	0.260	5.60×10^{-4}	2.350
	¾	3.7	0.481	4.70×10^{-5}	1.783
	Spray	0.425	0.643	5.38×10^{-8}	2.590
6	⅜	23.7	0.437	5.25×10^{-2}	1.796
	½	12.5	0.311	1.55×10^{-3}	1.600
	⅝	6.03	0.445	1.55×10^{-3}	1.445
	¾	3.08	0.513	1.55×10^{-3}	1.211
	1	1.42	0.580	1.55×10^{-3}	1.154
	Spray	0.364	0.610	5.2×10^{-6}	2.173

Table 2.—Raschig-ring Packing Properties

Nominal packing size, in.	Outside diameter, in.	Wall thickness, in.	Length, in.	Weight per piece, g	Volume per piece $\times10^5$, cu. ft.	Surface area per piece $\times10^2$, sq. ft.
¼	0.243	0.035	0.244	0.308	0.458	0.245
⅜	0.384	0.080	0.397	1.19	1.76	0.633
½	0.538	0.105	0.517	2.88	4.27	1.18
⅝	0.652	0.099	0.667	4.39	6.64	1.85
¾	0.756	0.129	0.772	7.75	11.3	2.46
1	1.14	0.136	1.14	15.0	28.3	5.59

above the packing. Operation was held constant and the flow rates were observed on the rotameters. After constant operations had been maintained for an hour, all the streams to and from the tower were simultaneously closed by means of rapid-shut-off solenoid valves.

The free holdup, the volume of dispersed toluene which is able to rise to the interface freely owing to density differences, was allowed ample time to rise, and in turn lower the interface. Additional aqueous phase returned the interface to its initial mark and in turn forced the excess toluene out through the graduated column. The differential volume of toluene in the graduated column was recorded as free holdup volume. By means of a pulsating action on the continuous phase, produced by the plunger rod, additional loosely entrapped droplets were freed from the interstices of the packing. After the interface was returned once again to its initial mark, the new differential volume of toluene in the graduated column was recorded as operational holdup. The manual pulsations were continued until further pulsations caused no increase in the differential volume. The column was then drained. After repeated washings of the packing, the collected drainage was separated and the total volume of toluene was measured. The total volume, corrected for the volume of toluene existing between the interface mark and the operating mark in the graduated column, was recorded as the total holdup volume.

The experiments were carried out at ambient room temperature which varied from 24° to 32°C. as extreme limits. It is evident from the results of Morello and Beckmann(*9*) that an over-all variation in temperature of this magnitude is not important for this system in this temperature range.

TYPES OF DISPERSED-PHASE HOLDUP OBSERVED

In the only previous extensive study on dispersed-phase holdup in a packed extraction column, Gayler and Pratt(*4*) presented data on two different types of holdup, normal and permanent. In a study of droplet behavior within a packed column, Lewis, Jones, and Pratt(*8*) observed that with ¼- and ⅜-in. packings the dispersed-phase droplets were normally retained within the interstices of the packing. The vertical motion of the entrapped drops resulted from continual impacts from the succeeding drops. On the basis of these results of Lewis, Jones, and Pratt(*8*) it would appear, for at least the ¼- and ⅜-in. packings, that a larger volume than the free-rising, normal holdup volume participates in the extraction operation.

Inasmuch as neither the normal nor the total holdup (i.e., sum of the normal and permanent holdup) can actually describe the volume of dispersed phase which is needed for active interfacial-area calculation, the present authors concluded that a third holdup, operational, must be actually involved in the mass transfer. Operational holdup includes the normal holdup volume plus an additional volume to account for the droplets temporarily retained by the packing, but having an over-all net movement through the packing. The latter droplets are normally freed during the course of the operation by impact from succeeding drops and by longitudinal thrusts from the descending continuous phase. As a result, holdup measurements were carried out to study the following three types of holdup:

1. *Free holdup,* the volume of dispersed phase which rises freely to the interface, owing only to the differences in density.
2. *Operational holdup,* the volume of dispersed phase which is considered to be the active portion of the dispersed phase taking part in the mass transfer.
3. *Total holdup,* the total volume of dispersed phase within the effective packing volume at any time.

EXPERIMENTAL HOLDUP RESULTS

Value of free, operational, and total holdups, reported as volume percentage of the total voids, are for the 3-in. I. D. column packed with ¼-, ⅜-, ½-, and ¾-in. Raschig rings and unpacked as a spray column for the 4-in. I. D. column packed with ⅜-, ½-, and ¾-in. Raschig rings and unpacked as a spray column, and for the 6-in. I. D. column packed with ⅜-, ½-, ⅝-,

Table 3.—Properties of the Packed Systems

Nominal packing size, in.	Run series	Ratio of column diameter to packing size	Number of packing pieces per cu. ft.	Superficial area of packing a_p, (sq. ft.)/(cu. ft.)	Void fraction F, (cu. ft.)/(cu. ft.)	Void volume, cc.	$\frac{a_p}{F^3}$
¼	3-1	12.0	90,566	222	0.585	3,512	1,110
⅜	3-2	8.0	23,490	148	0.587	3,514	732
⅜	3-2A	8.0	23,470	148	0.587	3,514	732
⅜	4-2	10.7	25,469	161	0.552	5,831	957
⅜	6-2	16.0	23,973	152	0.578	13,586	787
½	3-3	6.0	8,656	102	0.630	3,782	392
½	3-3A	6.0	8,678	102	0.630	3,782	392
½	3-3B	6.0	8,726	103	0.628	3,770	416
½	3-3C	6.0	8,585	101	0.633	3,800	398
½	4-3	8.0	9,517	112	0.594	6,275	534
½	6-3	12.0	8,795	104	0.625	14,691	426
⅝	6-4	9.6	4,692	86.8	0.688	16,161	267
⅝	6-4A	9.6	4,639	85.7	0.692	16,266	260
¾	3-5	4.0	2,547	62.7	0.712	3,843	174
¾	4-5	5.3	2,748	67.6	0.690	7,289	206
¾	6-5	8.0	2,771	68.2	0.687	16,148	215
1	6-6	6.0	1,111	62.1	0.686	16,125	201
Spray	3-0	...	....	....	....	6,004	
Spray	4-0	...	....	....	....	10,564	
Spray	6-0	...	....	....	....	23,506	

Note:—Packed volumes: 3-in. I. D. column = 0.212 cu. ft., 4-in. I. D. column = 0.373 cu. ft., 6-in. I. D. column = 0.830 cu. ft.

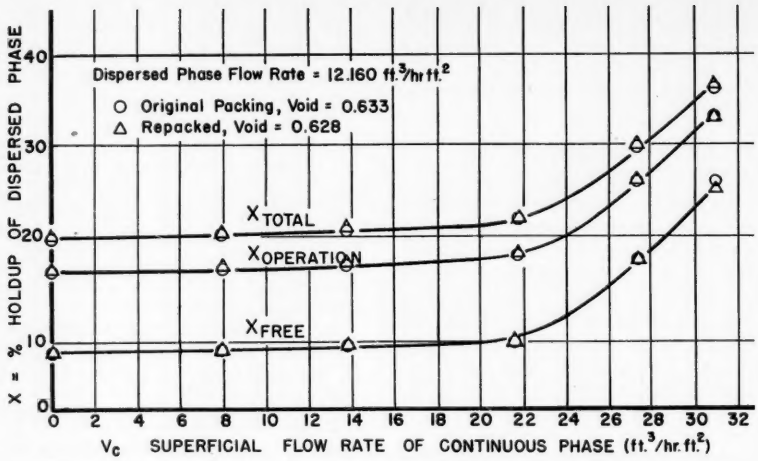
Dispersed Phase Flow Rate = 12,160 ft.³/hr ft.²
O Original Packing, Void = 0.633
Δ Repacked, Void = 0.628
X TOTAL
X OPERATION
X FREE
X = % HOLDUP OF DISPERSED PHASE
Vc SUPERFICIAL FLOW RATE OF CONTINUOUS PHASE (ft.³/hr.ft.²)

Fig. 3. Reproducibility of experimental data for measuring total holdup.

¾-, and 1-in. Raschig rings and unpacked as a spray column. Table 4 lists typical experimental results obtained for ¾-in. rings in the 6-in. I. D. column.*

REPRODUCIBILITY OF EXPERIMENTAL RESULTS

The total holdup results obtained for a specific packed bed are reproducible within 2% on a relative basis.† The operational holdup, being in the same range of magnitude, also showed a reproducibility within 2%. The free holdup results obtained for the packed beds are reproducible within 6%. The holdup results for the spray column are reproducible within 4%. This slightly higher percentage of reproducibility for the free and spray holdup is due primarily to the low numerical values of these results. The reproducibility of the data, as well as the internal consistency of the data, is illustrated in Figure 3.

In the initial phase of this investigation the column was packed randomly with no attempt being made to obtain the densest possible arrangement of the packing. This procedure followed the previously established manner of packing an extraction column. The results obtained for the unsettled ½-in. rings in the 3-in. I. D. column showed, upon repacking, that the total holdup data were reproducible within ± 15%; the free holdup data were reproducible within ± 19%. Dell and Pratt(3), Gayler and Pratt(4), and Leibson and Beckmann(7) encountered similar repacking difficulties in the reproducibility of flooding data, free holdup data, and mass transfer data, respectively.

The initial data obtained from a column packed to operate initially as a flooded absorber were generally erratic. This was undoubtedly due to the presence of air bubbles in some of the favorite droplet resting spots within the interstices of the packing. However, after several preliminary runs, during which the air was gradually removed, consistent results were obtained. When the 3-in. column was repacked in this manner with ½-in. rings, the total holdup data were reproducible to within 1.2%; the free holdup data to within 1.5%. For the ⅜-in. rings repacked in the 3-in. column the total holdup data were reproducible to within 2%; the free holdup data to within 5%. The total holdup data for the 6-in. column when it is repacked with ⅝-in. rings were reproducible to within 1.5%; the free holdup data to within 1.5%. Since all previous investigations in liquid-liquid extraction have failed to find a reproducible method of packing a column, it is suggested that this new procedure of settling the packing be used in mass transfer studies wherever it is particularly desirable to obtain the effect of packing on the variables.

CORRELATION OF HOLDUP DATA

An initial insight into the behavior of a physical system can often be obtained by a dimensional analysis of the variables that characterize the definite physical system. Dimensional analysis entails certain assumptions and limitations

*See footnote on page 426.
†The reproducibility of results will always be compared on a relative basis in this paper.

TABLE 4.—SAMPLE OF EXPERIMENTAL HOLDUP DATA

6-in. I. D. column — ¾-in. rings
Packed height: 48 in. — Void fraction: 0.687

Run	Flow rates, cu. ft./(hr.) (sq. ft.) Toluene Inlet	Toluene Exit	Water Inlet	Stream temperatures, °F. Toluene Inlet	Water Inlet	Holdup data, vol. % of total voids Free	Operation	Total
6–5–2	5.374	5.394	0.0	90	80	3.73	6.21	7.31
–3	5.374	5.394	0.0	87	80	3.72	6.16	7.36
–4	5.374	5.394	9.172	91	89	3.87	6.35	7.47
–5	5.374	5.394	15.009	87	83	4.07	6.56	7.64
–6	5.374	5.394	21.042	89	86	4.27	6.71	7.82
–7	5.374	5.394	27.124	91	88	4.44	6.86	7.98
–8	5.374	5.394	33.599	92	89	4.63	6.95	8.22
–9	5.374	5.394	40.220	94	91	4.81	7.13	8.43
–10	8.774	8.646	0.0	89	80	5.97	8.07	9.66
–11	8.774	8.646	9.184	91	88	6.21	8.32	9.83
–12	8.774	8.646	15.009	92	89	6.44	8.55	9.99
–13	8.774	8.646	21.042	90	86	6.71	8.85	10.19
–14	8.774	8.646	27.124	94	89	6.90	9.12	10.38
–15	8.774	8.646	33.599	87	87	7.10	9.40	10.57
–16	8.774	8.646	0.0	80	80	6.04	8.10	9.59

inherent in this method of correlation; and although it does not give the investigator any new information about the exact behavior of the situation, it is a powerful preliminary tool. In the case of dispersed-phase holdup in a randomly packed liquid-liquid contacting tower, the following factors may be considered to be of impartance:

$$X, d_o, V_D, \rho_C, \rho_D, V_C, \mu_C, \mu_D, D, h,$$

$$F, a_p, \sigma \text{ and } g_C$$

An analysis of these variables produces the following general equation:

$$\left(\frac{d_o}{D}\right)^a \left(\frac{h}{D}\right)^b \left(\frac{\rho_D}{\rho_C}\right)^c \left(\frac{\mu_D}{\mu_C}\right)^d \left(\frac{D\rho_C \sigma g_C}{\mu_C^2}\right)^e (a_p D)^f \left(\frac{D\rho_C V_D}{\mu_C}\right)^g \left(\frac{D\rho_C V_C}{\mu_C}\right)^h (X)^i + \ldots = 0 \quad (3)$$

This equation can be simplified, when only one system, one column diameter, one droplet diameter, and one packed height are dealt with, to the following equation:

$$A\,(a_p)^f \left(\frac{D\rho_C V_D}{\mu_C}\right)^g \left(\frac{D\rho_C V_C}{\mu_C}\right)^n (X)^i + \ldots = 0 \quad (3a)$$

Equation (3a) can be rearranged to be explicit in holdup:

$$X = \phi\left[A\,(a_p)^f \left(\frac{D\rho_C V_D}{\mu_C}\right)^g \left(\frac{D\rho_C V_C}{\mu_C}\right)^i\right] \quad (3b)$$

where ϕ signifies some function. Of course, if the equation were used for only one size and type of packing, the $(a_p)^f$ term could be grouped with the constant A term. From observation of the experimental data, the following final equation was chosen, which is directly obtainable from the foregoing equation:

$$X = \phi\left[C\,(V_D)^{g-y}\,(V_D)^y\,(V_C)^i\right] \quad (3c)$$

where C is a new constant, including A, $(a_p)^f$, and $(D\rho_c/\mu_c)^{g+i}$

Utilizing Equation (3c) and the data below the loading point yielded the following correlation for the total holdup in a specific packing and column:

$$X_T = A_1\,(V_D)^r + B_1\,(V_D)\,(V_C)^s \quad (4)$$

Table 1 presents the coefficients and the exponents for the packings and columns studied. It was generally found that the correlation permitted calculating total holdup to within ± 1.5% of the observed value. A few exceptional points, predicted to within ± 4%, were points in the vicinity of the loading point. The correlation presented here is applicable only to the system studied in this investigation. Further work with other systems is necessary before a more general correlation can be developed.

For a specific system a specific type of packing, the availability of a correlation between extraction variables, and some factor characterizing the size of the packing would extend the applicability off experimentally obtained data. Equation (3b) suggests the possibility of correlating holdup with an a_p term. A correlation of this type for the height of individual transfer unit for the toluene-diethylamine-water system was presented by Leibson and Beckmann (7) for Raschig rings ½ in. or larger. A similar correlation for the r exponent is presented on Figure 4 for the toluene-water system for packing sizes ½ in. or larger. This exponential term r was found to be proportional to $(a_p/F^3)^{-0.8}$. The work of Leibson and Beckmann (7) is also shown on Figure 4. Figure 5 reveals that the first coefficient, A_1, also has a dependency on the (a_p/F^3) term.

It is interesting to observe in the total holdup correlation the importance of the first term, $A_1(V_D)^r$. This term represents the total holdup obtained for zero continuous-phase rates. For all runs in which the continuous-phase rate differed from zero, the first term represents at least 90% of the numerical total holdup value. As a direct consequence of the magnitude of the first term, the evaluation of the residual term $B_1(V_D)\,(V_C)^s$, was made with relatively small numbers; a slight error in one or two of these numbers could possibly alter the numerical value of the coefficient and/or exponent of the term. The small magnitude of the residual term, $B_1(V_D)\,(V_C)^s$, did not permit a definite correlation of the coefficient B_1 or the exponent s.

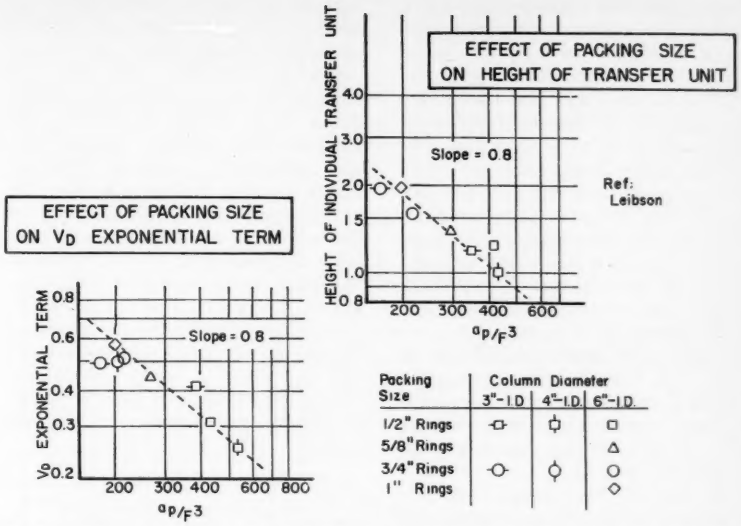

Fig. 4. Effect of packing size and column diameter on holdup and mass transfer.

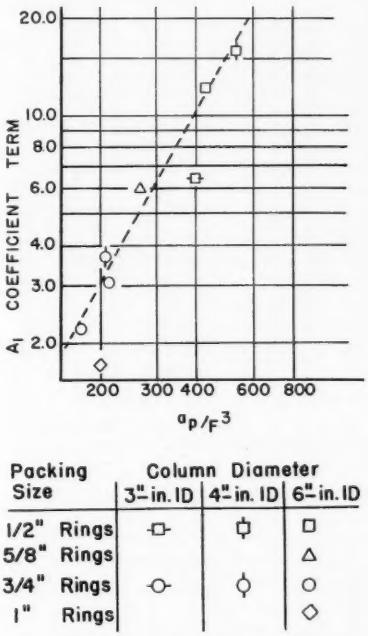

Fig. 5. Effect of packing size and column diameter on holdup.

A number of attempts to find a correlation between the phase flow rates and the free holdup were made, with only partial success. Figure 6 illustrates the linear dependency of the free holdup on the dispersed-phase rate when the continuous-phase rate was constant. Similar plots were obtained for the 3- and 4-in. I. D. columns. As with the total holdup data, these zero continuous-phase rate data account for 75 to 90% of the free holdup data in which the continuous-phase rate differs from zero. Owing to the relatively small magnitude of the actual free holdup values, the accuracy of the data did not allow a proper evaluation of the relationship of the continuous-phase rate to the free holdup.

As neither the normal nor the total holdup actually described the volume of dispersed phase which is involved in the over-all net movement through the packing, an attempt was made to measure the operational holdup. The freeing of the temporarily detained droplets was brought about by a manual pulsating of the continuous phase. This is undoubtedly only an approximation of what actually occurs during the column's operation; consequently, the obtained operational holdup data must be evaluated as only approximate operational holdup data. At the present time additional investigations are being made on this important holdup. Owing to the uncertainty of the relationship between the pulsating and the correct operational holdup, no separate correlation was developed for this pseudooperational holdup.

EFFECT OF PACKING SIZE ON HOLDUP

The appearance and behavior of the column with respect to variation in the packing size was quite similar to that observed by previous investigators (*4, 7, 8*). The column operation with ring sizes ½ in. and larger is markedly different from that with ¼-in. rings. The ⅜-in. rings behave as a critical or a transition packing between the ¼-in. rings and the ½-in. or larger sizes of packing.

In the case of the ½-in. and larger packing, the droplets of the dispersed phase visually appeared to be well defined and of a relatively constant size distribution independent of packing size. With these packings the operation of the column became steady early in the run and no difficulty was encountered in controlling the interface. However, severe channeling of the rising droplets was observed when the column diameter to packing size was less than 6.0.

The type of flow observed with the ¼-in. rings differs greatly from that described above. The droplets rise through the packing as irregularly shaped globules. Each droplet hangs in the interstices of the packing until impacted by the succeeding droplet. The drops emerge from the top of the packing at only a few different points. The position of these "active points" at the top of the packing varied with time. The droplets, leaving the packing, were well-defined drops. The length of time required to steady the operation of the column was considerably longer for the ¼-in. packing than for any other packing. Channeling of the droplets near the wall was not particularly noticeable.

The type of flow observed with the ⅜-in. rings may be classified as a transition between droplet behavior in the ¼-in. rings and that in the ½-in. or larger. At low flow rates the droplet flow in the ⅜-in. rings appeared to be the same as that observed for the ½-in. and larger rings. As the flow rates were increased, the droplet size increased markedly and the type of flow became similar to the flow in the ¼-in. rings. Erratic results were sometimes encountered in

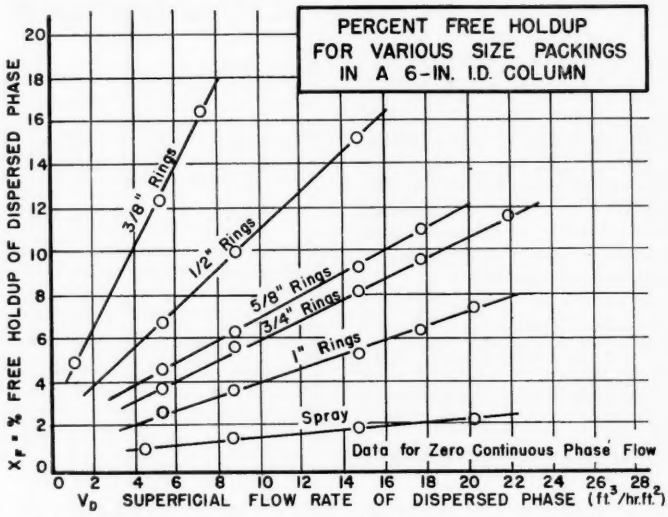

Fig. 6. Effect of flow rate (dispersed phase) on the free holdup for Raschig rings in a 6-in. column.

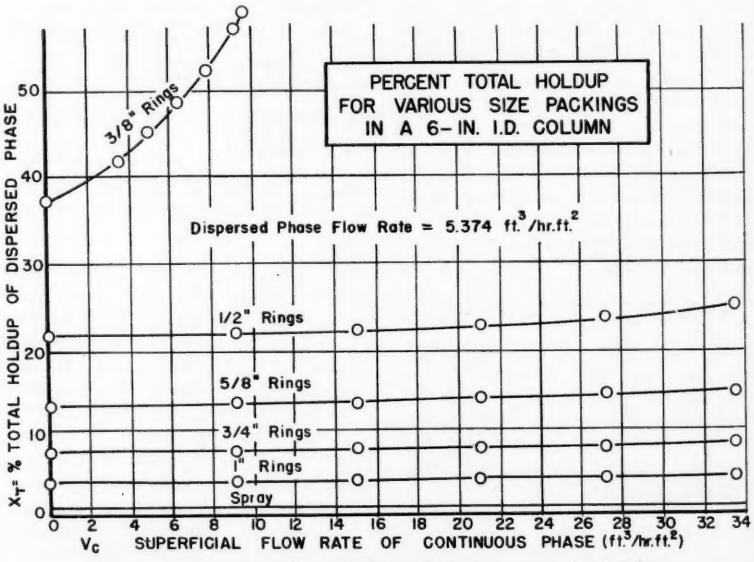

Fig. 7. Effect of continuous-phase flow rate on total holdup for Raschig rings in a 6-in. column.

columns packed with ⅜-in. rings. Possibly this may have been due to the transitional behavior of the packing.

For a given tower the holdup increases as the packing size is decreased. The effect upon the 6-in. I. D. column may be observed in Figure 7. This behavior is to be expected, as one of the main functions of the packing is to produce a series of baffles within the column. Thus, as the packing size decreases and the "baffling effect" increases, the holdup should increase.

FLOW-RATE EFFECTS ON HOLDUP

Although the correlation for the total holdup gives a mathematical relationship for the effect of the flow rates on total holdup, an additional important observation can be made from the data of this investigation. In plotting on logarithmic coordinates the total holdup vs. the continuous-phase flow rate for the various dispersed-phase flow rates, three zones of flow were observed. With the spray column, and also with some of the larger packing sizes, a zone of constant holdup occurred at low continuous-phase velocities. A zone, or zone of flow, as herein referred to is specifically concerned with the variation of holdup with either continuous- or dispersed-phase flow rate (the other phase flow rate being held constant) when the data are plotted in the conventional manner. These terms have no relationship to the visual behavior of the column. As the continuous-phase flow rate was increased, a secondary zone of gradually increasing holdup resulted. This increase in holdup appeared due to the drag placed on the droplets by the increasing flow of the continuous phase. The third zone, where the holdup increases exponentially with the increasing continuous-phase velocity, occurred after the loading point was reached. In the smaller packings the first zone was not observed, probably because of the relatively higher local velocities of the continuous-phase produced by the smaller voids in the packed sections.

SUMMARY

The effect of flow rates and of packing size and column diameter upon the holdup of a toluene dispersed phase, flowing countercurrent to a continuous water phase in packed columns, was investigated, and the results follow.

1. Consistent data were obtained for three different types of holdup: free, operational, and total. The free holdup includes the dispersed-phase drops that rise freely to the interface. The operational holdup includes the free-holdup volume plus the volume of the dispersed-phase droplets freed from the interstices of the packing by pulsations delivered to the continuous phase. The total holdup is the total volume of dispersed phase within the effective packing volume at any time.

2. The total holdup, below the loading point, has been correlated by the equation

$$X_T = A_1 (V_D)^r + B_1 (V_D) (V_C)^s$$

Tabulated values are given for the coefficients and the exponents. A dimensional analysis of the variables involved presents an equation in agreement with the correlating equation. For packing sizes ½ in. or larger, a graphical correlation of the effect of packing size on total holdup suggests that the exponential term r and the coefficient A_1 are related to a_p/F^3. The small magnitude of the residual term $B_1 (V_D) (V_C)^s$ did not permit a definite correlation of the coefficient B_1 or the exponent s.

3. The procedure adopted for randomly packing of the column gives reproducible results upon repacking of the column. Prior to this paper no satisfactory reproducible method of packing a column was observed.

4. The effect of packing size on holdup is in agreement with previous investigators. The column operating with ring sizes ½ in. and larger was observed to be markedly different from that with ¼-in. rings. The ⅜-in. rings behaved as a critical or transitional packing between ¼-in. rings and the sizes of packing ½-in. or larger. The holdup of the dispersed phase increased as the packing size decreased.

5. Two, and sometimes three, distinct zones of flow were found to occur. The increase in holdup with the increase in continuous-phase rate was found to differ in each zone.

NOTATION

A_1 = coefficient to first term in total holdup correlation
a = interfacial contact area/cu.ft. of column volume, sq.ft./cu.ft.
a_p = packing surface area/cu.ft. of column volume, sq.ft./cu.ft.
B_1 = coefficient to second term in total holdup correlation
D = inside diameter of the column, ft.
d_o = droplet diameter, ft.
D_N = nozzle diameter, ft.
F = void fraction of packing
g_C = gravitational constant, ft./sq.hr.
h = height of packing, ft.
H_t = height of transfer unit, ft.
V = superficial liquid velocity, cu. ft./(hr.)(sq.ft. of column cross section)
X = fractional holdup of the dispersed phase in that portion of the column volume which may be occupied by liquid
Δ = differential amount
μ = absolute viscosity, lb./(hr.)(sq.ft.)
ρ = density, lb./cu.ft.
σ = interfacial tension, lb./ft.
ϕ = any function

Subscripts

C = continuous phase
D = discontinuous phase
F = free
$flood$ = flooding
Op = operational
T = total

Exponents

r = exponent to first term, i.e., to (V_D), of total holdup correlation
s = exponent to second term, i.e. to (V_C), of total holdup correlation

LITERATURE CITED

1. Allerton, J., B. O. Strom, and R. E. Treybal, *Trans. Am. Inst. Chem. Engrs.*, **39**, 361 (1943).
2. Blanding, F. H., and J. C. Elgin, *Trans. Am. Inst. Chem. Engrs.*, **38**, 305 (1942).
3. Dell, F. R., and H. R. C. Pratt, *Trans. Inst. Chem. Engrs. (London)*, **29**, 89 (1951).
4. Gayler, R., and H. R. C. Pratt, *Trans. Inst. Chem. Engrs. (London)*, **29**, 110 (1950).
5. ————, N. W. Roberts, and H. R. C. Pratt, *Trans. Inst. Chem. Engrs. (London)*, **31**, 57 (1953).
6. Gier, T. E., and J. O. Hougen, *Ind. Eng. Chem.*, **45**, 1362 (1953).
7. Leibson, I., and R. B. Beckmann, *Chem. Engr. Progr.*, **49**, 405 (1953).
8. Lewis, J. B., I. Jones, and H. R. C. Pratt, *Trans. Inst. Chem. Engrs. (London)*, **29**, 126 (1951).
9. Morello, V. S., and R. B. Beckmann, *Ind. Engr. Chem.*, **42**, 1078 (1950).
10. Row, S. B., J. H. Koffolt, and J. R. Withrow, *Trans. Am. Inst. Chem. Engrs.*, **37**, 559 (1941).
11. Wehn, W. E., and N. W. Franke, *Ind. Eng. Chem.*, **41**, 2853 (1949).

(Presented at A.I.Ch.E. New York meeting)

Flow of Non-Newtonian Fluids—Correlation of the Laminar, Transition, and Turbulent-flow Regions

A. B. Metzner and J. C. Reed
University of Delaware, Newark, Delaware

All available data on flow of non-Newtonians in pipes have been correlated on the conventional friction factor — Reynolds number plot for Newtonian fluids. This correlation, theoretically rigorous in the laminar flow region, was tested with data on 16 different non-Newtonian materials covering the 2.1 × 10^9 range of Reynolds numbers from 6.3 × 10^{-5} to 1.3 × 10^5. Pipe diameters varied from ⅛ to 12 in. As the correlation does not depend on the type of fluid encountered, it may be used with Newtonian and non-Newtonian fluids alike.

In spite of the great range of the available experimental data, further work is necessary in the transition and turbulent-flow regions. No data at all were available on thixotropic, rheopectic, and dilatant fluids, and extension of the correlation to these materials should prove most illuminative from both theoretical and practical viewpoints.

Workers in the field of rheology have long classified non-Newtonian fluids as plastic (or Bingham plastic), pseudoplastic, dilatant, thixotropic, and rheopectic (*2, 9,* and *16*), and a few others, having found the foregoing divisions unsatisfactory, have added "general non-Newtonian" classifications (*12, 22,* and *23*). Engineering design procedures have then been developed on this basis, particularly for the first of the aforementioned fluid types (*4, 10, 12,* and *18*).

The classification of fluids into those categories constitutes a gross oversimplification of the facts. It has repeatedly been shown (*5, 6, 21,* and *26*) that the classification into which a fluid falls, and even the numerical values assigned its rheological properties, is extremely dependent upon the experimental conditions under which the measurements are made. Under certain narrow ranges of shear rate, for example, a given fluid may clearly appear to behave as a Bingham plastic; at slightly different rates of shear the pseudoplastic relationship is closely followed and, particularly at high shear rates, the same material may appear almost Newtonian.

The important consequences of these facts are two in number: first, large extrapolations of data to new conditions are not permissible where this system of classification is used and, second (and most important), design procedures for prediction of pressure drop in pipe lines become astronomically complex if they must be changed every time the fluid velocity in a pipe line (shear rate) is changed, which may be the case if the fluid exhibits a different type of flow behavior over every new region of shear rates.

It is obvious from the foregoing discussion that some method must eventually be developed which is universally applicable to all fluids —Newtonian and non-Newtonian alike. Several attempts to do this have been reported in the literature (*2, 16, 24,* and *28*). The second of these is limited because of its empirical nature and the last two require the assumption of equations relating fluid shear rate to shear stress. This is an eminently more useful procedure than the arbitrary classification of fluids into rheological types, but nevertheless these equations do not always correlate fluid properties with adequate precision. In addition, the first and last of these prior-art procedures are of considerable complexity. Therefore one major purpose of the present work was to provide a design procedure which might be completely general and rigorous yet as simple in form as the standard friction factor—Reynolds number correlations for Newtonian fluids.

The second severe limitation of these general prior-art methods is their unproved ability to predict accurately the point of onset of turbulence. In a few industries the non-Newtonian fluids encountered are invariably viscous pastes and this restriction is not important; in other industries turbulent flow is of common occurrence, particularly where it is needed to produce reasonably high rates of heat or mass transfer. The second major purpose of the present investigation, therefore, was to provide at least a tentative criterion for the onset of turbulence and to correlate all the available data on flow of non-Newtonian fluids outside the laminar flow region.

Very few of the prior-art publications in engineering deal with thixotropic or rheopectic fluids. It is also necessary to exclude these fluids from consideration in this work, but, as pointed out previously (*16*), this is not a serious limitation at the present time.

DEVELOPMENT OF CORRELATION

Rabinowitsch (*20*) developed an expression for the rate of shear of a fluid which is entirely independent of the fluid properties, provided thixotropy and rheopexy are eliminated. The complete development of this equation was also presented in a paper of Mooney (*17*). Their final expression takes the form

$$\left(\frac{-du}{dr}\right)_w = 3\left(\frac{8Q}{\pi D^3}\right) + \frac{D\Delta P}{4L} \cdot \frac{d\,(8Q/\pi D^3)}{d\,(D\Delta P/4L)} \qquad (1)$$

Since the bulk velocity V is equal to $4Q/\pi D^2$, Equation (1) can be rearranged as

$$\left(\frac{-du}{dr}\right)_w = \frac{3}{4}\left(\frac{8V}{D}\right) + \frac{1}{4}\left(\frac{8V}{D}\right) \frac{d\,(8V/D)}{d\,(D\Delta P/4L)} \Big/ \frac{(8V/D)}{D\Delta P/4L} \qquad (2)$$

$$= \frac{3}{4}\left(\frac{8V}{D}\right) + \frac{1}{4}\left(\frac{8V}{D}\right) \frac{d \ln (8V/D)}{d \ln (D\Delta P/4L)} \qquad (3)$$

In order to simplify Equation (3), the derivative will be denoted by the symbol $1/n'$. Rearrangement of Equation (3) then gives

$$\left(\frac{-du}{dr}\right)_w = \frac{3n' + 1}{4n'} \frac{8V}{D} \qquad (4)$$

It must be emphasized that Equation (4) is simply another form of Equations (1) to (3) and is therefore an entirely general expression of the relationship between rate of shear ($-du/dr$) and bulk flow rate of the fluid. It is preferable to the original Rabinowitsch relationship [Equation (1)] for two reasons, however:

1. It is in a simpler, more compact form.
2. The derivative n' represents the slope of a logarithmic plot of $D\Delta P/4L$ vs. $8V/D$ and has been found to be very nearly a constant over wide ranges of shear stress for a great variety of non-Newtonian fluids. From a calculational viewpoint it is much easier, therefore, to work with this parameter than with the derivative in Equation (1). An equation similar to Equation (4) was also developed by Schofield (*25*).

The definition of n' will next be rearranged to show the relationship of this physical property to other better known fluid properties.

Since

$$\frac{1}{n'} = \frac{d \ln 8V/D}{d \ln D\Delta P/4L}$$

one may write (over any range of shear stresses for which n' is constant)

$$\frac{D\Delta P}{4L} = K'\left(\frac{8V}{D}\right)^{n'} \qquad (5)$$

where K' is also a constant. It has been found experimentally that for most fluids K' and n' are constant over wide ranges of $8V/D$ or $D\Delta P/4L$. For some fluids this is not the case, however, and care must be taken to ensure that the range of integration is small, i.e., that the particular values of K' and n' used are valid for the actual $8V/D$ or $D\Delta P/4L$ with which one is dealing in a given design problem. Conceivably in the limiting case different values of K' and n' would have to be used for every value of $8V/D$ [in this case Equation (5) would be the equation of the tangent to the curve at a single point] but it must be emphasized that for almost all fluids the reverse is true and K' and n' are constant over wide ranges of $8V/D$.

On substituting for $8V/D$ in Equation (5) from Equation (4) and denoting the shear stress at the wall of a pipe ($D\Delta P/4L$) by T_w, one obtains

$$T_w = K'\left(\frac{4n'}{3n'+1}\right)^{n'}\left(\frac{-du}{dr}\right)_w^{n'} \qquad (6)$$

We are now in a position to appreciate the significance of the physical property n'. If it is a constant with the value of unity, Equation (6) becomes

$$T_w = K'\left(\frac{-du}{dr}\right)_w \qquad (7)$$

That is to say, the familiar linear relationship between shear stress and shear rate of Newtonian fluids appears, and K' is obviously equal to μ/g_c. If, on the other hand, n' is less than unity (but still constant) one obtains the Ostwald equation for pseudoplastic fluids, viz.,

$$T_w = K\left(\frac{-du}{dr}\right)^n \qquad (8)$$

Similarily, if n' is greater than unity the fluid is dilatant in character, a class of which the common starches are outstanding examples. (References *2, 9,* and *16,* among others, discuss these various types of non-Newtonian fluids in some detail.)

In summary of the preceding paragraphs it is seen that *the coefficient* n′ *is that physical property of a fluid which characterizes its degree of non-Newtonian behavior*: the greater the divergence of n' from unity (in either direction), the more non-Newtonian is the fluid in question. It is believed that this may be the first time that a quantitative and rigorous scale has been proposed by means of which the degree of non-Newtonian behavior of all fluids (other than time-dependent ones) may be established and compared.

Equation (5) is the basic relationship for relating pressure drop to flow rate by means of geometric parameters and the two physical properties of the fluid, K' and n'. Whereas n' defines the degree of non-Newtonian behavior of the fluid, K' defines its consistency: the larger the value of K' the "thicker" or "more viscous" the fluid.

The next step in the mathematical development is to relate ΔP in Equation (5) to the Fanning friction factor, in order to enable the computation of this parameter, and therefore for all fluids the Reynolds numbers and flow rates at which stable laminar flow no longer is found. The usual definition (*30*) of the former may be written as

$$f = \frac{D\Delta P}{4L} \Big/ \frac{\rho V^2}{2g_c} \qquad (9)$$

Substitution of $D\Delta P/4L$ from Equation (5) into Equation (9) gives

$$f = \frac{16\gamma}{D^{n'} V^{2-n'} \rho} \qquad (10)$$

where

$$\gamma = g_c K' 8^{n'-1} \qquad (11)$$

By letting $f = 16/N_{Re}$ as for Newtonian fluids in laminar flow, one defines a generalized Reynolds number:

$$N_{Re} = \frac{D^{n'} V^{2-n'} \rho}{\gamma} \qquad (12)$$

The significance of the foregoing equations cannot be overemphasized. They state that all fluids must follow the usual f vs. N_{Re} relationship in the laminar-flow region when one uses the generalized Reynolds number defined by Equation (12). As the only implicit assumption in this development is that of no "slip" at the wall of the pipe, this development is completely rigorous and may, in fact, be used to check the accuracy of experimental data. If perfect coincidence with the $f = 16/N_{Re}$ line is not obtained in the laminar-flow region, either the data or calculations are in error or the fluid exhibits evidence of thixotropic or rheopectic behavior.

For Newtonian fluids, $n' = 1.000$, $K' = \mu/g_c$, γ reduces to μ (the viscosity of the fluid), and N_{Re} [Equation (12)] reduces to the familiar $DV\rho/\mu$, showing that this traditional dimensionless group is merely a special restricted form of the more general one proposed here.

In order to make use of these relationships, it is necessary to obtain K' and n' for the fluid being considered. The easiest and the only perfectly rigorous method is to measure the pressure drop and flow rate of the material in any good capillary-tube viscometer and to apply Equation (5) to these data. Since K' and n' were independent of shear rate for all the fluids on which literature data were available, pressure-drop determinations at two flow rates are theoretically sufficient completely to define the physical properties of the fluid. (It may be noted in

passing that two experimental measurements are the minimum number which must be made on any non-Newtonian fluid in order to define its rheological properties adequately, as compared with the single measurement which suffices for Newtonians.) From a practical viewpoint, however, it is usually preferable to take more data because of the experimental difficulty of obtaining accurate, reproducible data on many non-Newtonian systems.

Rotational viscometers are also generally satisfactory for evaluation of K and n by means of Equation (8). [Krieger and Maron (*13*) have shown how $(-du/dr)_w$ may be obtained from data taken on such an instrument.) It must be noted, however, that K and n can be related to K' and n' only when these properties are constant over a reasonably wide (say, ten-fold) range of shear stresses. This has not been found to be a significant limitation on work to date but may be with certain other non-Newtonian materials. Accordingly, the over-all recommendation is to take data with a capillary-tube viscometer whenever this is convenient.

TRANSITION FROM LAMINAR TO TURBULENT FLOW

Although deviation from purely laminar or streamline motion has been observed to occur at Reynolds numbers as low as about 1,000 for Newtonian fluids (*19*), the formation of truly persistent eddies and substantial deviation of the velocity profile from the parabola of the laminar region occur rather suddenly over a narrow range of Reynolds numbers near 2,100 (*14* and *19*). Since the Reynolds number has been empirically found to define this transition region for Newtonian fluids, many workers have attempted to justify theoretically its use as a criterion for onset of turbulence by considering the Reynolds number to be a ratio of "inertial forces to viscous forces." It has been pointed out elsewhere (*19*) that this concept seems to be of little theoretical value.

The same is not true of the Fanning friction factor. As shown by Equation (9), it is indeed a ratio of forces—the viscous shear force (per unit wall area) divided by the average main-stream inertial force (per unit cross-sectional area). In the present work, therefore, f rather than N_{Re} will be generally used as the criterion for onset of turbulence. The two apparent disadvantages of such an approach are not believed to be of great importance: first, the problem of an increasing f in the transition region (at least for Newtonian fluids) must be noted only to avoid possible ambiguity, and the second shortcoming, that the inertial forces are average values, is common to almost all approaches of this type (since the various types of non-Newtonians will exhibit different velocity profiles, the averaging procedure is not uniform). In view of the unique relationship between f and N_{Re} for all fluids in the present correlation, it is still impossible to distinguish which of these criteria is rigorously correct.

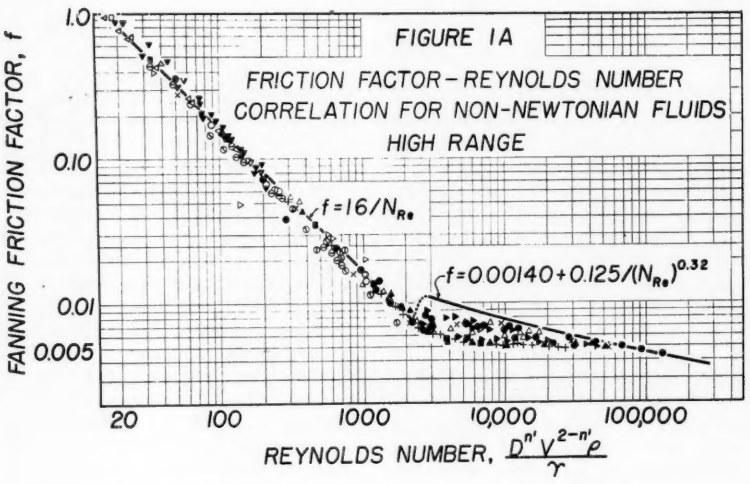

Fig. 1A. Friction-factor–Reynolds number correlation for non-Newtonian fluids—high range.

TABLE 1.—RHEOLOGICAL CONSTANTS FOR FLUIDS SHOWN IN FIGURE 1

Symbol used in Figure 1	Nominal pipe size, in.	Composition of fluid	Rheological constants n'	Rheological constants γ	Source of data
+	1	23.3% Illinois yellow clay in water	0.229	0.863	(*4*)
⊕	⅞ and 1½	0.67% Carboxy-methyl-cellulose (CMC) in water	0.716	0.121	(*24*)
⊖	⅞ and 1½	1.5% CMC in water	0.554	0.920	(*28*)
⊘	⅞ and 1½	3.0% CMC in water	0.566	2.80	(*28*)
⊘	⅞, 1½ and 2	33% Lime water	0.171	0.983	(*28*)
◁	⅞ and 1½	10% Napalm in kerosine	0.520	1.18	(*28*)
▼	8, 10 and 12	4% Paper pulp in water	0.575	6.13	(*1*)
△	¾ and 1½	54.3% Cement rock in water	0.153	0.331	(*31*)
▲	4	18.6% Solids, Mississippi clay in water	0.022	0.105	(*11*)
●	¾ and 1¼	14.3% Clay in water	0.350	0.0344	(*10*)
▷	¾ and 1¼	21.2% Clay in water	0.335	0.0855	(*10*)
x	¾ and 1¼	25.0% Clay in water	0.185	0.204	(*10*)
▽	¾ and 1¼	31.9% Clay in water	0.251	0.414	(*10*)
□	¾ and 1¼	36.8% Clay in water	0.176	1.07	(*10*)
■	¾ and 1¼	40.4% Clay in water	0.132	2.30	(*10*)
▶	¼, ¼, ½ and 2	23% Lime in water	0.178	1.04	(2)

RESULTS

Figure 1 shows a plot of f vs. $(D^{n'}V^{2-n'}\rho/\gamma$, which has been found to correlate all literature data on non-Newtonian fluids. Actually not all the data points used are shown on the figure; for example, the extensive data of Winding et al. (*32*) were found to correlate excellently, but their fluids were so nearly Newtonian (n' values of 0.885 to 0.985, as compared with 1.000 for a Newtonian fluid) that inclusion of these data would not have contributed significantly. The data of Wilhelm et al. (*31*) for 3-in. pipes were also omitted because of failure of this part of their system to give the correct results with

Newtonian liquids, and similar judgment was used in eliminating the data of many other authors. As it stands, Figure 1 includes data from eight independent investigators, covering sixteen different fluids, the properties of which are tabulated in Table 1. Pipe diameters varied from ⅛ to 12 in. (100-fold variation) and the data cover a 2.1×10^9 range of Reynolds numbers from 6.0×10^{-5} to 130,000. The fluid properties (K' and n') were obtained from rotational viscometers in the case of the *CMC* and lime slurry data of Salt(*24*) and Stevens(*28*) and from capillary-tube or pipe flow data in all other cases. The curves shown in Figure 1 are the commonly accepted relations for Newtonian fluids and the data points represent measurements on non-Newtonians.

Laminar Region. The scattering of the data is significant; although most of the laminar-region data fall with ±10% of the required $f = 16/N_{Re}$ line, several points deviate by 40% or more. As discussed earlier, this scattering must be due to experimental errors or errors in calculation, unless one makes the unlikely assumption that the fluids exhibited thixotropy or rheopexy. Since several of the authors whose data are shown in Figure 1 reported only nominal pipe sizes, it is likely that incorrect values for diameter were occasionally used. Similarily, fluid densities were not always reported accurately. In view of these possible errors the excellence of the correlation within the laminar region is remarkable.

Transition Region. If the previous discussion of the transition from laminar to turbulent flow is indeed valid, then the non-Newtonian data should begin to deviate appreciably from the laminar $f = 16/N_{Re}$ line at approximately the same ratio of viscous shear to inertial forces as do Newtonian data for smooth pipes, namely at $f = 0.008$. This is borne out remarkably well by all the data in this region on Figure 1. Furthermore, because of the close resemblance between highly non-Newtonian fluids at low shear rates and true solids, little eddies of the fluid in turbulent motion should behave more nearly like solid particles and, for example, not break up so readily as do the eddies of Newtonian fluids. The net effect of this difference would be a more diffuse transition from laminar to turbulent flow, mani-

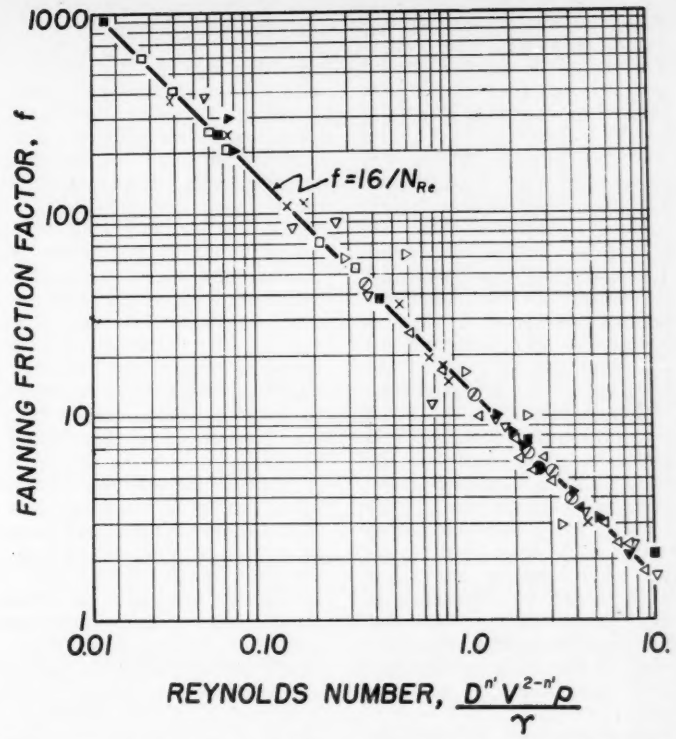

Fig. 1B. Friction-factor–Reynolds-number correlation for non-Newtonian fluids–medium range.

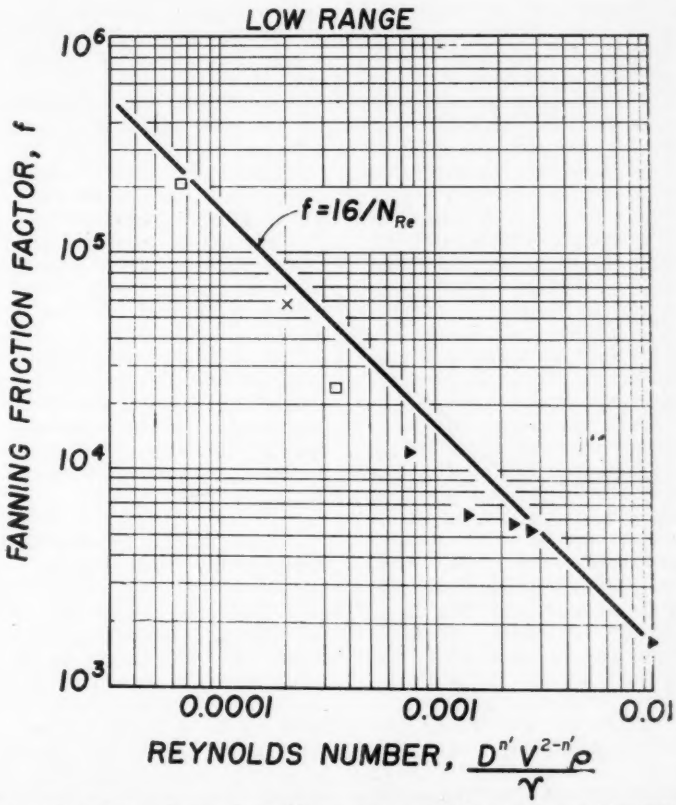

Fig. 1C. Friction-factor–Reynolds-number correlation for non-Newtonian fluids–low range.

fested by a much greater transition region than the 2,000 to 3,300 range of Reynolds numbers found (*14* and *27*) for Newtonian fluids. Whether or not turbulence is fully developed below the maximum Reynolds number of 130,000 (in Figure 1) will have to be shown by further experimental work. Qualitatively, however, the expected diffuse nature and great broadness of the non-Newtonian transition region have been experimentally confirmed by dye-injection studies (*29*) although no work to date has yet defined the actual extent of the transition region for these materials. Until this is done, our tentative approach is to assume that the breadth of the transition region increases as n' decreases and that for most of the fluids whose f–N_{Re} data are shown on Figure 1 the transition region extends approximately to N_{Re} = 50,000 to 70,000. This assumption, although tentative, is supported not only by the data of Figure 1 but also by the data on the less non-Newtonian fluids of Winding et al. (*32*).

It is interesting to compare the proposed criterion for onset of turbulence (i.e., when f first decreases to about 0.008) with the criteria suggested by other investigators. For Newtonian fluids it is obviously identical to the well-established criterion of N_{Re} = 2,000. For Bingham plastic non-Newtonian fluids, Caldwell and Babbitt (*4*) have given an equation which permits the calculation of a "lower critical velocity"—that velocity below which flow will always be laminar—in terms of the pertinent geometric variables and physical properties, which they checked by application to twenty-five different materials. Rearrangement of their equation to enable solving for f gives the identical criterion ($f = 0.008$) proposed in this paper. Hedstrom (*12*) suggested on the basis of extremely limited data that flow of Bingham plastic non-Newtonians becomes turbulent when the various laminar-region curves (for various values of the group $T_y D^2 \rho g_c/\eta^2$ intersect the line relating f and N_{Re} for Newtonian fluids. This is a significantly different criterion from the one proposed in this paper, but inspection of his graphs shows that the experimental data more nearly obey the present criterion than his. Winding et al. (*32*) have presented several criteria: one based on apparent viscosities at zero shear rate, which can obviously not apply to highly non-Newtonian fluids, and one for fluids to which the Williamson equation applies. This latter criterion, when rearranged into the form of a friction factor, again gives as the transition point f = 0.008. The same is also true of other criteria, presented by Toms (*29*) and Metzner (*16*), which make use of Reynolds numbers using apparent viscosities which are so defined as to give the correct pressure drop when substituted in Poiseuille's low. Ooyama and Ito (*18*) presented a criterion which is close to the proposed f = 0.008 but which is hard to compare in greater detail. They supported their criterion experimentally with a small fraction of the data incorporated in the present work; hence it may be concluded that, at least for these data, their criterion gives results identical to those of the more general present one. McMillen (*15*) presented a criterion for Bingham plastic fluids which predicts stable laminar flow at nearly three times the velocities calculated at the point f = 0.008. However, he states that his criterion is based on only two experimental measurements, one of which did not leave the laminar region except within the accuracy of the measurements. Accordingly, the discrepancy between his criterion and ours cannot be considered significant. A criterion suggested by Alves et al. (*2*) is too conservative to give the onset of turbulence with accuracy.

In summary, it has been proposed that both Newtonian and non-Newtonian fluids leave the region of stable streamline flow when f first drops to a value of about 0.008 or less or when $D^{n'}V^{2-n'}\rho/\gamma$ reaches a value of 2,000 to 2,500. All available data support this conclusion, and the many different prior-art criteria for onset of turbulence in non-Newtonian fluids which predict it accurately may be rearranged to give the single and perhaps universal criterion proposed here.

Turbulent Region. In view of the uncertainties surrounding the actual width of the transition region, little may be said concerning the difference between the accepted curve for Newtonian fluids in turbulent flow and the experimental non-Newtonian data in the same region of Reynolds numbers. However, if one accepts the foregoing assumption that fully developed turbulence may not occur until N_{Re}>50,000 for some fluids, then practically none of the available data fall into what is clearly the region of turbulent flow. Until further work defines the end of the transition region with certainty, it is recommended that the usual Newtonian curve be used for design purposes [with the form of Reynolds number shown in Equation (12)] regardless of the magnitude of N_{Re}. This procedure gives conservative values of pressure drop at N_{Re}>2,100, and since the maximum difference between the curve and data in this region is about 50%, Figure 1 is actually very useful even in this "transition" flow region as compared with methods suggested in the prior literature. Winding et al. (*32*) suggested use of the usual f vs. $DV\rho/\mu$ chart together with the evaluation of the viscosity at infinite shear rate, but in large pipes, where turbulence may set in at low velocities, the use of infinite shear-rate viscosities would lead to significant errors unless the fluids are nearly Newtonian in nature. Wilhelm (*31*), Binder (*3*), and Alves (*2*) suggest procedures which require empirical viscosity data in the turbulent region. It would appear that these may be satisfactory design methods if one is able to obtain the necessary data, but they do not permit the design of equipment from physical-properties measurements alone. Other authors (*4, 10, 12,* and *18*) have concerned themselves only with Bingham plastic fluids in turbulent flow; hence their work is limited in scope, but the excellent results of Winning (*10*) and Hedstrom (*12*) merit special consideration when fluids of this type are encountered.

COMMENTS ON USE OF CORRELATION

Although the development is perfectly general in that K' and n' were not assumed to be constants (independent of shear rate), it was found that for every fluid on which pipe-line data were available these rheological properties were indeed constant within the accuracy of the data. Had this not been the case, the design procedure to follow would be somewhat more complex; both γ and n' would have to be evaluated at the correct value of shear rate or shear stress. Within the laminar flow region this is not a serious difficulty as γ [Equation (11)] is not a very strong function of n'. Outside the laminar region, however, a trial-and-error procedure would be involved: after calculation of a pressure drop by use of Figure 1, it would be neces-

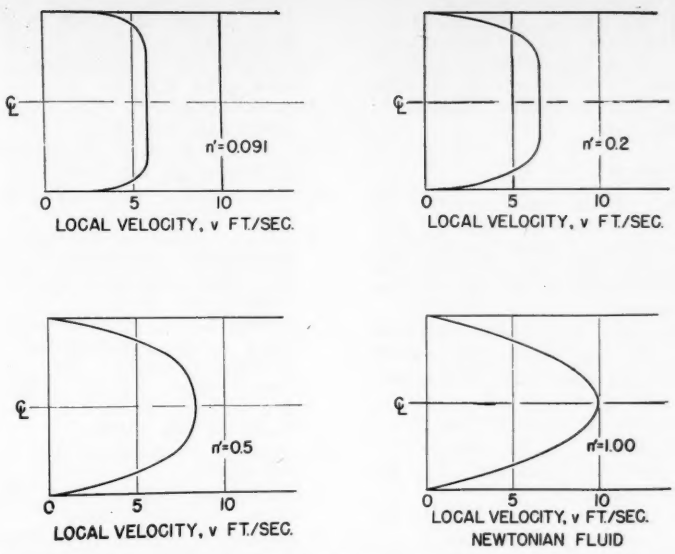

Fig. 2. Dependence of velocity distribution upon the fluid property n'.

sary to calculate T_w and to repeat this procedure until the calculated T_w is identical to that shear stress at which n' and γ were evaluated in obtaining N_{Re}.

Because K' and n' are very nearly constant for so many fluids over shear ranges of practical interest, the logarithmically linear relationship between shear stress and flow rate or shear rate depicted by Equations (5) and (8) constitutes perhaps the most useful means available for extrapolation of rheological data. Theoretical rheologists have long objected to the assumption of the validity of Equations (5) or (8), and Reiner (*23*) has given a particularly good review of their criticisms. Some of these, such as the fact that K' does not have units of viscosity, are irrelevant—N_{Re} as defined by Equation (12) is still rigorously dimensionless. Perhaps the most important apparent objection to the view that almost all fluids obey Equation (5), even when K' and n' are held constant, is the incompatability of this conclusion with the reported existence of materials which behave as Bingham plastics, the "plug flow" of these latter materials in tubes having been experimentally verified by Green (*7, 8* and *9*). However, Figure 2 shows that it is not necessary, as Green (*9*) states, for a material to be a Bingham plastic in order to exhibit plug flow well within experimental accuracy. Indeed, when $n' = 0.20$ it is seen that the velocity profile deviates markedly from the familiar Newtonian parabola and is within 1% of a true plug until r/R becomes greater than 0.4. Seven of the sixteen fluids whose properties are tabulated in Table 1 have values of n' well below 0.20. For these materials it is therefore to be expected that both Equation (5) and the Bingham plastic relationship between shear stress and shear rate apply equally well, a situation that further supports the shelving of classical non-Newtonian fluid definitions and extrapolating, when necessary, by use of Equation (5). The extent to which extrapolation is permissible must, however, be carefully considered in every case, as the rigor of the present treatment depends on the fact that n' and K' are permitted to vary with shear stress. In a sense the variation of these properties with shear stress is similar to the well-known variation of other physical properties with temperature or pressure.

It might appear that the designation of n and K as the true physical properties which describe a non-Newtonian fluid (at a particular shearing stress) would be preferable to the use of n' and K'. The support for this view arises from the fact that the former are independent of the type of apparatus in which the measurements are made, as true physical properties should be, and the latter are not. Actually n and n' are equal numerically for many fluids, and so this choice is not frequently an important one. When they are not equal, the engineering procedure recommended here is to use whichever is more closely related to the problem at hand—for flow in circular pipes this is n'; in other flow situations the use of n will undoubtedly be preferable.

Several important practical conclusions arising from the present work require emphasis. It is instructive to rearrange Equations (9) and (10) to solve for ΔP, whereby one obtains, for flow in the laminar region,

$$\Delta P = \frac{32\,\gamma\, LV^{n}}{g_c D^{n'+1}} \qquad (13)$$

For Newtonian fluids ($n' = 1.00$, $\gamma = \mu$) Equation (13) reduces to the usual Poiseuille relationship.

Since $V = 4Q/\pi D^2$,

$$\Delta P = \frac{32\,\gamma\, L}{g_c}\left(\frac{4Q}{\pi}\right)^{n} \cdot \frac{1}{D^{3n'+1}} \qquad (14)$$

If one wishes to reduce the pressure drop accompanying a given volumetric flow rate Q, it is well known that small increases in pipeline diameter are extraordinarily effective for Newtonian fluids as pressure drop varies inversely as diameter to the fourth power when $n' = 1.00$. On the other hand, for highly non-Newtonian systems n' approaches zero, and for such materials it is seen that pressure drop varies inversely as diameter to only the first power; so the designer must go to unusually large pipes before the reduction in pressure drop is appreciable. Increases in capacity of an existing plant, however, may frequently be obtained simply by increasing the pump speed, as the pressure drop is extremely insensitive to flow rate in which n' is small, As a matter of fact, for the slurry data reported by Gregory (*11*) (*see* Table 1) n' is almost zero; i.e., ΔP is very nearly independent of flow rate in the laminar flow region. For engineers familiar only with the peculiarities of Newtonian fluids, these differences are therefore both a hazard and an advantage, but observation of several piping systems installed to date indicates that the industries concerned have taken little advantage of the insensibility of pressure drop to flow rate. These comments must be restricted to the laminar flow region as too few of the present data extend into the region of well-developed turbulent flow to enable one to generalize for that case.

The second practical conclusion depends on the fact that Figure 1 constitutes a compilation of all the

available pipe-line data on highly non-Newtonian systems. As such, it clearly shows that the region of laminar flow is of major interest, as extremely viscous materials are the general rule. However, about one third of the data are outside the laminar region, and this proportion may be expected to increase as turbulence becomes necessary to produce high rates of mass or heat transfer, particularly in nuclear-reactor and similar high-output applications.

FUTURE WORK

The behavior of non-Newtonian fluids in both the transition and turbulent-flow regions should be defined more clearly than has been possible by use of literature data alone. In particular, the extent of the transition region must be clearly defined. A particularly instructive and critical test of of this correlation would be its extension to the turbulent flow of dilatant fluids, on which no data at all were available. Engineering correlations must also be developed at some future date for the more complex thixotropic and rheopetic systems.

SUMMARY

The recommended design procedure, supported by all available data, may be stated as follows:

1. *Data Required.* Rheological properties (K' and n') and fluid density are needed. The former should be measured with a capillary-tube viscometer but can frequently be approximated with essentially the same precision from rotational viscometric data. Measurements at only two shear rates (rotational speeds or flow rates) are theoretically sufficient although more are helpful to justify the absence of thixotropy and rheopecty and reduce the experimental errors which frequently tend to be large in this type of work.

2. *Calculations.* γ is obtained from K' and n' [Equation (11)], $N_{Re}(D^{n'}V^{2-n'}\rho/\gamma)$ is calculated, and f is obtained from the usual friction factor —Reynolds number plot. From this point the pressure-drop calculation is identical to the usual procedure for Newtonian fluids. The calculation will be rigorous if the Reynolds number is below 2,100 or if f is greater than 0.008 (laminar flow) and will be conservative in the transition and turbulent-flow regions. Outside the laminar-flow region, the foregoing conclusions may not apply to fluids exhibiting dilatancy.

ACKNOWLEDGMENT

This work was sponsored by the Office of Ordnance Research, U. S. Army. Of special value was the willingness of several authors whose data are included in this report to make their calculations and unpublished tabulations available. Comments of a highly constructive nature were received from G. E. Alves, D. F. Boucher, L. F. Brown, M. Mooney, R. E. Otto, S. Rankin, and R. L. Pigford.

NOTATION

Note: As the final correlation is based on dimensionless groups, any consistent set of units may be used. The units given in the following table merely represent those used by the authors.

du/dr = velocity gradient or shear rate, sec.$^{-1}$ $(-du/dr)_w$ refers to the shear rate at the wall of a pipe

D = inside diameter of pipe, ft.

f = Fanning friction factor, defined by Equation (9), dimensionless

g_c = conversion factor, 32.2 ft. lb. mass/(sec.^{2})(lb.force)

K' = coefficient in Equation (5), (lb.force)(sec.$^{n'}$)/(sq.ft.)

L = length of pipe or tube, ft.

n' = exponent in Equation (5), dimensionless. $n' = 1.000$ for Newtonian fluids, is between zero and unity for pseudoplastic non-Newtonians, and greater than unity for dilatant fluids

N_{Re} = Reynolds number, dimensionless. $N_{Re} = D^{n'}V^{2-n'}\rho/\gamma$ for all fluids, which reduces to $DV\rho/\mu$ for Newtonians

ΔP = pressure drop, lb.force/sq.ft.

Q = volumetric flow rate, cu.ft./sec.

r = distance or radial distance, ft.

R = inside radius of pipe, ft.

T = shear stress, lb.force/sq.ft. T_w denotes shear stress at the wall of a pipe and T_y refers to the yield strength of a Bingham plastic non-Newtonian

v = local velocity, ft./sec.

V = average or bulk velocity, ft./sec.

γ = generalized viscosity coefficient as defined by Equation (11), lb.mass/(ft.)(sec.$^{2-n'}$)

η = coefficient of rigidity of a Bingham plastic non-Newtonian fluid, lb.mass/(sec.)(ft.)

μ = viscosity of a Newtonian fluid, lb.mass/(ft.)(sec.)

ρ = density of fluid, lb.mass/cu.ft.

LITERATURE CITED

1. Allis-Chalmers Manufacturing Co. *Bull.* 1649.
2. Alves, G. E., D. F. Boucher, and R. L. Pigford, *Chem. Eng. Progr.*, 48, 385 (1952).
3. Binder, R. C., and J. E. Busher, *J. Appl. Mechanics*, 13, A101 (1946).
4. Caldwell, D. H., and H. E. Babbitt, *Trans. Am. Inst. Chem. Engrs.*, 37, 237 (1941).
5. Christiansen, E. B., private communication (1954).
6. Colgate-Palmolive Co., unpublished data (1952).
7. Green, H., *Proc. Am. Soc. Testing Materials*, 20, 451 (1920).
8. ———, and G. Hallam., *Ind. Eng. Chem.*, 17, 726 (1925).
9. ———, "Industrial Rheology and Rheological Structures," John Wiley and Sons, Inc., New York (1949).
10. Govier, G. W., and M. D. Winning, paper presented at the Montreal meeting, *Am. Inst. Chem. Engrs.* (Sept. 7, 1949); also Winning, M. D., M.Sc. thesis, Univ. Alberta (1948).
11. Gregory, W. B., *Mech. Eng.*, 49, 609 (1927).
12. Hedstrom, B.O.A., *Ind. Eng. Chem.*, 44, 651 (1952).
13. Krieger, I. M., and S. H. Maron, *J., Appl. Phys.*, 25, 72 (1954).
14. McAdams, W. H., "Heat Transmission," 3rd ed., McGraw-Hill Book Company, Inc., New York (1954).
15. McMillen, E. L., *Chem. Eng. Progr.*, 44, 537 (1948).
16. Metzner, A. B., *loc. cit.*, 50, 27 (1954).
17. Mooney, M., *J. Rheol.*, 2, 210 (1931).
18. Ooyama, Y., and S. Ito, *Chem. Eng. (Japan)*, 14, 96 (1950).
19. Prengle, R. S., D. Sc. thesis, Carnegie Inst. Technol. (1953).
20. Rabinowitsch, B., *Z. physik. Chem.*, 145A, 1 (1929).
21. Reed, J. C., M.Ch.E. thesis, Univ. Delaware (1954).
22. Reiner, M., "Ten Lectures on Theoretical Rheology," Rubin Mass, Jerusalem (1943).
23. ———, "'Deformation and Flow," H. K. Lewis and Co., London (1949).
24. Salt, D. L., M.S. thesis, Univ. Utah (1949).
25. Schofield, R., *J. Appl. Phys., IV*, 122 (1933).
26. Scott Blair, G. W., "Introduction to Industrial Rheology," J. and A. Churchill, Ltd., London (1938).
27. Senecal, V. E., and R. R. Rothfus, *Chem. Eng. Progr.*, 49, 533 (1953).
28. Stevens, W. E., Ph.D. thesis, Univ. Utah (1953).
29. Toms, B. A., *J. Colloid Sci.*, 4, 511 (1949).
30. Walker, W. H., W. K. Lewis, W. H. McAdams, and E. R. Gilliland, "Principles of Chemical Engineering," 3rd ed., McGraw-Hill Book Company, Inc., New York, (1937).
31. Wilhelm, R. H., D. M. Wroughton, and W. F. Loeffel, *Ind. Eng. Chem.*, 31, 622 (1939).
32. Winding, C. C., G. P. Baumann, and W. L. Kranich, *Chem. Eng. Progr.*, 43, 527, 613 (1947).

(Presented at A.I.Ch.E. New York meeting)

Capacity Factors in the Performance of Perforated-plate Columns

Charles d'Ancona Hunt, D. N. Hanson, and C. R. Wilke
University of California, Berkeley, California

A study was made of factors affecting the vapor-handling capacity of perforated-plate liquid-vapor contacting columns. Vapor-phase pressure drop across plates, liquid entrainment upward from plate to plate, and plate stability were investigated as functions of operational and geometric column parameters.

Gas-phase pressure drop across dry perforated plates was observed to follow functional relationships predicted from available information for single perforations. The presence of liquid on a plate increased the total pressure drop by the equivalent clear-liquid head plus a small residue which is nearly constant for a given liquid.

Entrainment was observed to be a function of column gas velocity, independent of gas velocity in the perforations. Weight rate of entrainment was also found to be proportional to the gas density, independent of liquid density, and inversely proportional to the liquid-surface tension. For a given system, entrainment was observed to be proportional to approximately the third power of the group, gas velocity divided by the distance between the liquid surface and the plate above.

The stability of perforated plates was observed to be adequate for many industrial and experimental applications, as also reported in recently published studies, but contrary to qualitative statements found in the earlier literature. Stability was found to increase with decreasing perforation diameter and decreasing total perforation area relative to column cross-sectional area; to increase with greater gas density, liquid surface tension, and liquid wetting power; and to be virtually independent of liquid density and viscosity.

Operating limits of vapor and liquid throughput are shown for a typical application of perforated plates in liquid-vapor contacting columns.

The industrial use of perforated-plate columns for countercurrent contacting of liquids and vapors was until recently limited mainly to applications where the liquids contained large quantities of solid matter. According to general opinion on column design, the perforated-plate type of contacting unit had a narrow stable operating range of gas flow; whereas a bubble-cap unit had no particular lower limit of gas flow except at relatively high liquid flow rates.

Recent studies by Mayfield, Church, Green, Lee, and Rasmussen (*10*), and Arnold, Plank, and Schoenborn (*1*) show that the perforated-plate column has definite economic advantages over the bubble-cap plate column and that the possible range of gas and liquid flows for stable operating conditions is sufficiently wide for many applications in the chemical processing field. According to Mayfield *et al.* perforated-plate columns are being used by the Celanese

C. d'A. Hunt is at present with Stauffer Chemical Company, Richmond, California.

Corporation for most new applications, and existing bubble-cap plates are being replaced by perforated plates in many units.

The present work was undertaken prior to the appearance of references 10 and 1 in order to clear up questions arising from previous work in this department related to pressure drop and plate stability. Another objective was to study entrainment in the perforated-plate column in order to determine upper limits of gas flow rate in the column imposed by excessive entrainment upward from plate to plate of liquid droplets in the gas stream. The experimental work was done in a 6-in.-diam. column.

In columns with liquid flowing across the plate and over a weir, the liquid head on the plate in the stable operating region is determined not only by the height of the overflow weir and the head of liquid required for the flow over the weir but also by the degree of aeration of the liquid on the plate. This aeration is the result of the flow of gas through the body of liquid and is fairly independent of gas flow rate in the stable operating region. However, the phenomenon of aeration is little understood at this time, and the degree of aeration can at best be predicted within ±20%.

In order to eliminate a large share of this uncertainty in the study of pressure drop across perforated plates, the liquid head on the plate was maintained by means of a constant-head tank connected to the column just above the plate. The head was then measured by means of a pressure tap located at the plate level. In this way the effect of many variables upon pressure drop could be determined without any interference from changing aeration of the liquid on the plate. Actually the liquid head on the plate constitutes an important part of the total pressure drop for the gas flowing up the column; so a complete prediction of gas pressure drop requires an accurate knowledge not only of the the effect of the variables studied in this work but also of the degree of aeration.

Because of the unreliability of the performance of liquid overflow weirs in a 6-in.-diam. column this study does not include any information on the effect of liquid flow rates across perforated plates.

EXPERIMENTAL PROCEDURE APPARATUS

Pressure drop, entrainment, and stability criteria were studied in a 6-in.-diam. perforated-plate column, using a nonflow constant-head system to maintain liquid on the plate and a totally enclosed gas-circulation system to provide gas flow through the perforated plate.

A diagram of the experimental system is shown in Figure 1. Both the gas-circulation system and the liquid constant-head system were enclosed and vented to the column in order to allow the use of other gases and liquids besides air and water. Provision was made for purging of manometers in the plate system with the liquid in use. A heat exchanger cooled by tap water served to remove heat added from the work of compression of the gas-circulation blower. Since the orifice measured the flow of gas between the blower and the heat exchanger, gas properties at both the orifice and the plate were measured in order to avoid significant systematic errors in gas density determination. The orifice was assembled according to A.S.M.E. standard specifications.

Gas entered the column through a trap designed to prevent the liquid which dumped through the perforations from filling up the gas ducts, flowed through a set of straightening screens designed to provide a 15:1 improvement in flow distribution, and impinged upon primary plate. The column was constructed of 1/16-in.-thick wall brass with plastic windows provided for observation of plate action and dumping. Pressure taps 6 in. below and 18 in. above the plate were constructed to avoid any possibility of drops of liquid affecting the pressure reading.

The liquid entrained from the primary plate was collected on a similar plate higher in the column and drained continuously into a vented receiver which was calibrated for determination of the volume of the liquid entrained as a function of time. Less than 1% of the liquid reaching this upper plate could be further entrained out of the tapered, baffled column section above this plate. All entrainment data were taken under conditions which assured little or no dumping of liquid from the catcher plate to the primary plate. The plate spacing was increased by adding glass spacer sections to the column just below the entrainment catcher plate. After the completion of the pressure-drop measurements the metal portion of the column above the plate was shortened to 8 in. in order to allow the determination of entrainment at small plate spacings.

The gas pressure at the entrance to the blower was maintained at slightly greater than atmospheric pressure in order to prevent inleakage of air in runs using other gases and to prevent excessive leakage of these gases through the inadequate seal around the blower shaft. Gas-flow velocity was controlled by means of a simple slide valve in the 4-in. ducting used throughout the remainder of the system. Liquid head on the plate was maintained constant within 0.3 in. by means of the adjustable overflow weir in the constant-head tank. The liquid was continuously circulated from a storage tank through the constant-head tank.

The manometers connected to the column and plate were assembled with glass and transparent plastic tubing in order to make visible any gas bubbles in lines which should have been full of liquid. The manometers were ¾ in. in diameter and vertical and could be read to 0.02 in. of water. The pressure drop at the orifice was

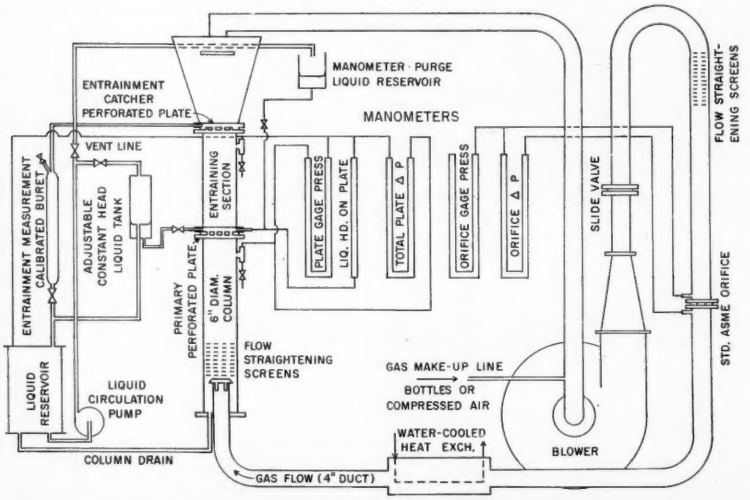

Fig. 1. Schematic diagram of experimental equipment.

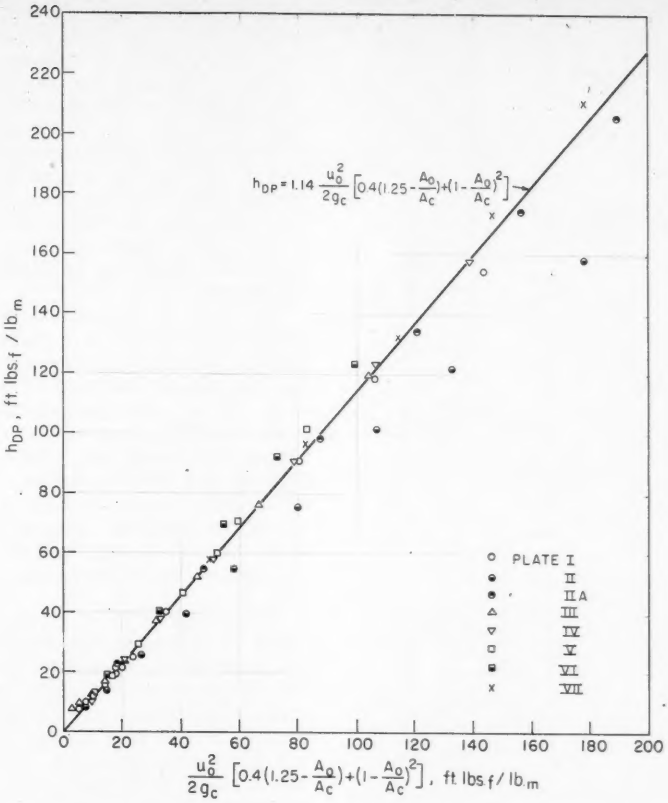

Fig. 2. Pressure drop for flow of air through dry plates.

TABLE 1.—CONFIGURATION OF PERFORATED PLATES

(All holes in equilateral triangular spacing)

Plate	Thickness, in.	Hole diam., in.	Hole spacing, in.	Number of holes	Area per hole, sq. ft.	Total hole area, sq. ft.	Percentage of total column area
I	1/8	1/8	1/4	433	0.0000852	0.0369	18.8
II	1/8	1/8	1/2	109	0.0000852	0.00929	4.9
III	1/4	1/4	1	31	0.000341	0.01056	5.4
IV	1/4	1/4	1/2	109	0.000341	0.0372	19.0
V	1/2	1/2	2	7	0.00136	0.00954	4.9
VI	1/2	1/2	1	31	0.00136	0.04226	21.5
VII	3/8	3/8	1 1/2	13	0.000767	0.00997	5.1
VIII	1/4	1/4	3/4	55	0.000341	0.0187	9.5
IIA	1/8	1/8	1/2	109	0.0000852	0.00929	4.9

measured with a standard Uehling inclined manometer.

Gas temperatures were measured with thermocouples immersed in the gas stream.

Plates of 20% relative perforation area were so unstable with respect to dumping that stabilizing screens had to be installed above these plates in order that a suitable liquid head might be maintained. The stabilizer consisted of three concentric cylinders, about 6 in. long, composed of 1/16-in. gauge wire woven into a 1/4-in. mesh screen. The stabilizer had no effect on pressure-drop measurements.

The trays used in the experiments are listed in Table 1. After reaming, micrometer measurements on the holes indicated the diameter to be within 0.001 in. of the nominal diameter.

Properties of the liquids used are listed on Figure 7.

Dry-plate Pressure Drop

Data on the pressure drop for gas flowing through perforated plates set in ducts were taken by both Arnold *et al.*(*1*) and Mayfield *et al.*(*10*). Arnold used relatively thin plates uniformly 0.029 in. thick with perforation diameters from 0.039 to 0.376 in. Mayfield used thicker plates, from 1/8 to 1/4 in., with perforations also from 1/8 to 1/4 in. Both investigators employed a simplified orifice equation to represent their data.

The plates used by Arnold *et al.* approximate sharp-edged orifices. It might be expected that the orifice coefficient obtained would be a function of Reynolds number, and this is borne out by the fact that Arnold found his pressure drop to be proportional to the 1.8 power of velocity through the perforations, rather than to the power 2, which would be required if the discharge coefficient were constant. On the other hand the plates used by Mayfield *et al.* approximate short tubes rather than sharp-edged orifices, and their data were correlated by use of the square of the velocity. Neither group of investigators generalized their correlation with plate geometry.

In preliminary studies Claypool (*4*) found that pressure drop through perforated plates with a single hole was correlated by the orifice relation if the ratio t/D_o, the plate thickness to the perforation diameter, were 0.9 or greater. The plates used by Mayfield *et al.* conform to this criterion with only one exception, where the ratio t/D_o was 0.67. It would be expected that the plates used in industrial practice would be relatively thick, to provide adequate mechanical strength and to ensure long freedom from the effects of corrosion. Accordingly, in the present study the ratio of t/D_o was held equal to unity, and plate thicknesses ranged from 1/8 to 1/2 in.

The pressure drop through a short tube running full may be interpreted as the sum of an entrance loss and an exit loss. For perforations with sharp edges at both entrance and exit this would be

$$h = \frac{u_o^2}{2g_c}\left[0.4\left(1.25 - \frac{A_o}{A_c}\right) + \left(1 - \frac{A_o}{A_c}\right)^2\right] \qquad (1)$$

where

h = head loss, ft. lb. force/lb. mass

u_o = velocity through the perforation, ft./sec.

g_c = 32.2 lb. mass.(ft.)/lb. force (sec.)^2

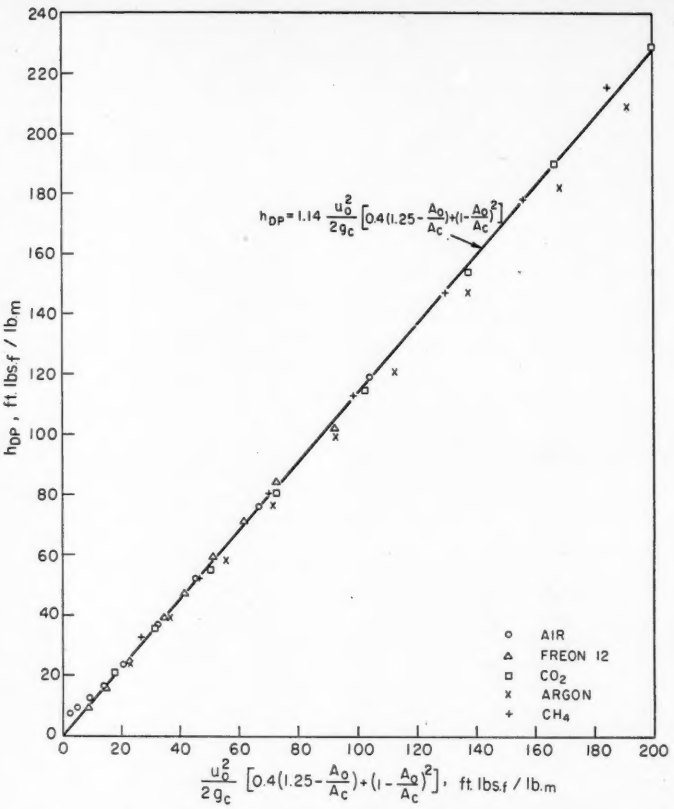

Fig. 3. Pressure drop for flow of various gases through dry plate; plate III.

A_o = total perforation area, sq.ft.
A_c = area of column available for gas flow, sq.ft.

Equation (1) is correct for circularly symmetric sudden enlargements and contractions but is not necessarily correct for perforated plates in ducts; however, studies by Baines and Petersen(*3*) on perforated plates composed of sharp-edged orifices in ducts have shown that flow through such plates can be correlated by the ordinary orifice relation, and it is reasonable to expect correlation of pressure drop for thick perforated plates by some relation like Equation (1).

The pressure drop for flow of air through plates I through VII, a range of perforation diameters from ⅛ to ½ in. and of A_o/A_c from 0.05 to 0.20, is shown in Figure 2. With one exception, plate II, the data are represented by Equation (2) within a few per cent.

$$h_{DP} = 1.14 \frac{u_o^2}{2g_c}\left[0.4\left(1.25 - \frac{A_o}{A_c}\right) + \left(1 - \frac{A_o}{A_c}\right)^2\right] \qquad (2)$$

Plate VI deviates from Equation (2) by +8%, the maximum deviation with the exception of plate II, which deviates by —18%. These deviations are attributable to defective drilling of the perforations. Plate II was the first plate made, and in the operation of reaming the holes to size, the plate was not rigidly clamped. All other plates were clamped during this operation. After the pressure-drop data were taken and the deviation of this plate was seen, a second plate, II*A*, was made exactly like plate II with the plate clamped during final reaming. It can be seen that plate II*A* is essentially on the line given by Equation (2).

Gases other than air were also used: Freon 12, carbon dioxide, argon, and methane. The data for these gases are shown in Figure 3, and it can be seen that Equation (2) holds within a few per cent. From these results it is felt that Equation (2) will accurately represent the dry-plate pressure drop for any gas flowing through a plate made up of sharp-edged holes on triangular centers for which the ratio of t/D_o is 0.9 or greater and will probably be adequate for $t/D_o = 0.67$. From the form of Equation (2) it might be expected that the pressure drop for commercial punched trays would be lower than that found here. The punching process will break the edge of the hole, and if this edge is used as the upstream edge a radius of curvature as low as 0.14 D_o will reduce the entrance loss effectively to zero and reduce the total loss by about one third(*12*).

The data of Mayfield *et al.* for all plates investigated in their 6-in. column fall approximately 14% below the values predicted by Equation (2), or essentially in accord with the theoretical values of entrance and exit loss. This difference may well be due to minor variations in hole size due to different methods of manufacture. Data from their large column are as much as 30% higher than Equation (2).

Jones and Pyle(*9*) report a curve of dry-plate pressure drop vs. *F* factor based on hole velocity for an 18-in. column with ⅛-in.-diam. holes. Equation (2), applied to their column specifications, gives dry-plate pressure drops approximately 25% lower than those represented by their curve. Their higher pressure drops are believed due to use of thin plates which approximate sharp-edged orifices. The data of Arnold *et al.*, also for thin plates, roughly agree with those of Jones and Pyle.

Wet-plate Pressure Drop

The presence of liquid on a perforated plate creates a static head of pressure at the plate surface which must be added to the other pressure drops experienced by the gas. The action of the bubbling gas aerates the liquid(*1, 7, 10*) to an extent dependent primarily on the liquid height. If liquid level on the tray is maintained by flow over a weir, the clear-liquid head equivalent to the aerated liquid is a function of weir height and liquid flow rate(*10*). No attempt was made in the present work to determine the degree of aeration. The liquid seal was maintained by a constant-head tank to counteract changes in head with change in gas flow. This aerated liquid head was measured in a manometer as equivalent clear liquid and subtracted from the total pressure drop. Essentially the same experiment was performed by Arnold *et al.* for one plate with air and water and by Mayfield *et al.* for one plate with air and three liquids.

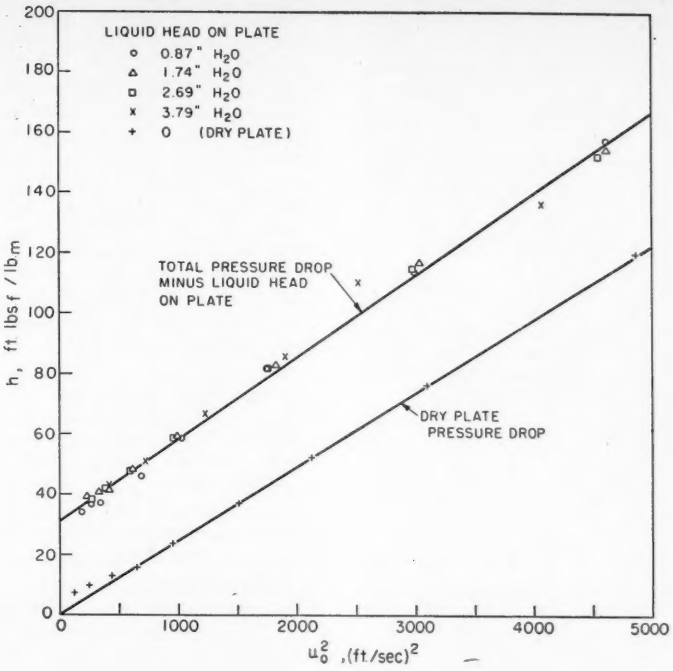

Fig. 4. Pressure drop with liquid on plate; air-water; plate III.

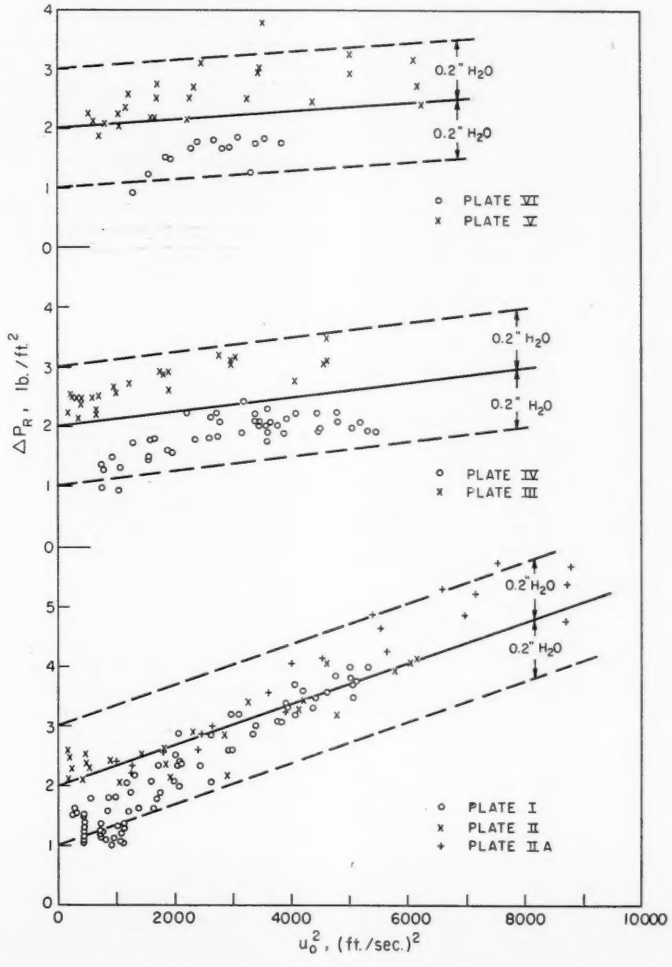

Fig. 5. Residual pressure drop with various plates; air-water.

The turbulent-expansion loss for gas flow across a dry plate would probably be little changed by the presence of liquid on the plate. Hence the total pressure drop for gas flow across a plate with liquid present would be expected to be at least as great as the sum of the equivalent clear-liquid seal and the dry-plate pressure drop. If a significant amount of energy is expended in the formation of bubbles, a corresponding additional pressure drop will be found.

In their experiments Arnold *et al.* found that the residual pressure drop unaccounted for by the sum of dry-plate drop and liquid seal was approximately 10% of the total drop, ranging from 0.1 in. of water to 0.5 in. Mayfield *et al.* found the residual to range from 0 to 0.2 in. of water and decided that it was insignificant in practical design.

In the present work the total pressure drop was measured for the system air-water for plates I through VI. In order to determine the effect of different gases and liquids total pressure drop was measured with plate III and water for all the gases used in the dry-plate experiments and with the air and the liquids listed in Figure 7.

The results of the air-water experiments with plate III are shown in Figure 4. The data for various liquid heads on the tray are shown. Liquid head was varied from 0.87 to 3.79 in. of water. The data obtained scatter at random around the line drawn for total drop minus liquid head. A similar scatter was obtained for all plates tested, leading to the conclusion that there is a residual pressure above that which can be accounted for by dry-plate drop plus liquid head, which is independent of values of liquid head normally encountered.

The residual pressure drop ΔP_R, defined as the total pressure drop minus the equivalent liquid head minus the dry-plate pressure drop, is shown in Figure 5 for all the

plates investigated. In the calculation of these residual pressure drops, the best lines through the dry-plate pressure-drop data for the individual plates were used in order to obtain as much accuracy as possible in the residual. The residual pressure drop is small in all instances, reaching a maximum value of about 5 lb./sq.ft., or 1 in. of water with plate II, a plate with ⅛-in. perforations on 4 D_o spacing. The residual appears to increase with increasing gas velocity, more so with ⅛-in. perforations and less with larger perforations. The residual also appears to be consistently higher for plates with the perforations spaced on $4D_o$ than for those with $2D_o$ spacing. There is little apparent difference in the residual pressure drop extrapolated to zero gas velocity for the various plates, the extrapolated residual being about 2 lb./sq.ft. or 0.4 in. of water for all the plates.

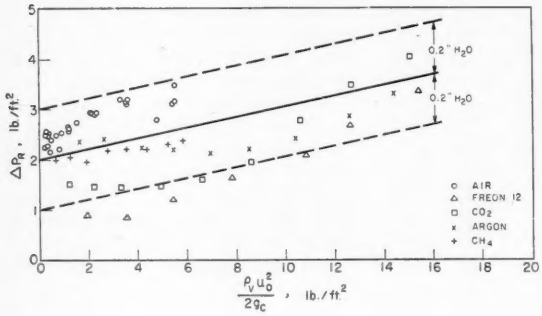

Fig. 6. Residual pressure drop with various gases and water; plate III.

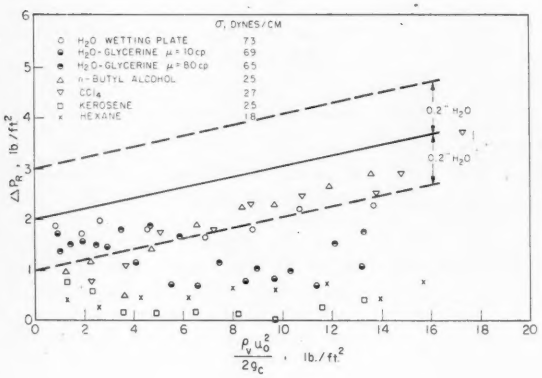

Fig. 7. Residual pressure drop with air and various liquids; plate III.

The residual pressure drop for various gases with water is shown in Figure 6. The data were all taken with plate III. The residual pressure-drop data correlate more satisfactorily as a function of the kinetic energy of the gas rather than as a function of gas velocity alone. The lines drawn on Figure 5 for air-water and for the same plate are redrawn on Figure 6, and it is apparent that the data for various gases are essentially within the same limits of scatter as the data on air-water.

Data were also taken with plate III for air with various liquids. Viscosity was varied from 1 to 80 centipoises, specific gravity from 0.67 to 1.60, and surface tension from 73 to 18 dynes/cm. The data as presented in Figure 7 show no consistent trend in the residual pressure drop with any of these variables. However, qualitatively it appears that systems with lower surface tension give lower residual pressure drops, as will be noted in comparing the data with the lines for the system air-water, which are also drawn on the figure.

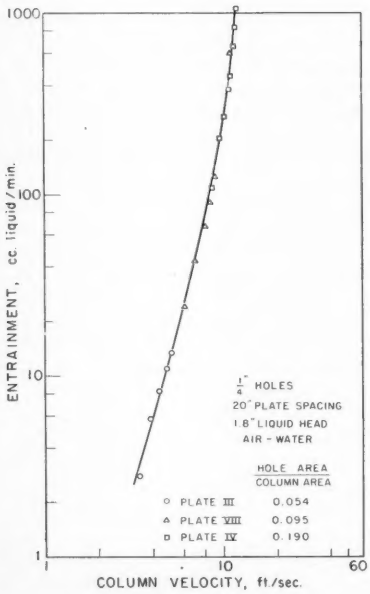

Fig. 8. Effect of velocity on entrainment.

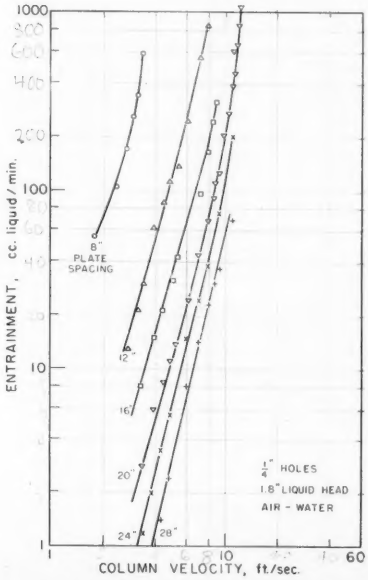

Fig. 9. Effect of plate spacing on entrainment.

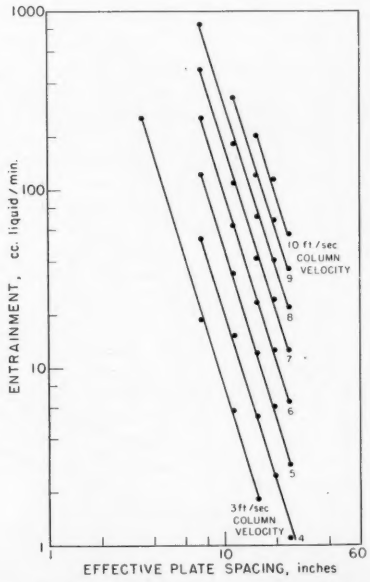

Fig. 10. Determination of relationship between effective plate spacing and entrainment.

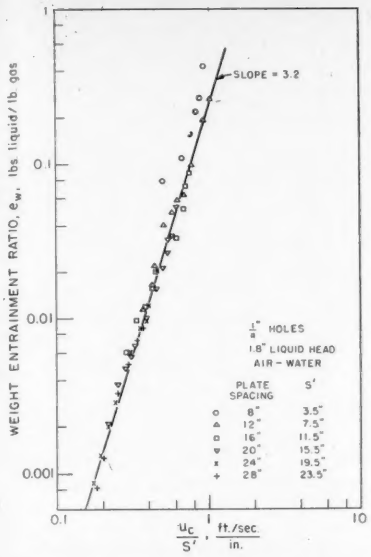

Fig. 11. Correlation of entrainment with column velocity and effective plate spacing.

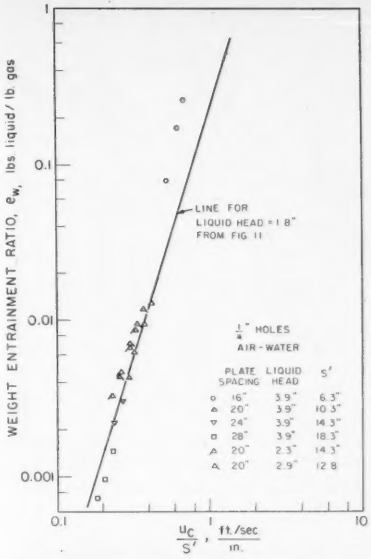

Fig. 12. Correlation of entrainment at various liquid heads.

Attempts to rationalize the residual-pressure-drop data with bubble formation have not been successful.

For practical design, in view of other uncertainties, the slight differences found in the residual pressure drop can probably be neglected. A constant residual of 2.5 lb./sq.ft. (0.5 in. of water) can be assumed, independent of velocity, plate geometry, and system, with a maximum error of approximately 0.5 in. of water over the entire range of variables investigated.

Entrainment

The entrainment of liquid drops by the rising gas was measured first with air and water in order to determine what geometrical factors were important. Previous investigations with bubble-cap plates (*2, 8, 11*) have shown slot velocity, column velocity, and plate spacing all to enter into the determination of the amount of entrainment.

The effect of hole velocity was investigated by the use of three ¼-in.-hole plates, plates with ratios of hole area to column area varying from 0.049 to 0.190. In all these runs the plate spacing was maintained at 20 in. and liquid head on the plate was held at 1.8 in. The data are shown on Figure 8 plotted vs. column velocity, and it is apparent from the fact that overlapping data at widely different hole velocities fall on the same curve that the entrainment is independent of hole velocity; for example, data taken at a column velocity of approximately 9 ft./sec. show the same entrainment although the hole velocities were as different as 95 ft./sec.. and 47 ft./sec. Data were also taken with ¼-in. hole plates at other values of plate spacing, again with liquid head held constant at 1.8 in. These data are shown on Figure 9 and indicate that entrainment is sharply dependent on plate spacing as well as column velocity, increasing exponentially with diminished plate spacing and increased column velocity.

It seemed intuitively correct that, barring a change in the character of the bubbling surface of aerated liquid with change in liquid depth, the entrainment should be a function of the distance between the bubbling surface and the plate above, i.e., the "effective plate spacing," and independent of the plate spacing itself. Unfortunately it was not possible to determine visually the foam height in the column used in order to calculate this effective plate spacing. Accordingly, runs were also made in which the liquid head was varied with and without variation in the plate spacing. From the results of these experiments it appeared that the foam density was between one third and one half of the true liquid density, independent of the gas velocity. An average value of 0.4 was assumed to hold for purposes of correlation. This value agrees well with the measurements of Bagnoli as reported by Gerster, Bonnet, and Hess (*7*), who found foam densities of 0.3 to 0.35 with air and water on plates with ⅛-in. holes. Bagnoli also found little or no effect of gas velocity. A more exact measurement of foam density is certainly desirable, but for purposes of determining entrainment at common plate spacings, the placement of the bubbling surface within 1 or 2 in. is sufficiently accurate. From the results of the work reported here the assumption of a density of 0.4 is within this accuracy.

The data of Figure 9 are cross-plotted on Figure 10 vs. effective plate spacing with column velocity as a parameter. Straight lines were obtained showing entrainment to be inversely proportional to the 3.2 power of the effective plate spacing, S'.

It might be noted that the straightness of the lines and the constancy of their slope lends support to the assumed foam density of 0.4 even though there is no reason *per se* to expect the entrain-

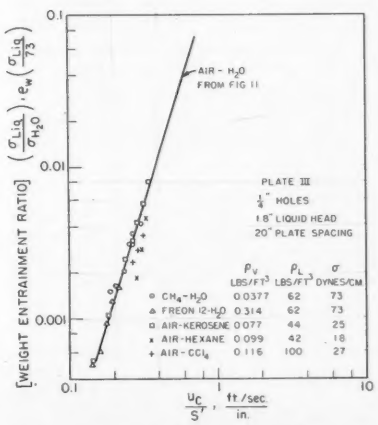

Fig. 13. Correlation of entrainment with various gases and liquids.

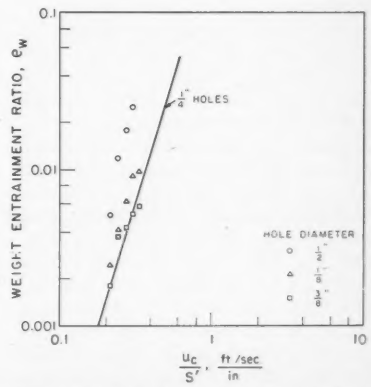

Fig. 14. Entrainment with varying perforation size.

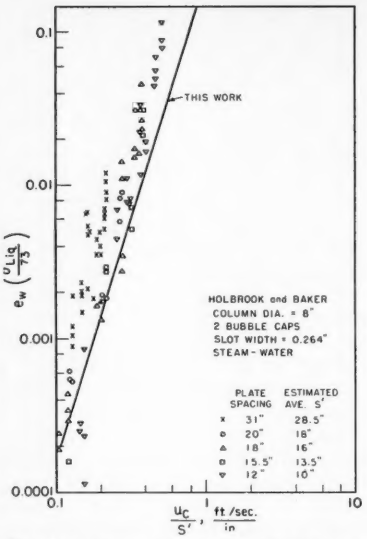

Fig. 15. Comparison of entrainment correlation with data of Holbrook and Baker.

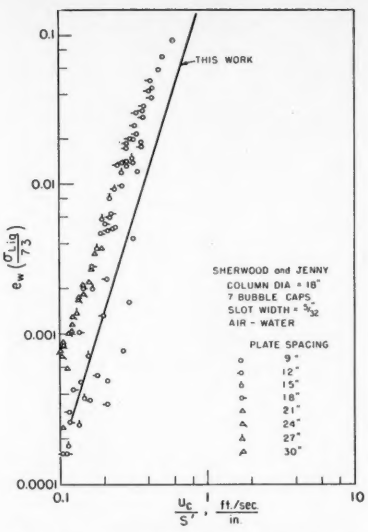

Fig. 16. Comparison of entrainment correlation with data of Sherwood and Jenny for bubble caps.

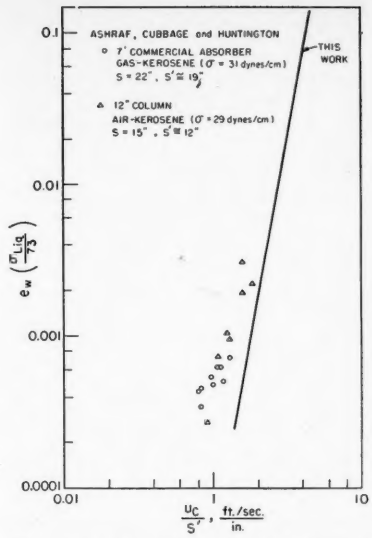

Fig. 17. Comparison of entrainment correlation with data of Ashraf *et al.* for bubble caps.

ment to be so simply related to the effective plate spacing.

Further data with other gases and liquids indicated that the weight entrainment ratio, pounds of liquid/pound of gas, was the proper variable to consider. It was found that adequate and simplified correlation could be obtained by plotting weight-entrainment ratio, e_w, vs. u_c/S'. From Figure 11 it can be seen that the correlation is satisfactory though limited to column velocities under 10 ft./sec., except for the data taken at 8-in. plate spacing, which are uniformly high. However, since the calculated effective plate spacing here is only 3.5 in., it would be expected that a small error in the location of the bubbling surface would have a large effect. To move the data for 8-in. spacing to the correlating line would require only the assumption of a foam density of 0.37 instead of 0.4.

The data at other values of liquid head are plotted vs. u_c/S' on Figure 12, and again except for the lowest effective plate spacing the correlation is adequate.

Data were also taken with water and the gases methane and Freon 12 and with air and the liquids kerosene, carbon tetrachloride, and hexane and are correlated on Figure 13. The data on other gases are seen to correlate well, indicating that the weight entrainment ratio is independent of the gas density. The data for other liquids deviate widely from the correlation if e_w is plotted vs. u_c/S'. However it was found that they correlate well if the ordinate is $e_w(\sigma_{liq}/\sigma_{H_2O})$ or $e_w(\sigma_{liq}/73)$ where σ_{liq} is the surface tension of the liquid on the plate in dynes/cm. It will be noted on Figure 13 that the data for kerosene are in excellent agreement, whereas the data for carbon tetrachloride and hexane are both low. The data for the latter two liquids are in some doubt because of evaporation losses from the entrainment collection plate. Although the gas circulation system was closed, leakage did occur and it was possible to estimate the evaporation losses only crudely. This problem was not present with kerosene owing to its low volatility.

A limited number of data for plates with other hole sizes were taken and are shown in Figure 14. The data for plates with ⅛-in. and ⅜-in. holes are seen to agree reasonably well with the correlation for ¼-in. holes, but the data for ½-in. holes are high. Visual observation of the bubbling surface of plates with ½-in holes indicated a higher degree of irregular splashing than was observed with the other hole sizes, and the higher entrainment is probably due to this effect. It is believed that the correlation obtained for ¼-in. holes will give satisfactory values for both ⅛- and ⅜-in. plates. The general correlation for weight entrainment ratio in pounds of liquid /pound of gas may be expressed by

$$e_w = 0.22\left(\frac{73}{\sigma_{liq}}\right)\left(\frac{u_c}{S'}\right)^{3.2}$$

where u_c is column velocity in feet/second and S' is effective plate spacing in inches, calculated as S, the actual plate spacing, minus 2.5 h_L, where h_L is the head of liquid on the tray in the bubbling zone expressed as inches of clear liquid.

Entrainment is apparently due primarily to splashing from wave action and/or the violent rupture of large bubbles at the top of the foam. High-speed photographs were made of the entrainment at a height of 20 in. above the lower plate, in addition to visual observations. In both observations large drops, up to ¼ in. in diameter, were observed to be thrown upward to at least this height. Counting the drops in the photographs showed that drops of about 0.2 in. comprised about 75% of the liquid visible in the photograph. At the same time the maximum size of drop which would be carried up by drag would be about 0.03 in. The marked dependence of entrainment on plate spacing also indicates that drag is unimportant.

Jones and Pyle(*9*) also determined entrainment for their sieve tray in distillation of acetic acid–water. Exact comparison of the present entrainment results with their data is not possible, as concentrations of the solutions were not given. If it is assumed that dilute aqueous solutions were used, the entrainment data are in substantial agreement.

Entrainment with bubble-cap plates has been studied at some length, notably by Holbrook and Baker(*8*), Sherwood and Jenny

(*11*), and Ashraf, Cubbage, and Huntington(*2*). Qualitative observations by Mayfield *et al.*(*10*) indicated that jetting and splashing were more severe with bubble caps than with perforated plates with resultant higher visual entrainment. The results of the three experimental studies are shown in Figures 15, 16, and 17 compared with the results of the present study. Foam heights were difficult to determine from the reported data, but it is believed the estimates made are accurate within about 2 in. The data of Holbrook and Baker scatter but are seen to have the same trend as the present data with column velocity. The effect of plate spacing appears to be smaller than found here. The precise data of Sherwood and Jenny show a varying effect of column velocity which is roughly the same as that found with perforated plates. Entrainment is found to be about three times higher with bubble caps. When cross-plotted $\bar{v}$ vs. S' at column velocities of 2 and 3 ft./sec. the data give straight lines of slope minus 3.1, almost exactly those found with perforated plates. The data of Ashraf *et al.* are of interest because they were obtained with kerosene as the liquid and include data on a 7-ft. diam. commercial absorber. Again they are higher by about a factor of 5 than the data obtained with perforated plates.

The effect of entrainment on plate efficiency has been derived by Colburn(*5*), who established the relationship describing entrainment which will give minimum column cost for any particular flows. Using the exponential relation found here and assuming the molal entrainment ratio equal to the weight entrainment ratio (roughly true for distillation columns) give this relation as

$$\left(e_w\right)_{opt} = \frac{L/V}{2E}$$

where L and V are liquid and vapor flows in moles and E is the Murphree vapor efficiency. As Colburn pointed out, the optimum entrainment is high. For example, for $L/V = 0.8$, $E = 0.8$, $(e_w)_{opt} = 0.5$ lb. liquid/lb. vapor. Such entrainments were not reached in the present study at plate spacings of 20 in. or more even at velocities of 10 ft./sec. in the column, and it is believed that entrainment is not a limiting capacity factor in ordinary columns, rather that excessive pressure drop will cause the column to flood before entrainment becomes seriously large.

Plate Stability

Stability of the plates with respect to liquid dumping was studied by measuring the quantity of liquid draining through the holes. Measurements were made for all the plates with varying gas velocity and liquid head. With a given plate and liquid head it was found that the rate of dumping increased first slowly as gas velocity decreased and then more and more rapidly, giving curves with more or less sharp breaks when plotted as dumping rate vs. gas velocity. For low liquid heads and widely spaced perforations very distinct breaks were found, indicating a lower limit to vapor velocity, i.e., "critical velocity," below which excessive liquid drainage would begin. At higher heads the breaks were less sharp, and at the lower values of hole spacing, specifically $2D_o$, dumping was found to be a smoothly ascending function of decreasing velocity, with considerable dumping going on at even moderate velocities. In Table 2 the critical velocities found for the various plates with air-water are recorded. The critical velocities in the perforations, calculated from the gas flow assuming all holes to be bubbling, are seen to increase in general as hole diameter increases. Plate *V*, with ½-in. holes spaced 4 D_o is an exception, showing greater stability than the corresponding 4 D_o ¼-in. hole plate. This discrepancy is believed to result from the fact that with this plate no holes were near the walls. A second plate, with ½-in. holes spaced on 6 D_o triangles, where some of the holes were as close as ½ in. to the wall, showed a critical velocity of 35 ft./sec., which is in line with the general trend. From the data obtained it appears that holes spaced 3 or 4 D_o apart give stable trays but that holes spaced on 2 D_o triangles are too unstable for general use except perhaps with holes as small as ⅛ in. diam.

Data at various liquid heads are shown in Table 3. Only the plates with holes spaced 3 D_o and 4 D_o are included, since the dumping found with the 2 D_o plates was high and the critical velocity was uncertain. The critical velocity is seen

Table 2.—Plate Stability Data

(1.8-in. liquid head)

Plate	Hole diam., in.	Hole spacing, in.	Gas	Liquid	Calculated critical gas velocity in holes, ft./sec.
I	⅛	¼	Air	Water	35
II	⅛	½	Air	Water	25
III	¼	1	Air	Water	30
IV	¼	½	Air	Water	>50
V	½	2	Air	Water	27
VI	½	1	Air	Water	>60
VIII	¼	¾	Air	Water	40
III	¼	1	Air	Water (wetting plate)	21
III	¼	1	Air	Water = glycerine (μ = 80 centipoises)	21
III	¼	1	Air	Water = glycerine (μ = 10 centipoises)	21
III	¼	1	Air	*n*-Butyl alcohol	23
III	¼	1	Air	Carbon tetrachloride	24
III	¼	1	Air	Kerosene	15
III	¼	1	Air	*n*-Hexane	14
III	¼	1	Freon 12	Water	15
III	¼	1	Methane	Water	32

Table 3.—Plate Stability Data, Varying Liquid Head, Air-Water

Plate	Hole diam., in., and spacing, in.	Calculated critical gas velocity in holes, ft./sec. h_L = 1.0 in.	h_L = 1.8 in.	h_L = 2.8 in.	h_L = 3.8 in.
II	⅛×4 D_o	5	25	32	35
III	¼×4 D_o	20	30	45	55
VIII	¼×3 D_o	27	40	55	70
V	½×4 D_o	25	27	27	30
V (modified)	½×6 D	30	35	40	45

to increase with increased head on the plate although the data scatter sufficiently that a functional relationship cannot be determined.

It is apparent from consideration of the data in Tables 3 and 4 that the stability is not markedly different for different hole sizes and that smaller holes do not in themselves contribute much greater stability to the plate. This is confirmed by Arnold, who found the minimum hole velocity to be substantially independent of hole size, being approximately 40 ft./sec. when hole spacing was about 4 D_o and about 30 ft./sec. when hole spacing was 3 D_o. They found little trend with weir height and liquid flow, but as pointed out by Mayfield the head of liquid in the bubbling zone is somewhat independent of these variables. Mayfield correlated data for stability of plates with 3/16-in. holes with dry-plate pressure drop. Their values are in the same region as those of this work and show the same trend with liquid head.

Data were also taken with plate III (¼ in. × 4 D_o) and various liquids and gases. From the data with Freon and water it appears that the gas-pressure drop in the holes is actually the important parameter. This conclusion was not completely borne out by the data on methane. However, operating data on commercial hydrocarbon columns reported by Eld(*6*) indicate satisfactory operation at velocities from 4 to 13 ft./sec. in the holes, with plates having up to 37% free area. These results are consistent with use of gas-pressure drop, which would be a function of $\rho_v {u_o}^2$, as the correct criterion of stability.

Data taken across a variety of liquid properties indicate little or no effect of viscosity and density but some effect of surface properties. From rough measurements of the wettability of the liquids on the plates, the stability appears to increase with increased wettability. Kerosene and hexane are very effective in wetting the plate, carbon tetrachloride and butyl alcohol next, and water with various amounts of glycerol somewhat effective compared to pure water. In all cases the stability was increased over that with water, and so the use of critical velocities based on air-water pressure drops should be conservative.

APPLICATION TO COLUMN DESIGN

The relations found in this work can be used in the design of operating columns. For this it is convenient to work the relations into charts which enable the designer to estimate quickly the size of the column; an example of such a chart is shown in Figure 18. The superficial vapor velocity, in feet/second, based on the cross section of the empty column shell, is plotted vs. liquid flow, gallons/minute/foot of column diameter. Lines corresponding to flooding and to minimum vapor flow for stability are shown. These operating limits are determined chiefly by vapor flow although they are affected to some extent by liquid flow. Maximum and minimum liquid flows are shown as those giving calculated heads over the weir of 3 and 0.5 in. respectively, the normal range of bubble-cap trays.

Because of the number of variables which affect the operating limits of a column, it is necessary to set arbitrarily a considerable number of these variables in order to obtain easily usable charts. In the construction of Figure 18 the variables set were

Plate spacing = $S = 24$ in.
Perforations: ¼-in. D_o spaced on 3 D_o equilateral triangles
Angle subtended at the center by the weir = 105°
Weir height = $H_w = 1.5$ in.
Minimum downcomer clearance at bottom = $H_d = 2.5$ in.

It is believed that all these chosen variables represent reasonable practice. However, many other values could have been used, and actual experience may prove some of those chosen to be less advantageous than other values. It will be noted that the downcomer clearance above the tray has been set an

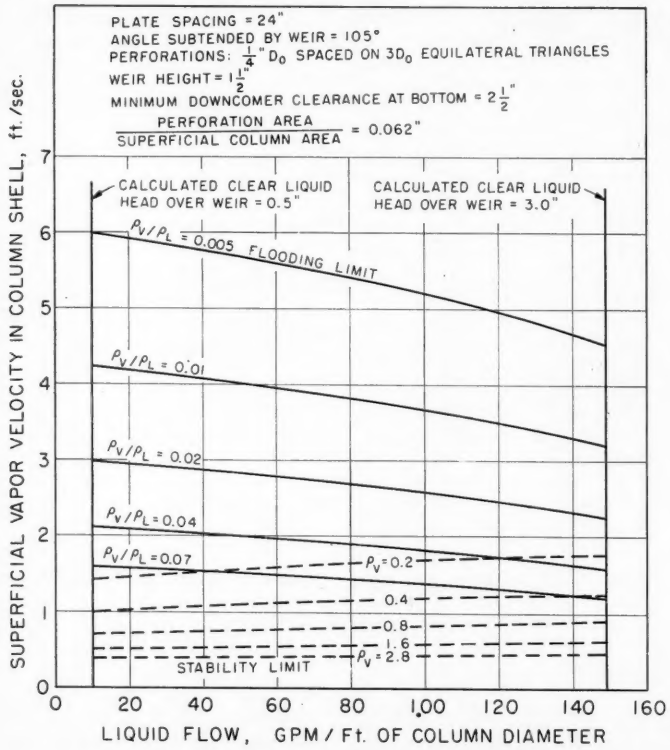

Fig. 18. Perforated-plate-column–operating limits.

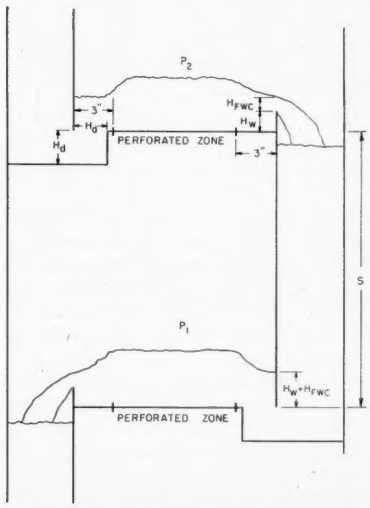

Fig. 19. Model for construction of Figure 18.

inch above the weir height, requiring the use of some sort of seal pot at the downcomer. Setting the clearance at 1.5 in. resulted in such high pressure drops at higher liquid flow rates that the vapor capacity was seriously reduced, and it appeared desirable to correct this feature. In addition to the variables above, an unperforated portion of the tray 3 in. wide was left at both downcomer and weir, in one case to leave room for the seal pot and in the other to act as a calming zone.

Figure 18 was constructed on the model shown in Figure 19. It was assumed that the hydraulic gradient across the tray was negligible, as experimentally shown by Mayfield, and that the height of partially aerated liquid at the downcomer was equal to the weir height plus the height of foam flowing over the weir, $H_W + H_{FWC}$. In addition it was assumed that the liquid in the downcomer, the liquid flowing over the weir, and the liquid just outside the downcomer were all partially aerated, i.e., still contained bubbles of vapor that had not escaped, and all had a density of 0.7 the density of clear liquid. No data are known to the authors on the density of liquid in downcomers, although unfortunately this density is of paramount importance in determining the capacity of a column. The density of 0.7 clear-liquid density assumed seemed a reasonable value from the figure of 0.4, which exists in the bubbling zone.

On the basis of Figure 19 and the assumptions made, the head balance at flooding in inches of clear liquid was taken as

$$0.7\,(S - H_{FWC}) = h_{total} + h_d$$

where S is plate spacing in inches; H_{FWC} is the height of foam flowing over the weir, in inches; h_{total} is the total head loss in the vapor flowing through the plate, inches of clear liquid; and h_d is the head loss in the liquid flowing through the constriction at the bottom of the downcomer, inches of clear liquid. Further,

$$h_{total} = 12\frac{\rho_V}{\rho_L}h_{DP} + \frac{12\Delta P_R}{\rho_L} + h_L.$$

where h_{DP} is the pressure drop for gas flow through the dry plate, ft. gas; ΔP_R is the residual pressure for flow through a wet plate, lb. force/sq.ft.; and h_L is the head of liquid in the bubbling zone. The terms h_{DP} and ΔP_R are functions of gas velocity in the perforations, which are related to superficial gas velocity through the ratio of hole area to shell area. The relationship is slightly dependent on column diameter for a constant weir angle. The ratio used in Figure 18, hole area/shell area = 0.062, is correct for a column diameter of 6 ft. and increases by only 7% up to a column diameter of 10 ft. Values of h_{DP} and ΔP_R were obtained from the relations previously given. The aeration factor of Mayfield *et al.* relating the liquid head in the bubbling zone to the calculated clear-liquid depth at the weir was used to obtain values of h_L. Values of H_{LWC} and h_{FWC} were calculated with the ordinary weir equation. The pressure drop due to liquid flow through the constriction at the bottom of the downcomer was calculated with the equation for a submerged sluice gate, correcting the velocity for the assumed density of 0.7. Entrainment also was calculated and found to be generally negligible. At the highest vapor velocity, over 6 ft./sec., for a liquid with a surface tension of 20 dynes/cm. the entrainment resulted in a calculated increase in head over the weir of about 0.1 in.

It will be noted that flooding was presumed to occur when the liquid level in the downcomer reached the top of the weir. For liquid levels above this, the weir action is changed to a submerged weir and the capacity is reduced for the same head over the weir. No particular effort was made to employ additional safety factors in the individual calculations; rather the pressure drops were calculated as accurately as possible and used without change. Because of this, and because of the high uncertainty in the density of liquid in the downcomer, a design at two thirds of the flooding limit is probably reasonable.

ACKNOWLEDGMENT

This work was sponsored by the University of California Radiation Laboratory.

NOTATION

A_c = area of column available for vapor flow, sq.ft.
A_o = total area of perforations, sq. ft.
D_o = diameter of perforation, in.
e_w = weight of liquid entrained/unit weight of vapor flowing
E = Murphree vapor efficiency
g_c = gravitational constant, 32.2 lb. mass (ft.)/(lb. force) (sec.^{2})
h = head loss, ft. or in. of fluid flowing
h_d = head loss from liquid flow through constriction at bottom of downcomer, in. clear liquid
h_{DP} = head loss in vapor flowing through dry plate, ft. vapor
h_L = head of liquid on tray in perforated zone, in. clear liquid
h_{total} = total head loss in vapor across tray, in. clear liquid
H_d = minimum width at bottom of downcomer for segmental downcomers, in.
H_{FWC} = height of foam flowing over weir, in.
H_{LWC} = calculated height of liquid flowing over weir based on clear-liquid flow rate in.
H_W = height of weir, in.
L = liquid flow, moles
ΔP_R = residual pressure drop, defined as total wet-plate pressure drop minus dry-plate pressure drop minus head of liquid on the tray, lb. force/sq.ft.
S = actual plate spacing, in.
S' = effective plate spacing, distance between top of foam and plate above, in.
t = plate thickness, in.
u_c = vapor velocity in column, ft./sec.
u_o = vapor velocity in perforations, ft./sec.
V = vapor flow, moles
ρ_L = liquid density, lb. mass/cu.ft.
ρ_v = vapor density, lb. mass/cu.ft.
σ = surface tension, dynes/cm.

LITERATURE CITED

1. Arnold D. S., C. A. Plank, and E. M. Schoenborn, *Chem. Eng. Progr.*, 48, 633 (1952).
2. Ashraf, F. A., T. L. Cubbage, and R. L. Huntington, *Ind. Eng. Chem.*, 26, 1068 (1934).
3. Baines, W. D., and E. G. Petersen, *Trans. Am. Soc. Mech. Engrs.*, 73, 467 (1951).
4. Claypool, D. C., M.S. thesis, Univ. California, Berkeley (1952).
5. Colburn, A. P., *Ind. Eng. Chem.*, 28, 526 (1936).
6. Eld, A. C., *Petroleum Refiner*, 32, 157 (May, 1953).
7. Gerster, J. A., W. E. Bonnet, and I. Hess, *Chem. Eng. Progr.*, 47, 523 (1951).
8. Holbrook, G. E., and E. M. Baker, *Trans. Am. Inst. Chem. Engrs.*, 30, 520 (1934).
9. Jones, J. B., and C. Pyle, *Chem. Eng. Progr.*, 51, 424 (1955).
10. Mayfield, F. D., W. L. Church, Jr., A. C. Green, D. C. Lee, Jr., and R. W. Rasmussen, *Ind. Eng. Chem.*, 44, 2238 (1952).
11. Sherwood, T. K., and F. J. Jenny, *Ind. Eng. Chem.*, 27, 265 (1935).
12. Vennard, J. K., "Elementary Fluid Mechanics," 3 ed., pp. 217-18, John Wiley and Sons., Inc., New York (1954).

Benedict Equation of State: Application to Vapor—Liquid Equilibria

Edward J. Cullen and Kenneth A. Kobe
University of Texas, Austin, Texas

The Benedict-Webb-Rubin equation of state(*3, 4, 5, 6*) has been used extensively and successfully by its authors to represent the *P-V-T* data of the hydrocarbons and to predict the vapor-liquid equilibria existing in binary and ternary mixtures of hydrocarbons (*6*). Sage and coworkers(*8, 12*) have subsequently shown the utility of this equation of state for hydrocarbons over much wider ranges of pressure. The equation has also been applied to the nitrogen–carbon monoxide system by Schiller and Canjar(*13*), who showed that it could satisfactorily predict vapor-liquid equilibria in that system. The latter investigation is the only one in systems outside the hydrocarbons and, as it was successful, the present authors decided to investigate the possibility of a general application of this equation of state to binary systems. The nitrogen–carbon monoxide system is a rather special case in that the two gases have isosteric molecules and consequently very similar physical properties. This is well illustrated by the similarity in the values of their constants in the equation of state. The more general system chosen for this work was that of carbon dioxide and propane, which have molecules differing both in molecular size and chemical type.

CONSTANTS FOR CARBON DIOXIDE

The method originally used by its authors for evaluating the constants is tedious, and a more refined technique using a statistical method has been developed by Sage and coworkers(*7*), who later facilitated the calculations by the use of a digital computing machine (*14*). Unfortunately the means to make use of these better methods were not available for this work, and so recourse had to be made to the original method of the authors. The details of the methods employed in this work are available in the literature(*3, 4*).

Kendall and Sage(*8*) have conveniently tabulated the isothermals for carbon dioxide in the temperature range from 40° to 460°F. and for pressures up to 10,000 lb./sq.in. abs., and these data were used to evaluate the constants. For the vapor pressure of liquid carbon dioxide the extensive data of Meyer and Van Dusen(*9*) in the temperature range from —60°F. to the critical temperature were used.

The constants for propane are available in the literature from two sources. The first source is in the summary of the original work by Benedict, Webb, and Rubin(*5*), in which they present values of the constants for twelve hydrocarbons. The second source is in the paper by Selleck *et al.*(*14*) in which a different set of constants is given, determined by the more refined technique and applicable over a wider range of pressures; the latter are consistent with those of Benedict, Webb, and Rubin up to pressures of about 4,000 lb./sq.in. abs., but deviate increasingly at higher pressures.

Since the method of Benedict, Webb, and Rubin was used to determine the values of the constants for carbon dioxide in this study, it was considered wiser to select their values. Then the two sets of constants used for the determination of the vapor-liquid equilibria in the carbon dioxide–propane system would be consistent in their method of determination. In any case, in the binary system investigated the pressure does not exceed 1,000 lb./sq.in. abs., and so the two sets of constants are consistent.

The equation of state may be written in the following form:

$$P = RTd + (B_oRT - A_o - C_o/T^2)d^2 + (bRT - a)d^3 + a\alpha d^6 + \frac{cd^3}{T^2}(1 + \gamma d^2)\, e^{-\gamma d^2} \qquad (1)$$

Subsequently for purposes of comparing the observed and predicted values, the pressure will be considered as the dependent variable.

Figures 1, 2, and 3 show the graphs from which the preliminary values of the constants were determined. An attempt was made to fit the equation to the vapor-pressure data, but it was impossible to adjust the constants A_o, B_o, and C_o so that the equation would represent the data over the whole range from —10° to 460°F. Therefore, it was decided to present two sets of constants to obtain adequate representation over the whole range of temperatures. Set *A*, to which vapor-pressure corrections have been applied, is to be used for the calculation of vapor pressures, the critical point, and pressures in the gaseous region up to 280°F. Set *B*, the preliminary values determined from Figures 1, 2, and 3, is to be used for the calculation of all pressures in the temperature range of 280° to 460°F. These constants are presented in Table 1.

Edward J. Cullen is at present at Cambridge University, Cambridge, England.

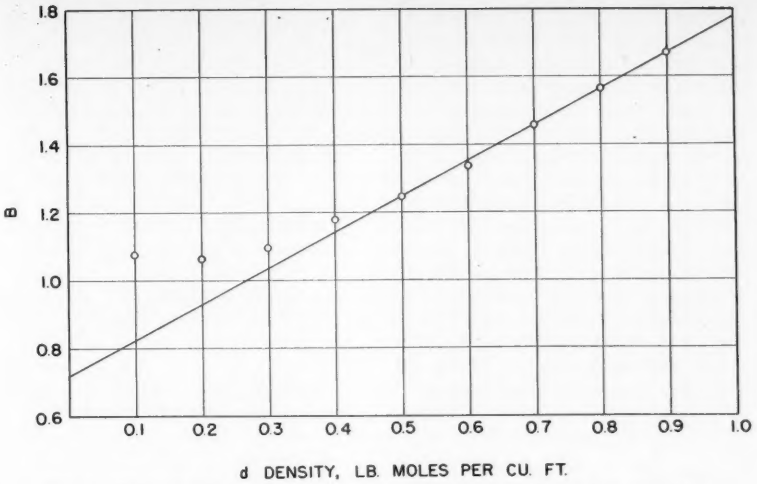

Fig. 1. Determination of function B for Benedict-Webb-Rubin equation of state for carbon dioxide.

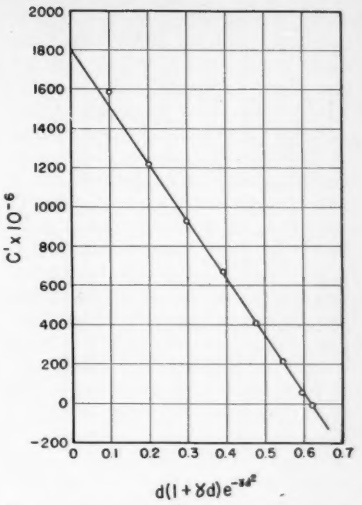

Fig. 2. Determination of function C' for Benedict-Webb-Rubin equation of state for carbon dioxide.

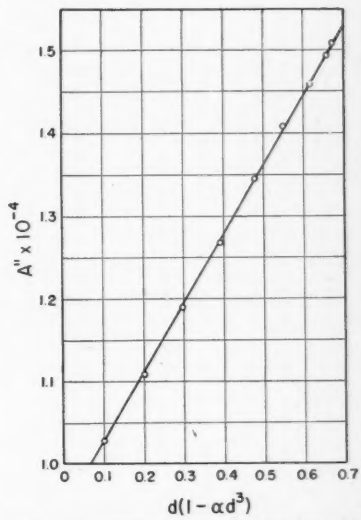

Fig. 3. Determination of function A'' for Benedict-Webb-Rubin equation of state for carbon dioxide.

The equation of state fits the P-V-T data on carbon dioxide with an over-all deviation in the dependent pressure variable of 0.32% up to densities of 0.9 mole/cu. ft. in the temperature range from the critical temperature up to 460°F. The maximum deviations occurred at the highest pressures along the isotherms close to the critical isotherm.

The equation fits the vapor-pressure data from —10°F. to the critical temperature with an average deviation of 0.57% and predicts a saturated liquid density in that temperature range with an average deviation of about 2.5%. A more detailed comparison of the properties of the saturated liquid are presented in Table 2.

VAPOR-LIQUID EQUILIBRIA IN THE CARBON DIOXIDE—PROPANE SYSTEM

Poettmann and Katz (*11*) studied the phase behavior of the carbon dioxide–propane system, and more recently Reamer, Sage, and Lacey (*12*) repeated their study. Fair agreement was realized between the two sets of data, but as it is believed that the more recent work is more accurate, it has been selected as a basis for comparison with the predicted vapor-liquid equilibria. The comparison was made through the predicted and observed vaporization ratios, commonly called K values. The observed K value was calculated from the equation

$$K_j(obs) = \frac{y_j}{x_j} \qquad (2)$$

At equilibrium the fugacities of any component in the liquid and vapor phases are equal; so Equation (2) may be changed thus:

$$K_j(calc) = \frac{f^L_j/x_j}{f^G_j/y_j} \qquad (3)$$

The fugacity coefficient f_j/x_j varies much less rapidly with the composition than the fugacity itself, and so it is convenient to use Equation (3) to calculate the predicted values.

It is assumed that the P-V-T properties and vapor-liquid equilibria of any mixture of carbon dioxide and propane can be repre-

TABLE 1.—VALUES OF THE CONSTANTS FOR CARBON DIOXIDE

	A	B
A_o	10322.8	9488.04
B_o	0.799496	0.719000
C_o	1.69301×10^9	1.80146×10^9
a	8264.46	8264.46
b	1.05820	1.05820
c	2.91971×10^9	2.91971×10^9
α	0.348000	0.348000
γ	1.38400	1.38400

Set A is to be used for the calculation of vapor pressures and for pressures in the gaseous phase up to 280°F. Set B is to be used for the calculation of pressures in the gaseous phase above 280°F.

TABLE 2.—THE PROPERTIES OF SATURATED LIQUID CARBON DIOXIDE

Temp., °F.	Vapor pressure, lb./sq. in. abs. Calc.	Obs.	Deviation, %	Liquid density, lb. moles/cu. ft. Calc.	Obs.	Deviation, %
85.0	1034.5	1032.2	−0.220	0.893	0.888	−0.563
80.0	970.6	969.4	−0.124	0.972	0.983	−1.170
50.0	652.7	652.9	+0.031	1.179	1.224	−3.676
20.0	417.7	422.0	+1.109	1.300	1.339	−2.913
−10.0	255.0	257.6	+1.010	1.395	1.437	−2.923

Critical Properties

	Calculated	Observed
Critical temperature, °R.	549.0	547.5
Critical pressure, lb./sq. in. abs.	1,093.2	1,069.9
Critical density, lb. mole/cu. ft.	0.685	0.664

sented by Equation (1). The parameters of this equation are functions of the composition and the individual constants of the pure components and they may be calculated by the relationships suggested by Benedict, Webb, and Rubin (*6*). These relationships are given as being most suitable for hydrocarbons but, though they have some basis in fact, they are largely empirical. It is conceivable that a more suitable method of determining these parameters for gases other than hydrocarbons might be found, but no attempt was made in this study. The determination of the fugacity coefficient for each component was begun by obtaining by trial, liquid and vapor densities which would represent several pressures for the range covered by the isotherm under investigation. This was done for the pure components where possible and for several intermediate compositions. The purpose was to obtain a scale of compositions by which fugacity coefficients might be interpolated to any other intermediate composition. By use of the values of the density so determined, fugacity coefficients for both phases were calculated from Equation (4) at their respective pressures and compositions.

$$RT\ln f_j/x_j = RT\ln RTd + \left[(B_o+B_{oj})\,RT - 2\,(A_oA_{oj})^{1/2} - 2\,(C_oC_{oj})^{1/2}T^{-2}\right]d + \frac{3}{2}\left[(b^2b_j)^{1/3}RT - (a^2a_j)^{1/3}\right]d^2 + \frac{3}{5}\left[a(\alpha^2\alpha_j)^{1/3} + \alpha\,(a^2a_j)^{1/3}\right]d^5 + \frac{3d^2}{T^2}(c^2c_j)^{1/3}\left[\left(\frac{1-e^{-\gamma d^2}}{\gamma d^2}\right) - \frac{1}{2}e^{-\gamma d^2}\right] - \frac{2d^2}{T^2}c\left(\frac{\gamma_j}{\gamma}\right)^{1/2}\left[\frac{1-e^{-\gamma d^2}}{\gamma d^2} - e^{-\gamma d^2} - \frac{1}{2}\gamma d^2 e^{-\gamma d_2}\right] \qquad (4)$$

The fugacity coefficients in both phases were plotted against pressure, with composition as a further parameter. From this plot it was possible to evaluate the fugacity coefficients at pressures and compositions corresponding to any

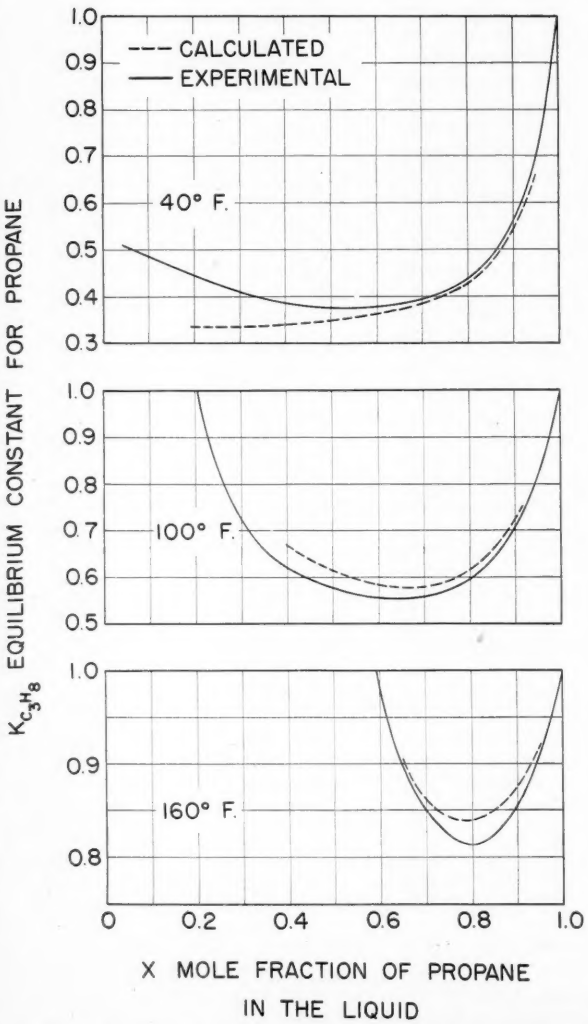

Fig. 4. Calculated and observed values of K for propane.

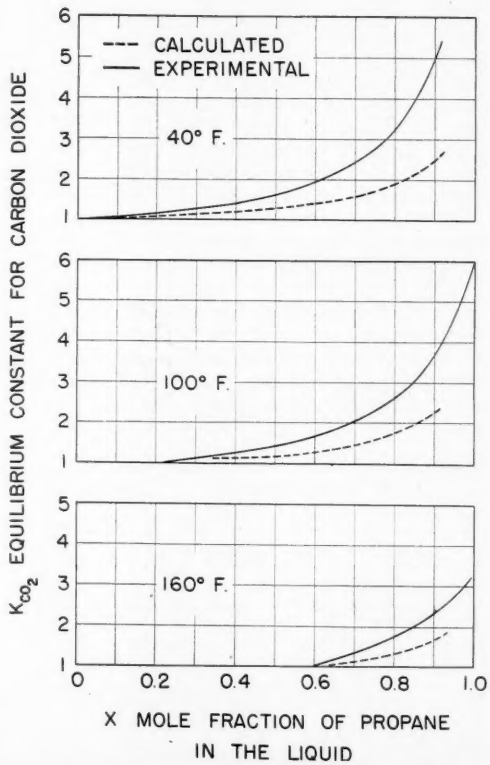

Fig. 5. Calculated and observed values of K for carbon dioxide.

given state of the system. The predicted K values were then calculated for three temperatures, 40°, 100°, and 160°F.

The graphical comparison of the observed and predicted K values given in Figures 4 and 5 shows that they differ markedly for carbon dioxide but less so for propane. As might be expected, the deviations are greatest at the lowest temperature. It is evident that this method gives calculated K values for this system which are outside the limits of experimental accuracy.

Benedict, Webb, and Rubin(*6*) point out that to be strictly correct the fugacity coefficients should be evaluated at the calculated equilibrium composition and not at the observed equilibrium composition; however, this calculation is a lengthy trial-and-error procedure and was not carried out in this study. They further point out that the error introduced by this assumption is small if calculated K values are close to the observed K values. This certainly was not the case for carbon dioxide, and so it is expected that the values will have an appreciable error, though nowhere nearly sufficient to account for the deviations observed.

DISCUSSION

The deviation found between the observed and calculated K values in the propane–carbon dioxide system is believed to be due to the method of expressing the dependence of the parameters of the equation on composition for a mixture. The authors of the equation(*6*) point out that the way they suggest is the most suitable for hydrocarbons and in such systems the method works extremely satisfactorily. It also works in some cases outside the hydrocarbons(*13*) but in others(*15*), including this work, it is not so successful.

The reason for the lack of success in certain cases is thought to be caused by the increased interaction of the molecules of the components in the liquid phase. For the systems in which the equation works successfully, the components have been either hydrocarbons or isosteric molecules, and in neither case would one expect much interaction in the liquid phase. In any case the interaction would be similar in both types of cases and it is satisfactorily represented by the suggested method of combining the individual parameters. When one or more of the components is dissimilar in chemical character from the others, however, then added interactions come into play, which are not accounted for by the present method, and one would hardly expect the equation as it stands to work successfully.

This does not mean however that the equation must be limited to very special cases. Presumably the interactions of molecules in the liquid phase can be classified into various types and if that is the case, then the possibility exists that a suitable method of combining the parameters appropriate to each type of interaction might be found. A good review of the various semitheoretical and empirical ways of combining the parameters which have been used is given by Beattie(*1*).

Another alternative which has been suggested by Benedict(*2*) for systems consisting of a gas, such as carbon dioxide and the hydrocarbons, is to correct one of the parameters, such as C_o, for the mixture to bring the oberved and calculated K values into agreement. It is hoped that this correction can then be generalized, so that it may be predicted for all the hydrocarbons. This method might obviously be extended so that the correction could cover a much wider range of gases, but owing to the extreme complexity of the interactions in the liquid phase this may not be possible. Stotler and Benedict(*15*) found that they could not correlate the liquid-vapor equilibria for the methane-nitrogen system using the original method, but by a suitable adjustment of the parameter A_o for the mixture a good agreement was obtained, indicating the feasibility of the foregoing method.

If either of the two methods discussed above can be made to work satisfactorily, then obviously the utility of the Benedict equation of state is greatly increased. Even with the assistance of electronic digital computors, to have to study each system individually would be extremely inconvenient, and it is considered that a thorough investigation of the preceding methods would be profitable.

SUMMARY

The Benedict equation of state has been applied to the prediction of the volumetric and phase behavior of carbon dioxide. Two sets of constants are presented; the first set predicts the vapor pressure and volumetric behavior in the temperature range from —10° up to 280°F.; the second set predicts the volumetric behavior for temperatures between 280° and 460°F.

The resulting equation fits the P-V-T data with an over-all deviation in the dependent pressure variable of 0.32% up to densities of 0.9 lb. mole/cu.ft. in the temperature range considered. The vapor pressures are represented with an average deviation of 0.57% in the temperature range from —10°F. to the critical temperature, and the critical properties are adequately represented.

In the binary system of carbon dioxide and propane predicted and observed K values are compared at 40°, 100°, and 160°F. The agreement is poor and deviations greater than 100% are found for carbon dioxide at the lowest temperature. In general the deviations are less for propane than for carbon dioxide. These deviations are believed to be due to the method of expressing the dependence of the parameters of the equation on composition.

NOTATION

A_o, B_o, C_o, a, b, c, d, α, γ = coefficients for the Benedict equation of state
P = pressure, lb./sq. inch abs.
R = universal gas constant, (lb./sq.in.) (cu.ft.) / (lb. mole (°R.)
T = absolute temperature, °R.
V = molal volume, cu.ft./lb. mole
K = vaporization ratio

LITERATURE CITED

1. Beattie, J. A., *Chem. Revs.*, **44**, 141 (1949).
2. Benedict, Manson, personal communication (March 16, 1955).
3. Benedict, Manson, G. B. Webb, and L. C. Rubin, *J. Chem. Phys.*, 8, 334 (1940).
4. *Ibid.*, **10**, 747 (1942).
5. ———, *Chem. Eng. Progr.*, **47**, 419 (1951).
6. *Ibid.*, **47**, 449 (1951).
7. Brough, H. W., W. G. Schlinger, and B. H. Sage, *Ind. Eng. Chem.*, **43**, 2442 (1951).
8. Kendall, B. J., and B. H. Sage, "The Volumetric Behavior of Carbon Dioxide," Am. Petroleum Inst. Research Project 37.
9. Meyer, C. H., and M. S. Van Dusen, *J. Research Natl. Bur. Standards*, **10**, 381 (1933).
10. Opfell, J. B., W. G. Schlinger, and B. H. Sage, *Ind. Eng. Chem.*, **46**, 1286 (1954).
11. Poettmann, F. H., and D. L. Katz, *loc. cit.*, **37**, 847 (1945).
12. Reamer, H. H., B. H. Sage, and W. N. Lacey, *loc. cit.*, **43**, 2515 (1951).
13. Schiller, F. C., and L. N. Canjar, *Chem. Eng. Progr. Symposium Ser.*, **49**, No. 7, 67 (1953).
14. Selleck, F. T., J. B. Opfell, and B. H. Sage, *Ind. Eng. Chem.*, **45**, 1350 (1953).
15. Stotler, H. H., and Manson Benedict, *Chem. Eng. Progr. Symposium Ser.*, **49**, No. 6, 25 (1953).

Gas Absorption Accompanied by Chemical Reaction

P. V. Danckwerts

United Kingdom Atomic Energy Authority, Risley, Warrington, Lancashire, England

This paper is concerned with the processes occurring on the liquid side of the interface when gases are absorbed by liquids, and by reactive liquids in particular. The mechanism of the transport of the solute gas up to the interface on the gas side is not considered. Reference will be made mainly to absorption in the type of equipment often used industrially, in which the absorbing liquid runs over an extended rigid surface, typical examples being ring- and grid-packed towers. However, much of what is said will have some bearing on absorption under other circumstances, for instance at the surface of a stirred liquid or rising bubble.

In the case of packed towers and similar equipment consideration will be confined to the processes occurring in a representative horizontal slice of packing (which will include at least one vertical unit of such ordered packings as grids or stacked rings). The paper will not be concerned with the progressive changes in the bulk compositions of the gas and liquid streams along the axes of flow, although this is of course an important aspect of the problem of designing complete pieces of equipment.

The interfacial partial pressure of the solute gas in the region considered is such that its saturated concentration at the surface of the liquid is c^* (this refers to *unreacted* gas in cases where the solute gas reacts with the absorbent). The effect of an interfacial resistance, which would prevent equilibrium at the interface, will not be considered. There is some evidence that such resistances may exist(*5, 6*); however, their magnitude appears to have little effect under conditions of practical interest(*5*), and their existence would in any case not affect the general conclusions reached here. The bulk concentration of unreacted dissolved gas in the region considered is c_o, and the effective area of liquid-gas interface per unit gross volume of the packed space is a. It is a well-established experimental fact that when no reaction occurs in the liquid the rate of absorption per unit gross volume, aN is given by an expression of the form

$$aN = k_L a\,(c^* - c_o) \qquad (1)$$

For the moment this equation may be taken as defining k_L, which will be used to mean the mass transfer coefficient for physical absorption into a nonreacting liquid. For a given gas and liquid $k_L a$ is constant under given hydrodynamic conditions (e.g., size and shape of packing, liquid flow rate, etc.). However, there is reason to suppose that the effective value of a is in general less than the geometrical surface of the packing and that both a and k_L change when the hydrodynamic conditions are varied. It is therefore not easy to assign values to a and k_L separately, and often only the product $k_L a$ is reported, as this can be directly determined from measurements of the volumetric absorption rate aN and a knowledge of c^* and c_o.

Several different types of model have been proposed for the processes which control the rate of absorption, and hence the value of k_L. Of these the two most familiar lead to the film and penetration theories of absorption.

THE FILM THEORY

The film theory was first put forward by Whitman(*26*); its implications are perhaps most clearly understood if absorption of gas into the horizontal surface of a stirred liquid is considered. Elaborating the original statement of the theory somewhat, one may suppose that the turbulence created in the main body of the liquid by stirring is damped out in the neighborhood of the surface, as it would be near a rigid surface. The scale of turbulence and the magnitude of the eddy diffusivity are supposed to become progressively smaller as the surface is approached, until transport by eddies becomes of negligible importance. There will thus be a region in the immediate neighborhood of the surface through which the solute is transported by molecular diffusion alone. Transport by eddy diffusion becomes increasingly important at greater depths, and the bulk of the liquid is kept virtually uniform in composition by large-scale eddies.

It is convenient for practical purposes to replace this picture by a simpler model (as is often done in the consideration of transfer from rigid surfaces) in which there is supposed to be a completely stagnant surface film of definite thickness B, which offers all the resistance to absorption and which overlies liquid having the bulk concentration c_o. Clearly this model very much oversimplifies the situation described in the preceding paragraph and must therefore be treated with caution if used to simulate the behavior of the real system. If the gas and liquid at the interface are in equilibrium, and steady-state diffusion through the film is assumed, the simplified model gives rise to the expression

$$N = \frac{D}{B}(c^* - c_o) \qquad (2)$$

whence

$$k_L = D/B \qquad (3)$$

D being the molecular diffusivity of the dissolved gas. It is found experimentally that k_L, and hence

B, is not uniquely determined by the hydrodynamic conditions, being roughly proportional to $D^{\frac{1}{2}}$ (*21*), but this might reasonably be regarded as a consequence of the simplifying assumption. [Similarly the effective film thickness for *solid*-liquid transfer under forced convection is found to vary as $D^{\frac{1}{3}}$ (*17*).]

The film model has been widely applied, perhaps with less plausibility, to absorption into the liquid running over the packing in an absorption tower.

THE PENETRATION THEORY

The penetration theory, proposed originally by Higbie (*7*) and modified by Danckwerts (*3*), supposes that turbulence extends to the surface of the liquid, so that eddies are constantly bringing macroscopic masses of fresh liquid from the interior to the surface, where they are exposed to the gas for a finite time before being replaced. Between its first exposure and ultimate replacement each element of liquid surface absorbs gas at a rate which is approximately the same as the rate of absorption into a stagnant liquid of infinite depth exposed to the gas for the same length of time; in general the absorption rate decreases with the time of exposure. Thus at a given moment the surface of a stirred liquid is a mosaic of elements of different "ages" which are absorbing at different rates. The average rate of absorption depends on the distribution of the elements of the surface among the various "age groups." In an absorption tower the liquid may be in laminar flow on the continuous surfaces of the packing and may be completely or partially mixed up at the points of discontinuity between packing elements. Each element of surface moving down the packing is supposed to absorb approximately as would a stagnant semiinfinite liquid over the same time interval and to be replaced sooner or later with fresh liquid of the bulk composition as the result of mixing at the discontinuities. Here again a representative slice of the packing will display at a given moment a spectrum of surface ages which will determine the average rate of absorption.

To find the average absorption rate per unit area of surface N, one multiplies the fraction of surface which has the age t by the stagnant-liquid absorption rate for an exposure time t and sums the product over all surface ages. It is convenient to define a distribution function $\phi(t)$ such that the fraction of the surface having ages between t and $(t+dt)$ is $\phi(t) \cdot dt$. If the amount of gas absorbed by unit area of stagnant surface at time t is $Q(t)$, we have then

$$N = \int_{t=0}^{\infty} \phi(t) \frac{dQ(t)}{dt} dt = \int_{t=0}^{\infty} \phi(t)\, dQ(t) \qquad (4)$$

Before the penetration theory can be used, the form of the surface-age distribution function $\phi(t)$ must be known or postulated. The two simplest models each lead to expressions for $\phi(t)$ characterized by a single parameter. Higbie postulated a simple situation in which each element of surface is exposed for the same length of time, θ, before being replaced. Thus $\phi(t) = 1/\theta$ for $t<\theta$, and $\phi(t) = 0$ for $t>\theta$. The average rate of absorption is then

$$N = Q(\theta)/\theta \qquad (5)$$

where $Q(\theta)$ is the amount of gas absorbed by unit area of stagnant surface in time θ (Figure 1).
For physical absorption

$$Q(\theta) = 2(c^* - c_o)\sqrt{D\theta/\pi},$$

and Higbie's model therefore leads to

$$k_L = 2\sqrt{D/\pi\theta} \qquad (6)$$

Danckwerts suggested that it might be more realistic, at any rate in the case of randomly arranged packings and stirred liquids, to suppose that there was no correlation between the age of an element of surface and its chance of being replaced. The distribution function $\phi(t)$ then has the form

$$\phi(t) = se^{-st} \qquad (7)$$

where s is the fractional rate of surface renewal. Inserting this expression for $\phi(t)$, and $Q(t)$ for physical absorption, into Equation (4), one finds

$$k_L = \sqrt{Ds} \qquad (8)$$

The distribution of ages in the Danckwerts model corresponds to that in a population in which the death rate s is independent of age; whereas Higbie's model corresponds to a population in which everyone dies at the same age θ. The Higbie and Danckwerts forms of $\phi(t)$ are compared in Figure 2, and it may be noted that they overlap to a considerable extent. Whatever form the age-distribution function is assumed to have, the penetration theory will always predict that k_L is proportional to $D^{\frac{1}{2}}$ and will give rise to the conventional rule for the addition of "resistances" in series (*19*).

EFFECTS OF CHEMICAL REACTION

In order to calculate the effect of a chemical reaction between absorbed gas and liquid on the basis of any one of the three models described, it is necessary to use the quantity k_L, which is the hypothetical mass transfer coefficient for absorption without reaction. The value of $(k_L a)$ may be found by measuring the absorption rate of a gas of known solubility and diffusivity into an inert liquid under identical hydrodynamic conditions; a liquid of the same viscosity and density as the reacting liquid must be used. The value of $(k_L a)$ thus found must be multiplied by the factor $(D_2/D_1)^{\frac{1}{2}}$, where D_1 is the diffusivity of dissolved gas in the inert liquid and D_2 that of unreacted dissolved gas in the reacting liquid. In view of the uncertainty involved in estimating D_2 (*see* below) and the fact that the diffusivities of many solutes in, for instance, aqueous solutions of equal viscosity are approximately equal, this correction may in practice often be omitted. Alternatively $(k_L a)$ may be estimated by means of some empirical formula, such as that of Sherwood and Holloway (*21*), based on experiments made under fairly similar hydrodynamic conditions. The value of k_L can be found from $(k_L a)$ only if there is some independent method of measuring a. Since a represents not necessarily the total wetted surface but that part of it which is effective in gas absorption, measuring it independently is clearly a matter of some difficulty. Various methods of measurement have been suggested, and the results embodied in formulas involving the hydrodynamic variables (*10*). The results are of doubtful significance, particularly in view of the conclusions reached later in the present discussion. An alternative method, described later, is the measurement of (aN) by use of, for instance, both an inert and a reacting solution. It will be assumed for the moment that unambiguous values of k_L and a can

be determined for a given system.

A knowledge of the following quantities is also required: c^*, the solubility of *unreacted* gas in the reacting liquid; D, the diffusivity of *unreacted* dissolved gas; the velocity constant of the reaction; and equilibrium constants (if reversible reactions occur). The quantities c^* and D are not accessible to direct measurement and must be estimated as well as possible; both will be influenced by the concentration and composition of the solution. The mechanism of the reaction between the dissolved gas and the solution may often be open to doubt. If it is known, the equations for diffusion accompanied by chemical reaction can be solved analytically only in certain simple cases. The reaction-velocity constant is often strongly dependent on the concentration and composition of the solution, and its value may have to be estimated by extrapolation from very different conditions. The calculation of equilibrium concentrations, particularly in systems involving ions, is complicated by the nonideal behavior of the reactants.

As explained later, explicit knowledge of the physicochemical quantities mentioned in the last paragraph may be unnecessary if the penetration theory in one of its forms is accepted as a valid basis for the calculation.

First-Order Reactions

As an example of the calculation of the effect of a reaction on the absorption rate N, the case of an irreversible first-order reaction (velocity constant r) may be considered. It leads to the destruction of the dissolved gas, the bulk concentration of this being taken as zero. The steady state and transient diffusion equations have been solved for this case and lead to the following expressions for N for the different models.

Film model (22)

$$N = c^* \sqrt{Dr} \,/\tanh B\sqrt{\frac{r}{D}} \qquad (9)$$

$$N = c^* \sqrt{Dr} \,/\tanh \sqrt{\frac{Dr}{k_L}} \qquad (9a)$$

Penetration model [*Higbie* (2)]:

$$N = c^* \sqrt{Dr}\left(1+\frac{1}{2r\theta}\right)\times$$

$$\operatorname{erf}\sqrt{r\theta} + e^{-\theta r}/\sqrt{\pi r\theta} \qquad (10)$$

$$N = c^* \sqrt{Dr}\left(1+\frac{k_L^{\,2}}{8Dr}\right)\times$$

$$\operatorname{erf}\frac{2}{k_L}\sqrt{\frac{Dr}{\pi}} + \frac{2}{k_L}\sqrt{Dr}\times$$

$$\exp\left(-4Dr/\pi k_L^{\,2}\right) \qquad (10a)$$

Penetration model [*Danckwerts* (3)]:

$$N = c^* \sqrt{D\,(r+s)} \qquad (11)$$

$$N = c^* \sqrt{Dr+k_L^{\,2}} \qquad (11a)$$

Equations (9*a*), (10*a*), and (11*a*) are obtained by substituting for B, θ and s respectively in terms of k_L for the appropriate model as given by Equations (3), (6), and (8).

The effect of this or any type of chemical reaction on the rate of absorption can be expressed as the ratio of the rate of absorption with chemical reaction to the rate of absorption in the absence of reaction, other things being equal; this ratio will be denoted by α. In the present case α is obtained by dividing the foregoing expressions for N by $(k_L c^*)$, which is the hypothetical rate of physical absorption when c_o is zero. Each of the three models predicts that α will depend on k_L as well as on (Dr), being greatest when k_L is small, and vice versa. In fact the effect of the reaction depends on the single parameter $(Dr/k_L^{\,2})$; α varies in each case from unity when this is small to $(\sqrt{Dr}/k_L)$ when it is large. In spite of the difference in mathematical form of the expressions based on the three models, they give numerically almost equal values for α, with a maximum divergence of less than 10% over the entire range of $(Dr/k_L^{\,2})$ from 0 to ∞ (*5*).

The dependence of α on k_L, and the numerical agreement among the three models, are also found in the expressions for irreversible first-order reaction with a finite value of c_o or for reversible first-order reaction (*5*).

Second-Order Reactions

If the dissolved gas is assumed to undergo a second-order reaction with a reagent which can diffuse through the liquid, the resulting diffusion equations cannot in general be solved analytically for either the steady state or the transient cases. However, van Krevelen and Hoftyzer (*11*) have used a step-by-step method to obtain solutions for the film model, and Perry and Pigford (*20*) have obtained expressions for transient absorption rates by means of an electronic computer. In both cases the calculations were simplified by assuming the diffusivities of the dissolved gas and the reagent to be equal. As with first-order reactions, there appears to be general numerical agreement among the predictions based on the film model and the two penetration models (*8, 12*).

Three extreme types of behavior are predicted under limiting conditions. If c'_o is the bulk concentration of the reagent (c^* and c'_o should be expressed in chemical equivalents) and r' is the second-order reaction-velocity constant between dissolved gas and reagent (c_o being assumed equal to zero), then

(*a*) if $\sqrt{Dr'\,c_o'}/k_L \ll 1$

then $N = k_L c^*$ (12)

i. e., $\alpha = 1$

(*b*) if $\sqrt{Dr'\,c_o'}/k_L \gg c_o'/c^*$

then $N = k_L\,(c^* + c_o')$

i. e., $\alpha = 1 + c_o'/c^*$ (13)

(*c*) if $1 \ll Dr'\,c_o'/k_L \ll c_o'/c^*$

then $N = c^* \sqrt{Dr'\,c_o'}$

i. e., $\alpha = \sqrt{Dr'\,c_o'}/k_L$ (14)

In case *a* the reaction is so slow or k_L so large that the reaction does not appreciably affect the absorption rate. In case *b* the reaction between the dissolved gas and the reagent is exceedingly fast, and the rate of absorption is controlled by the diffusion of the two substances to the site of the reaction within the film. In case *c* the concentration of the reagent is so high that the reaction is pseudo first order and so fast that the absorption rate is independent of k_L, as in the case of a true first-order reaction when $Dr/k_L^{\,2} >> 1$. In cases which do not fall into any of these limiting categories the value of α is in general dependent on k_L.

SIMPLE FILM AND PENETRATION MODELS INVALID

It has been pointed out that in cases where the calculations have been made the film model and the two simple penetration models lead to closely similar quantitative predictions concerning the effects of chemical reaction on the absorption rate. It might seem to be immaterial for practical purposes which type of model is used as a basis for calculation, as if any one of

the three is valid the use of the others would also be expected to give approximately correct results. However, the penetration models have a great advantage if it is possible to measure in the laboratory the transient rate of absorption of gas into stagnant liquid for short times of exposure (i.e., $Q(t)$ vs. t for small values of t). The Higbie or Danckwerts model can then be used to calculate N for absorption in conditions for which θ or s (i.e., k_L) is known, by use of Equation (4) with the appropriate form of $\phi(t)$. Explicit knowledge of such inaccessible quantities as c^*, D, r, etc., is not required, nor is it necessary to know the mechanism or order of the reaction. If absorption causes a rise in temperature at the surface of the liquid(*4*), this is also automatically allowed for. It is thus possible to make a comparison between the observed and predicted effects of reaction without introducing the uncertainties involved in the estimation of these various factors.

The Higbie model will be used to illustrate the process, since this is the simpler to follow. With the appropriate absorbing liquid and gas (the latter being at the right pressure or partial pressure to give the required value of c^*), $Q(t)$ is determined as a function of t by means of a rotating drum(*5*), a falling film(*6*), or some other technique. Absorption measurements are also made in, for instance, a packed tower by use of the same liquid and gas. If the exposure time of elements of liquid surface in the tower is θ, the average absorption rate N per unit area of interface is $Q(\theta)/\theta$ (Figure 1). The quantity actually measured in the column is the absorption rate per unit volume of packing(aN). There are thus two unknowns, a and θ. Comparing the results for two solutions which give Q vs. t curves of different shapes (e.g., absorption of carbon dioxide into an inert solution and a buffer solution) makes it possible to solve for both a and θ. If the Higbie model is valid, these same values should then enable one to predict the tower absorption rate (aN), under identical hydrodynamic conditions, for any other solution for which the Q vs. t curve is measured.

Kennedy(*5, 9*) has measured the transient rates of absorption of carbon dioxide into inert solutions, alkaline buffer solutions, and caustic soda solutions for times of exposure up to ¼ sec. Measurements were also made of the absorption rate (aN) in a tower packed with

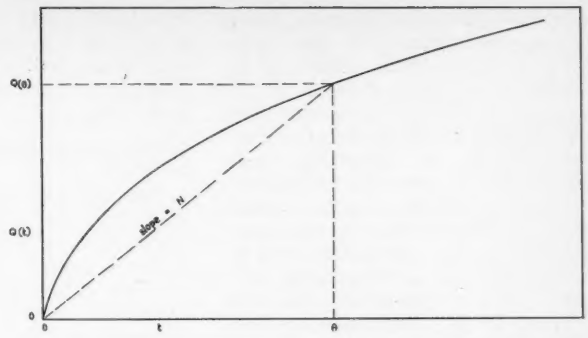

Fig. 1

½-in. Raschig rings under carefully standardized hydrodynamic conditions. It appears from these measurements that no single pair of values for a and θ will serve to correlate the observed absorption rates for different solutions in the tower in spite of the constancy of hydrodynamic conditions. For instance, the values of a and θ required to account for absorption into inert solutions and dilute caustic soda solutions appeared to be about 0.5 cm.$^{-1}$ and 0.15 sec. respectively, while the values for absorption into the buffer solutions were about 1.2 cm.$^{-1}$ and 1 sec. Thus the apparent wetted area varied from about 15% of the geometrical surface in the first case to about 30% in the second, and the corresponding apparent values of k_L could be estimated as about 0.13 and 0.05 cm./sec. Very similar conclusions were reached when the Danckwerts model was used as a basis of calculation.

A possible reason for this discrepancy is that the actual distribution of surface ages in the packing departs widely from that postulated in either the Higbie or the Danckwerts models. It seems likely that the "younger" elements of the surface may have a relatively greater rate of replacement than the "older" elements. In other words, there are regions in the packing where the flow is brisk and the rate of turnover high, and other parts where the liquid is relatively stagnant. The distribution of ages then corresponds to that in a population with a high infant mortality rate, and it may give a relatively greater weight to the older parts of the surface than either the Higbie or Danckwerts models, as indicated in Figure 2*c*.

Figure 3 shows calculated curves of $Q/c^*\sqrt{D}$ vs. t for (a) physical absorption, (b) absorption with irreversible first-order reaction ($r =$ 2.2 sec.$^{-1}$), (c) absorption with very fast first-order reaction ($r =$ 22 sec.$^{-1}$). In case (a) the absorption rate into the stagnant liquid falls off rapidly with exposure time, and so the absorption rate in the tower is strongly dependent on the rate of renewal of liquid surface. In case (b) (where the behavior is similar to that calculated and found experimentally for the absorption of carbon dioxide into buffer solutions of pH about 10.7) the transient absorption rate falls off at first and then becomes constant; the absorption rate in the tower is then less dependent on the surface-renewal rate. Finally, in case (c), the rate of absorption into the stagnant liquid is virtually constant, and the tower absorption rate is independent of surface renewal. It can be seen therefore that absorption into inert liquids in the tower will take place mainly in the regions where the rate of surface renewal is high. A first-order reaction, by maintaining the rate of absorption into older surfaces, enables a larger proportion of the absorption to occur in regions where the surface-renewal is low. In the limit a very fast first-order reaction gives the same rate of absorption into all regions of the wetted surface.

Without being committed to either the film or penetration models, one can say that the local value of k_L probably varies from one region to another in the packing. When k_L is determined for physical absorption, it is an average value which is obtained. If a reacting liquid is substituted, however, the reaction (if first order, for instance) will have more effect in the regions where k_L is small, and vice versa, and it is not possible to calculate the over-all effect unless the distribution of k_L values is known. In the case of an irreversible first-order reaction in which the reaction is so fast that $Dr/k_L^2 >> 1$ everywhere, the expressions for all three models agree [Equations (9*a*), (10*a*), (11*a*)] that N will be independent of k_L and equal everywhere to $c^*\sqrt{Dr}$.

Physical absorption, however, takes place predominantly in that fraction of the surface where k_L is large. If one takes a series of reacting solutions of increasing r, in effect more and more of the surface participates in absorbing gas. Similarly, in the case of a second-order reaction the effective wetted surface will be least in the cases where the local absorption rate is proportional to k_L [Equations (12) and (13)] and greatest in the case where it is independent of k_L [Equation (14)].

Since dissolved carbon dioxide undergoes, in effect, an irreversible first-order reaction with alkaline buffer solutions and since absorption into the dilute caustic soda solutions is believed to have been controlled by the diffusion of the reactants [the conditions of Equation (13)], Kennedy's observations are in general agreement with the foregoing arguments. Hoftyzer and van Krevelen(*8*) have shown that similar conclusions can be reached by considering some experiments by Tepe and Dodge(*24*) on the absorption of carbon dioxide in solutions of potassium hydroxide and caustic soda and by Comstock and Dodge(*1*) on the absorption of carbon dioxide in solutions of potassium carbonate and sodium carbonate, both in towers packed with Raschig rings. They have used a previous established equation for k_L as a function of flow conditions, packing diameter, diffusivity, etc., and have estimated the values of c^*, D and r' in the solutions considered. They show that certain of the measurements of Tepe and Dodge were made under conditions such that Equation (14) should be obeyed, with $c_o' = [OH']$. Calculating N on this basis, they used the experimental values of (aN) to calculate a, the effective wetted area per unit volume of packing, which appeared to be 40% of the geometrical surface. For other measurements Equation (13) was applicable, and in this case a was about 2% of the geometrical surface. Certain of the experiments carried out by Comstock and Dodge approached the limiting conditions represented by Equation (14) (with $c_o' = [CO^{3''}]$), and others by Equation (12). The values of a were again found to be about 40 and 2% respectively of the geometrical surface. The effective wetted surface therefore appears to be much less when the absorption rate is controlled entirely by diffusion, and thus proportional to k_L, than when it is independent of k_L. [The upper limit of 40% suggests that at best only about half the surface of a Raschig ring can be effectively irrigated(*8*).]

PROBLEMS OF INDUSTRIAL DESIGN

The nonuniformity of the value of k_L from one region of the packing to another makes it difficult to devise a generally valid procedure for the design of equipment for absorption accompanied by chemical reaction. If k_L were in fact uniform, and if the performance of the equipment for physical absorption under the appropriate hydrodynamic conditions were known, the effect of the reaction (i.e., the value of α) might be calculated in one of the following ways:

a. If the reaction mechanism is known and values of such physicochemical quantities as c^*, Dr, etc., can be estimated, then a solution of the equations for the film or penetration models leads to formulas such as Equations (9) to (14).

b. If the transient absorption rate of the gas into stagnant liquid is measured, the Higbie or Danckwerts model can be employed [Equation (4)].

c. The value of α, which would be the same for both systems, can be determined in a laboratory model having the same value of k_L as the full-scale equipment.

Modifications of these methods can be used if it is possible to discover the actual distribution of k_L values; this might conveniently be defined by a distribution function $\psi(k_L)$ such that the local value of the liquid-film coefficient lay between k_L and $(k_L + dk_L)$ over parts of the surface having an area corresponding to a fraction $\psi(k_L)$ $d(k_L)$ of the geometrical surface a_d. The volumetric rate of physical absorption would be given by

$$(aN) = (c^* - c_o)\, a_d \int_0^\infty k_L \cdot \psi(k_L) \cdot$$

$$d(k_L) = \bar{k}_L\, a_d\, (c^* - c_o) \qquad (15)$$

$\bar{k}_L$ being the average value of k_L over the entire geometrical surface. As already shown, the ratio α which determines the effect of reaction on absorption rate is in general a function of k_L, which may be written $\alpha(k_L)$, and will vary from one region to another. The average value $\bar{\alpha}$ for the surface as a whole would be given by

$$\bar{\alpha} = \int_0^\infty \alpha(k_L) \cdot \psi(k_L) \cdot d(k_L) \qquad (16)$$

There is not necessarily any simple relationship between $\bar{\alpha}$ and $\bar{k}_L$.

Alternatively, one may use the language of the penetration theory and say that the surface-age dis-

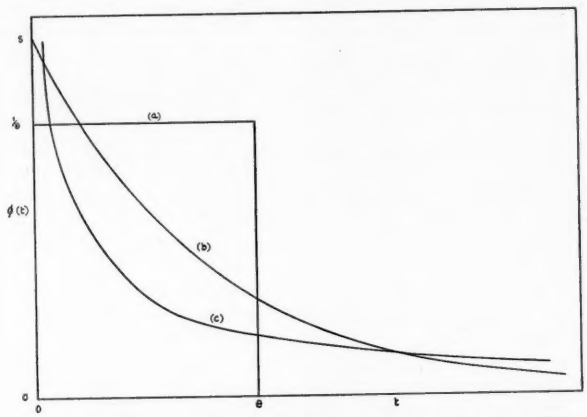

Fig. 2. Surface-age distribution functions $\phi(t)$; (a), Higbie, $\theta = 4D/\pi k_L^2$; (b) Danckwerts, $S = k_L^2/D$; (c) hypothetical case giving greater weight to older parts of the surface.

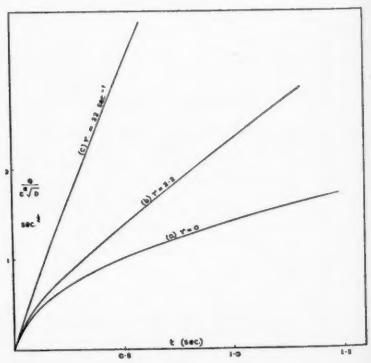

Fig. 3. Effect of first-order reaction on transient absorption.

tribution function $\phi(t)$ is not that of the Higbie or Daanckwerts models, but has some other form; if this were known, and $Q(t)$ known as a function of t by calculation or experiment, then $\bar{\alpha}$ could be found by evaluating Equation (4) for absorption with and without reaction.

An extension of Kennedy's work may make it possible to determine the actual distribution of k_L values or surface ages under the hydrodynamic conditions obtaining in his packed tower. It seems quite likely, however, that a change in hydrodynamic conditions (e.g., flow rate or packing size) might lead to an entirely different form for $\psi(k_L)$ or $\phi(t)$. The labor involved in determining these functions under all conditions of practical interest would then be prohibitive. Hoftyzer and van Krevelen(*8*) point out that investigations carried out under different sets of hydrodynamic conditions have led, for instance, to quite different conclusions about the effect of alkali concentration on the rate of absorption of carbon dioxide. These authors have suggested a simplified approximate design method for the case of second-order reaction, but its usefulness under various conditions requires to be tested by experiment.

The use of a laboratory model cannot be expected to give a value of $\bar{\alpha}$ which will be generally applicable to full-scale equipment, since the functions $\psi(k_L)$ or $\phi(t)$ are likely to have different forms in the two systems, even if the average coefficient $\bar{k}_L$ has the same value in both. Wetted-wall columns, "totem pole" columns, and stirred vessels do not give results which agree well with those for packed towers. Even geometrically similar models are unlikely to give satisfactory results because of the number of conditions which must be satisfied to ensure similarity in other respects. Thus in the case of an irreversible first-order reaction it appears that for a packing of a given shape $\bar{\alpha}$ will be a function of at least three dimensionless groups; for instance,

$$\bar{\alpha} = F\left\{\frac{dL}{\mu}, \frac{\mu^2 d^3}{\rho^2 g}, \frac{rd\rho}{L}\right\} \quad (17)$$

(where d is the particle diameter and L the mass velocity of the liquid).

If surface-tension effects are important, as they will be when the particles are sufficiently small, a fourth group must be added. A second-order reaction will require one or more further groups.

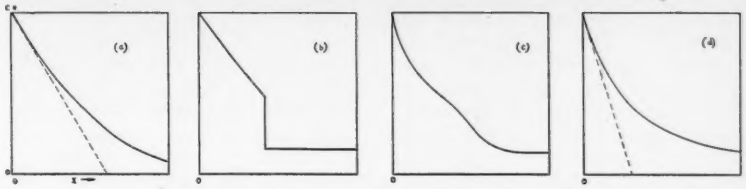

Fig. 4. Effect of discontinuity on concentration profile: (a) before discontinuity, (b) immediately after, (c) and (d) later stages.

However, there are certain circumstances in which laboratory experiments may be used to predict the effect of chemical reaction in industrial equipment. If the absorption rate per unit volume of packing (aN_A) is known for a given gas-liquid system A under specified hydrodynamic conditions, the absorption rate (aN_B) for some other gas-liquid system B under the same hydrodynamic conditions can be predicted provided the transient absorption curves (Q vs. t) for the two systems are geometrically similar, so that the ratio of Q_A to Q_B is constant. The following simple condition then holds:

$$\left(\frac{aN_B}{aN_A}\right) = \frac{Q_B}{Q_A} \quad (18)$$

The ratio Q_B/Q_A may be determined directly from transient absorption measurements, or it may be calculated if the data are available. Alternatively, the ratio $(aN_B)/(aN_A)$ may be determined in a model absorption apparatus, which need not have the same hydrodynamic characteristics as the full-scale equipment. For example, in the system A the gas might be absorbed in an inert liquid; the Q vs. t curve would then be parabolic:

$$Q_A = 2c^* \sqrt{D_A t/\pi} \quad (19)$$

In system B the dissolved gas might undergo an extremely rapid reaction with a reagent in the solution when

$$Q_B = 2\beta c_B^* \sqrt{D_B t/\pi} \quad (20)$$

β being a constant which is equal to $(1 + c'_o/c^*)$ when the diffusivities of the two reactants are equal(*23*). In such a case the ratio $(aN_B)/(aN_A)$ of the volumetric absorption rates for the two systems would be equal to $\beta c^*_B \sqrt{D_B}/c^*_A \sqrt{D_A}$, but it could be inferred directly from the Q vs. t curves without an explicit knowledge of the physical quantities involved. It could also be measured in a laboratory absorption apparatus if the two curves were known to be geometrically similar.

To take another example, the dissolved gas might in both systems undergo a very fast irreversible first-order or pseudo first order reaction. The Q vs. t curves would then be straight lines through the origin, of slope $c^*\sqrt{Dr}$, or $c^*\sqrt{Dr'c'_o}$, and $(aN_B)/(aN_A)$ would be equal to the ratio of the slopes.

The principle can be applied to all cases in which it is observed experimentally that the Q vs. t curves are geometrically similar, even when the mechanism of the absorption process is unknown. The method is easily justified if the penetration theory, in its most general form, is accepted, since from Equation (4)

$$N_B = \int_{t=0}^{\infty} \phi(t)\, dQ_B(t) =$$

$$\frac{Q_B}{Q_A} \int_{t=0}^{\infty} \phi(t)\, dQ_A(t) = \frac{Q_B}{Q_A} \cdot N_A \quad (21)$$

The justification does not depend on the form of the surface-age distribution function $\phi(t)$. However, if the two Q vs. t curves are only approximately similar, the accuracy of the method may depend on the form of $\phi(t)$. In such a case, if a model is used to determine the ratio $(aN_B)/(aN_A)$, the results should be treated with caution. Too little information is at present available to enable a more precise statement to be made.

OTHER MODELS OF THE ABSORPTION PROCESS

Since 1949 Kishinevskii and others(*13, 14, 15*) have been developing a theory of gas-absorption which assumes that the liquid surface is constantly being replaced by fresh material. A mean value of the exposure time is introduced, corresponding to the quantity θ in Higbie's model. However, it is assumed that molecular diffusion plays little or no part in determining the rate of absorption; the process envisaged may be described as one of surface re-

newal without penetration. It is supposed that a layer at the surface of the liquid becomes instantaneously saturated with the gas on exposure, and this saturated layer is subsequently carried away into the bulk of the liquid. If a chemical reaction occurs in solution, the surface layer is kept constantly saturated with *unreacted* gas during the time of exposure, while the concentration of *reacted* gas increases at a rate determined by the kinetics of the reaction. The thickness of the surface layer is not discussed, but it seems necessary for the validity of the theory that it should be confined to an adsorbed film on the surface of the liquid; a deeper layer could be formed only by the diffusion of dissolved gas molecules into the liquid, and this would lead back immediately to the penetration theory. A detailed critical survey of Kishinevskii's theory is not possible here, but it apparently implies that the influence of the diffusivity of the solute gas on k_L should be negligible. Evidence on this point is scanty, but Sherwood and Holloway's measurements (*21*) seem to provide strong evidence that (as between O_2 and CO_2 on one hand and H_2 on the other) k_L varies approximately as $D^{\frac{1}{2}}$. Further evidence on this point would be welcome. It is interesting that recent work by Lewis (*16*) appears to show that rates of transfer across a liquid-liquid interface under turbulent conditions are independent of diffusivity.

There is a certain amount of evidence in favor of what may be called "surface rejuvenation" rather than surface renewal. The passage of liquid over a discontinuity between two smooth surfaces, on both of which the flow is laminar, may be considered; as a simple example one may consider the flow over two contiguous spheres. Although it may be expected that over a wide range of flow conditions some type of eddy may form at the junction of the spheres, it appears that complete mixing and renewal of the surface does not occur. Lynn, Straatemeier, and Kramers, for instance, have found (*18*) that the rate of absorption into water flowing over a vertical column of contiguous spheres corresponds more closely to that to be expected if no mixing occurs at discontinuities than to the case of complete mixing. Experiments with totem-pole columns suggest that complete mixing does not occur at the junction points between the disks. Wagstaffe (*25*) (using the Higbie model) has shown that the average exposure time required to account for observed absorption rates is usually greater than the average retention time on a disk (calculated from flow rate and holdup); the ratio of apparent exposure time to retention time depends on the flow rate and the physical properties of the liquid, including its surface tension. Kennedy's measurements on a column packed with ½-in. Raschig rings (*5, 9*) indicate that the effective exposure time may be sufficient for liquid traveling with the mean vertical velocity to traverse several packing diameters. None of these observations are conclusive in themselves, but taken together they tend to suggest that when a film of liquid in laminar flow meets a discontinuity, a surface layer may under certain circumstances travel on relatively undisturbed even though eddying may cause mixing of the liquid beneath it. The liquid leaving the region of the discontinuity may then consist of an outer layer in which the original concentration profile is unchanged, overlying a layer in which the concentration is uniform (Figure 4). The result would be that owing to an increase in the concentration gradient at the surface, the absorption rate after the discontinuity would be higher than if the liquid had continued in undisturbed laminar flow, but not so high as if there had been complete mixing at the discontinuity. We may say that the surface has been rejuvenated rather than renewed. The net effect of passage over a series of discontinuities will be that the average value of the transfer coefficient k_L will remain constant, rather than decreasing progressively as it would in uninterrupted laminar flow. It is possible but by no means certain that the methods of the penetration theory might be applicable to a process of this kind, the surface-age distribution function $\phi(t)$ (unlike those functions discussed previously) having the value zero at $t = 0$. If the flow rate over the packing is sufficiently high and the uninterrupted paths are long enough, convective mixing of the liquid is likely to take place even on the continuous surfaces, either because of turbulence or through the action of ripples, which have a profound effect on liquid-film coefficients in wetted-wall columns (*6*).

Even if a liquid is in completely streamline flow, the fanning out of the stream lines and their subsequent convergence (particularly, for instance, in grid packings and totem-pole columns) are likely to play a major part in the process of gas absorption. As yet, the mechanics of flow of this kind have barely been considered.

CONCLUSIONS

In the present state of knowledge only rough estimates can be made of the performance of absorption equipment when reacting liquids are to be used (except in the special cases cited). The conventional methods fail because they employ oversimplified models of the hydrodynamic behavior of the liquid, involving only two parameters (k_L and a). It is possible that sufficiently accurate methods might be based on a rather more elaborate model, but there is not enough reliable information available to enable the theory to be developed further at the moment.

Much of the past research on absorption with reaction has been difficult to interpret because of lack of knowledge of the mechanism and rate of the reaction and other physicochemical data. It is recommended that any future work on absorption into agitated liquids should be coupled with the measurement of transient absorption rates into the same liquids; in this way many of the uncertainties would be resolved.

Gas absorption in packed towers depends on the flow of a layer of liquid over discontinuous surfaces, and very little is known about the mechanism of such flow. The study of this flow is essential to an understanding of the true mechanism of absorption.

ACKNOWLEDGMENT

Most of the ideas in this review are due wholly or in part to others. Sources in the literature have been indicated where possible, but the author has also gained much from informal discussions with his colleagues, with D. W. van Krevelen, P. J. Hoftyzer, H. Kramers, and Scott Lynn, and with S. P. S. Andrew, who suggested the concept of surface rejuvenation.

NOTATION

a = effective wetted surface area per unit volume of packing
a_d = geometrical surface area per unit volume of packing
B = effective liquid-film thickness
c^* = concentration of unreacted dissolved gas at surface of liquid
c_o = concentration of unreacted dissolved gas in bulk of liquid
c'_o = concentration of unreacted reagent in bulk of liquid

D = diffusivity of dissolved gas
d = diameter of packing particle
k_L = liquid-film coefficient for physical absorption
$\bar{k}_L$ = average value of k_L over entire surface of packing
L = liquid mass velocity
N = average rate of absorption per unit area of wetted surface in packing
$Q(t)$ = quantity of gas absorbed by unit area of stagnant liquid of effectively infinite depth in time t
r = first-order reaction-velocity constant
r' = second-order reaction-velocity constant
s = fractional rate of surface renewal
t = time of exposure of liquid to gas
α = ratio of N with reaction to N without reaction, other things equal
$\bar{\alpha}$ = average value of α over entire surface of packing
β = constant in Equation (20)
θ = effective exposure time of liquid on packing
μ = viscosity of liquid
ρ = density of liquid
$\phi(t)$ = distribution function for local surface ages
$\psi(k_L)$ = distribution function for local values of k_L

LITERATURE CITED

1. Comstock, C. S.. and B. F. Dodge, *Ind. Eng. Chem.*, **26**, 428 (1934).
2. Danckwerts, P. V., *Trans. Faraday Soc.*, **46**, 300 (1950).
3. ———, *Ind. Eng. Chem.*, **43**, 1460 (1951).
4. ———, *Appl. Sci. Research (A)*, **3**, 285 (1952).
5. ———, and A. M. Kennedy, Inst. Chem. Engrs., Symposium on Gas Absorption (April, 1954), in press.
6. Emmert, R. E., and R. L. Pigford, *Chem. Eng. Progr.*, **50**, 87 (1954).
7. Higbie, R., *Trans. Am. Inst. Chem. Engrs.*, **31**, 365 (1935).
8. Hoftyzer, P. J., and D. W. van Krevelen, Inst. Chem. Engrs., Symposium on Gas Absorption (April, 1954), in press.
9. Kennedy, A. M., Ph.D. thesis, Cambridge University (1954).
10. Krevelen, D. W. van, and C. J. van Hooren, Chim. et Ind., XXXIe Congrès Int. de Chim. Industrielle, Sept. 1948, p. 166.
11. Krevelen, D. W. van, and P. J. Hoftyzer, *Rec. trav. chim.*, **67**, 563 (1948).
12. ———, *Chem. Eng. Sci.*, **2**, 145 (1953).
13. Kishinevskii, M. Kh., and A. V. Pamfilov, *Zhur. Priklad. Khim.*, **22**, 1173 (1949).
14. Kishinevskii, M. Kh., *loc. cit.*, **24**, 542 (1951).
15. *Ibid.*, **27**, 382 (1954).
16. Lewis, J. B., *Repts. CE/R* 1118, 1119, Atomic Energy Research Establishment, Harwell (1954) (to be published in *Chem. Eng. Sci.*).
17. Lin, C. S., E. B. Denton, H. S. Gaskill, and G. L. Putnam, *Ind. Eng. Chem.*, **43**, 2136 (1951).
18. Lynn, S., J. R. Straatemeier, and H. Kramers, *Chem. Eng. Sci.*, **4**, 63 (1955).
19. Marshall, W. R., and R. L. Pigford, "Application of Differential Equations to Chemical Engineering Problems", Univ. of Delaware (1947).
20. Perry, R. H., and R. L. Pigford, *Ind. Eng. Chem.*, **45**, 1247 (1953).
21. Sherwood, T. K., and F. A. L. Holloway, *Trans. Am. Inst. Chem. Engrs.*, **36**, 39 (1940).
22. Sherwood, T. K., and R. L. Pigford, "Absorption and Extraction," p. 324, McGraw-Hill Book Company, Inc., New York (1952).
23. *Ibid.*, p. 332.
24. Tepe, J. B., and B. F. Dodge, *Trans. Am. Inst. Chem. Engrs.*, **39**, 255 (1943).
25. Wagstaffe, F. J., private communication.
26. Whitman, W. G., *Chem. & Met. Eng.*, **29**, 147 (1923).

(Presented at A.I.Ch.E. New York meeting)

Heat Transfer in Cylinders with Heat Generation

Leonard Topper

The Johns Hopkins University, Baltimore, Maryland

The prediction of temperatures has been studied for a tubular flow reactor when heat is generated at a rate which is a linear function of the local temperature. Analytical solutions are presented both for the case where the wall is isothermal and for the case where the exterior surroundings are isothermal and the heat transfer coefficient between the tube wall and the surroundings is constant. This analysis should be helpful for estimating local temperatures and also for predicting the transient response to changes in one of the independent operating variables.

One of the fundamental chemical engineering problems is the prediction of temperatures in a flow reactor. The temperature pattern is dictated by the inlet temperature of the fluid, heat generation within the fluid due to chemical or nuclear reaction, heat transfer to the surroundings, the velocity distribution and transport properties of the fluid, and the geometry of the reactor. Every case of this problem has some unique aspects, but there are enough common features to make a simplified theoretical analysis desirable. The present analysis should be helpful for estimating temperatures in a flow reactor and for predicting the transient response to changes in an operating variable.

The assumption that the rate of heat generation depends only on the local temperature is valid for chemical reactions only when they are of zero order. The linear temperature dependence of the heat source may be viewed as an approximation of the exponential variation of chemical reaction rate with temperature.

The reactor is taken to be a tube of radius s, through which the fluid

Leonard Topper is at present with Esso Research and Engineering Company, Linden, New Jersey.

flows at uniform and steady velocity V. The fluid enters the tube at a uniform and steady temperature t_o. Heat is generated within the fluid at a rate which is a linear function of the local temperature. The tube is surrounded by a medium at the constant temperature t_s, and the heat transfer coefficient between the fluid and its environment is a constant, h. When h is infinite, it is implied that the fluid in contact with the tube wall is always at the constant temperature t_s.

The differential equation of heat convection with a volume heat source is (*2*)

$$\frac{dt}{d\tau} = \frac{\partial t}{\partial \tau} + V_x \frac{\partial t}{\partial x} + V_y \frac{\partial t}{\partial y} + V_z \frac{\partial t}{\partial z} = \frac{q}{\rho c} + \alpha \nabla^2 t \qquad (1)$$

Here t is temperature; τ is time; V_x, V_y, V_z are the components of the velocity in the x, y, z directions; q is the rate of heat generation per unit volume and time; ρ is the density; c is the heat capacity; and α is the thermal diffusivity of the fluid. The conditions assumed are

a. Steady state.

b. Symmetry of temperature about the axis.

c. Fluid velocity in x direction only (axial velocity) and equal to V.

d. Physical properties of the fluid independent of temperature.

e. Axial conductivity negligible ($\partial^2 t/\partial x^2 << \partial^2 t/\partial r^2 + 1/r \ \partial t/\partial r$)

$$\left(\frac{\partial^2 t}{\partial x^2} \ll \frac{\partial^2 t}{\partial r^2} + \frac{1}{r}\frac{\partial t}{\partial r}\right)$$

f. Heat generation a linear function of temperature: $q/\rho c = At + B$.

Then by use of cylindrical coordinates,

$$V\frac{\partial t}{\partial x} = \alpha\left(\frac{\partial^2 t}{\partial r^2} + \frac{1}{r}\frac{\partial t}{\partial r}\right) + At + B \qquad (2)$$

The appropriate initial and boundary conditions for the differential equation (2) are (3) and either (4) or (5):

$$\text{At } x = 0, t = t_0 \qquad (3)$$

$$\text{At } r = s, t = t_s \text{ (isothermal wall)} \qquad (4)$$

$$\text{or } k\left(\frac{\partial t}{\partial r}\right)_{r=s} = -h\,(t - t_s)_{r=s} \qquad (5)$$

(heat loss to surroundings at constant temperature)

The solution to the problem of the constant source ($A = 0$) with boundary condition (4) has been presented (*3*) and is

$$\frac{t-t_s}{t_o-t_s} = \sum_{n=1}^{\infty} \frac{2}{\beta_n J_1(\beta_n)}\left[1 - \frac{Bs^2}{\alpha\,(t_o-t_s)\,\beta_n^2}\right] J_o(\beta_n w)\, e^{-\beta_n^2 \frac{\alpha}{sV}\frac{x}{s}} + \frac{Bs^2}{4\,\alpha\,(t_o-t_s)}(1-w^2) \qquad (6)$$

The J_0 and J_1 are Bessel functions of the first kind and of zero and first order respectively, and the β_n are the positive roots of the equation $J_0(\beta) = 0$. The first three β_n are 2.40 5.52 and 8.65.

When the boundary condition is (5) rather than (4) and the source term is constant ($A = 0$), the solution has the form

$$\frac{t-t_s}{t_o-t_s} = \sum_{n=1}^{\infty} N_n J_o(\lambda_n w) e^{-\lambda_n^2 \frac{\alpha}{sV}\frac{x}{s}} + \frac{1}{(t_o-t_s)}\left[\frac{B_s^2}{4\alpha}\left(1 + 2\frac{k}{sh} - w^2\right) - t_s\right] \qquad (7)$$

The λ_n are the positive roots of the equation

$$\lambda_n J_1(\lambda_n) - \frac{hs}{k} J_o(\lambda_n) = 0 \qquad (8)$$

These roots are tabulated as Table 3 of Carslaw and Jaeger (*1*). hs/k is a kind of Nusselt number, with h being the film heat transfer coefficient of the surroundings, and k the thermal conductivity of the fluid itself. The N_n are calculated to satisfy the initial condition (3). Use is made here of the Dini expansions of unity and of w^2 (*4*):

$$1 = 2\left(\frac{hs}{k}\right)\sum_{n=1}^{\infty} \frac{J_o(\lambda_n w)}{\left[\lambda_n^2 + \left(\frac{hs}{k}\right)^2\right] J_o(\lambda_n)} \qquad (9)$$

$$w^2 = 2\sum_{n=1}^{\infty} \frac{\left[2 + \frac{hs}{k} - 4\left(\frac{hs}{k}\right)\left(\frac{1}{\lambda_n}\right)^2\right] J_o(\lambda_n w)}{\left[\lambda_n^2 + \left(\frac{hs}{k}\right)^2\right] J_o(\lambda_n)} \qquad (10)$$

at $x = 0$

$$\frac{t-t_s}{t_o-t_s} = 1 = \sum_{n=1}^{\infty} N_n J_o(\lambda_n w) + \frac{1}{(t_o-t_s)}\left[\frac{Bs^2}{4\alpha}\left(1 + 2\frac{k}{sh} - w^2\right) - t_s\right] \qquad (11)$$

The Dini expansion on the right must equal

$$1 - \frac{Bs^2}{4\alpha\,(t_o-t_s)}\left(1 + \frac{2k}{sh} - w^2\right) + \frac{t_s}{(t_o-t_s)}$$

so that

$$N_n = \frac{2}{\left[\lambda_n^2 + \left(\frac{hs}{k}\right)^2\right] J_o(\lambda_n)}\left\{\frac{hs}{k}\left[1 + \frac{t_s}{t_o-t_s} - \frac{Bs^2\left(1 + \frac{2k}{sh}\right)}{4\alpha\,(t_o-t_s)}\right] + \frac{Bs^2\left[2 + \frac{hs}{k} - 4\left(\frac{hs}{k}\right)\left(\frac{1}{\lambda_n}\right)^2\right]}{4\alpha\,(t_o-t_s)}\right\} \qquad (12)$$

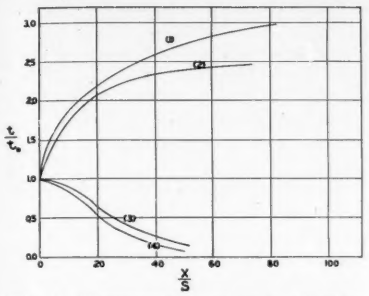

Fig. 1. Temperature at axis of tube. ($A = 0$, $t_s = 0$, $\alpha/sV = 10^{-2}$).

$$\frac{Bs^2}{\alpha t_o} = 10, \frac{hs}{k} = 10 \quad (1)$$

$$\frac{Bs^2}{\alpha t_o} = 10, \frac{hs}{k} = \infty \quad (2)$$

$$\frac{Bs^2}{\alpha t_o} = 0, \frac{hs}{k} = 10 \quad (3)$$

$$\frac{Bs^2}{\alpha t_o} = 0, \frac{hs}{k} = \infty \quad (4)$$

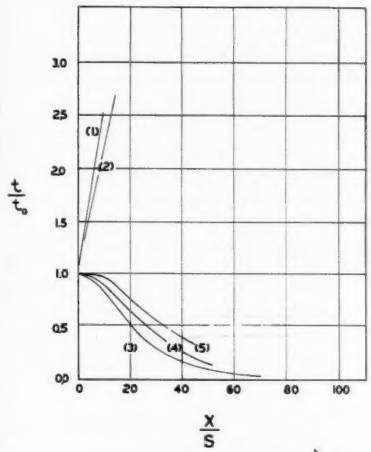

Fig. 2. Temperature at axis of tube, temperature-dependent volume heat source ($t_s = 0$, $B/A = 0$, $\alpha/sV = 10^{-2}$).

$$\frac{As}{V} = 10^{-1}, \frac{hs}{k} = 10 \quad (1)$$

$$\frac{As}{V} = 10^{-1}, \frac{hs}{k} = \infty \quad (2)$$

$$\frac{As}{V} = 0, \frac{hs}{k} = \infty \quad (3)$$

$$\frac{As}{V} = 10^{-2}, \frac{hs}{k} = \infty \quad (4)$$

$$\frac{As}{V} = 10^{-2}, \frac{hs}{k} = 10 \quad (5)$$

TABLE 1.—ROOTS *of* EQUATION (8)

hs/k	λ_1	λ_2	λ_3
0.01	0.141	3.83	7.02
0.1	0.442	3.86	7.03
1.0	1.26	4.08	7.16
10.0	2.18	5.03	7.6
∞	2.40	5.52	8.65

and the solution is

$$\frac{t-t_s}{t_o-t_s} = \frac{1}{t_o-t_s}\left[\frac{Bs^2\left(1+\frac{2k}{sh}-w^2\right)-t_s}{4\alpha}\right] + 2\sum_{n=1}^{\infty} \frac{hs}{k\left[\lambda_n^2+\left(\frac{hs}{k}\right)^2\right]J_o(\lambda_n)}$$

$$\left\{\left[1+\frac{t_s}{t_o-t_s}-\frac{Bs^2\left(1+\frac{2k}{sh}\right)}{4\alpha\,(t_o-t_s)}\right]+\frac{Bs^2}{4\alpha\,(t_o-t_s)}\left[\frac{2k}{sh}+1-\frac{4}{\lambda_n^2}\right]\right\}$$

$$J_o(\lambda_n w)e^{-\lambda_n^2\frac{\alpha}{sv}\frac{x}{s}} \quad (13)$$

Table 1 contains the first three roots of Equation (8) for some values of hs/k.

Figure 1 is a graphical representation of Equations (6) and (13) respectively in terms of various groups, $t_s = 0$ being assumed.

The solutions to the complete Equation (2) are somewhat more complex. When the wall is isothermal [boundary condition is Equation (4)], the solution has the form

$$t+\frac{B}{A} = \left(t_s+\frac{B}{A}\right)\frac{J_o\left[\left(\frac{As^2}{\alpha}\right)^{\frac{1}{2}}w\right]}{J_o\left[\left(\frac{As^2}{\alpha}\right)^{\frac{1}{2}}\right]} + \sum_{n=1}^{\infty}\left[\frac{2\left(t_o+\frac{B}{A}\right)}{\beta_n J_1(\beta_n)}\right.$$

$$\left.+N_n\right]J_o(\beta_n w)e^{-\frac{x}{v}\left[A-\alpha\left(\frac{\beta_n}{s}\right)^2\right]} \quad (14)$$

Equation (14) satisfies the boundary condition (4); it will satisfy the initial condition (3) if

$$\sum_{n=1}^{\infty} N_n J_o(\beta_n w) = -\left(t_s+\frac{B}{A}\right)\frac{J_o\left[\left(\frac{As^2}{\alpha}\right)^{\frac{1}{2}}w\right]}{J_o\left[\left(\frac{As^2}{\alpha}\right)^{\frac{1}{2}}\right]} \quad (15)$$

Use is made here of the Fourier-Bessel expansion of $J_o[(As^2/\alpha)^{\frac{1}{2}}w]$ (4):

$$J_o\left[\left(\frac{As^2}{\alpha}\right)^{\frac{1}{2}}w\right] = \sum_{n=1}^{\infty}\frac{2\,\beta_n J_o\left[\left(\frac{As^2}{\alpha}\right)^{\frac{1}{2}}\right]J_o(\beta_n w)}{\left(\beta_n^2-\frac{As^2}{\alpha}\right)J_1(\beta_n)} \quad (16)$$

Then the solution to the problem of linearly temperature-dependent heat sources in a fluid whose wall is maintained at a constant temperature is

$$\frac{t-t_s}{t_o-t} = \frac{t_s+\frac{B}{A}}{t_o-t_s}\left\{\frac{J_o\left[\left(\frac{As^2}{\alpha}\right)^{\frac{1}{2}}w\right]}{J_o\left[\left(\frac{As^2}{\alpha}\right)^{\frac{1}{2}}\right]}-1\right\}+\frac{2}{t_o-t_s}\sum_{n=1}^{\infty}\frac{1}{\beta_n J_1(\beta_n)}\left[\left(t_o\right.\right.$$

$$+\frac{B}{A}\Bigg)-\frac{\left(t_s+\frac{B}{A}\right)\beta_n^2}{\left(\beta_n^2-\frac{As^2}{\alpha}\right)}\Bigg]J_o(\beta_n w)\,e^{\frac{x}{v}\left[A-\alpha\left(\frac{\beta_n}{s}\right)^2\right]} \tag{17}$$

With boundary condition (5) instead of (4), the solution to differential equation (2) is of the type

$$t+\frac{B}{A}=\frac{\left(t_s+\frac{B}{A}\right)J_o\left[\left(\frac{As^2}{\alpha}\right)^{\frac{1}{2}}w\right]}{\left\{J_o\left[\left(\frac{As^2}{\alpha}\right)^{\frac{1}{2}}\right]-\frac{k}{sh}\left(\frac{As^2}{\alpha}\right)^{\frac{1}{2}}J_1\left[\left(\frac{As^2}{\alpha}\right)^{\frac{1}{2}}\right]\right\}}$$

$$+\sum_{n=1}^{\infty}\left\{\frac{2\left(t_o+\frac{B}{A}\right)\left(\frac{hs}{k}\right)}{\left[\lambda_n^2+\left(\frac{hs}{k}\right)^2\right]J_o(\lambda_n)}+N_n\right\}J_\rho(\lambda_n w)\,e^{\frac{x}{v}\left[A-\alpha\left(\frac{\lambda_n}{s}\right)^2\right]} \tag{18}$$

The N_n of (18) will satisfy the initial condition if

$$-\sum_{n=1}^{\infty}N_n J_o(\lambda_n w)=\frac{\left(t_s+\frac{B}{A}\right)J_o\left[\left(\frac{As^2}{\alpha}\right)^{\frac{1}{2}}w\right]}{\left\{J_o\left[\left(\frac{As^2}{\alpha}\right)^{\frac{1}{2}}\right]-\frac{k}{sh}\left(\frac{As^2}{\alpha}\right)^{\frac{1}{2}}J_1\left[\left(\frac{As^2}{\alpha}\right)^{\frac{1}{2}}\right]\right\}} \tag{19}$$

Use is made of the Dini expansion of

$$J_o\left[\left(\frac{As^2}{\alpha}\right)^{\frac{1}{2}}w\right]:$$

$$J_o\left[\left(\frac{As^2}{\alpha}\right)^{\frac{1}{2}}w\right]=$$

$$2\left(\frac{hs}{k}\right)\sum_{n=1}^{\infty}\frac{\lambda_n^2\left\{J_o\left[\left(\frac{As^2}{\alpha}\right)^{\frac{1}{2}}\right]-\frac{k}{sh}\left(\frac{As^2}{\alpha}\right)^{\frac{1}{2}}J_1\left[\left(\frac{As^2}{\alpha}\right)^{\frac{1}{2}}\right]\right\}J_o(\lambda_n w)}{\left[\lambda_n^2+\left(\frac{hs}{k}\right)^2\right]\left(\lambda_n^2-\frac{As^2}{\alpha}\right)J_o(\lambda_n)} \tag{20}$$

When (20) is used with (19), (18) becomes

$$\frac{t-t_o}{t_o-t_s}=\frac{t_s+\frac{B}{A}}{t_o-t_s}\left[\frac{J_o\left[\left(\frac{As^2}{\alpha}\right)^{\frac{1}{2}}w\right]}{\left\{J_o\left[\left(\frac{As^2}{\alpha}\right)^{\frac{1}{2}}\right]-\frac{k}{sh}\left(\frac{As^2}{\alpha}\right)^{\frac{1}{2}}J_1\left[\left(\frac{As^2}{\alpha}\right)^{\frac{1}{2}}\right]\right\}}-1\right]+$$

$$\frac{2}{t_o-t_s}\sum_{n=1}^{\infty}\frac{hs}{k\left[\lambda_n^2+\left(\frac{hs}{k}\right)^2\right]J_o(\lambda_n)}\left[\left(t_o+\frac{B}{A}\right)-\right.$$

$$\left.\frac{\left(t_s+\frac{B}{A}\right)\lambda_n^2}{\left(\lambda_n^2-\frac{As^2}{\alpha}\right)}\right]J_o(\lambda_n w)\,e^{\frac{x}{v}\left[A-\alpha\left(\frac{\lambda_n}{s}\right)^2\right]} \tag{21}$$

Equations (17) and (21) are presented in Figure 2, which plots the temperature at the axis of the tube as a function of the dimensionless distance downstream, the other variables of the problem being treated as dimensionless parameters.

An important aspect of solutions (17) and (21) is that the downstream temperature can increase out of bounds if $A>5.76\ \alpha/s^2$ [isothermal wall, Equation (17)] or if $A>\alpha(\lambda_1/s)^2$ [Equation (21), λ_1 is the smallest root of (8)]. The assumptions of uniform velocity and of heat transport in the radial direction by conduction only are not practical; however, the form of the results developed above should be useful for cases of turbulent flow if a turbulent eddy diffusivity for heat is used in place of the ordinary thermal diffusivity of the fluid.

NOTATION

A, B defined by $q/\varrho c = At + B$

J_0, J_1, J_2 = Bessel functions of the first kind and zero, first and second order

N_n = coefficient of various Fourier-Bessel and Dini expansions

V_x, V_y, V_z; V = local velocity in x, y, and z directions; uniform velocity in x direction

c = heat capacity

h = heat transfer coefficient in region exterior to fluid

k = thermal conductivity of fluid

q = rate of heat generation per unit volume

r = radial position coordinate

s = radius of tube

t, t_0, t_s = temperature, temperature at $x = 0$, temperature of surroundings $(r>s)$

$w = r/s$

α = thermal diffusivity $= k/\varrho c$

β_n = a zero of $J_0(\beta)$

λ_n = a zero of $\lambda J_1(\lambda) - hs/k\, J_0(\lambda)$

ϱ = density

τ = time

LITERATURE CITED

1. Carslaw, H. S., and J. C. Jaeger, "Conduction of Heat in Solids," Oxford University Press, New York (1947).
2. Jakob, Max, "Heat Transfer," John Wiley and Sons, New York (1949).
3. Topper, Leonard, "Chemical Engineering Science" (in press).
4. Watson, G. N., "A Treatise on the Theory of Bessel Functions," Cambridge University Press, Cambridge (1944).

Presented at A.I.Ch.E. Louisville meeting

Continuous Reactions in Distillation Equipment

Lothar H. Belck

E. I. du Pont de Nemours and Company, Inc., Waynesboro, Virginia

For hypothetical two- and three-component liquid-phase reversible reactions, continuous processes are described in which the products are obtained in essentially pure form by carrying out the reaction in a single distillation column. Methods for plate-to-plate calculations in such reaction-distillation systems and numerical solutions for two reactions are presented.

The desire for increased capacities, product uniformity, and simplified process control has frequently led to the development of continuous-processing methods in place of the batch processes formerly used. But in only comparatively few cases have processes been developed in which a liquid-phase reversible reaction is carried out simultaneously with a distillation and where the reaction and distillation rates are of the same order of magnitude. It is realized, of course, that such distillation-reaction processes are by no means generally applicable and that they can be used in comparatively few systems only. In most of these processes described so far, additional distillation columns are required besides the reaction column to obtain the products in their pure form (*1, 4*). It is desirable to devise processes in which at least one of the products is obtained in essentially pure* form without further purification, i.e., where only one column or two columns at the most are required. Such processes, e.g., for the preparation of esters, have been reported (*2, 5*) but without details of column design or calculation. This paper describes one-column processes leading to essentially pure products in hypothetical two- and three-component reactions and presents methods for plate-to-plate calculations in such systems.

Reversible reactions will be considered only; for irreversible reactions, it will in most cases be more economical to let the reaction go to completion and then to distill the reaction mixture. It will be assumed that the reaction takes place in the liquid phase only and requires the presence of a catalyst, the vapor pressure of which can be neglected. In view of the schematic character of the calculations, the heat of reaction as well as the influence of differences in temperature between various plates of a column on density, heat of vaporization, and reaction rate will be neglected. To further simplify calculations, deviations of the liquid mixture from ideal behavior will be disregarded, so that the average molar volume of the mixture, ϱ (liters/mole), will be the sum of the partial molar volumes of the components. It will also be assumed that the columns operate without heat losses and with a plate efficiency of 100%.

TWO-COMPONENT SYSTEMS

Low-boiling Product

In processes in which a high-boiling raw material A is to be converted into a low-boiling product B, the reaction is carried out in the reboiler of a distillation column (Figure 1). Per unit time, F moles of A is fed into the reboiler of the liquid volume V (liters) and an equivalent number of moles, D, of the product B is removed from the condenser at the top of the column. $(L+D)$ moles/min. is evaporated to supply the necessary reflux. The case where $F = D$ and where the reaction follows first-order kinetics will be considered.

$$\left[\frac{d\frac{B_o}{V}}{dt}\right]_{reaction} = \frac{k}{V}(A_o - KB_o) \quad (1)$$

where

A_o, B_o = number of moles in reactor

k = reaction rate constant, 1/min.

K = equilibrium constant

For the steady state in which reaction and distillation are superimposed, the composition of the liquid phase in the reboiler can be calculated (the volume change

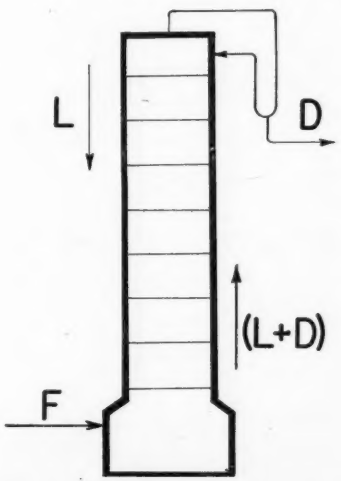

Fig. 1. Mass flow in two-component process with low-boiling product.

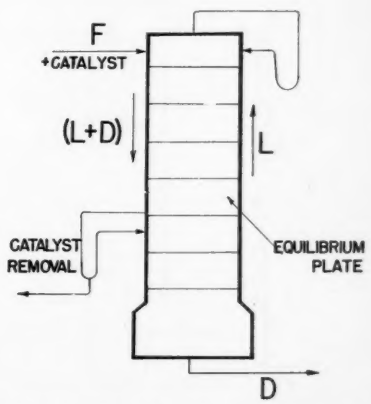

Fig. 1. Mass flow in two-component process with high-boiling product.

*The term *essentially pure* is used to indicate that products of any desired purity can be obtained by increasing the efficiency of the column (reflux, number of plates) without interfering with the principles of the process.

caused by the reaction being disregarded]:

$$\frac{dA_o}{dt} = -\frac{dB_o}{dt} = 0 = k(A_o - KB_o) - Db_n' \qquad (2)$$

b_n' = mole fraction of B in vapor leaving top plate
D = distillate rate = feed rate, moles/min.

This type of process is applicable not only to nonazeotropic systems, but also to systems with a maximum-boiling-point azeotrope, provided that under steady state conditions the mole fraction of B in the reboiler is higher than the azeotropic concentration.

The optimum operating conditions for such a process—i.e., lowest possible steam cost per unit quantity of B at the lowest possible equipment cost—can be calculated on the basis of the following considerations. If L moles/min. is refluxed to obtain D moles/min. of B of the purity b_n', the mole fraction of B in the vapor escaping from the reactor is $b_o' = Db_n'/(L+D)$. From this relationship and from the liquid-vapor equilibrium curve, the mole fraction of B in the reactor, b_o, can then be determined for constant values of D and b_n' but for varying values of L. This in turn makes it possible to calculate the amount of heat necessary to produce D moles/min. of B for various concentrations of B in the reboiler. Such curves—cost of heat per unit quantity of product vs. reactor concentration—are then determined for columns with varying plate numbers and efficiencies.

Rearranging (2), on the other hand, gives

$$k(A_o - KB_o) = Db_n' \qquad (3)$$

and since $b_o = B_o/(A_o + B_o)$, the required liquid holdup of the reactor, and consequently its cost, can thus be determined as a function of b_n'. Finally, heat requirements are compared with equipment cost (investment for column and reactor, maintenance, etc.), e.g., by plotting heat requirements plus equipment cost vs. the latter, in which case the minimum of the curve represents the optimum operating conditions.

High-boiling Product

Reactions of this type may be carried out in columns, not only in nonazeotropic systems but also under favorable conditions in certain minimum-boiling-point azeotropic systems. Such a process for the conversion of A (low-boiling raw material) into B (high-boiling product) by a reaction $nA \rightleftarrows mB$ is schematically shown in Figure 2. The column operates under total reflux, and F moles/min. of A, together with the catalyst, is fed into the top plate, while the equivalent number of moles of B, D, with a purity of b_o, is drawn off from the bottom. The plate on which the liquid composition is closest to that corresponding to chemical equilibrium is referred to as *equilibrium plate*. Since below the equilibrium plate the composition will exceed chemical equilibrium and the reverse reaction would predominate, it is necessary to remove or neutralize the catalyst from the liquid overflowing from this plate. To supply the necessary reflux, L moles is evaporated from the reboiler per unit time.

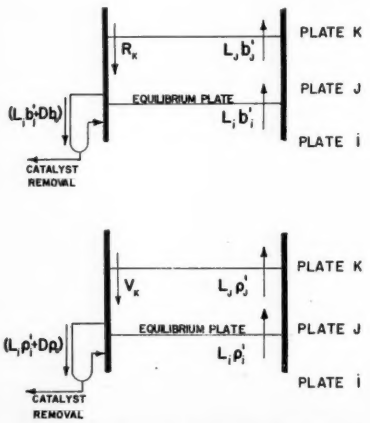

Fig. 3. Mass flow on equilibrium plate.

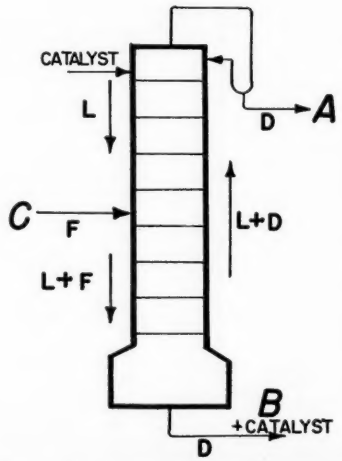

Fig. 4. Mass flow in three-component process: $2C \rightarrow A + B$.

Theoretically the same type of process could be used for reactions leading to low-boiling products. The catalyst would then be fed into the equilibrium plate and the raw product into the reboiler, and the product would be removed from the top of the column. But in this case a technical difficulty arises in that a liquid volume equal to that of the reflux from the lowest plate has to be drawn off from the reboiler per unit time and the catalyst removed from it to avoid a build-up in catalyst concentration. This catalyst circulation will most likely make the cost of this type of process for low-boiling products prohibitive.

If the composition of the liquid or vapor phase on one plate, e.g., the desired product purity, b_o, is known, the composition of the liquid phase on the other plates can be calculated from the process parameters (feed rate, reflux, reaction rate and equilibrium constants, liquid-vapor equilibrium curve, etc.). Any of the known graphical or plate-to-plate calculation methods can be used for the lower part of the column up to the equilibrium plate. A somewhat modified method, allowing for the chemical reaction, has to be used for the calculation of the composition of the reflux coming from the plate above the equilibrium plate (Figure 3). Since under steady state conditions the number of moles on the plate remains constant, R_k moles has to be refluxed onto the equilibrium plate per unit time, where

$$R_k = L_j b_j' + (L_i b_i' + Db_o) - L_i b_i' - \Delta B_j \text{ (moles } B\text{/min.)}$$

$$= L_j b_j' + Db_o - \Delta B_j \text{ (moles } B\text{/min.)} \qquad (4)$$

The subscripts refer to the plates from which liquid or vapor originates; ΔB_j = number of moles of B formed per minute on plate j owing to reaction; b = mole fraction of B in liquid; b' = mole fraction of B in vapor. On the other hand, the volume of reflux V_k onto the equilibrium plate is calculated upon the condition that there is no volume change under steady state conditions:

$$V_k = L_j \rho_j' + (L_i \rho_i' + D\rho_o) - L_i \rho_i' - m\Delta B_j \rho_B + n\Delta B_j \rho_A \text{ (liters/min.)}$$

$$= L_j \rho_j' + D\rho_o + \Delta B_j (n\rho_A - m\rho_B)$$

(liters/min.) (5)

Reaction rate constants
for $2A \rightarrow B$ (second-order reaction) $k_1 = 0.002$ liter/(mole) (min.)
for $B \rightarrow 2A$ (first-order reaction) $k_2 = 0.2$ 1/min.
Throughput 0.5 (moles B/min.)
Applied heat 30 kcal./min.
Liquid holdup of plates 1.0 liter
Product purity ($=b_o$) 0.99
A constant separation factor of $\alpha = 20$ is assumed.

Compounds	A	B
Density	0.7	0.9 kg./liter
Boiling point	60	165 °C.
Heat of vaporization	5.4	9.6 kcal./mole
Molecular weight	58	116

ρ_r = average molar volume of liquid on rth plate in liters/mole

---

Plate number	b	b'	Remarks
Reboiler	0.99	0.83	
1	0.85	0.22	
2	0.29	0.02	
3	0.10	0.005	Catalyst is removed
4 (Reaction plate)	0.09	0.005	between third and
5 (Reaction plate)	0.07	0.004	fourth plate
6 (Reaction plate)	0.06	0.003	
7 (Reaction plate)	0.03	0.001	

ρ_r' = average molar volume of condensate of vapor escaping from rth plate; ρA, ρB = molar volumes of A and B, respectively

The number of moles of B contained in V_k is obtained by multiplying (5) by b_k/ρ_k; this product then equals (4):

$$R_k = \frac{b_k}{\rho_k}\left[L_j \rho_j' + D\rho_o + \Delta B_j (n\rho_A - m\rho_B)\right] = L_j b_j' + Db_o -$$

$$\Delta B_j \text{ (moles } B\text{/min.)} \quad (6)$$

Rearrangement gives

$$\frac{b_k}{\rho_k} = \frac{L_j b_j' + Db_o - \Delta B_j}{L_j \rho_j' + D\rho_o + \Delta B_j (n\rho_A - m\rho_B)}$$

(moles/liter) (7)

from which b_k can be calculated easily, because b_k/ρ_k is a simple function of b_k. Essentially the same procedure is used for the other reaction plates.

To demonstrate the separation effects that can be expected from such a combination of distillation and reaction, a numerical computation was carried out for a hypothetical reaction $2A \rightleftarrows B$, where the properties of A and B and the the process parameters were selected as follows:

Plate-to-plate calculation as outlined above gave the following composition of liquid and vapor phases on the plates of the column:

Reactions of this type have so far been carried out in batch processes. As the results of the calculation indicate—a comparison of the heat requirements for this and a comparable batch process would go beyond the scope of this paper—such reactions can, at least theoretically, be carried out advantageously in a continuous process.

THREE-COMPONENT SYSTEMS

A considerably larger number of systems come under consideration if three compounds participate in the reaction. Depending on the boiling points of products and raw materials, six general types of three-component reactions are possible, only one of which will be considered here. Compounds A and B are produced from C, the boiling point of C being higher than that of A but lower than that of B. The reaction $2C \rightleftarrows A + B$ is carried out in a column where F moles/min. of C is fed into the proper plate in the middle part, and D moles/min. each of essentially pure A and B is removed from top and bottom, respectively. The catalyst is fed into the top plate and is removed together with B from the reboiler. The amounts of liquid and vapor, in moles/min., participating in the mass transfer in the column are shown in Figure 4. To simplify calculations, it will be assumed that there is no deviation from ideal behavior in the liquid-vapor equilibrium in the system A-B-C and that the reaction follows the simple kinetics:

$$\left[\frac{d\frac{A}{V}}{dt}\right]_{reaction} = k_1 \frac{C^2}{V^2} - k_2 \frac{AB}{V^2}$$

where A, B, and C are the number

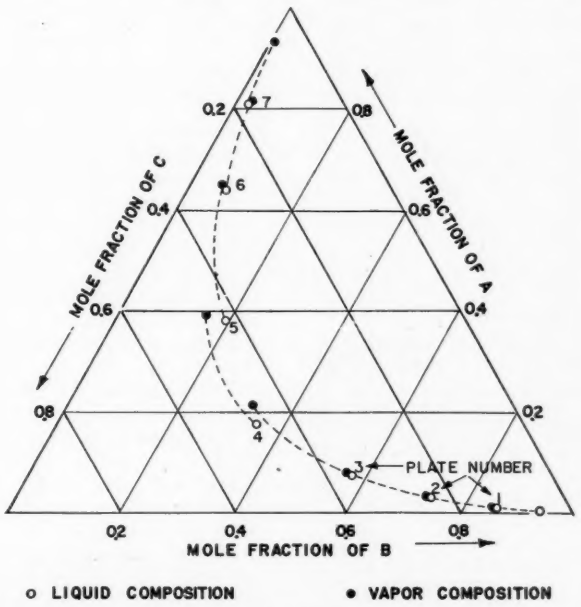

Fig. 5. Composition of liquid and vapor for three-component process: $2C \rightarrow A + B$.

of moles of the reactants and V is the liquid volume. To determine the composition of the reactant mixture on the various plates, a plate-to-plate calculation based on the same considerations as those leading to Equations (4) through (7) is carried out, starting with the desired composition of the bottom product. The composition of the reflux into the reboiler is again computed on the basis of constancy of volume and composition under steady state conditions:

$$A_o + B_o + C_o = \text{const.}:$$

$$R_1 = (L_o + D)\, a_1' + Da_o - \Delta A_o \qquad \text{(moles } A\text{/min.)} \qquad (8)$$

$$V_o = \text{const.}:$$

$$V_1 = (L_o + D)\, \rho_1' + D\rho_o - \Delta V_o \qquad \text{(liters/min.)} \qquad (9)$$

ΔA_o = number of moles of A formed by reaction/min.

ΔV_o = change in volume (liters/min) caused by reaction

Multiplication of Equation (9) by a_1/ρ_1, b_1/ρ_1, and c_1/ρ_1, respectively, and equating these expressions with (8) gives the composition of the reflux in moles/liter:

$$\frac{a_1}{\rho_1} = \frac{(L_o+D)\, a' + Da_o - \Delta A_o}{(L_o+D)\, \rho_o' + D\rho_o - \Delta V_o} \qquad \text{(moles } A\text{/liter)} \qquad (10a)$$

$$\frac{b_2}{\rho_1} = \frac{(L_o+D)\, b_o' + Db_o - \Delta A_o}{(L_o+D)\, \rho_o' + D\rho_o - \Delta V_o} \qquad \text{(moles } B\text{/liter)} \qquad (10b)$$

$$\frac{c_1}{\rho_1} = \frac{(L_o+D)\, c_o' + Dc_o + 2\Delta A_o}{(L_o+D)\, \rho_o' + D\rho_o - \Delta V_o} \qquad \text{(moles } C\text{/liter)} \qquad (10c)$$

from which the molar fractions can easily be calculated because of $a_1 + b_1 + c_1 = 1$. To let the reaction proceed in the desired direction, ΔA has to be > 0; this can be accomplished by proper choice of a_o, b_o, and c_o.

For a numerical calculation, the following physical data and reaction parameters were assumed:

Reaction rate constants

for $2C \rightarrow A + B$	$k_1 = 0.008$		liters/(mole) (min.)
for $A + B \rightarrow 2C$	$k_2 = 0.004$		liters/(mole)(min.)
Liquid hold-up of plates	1.6		liters
Applied heat	40		kcal./min.
Feed	1.0		moles of C/min.

Compounds	A	B	C	
Density	0.7	0.8	0.8	kg./liter
Molecular weight	78	106	92	
Boiling point	80	140	110	°C.
Heat of vaporization	6.8	8.0	7.3	kcal./mole

Liquid-vapor equilibrium data are based on the system benzene/toluene/xylene (*3*).

Plate-to-plate calculations gave the following results:

Plate	Liquid composition			Vapor composition			Δ	$\Sigma\Delta A$
	a	b	c	a'	b'	c'	(moles A/min.)	
0 (reboiler)	0.00^5	0.93	0.06^5	0.01	0.85	0.14	0.002	0.002
1	0.01	0.85^5	0.13^5	0.03	0.72	0.25	0.011	0.013
2	0.03	0.73	0.24	0.08^5	0.55	0.36^5	0.036	0.049
3	0.07^5	0.56^5	0.36	0.21	0.32	0.47	0.088	0.137
4 (feed plate)	0.17^5	0.34^5	0.48	0.39	0.15	0.46	0.164	0.301
5	0.38	0.19	0.43	0.64^5	0.05^5	0.30	0.126	0.427
6	0.63^5	0.06^5	0.30	0.82	0.02	0.16	0.056	0.483
7	0.81^5	0.02	0.16^5	0.93	0.002	0.06^5	0.016	0.500

These data are also shown in Figure 5. It deserves mentioning that, if no reaction takes place, the same number of plates is required if products of the same purity are to be distilled from a mixture of a corresponding composition. In other words, the reaction requires no additional cost—in equipment and operation—over the mere distillation. On the other hand, two columns instead of the one used in this process are required if pure C is allowed to react in a separate reactor and products of the same purity are to be obtained by distillation of the equilibrium mixture.

Similar processes can be devised for other suitable three-component systems. Whether or not such a process can be developed for a given system depends primarily on its liquid-vapor diagram. Under favorable conditions, it should be possible to react azeotropic systems by using the chemical reaction itself to overcome the azeotropic concentration.

Application of this type of process is of course not limited to two- or three-component systems. But as the complexity of the system increases, the calculation becomes increasingly difficult. Not only will it in most cases be necessary to work with more complex kinetical expressions and to consider deviations from ideal behavior with regard to density, vapor-phase composition, etc., but the uncertainty inherent in the experimental determination of reaction rate constants and liquid-vapor diagrams also tends to make the value of such calculations questionable. Whether or not the expenditures—in terms of experimental work and calculation time—for a detailed computation of such a process in a system with four or more components can be justified or not will then ultimately depend upon the economic importance of the products.

NOTATION

A, B, C = number of moles of compounds A, B, C in reactor

a, b, c = mole fractions of compounds A, B, C in liquid

a', b', c' = mole fractions of A, B, C in vapor

D = distillate rate, product draw-off rate, moles/min.

F = feed rate, moles/min.

K = equilibrium constant (chemical equilibrium)

k = reaction-rate constant, 1/min. or liters/(moles)(min.)

L = evaporation rate, moles/min.

R = reflux rate, moles/min.

V = liquid holdup of reactor, liters

V = reflux rate, liters/min.

α = relative volatility

ρ = molar volume of liquid, liters/mole

ρ' = molar volume of condensate, liters/mole

Subscripts refer to the plate from which vapors or liquids originate.

LITERATURE CITED

1. Berman, S., H. Isbenjian,, A. Sedoff, and D. F. Othmer, *Ind. Eng. Chem.*, **40**, 2139 (1948).
2. Burghart, L. M., U. S. patent 1,491,076 (April 22, 1924).
3. Kirschbaum, E., "Destillier—und Rectifiziertechnik," p. 33, Springer-Verlag, Berlin (1950).
4. Leyes, C. E., and D. F. Othmer, *Trans. Am. Inst. Chem. Engrs.*, **41**, 157 (1945).
5. Steffens, J. A., U. S. patent 1,433,308 (Oct. 24, 1922).

Kinetics of the Methane-steam Reaction

W. W. Akers and D. P. Camp, The Rice Institute, Houston, Texas

A kinetic study was made of the reaction of steam and natural gas over a reduced nickel catalyst at a temperature range of 637° to 1,180°F.

The rate of reaction is first order with respect to methane. The effect of temperature could be expressed by an Arrhenius type of equation. Both carbon monoxide and carbon dioxide are formed as primary reaction products.

The reaction of methane and steam has assumed a position of major importance as a source of hydrogen and as a synthesis gas for oxygenated derivatives such as alcohols, aldehydes, and ketones as well as high-molecular-weight hydrocarbons. The reforming of methane with steam followed by the Fischer-Tropsch synthesis provides a possible path for conversion of methane to higher hydrocarbons.

Numerous investigators have studied the catalytic reactions for the oxidation of methane with steam and with metal oxides (*2, 7, 9, 11, 12*) and the thermal decomposition of methane (*4, 5, 6, 10, 13, 14*), and various catalysts have been developed (*3, 7*). The reverse reaction has been studied extensively at the lower temperatures by several investigators (*1, 8, 15*). However, a kinetic study of the catalytic reaction of steam and methane has not been reported. The present study is concerned with the determination of the effect of the composition on the rate of reaction of steam and natural gas on a reduced nickel catalyst at a temperature of approximately 1,180°F. and 1 atm. pressure.

APPARATUS

A diagram of the apparatus is shown in Figure 1. In order to facilitate the description of the apparatus, it will be considered as in operation. Distilled water was fed from a constant-head source through a needle valve and a capillary orifice into the preheater, which consisted of a 1-in. pipe containing porous-clay chips; the pipe was inserted in a small electric furnace. The natural gas passed through a dry test meter to a small compressor equipped with a needle-valve by-pass arrangement. The compressor was operated only at high flow rates. The steam from the preheater then mixed with the natural gas and was admitted directly into the reactor.

The reactor consisted of a piece of 2-in. pipe with a welded connection at the upstream end and a blank flange at the downstream end inserted in a 2-kw. electric furnace. Passing through the blank flange was a ⅛-in. pipe to which was welded a small cup fitted with a screen upon which the catalyst was placed. A ¼-in. steel tube was also inserted in the blank flange to serve as a thermowell. A chromel-alumel thermocouple was placed in the thermowell immediately above the catalyst bed and a second thermocouple was placed in the center of the screen on the same level as the single layer of catalyst.

Upon entering the reactor the gases passed from the 2-in. pipe downward through the catalyst bed and out the ⅛-in. pipe to a water-cooled condenser. The condensate was removed continuously by a U-tube drain and weighed. The saturated product gases passed on through a sampling cock and then to a wet test meter.

The arrangement of the catalyst in the reactor was unique in that radiant heat supplied the energy necessary for the highly endothermic reaction. The catalyst bed was approximately 1.5 in. wide and 3.5 in. long. The bed was centered in the 2-in. pipe which formed the reactor wall. Thus the catalyst was exposed to radiant heat on all sides. It is believed that temperature variation in the bed was at a minimum.

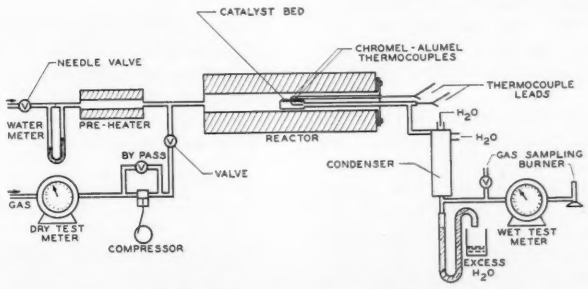

Fig. 1. Diagram of apparatus.

EXPERIMENTAL PROCEDURE

After the condenser and the thermocouple leads were disconnected, the flange was uncoupled and the catalyst assembly was removed from the reactor tube. A weighed amount of catalyst was placed on the screen. The area of the screen opening was varied by the use of sheet metal so that the catalyst completely covered the open area with a single layer. The catalyst assembly and connections were then placed back in the reactor.

The reactor then was brought up to temperature and the feeding of water begun. The water feed rate was adjusted prior to the introduction of the gas. For a series of runs the water feed rate was held constant while the natural-gas feed rate was varied to the desired feed compositions. Constant conditions were maintained for ½ hr. before sampling was begun. The rate of flow of gas through both meters, the water flow rate, the rate of water condensing from the product gases, and the temperatures of the gases in the catalyst bed were recorded. The product gases were analyzed according to standard procedures (*16, 18*). The carbon dioxide was determined by absorption in potassium hydroxide solution; the carbon monoxide and hydrogen by oxidation over copper oxide at 300°C.; the oxygen by absorption in Pyrogallol solution. The amounts of oxygen obtained were sufficiently small to be neglected. The ethane and heavier hydrocarbons in the product gases were not present in sufficient quantity to be detected by high-temperature oxidation techniques. Hence the gas remaining after carbon monoxide and hydrogen removal was taken as methane in all runs.

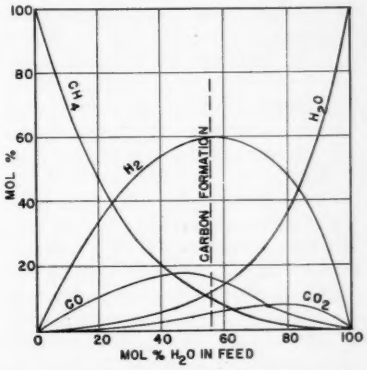

Fig. 2. Product equilibrium composition of methane-steam reaction at 1180°F.

MATERIALS

The catalyst used in this investigation was furnished by the Harshaw Chemical Company. It was a reduced nickel catalyst supported on Kieselguhr. The catalyst pellets were 1/8-in. cylinders. The bulk density was 93 lb./cu.ft. The composition of the natural gas is given in Table 1.

TABLE 1.—COMPOSITION OF NATURAL GAS

Component	Mole%
CO_2	00.80
CH_4	91.09
C_2H_6	5.02
C_3	1.85
iC_4	0.29
nC_4	0.24
nC_5	0.10
N_2	0.51
	99.90

EXPERIMENTAL RESULTS

The thermodynamic relationships of the methane-steam reactions fix within rather narrow limits the temperature for a kinetic study. At temperatures below 1,100°F. the equilibrium conversion of methane is so low that the reaction has little practical interest. As the temperature is increased, the conversion increases, but the possibility of forming carbon is also greatly enhanced. At temperatures above 1,800°F. the feed gas must contain a large excess of steam in order to prevent carbon formation and thereby limit greatly the range of composition that may be studied. For these reasons a temperature of approximately 1,180°F. was chosen. At this temperature feed compositions containing up to 42 mole % methane can be used without encountering conditions that are thermodynamically favorable to carbon formation; moreover, the equilibrium conversion of methane is high.

The experimental data for this investigation may be grouped into five series, each run within a series having the same feed composition. The first four series were obtained at a temperature of approximately 1,180°F. The fifth was run over the temperature range of 637° to 1,180°F. in order to determine the effect of temperature on the reaction. The data for the five series are presented in Table 2. The reaction time for the methane is directly proportional to the amount of catalyst and inversely with the methane feed rate. This reaction time is expressed as a time factor, defined as the weight of the catalyst divided by the feed rate of the natural gas expressed as moles per hour.

TABLE 2.—PARTIAL PRESSURES AT VARIOUS TIME FACTORS

Temperature, 1,180° F.

Run	Time factor	Partial pressure of products (atm.) CH_4	H_2O	CO_2	H_2	CO
100	0.00	0.089	0.911	0.000	0.000	0.000
101	1.49	0.079	0.865	0.010	0.046	0.001
102	2.94	0.069	0.839	0.013	0.079	0.002
103	4.47	0.060	0.812	0.023	0.103	0.003
104	5.96	0.052	0.793	0.028	0.127	0.004
105	11.42	0.032	0.698	0.041	0.220	0.009
106	8.90	0.041	0.712	0.036	0.204	0.007
200	0.00	0.167	0.833	0.000	0.000	0.000
201	0.74	0.149	0.749	0.016	0.083	0.003
202	1.47	0.120	0.722	0.022	0.132	0.005
203	2.23	0.111	0.668	0.035	0.178	0.008
204	2.98	0.096	0.621	0.046	0.227	0.011
205	5.71	0.055	0.498	0.070	0.353	0.024
206	6.12	0.062	0.487	0.067	0.361	0.024
300	0.00	0.222	0.777	0.000	0.000	0.000
301	0.49	0.199	0.668	0.020	0.108	0.005
302	0.99	0.162	0.623	0.029	0.175	0.011
303	1.49	0.151	0.575	0.043	0.223	0.012
304	1.99	0.134	0.523	0.050	0.274	0.019
305	3.81	0.161	0.355	0.076	0.458	0.050
306	5.86	0.044	0.353	0.078	0.480	0.045
307	6.12	0.071	0.343	0.076	0.466	0.044
400	0.00	0.280	0.720	0.000	0.000	0.000
401	0.37	0.245	0.605	0.022	0.128	0.008
402	0.74	0.198	0.544	0.033	0.208	0.017
403	1.12	0.193	0.512	0.040	0.236	0.019
404	1.49	0.173	0.468	0.047	0.289	0.024
405	5.86	0.062	0.247	0.077	0.545	0.071
406	6.12	0.070	0.230	0.078	0.560	0.063

Time factor = 2.98 for entire 500 series

	Temperature, °F.					
500		0.256	0.744			
501	637	0.239	0.719	0.009	0.033	0.000
502	749	0.218	0.635	0.026	0.114	0.007
503	842	0.197	0.552	0.042	0.205	0.005
504	943	0.158	0.504	0.054	0.272	0.012

In order to determine the effect of time on the activity of the catalyst, one run was made over a period of 6.5 hr. the temperature and feed rates being held constant. Samples of the product gas were analyzed periodically. During this period no change in the product-gas composition was noted. Since the catalyst was not in use more than 5 hr., the activity of the catalyst is assumed to be constant for all runs at the same temperature.

A component material balance was made for each of the runs. The average deviation for the carbon, hydrogen, and oxygen was 4.9%. The maximum deviation was 15.1%. In general, fewer atoms of carbon were measured in product gas than in the reactants, indicating that carbon was deposited in the reactor. However the hydrogen and oxygen balance did not necessarily substantiate this. No traces of carbon were observed in the reactor after a series of runs. Since the deviations were random in nature, showing no trend with composition or contact time, it is believed that they represent experimental error.

THERMODYNAMIC ANALYSIS

The over-all reaction of methane and steam to form carbon, carbon monoxide, carbon dioxide, and hydrogen may be represented by the following six equations:

$$CH_4 + H_2O \rightleftharpoons CO + 3H_2 \quad (1)$$

$$CH_4 + 2H_2O \rightleftharpoons CO_2 + 4H_2 \quad (2)$$

$$CH_4 \rightleftharpoons C + 2H_2 \quad (3)$$

$$CO + H_2O \rightleftharpoons CO_2 + H_2 \quad (4)$$

$$CO_2 + CH_4 \rightleftharpoons 2CO + 2H_2 \quad (5)$$

$$2CO \rightleftharpoons C + CO_2 \quad (6)$$

The heats and free energies of reaction for these six as computed by Wagmon et al.(*17*) were used. Using these values at 1,180°F. for reactions (1), (2), (4) and (5), the authors computed the equilibrium composition of the product gases for various feed compositions. The resulting composition diagram is shown in Figure 2. Then by means of these compositions, reactions (3) and (6) were checked to determine whether carbon might be present in an equilibrium mixture. With less than 58 mole % water in the feed, carbon may be deposited. At higher water concentrations carbon would not be present in an equilibrium mixture. This does not imply that carbon will not be formed when methane and steam react at concentrations greater than 58% water, merely that the equilibrium mixture will not contain carbon. As the reactions proceed to equilibrium, it is quite probable that carbon formation will be favored thermodynamically at one or more points along the way.

In order to determine the possible directions of the six reactions, the difference in free energy between the actual product composition and the equilibrium value for each of the six reactions was computed for the runs. The calculations indicated that

1. For all runs reactions (1) and (2) are proceeding to the right, approaching equilibrium at the longer contact times.

2. Reaction (3), if proceeding, will go to the right. However, several points taken at high contact time indicate the tendency for the reaction to reverse. This suggests that the reaction is proceeding at an extremely slow rate, or not at all.

3. In most of the runs reaction (4) has a tendency to go to the right. Points with higher inlet methane concentrations and longer contact times indicate a tendency to go to the left. This suggests that reaction (4), if proceeding, is going at a much slower rate than the reactions.

4. In all cases reaction (5) has a tendency to go to the right and reaction (6), to the left.

On the basis of these thermodynamic calculations, reactions (1) and (2) are the primary reactions and reaction (5) may be a secondary reaction. If reaction (4) is proceeding, the rate is slower. If carbon is formed, it is caused by the cracking of methane. However, it is probable that any carbon formed by reaction (3) would be consumed by the reverse of reaction (6).

In order to verify that both reactions (1) and (2) are primary reactions, the moles of carbon dioxide per mole of methane reacted for each series are plotted vs. time factor in Figure 3. The extrapolation of these curves to zero time factor indicates the initial products of reaction. From the plot it is evident that both carbon dioxide and carbon monoxide are primary reaction products. If either had been formed as a result of a secondary reaction [reaction (4)], the curves would have intersected the ordinate at unity or zero. The carbon dioxide is being formed at an initial rate of two to nine times the rate of carbon monoxide formation, depending on the inlet composition.

KINETIC ANALYSIS

If the reaction rate, r, is expressed as the moles of methane reacting per unit weight of catalyst per unit time, the relationship for a steady-flow system between conversion, weight of catalyst, and feed rate can be expressed:

$$-F\,dx = r\,dW$$

where

F = methane feed rate, moles/hr.
x = conversion, moles of methane reacted/mole of methane in feed
W = weight of catalyst
r = reaction rate, moles/unit weight of catalyst/unit time

This equation may be rearranged to give

$$r = -\frac{dx}{d\left(\frac{W}{F}\right)} = -\frac{d\frac{(CH_4)}{(CH_4)_F}}{d\,(T.F.)} \quad (1)$$

where T.F. is the time factor, weight of catalyst/mole of methane fed/hr.

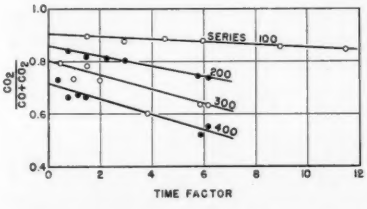

Fig. 3. Product-distribution plot.

In this study natural gas rather than pure methane was used because of the industrial interest in the reforming of natural gas to produce hydrogen. However, at even the shortest contact times none of the heavier hydrocarbons could be detected in the product gases. Thus the data constitute a kinetic study of the rate of reaction of methane. It was not possible to measure the rates of reaction of the heavier components by the techniques employed in this work; however, the presence of the components does not affect the study of the methane reaction.

If the moles of methane that have reacted per entering mole of methane are plotted vs. the time factor, the slope of the curve represents the rate of reaction at the conditions existing at that point. Although the method of slopes is, in general, subject to considerable error, the slope at the origin can be determined with a high degree of accuracy. This slope is the initial rate of reaction. The initial rate is dependent only upon the entering feed composition at a specified temperature and total pressure.

This analysis indicated that the initial rate of reaction was directly proportional to the partial pressure of methane; that is,

$$-\frac{d\frac{(CH_4)}{(CH_4)_F}}{d\,(T.F.)} = k p_{CH_4} \quad (2)$$

In order to determine whether the reaction rate was first order at appreciable concentrations of product, Equation (2) was integrated to give

$$-\int \frac{d\frac{(CH_4)}{(CH_4)_F}}{p_{CH_4}} = k\,(T.F.) \quad (3)$$

and the integral data used for correlation. The over-all reaction can be completely described by reactions (1) and (2) if no carbon is formed. In each of these reactions the change in the total number of moles per mole of methane reacted is two. The value of the integral of Equation (3), therefore, is independent of the relative amounts of carbon monoxide and carbon dioxide. Hence, a general plot of the integral vs. the fraction of methane converted for each of the four inlet compositions could be prepared without specific knowledge of the product composition. When the fraction of

methane converted from the product analysis was obtained, the corresponding value of the integral was read from the curve and plotted vs. the time factor. If the reaction is first-order over the whole range of compositions, the resulting curve would be a straight line with a slope equivalent to k, the reaction velocity constant. This plot is given in Figure 4. The data define a straight line quite well. The points not falling on the curve are at very low concentrations of methane, where small analytical errors are greatly magnified.

The rate of reaction being directly proportional to the methane partial pressure suggests two possible mechanisms as the rate-controlling step: (1) the mass transfer of the methane to the catalyst surface and (2) a first-order reaction, either the chemisorption of the methane on the active centers of the catalyst or the decomposition of the adsorbed methane to form free radicals. Of the two mechanisms, only the rate of mass transfer is dependent on the gas velocity through the catalyst bed. Since the diffusivities of methane, carbon dioxide, carbon monoxide, and water are of the same order of magnitude, it is not probable that the rate of diffusion of only one, methane, would be rate controlling. In order to check the effects of mass transfer, several runs were made in which the gas velocity through the bed was doubled but at the same time factor as the previous runs. For these runs the reaction velocity constant increased 10 to 15%, as compared to a theoretical increase of over 50% if mass transfer alone were rate controlling, thus indicating that mass transfer may have an appreciable effect. However, the reaction is highly endothermic, and an increase in gas velocity might quite easily result in an increased temperature at the catalyst surface, thus increasing the rate of reaction. It was not possible to make a systematic study of the effect of gas velocity in this experimental set-up. Consequently the only conclusion that can be drawn is that the gas velocity through the bed does have a slight effect on the rate of reaction and this effect is possibly due to mass transfer.

A first-order rate process would describe both the chemisorption of methane and the decomposition of the chemisorbed methane. In the former the rate of adsorption is directly proportional to the partial

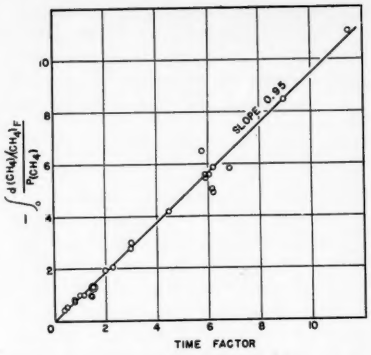

Fig. 4. First-order integral rate vs. time factor.

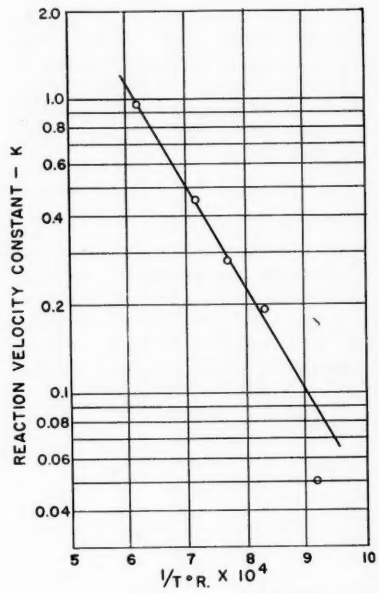

Fig. 5. Reaction-velocity constant vs. reciprocal of absolute temperature.

pressure if the surface is sparsely covered with methane. For the latter case the partial pressure of methane would be proportional to the concentration of the chemisorbed methane, since the adsorption step could be assumed to be at equilibrium. This first-order process is in agreement with the kinetics of the decomposition reaction of methane. Kassel(*10*) found that the thermal decomposition was first order and that the rate-controlling step was probably the reaction

$$CH_4 \rightleftarrows CH_2 + H_2$$

Moreover, the decomposition of higher hydrocarbons is generally first order for both thermal and catalytic reactions.

The reaction velocity constants can be expressed as a function of temperature by the Arrhenius equation

$$\frac{d \ln k}{dT} = \frac{Ea}{RT^2} \qquad (4)$$

or in the integrated form

$$k = Ae^{-\frac{Ea}{RT}}$$

where Ea is the apparent energy of activation for the reaction.

A series of runs was made at a constant-feed composition and a constant-time factor over the temperature range of 637° to 1,180°F. in order to measure the effect of temperature on the reaction velocity constant. The energy of activation, as defined by Equation (4), can be evaluated by measuring the slope of the curve $\ln k$ vs. the reciprocal of the absolute temperature. Such a plot is given in Figure 5. The reaction velocity constant can be represented by the equation

$$k = 127e^{-\frac{15{,}800}{RT}}$$

A kinetic analysis of the data reported by Bischel(*2*) using the same catalyst in a conventional fixed-bed reactor over the temperature range of 900° to 1,100°F. is in excellent agreement with these results.

The energy of activation of 15,800 B.t.u./lb. mole is of the same order of magnitude as that of radical formation for methane decomposition. If mass transfer were rate controlling, the rate constant would have increased less than twofold over the temperature range studied instead of tenfold, as found experimentally.

CONCLUSIONS

The rate of reaction of methane and steam over a reduced nickel is first order with respect to methane. The results indicate that the rate-controlling step is the decomposition of methane. Mass transfer, although not rate controlling, may exert an effect on the rate, but the data were not sufficient to evaluate this effect. Both carbon dioxide and carbon monoxide are primary reaction products, the carbon dioxide being formed from two to nine times faster than carbon monoxide. The water-gas shift reaction, if proceeding at all, is at a much slower rate.

NOTATION

A = constant of integration

Ea = apparent energy of activation, B.t.u./(lb. mole) (°R.)

F = feed rate, moles methane/hr.

T = temperature, °R.

T.F. = time factor, lb. catalyst/mole methane fed/hr.

W = weight of catalyst, lb.

(CH_4) = mole methane

k = reaction velocity constant, moles/(hr.)(lb. of catalyst)(atm.)

pCH_4 = partial pressure of methane, atm.

r = reaction rate, moles/(hr.)(lb. of catalyst)

x = conversion, moles/mole

Subscript

F = feed

LITERATURE CITED

1. Akers, W. W., and R. R. White, *Chem. Eng. Progr.*, 44, 553 (1948).
2. Bischel, K. H., M.S. thesis, Rice Inst. (1949).
3. Bridger, G. L, D C. Gernes, and H. L. Thompson, *Chem. Eng. Progr.* 44, 363 (1948).
4. Cantelo, R. C., *J. Phys. Chem.*, 30, 899 (1926).
5. *Ibid.*, 31, 124 (1927).
6. Gordon, A. S., *Ind. Eng. Chem.*, 38, 718 (1946).
7. Hawk, C. O., H. L. Golden, H. H. Storch, and A. A. Fieldner, *Ind. Eng. Chem.*, 24, 23 (1932).
8. Hightower, F. W., and R. R. White, *Ind. Eng. Chem.*, 20, 10 (1928).
9. Karzhavin, W. A., *Ind. Eng. Chem.*, 28, 1042 (1936).
10. Kassel, *J. Am. Chem. Soc.*, 54, 3949 (1932).
11. Lewis, W. K., E. R. Gilliland, and W. A. Reed, *Ind. Eng. Chem.*, 41, 1227 (1949).
12. Marek, L. F., and D. A. Hahn, "The Catalytic Oxidation of Organic Compounds in the Vapor Phase," Chemical Catalog Company, Inc., New York (1932).
13. Moore, R. L., *Ind. Eng. Chem.*, 24, 21 (1932).
14. Pease, R. N., and P. R. Chesebro, *J. Am. Chem. Soc.*, 50, 1464 (1928).
15. Randall, M., and F. Gerard, *Ind. Eng. Chem.*, 20, 1336 (1928).
16. Scott, Wilfred W., "Standard Methods of Chemical Analysis," 5 ed., D. Van Nostrand Company, Inc., New York (1939).
17. Wagmon, D. D., J. E. Kilpatrick, W. J. Taylor, K. S. Pitzer, and F. D. Rossini, *J. Research, Nat. Bur. Standards*, RD 1634 (1945).
18. White, A. H., "Technical Gas and Fuel Analysis," McGraw-Hill Book Company, Inc., New York (1920).

(Presented at A.I.Ch.E. New York meeting)

Graphical Solutions on Dimensionless-number Plots

Bryant Fitch

Dorr-Oliver, Incorporated, Westport, Connecticut

A graphical method for solving problems involving dimensionless-number plots is presented, and its application demonstrated for the relatively involved case of liquid cyclone scale-up.

Dimensionless-number plots frequently are awkward to use, in that the dependent variable, or unknown, may be contained in more than one of the dimensionless-number groups. In such a case there has been no direct way to solve for the unknown. Before the unknown could be evaluated, roundabout calculations have had to be made in order to locate the appropriate point on the dimensionless-number plot.

By way of example the familiar log-log plot of drag coefficient vs. Reynolds number, shown as Figure 1, may be considered. This relates to the free settling of spherical particles in a fluid. In actual problems which arise the unknown is most frequently either terminal settling velocity u_p or particle size D_p, both of which are included in each of the two dimensionless groups. When either u_p or D_p is unknown, the value for Re cannot be calculated directly, and neither can the value for C_R. Neither coordinate on the dimensionless-number graph, therefore, can be evaluated directly, and further means must be employed to find where on the graph the problem operation should be plotted.

One method for solving sedimentation problems when either u_p or D_p is unknown involves replotting the information of Figure 1 on a graph of Re vs. a new dimensionless function $C_R Re^n$, the exponent n being so chosen that the unknown variable, either u_p or D_p, cancels out of the function. Since the new function does not contain the unknown, it can be evaluated directly. The corresponding value of Re can thus be determined by means of the new graph, and the unknown calculated from the discovered value of Re.

There is also a graphical construction(*1*) for discovering the appropriate value of Re, in which the function

$$\log C_R = -n \log Re + \log C_R Re^n \quad (1)$$

is plotted in Figure 1. Here again the exponent n is chosen so that the unknown cancels from the final term, which can therefore be evaluated. The intersection of the plot of Equation (1) with that originally constituting Figure 1 locates the required Re value, namely, Re', from which the unknown can be calculated.

Neither of the methods described provides a graphical element to measure the value of the unknown. In this paper the graphical method will be elaborated to permit representing the unknown directly, and the particular utility of the method will be demonstrated in connection with solid-liquid cyclone scale-up problems.

GRAPHING AS A VECTOR ADDITION

Graphing, at least in Cartesian coordinates, may be regarded as a

vector addition. Each variable on a graph has been assigned not only a scale, but also a direction. Thus the value of each variable is represented in the graph by a vector. To plot a point (*see Figure* 2), one combines these chart vectors in typical vector fashion, starting at the origin. The outer end of the resultant is marked by the plotted point. In this view the axes are essentially only markers showing the direction and scale of the corresponding chart vectors.

The major variables of Figure 1 are C_R and Re. Each comprises several original or subordinate variables, three of which, namely, u_p, D_p and ρ_f, are included in each of the major variables. It can be shown that a chart direction and scale exist for each of the subordinate variables and further that a point which is plotted by summing the chart vectors for the two major variables (the normal plotting

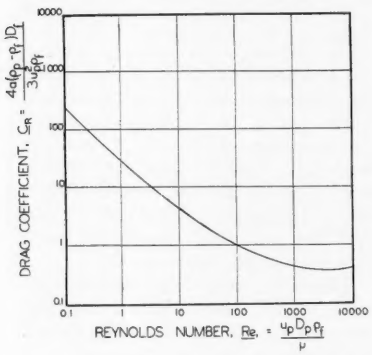

Fig. 1. Drag coefficient vs. Reynolds number for settling particles.

of C_R vs. Re) may also be plotted by summing chart vectors corresponding to the subordinate terms comprising them. By way of example it will be demonstrated that there exists a direction and scale corresponding to the variable u_p.

When u_p is eliminated between equations defining C_R and Re, it follows that

$$\log C_R = -2 \log Re + \log \frac{4a\,(\rho_p - \rho_f)\,D_p^{\,3}\,\rho_f}{3\mu^2} \qquad (2)$$

[This is Equation (1) with a value of 2 for the exponent n.] As the scales of Figure 1 are logarithmic, it will be seen that (2) is the equation of a family of straight lines with a slope of —2, the position of which depends upon the value of the parameter $4a(\rho_p - \rho_f)\,D_p^{\,3}\rho_f/(3\mu^2)$. As u_p is varied with all other subordinate variables held constant, the plotted point must always move along a straight line with a slope of —2. Therefore there is a chart direction corresponding to changes in value of the variable u_p.

There must be a scale corresponding to u_p proportional in module to that of Re, so that its projection upon the Re axis has the same module as the Re scale. This follows from the definition $Re = u_p D_p \rho_f/\mu$. If u_p is increased by a given factor (log u_p increased by a given amount and other variables held unchanged), then Re must change by the same factor (log Re increases by the same amount).

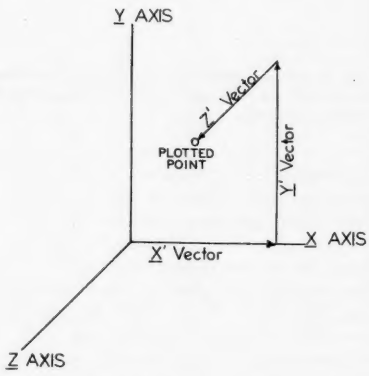

Fig. 2. Plotting as a vector operation.

As a chart direction and scale may be assigned to u_p, it may be represented by a chart vector and an axis drawn indicating this direction and scale.

In an analogous manner it can be shown that there exists a D_p axis with a slope of +1, and a ρ_f axis with a slope of —1, both having scales which when projected upon the Re axis are commensurable with the Re scale. [Note that ρ_f and $(\rho_p - \rho_f)$ are treated as though independent of one another; that is, the ρ_f chart vector will not take into account any change produced in the variable term $(\rho_p - \rho_f)$. This is treated as a separate entity.] The $(\rho_p - \rho_f)$ and a axes coincide in direction and scale with the C_R axis, as these variables do not appear in Re. The constant term 4/3 conventionally introduced into C_R must also be measured in this direction. The μ axis has the same scale module as that of Re but is rotated 180° from the Re axis.

Subordinate axes have been added on the conventional C_R vs. Re plot in Figure 3. Chart vector summations are shown for a set of values of subordinate variables (variables having values less than 1 and hence a negative log value are shown with dotted lines) and also for the corresponding values of the major variables. The two summations have the same resultant point. It will probably be obvious that they must but, if desired, this can be verified by summing projections of the subordi-

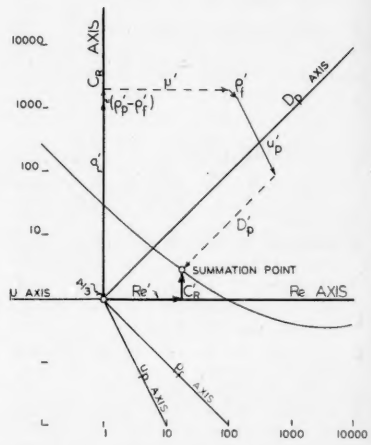

Fig. 3. Summation of major and subordinate vectors.

nate vectors along each of the major axes in turn. Summing the projections of the subordinate variable vectors along the Re axis and remembering that the thus-projected log scales of each of the subordinate vectors have the same module as the log Re scale except that the log μ scale is reversed makes it obvious that

$$-\log \mu' + \log \rho_f' + \log u_p' + \log D_p'$$

should be equal to log Re', which it is by identity.

The same method, taking into account the slopes of the various subordinate vectors, will show that the C_R coordinate of the subordinate vector summation must equal the sum of the projections of the subordinate vectors along the C_R axis.

In order to plot an unambiguous relationship between major variables, it is necessary that any plotted point be uniquely resolved into the chart vectors which were combined to locate the point. Therefore the direc-

tions or axes assigned to the different major variables must each have at least one directional component which is not shared by any of the others. This limits the number of major variables which can be fully plotted to the number of dimensions available for the graph. Points cannot be uniquely resolved into subordinate chart vectors, however, since these share graph dimensions.

Since the chart vectors for major variables always start at the coordinate zero on the corresponding scale, the coordinate of the terminal point measures the magnitude of the variable. Chart vectors for subordinate variables need not start at zero on their respective scales, and so the coordinate of the terminal point does not determine the length of the chart vector and therefore does not in itself determine the magnitude of the variable.

GRAPHICAL SOLUTION BY COMPLETING VECTOR ADDITION

The idea of subordinate vectors can be used to determine directly and graphically the value of any one of the subordinate or original variables if the values of all the others are specified.

The summation of chart vectors must always terminate on an appropriate C_R vs. Re curve. Also the chart vectors may be combined in any order to give the same summation point. Therefore, if all but some one of the subordinate chart vectors are combined, the point located by this partial or incomplete summation will be off the curve by an amount determined by the magnitude and direction of the missing chart vector. The value of the missing variable is measured directly by the distance from the incomplete summation point to the curve in the direction assigned to the missing variable. This permits solving graphically for any one of the variables if the others are known.

Example. If the unknown or dependent variable is particle size D_p, the coordinates of the summation point for all variables except D_p would be determined. The component of the summation incomplete by D_p in the C_R direction is equal to log $4a(\varrho_p - \varrho_f)/(3u_p^2\varrho_f)$, which is log C_R'/D_p. The component in the Re direction is log $u_p\varrho_f/\mu$, which is log Re'/D_p. The closing vector corresponding to D_p starts at this incomplete summation point, extends along the D_p vector direction with a slope of $+1$, and terminates on the curve at point C_R', Re', the values of which can be read directly from the log scales provided on the respective axes. The value of log D_p is then measured by the length of the closing vector, but since the projection of the D_p scale on the Re axis is commensurate with the Re scale, the scale length of the D_p vector can actually be determined from the Re coordinates; that is, the value of Re' is read from the log scale on the Re axis, and the value of Re'/D_p has already been determined. Obviously $D_p = Re'/(Re'/D_p)$.

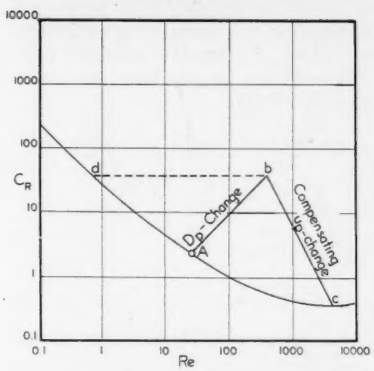

Fig. 4. Solution by compensating "change vectors."

SOLUTIONS BY COMPENSATING "CHANGE VECTORS"

A type of problem to which the proposed graphical solutions are particularly applicable arises in scale-up operations. In such cases the behavior of a model system is known. When the value of one or more variables in the operation are changed, there must be a compensating change in one or more of the others. It is desired to evaluate this compensating change.

On the graphical constructions, when one variable is changed by a fixed factor, its vector is changed by a corresponding fixed length, since log (variable $\times$ factor) = log (variable) + log (factor). The change factor itself can be considered as contributing a vector which is to be added to the vector representing the original value of the variable. Such "change vectors" may be manipulated in the constructions as independent entities.

A change in the value of any one variable in an operation, by a given factor, adds a corresponding "change vector" to the summation point lying on the curve of the dimensionless-number plot. Compensating "change vectors" must then also be added corresponding to compensating changes in one or more of the other variables, in order to bring the summation point back onto the curve. The magnitude of these compensating changes can be evaluated from the lengths of the corresponding change vectors.

Example. Point A in Figure 4 represents a certain known sedimentation operation. The size of the particles is to be increased by a factor of z. This adds a D_p-change vector Ab in the D_p direction of such length that Re_b is z times Re_A. If this is to be compensated by a change in settling rate u_p, as it would be if the properties of the fluid and particles remained the same, then the compensating u_p-change vector to return to the curve would be bc drawn parallel to the u_p axis. Because of the previously discussed projection relationships, the length of the u_p change vector corresponds to a change in u_p by a factor of Re_c/Re_b.

Alternatively, if the change in particle size were to be compensated instead by a change in viscosity of the liquid μ, then the compensating μ-change vector would be bd, and the viscosity would have to be changed (because of the reversed scale of μ) by a factor Re_b/Re_d.

SCALE-UP BY COMPENSATING VECTORS

The use of compensating vectors for scale-up will be illustrated by showing how the method might be used to predict the change in particle-size separation produced in liquid-solid or hydraulic cyclones when the size or scale of the cyclone is changed. In setting up the calculations, many assumptions have to be made concerning the flow patterns in cyclones. There will be no attempt in this paper to justify any of the cyclone assumptions, since the object is to present the graphical methods and the purpose of bringing in cyclone problems is purely to demonstrate the graphical methods.

In a cyclone new feed is injected tangentially at the periphery of the unit and is displaced inward toward the axis in a spiral path. The solid particles are subjected to a centrifugal force generated by the tangential components of flow and an opposing centripetal drag force resulting from the inward radial components of flow. Solids which develop a sufficiently high setting rate under the influence of the centrifugal field are flung against the bounding walls of the cyclone, from whence they are swept toward the apex of the conical end in a current induced by the drag of the walls. There they are discharged as a concentrated suspension through an apex opening. Solids developing insufficient settling rates to overcome the radial components of flow toward the axis are dragged by the fluid in toward the axis of the cyclone. They exit as a partially clarified overflow through a cylin-

drical duct or "vortex finder" concentric with the axis in the flat, or nonconical, end of the cyclone.

As the fluid spirals inward from the periphery and approaches the radius of the vortex finder, its tangential velocity increases in accord with the principles of vortex action. The increasing tangential velocity, combined with the decreasing radius of revolution, results in a rapid increase in the centrifugal force tending to make the solids settle toward the wall. At the same time the radial components of flow tending to drag particles into the overflow are also increasing, owing to the convergence of flow as radial distance from the axis is diminished.

In a conventional liquid-solid cyclone the balance of these centrifugal and drag forces on particles is such that the resultant tendency to settle toward the wall is greater at smaller distances from the axis.

It is now assumed that the particle classification in a cyclone takes place at a size D_{ps} which has at the radius of the vortex finder a settling velocity u_{ps} equal in magnitude to the radial flow component u_r, since particles settling more rapidly at this radius could not be dragged within it and thence into the overflow. It is also assumed that the radial flow velocity component is constant at all points having a radial distance from the axis equal to the radius of the vortex finder. Thus the developments to follow will treat particles of the diameter of separation and flow conditions at the surface of an imaginary cylinder which is within the cyclone, concentric with the axis, and of the same diameter as the vortex finder.

Scale-up will be treated as the sum of two operations each of which can be represented by a change vector in the particle C_R vs. Re chart. These are, first, a scale-up of the system at constant cyclone Reynolds number in which the pressure drop across the cyclone will be allowed to change to maintain the constant Re_{cyc}, and, second, a change of cyclone pressure drop back to the original value.

As a first step, it will be shown that a change in pressure drop across a cyclone can be represented by an appropriate change vector in the particle C_R vs. Re chart. If pressure drop p is the only cyclone variable changed independently, ϱ_p, ϱ_f, and μ will not be affected by the change. If D_{ps} is designated the compensating variable, it is not varied in determining the p-change vector. Thus the effect of changing p is to be evaluated in terms of changes in the remaining variables, a and u_{ps}. Under the specified conditions for a cyclone pressure change vector,

since

$$C_R = \frac{4a\,(\rho_p - \rho_f)\,D_{ps}}{3u_{ps}^2\,\rho_f}$$

by definition

$$C_R \propto a/u_{ps}^2 \qquad (3)$$

since ϱ_p, ϱ_f, and D_{ps} are not varied and since

$$Re = \frac{u_{ps}\,D_{ps}\,\rho_f}{\mu}$$

by definition

$$Re \propto u_{ps} \qquad (4)$$

since ϱ_f, μ, and D_{ps} are not varied.

But

$$a \propto u_c^2 \qquad (5)$$

centrifugal force at radius of vortex finder

And at any given point in a cyclone, assuming uniform distributions of radial flow components,

$$u_r \propto q \qquad (6)$$

According to the measurements of Kelsall(4) in a given cyclone,

$$u_c \propto q^{1.115} \qquad (7)$$

empirical relationship

$$p \propto q^{2.14} \qquad (8)$$

empirical relationship

$$a \propto u_c^2 \propto q^{2.23} \propto u_r^{2.23} \qquad (9)$$

from (5), (6), and (8)

In accordance with the assumption, u_{ps} is to be equal in magnitude to u_r at the radius of the vortex finder. At this radius

$$C_R \propto u_r^{2.3}/u_{ps}^2 = u_{ps}^{2.23}/u_{ps}^2 = u_{ps}^{0.23} \qquad (10)$$

from (3) and (9)

$$C_R \propto Re^{0.23} \qquad (11)$$

from (10) and (4)

From (11) it follows that log C_R varies as 0.23 log Re when changes in cyclone pressure drop cause variations in a and u_{ps}. This defines a direction on the particles C_R vs. Re chart.

A scale corresponding to the effect of changing p may be derived as follows:

$$Re \propto u_{ps} \propto q \propto p^{1/2.14} \propto p^{0.47} \qquad (12$$

from (4), (6), and (8)

or log Re varies as 0.47 log p along a pressure-change vector. Thus an axis can be drawn on a particle C_R vs. Re chart showing the direction and scale of a p-change vector. Provided that the model operation can be plotted on the C_R vs. Re curve, the effect of a change in cyclone operating pressure can be represented by the corresponding p-change vector, and its effect on separation size evaluated from a compensating D_{ps}-change vector.

The next step will be to show that the effect of scaling up the size of a cyclone at constant cyclone Reynolds number can also be represented by a corresponding change vector on the particle C_R vs. Re chart.

To the extent that gravitational forces may be disregarded in cyclone operation, the flow patterns in geometrically similar cyclone systems will be kinematically similar, with corresponding motions for corresponding particles, if operated at the same cyclone Reynolds number. In such cyclone systems, separation particle size would scale up in the same proportions as cyclone size. Therefore the change vector for cyclone size scale-up at constant cyclone Re_{cyc} would be equal and opposite in direction to that for D_{ps}-change.

To maintain constant cyclone Reynolds number with constant fluid properties, velocity must decrease by the same change factor as the linear scale increases, as $Re_{cyc} = D_c u \varrho_f/\mu$

where

D_c = linear scale of cyclone
u = velocity at any given location
Re_{cyc} = cyclone Reynolds number

From an energy balance it follows that the operating-head pressure must decrease by the square of the velocity change factor, since with dynamic symmetry, which also obtains at constant Reynolds number, the efficiency of conversion of pressure head to velocity remains constant. Thus when the cyclone is scaled up in size by a factor of z at constant Reynolds number, the pressure p drops by a factor of z^2

As a final step, scale-up of a cyclone at constant pressure may be evaluated as the sum of a scale up at constant Reynolds number, followed by a change in pressure back to its original value. Combining these change vectors analytically gives on a D_c-change vector

C_R varies as $z^{-0.78}$
Re varies as $z^{-0.06}$
Re varies as $C^{0.08}$

These relationships give the scale and direction of a D_c-change vector. Provided that the model operation can be located on the particle C_R vs. Re curve, the effect of a change on cyclone scale can, within the limits of the approximations tacit in the preceding development, be represented by a corresponding D_c-change vector, and its effect on separation size evaluated from a compensating D_{ps}-change vector.

In order to plot the model operation on an appropriate particle C_R vs. Re curve, it has been assumed, rather arbitrarily, that the radial components are distributed uniformly along the cyclone length. The average radial flow velocity at the diameter of the vortex finder was then calculated from cyclone geometry and feed flow. The separation size D_{ps} is known from the model operation, while the density and viscosity of the suspending liquid, water, were used as those of the medium. It will be recognized that this entails many approximations, but it will also be apparent from the shape of the C_R vs. Re curve that a very considerable error in evaluating Re will not change the shape of this vector construction much and hence should not lead to a serious error in scale-up.

Although methods based on the one given have been used successfully in predicting scale-up of liquid cyclones, it should be noted that considerations beyond the scope of this paper enter in most cases. For example, the C_R vs. Re curve shown in Figure 1 is valid only for spherical particles at infinite dilution, where particle diameter is taken as the measure of particle "size" or linear scale. At finite dilutions the curve would follow a different course, because of particle interferences. The curve for irregular particles would follow yet a different course, because of the influence of particle shape on settling rate, and the exact position of the plotted curve will further depend upon just what linear dimension of the particles is taken as a measure of its scale or size. (Dimensional analysis permits use of any characteristic linear dimension.) Thus, as textbooks show, there will be a family of C_R vs. Re plots for varying particle shapes and dilutions. Cyclone scale-up constructions must be built on an appropriate one of the family. Also the particle system

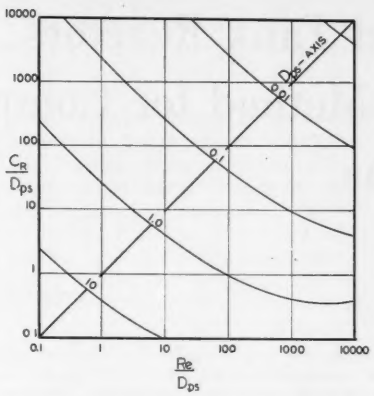

Fig. 5. Parametric representation of D_{ps}.

is usually not scaled up in toto as required for geometric symmetry of the systems, and relative particle size has an effect on separation (3).

PARAMETRIC REPRESENTATION

It often happens, as in cyclone scale-up problems, that some one of the variables will usually appear as the dependent or unknown one. In such cases a parametric representation of this variable is convenient.

If one subordinate variable, such as D_{ps}, has a fixed value, it follows that all summation points incomplete by the vector for this variable will be equidistant from the appropriate C_R vs. Re curve in a direction corresponding to that of the chart vector for the missing variable. The locus of all incomplete summation points for a given value of D_{ps} is therefore a curve of the same shape as the C_R vs. Re curve, but displaced along the D_{ps} axis by a distance corresponding to the fixed value of D_{ps}.

The summation of all variables except D_{ps} gives a component in the C_R direction (on a log scale) which is equal to that of C_R/D_{ps} and a component in the Re direction equal to that of Re/D_{ps}. Therefore, the locus of all points having a given value of D_{ps} can be plotted on a graph of log C_R/D_{ps} vs. log Re/D_{ps} (Figure 5) for various values of D_{ps} as parameter. The chart of Figure 5 is similar in general principle to the Fontein velocity chart described by Driessen (2) and might be considered a transformation from Fontein's chart. Its merit is that it permits subordinate axes to be assigned to all independent subordinate variables, while Fontein's representation of the same relationship does not. Constructions as previously described can be made on Figure 5 if D_{ps} is the dependent variable, but the length of the compensating D_{ps} vector is here indicated directly by the parametric D_{ps} scale. Obviously analogous parametric charts could be made with any other variable as the dependent one.

NOTATION

(Self-consistent units to be used throughout)

a = accelerating force acting on settling particle
C_R = drag coefficient for settling particle, a dimensionless number equal to $4a(\varrho_p - \varrho_f)D_p/(3u_p^2\varrho_f)$
D_c = linear scale (diameter) of cyclone
D_p = linear scale (diameter) of particle
D_{ps} = linear scale (diameter) of particle at which size separation is made
n = integral exponent
p = operating pressure drop across cyclone
q = feed rate of slurry to cyclone
Re = Reynolds number for settling particles, a dimensionless number equal to $u_p D_p \varrho_f/\mu$
Re_{cyc} = Reynolds number for cyclone, a dimensionless group equal to $D_c u \varrho_f/\mu$
u = any characteristic velocity in a cyclone
u_c = tangential component of flow velocity at any point in a cyclone
u_p = terminal settling velocity of particle
u_{ps} = terminal settling velocity of particle at which size separation is made
u_r = radial component of flow velocity in cyclone at radius of vortex finder
z = scale-up factor
ϱ_f = fluid density
ϱ_p = particle density
μ = fluid viscosity
$\propto$ = varies as

Superscript (′) denotes fixed value for variable.

LITERATURE CITED

1. Brown, G. G., *et al.*, "Unit Operations," p. 79, John Wiley and Sons, Inc., New York (1950).
2. Driessen, M. G., *Am. Inst. Mining Met. Engrs. Tech. Publ.* 2135, New York (1917).
3. Fitch, E. B., and E. C. Johnson, *Trans. Am. Inst. Mining Met. Engrs.*, 10, 304 (1953).
4. Kelsall, D. F., *Symposium on Mineral Processing*, Institution of Mining and Metallurgy (British), London (September, 1952).

Continuous Stirred Tank Reactors: A New Graphical Method for Complex Reactions and Reflux Designs

Olegh Bilous and Edgar L. Piret
University of Minnesota, Minneapolis, Minnesota

The usual graphical CSTR design methods are not adequate for the case of complex reactions involving competing or consecutive steps; therefore graphical design method based on the representation of batch data on a triangular diagram is given and illustrated by several examples. This method does not require a complete analysis of the kinetics of the reaction. Since material balances are easily represented on concentration spaces, the method is especially useful when the design includes recycling, or feed additions along a reactor chain.

Experiments on chemical reactions are most often performed batchwise in the laboratory, and design methods are needed to calculate the requirements for continuous operation. As there are important limitations to the available techniques for graphical design of stirred flow reactors, these methods require further development and clarification.

The available graphical methods (*3, 4, 7, 10*) all assume that a material balance on a single chemical component is sufficient for design purposes and, for instance, allows the complete determination of the outlet-stream composition when the feed-stream composition is known. This is true when the reaction taking place in the vessel is represented by a single relation, such as $A + B \rightarrow C$, but is not true in general when the reaction involves consecutive or parallel steps. It is therefore interesting to analyze in detail the case of consecutive or parallel reactions (which in the following discussion will be called "complex" reactions, as opposed to simple reactions) which are represented by a single relation like $A + B \rightarrow C$.

A graphical design method for the case of complex reactions has been developed as a result of this investigation. The method may be used when only batch data are available. It does not require a complete analysis for kinetics, as do the available algebraic methods (*3, 6, 8*), although a knowledge of the stoichiometry of the reaction is of course necessary. The method is especially suitable when recycles or side streams are used and might be extended to a three-dimensional space representation similar to representations employed for four-component extraction design.

COMPARISON OF BATCH AND CSTR PROCESSES

A reaction may be carried out batchwise or continuously, for instance in a continuous stirred tank reactor. In the batch process the composition of the reacting mixture changes with time, and therefore the reaction rate usually is not constant during the run. In a continuous stirred flow process, on the contrary, the reacting mixture is maintained at a steady state composition through the inflow of fresh feed and the outflow of product. The reaction occurs therefore at constant rate. The concentrations in all parts of the reactor are maintained uniform by sufficient agitation.

Another difference between the two processes concerns reaction time. In a batch run all fractions of the reacting mixture are processed during an equal time. In the continuous stirred flow process the different fractions of feed coming into the reactor do not stay for the same length of time. There is thus a distribution in residence times, the average residence time being the reactor holding time. These differences between the two groups of processes were described in detail long ago(*6, 2*). The viewpoint here is somewhat different, and in the following discussion the first object is to compare the products of a batch process and a continuous stirred flow process operating on the same feed.

A reaction process in which the rate depends on the concentrations of the chemical species involved will be considered. The rate may depend also on a score of other factors such as pressure, temperature, catalysts, ionic strength, and so on. All these other factors shall be assumed identically the same in the batch and continuous stirred tank reactor processes which will be compared.

It is assumed that a certain batch process is in operation, with a process time t and a certain feed introduced in totality at the beginning of the process. The problem may be summarized by the following question: Can one, using a feed of the same composition as the initial batch mixture, design a continuous stirred flow process, with a single tank operating with a holding time θ which will give a product stream of the same composition as the end product of the batch run? This is of course one of the first questions that arise whenever a reaction process is converted from batch to continuous operation. The answer is that such a conversion is possible for simple reactions and some special cases of complex reactions. In such cases there is, as will be seen, a definite relationship between t and θ, the batch process time and the equivalent CSTR holding time. When however the reaction scheme includes consecutive or parallel reactions, which are here called complex reactions, it is found generally that the batch product cannot be duplicated by continuous CSTR operation with the same feed, and thus the equivalent holding time cannot be defined. It is still possible, of course, in many ways to get the batch-product composition with a continuous stirred flow method, but a feed different from the batch process feed would be required.

A reaction described by a single relation, like $A + 2B \rightarrow C$, and proceeding in a batch system can be readily characterized by a degree of conversion $R(t)$ varying with time. Here C_1, C_2, C_3 will be called the concentration of the substances A, B, C at a time t after the start of the batch re-

Olegh Bilous is at present with the Laboratoire Centrale, Service des Poudres, Paris, France.

action and C_{10}, C_{20}, C_{30} the initial concentrations of A, B, C in the batch process feed. The degree of conversion $R(t)$ is defined as

$$R(t) = \frac{C_{10} - C_1}{1} = \frac{C_{20} - C_2}{2} = \frac{C_{30} - C_3}{-1}$$

The three terms on the right are equal because of the stoichiometric relations in the foregoing reaction scheme.

More generally, if one considers the reaction

$$\alpha_1 A_1 + \alpha_2 A_2 + \ldots + \alpha_p A_n \rightarrow \gamma P$$

where reactants A_1, $A_2 \ldots A_n$ contribute to the formation of a product P, one finds that

$$R(t) = \frac{C_{10} - C_1}{\alpha_1} = \frac{C_{20} - C_2}{\alpha_2} = \ldots + \frac{C_{no} - C_n}{\alpha_n} \qquad (1)$$

where, as before C_{10} and C_1 are the concentrations of component A_1 at time zero and at time t.

Such a relation exists for all reactions which are stoichiometrically described by a single relation, that is to say by single irreversible reactions as shown above or single reversible reactions of the type

$$\alpha_1 A_1 + \alpha_2 A_2 + \ldots + \alpha_p A_p \rightleftarrows (-\alpha_{p+1}) A_{p+1} + \ldots + (-\alpha_{p+q}) A_{p+q}$$

The stoichiometric coefficients α_i on the product side are taken as negative in order to keep the form of relation (1) valid for product compounds also.

The criterion which determines whether or not a single function $R(t)$, as defined by Equation (1), will describe the evolution of all components of a batch reaction is of course evident: the rates of reaction for all substances concerned should be proportional to each other during the whole course of the reaction. This condition is satisfied for a reaction like $A + 2B \rightarrow C$, where $dA/dT = (\frac{1}{2}\, dB/2dt) = (-dC/dt)$. It is not satisfied in general for what have been called complex reactions, like the scheme $2A \rightarrow B \rightarrow C + D$.

Since the test of proportionality of rates or of concentration changes is used generally to ascertain reaction stoichiometry, the distinction between the two types of reactions is easily established from analystical laboratory data.

Some reaction schemes involving parallel reactions may exceptionally be described by a single relation like (1). An important case is given by the formation of isomers having the same rate dependence on the reactant concentrations for each isomer.

Time Equivalence for Simple Reactions

If the concentrations present at various times in a batch process are plotted in concentration space, the result is a reaction path starting at the initial concentration point which can be graduated in terms of the reaction time t. A similar path, which will not necessarily coincide with the first, may be obtained by plotting, for different values of the reactor holding time θ, the product concentrations of a stirred flow reactor which receives a feed of the same composition as the initial batch mixture.

Relation (1) states that the reaction path of the batch process for a simple reaction is a straight line in concentration space, its direction parameters being the stoichiometric coefficients $\alpha_1, \alpha_2, \ldots \alpha_p$.

For the continuous stirred flow process, the concentration change across the reactor is given by a mass balance

$$\frac{C_i - C_{io}}{\theta} = \left[\frac{dC_i}{dt}\right]_{batch} \qquad (2)$$

where $[dC_i/dt]_{batch}$ is the reaction rate for component C_i for a batch process at the same composition and physical conditions as the steady state continuous process. Volume changes have been neglected for simplicity of presentation.

For the simple reaction the batch rate is, from relation (1),

$$\left[\frac{dC_i}{dt}\right]_{batch} = -\alpha_i \frac{dR(t)}{dt} \qquad (3)$$

Therefore, from relations (3) and (2) one can write for the CSTR path

$$\frac{C_{io} - C_i}{\alpha_i} = \theta \frac{dR(t)}{dt} \qquad (4)$$

TABLE 1.—TIME EQUIVALENCE FOR SEVERAL SIMPLE REACTIONS

Reaction	Kinetics	Time equivalence
$A \rightarrow P$	$\frac{dA}{dt} = -k$	$k\theta = kt$
$A \rightarrow P$	$\frac{dA}{dt} = -kA$	$k\theta = e^{kt} - 1$
$2A \rightarrow P$	$\frac{dA}{dt} = -kA^2$	$C_o k\theta = C_o kt\,(1 + C_o kt)$
$3A \rightarrow P$	$\frac{dA}{dt} = -kA^3$	$C_o^2\, k\theta = (1 + 2C_o^2\, kt)^{3/2} - (1 + 2C_o^2\, kt)$
$nA \rightarrow P$	$\frac{dA}{dt} = -kA^n$	$C_o^{n-1} k\theta = (1 + (n-1)\, C_o^{n-1} kt)^{n/n-1} - (1 + (n-1)\, C_o^{n-1} kt)$
$A \rightleftarrows B$	$\frac{dA}{dt} = k_2 B - k_1 A$	$(k_1 + k_2)\,\theta = e^{(k_1+k_2)t} - 1$
$\begin{cases} A \rightarrow B \\ A \rightarrow C \end{cases}$	$\frac{dA}{dt} = -(k_1 + k_2)\, A$	$(k_1 + k_2)\,\theta = e^{(k_1+k_2)t} - 1$

NOTE: C_o is the initial concentration of A.

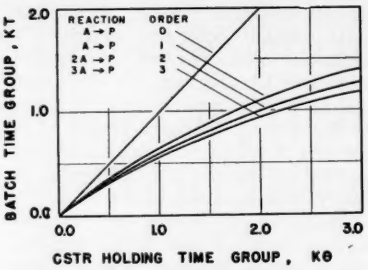

Fig. 1. Time equivalence for simple reactions. (The initial concentration of A is taken as unity.)

And, since (4) can be written for any component in the CSTR,

$$\frac{C_{10} - C_1}{\alpha_1} = \frac{C_{20} - C_2}{\alpha_2} = \cdots \frac{C_{p_0} - C_p}{\alpha_p}$$

But this is the same relation as (1), which describes the batch process path. Therefore the plot of CSTR operation in concentration space for simple reactions is a straight line, which is the same as for the batch process. Hence for the case of simple reactions, the batch product composition may also be obtained by continuous operation. Some general relations for simple reactions readily follow from the foregoing equations. Thus, the relation between the batch process time and the equivalent continuous reactor holding time is obtained from relations (1) and (4):

$$R(t) = \theta \frac{dR(t)}{dt}$$

and therefore

$$\frac{1}{\theta} = \frac{d \ln R(t)}{dt} \qquad (5)$$

The volumetric-CSTR-to-batch-efficiency ratio e, which is defined as the ratio of the amounts of product obtained in the same tank volume in equivalent CSTR and batch processes, may also be expressed in terms of $R(t)$. Assuming no dead time in batch operation, one has

$$e = \frac{Ft}{V} = \frac{t}{\theta} = \frac{t}{R(t)} \frac{dR(t)}{dt}$$

Therefore

$$e = \frac{d \ln R(t)}{d \ln t} \qquad (6)$$

Thus the slope of a log-log plot of concentration vs. time affords a convenient means of rapidly evaluating volumetric efficiencies.

Some examples of the time-equivalence relation (5) are given in Table 1 and plotted on Figure 1. The curves for first-, second-, and third-order reactions lie closely together, especially for low conversion. Rough estimations of time equivalence are therefore possible even when the order of the simple reaction considered is not known.

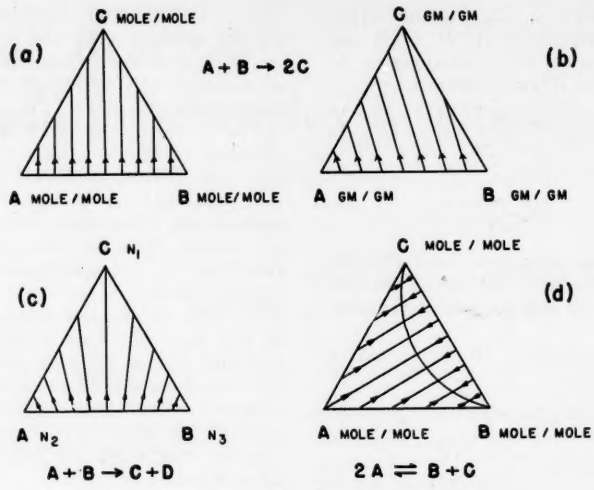

Fig. 2. Reaction paths for simple reactions.

Complex Reactions

When the process involves reactions of the type which have here been called complex, the batch reaction path is no longer described by expression (1), as from the definition of complex reactions the reaction rates for the different substances are no longer proportional to each other.

The path is therefore no longer a straight line. The same holds for the CSTR reaction path. Examples of such cases are given later and show that batch and CSTR reaction paths for the same feed do not coincide in the case of complex reactions. Thus for the case of complex reactions, the batch and CSTR products from a given feed will never have the same composition. This fact should be recognized and duly taken into account in the design of stirred flow reactors operating on complex reactions and in the selection of batch pilot plant data for such a design.

Especially in order to duplicate rate conditions in the projected continuous reactor, batch pilot-plant data should be taken with an initial batch mixture different from the projected CSTR feed. This will be seen from the samples presented.

PLOTTING OF REACTION PATHS

Below are some examples of batch reaction-path plots in concentration space representation. The design method for continuous operation is based on this type of plot.

The representation loses much of its practical interest when the number of independent components considered exceeds two. This allows the consideration of three linearly related components by means of a representation of the triangular diagram type. Usually the plotted quantities will be concentrations, expressed in mole/mole, gram/gram, or moles/liter of reactant mixture. Rectangular coordinates can also be used.

Example 1, Simple Reactions

The reaction $A + B \rightarrow 2C$ will be considered. The diagram of the reaction paths, with concentrations expressed in mole fraction, is shown in Figure 2*a*. The reaction paths are straight parallel lines. The same reaction can be plotted with concentrations in grams/grams of mixture. If it is assumed for instance that the mole weights of A, B, C are proportional to 1, 3, and 2, the diagram takes the form represented in Figure 2*b*.

Another example is the reaction $A + B \rightarrow C + D$, where D is a waste product of no interest, for instance water. Representations may be done in mole fractions on a selected component basis, excluding D. This procedure may be generalized to exclude more than one component. If C_1, C_2, C_3 are the mole fractions of A, B, C on the total basis, then the quantities to plot are

$$n_1 = \frac{C_1}{C_1 + C_2 + C_3}, \quad n_2 = \frac{C_2}{C_1 + C_2 + C_3}, \quad n_3 = \frac{C_3}{C_1 + C_2 + C_3}$$

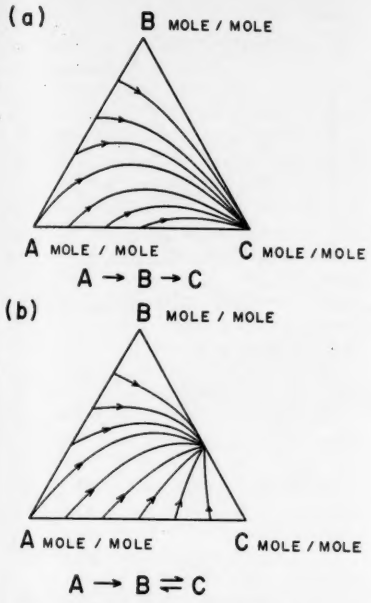

Fig. 3. Batch reaction paths for consecutive reactions.

The paths are given in Figure 2*c*. They converge at the point $n_1 = 1$, $n_2 = 1$, $n_3 = -1$. The existence of such a point is related to the stoichiometry of the reaction. Thus, for the reaction $\alpha A + \beta B \rightarrow \gamma C + \sigma D$ where α, β, γ, σ are the stoichiometric coefficients the coordinates of the common point of the reaction paths are

$$n_1 = \frac{\alpha}{\alpha + \beta - \gamma}, \quad n_2 = \frac{\beta}{\alpha + \beta - \gamma},$$

$$n_3 = \frac{-\gamma}{\alpha + \beta - \gamma}$$

As a last case of simple reactions the scheme $2A \rightleftarrows B + C$ may be examined. This is a reversible reaction, and equilibrium concentrations are related by

$$\frac{[A]^2}{[B]\,[C]} = K$$

This represents an equilibrium line on the diagram, which is given in Figure 2*d*. The reaction paths are still straight, in accordance with the general analysis.

Example 2, Consecutive Reactions

Until now the cases considered gave straight-line paths. The cases presented below are examples of curved paths. For instance the scheme $A \rightarrow B \rightarrow C$ will be considered. The paths plotted on a mole/mole basis are represented in Figure 3*a*. The curvature depends on the ratio of the rate constants in the two reactions.

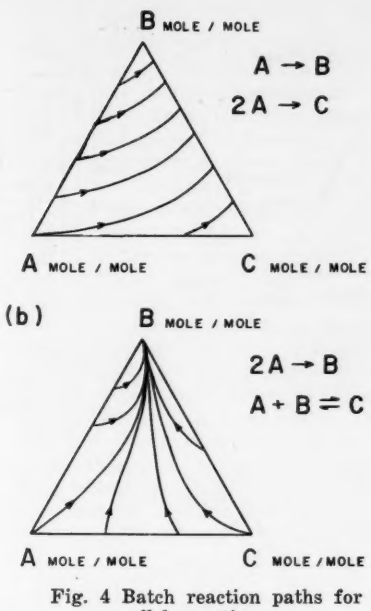

Fig. 4 Batch reaction paths for parallel reactions.

Another example is $A \rightarrow B \rightleftarrows C$. There is an equilibrium point, and the paths are curved (Figure 3*b*). Many variations could be found; however, the main features have been illustrated in Example 1, and the present example brings only the additional characteristic of curvature, which is also found below in the case of parallel reactions.

Example 3, Parallel Reactions

The scheme

$$\begin{cases} A \rightarrow B \\ 2A \rightarrow C \end{cases}$$

where the reactions are assumed to have different orders, is represented in Figure 4*a*.

Another example is the scheme shown in Figure 4*b*,

$$\begin{cases} 2A \rightarrow B \\ A + B \rightleftarrows C \end{cases}$$

GRAPHICAL DESIGN METHOD FOR THE CASE OF COMPLEX REACTIONS

The underlying assumption in the graphical CSTR design methods which have appeared in the literature is that the concentration vs. time plot taken during a batch process for one of the reaction components is enough to characterize the whole reaction.

From the general discussion, however, it appears, that this is true only for those kinetic schemes which have been classified as simple reactions. Eldridge and Piret have already pointed out(*5*) that their stepwise graphical procedure could not be used in all the cases. Instead they recommend an algebraic procedure for certain reaction schemes. A new graphical method can therefore be developed with advantage for the case of complex reactions. Such a method is presented below.

Determination of Product and Feed Compositions

A reaction with curved paths may be represented on a triangular diagram (A, B, C) in terms of the concentrations C_1, C_2, C_3 of the three components of interest A, B, C. The mass balances over a stirred flow reactor of holding time θ operating on the represented reaction are

$$C_1 - C_{10} = \theta \left[\frac{dC_1}{dt}\right]_{batch} \quad (7a)$$

$$C_2 - C_{20} = \theta \left[\frac{dC_2}{dt}\right]_{batch} \quad (7b)$$

$$C_3 - C_{30} = \theta \left[\frac{dC_3}{dt}\right]_{batch} \quad (7c)$$

With times eliminated, these relations may be written

$$\frac{[dC_1]}{C_1 - C_{10}} = \frac{[dC_2]}{C_2 - C_{20}} = \frac{[dC_3]}{C_3 - C_{30}} \quad (8)$$

The geometrical interpretation of these relations is the following. The quantities $[dC_1]$, $[dC_2]$, $[dC_3]$ determine the direction of the tangent to the batch reaction path at the product composition point (C_1, C_2, C_3), and relations (8) mean that the vector which has the projections $C_1 - C_{10}$, $C_2 - C_{20}$, $C_3 - C_{30}$ lies along this tangent. Therefore the feed composition point (C_{10}, C_{20}, C_{30}) lies on the

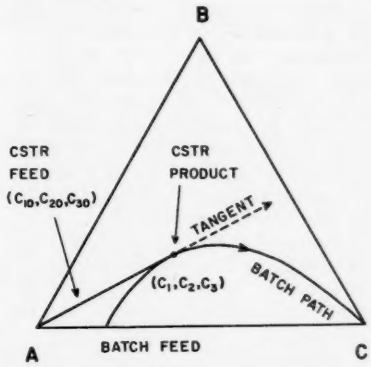

Fig. 5. Graphical CSTR design method.

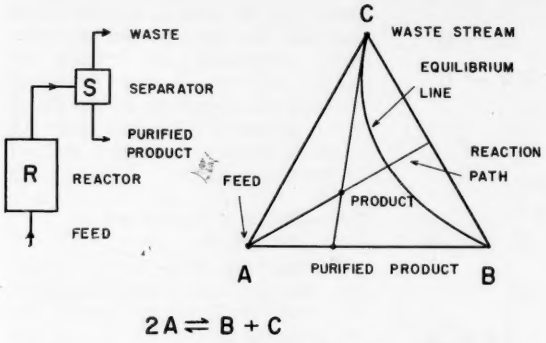

Fig. 6. CSTR design for the reaction $2A \rightleftarrows B + C$ (a single reactor).

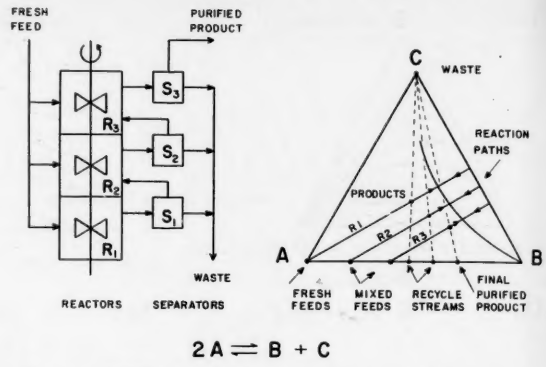

Fig. 8. CSTR design for the reaction $2A \rightleftarrows B + C$ (three reactors with purified product recycling).

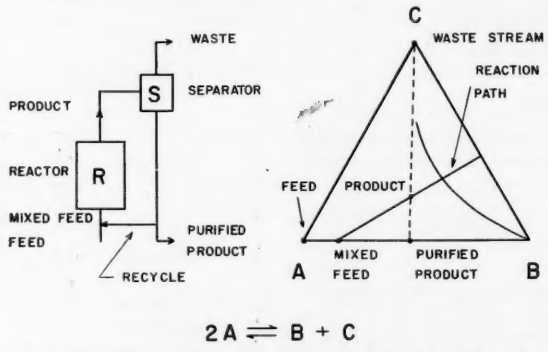

Fig. 7. CSTR design for the reaction $2A \rightleftarrows B + C$ (a single reactor with purified product recycling).

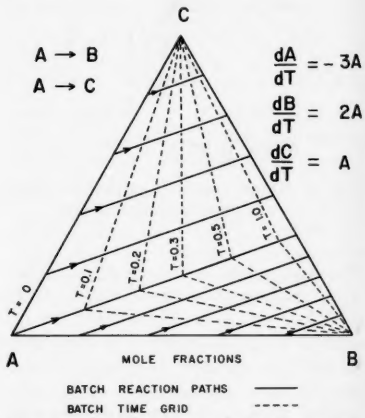

Fig. 9. Example of a batch reaction time grid.

tangent to the batch reaction path going through the desired product composition point (C_1, C_2, C_3).

The construction is illustrated in Figure 5. Actually only points which lie on the backward portion of the tangent are physically acceptable as CSTR feed-composition points. Any feed represented by a point lying on this portion of the tangent may thus be used to obtain the CSTR product of composition (C_1, C_2, C_3).

The construction holds as long as the mass balances (7*a*, *b*, *c*) are valid and generally is not affected by the method of plotting. Linear functions of the concentrations may be plotted instead of the concentrations themselves. The method is valid for instance if plotting is done on a selected-component basis. Thus for a reaction involving compounds *A*, *B*, *C*, *D*, a *D*-free representation of *A*, *B*, *C* in terms of the mole fractions may be used. Such a representation is of interest, however, only if *D*, or other excluded components, has no marked effect on reaction rates.

Holding Times and Reactor Volumes

In this presentation the emphasis has been placed on the concentrations of the different components and not on reaction time. Time dependence of the reaction may be indicated on the plot of the batch reaction paths in two ways.

1. *Indication of Reaction Rate.* Reaction rate for a given component, for instance *A*, may be indicated along the reaction paths. If extensive design is to be made, it may prove interesting to plot the whole grid of equal reaction-rate curves. The CSTR holding time is then obtained from the CSTR mass balance as

$$\theta = \frac{\Delta C_A}{R_A}$$

where ΔC_A is the concentration drop in reactant *A* across the reactor (which is known or which can be measured from the plot) and R_A is the reaction rate for component *A* at the desired CSTR product composition point. R_A may be obtained by interpolation from the rate grid. In this representation it is desirable to choose as components of interest those which most influence the reaction rate.

2. *Indication of Reaction Time.* This representation is less handy but is preferable when only a simple design is needed. Direct laboratory data on reaction time are marked along the batch reaction paths. The rate is then obtained by graphical differentiation of the batch curve only at the points where it is needed for design. The CSTR mass balance is then used as above for the calculation of the holding time. Again, in the case of extensive design, it may prove interesting to plot the whole grid of the equal reaction-time curves, the starting points being chosen for instance along the sides of the triangle.

ILLUSTRATIONS

The foregoing procedures may be illustrated by a few examples.

When design is concerned with simple reactions only, the triangular plots presented here are not necessary and other methods may be applied as well. Still even in these cases the triangular plot may be helpful for the presentation of data, especially when the design involves recycles or side streams, in close analogy with the methods

in use in solvent-extraction and separation processes.

In the case, already examined, of the reaction $2A \rightleftarrows B + C$, it may be assumed that C is a waste product which can be easily separated from the reacting mixture. It may be profitable then to recycle the purified product stream containing A and B only, in order to increase the conversion of A and the concentration of B in the reactor effluent. If the holding time proves too high, a series of reactors might be used, with side-stream addition of A and subtraction of C. The following designs are illustrated: a single reactor with product purification (Figure 6), a single reactor with recycling of purified product (Figure 7), and a series of three reactors with intermediate purification (Figure 8).

As an example of a time grid and also of a case of parallel reactions which have straight paths, Figure 9 shows two parallel first-order reactions:

$$A \rightarrow B, \text{ with } k_1 = 2$$

$$A \rightarrow C, \text{ with } k_2 = 1$$

Initial compositions are taken along two sides of the triangle. The time grid is represented by straight lines. Rates calculated from the equations of reference (*1*) have been used to illustrate the case of a rate grid. Figure 10 represents the monosulfonation of benzene. The rate is indicated in grams/gram of mixture/hour of benzene–sulfonic acid formed at 140°C. under 1 atm. of benzene. The components indicated are sulfuric acid, water, and benzene–sulfonic acid. Since the reaction paths are plotted on a selected component basis (benzene is excluded), the paths converge at a certain point.

In Figure 10 and in some subsequent figures an equilateral triangular plot has not been used simply to illustrate the point that of course other coordinates and representations of concentration space can be equally well used for the graphical procedures presented here.

Several cases of reaction schemes with curved reaction paths are presented below. In the case of the reaction $A \rightleftarrows B \rightarrow C$ with all reactions first order, the rate constant of the first forward reaction is $k_1 = 3$, the reverse rate is $k_2 = 2$, and the second forward reaction has a rate $k_3 = 2$. The paths are presented in Figure 11. To show the difference between batch reaction paths and CSTR reaction paths, a CSTR reaction path corresponding to an initial feed of pure A has been indicated.

It is seen from the figure that if B is the product of interest, the CSTR process will always give a lower concentration of B in its product than the batch process operating on the same feed.

If B is the product of interest, then a CSTR design where C is totally recycled will prevent any new formation of this waste component. Similar designs are possible whenever a waste compound is in equilibrium with a useful compound, provided that separation is economically feasible. Such an example is given in Figure 12 for the reaction $A \rightarrow B \rightleftarrows C$ with total recycling of C. Another instance where recycling may prove useful occurs for the case of reaction intermediates. The recycling of reaction intermediates maintains their concentration at the steady state value and prevents their loss in the effluent.

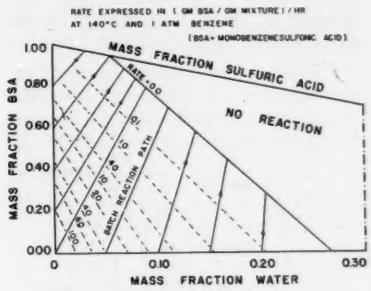

Fig. 10. Example of a rate grid [monosulfonation of benzene(*1*)].

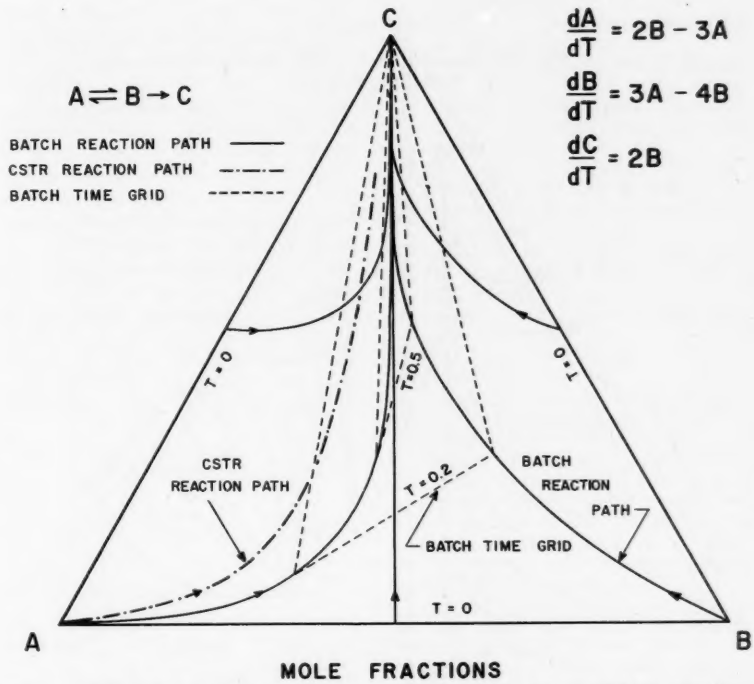

Fig. 11. Example of CSTR and batch reaction paths for a complex reaction.

TABLE 2.—GRAPHICAL DESIGN OF A STRAIGHT CSTR CHAIN

(Data from Figure 13)

	Tank 1			Tank 2			Tank 3			Tank 4		
	A	*B*	*C*	*A*	*B*	*C*	*A*	*B*	*C*	*A*	*B*	*C*
Feed composition, mole %	100	0	0	48.5	25	26.5	25.5	20.5	54	14	13	73
Product composition, mole %	48.5	25	26.5	25.5	20.5	54	14	13	73	5	5	90
Rate of production of *C*	50 moles/hr.			41 moles/hr.			26 moles/hr.			10 moles/hr.		
Increase in *C*	26.5 moles			27.5 moles			19 moles			17 moles		
Holding time	0.53 hr.			0.67 hr.			0.73 hr.			1.70 hr.		

Figure 13 shows the design of a straight chain of four continuous stirred tank reactors on the reaction $A \rightleftarrows B \rightarrow C$ the rate expressions of which are given in Figure 11. Table 2 shows the graphical data taken from Figure 13. The holding times are calculated as the ratio of the concentration increase of C across the reactor to the rate of production of C. This rate is proportional in the example to the mole fraction of B. For illustrative purposes the rates have been multiplied by 100, times being expressed in hours.

As a last example and somewhat of a generalization of the method, the case of a copolymerization reaction will be considered. The two monomers are styrene (S) and β chlorethylacrylate (A).

The differential equation of the batch reaction paths is, from reference (9),

$$\frac{dS}{dA} = \frac{S}{A}\,\frac{r_1 S + A}{S + r_2 A} \qquad (9)$$

with

$$r_1 = 0.59$$

$$r_2 = 0.08$$

The quantities plotted in Figures 15 and 17 are the mole percentage of monomers S and A and of monomers polymerized. Other ingredients of the reactive emulsion, such as catalyst, soap, and water, are not considered. The rate of this reaction is practically independent of monomer concentrations and may be assumed in the example to be 10 mole % of monomer converted/hr. The reaction paths, calculated from Equation (9), are presented in Figure 14.

Since polymer composition varies with the composition of the generating monomer mixture, according to Equation (9), which is plotted

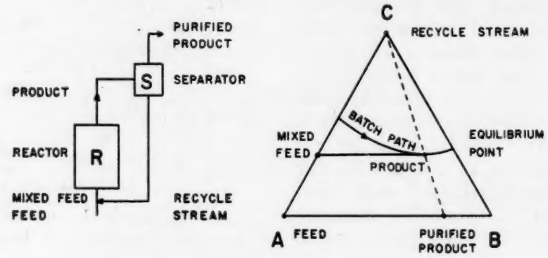

Fig. 12. Example of a CSTR design with recycling of waste.

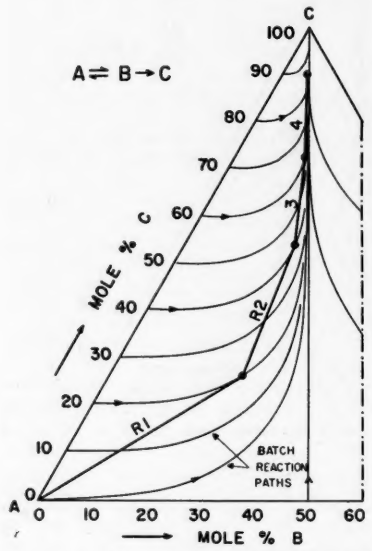

Fig. 13. Design of a straight chain of four CSTR's for the reaction $A \rightleftarrows B + C$.

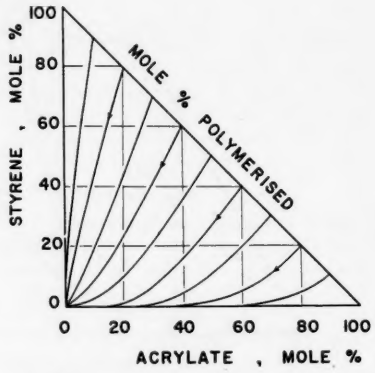

Fig. 14. Batch copolymerization reaction paths.

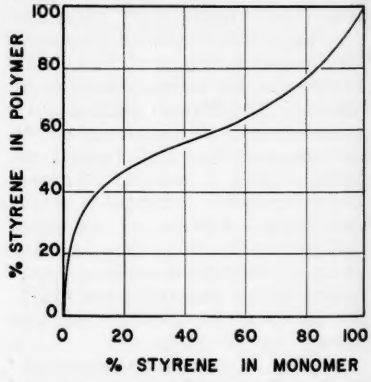

Fig. 15. Polymer-vs.-monomer-composition ratios for a copolymerization reaction.

TABLE 3.—GRAPHICAL DESIGN OF A CONTINUOUS COPOLYMERIZATION PROCESS

(Data from Figure 16)

	Tank 1				Tank 2				Tank 3				Tank 4			
Data	Moles/hour	S%	A%	P%	Moles/hour	S%	A%	P%	Moles/hour	S%	A%	P%	Moles/hour	S%	A%	P%
Side stream	0	0	0	0	8.3	100	0	0	8.7	100	0	0	5.8	100	0	0
Total feed	100	22.3	77.7	0	108.3	12.9	47.2	39.9	117.0	10.4	30	59.6	122.8	7.2	15.7	77.1
Product	100	5.7	51	43.3	108.3	3.6	32.3	64.1	117.0	1.83	16.5	81.7	122.8	0.55	5	94.5
Conversion of monomer feed		43.3%				40.3%				54.7%				76%		
Holding time based on monomer		4.33 hr.				4.03 hr.				5.47 hr.				7.6 hr.		

on Figure 15, it may be of interest, for example, to reduce viscosity and to control mixing or to design a chain of stirred low reactors with the same S/A monomer ratio in each vessel. As an illustration it may be assumed that one wishes to operate at a 10 mole % styrene concentration in the monomer, which yields from the plot of Figure 15 a polymer product with 38% styrene, 62% acrylate. The reactant mixture will be depleted in styrene, and therefore additional styrene side streams to each reactor are necessary. A final product containing 94.5% polymer is desired. The design for a chain of four reactors operating under such conditions, presented in Figure 16, is given as an example. Only the monomer and polymer flows have been determined, since they are the most important. Once these flows are determined, the other ingredients such as water, soap, and catalyst are added in known proportions, and the volume of the necessary tanks may be calculated. Thus, if one wishes to use tanks of equal size, a trial-and-error design should be made. Tabulated data from the graphical design of Figure 16 are presented in Table 3. Side-stream flows are calculated from a mass balance on styrene.

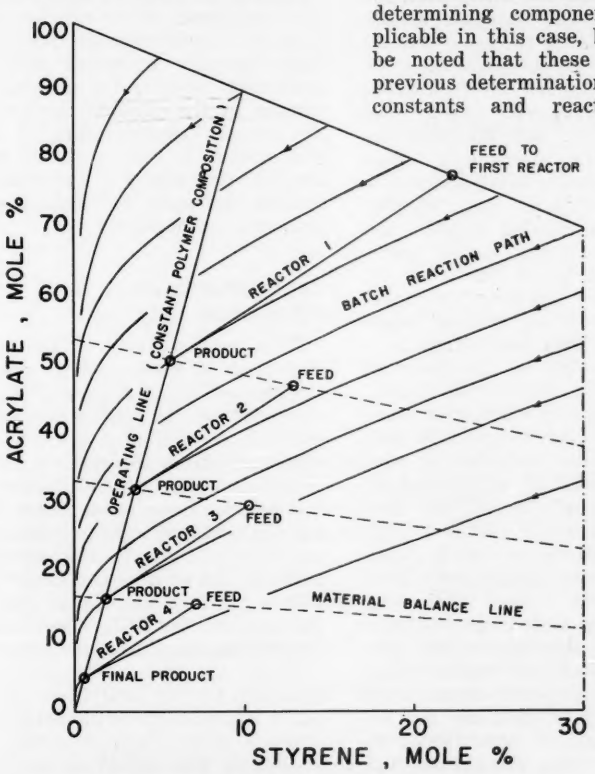

Fig. 16. Design of a CSTR chain for a copolymerization reaction.

CONCLUSIONS

In this development the difference between batch and CSTR processes has been carefully examined from the viewpoint of product compositions.

It was found that for single reversible or irreversible reactions and some special cases of parallel reactions the product compositions given by the two methods of operation from the same feed were comparable and an equivalence could be defined between batch process time and CSTR holding time. On the contrary, for complex reaction schemes, generally represented by consecutive and parallel reactions, the complete product compositions for the two processes are essentially different and no simple time equivalence could be defined. Thus for these complex reactions, adjusting the holding time in a CSTR does not result in the same product compositions obtained in a batch reactor.

This difference calls for a special graphical design method for the case of complex reactions, where the usual graphical methods (*4, 7, 10*) are not valid. Of course the algebraic methods previously presented (*3*), which are based upon the simultaneous solution of material balances on the several rate-determining components, are applicable in this case, but it should be noted that these require the previous determination of the rate constants and reaction orders. These last are obviously not always easily accomplished and hence the advantage of the graphical method.

A graphical method valid for complex reactions was developed on the basis of the representation of the reaction paths in concentration space. Triangular and other representations can be employed. The method is useful especially when side streams or recycles are involved and when the reaction can be sufficiently described in terms of two independent concentrations.

LITERATURE

1. Crooks, R. C., and R. R. White, *Chem. Eng. Progr.*, **46**, 249 (1950).
2. Denbigh, K. G., *Trans. Faraday Soc.*, **40**, 352 (1944).
3. Eldridge, J. W., and E. L. Piret, *Chem. Eng. Progr.* **46**, 290 (1950).
4. Jones, R. W., *Chem. Eng. Progr.*, **47**, 46 (1951).
5. Leclerc, V. R., *Chem. Eng. Sci.*, **2**, 213 (1953).
6. MacMullin, R. E., and J. Weber, Jr., *Trans. Am. Inst. Chem. Engrs.*, **31**, 409 (1935); see also *Chem. and Met. Eng.*, **52**, 101 (May 1945).
7. Provinteev, I. V., *Zhur. Priklad. Khim.*, **24**, 807 (1951).
8. Schoenemann, K., *Dechema Monographien*, **21**, 203 (1952).
9. Wall, F. T., C. J. Delbecq, and R. E. Florin, *J. Polymer Sci.*, **9**, 177 (1952).
10. Weber, A. P., *Chem. Eng. Progr.*, **49**, 26 (1953).

APPENDIX

Prediction of Continuous Stirred Tank Reactor Performance from Batch Reaction Data on Complex Reactions

Several batch reaction paths starting with various feed combinations are drawn on triangular coordinates. These paths are obtained by plotting the concentrations at different times of the three most important components of the reaction.

On this chart CSTR performance can be predicted. Beginning at the feed composition to be used in the continuous operation, any straight line is drawn, which is tangent to the one of the above-mentioned reaction paths. The coordinates found at the tangent point correspond to the composition of the CSTR product stream. The required holding time, and therefore the volume of the continuous reactor for a given production rate, is calculated from the batch rate of reaction data at this composition, i.e., $\theta = \Delta C_A / R_A$. For multistage CSTR design the procedure is repeated by drawing a series of tangent lines to the curves, each, of course, starting with the product composition of the previous reactor in the chain. The effects of recycle or side streams, if they are desired, may also easily be evaluated, as material balances appear as straight-line relations on these triangular plots.

Kinetics of the Liquid-phase Oxidation of Ethanol

John Klassen and R. S. Kirk
University of Wisconsin, Madison, Wisconsin

A study was made of the rate of liquid-phase oxidation of ethanol to acetic acid. An aqueous, basic solution of ethanol was allowed to trickle over a palladium-on-alumina catalyst in a packed tower while oxygen-containing gas was blown upward. The observed rates are described by an equation including a kinetic term and a mass transfer term for the diffusion of oxygen. Kinetic rate constants and gas- and liquid-film mass transfer coefficients are reported.

This paper reports the results obtained in a rate study of a reaction system in which both diffusion and kinetic effects are important. The object of the experiment was to determine the magnitude of both effects and to evaluate kinetic rate and mass transfer coefficients for the system. A solution of ethanol and sodium carbonate was allowed to trickle through a tower packed with palladium-on-alumina catalyst while oxygen-containing gas was blown upward through the tower. The ethanol was oxidized to acetic acid, which then reacted with the sodium carbonate to form sodium acetate. The reaction studied is as follows:

$$C_2H_5OH + O_2 + Na_2CO_3 \xrightarrow[Pd\ -Al_2O_3]{} NaOOCCH_3 + H_2O + NaHCO_3$$

In most cases the liquid rate to the tower was just sufficient to maintain a film of liquid on the catalyst. Liquid and gas flow rates; partial pressure of O_2; and concentration of ethanol, sodium carbonate, and sodium acetate were all varied to produce sufficient data from which the rate constants could be evaluated.

The oxidation of ethanol was chosen for investigation because it was known that the reaction proceeds smoothly at room temperature. Chemical analysis of the system would also be relatively accurate and simple. Furthermore it was hoped that the results of this work might be extended to the roughly analogous process of a trickling filter. From this viewpoint it was especially desirable to choose a reaction which can also be accomplished bacteriologically. The liquid rates were in the range used for trickling filters.

The choice of palladium as the catalyst was based on work of Mueller and Schwabe(*6*), who oxidized ethanol in a batch reactor using various platinum-group metals as catalysts. Their work indicated that any of these metals could be used as catalysts but all catalysts with the exception of palladium required an incubation period. As it was found that alumina would not interfere by catalyzing the reaction, a palladium-on-alumina catalyst containing 5% palladium was obtained. The alumina carrier was in the form of irregularly shaped particles, ⅛ to ¼ in. in size.

Mueller and Schwabe also tried acid, alkaline, and neutral reaction media. They found that in a neutral solution no reaction occurred; in acid solution, the ethanol was oxidized to acetaldehyde; and in basic solution, acetic acid was formed. It was desirable to produce acetic acid as the product of the reaction because of the simplicity of analysis. Thus it appeared necessary to use a basic solution for the experiments. Preliminary work showed that even dilute sodium hydroxide solutions attacked the alumina carrier. Ammonia inhibited the reaction completely. Various lower amines were tried, and while these did not inhibit the reaction they proved so volatile that extra precautions had to be taken to prevent substantial loss and consequent errors in analysis. Sodium carbonate was then tried and proved to be successful. Concentrations usually of the order of 0.1 molar were used. No attack on the carrier was noticed and the ethanol oxidized was completely converted to the acid. Infrared analysis and aldehyde tests showed that little or no acetaldehyde was being formed.

The equations used to correlate the data are derived in the following sections. First the kinetic rate equation, in terms of activities of the components at the catalyst surface, will be introduced. Then the mass transfer equations will be developed, relating the activity of oxygen at the catalyst surface to the oxygen concentration of the gas stream. It will be shown that the diffusion effects of the ethanol, sodium carbonate, and sodium acetate may be neglected.

DEVELOPMENT OF RATE EQUATIONS

This system involves the consideration of mass transfer across the gas and liquid films, a catalytic reaction on the surface of the catalyst, and diffusion of the products away from the catalyst. This is shown pictorially in Figure 1. Oxygen is transferred from the gas phase through the gas film and two liquid films to the catalyst surface. The ethanol and $CO_3^=$ ion diffuse through one liquid film to the catalyst; the HCO_3^- and AcO^- ions diffuse away from the catalyst.

There are many plausible rate equations for the catalytic reaction, but it is impossible to do more than select a most likely equation by inspection. The rate equations were developed by the methods suggested by Hougen and Watson(*4*).

John Klassen is with E. I. du Pont de Nemours Company, Ltd., Canada.

Complete tabular material has been deposited as document 4706 with the American Documentation Institute, Photoduplication Service, Library of Congress, Washington 25, D. C., and may be purchased for $1.25 for microfilm or photoprints.

The equation which best fits the data is

$$r = \frac{\mathbf{k}_t\, a_{ei}\, a_{bi}\, a_{oi}}{(1 + K_1 a_{oi} + K_2 a_{ai})^2} \quad (1)$$

where

r = rate of reaction, lb. moles/(hr.) (lb. of catalyst)

$\mathbf{k}_t$ = over-all kinetic rate constant

a_{ei}, a_{bi}, a_{oi} = activity at the catalyst surface of ethanol, carbonate ion, and oxygen, respectively

K_1 = adsorption equilibrium constant for oxygen

K_2 = adsorption equilibrium constant for acetate ion

This equation may be developed on the assumption that the reaction takes place by the following steps:

1. Adsorption of O_2 on a catalyst site

$$O_2 + l \rightarrow O_2 \cdot l$$

2. Reaction of ethanol with the adsorbed O_2, an active site, and carbonate ion to yield adsorbed acetate ion and water and free bicarbonate ion

$$l + \text{EtOH} + O_2 \cdot l + CO_3^{=} \rightarrow$$

$$l \cdot \text{AcO}^- + l \cdot H_2O + HCO_3^-$$

3. Desorption of the adsorbed acetate ion and water

$$l \cdot \text{AcO}^- \rightarrow l + \text{AcO}^-$$

$$l \cdot H_2O \rightarrow l + H_2O$$

Step 2 is a summation of several second-order reactions. Intermediates, including acetaldehyde and its hydroxylated form, are produced during reaction (3). For lack of information concerning the actual course of the reaction, the intermediate steps have been summarized in step 2.

The kinetic steps postulated above and their result, Equation (1), can be justified by the following information. When all variables except the partial pressure of oxygen were held constant, the rate of reaction increased with increasing O_2 partial pressure. The plot of these data suggested that the oxygen was adsorbed on the catalyst. It was also found that the rate was influenced by the concentration of the carbonate ion; this would indicate that step 2 above is the rate-controlling step. Equation (1) is based on step 2 being rate controlling. The thermodynamic data (7) for the reaction

$\text{EtOh}(aq.) + O_2(g) + Na_2CO_3(aq.) \rightarrow \text{NaAcO}(aq.) + NaHCO_3(aq.) + H_2O(l)$ shows that $\Delta G^o = -118.7$ kcal./g.mole. The equilibrium constant has a value of 1×10^{87}; consequently the reverse reaction may be neglected.

Equation (1) does not contain a water adsorption term because the water was present in large excess; its activity would be constant and the resulting rate equation would reduce to Equation (1). Correlation of the data indicated that ethanol was not adsorbed on the catalyst, and thus no term for ethanol adsorption appears in Equation (1).

When standard states of unit molarity are assigned for the ethanol, acetate ion, and sodium carbonate; 1 atm. pressure is assigned for the O_2; and ideal behavior is assumed, Equation (1) becomes

$$r = \frac{\mathbf{k}_t\, N_{ei}\, N_{bi}\, p_{oi}}{(1 + K_1\, p_{oi} + K_2\, N_{ai})^2} \quad (2)$$

where

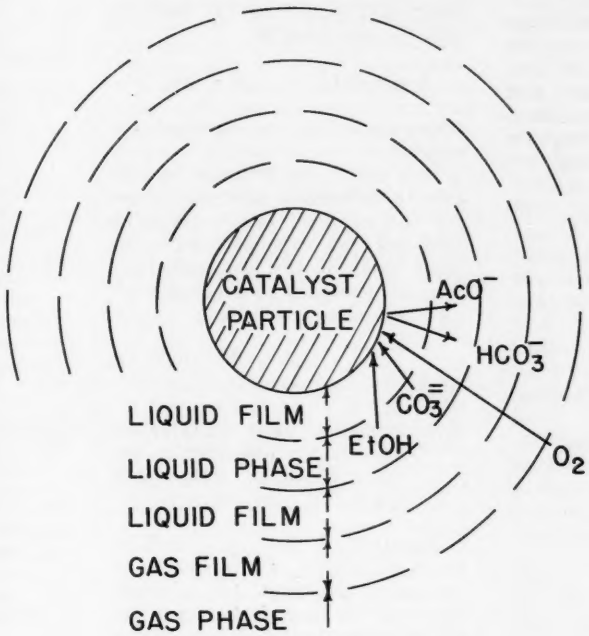

Fig. 1. Diagram of reactor mechanism.

N_{ei}, N_{bi}, N_{ai} = molarity at the interface of ethanol, sodium carbonate, and acetate/ion

p_{oi} = partial pressure of O_2 at the interface, atm.

Equation (2) is the basic equation used to correlate the data; however, the interfacial concentrations must be related to measurable quantities if this equation is to be useful.

MASS TRANSFER OF NONGASEOUS COMPONENTS

The concentrations of ethanol and carbonate were greater than 0.02 molar. The acetate concentration was either greater than 0.02 molar (when acetic acid was added to the feed) or so close to zero that the term $K_2 N_{ai}$ in Equation (2) was negligible. The oxygen was the limiting reactant, the maximum

concentration, corresponding to a saturated solution, being 0.0003 molar. Thus if all the oxygen in a saturated solution reacted, the maximum concentration difference of the other components across the liquid film surrounding the catalyst would be 0.0003 molar. The interfacial composition would then be about (0.02 — 0.0003), or approximately 0.02. As complete reaction does not occur, the concentration difference is even smaller; consequently the interfacial compositions of ethanol, carbonate, and acetate may be taken as the main stream compositions without introduction of serious error.

DIFFUSION OF OXYGEN

The sites of the major resistance to diffusion of the oxygen are the gas and liquid films at the gas-liquid interface and the liquid film at the catalyst surface. The following equation for gas-film transfer coefficients has been proposed (*5*):

$$k_G a = B L^m G^n \qquad (3)$$

where

$k_G a$ = gas-phase mass transfer coefficient, lb. moles/(hr.) (cu. ft. of packing) (atm.)
L = liquid mass velocity, lb./(hr.) (sq.ft.)
G = gas mass velocity, lb./(hr.) (sq.ft.)
B, m, n = empirical constants

A value of 0.8 is usually assigned to n. If Equation (3) is divided by the bulk density of the catalyst to convert to a basis of 1 lb. of packing

$$\mathbf{k}_G = BL^m G^{0.8} \qquad (4)$$

where

$\mathbf{k}_G$ = gas-phase mass transfer coefficient, lb.moles/(hr.) (lb. of catalyst) (atm.)

For liquid-film coefficients at a gas-liquid interface, the following equation is suggested (*5*)

$$\frac{k_L a}{D} = \alpha \left(\frac{L}{\mu}\right)^p \left(\frac{\mu}{\rho D}\right)^{0.5} \qquad (5)$$

where

$k_L a$ = liquid-phase mass transfer coefficient, lb. moles/(hr.) (cu.ft. of packing) (lb. moles/cu.ft.)
D = diffusion coefficient, sq.ft./hr.
μ = viscosity of liquid, lb./(ft.) (hr.)
ρ = density of liquid, lb./cu.ft.
α = constant
p = constant with a value of 0.5 to 0.7 for various packings

Van Krevelen and Krekels (*9*) studied mass transfer through a liquid film to a solid at low flow rates. They propose the following equation for the liquid-film mass transfer coefficient:

$$\frac{k_{Li} a}{D} = 1.8 \left(\frac{L}{a\mu}\right)^{0.5} \left(\frac{\mu}{\rho D}\right)^{1/3} \qquad (6)$$

where

$k_{Li} a$ = liquid mass transfer coefficient at the liquid-solid interface, lb.moles/(hr.) (cu.ft.) (lb.moles/cu.ft.)

For the system under investigation the diffusion coefficients and viscosity and density of the solutions remained approximately constant because the concentration of the solutions was not changed substantially. Equations (5) and (6) may be rewritten as

$$k_L a = Q_1 L^p \qquad k_{Li} a = Q_2 L^{0.5}$$

where Q_1 and Q_2 are empirical constants.

It is likely that it would be difficult to determine separate values for the exponent of L. Assuming that the two exponents have the same value, p, the two coefficients may be combined to give an over-all liquid-phase coefficient:

$$k_{Lt} a = QL^p \qquad (7)$$

where

$k_{Lt} a$ = combined mass transfer coefficient for diffusion in the liquid phase, lb. moles/(hr.) (cu.ft.) (lb.moles/cu.ft.)

Equation (7) may be divided by the bulk density of the packing to convert to a basis of 1 lb. of packing, and by Henry's constant for O_2 to convert the driving force from concentration units to partial-pressure units (atm.). The result is

$$\mathbf{k}_L = SL^p \qquad (8)$$

where

$\mathbf{k}_L$ = combined liquid-phase mass transfer coefficient, lb. moles/(hr.) (lb. of packing) (atm.)
S = a constant

Equations (4) and (5) may be combined to give an over-all mass transfer coefficient, $\mathbf{K}_o$,

$$\frac{1}{\mathbf{K}_o} = \frac{1}{\mathbf{k}_G} + \frac{1}{\mathbf{k}_L} \qquad (9)$$

The rate of reaction is equal to the rate of diffusion of O_2 from the gas phase to the catalyst surface, or

$$r = \mathbf{K}_o (p_o - p_{oi}) \qquad (10)$$

where

r = rate of reaction, lb. moles/(hr.) (lb. of catalyst)
$\mathbf{K}_o$ = over-all mass transfer coefficient, lb.moles/(hr.) (lb. of catalyst) (atm.)
p_o = partial pressure of oxygen in the gas phase, atm.
p_{oi} = partial pressure of oxygen at the catalyst surface, atm.

For purposes of correlation it is convenient to combine Equations (2) and (10) to give

$$p_o/r = \frac{(1 + \mathbf{K}_1 p_{oi} + K_2 N_a)^2}{\mathbf{k}_t N_b N_e} + \frac{1}{\mathbf{K}_o} \qquad (11)$$

Or, if the equivalent of $\mathbf{K}_o$ is substituted from Equations (4), (8), and (9),

$$p_o/r = \frac{(1 + K_1 p_{oi} + K_2 N_a)^2}{\mathbf{k}_t N_b N_e} + \frac{1}{SL^p} + \frac{1}{BL^m G^{0.8}} \qquad (12)$$

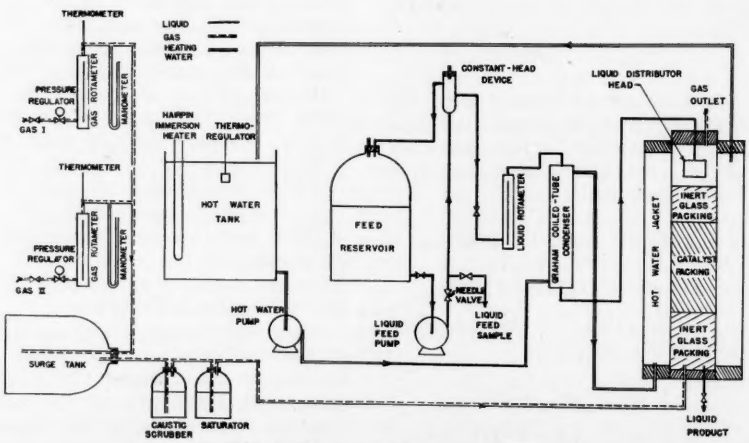

Fig. 2. Diagram of apparatus.

TABLE 1.—RANGE OF VARIABLES INVESTIGATED

Variable	Notation	Range
Gas flow rate	G	1-10 lb./(hr.)(sq. ft.)
Liquid flow rate	L	50-235 lb./(hr.)(sq. ft.)
Oxygen partial pressure in gas	p_o	0-1 atm.
Ethanol concentration	N_e	0.05-1.0 molar
Sodium carbonate concentration	N_b	0.1-0.3 molar
Acetate concentration	N_a	0-0.15 molar
Temperature	t	23° and 45° C.

where

N_a, N_b, N_e = molarity of acetate ion, sodium carbonate, and ethanol, respectively, in the main stream

Equations (11) and (12) are the completely developed forms of the rate equation (2), involving all the variables. The methods used to determine the constants in these equations are discussed in the following sections.

EQUIPMENT

A flow sheet of the equipment is shown in Figure 2.

The reactor consisted of a 20-in. length of 64-mm. glass tubing surrounded by a water jacket. The catalyst was palladium supported on alumina (5% palladium by weight); the particle size ranged from ⅛ to ¼ in. A bed depth of 7 in. was used (about 1 lb. of catalyst). A 7.5-in. layer of 4-mm. glass beads was placed above the bed and a similar 4-in. layer below the bed to ensure uniform gas and liquid flow patterns.

The liquid feed to the reactor entered at the top through a distributor equipped with four fine nozzles (orifice diameter = 0.0135 in.). The distributor was fed from a constant-head device to which liquid feed was pumped from the supply tank. Flow rates were measured with a rotameter. A Graham condenser was used as the feed preheater, warm water being the heating medium. A 1-in. depth of liquid was maintained at the bottom of the reactor to act as a gas seal.

Mixtures of air, oxygen, and nitrogen were used to produce various partial pressures of oxygen in the gas fed to the reactor. The air was taken from the laboratory service lines, the oxygen and nitrogen from cylinders. The gases passed through pressure-regulating valves to rotameters. The pressure was measured with a water manometer, temperature by thermometers. The gases after leaving the meters were combined and piped to a surge tank, from which they passed through a caustic scrubber to remove carbon dioxide and then to a saturator where the gases were bubbled through some of the liquid feed to minimize evaporation in the reactor. It was not necessary to adjust the temperature of the gas before it entered the reactor. The reactor temperature was controlled by pumping warm water from a thermostatted water bath through the various water jackets and condensers. Spun-glass insulation with an aluminum foil cover was used to insulate the jackets and water lines. All tanks and containers in the system were glass bottles. The piping, except for a few fittings on the pumps, was glass and Tygon tubing.

PROCEDURE

Three gallons of feed were made up for each run. First the warm water was circulated to the preheater and reactor jacket. Then the tanks, piping, and reactor were thoroughly flushed out with some of the feed solution to be used. The gas flow rates were adjusted to the desired values and then the gas was allowed to flow into the reactor to purge it. The liquid-feed tank was charged and the liquid admitted to the reactor at the desired rate, thus starting the run.

All runs were conducted for a period of 2 hr. when it was shown that after 2 hr. operation, steady-state conditions were reached. At the end of the 2 hr. samples of the feed and product solutions were withdrawn. The gas and liquid rates and temperatures were maintained constant throughout the run.

Less than 0.4°C. difference in temperature was found between the reactor bed at inlet and outlet and the water jacket surrounding the reactor. Thus the reactor temperature was measured by taking the jacket temperature. This procedure was justified for all gas and liquid flow rates and gas temperatures.

Experiments proved that no homogeneous reaction was occurring and that the alumina carrier was not dissolving.

CHEMICAL ANALYSIS OF FEED AND PRODUCT

The analytical procedure was based on the conversion of ethanol to acetic acid. Aldehyde and ketone tests gave negative results; analytical tests by the Chemistry Department at the University of Wisconsin confirmed the presence of acetate ions. Thus it could be safely assumed that all the ethanol converted was oxidized to acetic acid.

The conversion for any given run was determined from the difference of acetic acid content of the feed and product. The analysis for acetic acid involved the back titration of the alkaline sodium carbonate solutions with acetic acid by use of a glass-electrode pH meter to locate the end point of the titration. It was difficult to locate precisely the end point for each titration, but the titration curves for feed and product samples were parallel in the region of the end points. Thus the change in acetic acid concentration could be measured by taking the difference between the titration curves without a knowledge of the exact end points.

The total sodium carbonate concentration of the feed was determined by titration with hydrochloric acid to the methyl orange end point.

RESULTS

Table 1 shows the variables and their ranges, which were investigated.

Calculation Procedures

In the evaluation of the constants of Equation (12), mean values of the concentration terms were used as the reaction caused a change in concentration. This change was of the order of 4%; because it was so small, the arithmetic average of inlet and outlet concentrations was used as the mean. Table 2 contains the data from a sample run, run 120.

Temperature corrections were introduced in the correlation of data from those runs which could not be maintained at the desired temperature. The values of the constants at the lower temperature are reported for the average of the

TABLE 2.—SAMPLE DATA—RUN 120

$G = 10.72$ lb./(hr.) (sq. ft.) $\quad p_o = 0.205$ atm.
$L = 145$ lb./(hr.) (sq. ft.) $\quad t = 32.0$ °C.
$r = 1.943 \times 10^{-5}$ lb. moles acetate formed/(hr.) (lb. of catalyst)

	Concentrations (molarity)		
	Inlet	Outlet	Average
N_e	0.200	0.196	0.198
N_b	0.0984	0.0940	0.0962
N_a	0.0466	0.0510	0.0488

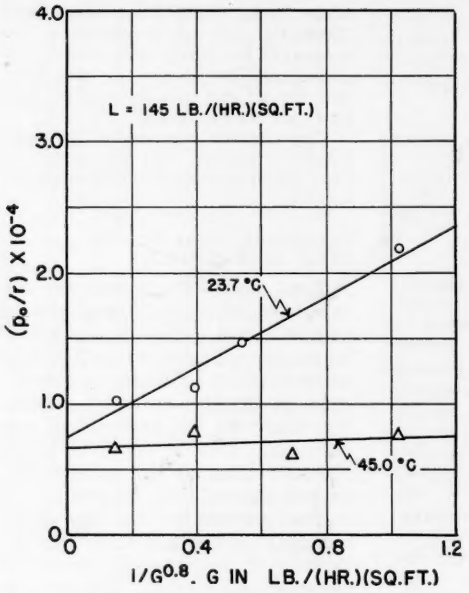

Fig. 3. Correlation of reaction rate with gas mass velocity.

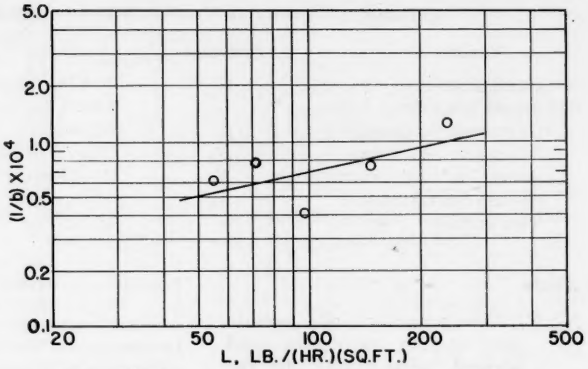

Fig. 4. Effect of liquid mass velocity on gas-phase mass transfer coefficients.

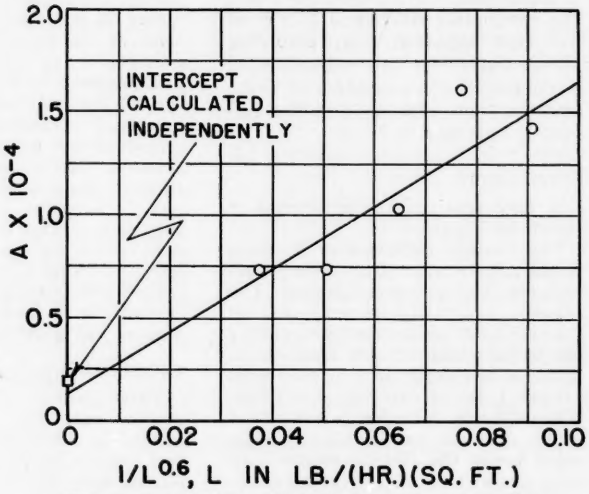

Fig. 5. Correlation of liquid phase mass transfer coefficients at 23.7°C.

TABLE 3.—CONSTANTS OF EQUATION (14) AT 23.7°C.

Liquid flow rate, lb./(hr.) (sq. ft.)	$A \times 10^{-4}$	$b \times 10^{-4}$
234	0.733	0.807
145	.734	1.359
96.2	1.033	2.415
71.6	1.602	1.304
54.6	1.419	1.621

temperatures of the runs used in a particular correlation.

The actual mathematical evaluation of the constants was done by the method of least squares.

Gas-phase Mass Transfer Coefficients

For a given liquid rate, if the concentrations of the reactants and products are held constant, Equation (12) reduces to

$$p_o/r = A + \frac{b}{G^{0.8}} \qquad (13)$$

where A and b are constants.

This incorrectly presumes that p_{oi} will remain constant. Variations in gas rate will affect the rate of transfer of oxygen, and thus p_{oi}. It is extremely difficult to evaluate the constants in Equation (12) without making this assumption. The later correlations show that R, the resistance to reaction of the chemical terms $[R = A - (1/SL^p)]$ is about 0.13×10^4; whereas the total resistance (p_o/r) varies between 0.8×10^4 and 3.5×10^4. Thus the assumption of constant p_{oi} in this correlation does not introduce a large error.

Then by varying only the gas flow rate, the constants A and b of Equation (13) may be evaluated. Table 3 reports the values obtained for various constant liquid rates. Figure 3 illustrates the data for a liquid mass velocity of 145 and temperatures of 23.7 and 45.8°C.

From Equation (12) the parameter b is related to the liquid rate by $1/b = BL^m$.

The values of the constants B and m may be determined from the data of Table 3 by plotting log $(1/b)$ vs. log L. This is shown in Figure 4. At 23.7°C. these values are

$B = 0.098 \times 10^{-4}$
$m = 0.4$

Similarly at 45°C. $m = 0.4$ and $B = 0.055 \times 10^{-4}$

Liquid-phase Mass Transfer Coefficients

The term A of Equation (13) may be written as $A = R + 1/SL^p$ where R represents the chemical reaction terms. Again assuming R constant, R, S, and p were evaluated from the data of Table 3. Values of p from 0.4 to 0.8 were assumed and R and S were evaluated. The best fit was obtained for $p = 0.6$, although the other values correlated reasonably well. Figure 5 illustrates the data for 23.7°C. The term R initially was found to be zero; subsequently it was found that $R = 0.136 \times 10^4$. Using this value of R and recalculating give the constants at 23.7°C. as

$R = 0.136 \times 10^4$
$p = 0.6$
$S = 6.63 \times 10^{-6}$

Similarly at 45°C.

$R = 0.136 \times 10^4$
$p = 0.6$
$S = 9.18 \times 10^{-6}$

Oxygen Adsorption Equilibrium Constant K_1

The most convenient form of Equation (1) for determining the oxygen adsorption equilibrium constant K_1 is

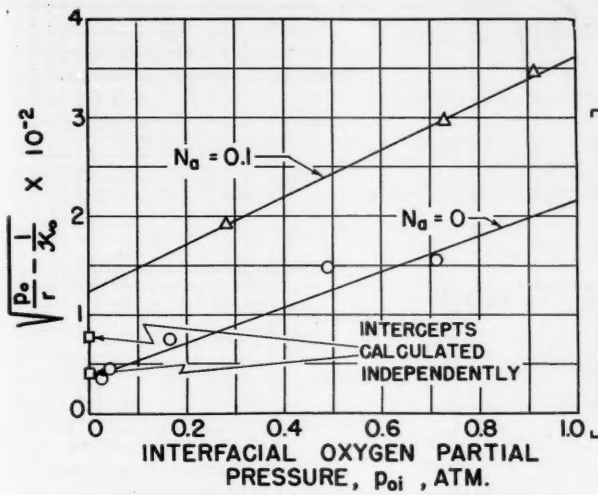

Fig. 6. Correlation of reaction rate with oxygen partial pressure at 28.6°C.

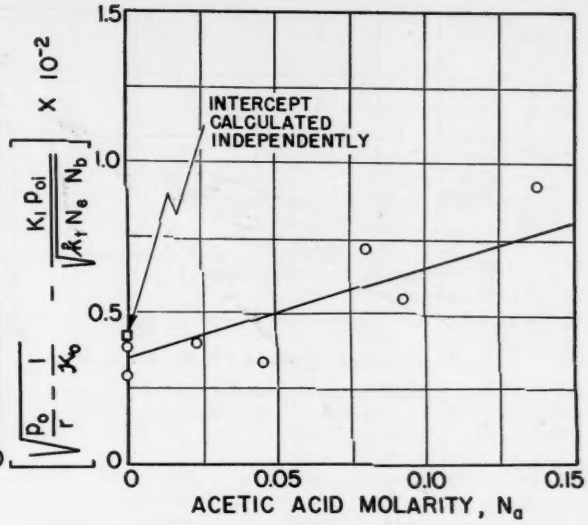

Fig. 7. Correlation of reaction rate with acetic acid concentration at 29.3°C.

$$\sqrt{\frac{p_o}{r}-\frac{1}{\mathbf{K}_o}}=\frac{1+K_2N_a}{\sqrt{\mathbf{k}_t N_e N_b}}+\frac{K_1 p_{oi}}{\sqrt{\mathbf{k}_t N_e N_b}} \quad (14)$$

and

$$p_{oi}=p_o-r/\mathbf{K}_o$$

Values of $\mathbf{K}_o$, the over-all mass transfer coefficient, may be calculated from the previously determined quantities by the equation

$$\frac{1}{\mathbf{K}_o}=\frac{1}{SL^{0.6}}+\frac{1}{BL^{0.4}G^{0.8}} \quad (15)$$

The lower temperature of 23.7°C. could not be maintained at this time. The average temperature rose to 28.6°C. Interpolating for the proper values of B and S, gave $1/\mathbf{K}_o = 0.925 \times 10^4$ at 28.6°C. and $1/\mathbf{K}_o = 0.590 \times 10^4$ at 45°C.

The operating variables, except p_o were held constant; under these circumstances Equation (14) reduced to a linear equation. If $\sqrt{p_o/r - 1/\mathbf{K}_o}$ is plotted vs. p_{oi}, a straight line should be obtained with a slope of $K_1/\sqrt{\mathbf{k}_t N_e N_b}$ and an intercept of $(1+K_2N_a)/\sqrt{\mathbf{k}_t N_e N_b}$. This is shown in Figure 6. The value of K_1 is obtained by dividing the slope by the intercept of the curve when $N_a = 0$. From the average of the slopes of the two curves of Figure 6, at 28.6°C. $K_1 = 5.3$. Similarly at 45°C. $K_1 = 4.3$.

Acetic Acid Adsorption Equilibrium Constant, K_2

If Equation (11) is written in the form

$$\sqrt{\frac{p_o}{r}-\frac{1}{\mathbf{K}_o}}-\frac{K_1 p_{oi}}{\sqrt{\mathbf{k}_t N_e N_b}}=\frac{1}{\sqrt{\mathbf{k}_t N_e N_b}}+\frac{K_2 N_a}{\sqrt{\mathbf{k}_t N_e N_b}}$$

it will be seen that the equation is linear with respect to N_a provided the value of $\sqrt{\mathbf{k}_t N_e N_b}$ is constant. The operating conditions were such that the value of $\sqrt{\mathbf{k}_t N_e N_b}$ would be the same as in the previous section.

Figure 7 is the graph of Equation (16) at 29.3°C. The value of K_2 is obtained by dividing the slope of the line by the intercept.

The results of this correlation are
$K_2 = 9.05$ at 29.3°C.
$= 25.9$ at 45.0°C.

TABLE 4.—SUMMARY OF RESULTS

$$r=\frac{\mathbf{k}_t N_e N_b p_{oi}}{(1+K_1 p_{oi}\times K_2 N_a)^2}$$

$$p_{oi}=p_o-r/\mathbf{K}_o$$

$$\frac{1}{\mathbf{K}_o}=\frac{1}{\mathbf{k}_G}+\frac{1}{\mathbf{k}_L}$$

$$\ln k_t=\frac{-17{,}000}{RT}+\frac{49.3}{R}$$

$$\ln K_1=\frac{-2.375}{RT}+\frac{4.35}{R}$$

$$\ln K_2=\frac{-12{,}750}{RT}+\frac{46.0}{R}$$

Temperature range of 23.7° to 45.0° C

Temperature = 23.7° C.

$\mathbf{k}_G = 0.098\times10^{-4}\ L^{0.4}G^{0.8}$
$k_G a = 4.46\times10^{-4}\ L^{0.4}G^{0.8}$
$\mathbf{k}_L = 6.63\times10^{-6}\ L^{0.6}$
$k_L a = 3.62 L^{0.6}$

Temperature = 45.0° C.

$\mathbf{k}_G = 0.055\times10^{-4}\ L^{0.4}G^{0.8}$
$k_G a = 2.50\times10^{-4}\ L^{0.4}G^{0.8}$
$\mathbf{k}_L = 9.18\times10^{-6} L^{0.6}$
$k_L a = 6.85 L^{0.6}$

Kinetic Rate Constant, $\mathbf{k}_t$

The value of the rate constant $\mathbf{k}_t$ is obtained directly from Equation (11):

$$p_o/r=\frac{1}{\mathbf{K}_o}+\frac{1}{\mathbf{k}_t}\left[\frac{(1+K_1 p_{oi}+K_2 N_a)^2}{N_e N_b}\right] \quad (11)$$

All the constants but $\mathbf{k}_t$ have been determined so that all the terms in the equation may be calculated.

Then if p_o/r is plotted vs. $(1+K_1 p_{oi}+K_2N_a)^2/N_eN_b$ a straight line should result with a slope of $1/\mathbf{k}_t$ and an intercept of $1/\mathbf{K}_o$. The plot of the data at 29.5°C. is shown in Figure 8. Five points falling within the labeled square were omitted from the correlation, with the result that
$\mathbf{k}_t = 0.032$ at 29.5°C.
$= 0.128$ at 45.0°C.

Temperature Effects

The constants K_1, K_2 and $\mathbf{k}_t$ may be related to the temperature

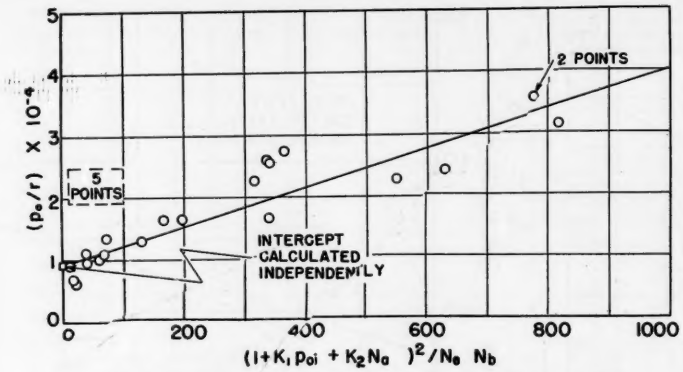

Fig. 8. Correlation of reaction rate with ethanol and sodium carbonate concentrations at 29.5°C.

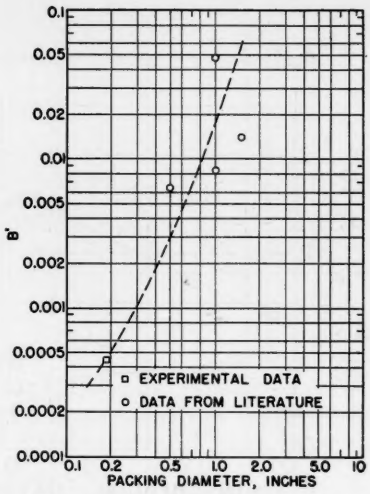

Fig. 9. Comparison of gas mass transfer correlations.

change by the equation

$$\ln K = -\frac{\Delta H}{RT} + \frac{\Delta S}{R}$$

where

ΔH = enthalpy change of reaction or activation

ΔS = entropy change of reaction or activation

The appropriate equations are reported in the summary, Table 4.

DISCUSSION OF RESULTS

Independent Calculation of Intercepts

The intercepts of Figure 4 through 7 may be calculated from the known values of the constants. This serves as a check on the calculations. The calculated and graphically determined values are listed in Table 5.

Comparison of Calculated and Experimental Rates of Reaction

The rate of reaction for any run may be calculated by a trial-and-error procedure by use of the determined values of the constants. The average percentage of error between calculated and experimental values is 27.2. A total of sixty-seven runs was used in the calculations; of these, two runs had errors in excess of 100%.

The differences between calculated and experimental rates of reaction may be ascribed to temperature variations, the chemical nature of the system, and the method of analysis.

The correlations show that the constants change appreciably with temperature. Better results could be obtained by maintaining constant temperature; the agreement between calculated and experimental rates is much better for the 45°C. runs than for the lower temperature runs, where the temperature varied. Inspection of the data indicates that large variations in the feed concentrations (as is necessary to evaluate the constants) frequently caused unusual rates of reaction. It is felt that the buffering action of the acetate-carbonate system obscured rate changes caused by changes in the feed composition. A more positive means of analysis would also be desirable, as duplicate runs had as much as 15% difference in conversion.

Within the limits of analysis, the catalyst showed constant activity during the period of experimentation.

Comparison of Results with Published Data

Most data on gas-phase mass transfer coefficients have been obtained from the study of the ammonia-air-water system. Sherwood and Holloway (*8*) showed that different solutes affect the coefficients only in proportion to the 0.17 power of the diffusivities. Thus the results reported in this paper for oxygen absorption may be compared directly with the ammonia results.

Gas-film mass transfer coefficients have been correlated with the following equation (*2, 5*):

$$k_G a = B' L^m G^{0.8} \qquad (3)$$

B' is a constant dependent on the size of the packing. The value of m reported is about 0.4, the same value determined in this paper.

It is interesting to compare a plot of B' vs. the nominal diameter of the packing, as shown in Figure 9. The value of B' for the packing used in this experiment is 0.00045, and the diameter is assumed to be the average of the particle-size range (⅛ to ¼ in.), or 0.188 in.

Liquid-phase mass transfer coefficients have been correlated by the equation (*5*):

Table 5.—Comparison of Graphical and Calculated Intercepts

Figure	Temp.°C.	N_a	Formula	Intercept: Calculated value	Intercept: Graphical value
4	23.7	—	$\frac{(1+K_1 p_{oi})^2}{\mathbf{k}_t N_e N_b}$	0.2×10^4	0.136×10^4
	45.0	—		0.066×10^4	0.136×10^4
5	28.6	0	$\frac{1+K_2 N_a}{\sqrt{\mathbf{k}_t N_e N_b}}$	41.3	39.8
		0.0974		77.1	120
	45.0	0		21.4	31.4
6	29.3	—	$\frac{1}{\sqrt{\mathbf{k}_t N_e N_b}}$	40.5	34.8
	45.0	—		20.4	26.8
7	28.6	—	$\frac{1}{\mathbf{k}}$	0.925×10^4	0.924×10^4
	45.0	—		0.590×10^4	0.631×10^4

$$\frac{k_L a}{D} = \alpha \left(\frac{L}{\mu}\right)^p \left(\frac{\mu}{\rho D}\right)^{0.5} \quad (5)$$

where α is a constant dependent on packing size and p is a constant of value 0.5 to 0.8

The value of $p = 0.6$ reported here for oxygen absorption seems reasonable when compared with the foregoing values. Figure 10 shows a plot of α vs. packing diameter. From the data given in Perry (*7*) for D and N_{Sc}, α for this packing is calculated to be 3,190.

It is difficult to estimate the individual liquid-film coefficients at the gas-liquid and liquid-solid interfaces, but the apparent agreement between the results and Molstad's correlations would indicate that the major resistance to mass transfer in the liquid phase is at the gas-liquid interface. This may be corroborated by estimating a coefficient for the other liquid film from Equation (6). Brown (*1*) indicates that the surface area per volume of packing is approximately six times the area of a sphere of the same diameter as the packing (0.188 in.). Coefficients calculated on this basis are about four times as large as the experimental values, an indication that the liquid film at the gas-liquid interface offers more resistance to mass transfer than does the liquid film at the catalyst surface.

CONCLUSIONS

It may be concluded that the equations presented in Table 3 correlate the data reasonably well. The various parameters in the mass transfer equations agree with previously published work (*2, 5*). Figures 9 and 10 indicate that packing size may have a considerable effect on mass transfer coefficients.

It has been shown that for this system—oxidation of dilute alcohol solutions trickling over a palladium catalyst countercurrent to a flow of oxygen-containing gas—appreciable resistance to reaction is encountered in both gas and liquid films. Increased rates of reaction may be obtained by increasing the gas or liquid flow rates and also by increasing the oxygen content of the gas.

ACKNOWLEDGMENT

The authors wish to acknowledge the financial assistance given by the Wisconsin Alumni Research Foundation, the National Research Council of Canada, and the Engineering Experiment Station of the University of Wisconsin.

The counsel of O. A. Hougen, W. R. Marshall, Jr., and R. B. Bird is gratefully acknowledged. Thanks are due J. A. Fairall, formerly of U.S.P.H.S., from whose suggestion this project developed.

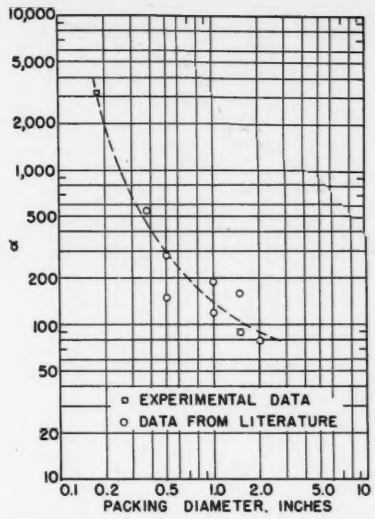

Fig. 10 Comparison of liquid mass transfer correlations.

NOTATION

$A = (1 + K_1 p_{oi} + K_2 N_a)^2 / \mathbf{k}_l N_e N_b + 1/SL^p$

a = interfacial packing area, sq. ft./cu.ft.

$a_{ai}, a_{bi}, a_{ei}, a_{oi}$ = activity of acetate ion, carbonate ion, ethanol and oxygen, respectively, at the catalyst surface

B = empirical constant

b = empirical constant

D = liquid diffusion coefficient, sq. ft./hr.

G = gas mass velocity, lb./(hr.) (sq.ft.)

H = Henry's law constant, atm./(lb. moles/cu.ft.); for oxygen, $H = 1.20 \times 10^4$

ΔH = enthalpy change of reaction or activation, cal./g. mole

$\mathbf{K}_o$ = over-all mass transfer coefficient, lb. moles/(hr.) (lb. of catalyst) (atm.)

K_1 = adsorption equilibrium constant for oxygen

K_2 = adsorption equilibrium constant for acetate ion

k_G = gas-film mass transfer coefficient, lb. moles/(hr.) (sq.ft.) (atm.)

$\mathbf{k}_G$ = gas-film mass transfer coefficient, lb. moles/(hr.) (lb. of catalyst) (atm.)

k_L = liquid-film mass transfer coefficient, lb. moles/(hr.) (sq. ft.) (lb. moles/cu.ft.)

k_{Li} = liquid-film mass transfer coefficient at a solid-liquid interface, lb. moles/(hr.) (sq. ft.) (lb. moles/cu.ft.)

K_{Lt} = effective mass transfer coefficient for all diffusion in the liquid phase, lb. moles/(hr.) (sq.ft) (lb. moles/cu.ft.)

$\mathbf{k}_L$ = effective mass transfer coefficient for all diffusion in the liquid phase, lb. moles/(hr.) (lb. of packing) (atm.)

$\mathbf{k}_l$ = over-all kinetic rate constant

l = symbol for a single active site on the catalyst

m = empirical constant

N_a, N_b, N_e = average molarity in the main liquid stream of acetate ion, carbonate ion, and ethanol, respectively

N_{ai}, N_{bi}, N_{ei} = average molarity at the catalyst surface of acetate ion, carbonate ion, and ethanol, respectively

p = empirical constant

p_o = partial pressure of oxygen in the main gas stream, atm.

p_{oi} = partial pressure of oxygen at the catalyst surface, atm.

Q = empirical constant

$R = (1 + K_1 p_{oi} + K_2 N_a)^2 / \mathbf{k}_l N_e N_b$

R = gas constant = 1.987 cal./g. mole) (°K.)

r = rate of reaction, lb. moles/(hr.) (lb. of catalyst)

S = empirical constant

ΔS = entropy change of reaction or activation, cal./(g.mole) (°K.)

T = absolute temperature, °K.

t = temperature, °C.

α = empirical constant

μ = liquid viscosity, lb./(ft.) (hr.)

ρ = liquid density, lb./cu.ft.

ρ_B = bulk density of catalyst, lb./cu.ft. = 45.5

LITERATURE CITED

1. Brown, G. G., and associates, "Unit Operations," John Wiley and Sons, Inc., New York (1950).
2. Dwyer, O. E., and B. F. Dodge, *Ind. Eng. Chem.*, **33**, 485 (1941).
3. Egloff, G., in "Organic Chemistry," edited by H. Gilman, vol. I, John Wiley and Sons, Inc., New York (1943).
4. Hougen, O. A., and K. M. Watson, "*Chemical Process Principles*," III, John Wiley and Sons, Inc., New York (1947).
5. Molstad, M. C., J. F. McKinney, and R. G. Abbey, *Trans. Am. Inst. Chem. Engrs.*, **39**, 605 (1943).
6. Mueller, E., and K. Schwabe, *Kolloid-Z.*, **52**, 163 (1930).
7. Perry, J. H., ed., "Chemical Engineer's Handbook," 3 ed., McGraw-Hill Book Company, Inc., New York (1950).
8. Sherwood, T. K., and F. A. L. Holloway, *Trans. Am. Inst. Chem. Engrs.*, **36**, 39 (1940).
9. Van Krevelen, D. W., and J. T. C. Krekels, *Rec. trav. chim.*, **67**, 512 (1948).

(Presented at A.I.Ch.E. Houston meeting)

Activity Coefficients at Infinite Dilution

M. F. Gautreaux, Jr., and Jesse Coates
Louisiana State University, Baton Rouge, Louisiana

Equations are derived for obtaining activity coefficients at infinite dilution in binary systems by use of one of the following: (1) an isobaric temperature—liquid composition diagram, (2) an isobaric temperature—vapor composition diagram, (3) an isothermal pressure—liquid composition diagram, or (4) an isothermal pressure—vapor composition diagram. The derived equations are thermodynamically exact, and application involves no doubtful extrapolation of experimental data, as has heretofore been the case.

Each equation involves the slope of one of the diagrams at the point corresponding to the pure component. Attention is called to the fact that data on the compositions of both the vapor and liquid phases in equilibrium are not required. Use of the equations is illustrated.

Vapor-liquid equilibrium data are frequently correlated in terms of activity coefficients. An activity coefficient, γ, is a thermodynamic quantity which is related to the fugacity, f, of a component in solution by an expression such as Equation (1):

$$\gamma_{1L} = \frac{f_{1L}}{x_1 f^o_{1L}} \qquad (1)$$

Subscript 1 refers to component one; subscript L refers to the liquid phase. [An equation analogous to Equation (1) could be written for component one in the vapor phase.] The subscript 0 refers to the chosen standard state. It is convenient to choose pure liquid and pure vapor at the temperature and pressure of the system for liquid- and vapor-phase standard states, respectively. These standard states are used throughout this paper. Usually at the temperature and pressure of the system the pure component will be either liquid or vapor, and one of the standard states will be hypothetical.

As the mole fraction of component one approaches zero in solution, its activity coefficient approaches a definite limit. This limiting value is frequently termed the "activity coefficient of component one at infinite dilution." The condition of infinite dilution will be designated by the subscript $x_1 = 0$. Thus

$$(\gamma_{1L})_{x_1=0} = \lim_{x_1 \to 0} \gamma_{1L} \qquad (2)$$

This coefficient is of considerable practical and theoretical interest. In extractive and azeotropic distillations important components frequently appear in very low concentrations in the liquid phase. The activity coefficient at infinite dilution is of aid in the determination of vapor-liquid equilibrium in these regions. Similarly the activity coefficient at infinite dilution is important because its logarithm generally appears as a constant in empirical equations which relate $\log \gamma$ and x (*1*). The coefficient is of interest to the scientist who is attempting to relate the structures of pure components and the nonidealities of solutions. This relation is probably most easily made at infinite dilution where there is absolutely no interaction among solute molecules in solution (*10*). Thus the partial molal excess free energy at infinite dilution is obtained (*3*) directly from Equation (3):

$$(\bar{G}^E = RT \ln \gamma)_{x=0} \qquad (3)$$

The partial molal excess enthalpy at infinite dilution is obtained by determining the rate of change of the coefficient with temperature:

M. F. Gautreaux, Jr., is at present with Ethyl Corporation, Baton Rouge, Louisiana.

TABLE 1.—EXACT EQUATIONS FOR $(\gamma_{1L}/\gamma_{1V})_{x_1=0}$

Type of diagram	Applicable thermodynamically exact equation* $(\gamma_{1L}/\gamma_{1V})_{x_1=0}$ equals	Applicable low-pressure equation* $(\gamma_{1L})_{x_1=0}$ equals
I. Isobaric temperature–liquid composition diagram†	$\frac{f^o_{1V}}{f^o_{1L}}\left[1-\left(\frac{\partial T}{\partial x_1}\right)_\pi\left(\frac{d\ln P_2}{dT}\right)\left(\frac{V_{2V}\pi}{RT}-\frac{V_{2L}\pi}{RT}\right)\right]$	$\frac{\pi}{P_1}\left[1-\left(\frac{\partial T}{\partial x_1}\right)_\pi\left(\frac{d\ln P_2}{dT}\right)\right]$
II. Isobaric temperature–vapor composition diagram†	$\frac{f^o_{1V}}{f^o_{1L}}\left[\frac{1}{1+\left(\frac{\partial T}{\partial y_1}\right)_\pi\left(\frac{d\ln P_2}{dT}\right)\left(\frac{V_{2V}\pi}{RT}-\frac{V_{2L}\pi}{RT}\right)}\right]$	$\frac{\pi}{P_1}\left[\frac{1}{1+\left(\frac{\partial T}{\partial y_1}\right)_\pi\left(\frac{d\ln P_2}{dT}\right)}\right]$
III. Isothermal pressure–liquid composition diagram	$\frac{f^o_{1V}}{f^o_{1L}}\left[1+\left(\frac{\partial \pi}{\partial x_1}\right)_T\left(\frac{V_{2V}}{RT}-\frac{V_{2L}}{RT}\right)\right]$	$\frac{\pi}{P_1}\left[1+\frac{1}{\pi}\left(\frac{\partial \pi}{\partial x_1}\right)_T\right]$
IV. Isothermal pressure–vapor composition diagram	$\frac{f^o_{1V}}{f^o_{1L}}\left[\frac{1}{1-\left(\frac{\partial \pi}{\partial y_1}\right)_T\left(\frac{V_{2V}}{RT}-\frac{V_{2L}}{RT}\right)}\right]$	$\frac{\pi}{P_1}\left[\frac{1}{1-\frac{1}{\pi}\left(\frac{\partial \pi}{\partial y_1}\right)_T}\right]$

*All terms evaluated at conditions corresponding to $x_1 = 0$.

† $\frac{d\ln P_2}{dT}\left(\frac{V_{2V}\pi}{RT}-\frac{V_{2L}\pi}{RT}\right)\frac{\lambda_2}{RT^2}$ (Clapeyron equation)

$$\left[\left(\frac{\partial \ln \gamma}{\partial T}\right)_\pi = \frac{-\overline{H}^E}{RT^2}\right]_{x=0} \quad (4)$$

And the partial molal excess entropy can then be obtained from

$$(\overline{G}^E = \overline{H}^E - T\overline{S}^E)_{x=0} \quad (5)$$

Activity coefficients at infinite dilution have been calculated in a variety of ways, perhaps most frequently from van Laar or similar constants obtained after vapor-liquid equilibrium data were correlated. For example, the van Laar constant A is related to the activity coefficient of component one (*3*) by the equation

$$A = (\log \gamma_{1L})_{x_1=0} \quad (6)$$

If vapor-liquid equilibrium data are available in the region $x_1 = 0$, graphical extrapolation by eye of γ_{1L} to $x_1 = 0$ is often used to obtain $(\gamma_{1L})x_1 = 0$. Carlson and Colburn (*1*) suggest using an isothermal pressure-composition diagram or an isobaric temperature-composition diagram and calculating an "apparent" activity coefficient which may be extrapolated to $x_1 = 0$ to obtain $(\gamma_{1L})x_1 = 0$.

The object of this paper is to derive *thermodynamically exact* relations for activity coefficient at infinite dilution in binary systems. No assumptions will be made concerning the idealities of the vapors or the vapor-phase solutions. Nor will the assumptions be made of a negligible heat of mixing and of a negligible effect of temperature on activity coefficients. Relations will be derived for utilization of vapor-liquid equilibrium data, isobaric temperature-composition diagrams, and isothermal pressure-composition diagrams. Usually it is simpler experimentally to obtain the two diagrams.

DERIVATION OF EQUATIONS

At equilibrium, $f_{1L} = f_{1V}$, Equation (7) results:

$$\frac{\gamma_{1L}}{\gamma_{1V}} = \frac{y_1 f^o_{1V}}{x_1 f^o_{1L}} \quad (7)$$

As x_1 approaches zero, the right-hand member (RHM) approaches the form 0/0. Applying L'Hospital's rule yields

$$\left(\frac{\gamma_{1L}}{\gamma_{1V}}\right)_{x_1=0} = \left[\left(\frac{\partial y_1}{\partial x_1}\right)\left(\frac{f^o_{1V}}{f^o_{1L}}\right)\right]_{x_1=0}$$

$$= \left[K_1\left(\frac{f^o_{1V}}{f^o_{1L}}\right)\right]_{x_1=0} \quad (8)$$

where K is the familiar equilibrium vaporization ratio.

Equation (8) is an exact thermodynamic relation for $(\gamma_{1L}/\gamma_{1V})$ $x_1 = 0$. It is independent of the number of components under consideration and applies to both constant temperature and constant pressure data. However, Equation (8) involves determinations of y and x in equilibrium at low values of y and x. These determinations are experimentally difficult.

Further derivations will be made to obtain $(\gamma_{1L}/\gamma_{1V})x_1 = 0$ in terms of information available from the more easily obtained isobaric temperature-composition diagrams and isothermal pressure-composition diagrams. A binary system will be considered.

When an equation for component two analogous to Equation (7) is utilized,

$$y_1 = 1 - y_2 = \frac{\gamma_{2V} f^o_{2V} - \gamma_{2L}\, x_2 f^o_{2L}}{\gamma_{2V} f^o_{2V}} \quad (9)$$

Differentiating with respect to x_1 and noting that at $x_1 = 0$, $\gamma_{2V} = \gamma_{2L} = 1.0$, $f_{2V}{}^\circ = f_{2L}{}^\circ = f_2{}^\circ$, $\partial\gamma_{2V}/\partial x_1$

TABLE 2.—EXACT RELATIONS BETWEEN $\partial T/\partial x_1$ AND $\partial T/\partial y_1$ AND $\partial \pi/\partial x_1$ AND $\partial \pi/\partial y_1$

Type of diagram	Relation*
I. Isobaric temperature-composition diagram	$\frac{1}{\left(\frac{\partial T}{\partial x_1}\right)_\pi} - \frac{1}{\left(\frac{\partial T}{\partial y_1}\right)_\pi} - \frac{d \ln P_2}{dT}\left(\frac{V_{2V}\pi}{RT} - \frac{V_{2L}\pi}{RT}\right) = 0$
II. Isothermal pressure-composition diagram	$\frac{1}{\left(\frac{\partial \pi}{\partial x_1}\right)_T} - \frac{1}{\left(\frac{\partial \pi}{\partial y_1}\right)_T} + \left(\frac{V_{2V}}{RT} - \frac{V_{2L}}{RT}\right) = 0$

*All terms evaluated at conditions corresponding to $x_1 = 0$.

$= \partial \gamma_{2L}/\partial x_1 = 0$ (*see* Appendix 4) gives Equation (10):

$$\left(\frac{\partial y_1}{\partial x_1}\right)_{x_1=0} = \left[\frac{f_2^o + \frac{\partial (f_{2V}^o - f_{2L}^o)}{\partial x_1}}{f_2^o}\right]_{x_1=0} \quad (10)$$

This equation is applicable to both constant-pressure and constant-temperature data.

At constant pressure one may write

$$\left[\frac{\partial (f_{2V}^o - f_{2L}^o)}{\partial x_1}\right]_\pi = \left[\frac{\partial (f_{2V}^o - f_{2L}^o)}{\partial T}\right]_\pi \left(\frac{\partial T}{\partial x_1}\right)_\pi \quad (11)$$

where $\partial T/\partial x_1$ will be recognized as the slope of an isobaric temperature-liquid composition diagram. As a result of the standard states chosen, the following thermodynamically exact expressions apply:

$$f_{2V}^o = v_{\pi, T}\,\pi \quad (12)$$

$$f_{2L}^o = v_{P_2, T}\, P_2 e^{V'_{2L}(\pi - P_2)/RT} \quad (13)$$

When (12) and (13) are utilized in Equation (11) at $x_1 = 0$, Equation (14) results:

$$\left\{\left[\frac{\partial (f_{2V}^o - f_{2L}^o)}{\partial x_1}\right]_\pi = f_2^o \left(\frac{\partial T}{\partial x_1}\right)_\pi \left(-\frac{d \ln P_2}{dT}\right)\left(\frac{\pi V_{2V}}{RT} - \frac{\pi V_{2L}}{RT}\right)\right\}_{x_1=0} \quad (14)$$

Combining (14), (10) and (8) yields the desired result:

$$\left\{\frac{\gamma_{1L}}{\gamma_{1V}} = \frac{f_{1V}^o}{f_{1L}^o}\left[1 - \left(\frac{\partial T}{\partial x_1}\right)_\pi \left(\frac{d \ln P_2}{dT}\right)\left(\frac{\pi V_{2V}}{RT} - \frac{\pi V_{2L}}{RT}\right)\right]\right\}_{x_1=0} \quad (15)$$

Equation (15) is a thermodynamically exact relation for obtaining $(\gamma_{1L}/\gamma_{1V})x_1 = 0$ from the slope of an isobaric temperature-liquid composition diagram at $x_1 = 0$.

By mathematics paralleling that above, equations can be derived which utilize slopes at infinite dilution of an isobaric temperature-vapor composition diagram, an isothermal pressure-liquid composition diagram, and an isothermal pressure-vapor composition diagram. Table 1 summarizes these equations.

As previously noted, there are no assumptions involved in the equations of Table 1. They apply even if the pure vapors are nonideal and if the vapors form a nonideal solution. Furthermore, the effect of temperature on liquid phase activity coefficients has not been neglected.

Redlich and Kister(*8*) have derived relations among $\partial T/\partial x$ and $\partial T/\partial y$, the relative volatility and vapor pressures. Their derivations were made for conditions of low pressure, negligible effect of temperature on activity coefficients and

TABLE 3.—EXACT EQUATIONS FOR CALCULATING K_1 AT $x_1 = 0$

Type of diagram	Equation*
I. Isobaric temperature–liquid composition diagram	$1 - \left(\frac{\partial T}{\partial x_1}\right)_\pi \left(\frac{d \ln P_2}{dT}\right)\left(\frac{V_{2V}\pi}{RT} - \frac{V_{2L}\pi}{RT}\right)$
II. Isobaric temperature–vapor composition diagram	$\frac{1}{1 + \left(\frac{\partial T}{\partial y_1}\right)_\pi \left(\frac{d \ln P_2}{dT}\right)\left(\frac{V_{2V}\pi}{RT} - \frac{V_{2L}\pi}{RT}\right)}$
III. Isothermal pressure–liquid composition diagram	$1 + \left(\frac{\partial \pi}{\partial x_1}\right)_T \left(\frac{V_{2V}}{RT} - \frac{V_{2L}}{RT}\right)$
IV. Isothermal pressure–vapor composition diagram	$\frac{1}{1 - \left(\frac{\partial \pi}{\partial y_1}\right)_T \left(\frac{V_{2V}}{RT} - \frac{V_{2L}}{RT}\right)}$

*All terms evaluated at conditions corresponding to $x_1 = 0$.

negligible effect of pressure on liquid-phase fugacities. Nord (7) derived an equation in terms of $\partial T/\partial y$ which can be reduced to the equation in terms of $\partial T/\partial y$ in Table 1. Nord's equation is thermodynamically exact except for the assumption that the vapor phase is an ideal solution. Ibl and Dodge (4) have derived thermodynamically exact equations in terms of $\partial\pi/\partial y$ and $\partial T/\partial y$ which can be used to derive the equations in Table 1 involving $\partial\pi/dy$ and $\partial T/dy$.

Combination of the equations in Table 1 yields relations between $\partial T/\partial x_1$ and $\partial T/\partial y_1$ and $\partial\pi/\partial x_1$

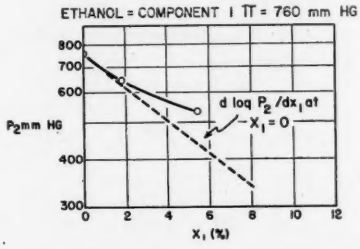

Fig. 1. Plot of P_2 vs. x_1 at 760 mm. Hg for ethanol (component 1)—water. Dotted line is $(\partial \log P/\partial x_1)\pi$ at $x_1 = 0$.

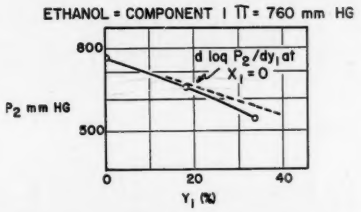

Fig. 2. Plot of log P_2 vs. y_1 at 760 mm. Hg. Dotted line is $(\partial \log P_2/\partial y_1)\pi$ at $x_1 = 0$.

and $\partial\pi/\partial y_1$ which must be fulfilled for thermodynamic consistency. These relations are summarized in Table 2.

Combining equations such as (15) and (8) makes it possible to determine $(K_1)_{x_1=0}$. These relations are summarized in Table 3. Thus the slope of the x-y diagram is also rigorously determined at $x_1 = 0$. It is important to note that it frequently happens that at the temperature and pressure corresponding to pure component two, component one will have a hypothetical standard state. This factor has no bearing on the relations in Table 2 or 3. Indeed, the relations are valid even if component one is above its critical point at the condition corresponding to $x_1 = 0$.

The relations in Tables 2 and 3 serve as thermodynamic consistency checks when vapor-liquid equilibrium data are available. These relations are exact. Indeed they are the only *exact* relations which are applicable when just vapor-liquid equilibrium data and pure component data are available. For example, the *exact* application of the Gibbs-Duhem equation at other values of x requires knowledge of the vapor-phase-solution nonideality and either the heat of mixing (isobaric data) or volume change

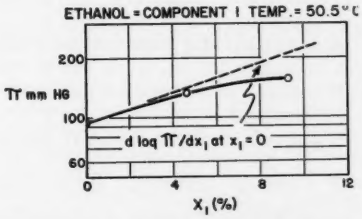

Fig. 3. Plot of log π vs. x_1 at 50.5°C. for ethanol (component 1)—water. Dotted line is $(\partial \log \pi/\partial x_1)_T$ at $x_1 = 0$.

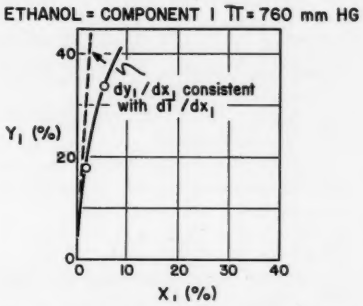

Fig. 4. x-y diagram for ethanol (component 1)—water at 760 mm. Hg. Dotted line is $(\partial y_1/\partial x_1)\pi$ thermodynamically consistent with $(\partial T/\partial x_1)\pi$.

upon mixing (isothermal data) (2, 4, and 7).

Latent heats of vaporization may be rigorously introduced by the relation in a footnote to Table 1.

At low pressures $f^\circ_{1V} = \pi, f^\circ_{1L} = P_1$, $V_{2L}\pi/RT << 1.0$, $V_{2V}\pi/RT$ approaches unity, and γ_{1V} approaches unity. The exact equations in Table 1 then reduce to the "low-pressure" equations tabulated in the last column of Table 1.

The equations for isobaric and isothermal data may be put in similar forms by simple rearrangement. As an illustration for liquid composition diagrams at $x_1 = 0$:

Isobaric:

$$\left\{\frac{\gamma_{1L}}{\gamma_{1V}} = \frac{f^\circ_{1V}}{f^\circ_{1L}}\left[1 - \left(\frac{\partial \ln P_2}{\partial x_1}\right)_\pi \left(\frac{V_{2V}\pi}{RT} - \frac{V_{2L}\pi}{RT}\right)\right]\right\}_{x_1=0} \quad (16)$$

Isothermal:

$$\left\{\frac{\gamma_{1L}}{\gamma_{1V}} = \frac{f^\circ_{1V}}{f^\circ_{1L}}\left[1 + \left(\frac{\partial \ln \pi}{\partial x_1}\right)_T \left(\frac{V_{2V}\pi}{RT} - \frac{V_{2L}\pi}{RT}\right)\right]\right\}_{x_1=0} \quad (17)$$

Illustrative Example

Application of the derived equations to experimental data is not difficult. The isobaric and isothermal data of Jones, Schoenborn and Colburn (5) for ethanol-water is used here. Ethanol has been chosen as component one.

TABLE 4.—ISOBARIC AND ISOTHERMAL DATA FOR ETHANOL-WATER*

Isobaric at 760 mm.Hg

Temp., °C.	x_1	y_1
100	0	0
95.5	0.018	0.179
90.6	0.054	0.338

Isothermal at 50.5°C.

Press., mm.Hg	x_1	y_1
94.8	0	0
133	0.046	0.290
157	0.093	0.424

*Ethanol is component 1.

Isobaric Data. T-x_1 data are in Table 4 for 760 mm.Hg total pressure. One has the option of plotting T vs. x_1 and obtaining $(\partial T/\partial x_1)\pi$ at $x_1 = 0$, or of obtaining P_2 for each value of x_1 and plotting ln P_2 vs. x_1 and obtaining $(\partial \ln P_2/\partial x_1)\pi$. The latter route, which usually results in more accurate slope taking, is used in Figure 1 with the vapor pressure of water from Keenan (6).

From Figure 1 $(\partial \ln P_2/\partial x_1)\pi = -14.34$; and, with the appropriate "low-pressure" equation and the vapor pressure of ethanol from Stull (9),

$$\left\{\gamma_{1L} = \frac{\pi}{P_1}\left[1 - \left(\frac{\partial \ln P_2}{\partial x_1}\right)_\pi\right]\right\}_{x_1=0} \quad (18)$$

$$(\gamma_{1L})_{x_1=0} = \frac{760}{1{,}685}(15.34) = 6.92 \quad (18a)$$

[This value is a reasonable extrapolation of the plot of log γ_{1L} vs.

x_1 in the original reference(5).]

In Figure 2 $(\partial \ln P_2/\partial y_1)\pi$ has been determined as —0.846. With the appropriate low-pressure equation.

$$\left\{\gamma_{1L}=\frac{\pi}{P_1}\left[\frac{1}{1+\left(\frac{\partial \ln P_2}{\partial y_1}\right)_\pi}\right]\right\}_{x_1=0} \tag{19}$$

$$(\gamma_{1L})_{x_1=0}=\frac{760}{1{,}685\ (0.154)}=2.93 \tag{19a}$$

This brings out an important point. The value 2.93 is not close to 6.92; however, determination by means of $(\partial \ln P_2/\partial y_1)\pi$ is subject to considerable error because the *difference* between unity and $(-\partial \ln P_2/\partial y_1)\pi$ is involved. Thus, using $(\partial \ln P_2/\partial y_1)\pi$ is not a desirable route. This conclusion is valid for all systems wherein $(\partial \ln P_2/\partial y_1)\pi$ is *negative* (e.g., minimum boiling azeotropes). For systems where $(\partial \ln P_2/\partial y_1)\pi$ is *positive*, use of $(\partial \ln P_2/\partial y_1)\pi$ is preferred. Similar considerations apply when constant-temperature data are used.

Isothermal Data. In Figure 3 $(\partial \ln\pi/\partial x_1)_T$ is determined for the 50.5°C. data. With the appropriate low-presure equation, $\gamma_{1L}=4.01$. [This value is a reasonable extrapolation of the plot of log γ_{1L} vs. x_1 in the original reference(5).]

Consistency Check. To illustrate a thermodynamic consistency check, the value of $(\partial y_1/\partial x_1)\pi$ consistent with $(\partial T/\partial x_1)\pi$ is shown in Figure 4 for the 760 mm.Hg data. There is clearly no inconsistency. Other checks which can be made are $(\partial T/\partial y_1)\pi$ consistent with $(\partial T/\partial x_1)\pi$ (and vice versa), by means of Table 3; $(\partial y_1/\partial x_1)\pi$ consistent with $(\partial T/\partial y_1)\pi$; and a similar set of checks for the isothermal data.

Discussion

Several additional points warrant comment.

The meager data required to establish these slopes are emphasized. Only two experimental points are required for the mixtures, and the composition of only a single phase need be considered.

The equations provide certain limits for any particular system. For example, since $(\gamma_{1L}/\gamma_{1V})$ must be positive, $(\partial T/\partial x_1)_{\pi x_1=0}$ has a certain maximum value above which it cannot go.

To date little use has been made of isothermal pressure–liquid composition and isobaric temperature–liquid composition diagrams. The derived equations strongly suggest more use of these at least to obtain activity coefficients at infinite dilution.

ACKNOWLEDGMENT

The authors wish to acknowledge a critical review of this paper by L. C. Matsch and J. Wang of Linde Air Products.

NOTATION

A = dimensionless constant in the van Laar equation
e = base of natural logarithms
f = fugacity, atm.
G^E = excess free energy, B.t.u./lb.-mole
H^E = excess enthalpy, B.t.u./lb.-mole
K = equilibrium vaporization ratio $= y/x$
P = vapor pressure of a pure component, atm.
R = gas-law constant=1.987 B.t.u./(lb.-mole) (°R.)
S^E = excess entropy, B.t.u./(lb.-mole) (°R.)
T = absolute temperature, °R.
V = molal volume of pure component, cu.ft./lb.-mole
V' = an average molal volume of the pure component over the pressure range π to P, cu.ft./lb.-mole
x = mole fraction in liquid phase
y = mole fraction in vapor phase
γ = activity coefficient
λ = latent heat of vaporization, B.t.u./lb.-mole
ν = fugacity coefficient $= f/\pi$
π = total pressure of the system, atm.

Subscripts

1, 2 refers to components one and two
L refers to liquid phase
V refers to vapor phase
$x_1=0$ refers to conditions at $x_1=0$
π, T and
P_2, T refer to the temperatures and pressures at which fugacity coefficients are evaluated

Superscripts

° refers to the standard state
— denotes a partial molal quantity (e.g., $\overline{G}^E$)

LITERATURE CITED

1. Carlson, H. C., and A. P. Colburn, *Ind. Eng. Chem.*, 34, 581 (1942).
2. Gautreaux, M. F., M. S. thesis, Louisiana State University, Baton Rouge (1951).
3. Hougen, O. A., and K. M. Watson, "Chemical Process Principles," Part II, p. 649, John Wiley and Sons, Inc., New York (1947).
4. Ibl, N. V., and B. F. Dodge, *Chem. Eng. Science*, 2, 120-126 (1953).
5. Jones, C. A., E. M. Schoenborn, and A. P. Colburn, *Ind. Eng. Chem.*, 35, 666 (1943).
6. Keenan, J. H., and F. G. Keyes, "Thermodynamic Properties of Steam," 1 ed., John Wiley and Sons, Inc., New York (1936).
7. Nord, M., *Chem. Eng. Progr. Sym. Series* No. 3, 48, 55 (1952).
8. Redlich, O., and A. T. Kister, *Ind. Eng. Chem.*, 40, 341 (1948).
9. Stull, D. R., *Ind. Eng. Chem.*, 39, 514 and 536 (1947).
10. Wood, S. E., *J. Chem. Phys.*, 15, 358 (1947).

APPENDIX

Proof That $(\partial\gamma_{2L}/\partial x_1)\pi$ Equals Zero at $x_1=0$

γ_{2L} is a function of T, π, and x_1. Therefore

$$d\ln\gamma_{2L}=\left(\frac{\partial \ln\gamma_{2L}}{\partial T}\right)_{\pi,\,x_1}dT+\left(\frac{\partial \ln\gamma_{2L}}{\partial \pi}\right)_{T,\,x_1}d\pi+\left(\frac{\partial \ln\gamma_{2L}}{\partial x_1}\right)_{T,\,\pi}dx_1 \tag{1}$$

For constant pressure

$$\left(\frac{\partial \ln\gamma_{2L}}{\partial x_1}\right)_\pi=\left(\frac{\partial \ln\gamma_{2L}}{\partial T}\right)_{\pi,\,x_1}\left(\frac{\partial T}{\partial x_1}\right)_\pi+\left(\frac{\partial \ln\gamma_{2L}}{\partial x_1}\right)_{T,\,\pi} \tag{2}$$

But at $x_1=0$

$$\left(\frac{\partial \ln\gamma_{2L}}{\partial T}\right)_{\pi,\,x_1}=-\left(\frac{\overline{H}_2-H_2^\circ}{RT^2}\right)=0 \tag{3}$$

$$\left(\frac{\partial \ln\gamma_{2L}}{\partial x_1}\right)_{T,\,\pi}=-\frac{x_1}{x_2}\left(\frac{\partial \ln\gamma_{1L}}{\partial x_1}\right)_{T,\,\pi}=0 \tag{4}$$

Thus,

$$\left(\frac{\partial \ln\gamma_{2L}}{\partial x_1}\right)_\pi=\frac{1}{\gamma_{2L}}\left(\frac{\partial\gamma_{2L}}{\partial x_1}\right)_\pi=\left(\frac{\partial\gamma_{2L}}{\partial x_1}\right)_\pi=0 \tag{5}$$

A similar argument holds for $(\partial\gamma_{2V}/\partial x_1)\pi$ at $x_1=0$. Also a similar argument holds if temperature rather than pressure is held constant.

(Presented at A.I.Ch.E. Houston meeting)

Heat Transfer to Water in an Annulus

Philip Miller, James J. Byrnes, and David M. Benforado
Walter Kidde Nuclear Laboratories, Inc., Garden City, New York

A limited number of measurements were made of the heat transfer coefficient from an electrically heated rod to water flowing in an annulus. Tests were performed at Reynolds numbers ranging from 5,000 to 22,000 (based on equivalent diameter), water temperatures of 70° and 125°F., and relatively high heat fluxes of 52,000 to 208,000 B.t.u./(hr.) (sq. ft.). The annulus dimensions were 0.625 in. I.D. and 0.840 in. O.D. The coefficients varied as the 0.8 power of the velocity; they were 20% higher than predicted by use of Colburn's equation for flow inside pipes with the equivalent diameter. Over the range of conditions studied, it was found that the thermal boundary layer was fully developed in 1⅛ in. ($L_h/D_e=5$).

In the course of a study of heat transfer to water flowing parallel to a bundle of rods (which will be reported separately), a few measurements were made under annular-flow conditions by means of the heated test rod developed for the general study. These measurements were made at high heat fluxes and moderate Reynolds numbers. Since the literature contains only a limited amount of data for annular-flow heat transfer, it seemed worth while to present the results of these tests, in spite of their limited scope (including the use of a single geometry and the absence of pressure - drop measurements). Tests were made at Reynolds numbers (D_eG/μ) ranging from 5,000 to 22,000; at heat fluxes from 52,000 to 208,000 B.t.u./(hr.)(sq.ft); at water temperatures 70° and 125°F.; and at a single ratio of $D_2/D_1 = 1.34$. Three different heater rods were tested.

Equipment and Procedure

Figure 1 shows a diagram of the annulus test section. A vertical glass tube, 16 in. long and with a measured I.D. of 0.840 ± 0.001 in. enclosed the middle section of the 0.625-in. O.D. heater rod (for rods 15 and 19; for rod 20 the glass tube was 17 in. long and $0.865 \pm .001$ in. I.D.). The rod was centered in the tube by means of two perforated aluminum collars, which had about 50% free-flow area. For rod 15 the bottom collar was 3½ in. below the bottom of the heated section; for rod 19 this distance was 2 in.; and for rod 20 it was 3¾ in. Standard ¾-in. pipe tees formed inlet and outlet headers for the water, which flowed upward; the tees were connected to the glass tubes by heavy-wall rubber tubing and were sealed at the outer end by rubber stoppers through which the heater rod passed.

Figure 2 gives a flow diagram of the system. For convenience, an available overhead 1,000-gal. storage tank of a laboratory-waste-water-treatment system, which contained deionized water, was used as a feed tank. To obtain the required flow rate, an air pressure between 38 and 39 lb./sq.in. gauge was maintained automatically in the upper part of this tank; the flow rate was adjusted by means of a throttling valve in the tank discharge line, which was connected to the test section by means of rubber hose. The water leaving the test section discharged to the atmosphere through a throttling valve, which was adjusted to give a convenient pressure reading in an open-ended vertical glass tube inserted in the discharge line, which served as an indication of the uniformity of flow rate. The flow rate was measured by the time required to fill a calibrated 5-gal. bottle, and the temperature of the discharge water was measured to 0.2°C. with a glass thermometer. The flow-rate measurement was reproducible to better than 2%.

An ice bath was used for the reference junction for all thermocouple measurements. The water temperature was raised appreciably by the heat from the test rod; the temperature rise was about 5°F. at a velocity of 3 ft./sec. and a power input of 1,650 watts. A proportionate part of this temperature rise was subtracted from the measured outlet temperature of the water to obtain the appropriate water temperature for calculating ΔT. Since both the temperature rise and ΔT are proportional to the power input, the percentage correction in ΔT is independent of power; it amounted to about 2% for a thermocouple at the midpoint of a 4-in. heated section. The thermocouple voltages were read with a Leeds and Northrup type K-2 potentiometer and D.C. (No. 2430) galvanometer. The surface thermocouples were calibrated in flowing water against a chromel-alumel thermocouple that had been calibrated in an oil bath against Anshutz precision thermometers.

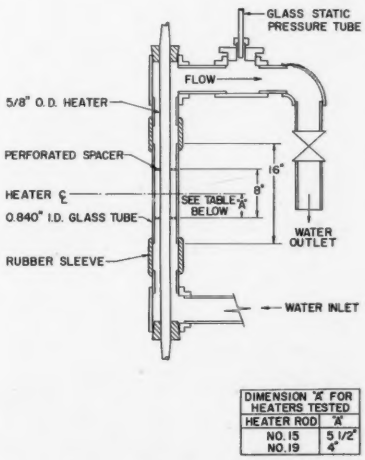

Fig. 1. Diagram of annulus test section.

The test element was heated with D.C. current from a Westinghouse type R.A. arc welder. This unit was rated to supply 200 amp. at 40 volts. The maximum power input obtainable with the heaters used (close to 1-ohm resistance) was approximately 3.2 kw., corresponding to a current of 56.5 amp. and a voltage drop of 56.5 volts across the heater. The power input was measured with a Weston model 310 Wattmeter, which had scales of 1,000, 2,000, and 4,000 watts graduated in divisions of 10, 20, and 40 watts. Independent calibration of this meter by the vendor and by an outside laboratory showed the maximum error on any scale to be less than ¼ of 1% of full scale value. The meter readings required no correction, since the voltage leads were connected directly to the ends of the heating coil.

The cooling water was at room temperature, except for one set of measurements made with rod 15 and water at 125°F. In that test the inlet stream was preheated continuously with steam by means of a Heliflow heat exchanger suitably connected.

After a smooth flow rate had been established and the system was visually free of air bubbles, power was applied to the heater (at 825, 1,650, or 3,200 watts, for a 4-in.

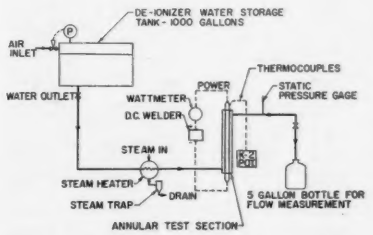

Fig. 2. Flow diagram for annular-flow heat transfer tests.

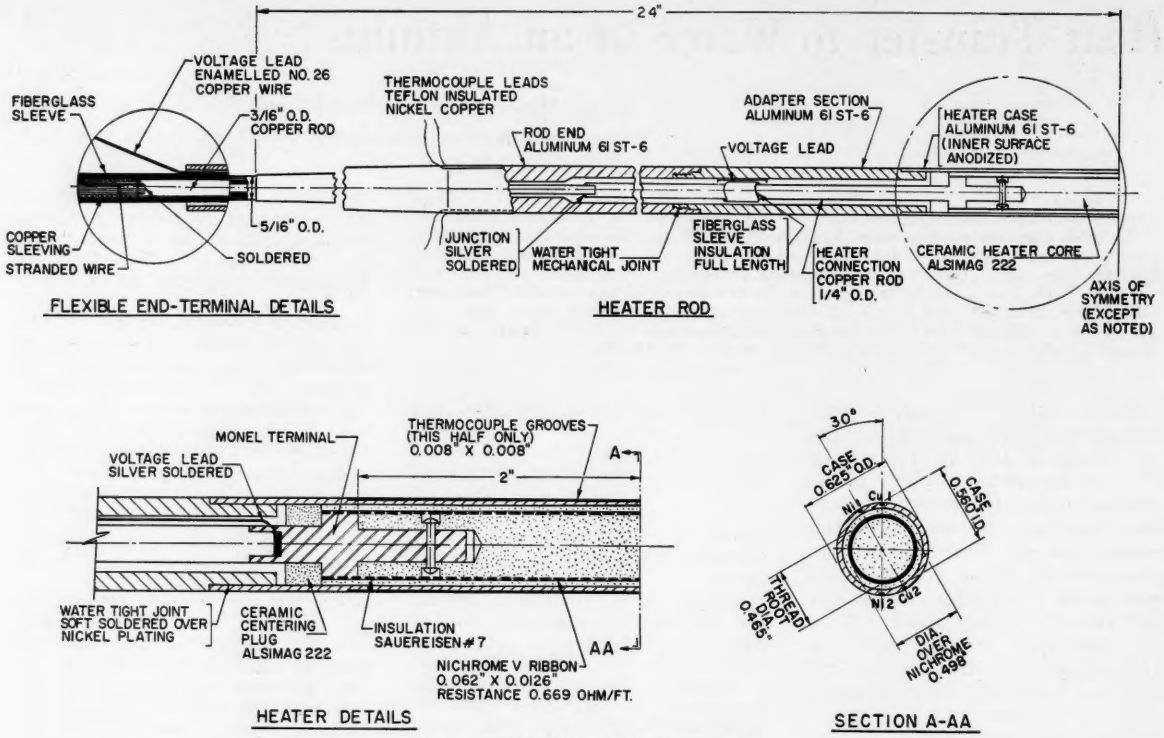

Fig. 3. Construction of heater rod 15.

heated length). Thermocouple readings were then taken until a steady state was indicated by the absence of a trend. Generally three sets of consecutive readings were sufficient, and an average of the last two sets was taken as the result. Table 1 gives a typical data sheet.

Description of Heater Rod

The construction of the heated test rod is shown in Figure 3. Heat was generated in a nichrome resistance element wound on a threaded ceramic core and encased in an aluminum jacket from which it was insulated electrically by a 31-mil layer of Sauereisen (type 7) refractory ce-

TABLE 1.—TYPICAL DATA SHEET (TEST A3-ROD 15)

Time	Cold junction, °C.	Thermocouple reading, mv. CuNi 1	CuNi 2	Outlet water temp., °C.	Flow rate	Air pressure, lb./sq. in. gauge	Wattmeter Read.	Scale	Factor	Power, watts
9:05	—0.2	0.374	0.374	19.75	125 sec. ≈ 5.15 gal.	39	OFF			
9:11		0.374	0.375	19.75						
9:25							805	75 Par.	1.0	805
9:27		1.020	0.943	21.5			810			810
9:28		1.025	0.945	21.5			810	75 Par.	1.0	810
9:30		1.029	0.948	21.5	127 sec. ≈ 5.15 gal.	39	810	75 Par.	1.0	810
9:33		1.027	0.947	22.0			810	75 Par.	1.0	810
9:35							1,650			1,650
9:37		1.624	1.444	23.2			1,640	75 Par.	1.0	1,640
9:38	—0.2	1.645	1.471	23.2		38	1,650			1,650
9:41		1.647	1.470	23.5			1,650	75 Par.	1.0	1,650
9:42		1.652	1.488	23.2	128 sec. ≈ 5.15 gal.		1,650			1,650
			1.496							
9:48		1.659	1.514				1.650	75 Par.	1.0	1,650
9:50		1.661	1.518				1,650			1,650
9:55		1.124	0.990	22.2	67 sec. ≈ 5.15 gal.		1,650	75 Par.	1.0	1,650
9:59	—0.2	1.126	0.986				1,650			1,650
10:01		1.126	0.985	22.0			1,650	75 Par.	1.0	1,650
10:03							840	75 Par.	1.0	840
10:05		0.768	0.699	22.0			840	75 Par.	1.0	840
10:08		0.770	0.700	22.0			840	75 Par.	1.0	840
10:09		0.770	0.700	22.0	66 sec. ≈ 5.15 gal.		840			840

ment. The core was made of Alsimag 222, a ceramic which can be machined quite easily and which does not change its dimensions upon subsequent heating to high temperatures. The core was doubly threaded in order to use two nichrome windings in parallel, which was a convenient way of reducing the resistance without changing the type of nichrome ribbon used (nichrome V, cross section 0.062×0.0126 in., resistance 0.669 ohm/ft.). The heated section was 4 in. long, and the heater resistance was 0.919 ohm. The ceramic core was extended for ¼ in. at each end with a cylindrical Monel terminal piece of the same O.D. and threaded continuously with the ceramic core. The ends of the nichrome windings were anchored to the Monel pieces by peening the thread walls down over the nichrome ribbon. The Sauereisen cement was brushed on as a paste, air-dried at room temperature overnight, ground on a lathe to the I.D. of the aluminum jacket, then baked overnight at 120°C.

The aluminum jacket was a 6-in. length of commercially available 61ST-6 tubing of 0.625 in. O.D. and 32-mil wall thickness. It was anodized on the inside to provide additional electrical insulation, and was fastened by soft-soldering to two hollow aluminum end pieces of equal length. Aluminum surfaces to be soldered were first nickel plated.

Separate power leads and voltage leads were fastened to the Monel terminal pieces and were carried out through the hollow aluminum end pieces.

Two copper-nickel thermocouples were attached to the surface of heater rod 15, with both junctions at the midlength of the heated section and 180° apart on the circumference. For each thermocouple the two wires were inserted in separate grooves and were insulated from the jacket metal except at the tip, where a junction was made by swaging ¼ in. of exposed wire into the groove with cold solder, then smoothing the surface. The thermocouple circuit was completed by the jacket. The grooves were 8 mils wide by 8 mils deep and 30° apart and extended back for 2 in. from the junction. Beyond this point the wires were cemented to the surface of the rod. The copper wire was 7 mils in diameter and the nickel wire was 3.5 mils in diameter; both were insulated with an integral Teflon coating. Void space in the grooves not occupied by the wires was filled in with Pliobond cement.

Heater rod 19 was similar to rod 15, except that it was provided with a single thermocouple mounted as nearly flush with the surface as was feasible. This was done to determine whether the 8-mil depth of the rod-15 thermocouples caused any significant difference in reading. The rod-19 thermocouple was installed by squeezing the wires into slits only 1 to 2 mils deep made with a razor blade. Then a ⅛-in. band of nickel less than ½-mil thick was plated around the circumference over the wire tips to anchor them and ensure electrical and thermal contact. (This method of installation did not prove rugged enough for general use.) The thermocouple junction was located ⅞ in. below the midlength of the heated section.

Heater rod 20 had an 8-in. heated length and was copper jacketed. It was provided with six thermocouples spaced axially along the rod. Each thermocouple required only a single groove, for a nickel wire, since the copper jacket completed the thermocouple circuit. The nickel wires were 45° apart on the circumference.

The surface of the heater rods is believed to have been equivalent to that of a smooth tube. In a long series of experiments (not annular flow), coefficients measured with rod 15 showed no trend, indicating that the surface remained smooth. This was confirmed by physical appearance.

RESULTS AND DISCUSSION

The results of the heat transfer measurements are listed in Table 2. For heater rod 15 the readings of the two thermocouples were averaged to calculate the temperature difference between the heated surface and the water. The two thermocouples consistently differed by about 10%; from other work with this heater rod it was concluded that this difference was probably due to a peripheral variation in heat flux, caused by a variation in thickness or thermal conductivity of the layer of Sauereisen insulation. Since there was an estimated drop of as much as 1500°F. across this layer, relatively small differences in thermal resistance could cause an uneven flux pattern. In several measurements the glass outer sleeve was rotated 180° as a means of detecting any annulus eccentricity not disclosed by the measurement of the dimensions. No significant changes were observed.

The heat ransfer results are believed to be accurate to ±8%.

The effect of heated length on heat transfer coefficient was investigated in tests made with rod 20. This rod had an 8-in. heated length, with six thermocouples spaced axially along the rod from 1⅛ to 6 in. past the upstream end. The upstream unheated length was 3¾ in., and the jacket diameter was 0.865 in. I.D. (compared with 0.840 in. in the other tests). Tests were made at two velocities with room-temperature water, the heat flux being varied at the lower velocity.

Figure 4 gives a plot of h vs. heated length. The measured heat

TABLE 2.—MEASURED HEAT TRANSFER COEFFICIENTS FOR ANNULAR FLOW

Test	Heater rod	Outlet water temp., °F.	Water velocity, ft./sec.	Heat flux, B.t.u./(hr.)(sq. ft.)	Corrected† ΔT, °F.	h, B.t.u. (hr.)(sq. ft.)(°F.)
*A*3	15	70.8	3.15	50,600	50.1	1,010
		73.8	3.13	103,000	97.5	1,060
		71.6	6.06	52,400	27.8	1,880
		71.6	5.98	103,000	55.2	1,870
		73.4*	6.06	105,500	55.4	1,900
*A*6	15	75.8*	6.68	104,600	44.9	2,330
		126.2	6.91	104,300	36.0	2,900
		126.2	6.91	103,600	35.0	2,960
		130.6	6.91	199,800	69.0	2,900
*A*4	19	74.3	3.21	51,200	44.9	1,140
		76.3	3.21	104,300	86.5	1,210
		69.2	6.37	50,900	28.8	1,770
		73.8	6.26	104,300	51.4	2,030
		73.8*	6.37	103,000	54.9	1,880
		73.4*	12.52	102,700	31.1	3,300
*A*17	20	80.6	2.82	38,200	39.7	960
		82.9	2.82	62,600	62.9	995
		86.0	2.82	100,800	94.5	1,070
*A*15	20	75.3	5.98	98,900	55.4	1,790

*For these tests the glass outer tube was rotated 180° compared with the unstarred tests.

†For rod 15 the reported ΔT is based on an average of two thermocouples; for rod 20, an average is taken for six thermocouples; rod 19 had a single thermocouple.

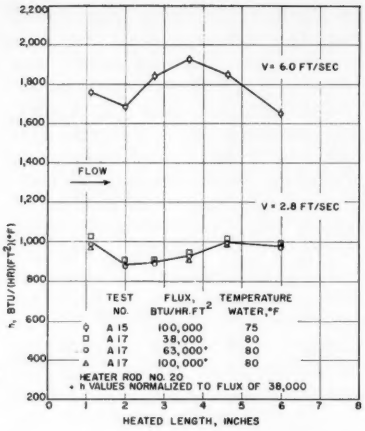

Fig. 4. Effect of heated length.

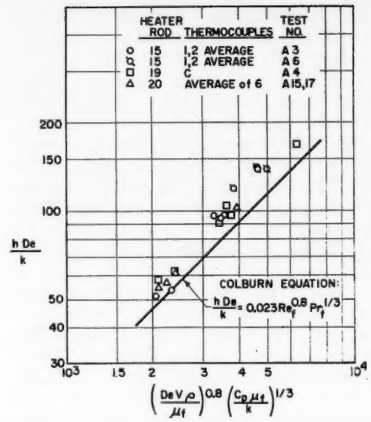

Fig. 5. Annular-flow heat transfer data compared with Colburn equation.

transfer coefficients increased with increasing flux, as would be expected from the effect of increased film temperature and reduced viscosity. To place the data for the lower velocity on a comparable basis, the values in Figure 4 have been "normalized" to a constant film temperature by use of the relation that h is inversely proportional to $\mu_f^{0.467}$, derived from the Colburn equation [Equation (1)].

The values of h show no consistent trend with heated length. The average deviation of a single value from the mean of the six values was less than 5% at each velocity. It appears that for a heated length greater than 1⅛ in. ($L_h/D_e > 4.7$, where L_h is heated length) the thermal boundary layer was fully developed within the accuracy of the experiments. Likewise, for $L/D_e > 20$ the hydraulic boundary layer was fully developed.

(A measurement was also made at a heated length of ⅝ in. in one test, which indicated a higher value of h; however, it was calculated that axial heat conduction would be sufficient to lower the surface temperature significantly at this point. For this reason, the value is not reported.)

Rod 15 had a 2-in. heated length upstream of the thermocouples, and for rod 19 this distance was 1⅛ in. Consequently, all the results represent a fully developed thermal boundary layer.

These results are not in agreement with those reported by McAdams et al. (*1*) for annular heat transfer to water. They report the results of a test, over an 11.5-in. heated length, in which the coefficient dropped almost linearly by 35%, in going from 2 to 10 in. (corresponding to a range of 4 to 19 for L_h/D_e). The heated rod was 0.25 in. in diam., the jacket was 0.77 in. I.D., the velocity was 1 ft./sec., water temperature was 270°F. ($Re = 17{,}600$, based on D_e), and there was an upstream unheated section 3 in. long.

The data in Table 2 are plotted in Figure 5 for comparison with the modified Colburn equation, which is recommended by Perry for annular heat transfer (*2*):

$$\frac{hD_e}{k} = 0.023\left(\frac{D_eG}{\mu_f}\right)^{0.8}\left(\frac{C_p\mu_f}{k}\right)^{1/3} \quad (1)$$

On the average, the experimental values fall about 20% above the straight line representing Equation (1). The values obtained with heater rod 19 (squares) fall quite close to a straight line parallel to the Colburn equation. The other values show somewhat more scatter, particularly at the low velocities, but are in general agreement with the rod-19 results. This was taken to indicate that the method of mounting the thermocouples used on heater rods 15 and 20 did not introduce any significant error into the measured surface temperatures.

Perry (*2*) gives the following dimensional equation for heat transfer to water in turbulent flow inside tubes:

$$h = \frac{160\,(1 + 0.012\,t_f)\,(V_s)^{0.8}}{(D')^{0.2}} \quad (2)$$

When one applies this equation to the conditions of Table 2, using D_e, values of h are calculated which, on the average, are 6% higher than the experimental values. Equation (2), which is confined to water, is perhaps a better basis of comparison than Equation (1), which represents the average behavior of a large variety of fluids over a wide range of conditions.

It is concluded that the present results, within their limited scope, indicate that annular-flow heat transfer can be predicted by the accepted equations for flow inside tubes, by means of the equivalent diameter.

ACKNOWLEDGMENT

The results reported in this paper were obtained during work performance by the Walter Kidde Nuclear Laboratories, Inc., under Contract AT(30-1)-1374 for the United States Atomic Energy Commission. The permission of the A.E.C. to publish this paper is hereby gratefully acknowledged.

The authors are indebted to Mr. George G. Bartolomei for construction of the heated test rods.

NOTATION

C_p = specific heat of water at bulk temperature, B.t.u./(lb.) (°F.)
D_1 = outside diameter of rod, ft.
D_2 = inside diameter of annulus jacket, ft.
D_e = equivalent diameter, ft. = 4x flow area/wetted perimeter = $D_2 - D_1$
D' = diameter, in.
G = mass velocity of water = $V\varrho$, lb./(hr.) (ft.²)
h = heat transfer coefficient, B.t.u./(hr.) (ft.²) (°F.)
k = thermal conductivity of water at bulk temperature, B.t.u./(hr.) (ft.) (°F.)
L = upstream length, ft.
L_h = upstream heated length, ft.
T = temperature, °F.
T_f = average film temperature, °F.
ΔT = temperature difference from rod surface to bulk water, °F.
V = water velocity, fps.
V_s = water velocity, fps., based on $\varrho = 62.3$ lb./ft.³
μ = viscosity of water at bulk temperature, lb./(ft.) (hr.)
μ_f = viscosity of water at average film temperature, lb./(ft.) (hr.)
ϱ = density of water at bulk temperature, lb./ft.³
Re = Reynolds number, D_eG/μ
$Re_f = D_eG/\mu_f$

LITERATURE CITED

1. McAdams, W. H., W. E. Kennel, C. S. Minden, R. Carl, P. M. Picornell, and J. E. Dew, *Ind. Eng. Chem.*, 41, 1945 (1949).
2. Perry, J. H., "Chemical Engineers' Handbook," 3 ed., p. 470, McGraw-Hill Book Company, Inc., New York (1950).

Numerical Solution of Two-dimensional Heat-flow Problems

JIM DOUGLAS, JR., and D. W. PEACEMAN
Humble Oil and Refining Company, Houston, Texas

Two-dimensional heat flow frequently leads to problems not amenable to the methods of classical mathematical physics; thus, procedures for obtaining approximate solutions are desirable. A recently introduced finite-difference method, known to be applicable to problems in a rectangular region and involving much less calculation than previous methods, is extended by example to cases of more practical interest. Although all three examples given are steady state, unsteady state problems may also be attacked successfully by the method. The first example is that of flow around a corner and indicates that a more complicated region than a rectangle can be treated. Then a problem involving a radiation-boundary condition is given; as this condition is nonlinear, the method is extended to more general equations. The last example involves point heat sources and sinks in an elliptical region and so extends the method to treat curved boundaries (as distinguished from polygonal domains) and singular points. It is believed that materially less calculation is necessary by this method than for previous procedures.

Many cases of heat conduction in three dimension may be reduced by symmetry to problems involving only two-space variables. Further reduction to a one-space variable is frequently not possible. Unless the geometry and boundary conditions are very simple, analytical solutions of the differential equation of heat conduction in two dimensions are either very cumbersome or impossible to obtain. Approximate solutions may be obtained by numerical, graphical, or experimental methods. The rapid development of high-speed electronic computers in the past few years has stimulated interest in numerical methods for the solution of a wide class of problems. In this paper a recently introduced numerical procedure which is known to be applicable to problems in a rectangular region is extended by example to cases of more practical interest. Although this procedure was developed for the purpose of solving problems involving fluid flow through porous media in two-dimensional reservoirs, it can also be used for two-dimensional problems in many other fields such as heat conduction and diffusion.

PREVIOUS NUMERICAL METHODS

Heat-conduction problems can be divided into two categories: unsteady state and steady state. The differential equation describing unsteady state heat flow is(*8*)

$$\frac{k}{c\rho}\left(\frac{\partial^2 T}{\partial x^2}+\frac{\partial^2 T}{\partial y^2}\right)=\frac{\partial T}{\partial \theta} \quad (1)$$

while that governing steady state heat flow is

$$\frac{\partial^2 T}{\partial x^2}+\frac{\partial^2 T}{\partial y^2}=0 \quad (2)$$

All numerical methods for the solution of these equations involve replacement of the continuous derivatives by ratios of finite differences and solution of the resulting difference equations. To formulate the difference equations, the two-dimensional region in which the integration is to be carried out has placed over it an integration net with mesh widths Δx and Δy, as shown in Figure 1. Usually

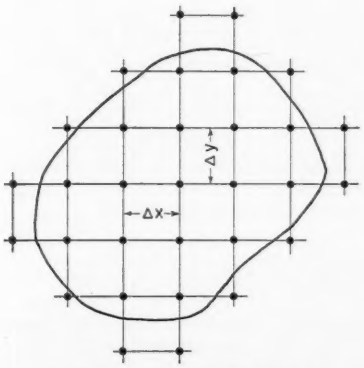

Fig. 1. Integration net.

Δx and Δy are set equal to each other. The second derivatives are then replaced by second differences. For example, at the point x, y, $\partial^2 T/\partial x^2$ is replaced by

$$\frac{\dfrac{T(x+\Delta x)-T(x)}{\Delta x}-\dfrac{T(x)-T(x-\Delta x)}{\Delta x}}{\Delta x}$$

which is equal to

$$\frac{1}{(\Delta x)^2}[T(x-\Delta x)-2T(x)+T(x+\Delta x)]$$

Thus, if $\Delta x=\Delta y$, the difference equation corresponding to the steady state Equation (2) is

$$T(x-\Delta x,y)+T(x+\Delta x,y)+T(x,y-\Delta y)+T(x,y+\Delta y)-4T(x,y)=0 \quad (3)$$

In the carrying out of a numerical solution of the unsteady state Equation (1), the time coordinate is also divided into finite increments, $\Delta\theta$, not necessarily equal. It is assumed that a solution has been obtained for time θ, and a difference equation is used to obtain the solution at time $\theta+\Delta\theta$.

Jakob(*4*) and Milne(*5*) describe several methods for the numerical solution of Equations (1) and (2). The three chief ones are relaxation, explicit, and implicit methods. Relaxation is rapid and convenient for hand calculation with a small number of points, but when it is desired to evaluate the solution at a large number of points by use of a computing machine, relaxation is inconvenient because of its non-mechanical nature.

The terms *explicit* and *implicit* have somewhat different meanings for the unsteady and steady state

cases. In the unsteady state case, an explicit difference equation may be solved explicitly for the unknown function at time $\theta + \Delta\theta$ in terms of the known values of the function at time θ. For example, an explicit difference equation may be obtained by replacing the second derivatives of Equation (1) by second differences evaluated at time θ. Thus, if $\Delta x = \Delta y$,

$$\frac{k}{c\rho(\Delta x)^2}[T(x-\Delta x, y, \theta) + T(x+\Delta x, y, \theta) + T(x, y-\Delta y, \theta) + T(x, y+\Delta y, \theta) - 4T(x, y, \theta)] = \frac{1}{\Delta\theta}[T(x, y, \theta+\Delta\theta) - T(x, y, \theta)] \quad (4)$$

This equation may be solved explicitly for $T(x, y, \theta+\Delta\theta)$ at each point of the integration net. Starting with known initial values of T at $\theta = 0$, the solution may be carried forward to any time, θ.

Implicit methods for the unsteady state case, on the other hand, are characterized by having the unknown values of the desired function at time $\theta + \Delta\theta$ bound together by systems of simultaneous equations. For example, an implicit difference equation may be obtained by replacing the second derivatives of Equation (1) by second differences evaluated at time $\theta + \theta\Delta$. Thus, if $\Delta x = \Delta y$.

$$\frac{k}{c\rho(\Delta x)^2}[T(x-\Delta x, y, \theta+\Delta\theta) + T(x+\Delta x, y, \theta+\Delta\theta) + T(x, y-\Delta y, \theta+\Delta\theta) + T(x, y+\Delta y, \theta+\Delta\theta) - 4T(x, y, \theta+\Delta\theta)] = \frac{1}{\Delta\theta}[T(x, y, \theta+\Delta\theta) - T(x, y, \theta)] \quad (5)$$

When this equation is written for each point in the integration net, N simultaneous equations are obtained, where N is the number of interior points in the net. These N equations must be solved at each time step.

When the steady state case is considered, the difference Equation (3) is written for each point in the integration net. A set of N simultaneous equations is obtained, most of which have five unknowns in them. Simultaneous equations of this type are most successfully attacked by iterative methods, most of which can be shown to be analogous to a solution by finite differences of a related unsteady state problem. An iteration method is explicit if each iteration involves solving explicitly for the unknown function at each point, while it is implicit if the unknown values of the function are tied together by simultaneous equations.

For the solution of the unsteady state problem on a computing machine, the explicit Equation (4) is easy to use because of its simplicity, but it suffers from a severe disadvantage. If the size of the time increment, $\Delta\theta$, is taken too large, the computations become unstable in the sense that small errors introduced at the beginning of the calculations are amplified and eventually become so large as to swamp the calculations. To avoid this, it is necessary to satisfy the relationship

$$\Delta\theta \leqslant \frac{c\rho(\Delta x)^2}{4k} \quad (6)$$

This instability of explicit difference equations for large time increments is discussed by O'Brien, Hyman and Kaplan(*6*) and Milne (*5*). This restriction on $\Delta\theta$ means that a large number of small time steps must be taken to carry the solution to a given time θ. If it is desired to increase the accuracy of the solution by using more points in the integration net, it is necessary to decrease $\Delta\theta$ in accordance with Equation (6), so that the number of computations increases as the square of the number of points.

The implicit difference Equation (5), on the other hand, has the advantage of being stable for any size time increment(*1, 6*). In the carrying out of an unsteady state solution by an implicit procedure, $\Delta\theta$ is restricted not by stability but only by the allowable truncation error, and for a specified accuracy, fewer time steps are required than for the explicit procedure. The reduction of the number of time steps more than compensates for the additional labor required to solve by iteration the N simultaneous equations at each time step, so that, from the point of view of computational labor, the implicit procedure is considerably superior to the explicit procedure for the solution of unsteady state problems(*7*).

For the solution of the steady state problem on computing machines, various explicit methods have been proposed for iterating the simultaneous equations which occur when Equation (3) is written for each point in the integration net. Probably the best explicit iterative method known is the extrapolated Liebmann method (also known as the successive overrelaxation method). The computational labor required for this method is discussed by Frankel(*3*). No implicit methods for iterating simultaneous equations have previously been proposed.

ALTERNATING-DIRECTION IMPLICIT METHOD

Application to Unsteady State Problem

Peaceman and Rachford(*7*) proposed an alternating-direction implicit procedure for the solution of Equation (1) which is stable for any size of time increment and yet avoids the necessity for iteration at each time step. The difference equations are obtained by replacing only one of the second derivatives, say $\partial^2T/\partial x^2$, by a second difference evaluated in terms of the unknown values of T at time $\theta + \Delta\theta$, while replacing the other second derivative, $\partial^2T/\partial y^2$, by a second difference evaluated in terms of known values of T at time θ. Comparatively small sets of simultaneous equations, each containing no more than three unknowns, are formed which are said to be implicit in the x direction. These equations are of a form that can be solved easily without iteration. If the procedure is then repeated for a second time step of equal size, with the difference equations implicit in the y direction, the over-all procedure for the two time steps is stable for any size of time increment.

Thus two difference equations are used, one for the first time step, the other for the second time step:

$$\frac{\kappa}{c\rho(\Delta x)^2}[T(x-\Delta x, y, \theta+\Delta\theta) - 2T(x, y, \theta+\Delta\theta) + T(x+\Delta x, y, \theta+\Delta\theta)] + \frac{k}{c\rho(\Delta y)^2}[T(x, y-\Delta y, \theta) - 2T(x, y, \theta) + T(x, y+\Delta y, \theta)] = \frac{1}{\Delta\theta}[T(x, y, \theta+\Delta\theta) - T(x, y, \theta)] \quad (7)$$

ERRATA

Volume 1, Number 1, page 25: The values of k in Table 1 should be higher by a factor of 10.

Volume 1, Number 1, page 76: In the legend of Figure 1 $p_r = p^b{}_o/R(\varepsilon/k)$ should be $p_r = pb_o/R(\varepsilon/k)$.

Volume 1, Number 2, page 146: Equation (26) should read $(d^3P/dV^3)_T \leqslant 0$ at critical.

$$\frac{k}{c\rho\,(\Delta x)^2}[T(x-\Delta x, y, \theta+\Delta\theta)-2T(x, y, \theta+\Delta\theta)+T(x+\Delta x, y, \theta+\Delta\theta)]+\frac{k}{c\rho\,(\Delta y)^2}\cdot[T(x, y-\Delta y, \theta+2\Delta\theta)-2T(x, y, \theta+2\Delta\theta)+T(x, y+\Delta y, \theta+2\Delta\theta)]=\frac{1}{\Delta\theta}[T(x, y, \theta+2\Delta\theta)-T(x, y, \theta+\Delta\theta)] \quad (8)$$

If $\Delta x=\Delta y$, and $\alpha=c\rho(\Delta x)^2/k\Delta\theta$, these equations may be arranged in the following form, which is more suitable for calculation:

$$-T(x-\Delta x, y, \theta+\Delta\theta)+[2+\alpha]T(x, y, \theta+\Delta\theta)-T(x+\Delta x, y, \theta+\Delta\theta)=T(x, y-\Delta y, \theta)+[\alpha-2]\,T(x, y, \theta)+T(x, y+\Delta y, \theta) \quad (9)$$

$$-T(x, y-\Delta y, \theta+2\Delta\theta)+[2+\alpha]\,T(x, y, \theta+2\Delta\theta)-T(x, y+\Delta y, \theta+2\Delta\theta)=T(x-\Delta x, y, \theta+\Delta\theta)+[\alpha-2]\,T(x, y, \theta+\Delta\theta)+T(x+\Delta x, y, \theta+\Delta\theta) \quad (10)$$

Use of Equation (9) or (10) for each point in the integration net leads to as many sets of simultaneous equations as there are lines in the net, each set having as many equations and unknowns as there are points on the line. When the boundary conditions are taken into account, these equations may always be arranged in the form

$$B_1 T_1 + C_1 T_2 = D_1$$

$$A_i T_{i-1} + B_i T_i + C_i T_{i+1} = D_i \qquad 2 \leqslant i \leqslant n-1$$

$$A_n T_{n-1} + B_n T_n = D_n \quad (11)$$

The solution of these equations is obtained by a straightforward technique proposed by L. H. Thomas of the Watson Scientific Computing Laboratory. Let

$$w_1 = B_1$$

$$w_i = B_i - \frac{A_i C_{i-1}}{w_{i-1}} \qquad 2 \leqslant i \leqslant n \quad (12)$$

and

$$g_1 = \frac{D_1}{w_1}$$

$$g_i = \frac{D_i - A_i g_{i-1}}{w_i} \qquad 2 \leqslant i \leqslant n \quad (13)$$

The solution is

$$T_n = g_n$$

$$T_i = g_i - \frac{C_i T_{i+1}}{w_i} \qquad 1 \leqslant i \leqslant n-1 \quad (14)$$

Thus w and g are computed in order of increasing i, and T is computed in order of decreasing i.

For the integration of Equation (1) in a square by this method, approximately $9N$ operations must be performed for each time step (7). For the complete solution with $N=196$ the work required by the alternating-direction implicit method was found to be 1/7 of the work required by the use of the implicit Equation (5) with extrapolated Liebmann iteration, and 1/25 of the work required by the use of the explicit Equation (4). The comparison is even more favorable for the alternating-direction implicit method for larger values of N. Douglas (1) has shown that as the mesh width is decreased, the solution obtained converges to the solution of the differential equation.

Application to Steady State Problem

The alternating-direction implicit method may be used to iterate to the solution of the steady state Equation (2), since the steady state solution may be regarded as the limiting case of the solution of a corresponding unsteady state problem. In this case each stage of the iteration may be regarded as a time step of the unsteady state problem, while the starting values used for the first iteration correspond to the initial condition. Equations (9) and (10) are used for alternate stages of the iteration with α serving as an iteration parameter. For the solution of Equation (2) in a square, it was found (7) that a sequence of α's can be chosen such that this method requires about $\ln N/N^{\frac{1}{2}}$ as many calculations as the extrapolated Liebmann method.

Examples

The alternating-direction implicit procedure has been applied (7) in the solution of two simple problems involving square boundaries. The first problem considered was that of unsteady state heat flow in a square wherein the boundaries are maintained at zero temperature and the square initially has a temperature of unity. The second problem was that of determining the steady state temperature distribution in a square in which two opposite faces are at zero temperature and the remaining two faces have a temperature of unity.

It has been shown (1, 7) that the alternating-direction implicit procedure is stable for the case of a square or rectangular boundary, but stability has not been demonstrated for a more general class of boundaries. It is the purpose of this paper to show by example the application of the new procedure to problems involving more complicated boundaries. Three examples will be cited, all of which were calculated by means of eight-digit, floating-decimal arithmetic. The examples were so chosen as to keep the number of points in the integration nets small in order not to overrun the small internal storage capacity of the computer used. Although this limitation did prevent the examples from being more practical than they were, they are sufficient to show that a wide variety of boundary conditions can be treated satisfactorily by the new procedure.

All the examples discussed are steady state problems; however, the difference equations are set up as if the problems are unsteady state in nature. Thus it is shown that as far as setting up the equations is concerned, there is no difference between steady and unsteady state problems. The only difference is in the choice of the parameter, α, and the discussion of this choice will be deferred to the next section.

Flow Around a Corner. The problem of flow of heat around a corner was chosen in order to demonstrate that a more complicated region than a rectangle can be treated. The equation describing this process also describes the flow of an ideal fluid around a corner; hence this application of the alternating-direction implicit procedure should be of interest in hydrodynamics.

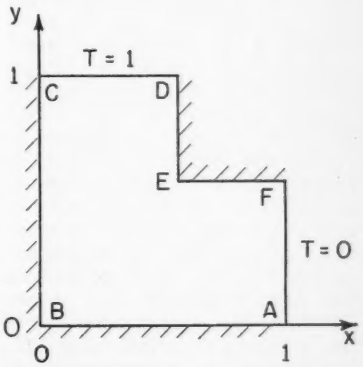

Fig. 2. Flow around corner.

In the shape in Figure 2 edge AF is maintained at zero temperature; edge CD is maintained at a temperature of unity; at all other edges no heat flows across the boundary. Equation (2) applies to the interior of this region, and the following boundary conditions apply:

$$\text{Edge } AF \qquad T = 0$$

$$\text{Edges } AB \text{ and } EF \quad \frac{\partial T}{\partial y} = 0 \qquad (15)$$

$$\text{Edges } BC \text{ and } DE \quad \frac{\partial T}{\partial x} = 0$$

$$\text{Edge } CD \qquad T = 1$$

Figure 3 shows the integration net with each of the points labeled with an index number.

Fig. 3. Integration net for flow around corner.

First one considers the time step in which the difference equations are implicit in the x direction. Equation (9) applies to each of the interior points. At the boundaries which are adiabatic, the temperature gradient in the direction perpendicular to the boundaries is zero, and the so-called "reflection" boundary condition can be used; that is, a set of fictitious points are imagined to exist, Δx, outside the boundary, and these points are assumed to have the same values as the points located a distance Δx inside the boundary. Figure 4 shows how this applies to some of the points on edge BC. When Equation (9) is written for a point on BC, only two unknowns appear, and so this becomes the first equation for that particular line. When Equation (9) is written for one of the points just inside edge AF, again only two unknowns appear, and the last equation for that line

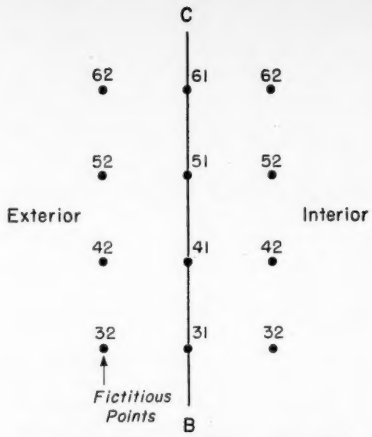

Fig. 4 Reflection boundary condition.

is obtained. Below are written the equations for the first, second, sixth, and seventh lines to illustrate how all the equations are set up. T represents a known value of temperature at time θ; T^* represents an unknown value of temperature at time $\theta + \Delta\theta$; the subscripts are the index numbers of the points.

First Line

$$(2+\alpha)\,T^*_{11} - 2\,T^*_{12} = 2\,T_{21} + (\alpha-2)\,T_{11}$$

$$-T^*_{11} + (2+\alpha)\,T^*_{12} - T^*_{13} = 2\,T_{22} + (\alpha-2)\,T_{12}$$

$$-T^*_{12} + (2+\alpha)\,T^*_{13} - T^*_{14} = 2\,T_{23} + (\alpha-2)\,T_{13}$$

$$-T^*_{15} + (2+\alpha)\,T^*_{16} - T^*_{17} = 2\,T_{26} + (\alpha-2)\,T_{16}$$

$$-T^*_{16} + (2+\alpha)\,T^*_{17} - 0 = 2\,T_{27} + (\alpha-2)\,T_{17}$$

These seven equations with seven unknowns may now be solved for the unknown temperatures on the first line by use of Equations (12) to (14).

Second Line

$$(2+\alpha)\,T^*_{21} - 2\,T^*_{22} = T_{11} + (\alpha-2)\,T_{21} + T_{31}$$

$$-T^*_{21} + (2+\alpha)\,T^*_{22} - T^*_{23} = T_{12} + (\alpha-2)\,T_{22} + T_{32} - T^*_{25} + (2+\alpha)\,T^*_{26} - T^*_{27} = T_{16} + (\alpha-2)\,T_{26} + T_{36}$$

$$-T^*_{26} + (2+\alpha)\,T^*_{27} - 0 = T_{17} + (\alpha-2)\,T_{27} + T_{37}$$

Sixth Line

$$(2+\alpha)\,T^*_{61} - 2\,T^*_{62} = T_{51} + (\alpha-2)\,T_{61} + T_{71}$$

$$-T^*_{61} + (2+\alpha)\,T^*_{62} - T^*_{63} = T_{52} + (\alpha-2)\,T_{62} + T_{72} - 2\,T^*_{64} + (2+\alpha)\,T^*_{65} = T_{55} + (\alpha-2)\,T_{65} + T_{75}$$

Seventh Line

$$(2+\alpha)\,T^*_{71} - 2\,T^*_{72} = T_{61} + (\alpha-2)\,T_{71} + 1$$

$$-T^*_{71} + (2+\alpha)\,T^*_{72} - T^*_{73} = T_{62} + (\alpha-2)\,T_{72} + 1 - 2\,T^*_{74} + (2+\alpha)\,T^*_{75} = T_{65} + (\alpha-2)\,T_{75} + 1$$

Thus, line-by-line, the values of T at $\theta + \Delta\theta$ are obtained. For the next time step, the difference equations are implicit in the y direction and the same value of α is used. Equation (10) is now used for each of the interior points, and the equations are set up in exactly the same way as on the previous step. T now represents a known value of temperature at time $\theta + \Delta\theta$; T^* represents an unknown value at time $\theta + 2\theta\Delta$. Just the first line will be written.

First Line

$$(2+\alpha)\,T^*_{11} - 2\,T^*_{21} = 2\,T_{12} + (\alpha-2)\,T_{11}$$

$$-T^*_{11} + (2+\alpha)\,T^*_{21} - T^*_{31} = 2\,T_{22} + (\alpha-2)\,T_{21}$$

$$-T^*_{21} + (2+\alpha)\,T^*_{31} - T^*_{41} = 2\,T_{32} + (\alpha-2)\,T_{31}$$

$$-T^*_{61} + (2+\alpha)\,T^*_{71} - 1 = 2\,T_{72} + (\alpha-2)\,T_{71}$$

The values of T at $\theta + 2\Delta\theta$ are obtained, again line by line. Then then entire procedure is repeated, first the equation implicit in the x direction being used, then the equations implicit in the y direction. A different value of α may be used for each of the double steps, but it must be the same for both halves of the double step.

By use of these equations, the steady state solution was obtained by iteration; the starting values, by use of the arbitrary equation

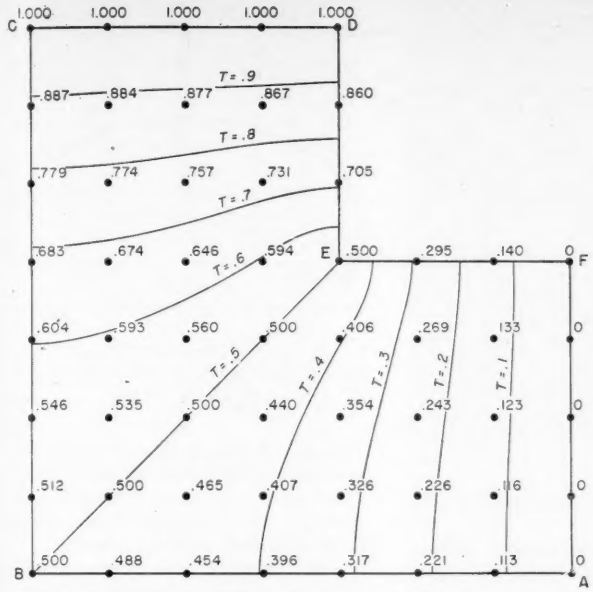

Fig. 5. Temperature distribution for heat flow around corner.

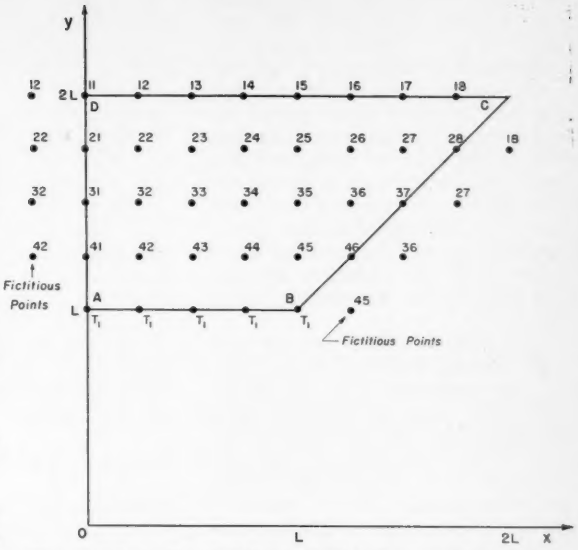

Fig. 6. Integration net for radiation from square pipe.

$$T = 0.5\,(1-x)/(1-y)$$

for all points to the right of the line $x = y$, and the equation

$$T = 1 - 0.5\,(1-y)/(1-x)$$

for all points above the line $x = y$. The values of α used were 4, 2, 1, 0.5, 4, 2, 1, 0.5 . . . with the cycle of four values of α being repeated.

To check the progress of the iteration after each double step, the residual, δ, was calculated for each interior point by the equation

$$\delta = T\,(x-\Delta x, y) + T\,(x+\Delta x, y) + T\,(x, y-\Delta y) + T\,(x, y+\Delta y) - 4\,T\,(x, y) \qquad (16)$$

and the sum of the squares of the residuals, $\Sigma\delta^2$, evaluated. A plot of log $\Sigma\delta^2$ vs. number of double steps fell approximately on a straight line for the first nine double steps, with $\Sigma\delta^2$ decreasing from 0.187 to 1.04×10^{-9}. Twelve double steps reduced $\Sigma\delta^2$ to 2×10^{-10}, corresponding to about five digits' accuracy. Upon further iterations, the solution continued to converge, but at a much slower rate, with $\Sigma\delta^2$ reduced to 10^{-12} after twenty-eight double steps, corresponding to about six digits' accuracy. The solution is shown in Figure 5. The isotherms in this figure were obtained by graphical interpolation between the points.

Radiation from Square Pipe. The second example is that of determining the temperature distribution in a square pipe, the inside surface of which is maintained at a constant temperature, t_1, while the outside surface is radiating heat to surroundings maintained at temperature t_2. This problem is of interest because it contains a nonlinear boundary condition involving radiation and also because it introduces a diagonal boundary. The ability of the new numerical procedure to handle nonlinear boundary conditions is important for furnace-design problems, as well as for problems with heat transfer to fluids in which the heat transfer coefficient is not constant.

Because of symmetry, only one eighth of the cross section of the pipe need be considered. By this use of symmetry, it is possible to calculate the temperature distribution in the whole pipe with many fewer points. The integration net used is shown in Figure 6. The bore of the pipe is assumed to be a square $2L$ across, the outside a square $4L$ across.

The equation

$$\frac{\partial^2 t}{\partial x^2} + \frac{\partial^2 t}{\partial y^2} = 0 \qquad (17)$$

holds in the interior of the region, and the boundary conditions are

Edge AB: $t = t_1$

Edge BC: $\partial t/\partial n = 0$

where n is distance in a direction perpendicular to the edge

Edge CD: $-k\dfrac{\partial t}{\partial y} = \sigma\,(t^4 - t_2^4)$

Edge AD: $\dfrac{\partial t}{\partial x} = 0$ (18)

Because of the symmetry, edges BC and AD have reflection boundary conditions. The fictitious points associated with these edges are also shown in Figure 6.

In order to make the functions dimensionless, the following substitutions may be made:

$$X = x/L \qquad (19)$$

$$Y = y/L \qquad (20)$$

$$T = (\sigma L/k)^{1/3} t \qquad (21)$$

Equation (17) becomes

$$\frac{\partial^2 T}{\partial X^2} + \frac{\partial^2 T}{\partial Y^2} = 0 \qquad (22)$$

and the upper and lower boundary conditions become

Edge AB: $T = T_1 = (\sigma/kL)^{1/3} t_1$ (23)

Edge CD: $-\dfrac{\partial T}{\partial Y} = T^4 - T_2^4$ (24)

In the setting up of the difference equations, no new difficulties are introduced at the boundaries AB

and AD. When the difference equations are set up for the points on the diagonal boundary, the temperature at the fictitious points are introduced as unknowns. If the calculations are carried out so that the long lines are solved before the short ones, it always turns out that the temperature at each fictitious point has been obtained during the solution of the previous line. Thus only two unknowns appear in the equation for the diagonal boundary point, and this equation becomes the last one for the corresponding line.

The difference Equations (9) and (10) are not written for the points on the boundary CD. Instead, a difference equation corresponding to Equation (24) is written. In order that this difference equation be linear in T, the T^4 term is split into two factors, T^3 T^*, where T is the known value of temperature obtained from the last time step and T^* is the unknown value. The boundary difference equation is then

$$\frac{T^*_{2i} - T^*_{1i}}{\Delta Y} = T^3_{1i}\, T^*_{1i} - T_2$$

or

$$-T^*_{2i} + (1 + T^3_{1i}\Delta Y)\, T^*_{1i} = T^4_2 \Delta Y \qquad (25)$$

Consider first the difference equations implicit in the x direction. Line 21-28 is solved first, by use of the following equations.

Second Line

$$(2+\alpha)\, T^*_{21} - 2\, T^*_{22} = T_{11} + (\alpha - 2)\, T_{21} + T_{31}$$

$$-T^*_{26} + (2+\alpha)\, T^*_{27} - T^*_{28} = T_{17} + (\alpha - 2)\, T_{27} + T_{37}$$

$$-T^*_{27} + (2+\alpha)\, T^*_{28} - T^*_{18} = T_{18} + (\alpha - 2)\, T_{28} + T_{27}$$

$$-T^*_{28} + (1 + T^3_{18}\, \Delta Y)\, T^*_{18} = T^4_2\, \Delta Y$$

In addition to T^*_{21} through T^*_{28}, T^*_{18} is obtained. By use of Equation (25) T^*_{11} through T^*_{17} may be solved for directly. The remaining lines offer no difficulty.

In the setting up of the difference equations implicit in the y direction, Equation (25) is used as the first equation for each line. Otherwise the equations for the second half of the double time step are quite straightforward.

In order to carry out a numerical solution of these equations, values were assigned to the constants T_1 and T_2. It was assumed that $L = 4$ in., $k = 30$ B.t.u./(hr.)(ft.)(°F.), $t_1 = 1033$°F. $= 1493$°R., and $t_2 = 100$°F. $= 560$°R. σ is equal to 0.173×10^{-8} B.t.u./(sq.ft.)(hr.)(°R.)^4. Then $T_1 = 0.4$ and $T_2 = 0.15$. ΔY is equal to 0.25.

The starting values for the iteration were obtained by solving for the temperature distribution that would exist in an infinite plate of thickness L with the same upper and lower boundary conditions. This gave at the upper edge $T = 0.37971694$. Intermediate starting temperatures were obtained by use of the relation

$$T = 0.4 - (0.4 - 0.37971694)\,(Y - 1)$$

Residuals for the interior points were calculated by Equation (16), and the sum of squares of the residuals were evaluated after each double step. The values of α used were 4, 2, 1, 0.5, 0.2, 4, 2, 1, 0.5, 0.2, 10, 4, 10, 20, 10, 4, 2, 1, 0.5, 0.2, 0.1, 20, 10. A plot of log $\Sigma\delta^2$ vs. number of steps was approximately straight for the first twelve double steps, with $\Sigma\delta^2$ decreasing from 3.06×10^{-4} to 7.66×10^{-11}; the portion of the plot from twelve to twenty-three double steps was also approximately straight, with $\Sigma\delta^2$ decreasing to 1.51×10^{-13}. The solution, with temperatures in degrees Fahrenheit, is presented in Figure 7.

Heat Sources and Sinks in an Elliptical Plate. Although the examples discussed above have straight boundaries, the boundaries of many problems that occur in engineering are curved. In addition, some problems involve point sources and sinks, wherein heat or fluid is added or removed at a point. These two features are introduced in the third example, which is that of determining the temperature distribution in an elliptical plate which has two heat sources and two heat sinks. (*See* Figure 8.)

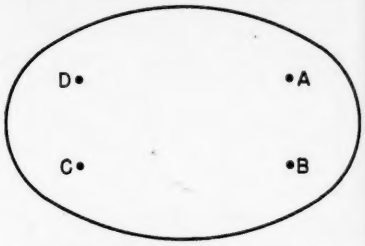

Fig. 8. Heat sources and sinks in an elliptical plate.

The elliptical boundary is adiabatic, and heat is injected at equal constant rates at points A and B and removed at equal constant rates from points C and D.

This example has been formulated as a heat-conduction problem, but it may also be formulated as an equivalent electrical problem, where current flows into the plate at points A and B and flows out at points C and D, and it is desired to compute the potential distribution. Another important analogy occurs in reservoir engineering, wherein it is desired to obtain the pressure distribution in an elliptical reservoir in which fluid is injected at wells located at points A and B and produced from wells located at points C and D. Because well diameters are usually very small compared with the dimensions of a reservoir, they must be considered as points. This example shows the application of the new method to reservoir engineering, since reservoirs almost always have curved boundaries and have many wells located at various points within.

The problem as stated above has only derivatives specified at the boundaries, and so the solution is unique except for an arbitrary con-

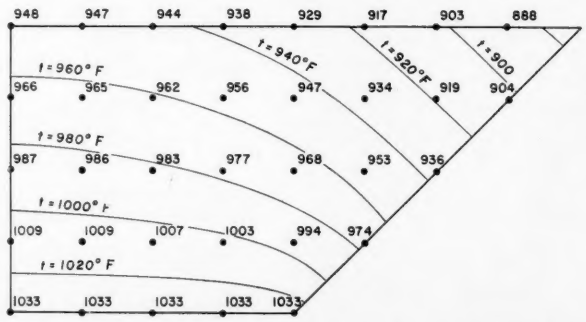

Fig. 7. Temperature distribution in a square pipe with radiation from outer surface.

stant. From symmetry it can be seen that the temperature will be constant along the minor axis; a zero value will be arbitrarily assigned to this constant temperature. The solution will be symmetric with respect to y and antisymmetric with respect to x, and so it will be sufficient to consider only the upper right-hand quadrant. Figure 9 shows the integration net used. Since the major axis is now a reflection boundary, fictitious points have been added below the major axis. Fictitious points have also been added outside the curved boundary in such a way that every interior point is surrounded by four mesh points.

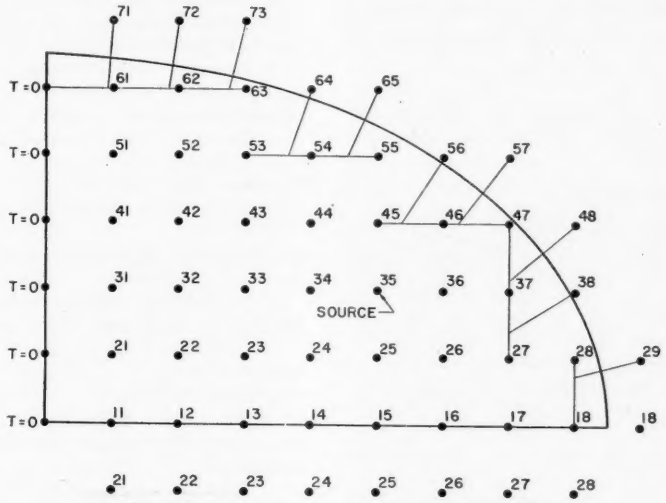

Fig. 9. Integration net for elliptical plate problem.

The problem now exists of evaluating the temperature at the fictitious points outside a curved boundary at which the normal derivative is zero. The device proposed by Fox(*2*), who was concerned with applying the relaxation method to the solution of problems with curved boundaries at which the normal derivative is specified, is applicable here. The device is to draw a line from each fictitious point perpendicular to the curved boundary and to extend it until it intersects a line which joins two mesh points completely within the boundary. This has been done in Figure 9. Since the normal derivative of the temperature is specified to be zero at the boundary, the temperatures at both ends of the perpendicular lines are taken to be equal. Linear interpolation along the line joining the two mesh points within the boundary is then used to evaluate this temperature. For example, the perpendicular from point 73 intersects the line approximately one-quarter of the way from point 63 to point 62. Then one writes

$$T_{73} = 0.25\,T_{62} + 0.75\,T_{63} \quad (26)$$

When Equation (9) or (10) is written about a point just inside the boundary, a fictitious point will be involved on either the left- or right-hand side of the difference equation. If it is on the right side, it is necessary to use the old values of the two interior temperatures used to evaluate the fictitious point. For example, if T_{73} occurs on the right side, Equation (26) is used. On the other hand, if the fictitious temperature occurs on the left-hand side of the difference equation, new or unknown values of the interior temperatures must be used. Thus, if T^*_{73} occurs on the left side, one must write

$$T^*_{73} = 0.25\,T^*_{62} + 0.75\,T^*_{63} \quad (27)$$

It frequently occurs that an unknown value of T^* from a different line will be introduced by such a difference equation. It will always be from a longer line, however, and so if the lines are solved in order of decreasing length, this T^* will have just been solved for on the previous line.

It remains now to take into account the point source occurring at point 35. While the final solution satisfies Equation (3) everywhere else in the interior of the region, it does not satisfy it at a point source or sink because this equation expresses the condition that the net heat flow into the region around a point is zero. To obtain the correct expression, one must consider Figure 10. If heat is injected at point 0 at the rate q, the heat flow across the line ab is approximately

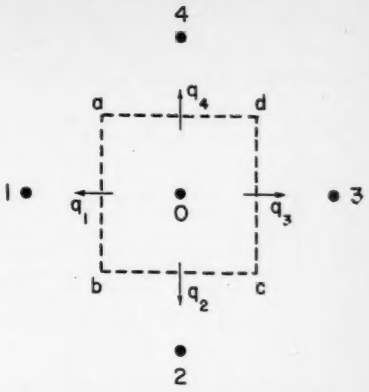

Fig. 10. Heat source at a point.

$$q_1 = k\,\Delta y\,(T_0 - T_1)/\Delta x \quad (28)$$

Similarly for each of the other sides of the square $abcd$. Since $\Delta x = \Delta y$, the total flow into the square is

$$q = k\,(4T_0 - T_1 - T_2 - T_3 - T_4) \quad (29)$$

Let $Q = q/k$. Then, if the heat source is located at the point x,y, it will be required that the steady state solution satisfy the relation

$$-T(x-\Delta x, y) - T(x+\Delta x, y) - T(x, y-\Delta y) - T(x, y+\Delta y) + 4T(x, y) = Q \quad (30)$$

while satisfying Equation (3) elsewhere. The iteration Equations (9) and (10) must then be modified at the heat source point in order to converge to this solution. They become, respectively,

Implicit in x *direction,*

$$-T^*(x-\Delta x, y) + (2+\alpha)\,T^*(x, y) - T^*(x+\Delta x, y) = Q + T(x, y-\Delta y) + (\alpha-2)\,T(x, y) + T(x, y+\Delta y) \quad (31)$$

Implicit in y *direction,*

$$-T^*(x, y-\Delta y) + (2+\alpha)\,T^*(x, y) - T^*(x, y+\Delta y) = Q + T(x-\Delta x, y) + (\alpha-2)\,T(x, y) + T(x+\Delta x, y) \quad (32)$$

Equations (31) and (32) may also be used as difference equations for unsteady state solutions.

To start the iteration, a temperature of zero was assigned to every point. As before, after each double step residuals were calculated at every interior point by

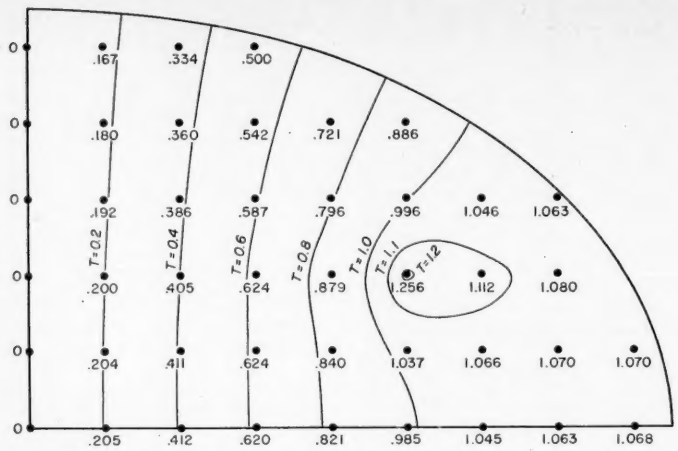

Fig. 11. Temperature distribution in an elliptical plate with a point heat source.

use of Equation (16), with the exception of the source point, where Equation (33) was used.

$$\delta_{35} = T_{34} + T_{36} + T_{25} + T_{45} - 4\,T_{35} + Q \qquad (33)$$

The values of α used were 4, 2, 1, 0.7, 0.4, 0.2, 0.1, 0.07, 0.04, 7, 4, 2, 1, 0.4, 0.1, 0.07, 0.04, 0.03, 10, 4, 1, 0.4, 0.1, 0.07, 7, 2, 0.7. A plot of log $\Sigma\delta^2$ vs. number of steps was approximately straight, with $\Sigma\delta^2$ decreasing from 1.0 to 5.23×10^{-13} in twenty-seven double steps. The solution is presented in Figure 11.

CHOICE OF ITERATION PARAMETER

For iteration to the steady-state solution of the heat-flow equation with a square boundary, a procedure has been suggested (7) for selection of a set of values of α. Such a procedure has not been obtained, however, for other types of boundaries. The sets of values of α used to iterate these three examples by no means represent an optimum choice, and it appears that more experience with the alternating-direction implicit method will be required before an optimum procedure for choosing α can be found.

Some general statements can be made, however. In the first place, it is desirable to calculate the sum of squares of the residuals, in order to keep track of the progress of the iteration. Second, it is advantageous to use several different values for α rather than continuing to use the same value repeatedly. A satisfactory procedure appears to be the following: to start, an α between 4 and 10 is chosen; on each double step α is divided by 2 or 4, until the rate of decrease of $\Sigma\delta^2$ becomes small. The cycle is then repeated as many times as necessary to reduce the residuals to as low a level as desired. One or two such cycles should be sufficient for engineering accuracy in the solution.

CONCLUSION

The chief advantage of the alternating-direction implicit method developed by Peaceman and Rachford (7) is that both unsteady and steady state problems in the flow of heat in two dimensions can be solved on a computing machine to a given degree of accuracy with less computing labor than that required by previously available numerical techniques. This reduction in labor is brought about by the fact that the new method is stable for any size of time increment and yet does not require iteration for solution of the simultaneous equations obtained.

Because it has not been possible to prove rigorously that the alternating-direction implicit method will work for nonrectangular boundary condition, it is necessary to rely upon actual numerical examples to determine the usefulness of the method for various engineering problems having realistic boundary conditions. The main purpose of this paper has been to present a few examples with a wide variety of boundary conditions in order to show the usefulness of the method for these problems. While it is not possible to say in advance that the new technique is applicable to any problem different from the ones described here, the success of the method with these problems, as well as the fact that no problems have yet been found where it is unsuccessful, are strong indications that the method may be applied to other heat flow or diffusion problems in two dimensions.

NOTATION

A,B,C,D = coefficients of simultaneous equations
c = heat capacity, B.t.u./(lb.)(°F.)
g = intermediate quantity in solution of simultaneous equations
k = thermal conductivity, B.t.u./(hr.)(ft.)(°F.)
L = basic length, ft.
N = number of interior points of integration net
n = distance in direction perpendicular to boundary
Q = dimensionless rate of heat input, q/k
q = rate of heat input, B.t.u./(hr.)(ft.)
T = dimensionless temperature
t = temperature, °R.
w = intermediate quantity in solution of simultaneous equations
X = dimensionless distance, x/L
x = distance in horizontal direction, ft.
Y = dimensionless distance, y/L
y = distance in vertical direction, ft.
α = iteration parameter in steady state problems; $c\rho(\Delta x)^2/k\Delta\theta$ in unsteady state problems
$\Delta x, \Delta y, \Delta\theta$ = increment of x, y, and θ, respectively
δ = residual
θ = time, hr.
ρ = density, lb./cu.ft.
σ = Stefan-Boltzmann constant

Superscript

* = unknown values of T

Subscripts

i = index number for simultaneous equations
1 = inside of pipe
2 = surroundings

LITERATURE CITED

1. Douglas, J., Jr., *J. Ind. Appl. Math.*, 3, 42 (1955).
2. Fox, L., *Quart. Appl. Math.*, 2, 251 (1944).
3. Frankel, S. P., *Math. Tables and Other Aids to Computations*, 4, 65 (1950).
4. Jakob, M., "Heat Transfer," vol. I., pp. 365-79, John Wiley & Sons, Inc., New York (1949).
5. Milne, W. E., "Numerical Solution of Differential Equations," pp. 119, 200, John Wiley & Sons, Inc., New York (1953).
6. O'Brien, G. G., M. A. Hyman, and S. Kaplan, *J. Math. Phys.*, 29, 223 (1951).
7. Peaceman, D. W., and H. H. Rachford, *J. Ind. Appl. Math.*, 3, 28 (1955).
8. Sherwood, T. K., and C. E. Reed, "Applied Mathematics in Chemical Engineering," 1 ed., p. 217, McGraw-Hill Book Company, Inc., New York (1939).

(Presented at A.I.Ch.E. Houston meeting)

Chemical Reactor Stability and Sensitivity

Olegh Bilous and Neal R. Amundson, University of Minnesota, Minneapolis, Minnesota

The purpose of this paper is to consider the well agitated continuous reactor from the standpoint of stability of the steady state. It has been shown in the past that chemical-reaction systems may be unstable in the sense that on slight perturbation they tend to move to a more stable state or that they are stable in their steady states, small perturbations being self-correcting so that the system possesses autoregulation. In this paper methods of developing criteria for the quantitative determination of stability or instability are presented and applied to some simple problems. In order that the effect of large perturbations on the system may be determined, complete solutions of the rigorous equations are obtained on the analogue computer (R.E.A.C.). A complete plot of reaction paths in the concentration-temperature plane may be obtained in this manner. Because of the nonlinearity of the system one cannot predict with certainty what steady state will be approached after a given large perturbation, multiple steady states being assumed possible. From the phase plot of reaction paths the regions in the plane which lead to certain steady states are delineated. Also it is shown that the natural behavior of a reactor is not to approach an unstable state. So far as the reactor is concerned, the unstable state does not exist. The stability of the system is important to the engineer, as control will be easy or difficult and product quality will be satisfactory or not depending upon the relative stability of the steady state. An unstable state would require more elaborate control than a stable state.

The rational design of chemical reactors is a problem of primary interest to the chemical engineer. The theory and practice of catalytic-reactor design is still in a somewhat awkward stage; however, the design of homogeneous reactors can be approached with some confidence whether they be tubular, batch, or the well-agitated continuous type. In particular, the behavior of the continuous stirred tank reactor because of its simplicity and constancy of conditions may be predicted with ease. These reactors have been discussed in detail by MacMullin and Weber(*10*), Denbigh(*2*), Denbigh, Hicks and Page(*3*), Eldridge and Piret(*4*), and Tiller(*16*), all of whom concerned themselves with the steady state. Mason and Piret(*11*) considered the transient behavior of linear systems, that is, isothermal systems in which all reactions are kinetically of the first order. Van Heerden(*17*) considered the nature of the steady state and showed that steady states may be of different types, being stable, autoregulatory, or unstable, the stability manifesting itself in the tendency of the reactor to stay at that state. Salnikov(*15*) has discussed the problem of periodic phenomenon in reaction systems and Frank-Kamenetski(*5, 6, 7*) and Gevart(*7*) have considered similar problems.

It is the purpose of this paper to investigate these problems more deeply and to develop methods of calculation and criteria for the stability or instability of the system. Analytic solutions of the transient behavior will not be developed or needed even though the term *instability* has inherent in it the notion of time. Rather, the methods of nonlinear mechanics as developed and used by Poincare(*13, 14*), Liapounoff(*9*), Minorsky(*12*), and others will be used. These methods are useful in investigating the effect of a small perturbation on the system. In order to investigate the effect of large perturbations an analogue computer has been used to generate solutions of the differential equations and to show very graphically the nature of the approach to the steady state.

It should be pointed out that this paper will deal with the chemical system alone and does not involve instabilities introduced by a control element operating at a time lag. This is another problem altogether and will be treated at another time. The problem here is that of a chemical reaction, exothermic in nature, and the effect on it of large or small perturbations in the conditions under which the reaction is carried out.

In general for stability problems there are two techniques available. The frequency-response technique has been for years widely used by electrical engineers in circuit analysis and feedback amplifier design. Problems in mechanics have been analyzed by perturbation methods. Both these methods will be used in this paper and the succeeding ones. In addition, the whole phase plane may be produced by the use of the analogue computer. These problems should be of interest to the engineer concerned with automatic control, for it is obvious that if the steady state is unstable the difficulty of control will be increased. Stable states, as will be shown, are states in which the reactor tends to remain; the system then possesses autoregulation, and control should be simple.

Most of the analysis, for the sake of illustration only, will be on a very simple system, but the methods do not have this restriction. The perturbation method can be applied to systems of arbitrary complexity, and the use of the analogue computer is limited only by the particular machine available.

Olegh Bilous is at present with the Laboratoire Central des Poudres, Paris, France.

THE PERTURBATION METHOD

Consider a well-agitated continuous reactor as shown in Figure 1. This may be a single reactor or it may be one of a series of many such. In a reaction $A \rightarrow B$, irreversible, exothermic, and kinetically of the first order, q is the volumetric flow rate of the influent, k the specific reaction velocity constant, T_s the temperature of operation, T' the average temperature of the coolant in the coil, and U the product of area and heat transfer coefficient. A_o is the concentration of A in the influent and A_s the concentration in the reactor. If V is the volume of the reactor, a mass balance gives

$$qA_o - qA_s - k_s V A_s = 0$$

from which

$$A_s = \frac{qA_o}{q + k_s V} \qquad (1)$$

Implicit here is that T_s has been specified so that k_s is fixed. A steady state heat balance gives

$$qc\rho\,(T_o - T_s) - k_s A_s V\,(\Delta H) - U\,(T_s - T') = 0 \qquad (2)$$

and therefore the remainder of the parameter must be fixed in order to satisfy this condition. The two numbers which emerge from the calculation are A_s and T_s.

If the parameters which were previously fixed remain fixed except for the temperature T and concentration A, Equations (1) and (2) may then be combined to give a single equation

$$qc\rho\,(T - T_o) - U\,(T' - T) = -V\,(\Delta H)pe^{-E/RT}\frac{qA_o}{q + Vpe^{-E/RT}} \qquad (3)$$

where

$$k = pe^{-E/RT}, \quad -\Delta H > 0$$

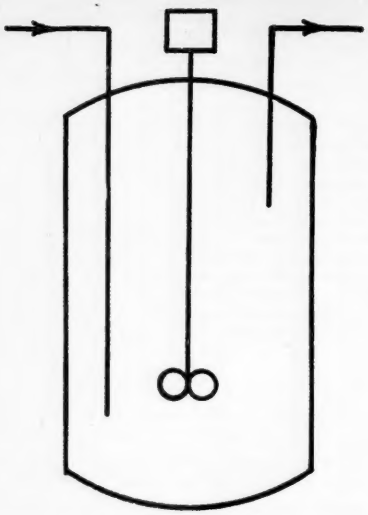

↑Fig. 1. Schematic diagram of well-agitated continuous reactor.

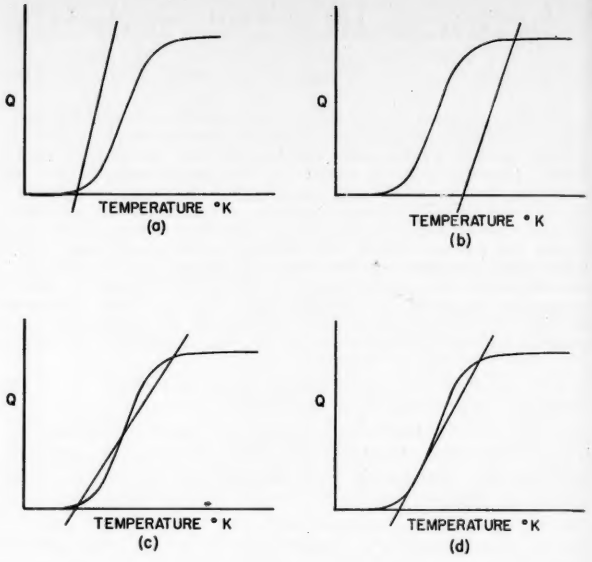

Fig. 2. Schematic plots of heat generation and heat consumption vs. temperature; six possible cases.→

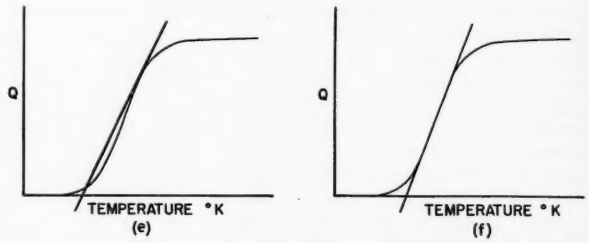

↓Fig. 3. Schematic plots for (a) $A \rightarrow B, -\Delta H > 0$, (b) $A \rightarrow B \rightarrow C$—both reactions exothermal; (c) and (d) $A \rightarrow B \rightarrow C$—one reaction exothermal and one endothermal.

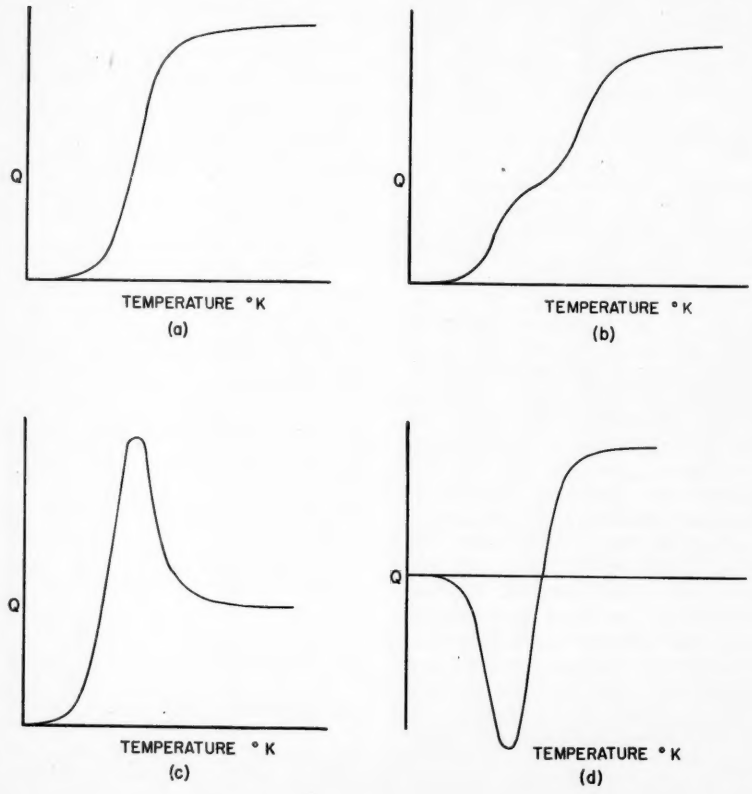

This is an algebraic equation from which one can determine the temperature of operation. The left-hand side of Equation (3) represents the rate of heat consumption in the reactor and the right-hand side is the rate of heat generation. When q, c ρ, U are assumed constants, the left-hand side is a linear function of T and the right-hand side has a sigmodial shape, as shown in Figure 3*a*. Figure 2*a* shows the left- and right-hand sides plotted as functions of T, and the temperature of operation is certainly given by the intersection of the two curves. It is readily apparent that there are six possible cases as shown in Figure 2. The analysis of van Heerden (*17*) may be applied. If there is a single intersection as in Figures 2*a* and *b* the reactor is stable. Three distinct intersections as in Figure 2*c* produce two stable points and the middle unstable point. Figures 2*d* and *e* have each a stable point and a tangency implying a one-sided stability, which really implies instability. Figure 2*f* contains a tangent at the point of inflection, and by van Heerden's analysis is stable although a reactor operated

under these conditions would probably show sustained oscillations if perturbed. This point is unsettled at the moment. Thus three distinct intersections always produce one unstable point in the middle. Single intersections are always stable. Other pathological cases produce instabilities which probably would not occur in practice.

Systems of other types may be analyzed by this method although the sigmoidal curve may change its shape under some conditions, usually extreme. In Figure 3 are given three other than the one considered above. They arise from the following situations where the reaction is of the general form:

$$\begin{matrix}(1) & (2)\\ A \rightarrow & B \rightarrow C\end{matrix}$$

Figure 3*b* $(-\Delta H_1) > 0$, $(-\Delta H_2) > 0$
Figure 3*c* $(-\Delta H_1) > 0$, $(-\Delta H_2) < 0$
Figure 3*d* $(-\Delta H_1) < 0$, $(-\Delta H_2) > 0$

and with suitable activation energies. It is easy to see that a multiplicity of states might arise with stable and unstable states in close proximity. In Figure 3*b* if the number of reactions is increased the number of bumps on the curve may be increased for suitable activation energies, and a profusion of stable and unstable states may result. The existence of a real reaction system as in Figure 3*b* is questionable.

This sort of stability is defined in terms of a small perturbation of the system and the return of the system to its original unperturbed state. If the system exhibits a desire to go elsewhere after slight irritation, perhaps to some more desirable state, the system is said to be unstable. This psychoanalysis of the reactor is essential, since the engineer must choose a control instrument which will live in harmony with the reactor.

In order to investigate the instability analytically, Equations (1) and (2) will be rewritten in their transient forms; thus

$$qA_o - qA - pVe^{-E/RT}A = V\frac{dA}{d\theta} \tag{4}$$

$$qc\rho\,(T_o - T) - pe^{-E/RT}AV\,(\Delta H) - U\,(T - T') = Vc\rho\frac{dT}{d\theta} \tag{5}$$

These equations are nonlinear and their analytic solutions probably unobtainable. However, they are of a form which appears in much of the theory of nonlinear mechanics (*12*). The equations can be linearized by taking their first-order linearization by Taylor series about the steady state position. Then it may be supposed that

$$a = A_s - A$$
$$t = T_s - T$$

and the linearization may be taken by the rule

$$f(x_o + h, y_o + k) = f(x_o, y_o) + h\left(\frac{\partial f}{\partial x}\right)_{x_o,\,y_o} + k\left(\frac{\partial f}{\partial y}\right)_{x_o,\,y_o}$$

Equations (4) and (5) then can be written in the form

$$\frac{da}{d\theta} = -a_{11}a - a_{12}t \tag{6}$$

$$\frac{dt}{d\theta} = -a_{21}a - a_{22}t \tag{7}$$

with

$$a_{11} = \frac{q}{V} + pe^{-\frac{E}{RT_s}},\quad a_{12} = pA_s\frac{E}{RT_s^2}e^{-\frac{E}{RT_s}},\quad a_{21} = p\frac{\Delta H}{c\rho}e^{-\frac{E}{RT_s}},$$

$$a_{22} = \frac{q}{V} + p\frac{\Delta H}{c\rho}A_s\frac{E}{RT_s^2}e^{-\frac{E}{RT_s}} + \frac{U}{Vc\rho}$$

Equations (6) and (7) are simple linear equations which may be solved with ease. The solution, however, is not needed. If the steady state is to be stable, that is, if the system is to return to that steady state after being perturbed, these small perturbations, a and t, must damp out to zero with increasing time. Since the solution to Equations (6) and (7) occurs in the form of exponentials, stability may be expected only if the characteristic equation has roots whose real parts are negative; i.e.

$$\begin{vmatrix} -a_{11} - \gamma & -a_{12} \\ -a_{21} & -a_{22} - \gamma \end{vmatrix} = 0$$

has two roots γ_1 and γ_2 with negative real parts. In this case the characteristic equation is a quadratic

$$\gamma^2 + (a_{11} + a_{22})\gamma + a_{11}a_{22} - a_{12}a_{21} = 0$$

and

$$\gamma_1, \gamma_2 = \frac{-(a_{11}+a_{22}) \pm \sqrt{(a_{11}+a_{22})^2 - 4\,(a_{11}a_{22} - a_{12}a_{21})}}{2}$$

The roots will have negative real parts if, and only if,

$$a_{11} + a_{22} > 0$$

$$a_{11}a_{22} - a_{12}a_{21} > 0$$

or

$$\frac{2q}{V} + k_s + \frac{U}{Vc\rho} > k_s\left(\frac{-\Delta H}{c\rho}\right)A_s\frac{E}{RT_s^2} \tag{8}$$

$$\frac{q}{V} + k_s + \frac{U}{Vc\rho} + k_s\frac{U}{qc\rho} > k_s\left(\frac{-\Delta H}{c\rho}\right)A_s\frac{E}{RT_s^2} \tag{9}$$

and these are necessary and sufficient conditions. Note that the criteria for stability or instability are given in terms of steady state values and no transients need be calculated. Therefore the calculations made for steady state design are also sufficient for the determination of the stability. Equations (8) and (9) taken together give necessary and sufficient criteria for the determination of the stability or instability of the system provided that the linearized equations decribe the nonlinear system. It is not obvious that it should be so, and Liapounoff (*9*) showed that the linearization about the steady state and the subsequent analysis of the linear system was a valid operation and described the physical system in the neighborhood of the steady state, provided the system was either definitely stable or unstable. Perhaps this seems so obvious that the reader doubts the necessity of pressing the point. To illustrate that there is some difficulty here, one sees that if the characteristic equation has pure imaginary roots, i.e., if $a_{11} + a_{22} = 0$, $a_{11}a_{22} - a_{12}a_{21} > 0$, the linear system would exhibit sustained oscillations since the solution would be expressed in terms of trignometric functions, and one would be tempted to say that the nonlinear system must also exhibit oscillations. One has only to recall the treatment of the pendulum in elementary mechanics to fall into such a

mistake. However, Liapounoff's theorem holds only for systems which are definitely stable or unstable and it may be shown that when the linearized system exhibits oscillations the nonlinear system may have any of the three behaviors; i.e., stable, unstable, or oscillatory.

Hence in order to examine for stability one must investigate the characteristic equation, to determine the nature of the roots. The system is stable if all roots have negative real parts and unstable if there is one root with a positive real part. For example, if a chemical system has reactions, both simultaneous and consecutive, taking place with chemical species A_i, the system of linearized equations will be of the form

$$\frac{da_1}{d\theta} = a_{11}a_1 + a_{12}a_2 + \cdots + a_{1,n-1}a_{n-1} + a_{1,n}t$$

$$\frac{da_2}{d\theta} = a_{21}a_1 + a_{22}a_2 + \cdots + a_{2,n-1}a_{n-1} + a_{2,n}t$$

$$\vdots$$

$$\frac{da_{n-1}}{d\theta} = a_{n-1,1}a_1 + a_{n-1,2}a_2 + \cdots + a_{n-1,n-1}a_{n-1} + a_{n-1,n}t$$

$$\frac{dt}{d\theta} = a_{n,1}a_1 + a_{n,2}a_2 + \cdots + a_{n,n-1}a_{n-1} + a_{n,n}t$$

with a_{ij} dependent upon the steady state parameters. If the roots of

$$\begin{vmatrix} a_{11}-\gamma & a_{12} & \cdots & a_{1,n} \\ a_{21} & a_{22}-\gamma & \cdots & a_{2,n} \\ \vdots & & & \\ a_{n,1} & a_{n,2} & \cdots & a_{n,n}-\gamma \end{vmatrix} = 0$$

have negative real parts the system is stable. This is a polynomial of the nth degree of the form

$$b_0\gamma_n + b_1\gamma^{n-1} + \cdots + b_{n-1}\gamma + b_n = 0.$$

The Routh-Hurwitz (8) criterion may be used to determine the character of the roots. The necessary and sufficient condition that this polynomial have roots with negative real parts is that the successive determinants

$$\Delta_1 = b_1;\ \Delta_2 = \begin{vmatrix} b_1 & b_0 \\ b_3 & b_2 \end{vmatrix};$$

$$\Delta_3 = \begin{vmatrix} b_1 & b_0 & 0 \\ b_3 & b_2 & b_1 \\ b_5 & b_4 & b_3 \end{vmatrix};\ \text{etc.}$$

and in general

$$\Delta_r = \begin{vmatrix} b_1 & b_0 & 0 & 0 & 0 & 0 & 0 \\ b_3 & b_2 & b_1 & b_0 & 0 & 0 & 0 \\ b_5 & b_4 & b_3 & b_2 & b_1 & b_0 & 0 \\ \vdots & & & & & & \\ b_{2r-1} & b_{2r-2} & b_{2r-3} & & & & b_r \end{vmatrix}$$

should all be positive, it being understood that where $b_r, r > n$ appears in the determinant, it is to be replaced by zero. There are other methods for determining the character of the roots of such an equation, and these can be found in standard works on servomechanism theory. It should be noted that the Routh-Hurwitz criterion leads in the case considered above to Equations (8) and (9). It would be desirable to have a method for the determination of the character of the latent roots of a matrix directly without the polynomial reduction, but no general method is available. There are some special results in this direction, but the matrix of coefficients which arises generally possesses no special simplifying properties.

Example 1. A reactor operates on the simple first-order, irreversible, exothermic reaction, $A \rightarrow B$. The following values of the parameters have been fixed:

$\rho = 1$ g./cc.
$c = 1$ cc./(g.) (°C.)
$q = 10$ cc./sec.
$V = 2000$ cc.
$U = 1.356$ cal./(°C.) (sec.)
$-\Delta H = 10{,}000$ cal./mole
$T_0 = 300$°K.
$A_0 = 0.005$ mole/liter
$k = 7.86\ (10^{12}) \exp(-22{,}500/RT)$
$T' = 305$°K.

The graphical or algebraic method will show that there are three intersections or steady states with these parameters

$A_s \times 10^3$	T_s	k_s
4.42	306	6.6×10^{-4}
1.67	330	1.00×10^{-2}
1.57	330.8	1.09×10^{-2}

Direct computation will show that Equations (8) and (9) are satisfied simultaneously for the lowest and highest conversions but are not satisfied for the intermediate case. This example is interesting because of the closeness of the two upper states. It is apparent that difficulty of operation would result at any but the state of lowest conversion.

Example 2. Suppose the following reactions are carried out.

$$A + B \underset{k_2}{\overset{k_1}{\rightleftarrows}} C + F, \quad \Delta H_1$$

$$C \xrightarrow{k_3} E, \quad \Delta H_2$$

The transient equations which describe an arbitrary displacement from the steady state are

$$hA_0 - hA - k_1AB + k_2CF = \frac{dA}{d\theta}$$

$$hB_0 - hB - k_1AB + k_2CF = \frac{dB}{d\theta}$$

$$hC_0 - hC + k_1AB - k_2CF - k_3C = \frac{dC}{d\theta}$$

$$hF_0 - hF + k_1AB - k_2CF = \frac{dF}{d\theta}$$

$$h(T_0 - T) - (k_1AB - k_2CF)\left(\frac{\Delta H_1}{c\rho}\right) - k_3C\left(\frac{\Delta H_2}{c\rho}\right) - \frac{U}{Vc\rho}(T - T') = \frac{dT}{d\theta}$$

If the perturbations from the steady state are defined by

$$t = T - T_s$$
$$a = A - A_s$$
$$b = B - B_s$$
$$c = C - C_s$$
$$f = F - F_s$$

the linearized perturbations about the steady state may be written. These will constitute a homogeneous set of first-order linear differential equations. The matrix whose latent roots must have negative real parts to ensure stability is

$$\begin{bmatrix} -h-k_{1s}B_s & -k_{1s}A_s & k_{2s}F_s & k_{2s}C_s & -X_s \\ -k_{1s}B_s & -h-A_sk_{1s} & k_{2s}F_s & k_{2s}C_s & -X_s \\ k_{1s}B_s & k_{1s}A_s & -h-k_{2s}F_s-k_{3s} & -k_{2s}C_s & -X_s \\ k_{1s}B_s & k_{1s}A_s & -k_{2s}F_s & -h-k_{2s}C_s & X_s \\ M_s & N_s & P_s & Q_s & -h-Z_s \end{bmatrix}$$

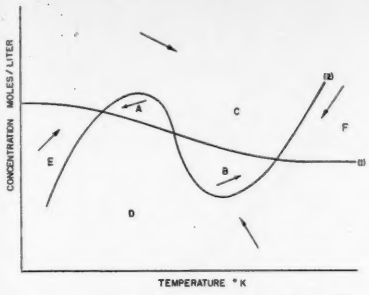

Fig. 4. Qualitative plot showing trends of reaction paths.

where

$$M_s = -k_{1s}B_s\frac{\Delta H_1}{c\rho}$$

$$N_s = -k_{1s}A_s\frac{\Delta H_1}{c\rho}$$

$$P_s = k_{2s}F_s\frac{\Delta H_1}{c\rho} - k_{3s}\frac{\Delta H_2}{c\rho}$$

$$Q_s = k_{2s}C_s\frac{\Delta H_1}{c\rho}$$

$$X_s = k_{1s}A_sB_s\frac{E_1}{RT_s^2} - k_{2s}C_sD_s\frac{E_2}{RT_s^2}$$

$$Y_s = X_s - k_{3s}\frac{E_3}{RT_s^2}C_s$$

$$Z_s = -X_s\frac{\Delta H_1}{c\rho} - \frac{U}{Vc\rho} - k_{3s}\frac{E_3}{RT_s^2}C_s\frac{\Delta H_2}{c\rho}$$

Five equations must be written as the perturbations must be arbitrary. The task of determining the latent roots of a matrix of large order can be carried out with facility with new high-speed computation equipment.

It may be of interest to consider the stability of the corresponding isothermal system; that is, to consider only perturbations which alter the concentrations, on the assumption that temperature control and mixing are instantaneous. The secular determinant is then

$$\begin{vmatrix} -h-\bar{a}-\gamma & -\bar{b} & \bar{c} & \bar{f} \\ -\bar{a} & -h-\bar{b}-\gamma & \bar{c} & \bar{f} \\ \bar{a} & \bar{b} & -h-\bar{c}-\bar{g}-\gamma & -\bar{f} \\ \bar{a} & \bar{b} & -\bar{c} & -h-\bar{f}-\gamma \end{vmatrix} = 0$$

with

$$\bar{a} = k_{1s}B_s, \bar{b} = k_{1s}A_s, \bar{c} = k_{2s}F_s,$$

$$\bar{f} = k_{2s}C_s, \bar{g} = k_{3s}.$$

This determinant may be expanded to give

$$(h+\gamma)^2\left[(h+\gamma)^2 + (h+\gamma)(a+b+c+f+g) + g(a+b+f)\right] = 0$$

and the γ's satisfying this equation have negative real parts. Thus the isothermal system is always stable.

Certainly these methods may be generalized to any chemical system for the continuous stirred reactor, however complex may be the kinetics. The physical mechanism of instability is clear and needs no elucidation. It would be interesting to investigate the oscillatory state, but from a practical point of view this cannot be much more than a curiosity since, seemingly, it would require a coincidental choice of parameters.

NATURE OF THE APPROACH TO THE STEADY STATE

Reactors are generally brought to a steady state in practice by a coaxing and coercing process bringing temperatures and concentrations to the desired point. This may be easy or difficult and it is the purpose of this section to study in detail, not this process, but rather the natural behavior of a reactor in the region or neighborhood of its steady states. For simplicity only the simple case $A \rightarrow B$, first order, will be considered, but the generalization to more complex systems may be carried out. The two transient equations (4) and (5) may be written in the form

$$\frac{dA}{d\theta} = a_1 - b_1A - c_1Ae^{-E/RT} \quad (10)$$

$$\frac{dT}{d\theta} = a_2 - b_2T + c_2Ae^{-E/RT} \quad (11)$$

$$a_i > 0, b_i > 0, c_i > 0$$

For the plane A, T, if in Equations (10) and (11) $dA/d\theta$ and $dT/d\theta$ are set equal to zero, two equations result which may be plotted in this A, T plane to give, respectively, the curves 1 and 2 in Figure 4. On curve 1, $dA/d\theta = 0$, and on curve 2, $dT/d\theta = 0$. For fixed T, as A is increased

$$a_1 - b_1A - c_1Ae^{-E/RT}$$

decreases. Similarly, for fixed T, as A is increased

$$a_2 - b_2T + c_2Ae^{-E/RT}$$

increases. Therefore above curve 1 $dA/d\theta < 0$, and below curve 1, $dA/d\theta > 0$, since it is zero on curve 1. Likewise above curve 2, $dT/d\theta > 0$, and below curve 2, $dT/d\theta < 0$. In the six regions of the A, T plane the following values appear:

	$dA/d\theta$	$dT/d\theta$
A	neg	neg
B	pos	pos
C	neg	pos
D	pos	neg
E	pos	neg
F	neg	pos

The steady state for the reactor is defined by the parameters a_i, b_i, and c_i and there are three such states at the three intersections. From the earlier argument the two extreme states are stable but the middle one is unstable. Any point on the A, T plane is a possible transient state for the reactor, and in undergoing the transient the reactor must ultimately end at one of the three states. Attached to every point on this plane is a vector pointing in the direction which the reactor coordinates will move on this plane. In region C, $dA/d\theta < 0$, $dT/d\theta > 0$, and hence the reactor must move in the general direction indicated by the arrow. It must continue to move in this direction until it crosses over into region F, where, because of the sign of the derivatives, it must move as the arrow indicates. In region B the arrow points upward and to the right and it appears that the right-hand steady state will be approached perhaps even by transient states, which are initially closer to the left-hand steady state. In regions A and B the vectors will point away from the unstable state, and hence this appears to be a state toward which a reactor would never naturally tend. It is clear that this method could be made quantitative by a numerical scheme and the whole plane could be filled in with reaction paths. Thus one could consider any point on the plane as an initial point, resulting from start up or from a large perturbation, and could calculate and plot on such a diagram the time history of the reactor in its approach to the steady state. This would be a difficult task and it is easier and quicker to accomplish this on an analogue computer.

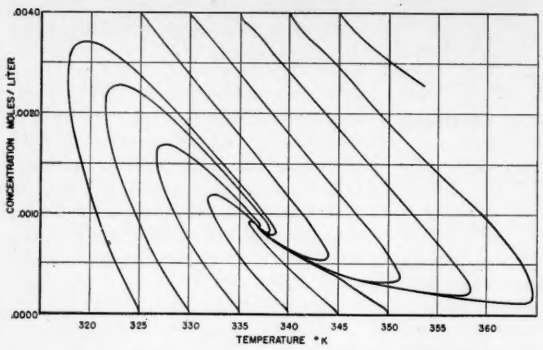

Fig. 5a. Reaction paths for a single stable state.

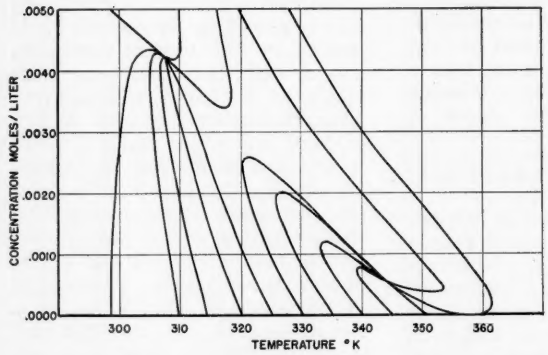

Fig. 5b. Reaction paths for a system with three steady states; $q = 10$ cc./sec.

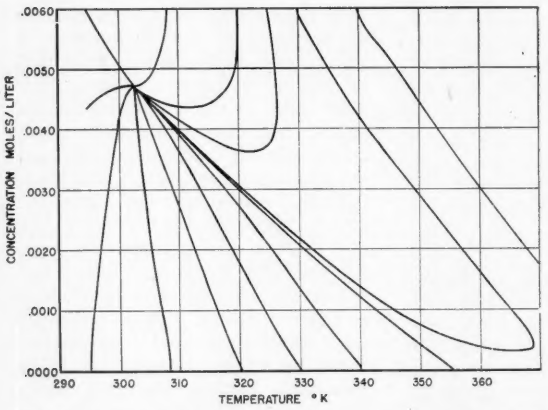

Fig. 5c. Reaction paths for a system with one stable state; data same as in Figure 5b except that $q = 20$ cc./sec.

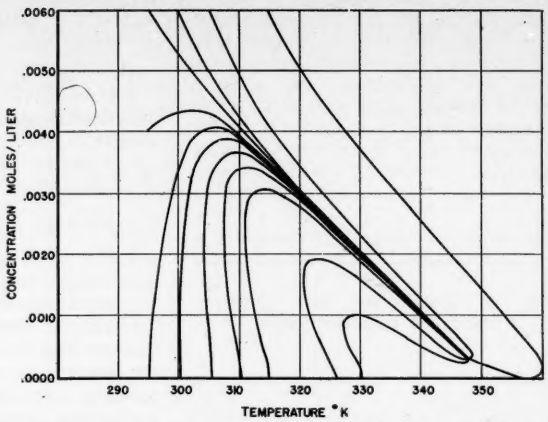

Fig. 5d. Reaction paths for a system with one stable state; data same as in Figure 5b except that $q = 5$ cc./sec.

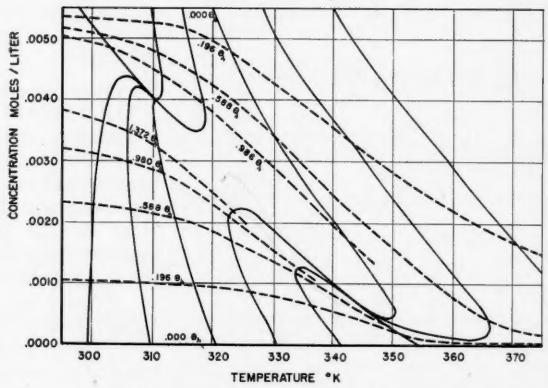

Fig. 5e. Reaction paths for a system with two stable states with a superimposed time grid, $\theta_h = V/q$.

With this end in view Equations (10) and (11) were programmed for the Reeves electronic analogue computer (R.E.A.C.) (*1*) and the reaction paths obtained. Figure 5 was obtained by this method and the curves shown are the actual traces made by the pen on the plotting board. On the R.E.A.C. one may obtain the two plots A vs. θ and T vs. θ, or one may use the plotting board and feed A and T to pens to obtain the reaction paths directly. The latter method was chosen as it illustrates more graphically reactor behavior.

In Figure 5*a* are shown the reaction paths for a single intersection at a high temperature such as in Figure 2*b*. The numerical data used are not important; suffice it to say that they are not much different from those of Example 1. All transient states lead to the same stable steady state. In Figure 5*b* the data would produce three steady states, one of which is unstable. In this case a flow rate of $q = 10$ cc./sec. was used, and this plot bears out the qualitative argument used above. The unstable state is approached on no reaction path and the plane seems to be divided into two domains by a line (not drawn) such that all transients in one part lead to one steady state while all transients in the other part lead to the other steady state. Two transient states

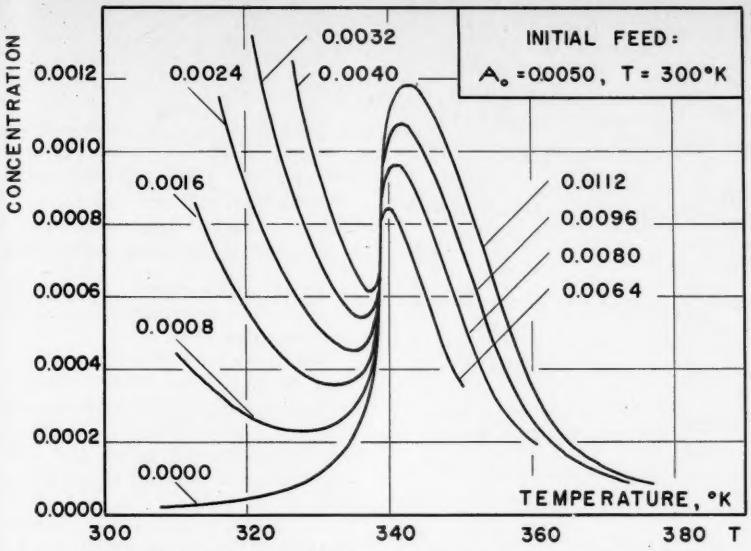

Fig. 6. Transient behavior caused by a step function in the feed showing overshoot. Numbers on curves refer to new feed concentration.

which are very close initially might lead to widely different steady states.

If the data for Figure 5*b* are kept unchanged except that the flow rate is increased to $q = 20$ cc./sec., then Figure 5*c* results. The high-conversion steady state is wiped out completely, as it should be, because the slope of the heat-consumption curve increases. There are some transient states however at which the reactor appears to be seeking a high-conversion steady state. None existing, it must then return to the low conversion state.

If the flow rate instead of being doubled is cut in half, $q = 5$, the low-conversion state is wiped out, and the reactor approaches only the high conversion state, as shown in Figure 5*d*. It appears, however, that transients would prefer to go to a low-conversion steady state but are forced to converge to a high-conversion state.

On each reaction path there is implicit a time scale and in theory it would require infinite time to traverse a single path, the speed along the path becoming less and less as the steady state is approached. This manifests itself on the computer in exactly the same way. In Figure 5*e*, Figure 5*b* is essentially reproduced except that during the course of tracing out the reaction paths a record was kept of the elapsed time and a time grid then superimposed on the totality of reaction paths. In this way the time for various transients can be compared.

One further study was made in connection with the transient from one steady state to another. It was supposed that the reactor had been operated at an influent concentration $A_o = 0.005$ and $T_o = 300°K$. At $\theta = 0$ a step change in feed concentration is made. As shown in Figure 6, if the step is positive the concentration in the reactor always increases over the prior steady state value and then damps off to a higher conversion, higher temperature steady state. When the step is negative, these trends are inverted.

All these reaction paths show overshoot and false-start phenomena which seem a little surprising. However such systems have been observed by Denbigh, Hicks, and Page (*3*).

It would be interesting to consider other types of steady states such as were discussed in connection with Figures 3 and 2*d*, *e*, and *f*. Some effort was put on this but the practicality of such a discussion is limited and it was decided to put no more time on it since the technique was now clear and reactor behavior had been illustrated and elucidated. These special states are difficult to produce as they require a coincidental choice of parameters. Systems with a high degree of instability are difficult to simulate on the analogue computer and the reason is not hard to find. For if the simulation is a real analogue, one must expect the electric circuit to become unstable also. This seemed to be the case in some of the work since more often than not

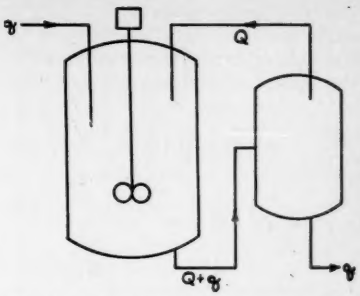

Fig. 7. Schematic diagram of reactor with recycle stream.

the capacity of the machine was exceeded in these special cases. A great deal of time was put on the case corresponding to Figure 2*f*. No conclusive results were obtained but indications were that this case would exhibit oscillatory or periodic (limit cycle) reaction paths.

In the language of nonlinear mechanics the points of stability appear to be stable nodal points. The points of instability are either saddle points or unstable nodal points. Focal points have not been noticed, but these probably exist in some problems of the type considered here.

One sees thus that the approach to a steady state is not a straightforward procedure but may be rather involved. The unstable state is also recognized as a state which a reactor will not naturally approach. If a perturbation is large, it is also evident that the reactor of its own accord might shift to a new steady state. At stable states the system is autoregulatory, always returning after small perturbations to the same state. Control is thus a simple problem. At unstable states the control must be good as the reactor must be maintained in a state to which it has no natural tendency.

A REACTOR WITH A RECYCLE STREAM

The product from a stirred reactor, R, may be supposed to pass to a separating unit, S. From this unit a stream rich in unreacted feed is recycled into the reactor while the enriched product passes out. The external and recycle flows are q and Q respectively. The separating unit might be a distillation column, extractor, crystallizer, settler, etc. The simple reversible reaction, $A \rightleftarrows B$, first order in each direction, is carried out in the schematic system of Figure 7. A linear equilibrium is assumed in the separator and the rate of separation in the separator is the usual

one for mass transfer. A and B stand for concentrations as well as chemical species. The transient isothermal equations are easily set up:

$$V\frac{dA}{d\theta} = qA_0 + QA' - (q+Q)A - V(k_1 A - k_2 B) \quad (12)$$

$$V\frac{dB}{d\theta} = QB' - (q+Q)B + V(k_1 A - k_2 B) \quad (13)$$

$$H\frac{dA'}{d\theta} = (q+Q)A - QA' - SK_A(A' - \alpha A) \quad (14)$$

$$H\frac{dB'}{d\theta} = (q+Q)B - QB' - SK_B(B' - \beta A_1) \quad (15)$$

$$h\frac{dA_1}{d\theta} = SK_A(A' - \alpha A_1) - qA_1 \quad (16)$$

$$h\frac{dB_1}{d\theta} = SK_B(B' - \beta B_1) - qB_1 \quad (17)$$

The symbols are defined completely at the end of the paper. The first pair of equations describes the reactor. Equations (14) and (15) describe the lean phase where H is the holdup, SK_A is the over-all mass transfer factor, and α is the equilibrium constant for the phase equilibrium. Equations (16) and (17) describe the rich phase. This system of equations could be solved analytically, but the solving of a sixth-order system is a little tedious and so will be omitted. The solution can easily be obtained on the analogue computer, and in fact systems in which the kinetics are more complicated or in which the separation is more complex may also be treated. A particular example will be considered to illustrate what may be done.

Let $\gamma = Q/q$
which may be called a reflux ratio.
Suppose
$V = 2000$ liters
$q = 1000$ liters/hr.
$Q = \gamma q$
$h = 500$ liters
$H = 500$ liters
$k_1 = 1.00$ hr.$^{-1}$
$k_2 = 2.00$ hr.$^{-1}$
$SK_A = 1000$ liters/hr.
$SK_B = 2000$ liters/hr.
$\alpha = 5$; $\beta = 0.2$
$A_0 = 1$ mole/liter
$B_0 = 0$

The transient equations may then be written

$$\frac{dA}{d\theta} + (1.5 + 0.5\gamma)A = 0.5A_0 + 2B + 0.5\gamma A' \quad (18)$$

$$\frac{dB}{d\theta} + (2.5 + 0.5\gamma)B = A + 0.5\gamma B' \quad (19)$$

$$\frac{dA'}{d\theta} + (2 + 2\gamma)A' = 2(1+\gamma)A + 10A_1 \quad (20)$$

$$\frac{dB'}{d\theta} + (4 + 2\gamma)B' = 2(1+\gamma)B + 0.8B_1 \quad (21)$$

$$\frac{dA_1}{d\theta} + 12A_1 = 2A' \quad (22)$$

$$\frac{dB_1}{d\theta} + 2.8B_1 = 4B' \quad (23)$$

and the steady state solution is

recycle

$$A_s' = 6A_{1s}$$
$$B_s' = 0.7B_{1s}$$

reactor product

$$A_s = \frac{1+6\gamma}{1+\gamma}A_{1s}$$

$$B_s = \frac{1+0.7\gamma}{1+\gamma}B_{1s}$$

separator product

$$A_s = \frac{2.50 + 1.90\gamma}{3.50 + 7.90\gamma}A_0$$

$$B_{1s} = \frac{1+6\gamma}{3.50 + 7.90\gamma}A_0$$

The product yield increases with the reflux ratio γ,

γ	0	0.50	1.00	2.00	∞
B_1/A_0	0.286	0.537	0.615	0.675	0.760

In practice the reflux ratio would have to be determined by some optimizing process.

The transient, as stated above, was developed on the analogue computer, and Figure 8 shows the effect of a step change in the feed concentration and gives the two concentrations A_1 and B_1 as functions of the time for the case $\gamma = 1$. Each of these curves will become asymptotic to a line which can be calculated from the steady state solution.

In order to study the stability of the system the methods used above could be applied, but it is interesting to approach the problem from the frequency-response technique. For such a system, from control theory, it is known that if L denotes the Laplace transform operator, then the transfer function of the system is

$$G(s) = \frac{L(\text{output})}{L(\text{input})}$$

where s is the Laplace transform parameter. The product of $G(jw)$, where $j = \sqrt{-1}$ and w is the frequency of the input signal, and the input signal gives the output signal. In this case

$$G(s) = \frac{\begin{vmatrix} 1.5+0.5\gamma+s & -2 & -0.5\gamma & 0 & 0 & 0.5 \\ -1 & 2.5+0.5\gamma+s & 0 & -0.5\gamma & 0 & 0 \\ -2(1+\gamma) & 0 & 2(1+\gamma)+s & 0 & -10 & 0 \\ 0 & -2(1+\gamma) & 0 & 4+2\gamma+s & 0 & 0 \\ 0 & 0 & -2 & 0 & 12+s & 0 \\ 0 & 0 & 0 & -4 & 0 & 0 \end{vmatrix}}{\begin{vmatrix} 1.5+0.5\gamma+s & -2 & -0.5\gamma & 0 & 0 & 0 \\ -1 & 2.5+0.5\gamma+s & 0 & -0.5\gamma & 0 & 0 \\ -2(1+\gamma) & 0 & 2(1+\gamma)+s & 0 & -10 & 0 \\ 0 & -2(1+\gamma) & 0 & 4+2\gamma+s & 0 & -0.8 \\ 0 & 0 & -2 & 0 & 12+s & 0 \\ 0 & 0 & 0 & -4 & 0 & 2.8+s \end{vmatrix}}$$

and after reductions

$$G(s) = \frac{4+24\gamma+(14+2\gamma)\,s+s^2}{P_6(s)}$$

where $P_6(s)$ is a polynomial of the sixth degree in s. System stability may be discussed by applying the Routh-Hurwitz criterion to $P_6(s)$. Also theoretical Nyguist and Bode diagrams may be calculated from the expression for $G(jw)$. If, for example $\gamma = 1$ and the frequency $w = 1$ radian/hr., then

Amplitude ratio $= G(jw) = 0.70$
Phase lag $= \phi = 130°$

These considerations will not be given in more detail here since the elucidation of the method of solution was all that was intended. Clearly the inclusion of heat effects for exothermic reactions, etc., will cause only a complication and in no way alters the method. For recycle systems one should expect instabilities in the system as well as increased sensivity, as a recycle stream in chemical operations would play the same role as feedback in electric circuit and amplifier design.

SUMMARY

In this paper the general character of the steady state operation of the continuous stirred-tank reactor has been considered. It has been shown, after the method of van Heerden, that instabilities may exist in these steady states. Analytical criteria for the determination of stability or instability have been developed. The nature of the approach to the steady state has been investigated both qualitatively and by the use of the R.E.A.C., an analogue computer. It cannot be decided on *a priori* grounds to what steady state a given transient state will lead. This may have been expected by some because of the high degree of nonlinearity of the transient equations. The approach to the steady state is not, in general, simple, and the reaction paths traced by the R.E.A.C. show that unstable states are not approached at all along any reaction paths. As far as the natural behavior of the reactor is concerned, the unstable states do not even exist and, in fact, a reactor which finds itself in the neighborhood of an unstable state makes an effort to leave that neighborhood. This poses problems in the control of such reactors and may explain in part some of the difficulties encountered in their control. It is the conclusion of this paper that steady states should be investigated for stability. It is also the conclusion that an investigation of the reaction path may shorten transient times by a proper juggling of initial conditions.

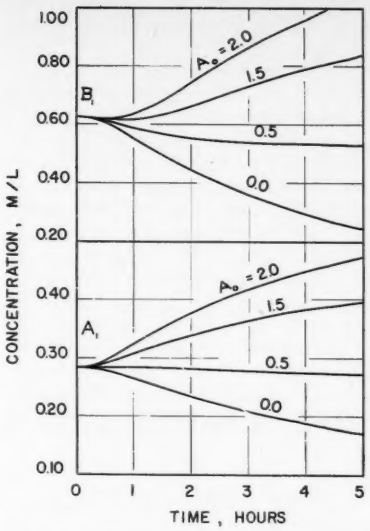

Fig. 8. Effect of step change on the feed with a system with a recycle ratio equal to 1.

The methods of this paper may be extended to systems with arbitrary kinetics and heat effects. The problems were chosen as simply as possible here in order to illustrate the method.

ACKNOWLEDGMENT

The authors are indebted to the Computer Center at the University of Minnesota for advice and counsel and for the extensive use of the R.E.A.C. in the preliminary stages of the research.

A portion of this paper was written while N. R. Amundson was a Fulbright Scholar in the Department of Chemical Engineering at Cambridge University, England.

NOTATION

A,B,C,F, etc. = chemical specie and concentrations in the reactor
A_o,B_o,C_o,F_o, etc. = influent concentration or corresponding specie
A_s,B_s,C_s,F_s, etc. = steady state concentration of corresponding specie
A_1,B_1 = concentration in the rich phase (rich in B)
A',B' = concentration in the lean phase
a,b,c, etc. = perturbations from steady state values
c = specific heat
ΔH = heat of reaction ($-\Delta H > 0$, exothermic)
E = activation energy
k = reaction velocity constant
k_s = reaction velocity constant at temperature of steady state
q = influent flow rate
Q = recycle flow rate (recycle problem)
p = frequency factor in reaction velocity constant
SK_A, SK_B = separation-rate constants in separator
T = reactor temperature
T_s = reactor steady state temperature
T' = average coolant temperature in reactor cooling coil
T_o = influent temperature
s = Laplace transform variable
U = product of heat transfer coefficient and surface area in reactor
V = reactor volume

Greek Letters

α,β = equilibrium constant in separator
γ = root of characteristic equation (stability) or recycle ratio (recycle problem)
ρ = density
θ = time

LITERATURE CITED

1. Acrivos, A., and N. R. Amundson, *Ind. Eng. Chem.*, **45**, 467 (1953).
2. Denbigh, K. G., *Trans. Faraday Soc.*, **43**, 648 (1947).
3. ———, M. Hicks, and F. M. Page, *loc. cit.*, **44**, 479 (1948).
4. Eldridge, J. W., and E. L. Piret, *Chem. Eng. Progr.*, **46**, 290 (1950).
5. Frank-Kamenetski, D. A., *Zhur. Fiz. Khim.*, **14**, 30 (1940).
6. ———, *Uspekhi Khim.*, **10**, 373 (1941).
7. Gevart, Y. G., and D. A. Frank-Kamenetski, *Izvest. Akad. Nauk S.S.S.R., Otdel. Khim. Nauk*, **4**, 210 (1942).
8. Hurwitz, A., *Math. Ann.*, **46**, 273 (1895).
9. Liapounoff, M. A., "General Problem of Stability of Motion," Annales de Toulouse, Vol. 9, Paris (1907).
10. MacMullin, R. B., and M. Weber, *Trans. Amer. Inst. Chem. Engrs.*, **31**, 409 (1935).
11. Mason, D. R., and E. L. Piret, *Ind. Eng. Chem.*, **42**, 817 (1950); **43**, 1210 (1951).
12. Minorsky, N., "Non-linear Mechanics," J. W. Edwards, Ann Arbor (1947).
13. Poincare, H., "Oeuvres," Vol. 1, Gauthier Villars, Paris (1928).
14. ———, "New Methods in Celestial Mechanisms," Vol. 1, Gauthier Villars, Paris (1892).
15. Salnikov, I. E., *Doklady Acad. Nauk S.S.S.R.*, **60**, (3), 405 (1948); **60**, (4), 611 (1948).
16. Tiller, F. M., *Chem. Eng. Progr.*, **44**, 299 (1948).
17. Van Heerden, C., *Ind. Eng. Chem.*, **45**, 1242 (1953).

Ion Diffusion in Mass Transfer Between Phases

T. K. SHERWOOD and J. C. WEI
Massachusetts Institute of Technology, Cambridge, Massachusetts

Mass transfer between phases has become a subject of broad technical importance, particularly in industrial operations involving gas absorption, extraction, ion exchange, and other separation processes. Many such operations involve simultaneous mass transfer and chemical reaction, as in the absorption of carbon dioxide by an alkaline solution, the absorption of hydrogen sulfide by amine solutions, or the absorption of NH_3 by sulfuric acid. The theory of such cases has been discussed in recent years by many writers, notably by Danckwerts (*2*) and by Pigford (*6*), and a considerable amount of experimental data has been collected, especially by Van Krevelen (*8*) and by Pozin (*7*).

The general mechanism of simultaneous mass transfer and chemical reaction was outlined by Hatta (*4*) in 1928. Hatta pictured the solute A entering a phase with a concentration p at the phase boundary and reacting with a second solute B present in concentration q in the bulk of the fluid. In the special case of a rapid irreversible reaction between A and B, the reaction is presumed to occur at a plane near the interface where the concentrations of both A and B are zero: A diffuses to this zone as a result of the concentration potential (p-0) and B as the result of the concentration difference (q-0). This relatively simple picture leads to the rate equation

$$N_A = \frac{D_A p + D_B q}{x_L}$$

$$= k^\circ_{LA}\left(p + \frac{D_B}{D_A} q\right) \qquad (1)$$

where N_A represents the flux as gram moles/(day) (square centimeter), D_A and D_B are the effective diffusion coefficients of A and B, square centimeter/day, and x_L is the "effective thickness" of the "stagnant film," which corresponds to the diffusional resistance. k°_{LA} is the coefficient of mass transfer of A into the phase when B is not present and no reaction occurs.

This picture has been described many times, usually in terms of the oversimplified stagnant-film model. The basic concept, however, permits allowance for combined molecular and eddy diffusion provided D_A, D_B, and x_L are properly defined, without reference to the molecular-diffusion – stagnant-film model. Danckwerts's surface-renewal theory (*2*), for example, leads to a more complex relation but gives approximately the same quantitative relationship between N_A and $(D_A p + D_B q)$.

DIFFUSION IN MIXED ELECTROLYTES

In cases of neutralization involving ionic reactions, as, for example, the absorption of hydrochloric acid gas by an aqueous solution of sodium hydroxide, it is diffusion of ions that is important, and allowance must be made for the fact that individual ions in the presence of other ions may diffuse at rates which are quite different from those of their original "partners." Allowance for this effect is the subject of the present paper. The subject will be developed within the framework of the classical stagnant-film picture presented by Hatta, with later comments on the errors in this approach.

Diffusion in mixed electrolytes has been discussed by several authors (*3, 5*); the treatment of Vinograd and McBain (*9*) will be used here. Following the Nernst theory, these authors write diffusion equations for each ion, the diffusion potential for each involving both the concentration gradient of the particular ion and the gradient of the electrical potential in the solution. Imposing the condition of electrical neutrality for the ion mixture, they obtain the following equation for diffusion of cations:

$$n_+ N_+ = -\frac{RT}{F}\frac{u_+}{n_+}\left(G_+ - n_+ C_+ \frac{\Sigma u_+ G_+/n_+ - \Sigma u_- G_-/n_-}{\Sigma u_+ C_+ + \Sigma u_- C_-}\right) \quad (2)$$

A similar relation is given for anions, the minus becoming a plus within the parenthesis. Here N_+ is the ion flux of a particular cation of valence n_+, concentration C_+, and mobility u_+; G_+ is the concentration gradient dC_+/dx of this cation in the direction of diffusion; and the minus signs as subscripts refer to anions. The derivation is subject to the limitation that activity coefficients and collision effects are ignored, as are the effects of ion pairs or ionic complexes. Such approximations are well within the precision of an approach to mass transfer problems by use of the stagnant-film model.

Vinograd and McBain demonstrate the use of these equations in the analysis of data on simultaneous diffusion of barium chloride and hydrogen chloride and of potassium chloride and hydrogen chloride in the same direction through the fritted-glass disk of a diffusion cell. Since the concentration gradient G varies with distance x through the disk, the calculation is simplified if G is assumed to be represented by $\Delta C/\Delta x$; furthermore, C is taken as the arithmetic mean of the concentrations of the ion in the bulk fluid on the two sides of the cell, and ionization is assumed to be complete. In spite of these several simplifying assumptions, the data and theory are found to check within a few per cent.

In the barium chloride–hydrogen chloride system, D for the H^+ ion decreased from 10.6 to 4.2 sq.cm./day as the ratio of H^+ to Ba^{++} was increased from 0 to 1.3; these values may be compared with the value for free H^+ ion, which is 8.05 sq.cm./day, and the value 2.87 sq.cm./day for hydrogen chloride at the same temperature (25°C.). The presence of the slow-moving Ba^{++} ion accelerates the H^+ ion; hydrogen chloride retards the Ba^{++} ion. D for Cl^- increases with increase in the ratio H^+/Ba^{++}, and D for Ba^{++} decreases and even becomes negative. Similar data are quoted for the system hydrogen chloride–potassium chloride.

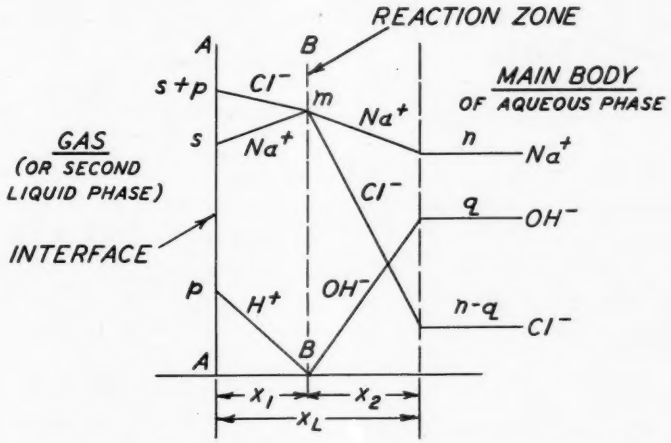

Fig. 1. Concentrations in double film during absorption of hydrochloric acid by aqueous sodium hydroxide.

Ions of a single ionized solute, such as hydrogen chloride, must diffuse at the same rate to maintain electrical neutrality at any plane in the solution. Under such circumstances it is allowable to define a molecular diffusivity of the compound hydrogen chloride, even though ions rather than molecules are diffusing. In a system of mixed ions, as in the simultaneous diffusion of hydrogen chloride and sodium chloride, the faster moving H^+ may move ahead of its Cl^- partner, essential electrical neutrality being maintained by the presence of the slower moving Na^+ ions, which now lag behind their own Cl^- partners. At very low H^+ concentration in a solution of sodium chloride the electrical potential in the direction of diffusion may cause the effective diffusivity of H^+ to be even greater than that of a free hydrogen ion.

STEADY STATE DIFFUSION OF HYDROGEN CHLORIDE INTO SODIUM HYDROXIDE

An example of a possible approach to the problem of absorption with chemical reaction is the case of steady state absorption of hydrogen chloride gas from air by an aqueous solution of sodium hydroxide. The modified Hatta picture is illustrated by Figure 1, where *A-A* is the gas-liquid interface and *B-B* the zone in the liquid where H^+ and OH^- ions meet. Concentrations of the several ions at different planes are represented by the symbols shown on the figure. The symbol p, for example, represents the H^+ ion concentration at the liquid surface, and q is the OH^- ion concentration in the main bulk of the alkaline solution. Na^+ and Cl^- concentrations must be equal at the reaction zone in order to maintain electrical neutrality.

In order to make the analysis more understandable, specific values of the several variables will be assumed and the results compared quantitatively with the simple Hatta theory. Thus for the system hydrogen chloride–sodium hydroxide at 25°C. the mobilities are $u_+(H^+) = 350/F$, $u'_+(Na^+) = 50/F$, $u_-(Cl^-) = 76/F$, and $u'_-(OH^-) = 198/F$ sq.cm./(sec.)(volt), where F is the Faraday. The assumptions employed by Vinograd and McBain regarding linear concentration gradients and arithmetic mean concentrations will be adopted. First is considered the region near the interface in film of thickness x_1:

$$G_+ = -\frac{p}{x_1}; G'_+ = \frac{m-s}{x_1};$$

$$G_- = \frac{m-s-p}{x_1}$$

$$C_+ = p/2; C'_+ = \frac{m+s}{2};$$

$$C_- = \frac{m+s+p}{2}; C'_- = 0$$

Substituting in Equation (2) and simplifying give

$$N_+ = 8.05\frac{p}{x_1}\left[\frac{100m+152s+152p}{426p+126m+126s}\right] \quad (3)$$

Here the number 8.05 is the diffusion coefficient for free H^+ ion (RTu_+/Fn_+) and has the units sq.cm./day; N_+ is expressed as g. equivalents/(day)(sq.cm.)

Similar equations are obtained for Na^+ and Cl^- diffusion. Since

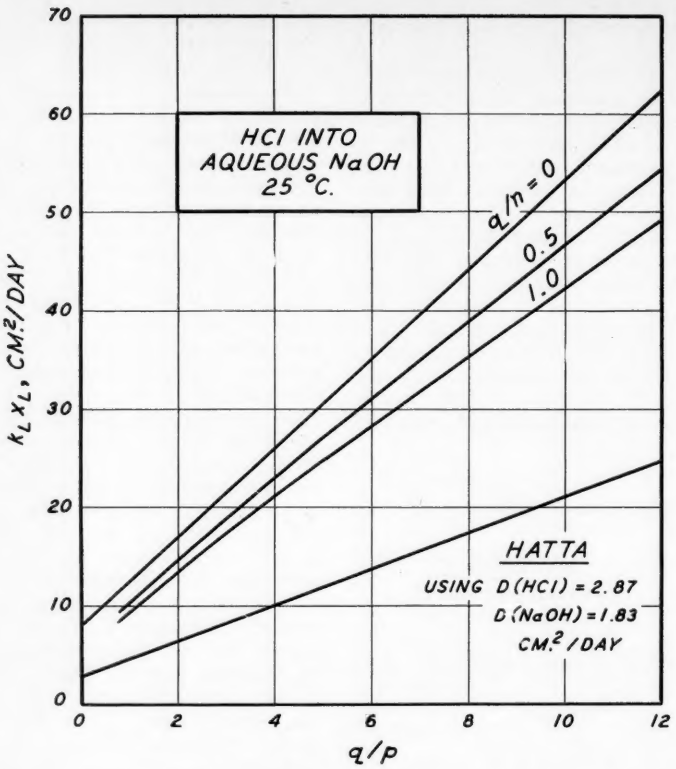

Fig. 2. Comparison of ion-diffusion theory with original version of Hatta theory; effect of sodium hydroxide concentration on rate of hydrochloride absorption.

there is no net diffusion of Na^+ in this region, N'_+ may be set equal to zero; whence

$$s = -\frac{p}{2} + \sqrt{\frac{p^2}{4} + m^2 + 4.61\,pm} \qquad (4)$$

This same relation is obtained by equating N_+ and N_- (H^+ and Cl^-).

Following this procedure, diffusion equations are written for the x_2 region, for OH^-, Na^+, and Cl^-. Since Na^+ is not diffusing, N'_+ is again set equal to zero; whence

$$m = n\sqrt{1.605\frac{q}{n} + 1} \qquad (5)$$

which is also obtained by equating N'_- and $-N_-$.

If N is the rate of absorption of hydrogen chloride and k_L the mass transfer coefficient for hydrogen chloride crossing the liquid layer x_L then

$$k_L x_L = \frac{N x_L}{p} = \frac{N_+ x_1 = N'_- x_2}{p} \qquad (6)$$

It follows from Equation (5) that m/n is a function of q/n, and from Equation (4) that s/m is a function of the product $p/q \cdot q/n \cdot n/m$. The fraction in square brackets in Equation (3) can, therefore, be expressed in terms of q/p and q/n. The corresponding term in the equation for N'_- is a function of q/n only but is multiplied by q instead of p. From Equation (6) then

$$k_L x_L = 4.54\frac{q}{p} f_1\left(\frac{q}{n}\right) + 8.05 f_2\left(\frac{q}{n}, \frac{p}{q}\right) \qquad (7)$$

where the number 4.54 is the diffusion coefficient RTw'_-/Fn'_- for OH^- ion, corresponding to the 8.05 for H^+ ion.

Figure 2 shows values calculated from this relation for the diffusion of hydrogen chloride into aqueous sodium hydroxide at 25°c., by use of the values of ion mobilities quoted earlier. For comparison with the simple form of the Hatta theory, values of $k_L x_L$ are also shown as the lowest line on the graph. These are calculated from Equation (1) in the form

$$k_L x_L = \frac{N_A x_L}{p} = D_A\left(1 + \frac{D_B}{D_A}\frac{q}{p}\right) \qquad (8)$$

D_A for molecular hydrogen chloride and D_B for sodium hydroxide are calculated from the Nernst equation to be 2.87 and 1.83 sq. cm./day, respectively.

Figure 2 indicates that the rapid diffusion of H^+ and OH^- ions in the presence of Na^+ and Cl^- ions may lead to an absorption rate more than twice that predicted by the use of molecular diffusion concepts and the Hatta theory. The limiting value of $p = 0$, at which the gas-side resistance controls, is

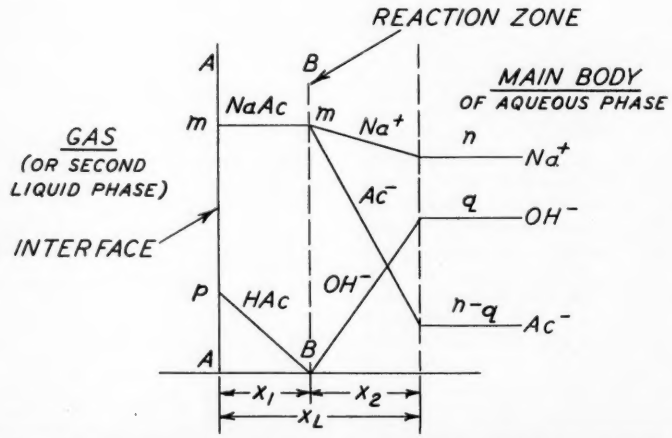

Fig. 3. Concentrations in double film during absorption of nonionizing acetic acid by aqueous sodium hydroxide.

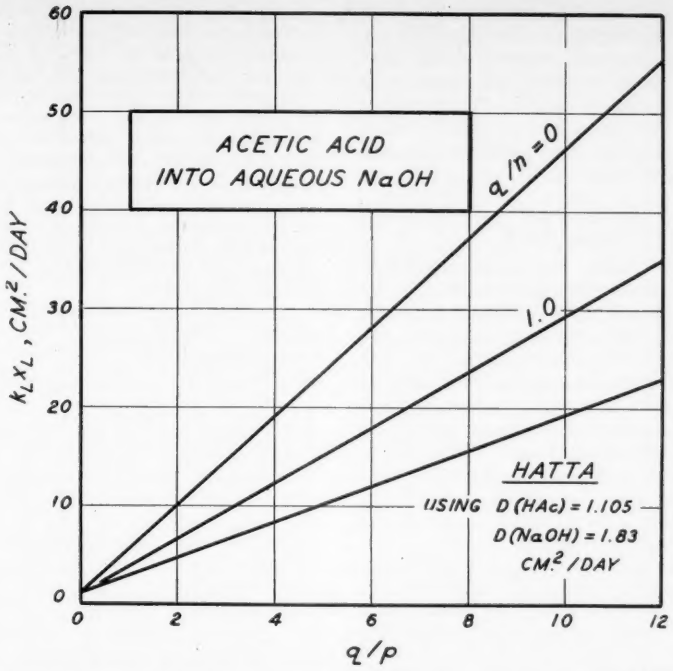

Fig. 4. Effect of sodium hydroxide concentration on rate of absorption of acetic acid.

reached at a lower value of q (or C_B) than predicted by the Hatta theory by use of diffusion coefficients for pure compounds.

In the calculation of the values plotted in Figure 2 it is noted that m, the sodium normality at the reaction zone, varies from n at $q = 0$ to about $1.6n$ at $q = n$. Because chloride ion diffuses more slowly than the H^+ ion, sodium ion tends to accumulate near the interface in concentrations greater than in the bulk liquid. The concentration s at the liquid surface may be more than twice that in the bulk liquid.

STEADY STATE DIFFUSION OF ACETIC ACID INTO SODIUM HYDROXIDE

There are several possible variations of the hydrogen chloride–sodium hydroxide case, as, for example, to allow for different valences. Allowance for the variation of ionization with concentration might be made, although this would be difficult. One of the reacting solutes may not dissociate, whereupon the ion diffusion equations apply only to part of the film. As an example of this last possibility, one may consider the diffusion of acetic acid into aqueous caustic, neglecting the ionization of acetic acid in layer x_1. The picture of the double diffusion layer is given in Figure 3.

As in the previous illustration, steady state will be assumed, with p, the surface concentration of acetic acid, held constant. Then in region x_1

$$N_A = \frac{D_A}{x_1} p \qquad (9)$$

where the subscript A now refers to acetic acid. In the region x_2

$$\text{for } Na^+,\ u'_+ = \frac{50}{F};\ G'_+ = \frac{n-m}{x_2};$$

$$C'_+ = \frac{n+m}{2}$$

$$\text{for } OH^-,\ u'_- = \frac{198}{F};\ G'_- = \frac{q}{x_2};$$

$$C'_- = \frac{q}{2}$$

$$\text{for } Ac^-,\ u_- = \frac{41}{F};\ G_- = \frac{n-q-m}{x_2};$$

$$C_- = \frac{m+n-q}{2}.$$

Substituting these values into Equation (2) (and the corresponding equation for anions) yields for the OH^- ion:

$$N'_- = -\frac{4.54}{x_2}\left[\frac{50nq+41mq}{45.5m+45.5n+78.5q}\right] \qquad (10)$$

with similar equations for Na^+ and Ac^-. Since Na^+ does not diffuse, N'_+ may be set equal to zero (or N'_- put equal to $-N_-$), whence

$$m = n\sqrt{3.82\frac{q}{n} + 1} \qquad (11)$$

For the entire layer x_L

$$N_{HAc} x_L = N_{HAc} x_1 = N_{OH} - x_2 \qquad (12)$$

and

$$k_L x_L = \frac{N_{HAc}\, x_L}{p} = D_{HAc} + \frac{4.54q}{p}\left[\frac{50n+41m}{45.5n+45.5m+78.5q}\right] \qquad (13)$$

As in the case of hydrogen chloride–sodium hydroxide, $k_L x_L$ is seen from Equations (10) and (12) to be a function of q/p and q/n, but the relation is not only simpler, but, as shown by Figure 4, the rate is somewhat nearer that predicted by the simple Hatta theory for molecular diffusion.

OVER-ALL COEFFICIENTS

The effect of ion diffusion has been illustrated by considering its effect on the aqueous-side mass transfer coefficient k_L. Over-all mass transfer coefficients may be defined for cases where the transfer is to or from a second gas or liquid phase, and these are easily related to the individual coefficients k_L and k_G if Henry's law applies.

Let the gas solubility at the interface be represented by $P_i = Hp$, and let C^* be the aqueous concentration corresponding to the main gas composition P_G. For the hydrogen chloride–sodium hydroxide illustration, K_L is defined as $N/C^* - 0$). Then if the gas-side transfer coefficient is k_G, it follows that

$$\frac{1}{K_L} = \frac{C^*}{N} = \frac{1}{Hk_G} + \frac{D_A}{k^\circ_L (k_L x_L)} \qquad (14)$$

and

$$\frac{K_L}{K^\circ_L} = \frac{Hk_G + k^\circ_L}{k^\circ_L + \dfrac{Hk_G D_A}{(k_L x_L)}} \qquad (15)$$

Here k°_L is the aqueous-side transfer coefficient D_A/x_L for *molecular* diffusion of solute A and K°_L is the corresponding over-all coefficient.

Figure 2 illustrates the dependence of $k_L x_L$ on p, q, and n; p may be eliminated by combining this with Equation (14) and the division of C^* into parts proportional to resistances:

$$p = \frac{C^* D_A K_L}{k^\circ_L (k_L x_L)} \qquad (16)$$

The expression for the over-all coefficient in the acetic acid–sodium hydroxide case is simpler. $k_L x_L$ is represented by

$$k_L x_L = D_A + \frac{q}{p} Q \qquad (17)$$

where Q is defined by comparison with Equation (13). Then from Equation (14)

$$K_L = \frac{\left(1 + \frac{qQ}{C^* D_A}\right)}{\frac{1}{Hk_G} + \frac{1}{k_L^\circ}} = K^\circ_L \left(1 + \frac{qQ}{C^* D_A}\right) \qquad (18)$$

In this case Q does not depend on p, and so no trial-and-error method is required. In both examples, however, the Henry-law constant H is properly defined as the solubility of the diffusing substance in the aqueous solution at the interface. This may in some instances be a rather strong electrolyte, containing more sodium, for example, than the main bulk of the solution.

The discussion has emphasized that allowance for ion diffusion may increase the rate of transfer above values predicted from the Hatta theory or other analyses based on molecular diffusion. It should be pointed out that the reverse can also happen, as in cases involving chemical reaction of a metal ion which, in the presence of other ions, has an effective diffusivity less than that for the unionized molecule.

IONIC REACTIONS IN DIFFUSION CELLS

The Hatta model can evidently be represented experimentally by the operation of a diffusion cell in which two reacting solutions are used. Preliminary studies of this kind have been made by means of the standard type of porous-glass disk apparatus commonly employed in measurements of diffusion coefficients in liquids. Several tests were made in which sodium hydroxide was neutralized by acetic and by hydrochloric acids.

The apparatus consisted of a vertical glass cylindrical vessel divided into two halves by a porous glass disk approximately 2 mm. thick. The solutions were placed in the two compartments, and the whole was placed in a bath at 25 ± 0.02°C. for 14 to 24 hr., when the solutions in both compartments were withdrawn and analyzed. Cell constants were obtained by preliminary tests using 0.1N potassium chloride and water, by reference to the established values of the integral diffusion coefficient for potassium chloride. The two liquids were not stirred, but natural convection was assisted by placing the heavier sodium hydroxide solution in the upper compartment and the lighter acid in the lower compartment. The lower compartment was first filled with the acid solution to the top of the porous disk. The upper compartment was rinsed and then filled with the alkaline solution, the volumes of both solutions being 68.0 ml. Inclusion of air bubbles was carefully avoided. At the end of the test the solutions were titrated with standard sodium hydroxide, hydrogen chloride, and silver nitrate to determine OH^-, H^+, and Cl^-. Bulk flow between the two compartments, resulting from volume changes of the solutions, was estimated and found to be negligible. Results are shown in Table 1, which gives the arithmetic average rate of neutralization for the period of the test.

Application of the ion diffusion theory is complicated by the fact that a steady state does not prevail. Figures 1 and 3 illustrate the conditions in the porous disk at any instant, but the concentrations change continuously with time. For the sodium hydroxide–hydrogen chloride case Equation (2) may be employed for both H^+ and Na^+ in region x_1 but the corresponding equation for Cl^- is not independent. In region x_2 independent rate equations may be written for Na^+ and OH^-. In addition to these four rate equations, the following apply:

$$N_{Na^+} \text{ through } x_1 = N_{Na^+} \text{ through } x_2 \qquad (19)$$

$$N_{H^+} = -N_{OH^-} \qquad (20)$$

$$x_1 + x_2 = x_L \qquad (21)$$

$$(p_o - p)\, V_L = \int_0^\theta N_+ \, d\theta \qquad (22)$$

TABLE 1.—RESULTS OF NEUTRALIZATION TESTS IN DIFFUSION CELLS

Run	Measured concentrations, normality: Initial, Upper	Initial, Lower	Final, Upper	Final, Lower	Time, hr.	Average neutralization rate, m. e. / (liter) (day): Obs.	Calc.
1	0.0971 NaOH	0.1046 HCl	0.0768 OH− 0.0123 Cl−	0.0844 H+ 0.0925 Cl−	23.7	0.0204	0.0225
2	0.0486 NaOH	0.1046 HCl	0.0339 OH− 0.0101 Cl−	0.0900 H+ 0.0954 Cl−	23.2	0.0151	0.0174
3	0.0971 NaOH	0.1082 HAc	0.0837 OH−	0.0959 HAc	23.87	0.0124	0.0128
4	0.0971 NaOH	0.0523 HCl	0.0822 OH− 0.0078 Cl−	0.0377 H+ 0.0452 Cl−	22.35	0.0157	0.0158
5	0.0486 NaOH	0.1082 HAc	0.0392 OH−	0.0991 HAc	23.72	0.00922	0.00891
6	0.4898 NaOH	0.4935 HCl	0.431 OH−	0.437 H+	13.85	0.102	0.113
7	0.0924 NaOH	0.0936 HCl	0.0701 OH−	0.0730 H+	21.5	0.023	0.0222

*Test 7 was carried out by Thibaut Brian (*1*) with magnetic stirring of both compartments and $V_L = 75$ ml. Calibration tests with potassium chloride to obtain the cell constant with and without stirring checked within 1%. However, the material balance in this test is off by 8%, as was true of run 3; the other balances checked within 4% for the acetic acid tests and within 2% when HCl was used.

$$sV_L = -\int_0^{\theta} N'_+ d\theta \qquad (23)$$

Equation (19) neglects holdup in the porous disk. Equation (21) relates x_1 and x_2 to x_L, obtainable from the cell constant (in terms of the unknown cross section of the diffusion path). Equation (22) assumes the bulk concentration of H^+ ion in the lower compartment to be the same as the surface concentration p of Figure 1. This compartment has an initial H^+ concentration p_o and a volume V_L ml.

With the variable p retained, these nine equations may be solved simultaneously to obtain the neutralization rate $dp/d\theta$ for any specific values of p, s, q, and n. New concentrations can be calculated after a short time increment, and numerical stepwise integration employed to relate all concentrations to time.

In comparison of the theory with the test results, the foregoing procedure was followed to calculate the neutralization rate at the beginning and end of each test, and the average of these two calculated rates is shown in Table 1. As in the earlier discussion, linear concentration gradients and average concentrations were assumed in applying the ion-diffusion-rate equations.

The deviation of the calculated from the observed average rates averages 7.7%, which is believed to be excellent in view of the several approximations made to simplify the application of the Vinograd-McBain equations. By contrast, the neutralization rates predicted by the Hatta theory, by use of molecular diffusivities, show an average deviation of 18% from the experimental values. In the light of these results it must be concluded that allowance for the effects of multiple-ion diffusion requires a substantial modification of the Hatta picture of mass transfer with chemical reaction in electrolytes, as in the neutralization of an acid by a base. As suggested by Figure 3, the deviation from the Hatta theory under some circumstances may be much greater than in the diffusion-cell tests here reported.

APPLICATION TO MASS TRANSFER WITH TURBULENCE

As applied to mass transfer into a stirred or moving fluid, the Hatta model is, of course, an incorrect idealized picture of the actual situation. Transfer is accomplished in large part by mixing or eddy diffusion, though final contact of reacting molecules or ions must be accomplished by molecular or ion diffusion. Eddies are damped out by the presence of the surface, and so equations for molecular or ion diffusion apply only in the limit as the distance from the surface approaches zero.

One can only speculate as to the effect of mixed ion diffusion in the case of mass transfer with chemical reaction in a moving liquid. It is not obvious, for example, that the stipulation of electric neutrality would be valid for macroscopic eddies. A rough approximation might be made by dividing the phase-boundary resistance arbitrarily into two parts (*10*), one involving D to the first power and one not involving D, and then applying the corrections indicated by Figures 2 and 4 to the first of these. In such cases as that illustrated by Figure 3, however, the effect of ion diffusion might be expected to be minor because ionization is small in the region near the interface, where D is important.

Attempts have been made in this laboratory to study the applicability of the ion-diffusion theory to the case of mass transfer between two stirred immiscible liquids with acid-base neutralization of diffusing solids. These have failed because in such cases the interface is violently agitated by the tendency of the phases to emulsify spontaneously and it would appear that no diffusion equations apply. The results, which throw considerable light on phenomena of solvent extraction with simultaneous chemical reaction, will be reported at another time.

ACKNOWLEDGMENT

The investigation described was supported by a research grant from The National Science Foundation.

NOTATION

C = concentration, g. equiv./cu.cm.
C^* = liquid concentration in equilibrium with other phase, g. moles/cu.cm.
D = diffusivity, sq.cm./sec., or sq. cm./day, diffusion rate per unit area per unit of concentration gradient, where the concentration employed is that of the species (ion or molecule) diffusing
F = Faraday = 96,500 coulombs/g. equiv.
G = concentration gradient, g. equiv./cm.^{4}
H = Henry's law constant, g.moles/(cu.cm.)(atm.)
k_L = mass transfer coefficient, cm./day
k°_L = mass transfer coefficient in absence of chemical reaction, cm./sec. or cm./day
K_L = over-all coefficient in absence of chemical reaction, cm./sec. or cm./day
m = sodium ion concentration, g. equiv./cu.cm.
n = valence
N = mass transfer rate, g.moles/(sec.)(sq.cm.) or g.moles/(day)(sq.cm.)
p = concentration of reactant A at boundary, g.moles/cu.cm.
q = concentration of reactant B at boundary, g.moles/cu.cm.
Q = quantity in square brackets in Equation (13)
R = gas constant, joules/(°K.)(g. mole)
T = temperature, °K.
u = ion mobility, sq.cm./(sec.)(volt)
V_L = diffusion cell volume, cu.cm.
x = distance normal to diffusion flux, cm.
x_L = effective film thickness, cm.
θ = time, sec. or days

LITERATURE CITED

1. Brian, Thibaut, personal communication (December, 1954).
2. Danckwerts, P. V., *Trans. Inst. Chem. Eng., (London)*, **32**, Suppl. No. 1, p. S49 (1954).
3. Dean, R. B., *J. Amer. Chem. Soc.*, **67**, 31 (1945).
4. Hatta, S., *Tech. Repts. Tohôku Imp. Univ.*, **8**, 1 (1928): **10**, 119 (1932).
5. Hartley, G. S., and C. Robinson, *Proc. Roy. Soc. (London)*, **134A**, 20 (1931).
6. Pigford, R. L., in T. K. Sherwood and R. L. Pigford, "Absorption and Extraction," 2nd ed. McGraw-Hill Book Company, Inc., New York (1952).
7. Pozin, M. E., series of articles in *J. Appl. Chem. (U.S.S.R.)* (1947 to date).
8. Van Krevelen, D. W., numerous articles, especially in *Rec. trav. chim.* (1947 to date).
9. Vinograd, J. R., and J. W. McBain, *J. Amer. Chem. Soc.*, **63**, 2008 (1941).
10. Walker, W. H., W. I. Lewis, W. H. McAdams, and E. R. Gilliland, "Principles of Chemical Engineering," 3rd ed. p. 448, McGraw-Hill Book Company, Inc., New York (1937).

Equivalent Isothermal Temperatures for Nonisothermal Reactors

JOHN B. MALLOY and HERMAN S. SEELIG, Standard Oil Company (Indiana), Whiting, Indiana

A simple procedure has been developed for evaluating the equivalent isothermal temperature for nonisothermal reactors. Reaction-rate constants determined from a kinetic study are averaged by a simplified integration method; the average rate constant defines the equivalent isothermal temperature. Use of this equivalent temperature permits direct comparison of experiments carried out in reactors having widely different temperature profiles.

Temperature so strongly influences the rate of chemical reaction that in any reaction study temperature must be accurately known. Ideally such studies are carried out in isothermal systems where the reaction temperature is known without question. When the reaction absorbs or evolves much heat, however, isothermal operation at practical conversion levels is almost impossible. Different parts of the reacting system are at widely different temperatures, and determining average reaction temperature becomes a real problem.

Endothermic reactions, for example, are often carried out commercially in a number of adiabatic reactors in series. A large variation in temperature exists in each reactor. Figure 1 shows a temperature profile typical of such a system. Pilot-plant studies attempt to duplicate the commercial operation and therefore operate with the same type of temperature profile. In smaller scale reactors it is extremely difficult to carry out reactions with large heat effects either adiabatically or isothermally. Small-scale reactors operate with quasiisothermal profiles such as the profile shown in Figure 2. In this example temperature drops rapidly in the inlet end of the bed because the reaction absorbs heat faster than it can be supplied through the reactor walls. This situation is reversed as the reaction slows down, and temperature rises in the exit end of the bed. Changes in feed composition, reaction conditions, size and location of reactor heaters, and dilution of the catalyst bed with inert material obviously make a wide variety of temperature profiles possible.

Researchers are thus confronted with the problem of comparing experiments performed in reactors that have widely different temperature profiles. Direct comparison is possible only if each temperature profile can be expressed by a single equivalent temperature —the equivalent isothermal temperature. This important concept of equivalent temperature has been recognized but rarely used. Previous authors (*1, 2*) developed algebraic solutions for the equivalent temperature for cases in which temperature can be related algebraically to reaction time or to distance through the catalyst bed. However, these solutions are complex. Calculating equivalent temperature for anything more than a handful of experiments is so time consuming that the concept has been little used. This paper presents a simple method for calculating equivalent temperatures that can be readily applied to a large number of experiments.

EQUIVALENT ISOTHERMAL TEMPERATURE

A reaction-rate equation can usually be expressed in the following form:

$$\frac{dn_A}{d\theta} = k\,\phi\,(p_A, p_B, \ldots) \qquad (1)$$

where the effect of temperature on reaction rate is contained in the rate constant k. Conversion is obtained by integrating Equation (1):

$$\int \frac{dn_A}{\phi\,(p_A, p_B, \ldots)} = \int k d\theta = k_{avg} \int d\theta \qquad (2)$$

For any nonisothermal reactor, Equation (2) shows that the effect of temperature is given by the average rate constant. The equivalent isothermal temperature is the temperature that corresponds to this average rate constant; it is the temperature at which an equivalent isothermal reactor would give the same conversion as the nonisothermal reactor.

To average rate constants the relation between temperature and rate constant must first be determined by a kinetic study. This relation is usually expressed by the Arhennius equation

$$k = Ae^{-\Delta E/RT} \qquad (3)$$

If radial temperature gradients are ignored, the average rate constant in the catalyst bed is

$$k_{avg.} = \int_0^1 k ds \qquad (4)$$

where s is the fractional distance through the bed. Equivalent isothermal temperature is obtained by substituting k_{avg} into Equation (3). To determine the equivalent temperature for the profile shown in Figure 2, for example, the profile is replotted in terms of rate constant and fractional bed length, as shown in Figure 3. The average rate constant is obtained by integration and is equal to the area under the curve. Equivalent temperature is obtained from the average rate constant and Equation (3).

Equivalent temperatures have seldom been used because of the labor and time involved in this integration. In its place a simple arithmetic average temperature, or some other arbitrary temperature —such as that of the inlet, outlet, or an intermediate point in the bed or reactor wall—is often used. Such temperatures are usually poor substitutes for the true equivalent temperature. They lead to inconsistent correlations, particularly when changes in conversion, space velocity, pressure, feed stock, etc., cause changes in the temperature profile.

SIMPLIFIED INTEGRATION METHOD

Integrating rate-constant profiles is greatly simplified by a technique devised by Gauss (*3*). The method integrates exactly a polynomial of degree $2n$-1 from n predetermined ordinates in the interval of integration. To apply the method to averaging reaction-rate constants, it is necessary only to determine how high the degree of the polynomial must be to describe with fair accuracy the relation between rate constant and bed length. For temperature profiles of the type shown in Figure 2, a seventh-degree polynomial is adequate, and a four-point integration applies:

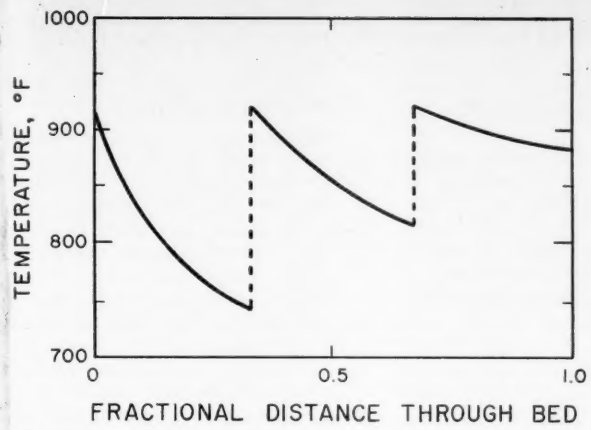

Fig. 1. Temperature profile in a multireactor system.

$$k_{avg} = 0.174\,k_{0.07L} + 0.326\,k_{0.33L} + 0.326\,k_{0.67L} + 0.174\,k_{0.93L} \qquad (5)$$

where $k_{0.07L}$ is the value of k at a point 7% of the distance through the bed, etc.

The constants of the polynomial need not be evaluated; it is necessary only to ensure that the degree is high enough to represent adequately the relation between k and position in the bed. This requirement is easily checked by progressively increasing the number of points used in the method until the result agrees with a careful graphical integration.

Calculation of equivalent isothermal temperature by this simple procedure is illustrated by an example from the Ultraforming process. The average activation energy for the predominant reactions has been established in kinetic studies as 96,000 B.t.u./mole. This value fixes the relation between temperature and reaction-rate constant. To calculate the equivalent isothermal temperature for the temperature profile shown in Figure 2, the k's are determined at the four points required by Equation (5). Substituting these k's into Equation (5) gives an equivalent isothermal temperature of 915°F., which agrees exactly with a careful graphical integration. A two- and a three-point integration of this profile would have given temperatures of 920° and 917°F. respectively. If the four-point integration had not agreed with the graphical integration, one could either use more points or divide the catalyst bed into two sections and apply Gauss's method to each section.

When a large number of equivalent temperatures are to be calculated, the procedure can be simplified even further by a nomographic solution of Equation (5). The nomograph is graduated directly in temperature rather than k. With such a nomograph, equivalent isothermal temperature can be calculated on a routine basis in about a minute.

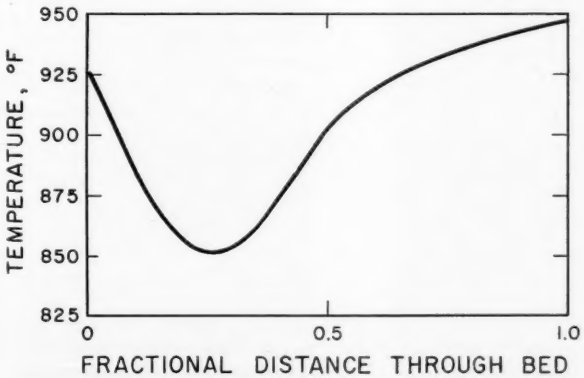

Fig. 2. Temperature profile in a quasiisothermal reactor.

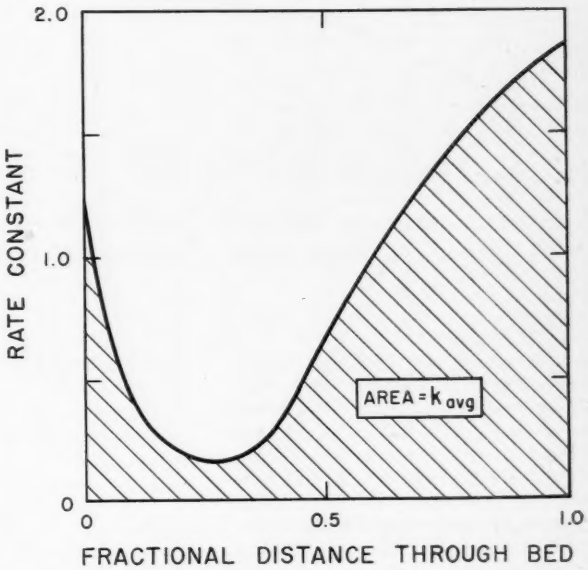

Fig. 3. Rate constant profile in a quasiisothermal reactor.

APPLICATION TO COMPLEX SYSTEMS

In systems involving simultaneous reactions an exact definition of equivalent isothermal temperature is not generally possible because the individual reactions have different activation energies. For these systems equivalent temperature is an approximation of the

influence of temperature on the several reactions. The degree to which equivalent temperature measures the temperature effect depends on the number of major reactions, and the difference between their activation energies. By suitable choice of ΔE, the equivalent temperature can be made to approximate quite closely the over-all temperature effect.

Although the number of simultaneous reactions involved in a given system may be large, it will almost always be true that only one or two control conversion, yield, or product quality. This is particularly true if conversion is high. By using the average ΔE of the controlling reactions, the equivalent temperature becomes a close measure of the over-all temperature effect.

If different reactions control in different operating ranges, one should use the appropriate ΔE in each range. Equivalent temperature is not sensitive to ΔE, however, and unless the controlling reactions have widely different ΔE's use of a single value over the whole range is justified. Figure 4 shows the small change for the profile shown in Figure 2 as ΔE varies from 30,000 to 120,000 B.t.u./mole. Between 60,000 and 120,000 B.t.u./mole, equivalent temperature changed only 0.7°F. 10,000 B.t.u./mole change in ΔE. The solution for equivalent temperature involves raising $e^{-1/RT}$ for each increment of the bed to the ΔE power and taking the ΔE root of the sum. Raising the individuals to the ΔE power and extracting the same power from the sum causes equivalent temperature to be insensitive to ΔE. Hence, even in the absence of accurate kinetic data, reliable equivalent temperatures can still be calculated from approximate values of ΔE.

The only problem radial gradients introduce is determining k at the points along the axis of the reactor required by Equation (5). For a cylindrical reactor of radius R in which the radial gradient is symmetrical, k_{avg} for an element of catalyst perpendicular to the axis of the reactor is

$$k_{avg} = \frac{\int k dV}{\int dV} = 2 \int_0^1 k\left(\frac{r}{R}\right) d\left(\frac{r}{R}\right) \qquad (6)$$

where r is the distance along the radius. Gauss's method may also be used for this integration. The value of the group kr/R is needed at n points along the radius. Again, the number of points needed depends on the complexity of the radial gradient. Values of k_{avg} are determined for the positions in the bed required by Equation (5). The average rate constant for the entire bed is then calculated as before.

When a reaction is carried out in a series of catalyst beds, discontinuities in the temperature profile occur and the relation between rate constant and position in the bed cannot be represented by a single polynomial. The three-bed profile of Figure 1 is an example. In this case an average k must be computed for each bed. Equivalent temperature corresponds to an average of the k's for the individual beds, weighted according to the amount of catalyst in each bed.

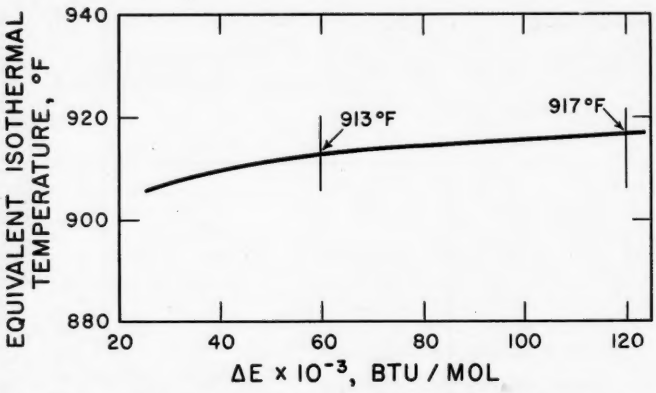

Fig. 4. Effect of activation energy on equivalent isothermal temperature.

TEST OF THE METHOD

Different reactors give the same product when they are operated under the same reaction conditions. If reactors having different temperature profiles are made to yield the same product under otherwise identical conditions, then their equivalent isothermal temperatures must be equal. This fact serves as a test of the method. Ultraforming reactors with temperature profiles shown in Figures 1 and 2 have been operated with aliquots of the same catalyst to give identical products. The equivalent isothermal temperatures calculated for two such tests are

	Adiabatic multibed	Quasi-isothermal one bed
Test A	912°F.	911°F.
Test B	912°F.	908°F.

The good agreement between the calculated temperatures shows that equivalent isothermal temperature is a valid measure for comparing catalyst beds having widely different temperature profiles. Furthermore, because the Ultraforming process involves a number of simultaneous reactions, these tests also demonstrate that the concept of equivalent temperature can be useful in complex reaction systems.

NOTATION

A = constant
ΔE = activation energy
L = length of catalyst bed
R = gas law constant, radius of catalyst bed
T = absolute temperature
V = volume
k = reaction-rate constant
n_A = moles of component A
r = distance along radius from axis of reactor
s = fractional distance through catalyst bed
θ = reaction time
$\phi(p_A, p_B \ldots)$ = function of partial pressures of components A, B, ..

LITERATURE CITED

1. Otake, T., E. Kunugida, and H. Kobayashi, *Chem. Eng.* (*Japan*), 18, 413 (1954).
2. Sherman, J., *Ind. Eng. Chem.*, 28, 1026 (1936).
3. Sherwood, T. K., and C. E. Reed, "Applied Mathematics in Chemical Engineering," p. 272, New York, McGraw-Hill Book Company, Inc., New York (1939).

(Presented at A.I.Ch.E. New York meeting)

Dynamics of Vapor Bubbles and Boiling Heat Transfer

H. K. Forster and N. Zuber, University of California, Los Angeles

Analytical expressions for bubble radii and growth rates derived by the authors are applied in an analysis of surface boiling at high heat transfer rates. It is shown that the product of bubble radius and radial velocity is a constant, independent of the bubble radius. This circumstance permits the formulation of a Reynolds number for the flow in the thin superheated liquid layer adjacent to the heating surface. The result of the analysis is then applied to maximal heat transfer rates in pool boiling.

Modern technological developments in the fields of rocket engines and nuclear reactors, with their high heat transfer rates, have created renewed interest in the field of boiling heat transfer.

Most investigations are concerned with experiments on heat transfer rates and burnout conditions for pool boiling, forced convection with various degrees of subcooling, and natural-circulation evaporation.

It is generally agreed that the high heat transfer rates encountered with nucleate boiling are not a consequence of the latent heat transport but are due to the turbulence in the superheated liquid boundary created by bubble dynamics. In order to obtain a quantitative understanding of nucleate boiling, it is therefore necessary to take into account the mechanism of bubble formation and growth.

The authors have developed a theory for the growth of a vapor bubble in a superheated liquid (*1*) which is in good agreement with experimental data (*2*). The analysis has also been extended to volume boiling (*3*). In the present paper the results of the analysis are used in a quantitative formulation of the microconvection in surface boiling. To facilitate the presentation, experimental results of nucleate boiling are discussed and the theory of bubble growth is briefly reviewed.

NUCLEATE BOILING

Developments in nuclear reactors and rocket engines, where exceedingly high heat quantities are generated in comparatively small volumes, focused attention on nucleate boiling as a mode of transferring heat at high rates at an almost constant temperature of the heat transfer surface.

Jakob (*4*) proposed that this increase in heat transfer in nucleate boiling was due to agitation of the liquid near the wall caused by detaching bubbles. From a photographic study of nucleate boiling in subcooled water Gunther and Kreith (*5, 6*) showed the existence of a highly superheated (53°F.) film (0.005 in. in thickness) next to the heating surface. The high thermal resistance of this film is removed by the growth and collapse of vapor bubbles. Radial velocities of 8 to 15 ft./sec. were reported, indicating the importance of bubble agitation. From photographic bubble counts Gunther and Kreith quantitatively showed (*6*) that neither the latent heat transport by the growing bubbles nor a mechanism of simultaneous evaporation at the equatorial region and condensation at the bubble cap can account for the measured heat transfer rates. When they inserted the measured radial velocity and film thickness in the Sieder-Tate convective heat transfer equation, agreement with the experimental heat flux was obtained. The small contribution of the latent heat transport was also confirmed by Rohsenow and Clark (*7*).

In his studies on the mechanism of boiling heat transfer, Ellion (*8*) measured bubble radii and radial velocities in subcooled water and in carbon tetrachloride at atmospheric pressure. He used these measured values as the characteristic velocity and length in the Reynolds and Nusselt numbers and obtained good agreement with experimental heat fluxes. He also observed in his photographic studies that bubbles were ejected from the lower side of a horizontal heating strip—a motion which cannot be attributed to buoyant forces. At higher superheats the diameter of a bubble at departure is therefore governed by a different mechanism, which indicates the importance of the radial velocity of a bubble while it is still attached to the heating strip.

Corty and Foust (*9*) made photographic studies of nucleate boiling and demonstrated the importance of the size and distribution of the microroughness in determining the liquid superheat and boiling heat flux. A small increase of superheat in the nucleate region activates a very large number of nucleating centers, reflecting the extreme sensitivity of heat flux to nucleation. They also showed experimentally that the dimensions of the active surface cavities are closely represented by the critical radii as given by Gibbs's equation.

These experimental findings indicate that the large heat transfer rates associated with nucleate boiling are a consequence of the microconvection in the superheated sublayer. In order to arrive at a quantitative understanding of the process the dynamics of the vapor bubbles must be taken into account in formulating the analysis.

BUBBLE DYNAMICS

The first important work in bubble dynamics was done by Lord Rayleigh (*10*), who formulated it as a problem of the dynamics of an incompressible, inviscid fluid, obtaining the equation that now bears his name:

$$R\ddot{R} + \frac{3}{2}\dot{R}^2 + \frac{2\sigma}{\rho_L R} = \frac{P_v - P_\infty}{\rho_L} \qquad (1)$$

As discussed by Frenkel (*11*), one condition for the breakdown of the liquid (boiling), is the existence of an embryonic bubble with critical radius defined by

$$R_o = \frac{2\sigma}{P_v - P_\infty} \qquad (2)$$

The temperature at which the process of boiling can start must be higher than the saturation temperature T_∞ corresponding to the external pressure P_∞ (pressure on the system). In the case of an embryonic bubble with radius R_o this "starting" temperature T_o must exceed T_∞ by an amount corresponding to the excess value of P_v with respect to P_∞, i.e., by the capillary pressure $2\sigma/R_o$. The temperature of the bubble wall necessarily decreases owing to evaporation at the interface, whereby P_v on the right side of Equation (1) becomes time dependent. The temperature of the vapor within the bubble is practically the same as the temperature of the bubble wall. The determination of the latter temperature involves the solution of a problem of heat conduction in

a moving medium with given motion of the boundaries. The analysis (*12*) furnishes the instantaneous temperature $T_v(t)$ inside the vapor bubble, which at time zero was situated in an infinite liquid of temperature T_o and which then increased in size owing to evaporation, attaining radius $R(z)$ at time z during the interval $0 \leqslant z \leqslant t$

$$T_v(t) - T_o = -\frac{L\rho_v}{C\,\rho_L\sqrt{\pi a}} \int_o^t \frac{R(z)\,\dot{R}(z)}{R(t)\sqrt{t-z}}\,dz \qquad (3)$$

It was pointed out by Forster (*13*) that a rather general class of problems of heat transfer in moving media with given motion of the boundaries may be solved by an extension of the foregoing method.

Combining Equations (1) and (3) and the Clausius-Clapeyron equation yields the integrodifferential equation which describes the growth of a spherical bubble in a superheated liquid:

$$R\ddot{R} + \frac{3}{2}\dot{R}^2 + \frac{2\sigma}{\rho_L R} = \frac{L}{\rho_L T(V_v - V_L)}\left[T_o - T_\infty - \frac{L\rho_v}{C\,\rho_L\sqrt{\pi a}} \int_o^t \frac{R(z)\,\dot{R}(z)}{R(t)\sqrt{t-z}}\,dz\right] \qquad (4)$$

Based on mathematical arguments, the inertia of the liquid, represented by the terms $(R\ddot{R} + 3/2\,\dot{R}^2)$, was shown to be of minor importance in determining bubble growth. Were this not the case, the complexity of the solution of Equation (4) would forbid the application of the results to bubble populations as encountered in boiling. Since this point is important for the present analysis, it is here further considered from the point of view of thermodynamics.

While the bubble of radius R expands by dR, heat energy δQ is taken from the surroundings and $\delta Q > L\rho_v 4\pi R^2 dR$; most of δQ is used to increase the internal energy of the system and to do work against the atmospheric pressure. The mechanical work δW_m done against combined surface tension and liquid inertia is bounded by $\delta W_m \leqslant \Delta P 4\pi R^2 dR$ because the pressure in the bubble is at most ΔP above atmospheric. The ratio $\delta W_m/\delta Q$ therefore remains smaller than $\Delta P/L\rho_v$ and the latter expression is equal to $\Delta T/T$ by Clausius-Clapeyron's equation. Hence, of the energy reaching the bubble, less than the fraction $\Delta T/T$ is at any time available for doing work against surface tension and liquid inertia combined. For boiling liquids this fraction is of the order of a few per cent.

We want to find a bound for the fraction of the energy available for doing work against the liquid inertia alone. During expansion by dR the work done against surface tension δW_s equals $8\pi\sigma R dR$ and with $2\sigma = R_o\Delta P$ this work equals $4\pi R R_o \Delta P dR$; thus $\delta W_s/\delta W_m$ equals R_o/R. The fraction η of δQ, which is available for accelerating the liquid, is therefore bounded by the inequality

$$\eta \leqslant \frac{\Delta T}{T}\left(1 - \frac{R_o}{R}\right) \qquad (5)$$

In the initial stage of growth, while the temperature of the bubble wall is still close to T_o, the radius R is also still close to the initial radius R_o and therefore the factor $(1 - R_o/R)$ in *Equation* (5) is then close to zero. Later, when R has grown sufficiently to make this factor of order unity the other factor $\Delta T/T$, which was small at the start, has further decreased and is approaching zero just as the bubble-wall temperature decreases and approaches T_∞. The fraction of the energy available for accelerating the liquid is thus seen to start at zero, to be always bounded by a theoretical boun a few per cent, and to appr zero again. It may be concl that the liquid inertia is n a controlling factor in the growt a vapor bubble if the growth t es place by evaporation. Statem ts to the contrary which appeare in the literature without proof) are therefore in error.

Considerations similar to t se here presented facilitate the ma hematical analysis to such an ex t that a solution of the proble n closed form can be obtained (*1*)

$$r + \ln\frac{r-1}{r_1-1} = C\sqrt{t}\,;\; r > r_1 \qquad (6)$$

$$t > \frac{r_1^2}{C^2}$$

where

$$r = \frac{R}{R_o},\quad R_o = \frac{2\sigma}{\Delta P} \qquad (7)$$

The bubble-growth coefficient is

$$C = \frac{\Delta T_c\,\rho_L\sqrt{\pi a}}{L\,\rho_v\,R_o} \qquad (8)$$

The radius r_1 is not arbit ry but calculable, and it turns ou to be only 1 or 2% above the cri al radius $(r = 1)$. Bubble radii as predicted by Equation (6) id compared with experiment (*2*) re shown in Figure 1 for illustra on (cf. reference *1*).

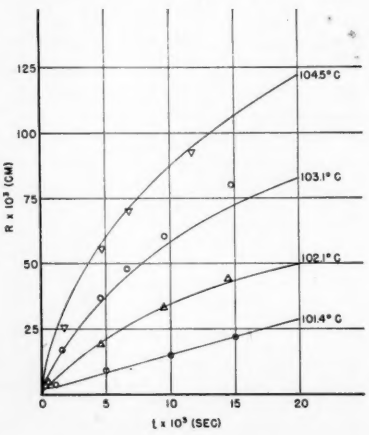

← Fig. 1. Radius-time relation for vapor bubbles growing in superheated water as given by Equation (6). [Circles and triangles show experimental values by Dergarabedian (*2*).]

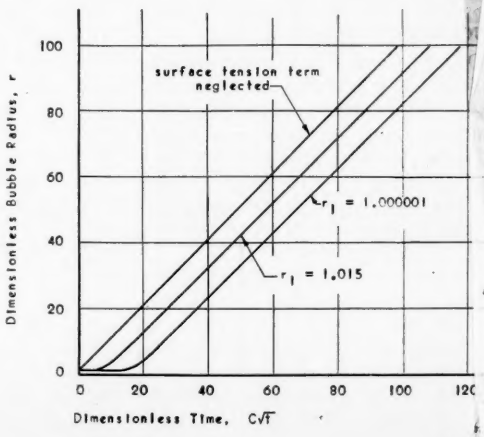

→ Fig. 2. Dimensionless bubble radius as function of dimensionless time, from Equation (6).

The logarithmic term in Equation (6) stems from the surface-tension term in Equation (4). It may be seen from its logarithmic nature that it is most important only while the bubble radius has increased by less than an order of magnitude. Afterward its influence consists mainly in a shift along the time axis, leaving practically unaffected the growth rate of bubbles considerably larger than the critical. This fact is illustrated in Figure 2.

It was shown(*15*) that to the extent that the inertia term is unimportant the bubble-wall temperature T_v is given by

$$T_o - T_v = (T_o - T_\infty)\left(1 - \frac{1}{r}\right) \quad (9)$$

Hence the vapor temperature approaches the saturation temperature T_∞ as soon as r has grown by an order of magnitude.

In the foregoing considerations the relative importance of the various factors influencing bubble growth was evaluated and compared. It was demonstrated that the growth of a vapor bubble in a superheated liquid [Equation (6)] is essentially determined by the single coefficient C given by Equation (8).

The question now arises whether the former analysis can be applied to the nonspherically symmetric bubble next to the heating surface. The following comparison of measured and predicted initial radial velocities of bubbles still attached to the heating surface is therefore significant.

Ellion(*8*) reported a typical initial growth rate of 10 ft./sec. for a bubble-radius increase from 0.001 to 0.010 in. in degassed, subcooled water at a temperature of 135°F. and 74% of peak (burnout) flux. The peak flux for this temperature is 3 B.t.u./(sq.in.)(sec.); hence for 2.22 B.t.u./(sq. in.)(sec.) the corresponding excess wall temperature (maximum superheat) is 48°F. (cf. reference 8, Figures 38 and 39).

It was previously shown that the influence of the surface-tension term on the rate of growth is small in the domain here considered. Therefore it follows from Equations (6) and (8) that the radial velocity is given with good approximation by

$$\dot{R} = \frac{\Delta T c \rho_L \sqrt{\pi a}}{L \rho_v} \frac{1}{2\sqrt{t}} \quad (10)$$

If the properties of the liquid at the superheat temperature and those of the vapor at the saturation temperature are evaluated, the coefficient $\Delta T c \rho_L \sqrt{\pi a}/L\rho_v$ for a superheat of 48°F. is 4.54 cm./$\sqrt{}$sec.; the time period in Ellion's experiment is 75×10^{-6} sec. Equation (10) then predicts a velocity of 11.2 ft./sec., which is to be compared with the measured initial growth rate of 10 ft./sec. The predicted velocity could have been expected to be larger than the average experimentally measured velocity, since the computation was based on the maximum superheat. The bubble actually grows through a film region where a high-temperature gradient exists, and so in reality it experiences a somewhat lower mean superheat. With a mean superheat of, say, 38°F. the predicted initial growth rate would be 8.75 ft./sec. Similar agreement is obtained with experimental data reported in references 5 and 6. It may thus be seen that the theory compares favorably with experiment.

It should be noted that the coefficient $\Delta T c \rho_L \sqrt{\pi a}/L\rho_v$ decreases rapidly with an increase in pressure; thus the agitation from one nucleating center is greatly reduced at elevated pressure. Similarly, if the Laplace constant $[2\sigma/g(\rho_L - \rho_v)]^{\frac{1}{2}}$ be a measure of the agitation introduced by a departing bubble from *one* nucleating center, its agitation effect per unit time would again decrease with pressure because the Laplace constant changes by less than an order of magnitude and the growth rate decreases in the same pressure range by several orders of magnitude. Both facts indicate that the higher heat flux at higher pressures must be due to an increase in the number of nucleating centers as pressure is increased.

One may see the physical reason for this increase in the number of nucleating centers with an increase in pressure by considering how (for a given roughness distribution and temperature difference) the nucleation propensity depends on the surface tension (which decreases) and the slope of the vapor pressure-temperature curve (which increases).

MICROCONVECTION AND BOILING HEAT TRANSFER

Application of the theory of similarity to the differential equations of heat transfer and fluid flow(*16, 17*) yields the result that for the heat transfer from a solid boundary to a fluid, in similar systems, a relation

$$Nu = \phi\,(Re, Pr) \quad (11)$$

will exist. The function ϕ may be formulated from experimental data, and for purposes of design, an empirical expression of the form

$$Nu = \alpha\, Re^m Pr^n \quad (12)$$

is usually employed.

It is surmised that an expression of the form of Equation 12 will describe the process of heat transfer in boiling; the problem is to formulate the Reynolds and Nusselt numbers in terms of those parameters which are most descriptive of the essential features of the physical system.

For the Reynolds number a characteristic length and velocity must be found. Various authors (*18, 19*) chose for their characteristic length the diameter of the bubble at departure from the heating surface, which is specified by the Laplace constant and the contact angle; this diameter multiplied by the frequency of bubbles leaving the surface was used as a characteristic velocity. The physical significance of the length thereby obtained consists in its relation to the largest size of bubble for which buoyant and adhesive forces are still in equilibrium. Although the equilibrium of these static forces is certainly physically significant at low superheats and low levels of agitation, it must be expected that for high superheat and high levels of agitation the dynamic forces due to fluid motion will be more important. In this connection recent studies by Yamagata (*20, 21*) and coworkers are of interest because they show the mutual interaction of bubbles at high heat fluxes. The characteristic velocity, arrived at as mentioned above, is of the order of 1,000 ft./hr. while the experimental and analytical evidence, as discussed previously, gives radial velocities of the order of 36,000 ft./hr.

Inasmuch as the state of liquid motion is most important in the thin layer of fluid adjacent to the heating surface, where also most of the temperature drop occurs, it is plausible that the bubble radii and radial velocities should furnish the characteristic length and velocity for the Reynolds number of the flow system. As mentioned be-

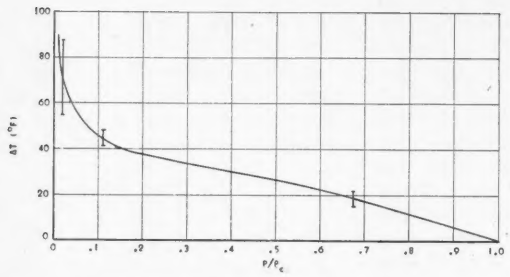

Fig. 3 Empirical correlation of maximum temperature difference (superheat) at peak flux in pool boiling by Cichelli and Bonilla(*22*).

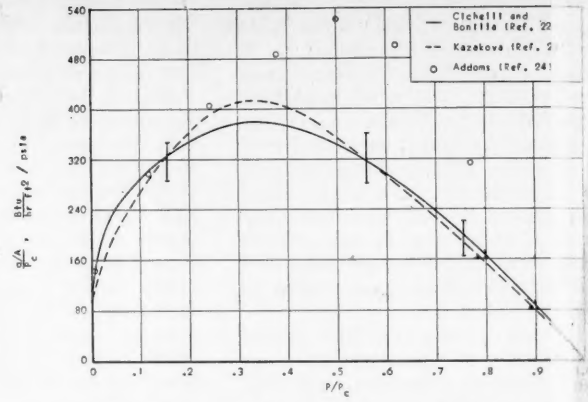

Fig. 4 Empirical correlation of maximum heat flux in p[ool] boiling by Cichelli and Bonilla(*22*).

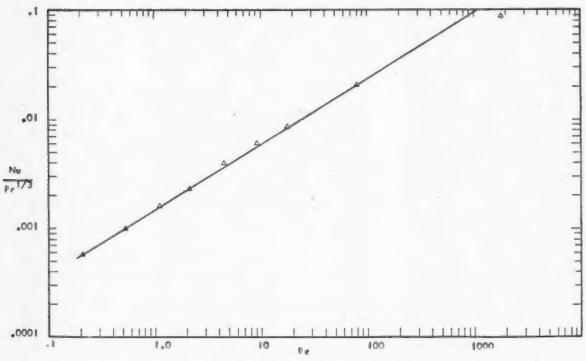

Fig. 5. Correlation of data for ethanol at maximum heat flux and temperature in pool boiling, from Equation (17).

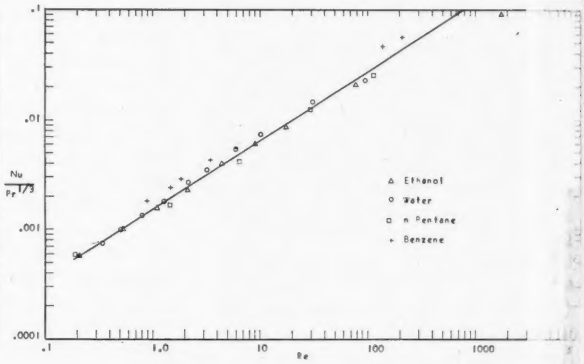

Fig. 6. Correlation of data for various liquids a[t] maximum heat flux and temperature in pool boiling from Equation (17).

fore, Ellion(*8*) in his Ph.D thesis with Professor Sabersky used such bubble radii and radial velocities, which he had to obtain from averages over many bubbles photographically observed in boiling water and carbon tetracloride at atmospheric pressure. The present theory gives mathematical expressions for the bubble radii and, significantly, the question of which bubble radius and which velocity should be chosen does not arise: As follows from the analysis given previously, the product

$$2R\dot{R} = \left[\frac{\Delta T\, c\, \rho_L \sqrt{\pi a}}{L\rho_v}\right]^2 \quad (13)$$

is constant for a given superheat and pressure and is a function of the thermodynamic properties of the liquid and vapor only. Physically, the relation expressed by Equation (13) means that small bubbles grow faster and large bubbles grow slower in such a way that their contribution to the agitation of the fluid remains constant. The Reynolds number for the flow system (the superheated sublayer) is then

$$Re = \frac{\rho_L}{\mu}\left(\frac{\Delta T\, c\, \rho_L \sqrt{\pi a}}{L\rho_v}\right)^2 \quad (14)$$

The Nusselt number for the system is

$$Nu = \frac{q/a\, R}{(T_w - T_L)\, k} \quad (15)$$

where the length R is obtained from considerations of bubble dynamics and is given by

$$R = \frac{\Delta T\, c\, \rho_L \sqrt{\pi a}}{L\rho_v}\sqrt{\frac{2\sigma}{\Delta P}}\sqrt[4]{\frac{\rho_L}{\Delta P}} \quad (16)$$

The time constant represented by the roots in Equation (16) is not the only one that may be significant; other possibilities are at present under consideration.

Equations (12), (14), and (15) then yield a relation between the heat flux and the superheat in terms of the thermodynamic properties of the vapor and the liquid:

$$\frac{q/a}{(T_w - T_L)\, k}\left(\frac{\Delta T\, c\, \rho_L \sqrt{\pi a}}{L\rho_v}\sqrt{\frac{2\sigma}{\Delta P}}\sqrt[4]{\frac{\rho_L}{\Delta P}}\right) = \alpha\left[\frac{\rho_L}{\mu}\left(\frac{\Delta T c\, \rho_L \sqrt{\pi a}}{L\rho_v}\right)^2\right]^m \left[\frac{\mu c}{k}\right]^n \quad (17)$$

If the considerations which led to the formulation of Equation (12) are still valid for the process here considered, the exponent for the Reynolds number should be in the range $0.5 < m < 0.8$ and the exponent for the Prandtl number should be around 1/3.

COMPARISON WITH EXPERIMENTS

Many experiments on heat transfer in pool boiling are reported in the literature. Conditions of maximum heat flux (i.e., burnout conditions) are of great interest to the designer. Cichelli and Bonilla (*22*) have shown that the experimentally determined superheats of

various organic liquids at burnout can be represented by a single curve giving the burnout superheat as a function of the reduced pressure (cf. Figure 3). They also showed that the burnout heat fluxes may similarly be correlated as a function of the reduced pressure (cf. Figure 4).

The validity of the theoretical considerations presented in the previous section can now be tested by investigating whether or not one equation [Equation (17)] with superheats inserted from Figure 3 yields heat-flux values in agreement with Figure 4.

Such calculations were first carried out for one liquid: ethanol. Superheats and corresponding heat fluxes were taken from the curves in Figures 3 and 4. Figure 5 shows the relation between the Nusselt, Reynolds, and Prandtl numbers as given by Equation (17) for a pressure range of 0.015 P_{crit} to 0.8 P_{crit}, that is, from 14.7 to 743 lb./sq.in.abs.* The linearity of the relationship indicates the constancy of the exponent m for which the value of 0.61 is found. A few words may be said about the point corresponding to atmospheric pressure, which deviates from the straight line. The superheat plotted in Figure 3 represents the difference between wall and saturation temperatures, i.e., the maximum superheat in the fluid. The bubble spends most of its time in surroundings below the maximum temperature, and, inasmuch as in the low-pressure region high superheats occur, errors in superheat values are most important in this region. A reduction of superheat by 10% would bring the point in question down to the straight line.

The results of the analysis as applied to n-penthane, benzene, ethanol, and water are presented in Figure 6. It may be seen that the various liquids follow closely the same relationship, given by

$$Nu = 0.0015\, Re^{0.62}\, Pr^{0.33} \quad (18)$$

where the dimensionless groups are given by Equation (17). Since Equation (17) is very sensitive to the superheat used, the foregoing correlation is in additional support of the analysis.

In the literature two sets of experimental data for water at burnout conditions at high pressure are reported, one by Kazakova (*23*) and one by Addoms, as reported by McAdams (*24*); both are shown in Figure 3. Kazakova's data are seen to follow closely the curve given by Cichelli and Bonilla. Kazakova also points out that the effects of rapid heat corrosion and salt deposition in increasing burnout heat transfer values become very pronounced at pressures above 64 atm. (0.3 P_{crit}). It is seen that the data reported by Addoms start to deviate from the data of Cichelli and Bonilla and those of Kazakova in just that pressure range. Inasmuch as the experimental conditions under which Addoms's data were obtained are not published, Kazakova's data for the pressure range 0.1 P_{crit} to 0.8 P_{crit} were used in the calculations for water represented on Figure 6.

The thermodynamic properties of liquids and vapors used in this paper were taken from the International Critical Tables and reference *22*. Liquid properties were evaluated at superheat temperatures; those of the vapor were taken at saturation temperature.

The considerations here presented, which compare favorably with experimental results, should prove helpful in the analysis of boiling of subcooled liquids. The bubble-growth coefficient, the importance of which in pool boiling was here demonstrated, should be equally significant for other conditions of boiling.

*In the graphs low Reynolds numbers correspond to high pressures.

ACKNOWLEDGMENT

This paper was presented at the 1955 Conference on Nuclear Engineering at the University of California, Los Angeles, California, April 27 to 29, 1955.

NOTATION

a = thermal diffusivity
$c_p = c$ = specific heat at constant pressure
g = acceleration due to gravity
k = thermal conductivity
L = latent heat of vaporization
P = pressure
$\Delta P = P_o - P_\infty$ = vapor - pressure difference corresponding to the superheat temperature
$r = R/R_o$ = dimensionless bubble radius
R = bubble radius
$R_o = 2\sigma/\Delta P$ = radius of critical bubble
t = time
T_w = temperature of the heating surface
T_o = temperature of the liquid
T_∞ = saturation temperature corresponding to pressure on system P_∞
$\Delta T = T_o - T_\infty$ = superheat temperature
v = specific volume
ρ = mass density
σ = surface tension
μ = viscosity

Subscripts

L = liquid
v = vapor

LITERATURE CITED

1. Forster, H. K., and N. Zuber, *J. Appl. Phys.*, 25, 474, 1954.
2. Dergarabedian, P., *J. Appl. Mech.*, 75, 537 (1953).
3. Lipkis, R. P., C. Liu, and N. Zuber, paper presented at A.I.Ch.E. and A.S.M.E. Heat Transfer Symposium, A.I.Ch.E. National Meeting, Louisville (1955).
4. M. Jakob, "Heat Transfer," p. 642, John Wiley and Sons, New York (1949).
5. Gunther, F. C., and F. Kreith, *Heat Transfer and Fluid Mechanics Institute*, Berkeley, Calif. (1949).
6. ———, *Progr. Rept.* 4-120, Jet Prop. Lab., Calif. Inst. Technol. (March, 1950).
7. Rohsenow, W. M., and J. A. Clark, *Trans. Am. Soc. Mech. Engrs.*, 73, 609 (1951).
8. Ellion, M. E., Ph.D. thesis, California Inst. Technol. (1953; see also Memo. 20-88, Jet Prop. Lab., Calif. Inst. Technol. (March, 1954).
9. Corty, C., and A. S. Foust, *Chem. Eng. Progr. Symposium Series* No. 51, (1955).
10. Rayleigh, Lord, *Phil. Mag.*, 34, 94 (1917).
11. Frenkel, J., "Kinetic Theory of Liquids," p. 366, Oxford Univ. Press (1946).
12. Forster, H. K., *J. Appl. Phys.*, 25, 1067 (1954).
13. ———, *Phys. Rev.*, 99, 660 (1955).
14. Plesset, M. S., and S. A. Zwick, *J. Appl. Phys.*, 25, 493 (1954).
15. Zuber, N., M.Sc. thesis, Univ. Calif., Los Angeles (1954).
16. Von Karman, T., *Trans. Am. Soc. Mech. Engrs.*, 61, 705 (1939).
17. Boelter, L. M. K., R. C. Martinelli, and F. Jonassen, *loc. cit.*, 63, 447 (1941).
18. Jakob, M., *op. cit.*, p. 642.
19. Rohsenow, W., *Trans. Am. Soc. Mech. Engrs.*, 74, 969 (1952).
20. Yamagata, K., F. Hirano, K. Nishikawa, and H. Matsuoka, *Japan Sci. Rev.*, 14, No. 4 (1952).
21. Yamagata, K., F. Hirano, K. Nishikawa and H. Matsuoka, Mem. Fac. Eng., Kyushu Univ., 15, No. 1 (1955).
22. Cichelli, M. T., and C. F. Bonilla, *Trans. Am. Inst. Chem. Engrs.*, 41, 755 (1945).
23. Kazakova, E. A., *The Engineer's Digest*, 12, No. 3, p. 81 (1951).
24. McAdams, W. H., "Heat Transmission," p. 382, McGraw-Hill Book Company, Inc., New York (1954).

Plant Performance of a 13-ft.-diameter Extractive-distillation Column

J. A. Gerster and Tokuro Mizushina
University of Delaware, Newark, Delaware

T. N. Marks and A. W. Catanach
Neches Butane Products Company, Port Neches, Texas

Plant performance data are presented for a 13-ft.-diam., 100-tray furfural extractive-distillation column separating iso- and *n*-butane from 1- and 2-butene. In addition to composition, temperature, pressure, and flow rate of the external streams, values are presented for vapor and liquid compositions and flow rates at a number of different locations within the tower. With the exception of the vapor compositions, which were determined experimentally, the internal conditions were determined by heat and material balances. These data permitted calculation of plate efficiency over various small sections of the column. In the 50-tray rectifying section, plate efficiency for the isobutane—1-butene separation was constant at 20%, and in the stripping section the plate efficiency varied from 25 to 45%. The average for the entire column was 25%.

The furfural-column plate efficiencies compare favorably with those predicted from laboratory tests made before the construction of the column to evaluate the performance of the tray design to be employed. The laboratory plate efficiencies were obtained for the desorption of oxygen from oxygen-rich water with air at the same conditions of volumetric gas and liquid rates to be encountered in the furfural column. When these values were suitably corrected for physical property differences between the two systems, the point efficiencies predicted from the laboratory data for the furfural column ranged from 35% near the top of the column to 25% near the bottom of the column, the average value being 29%.

Operating data have recently been obtained for a newly completed furfural extractive-distillation column at the Neches Company's butadiene plant(*15*). The tray design for this column was essentially the same as that recommended by the University of Delaware for the conditions of high loading and low gas throughput encountered in such columns. The Delaware recommendations were based on laboratory efficiency measurements for the desorption of oxygen from oxygen-rich water with air on a tray of this design (*4*). The purpose of this report is to compute the plate efficiency of the plant column from the operating data and to compare the result with the plate efficiency anticipated from the laboratory measurements.

NECHES TRAY DESIGN

The new Neches column trays were designed to give as good a vapor distribution as possible in spite of the conditions of high liquid loading and low vapor throughput found in furfural extractive columns. Tunnel caps placed parallel to the direction of liquid flow were shown to be superior to any other type of bubble cap for minimizing hydraulic gradient, and these caps were employed in the final design. Hydraulic gradients were further minimized by utilizing comparatively short lengths of liquid travel. In the 13-ft.-diam. tower required by Neches, a double split-flow system was used; that is, the liquid was split into four separate streams flowing across each tray. With this scheme the distance between inlet and outlet weirs for any one liquid stream was 20¼ in.

The caps themselves were 4 in. high 2½ in. wide, and 20 in. long, with 1-in.-high slots on ½-in. spacing. The slots were 5/16 in. wide at the bottom and 5/32 in. at the top. The outlet-weir height employed with these caps was 2½ in. To ensure as high an efficiency as possible with the extractive system where the mass transfer rate within the liquid phase is controlling, the liquid residence time on the tray was increased by use of a wide spacing between adjacent tunnel caps. The distance between adjacent cap faces was 4 in. The laboratory tests showed that even with this rather wide spacing, all the liquid was well contacted by the gas and the efficiency did not suffer. Complete results of the laboratory tests for this tray design have already been reported(*4*).

NECHES-COLUMN OPERATING DATA

The operating data taken in the plant are summarized in Tables 1 and 2. The column consists of two 50-tray units operated in series. The feed, mainly butanes and butenes, enters as a vapor below the fiftieth tray. The furfural-water extractive solvent enters onto the fifth tray from the top of the column and, being essentially nonvolatile, is removed from the bottom of the column along with the butenes. The solvent is recovered from the bottoms in a separate stripper column.

Table 1 shows the flow rate, temperature, and pressure of the various streams entering and leaving the tower. The large quantity of solvent required for this column is evident from this table.

Table 2 shows the composition of the various streams entering and leaving the tower. The main separation is between isobutane and 1-butene. The water content of the furfural is seen to be appreciable on a molar basis. Table 2 also summarizes the component and over-all material balances for the tower. Except for the components present in small amounts, the agreement between input and output is good and indicates that the plant data are accurate. For the purpose of making over-all enthalpy balances, the flow rates were slightly adjusted to give perfect material balance.

In the over-all enthalpy balance made for the column the enthalpies of the various streams were computed from the plant data given in Tables 1 and 2 and from enthalpy data for the C_4 hydrocarbon-furfural-water system(*11*). These enthalpies include the rather appreciable-heat-of-solution values for C_4 hydrocarbon in furfural-water(*16*). When enthalpies were based upon the pure liquid at 32°F. and 1-atm. total pressure and expressed in the units of British thermal units $\times 10^{-6}$/.24-hr. day, it was found that the heat added by the reboiler was 2,583; the enthalpy of the solvent feed stream was 1,082; the enthalpy of the hydrocarbon feed stream was 287; and the enthalpy of the hydrocarbon reflux stream to the tower was 44. The sum of the input enthalpy quantities was 4,196. The output enthalpy quantities consisted of 3,783, which was the enthalpy of the bottoms product to the stripper, and 364, which was the enthalpy of the overhead vapor stream to the condenser, giving a total of 4,147. These figures show good agreement between input and output enthalpy quantities, again confirming the validity of the plant operating data. The computed enthalpies were adjusted slightly to obtain perfect balance, and these self-consistent values

Tokuro Mizushina is at present at Kyoto University, Kyoto, Japan.

TABLE 1.—OPERATING CONDITIONS FOR FURFURAL EXTRACTIVE TOWER AND SOLVENT STRIPPER

Process stream	Total flow rate as metered, lb. moles/24-hr. day	Pressure, lb./sq. in. gauge	Temperature, °F.
C_4 Hydrocarbon feed (Fed as vapor below tray 50)	24,300	...	166
C_4 Hydrocarbon overhead product	13,950	86	112*
C_4 hydrocarbon reflux to tower	20,820	86	98
Solvent feed (fifth tray down from top)	411,500	...	130.5
Liquid transfer from bottom of upper 50-tray column to top of lower 50-tray column	465,000	91	144
Bottoms product to solvent stripper	429,860	98.5	292
Stripper overhead product	10,810	52	105*
Stripper reflux	33,960	52	84
Stripper bottoms product	418,300	58	315

*Condensation temperature.

are used in later calculations of vapor and liquid flow rates within the column.

VARIATION OF CONDITIONS WITHIN THE TOWER

A constant molar flow rate for vapor and liquid within the tower cannot be assumed in the present case and so for the purpose of computing the plate efficiency it is necessary to know the local operating conditions within the extractive column. Local values of vapor composition, temperature, and pressure were obtained in the plant test, and from these data and the known conditions external to the column, it was possible by heat and material-balance calculations to compute the liquid and vapor flow rates and liquid compositions within the tower. A sample calculation for this procedure is given in the Appendix. Results are given in Tables 3, 4, and 5. A check on the accuracy of the calculation may be made by comparing the computed total liquid flow rate at tray 51 with the metered flow rate of the liquid stream pumped from the bottom of the first 50-tray column section to the top of the second 50-tray column section. The two values are seen to agree within 3% in Table 3.

Table 3 also shows that although the liquid flow rates range from about 65 to 85 gal./(min.) (ft. of weir length), the corresponding vapor rates are only from 0.6 to 1.0 ft./sec. The high liquid rates result from the presence of the large quantities of solvent added to the column; the liquid on the trays contains 91 mole % furfural-water near the top of the column and 81 mole % furfural-water at the bottom. The furfural is essentially nonvolatile and the water only slightly so, which gives a vapor consisting mainly of C_4 hydrocarbons. The vapor flow rate is thus quite small compared with the liquid flow rate, which makes it more difficult to obtain good hydraulic characteristics and high plate efficiency for columns of this type. These factors are considered in more detail in a later section.

Table 3 shows that the vapor and liquid flow rates not only are unusual in magnitude but both increase considerably in proceeding from the top to the bottom trays of the tower. The change in liquid flow rate is wholly due to the change in flow of the C_4 hydrocarbons, rather than to any change in flow of solvent, which is essentially nonvolatile and constant in rate. The changes in C_4 hydrocarbons flow rate within the column are due to the highly nonideal nature of the multicomponent solution present. Isobutane and *n*-butane, which concentrate near the top of the column, are more nonideal with respect to furfural-water than the butenes, which concentrate near the bottom of the column; being more nonideal, the butanes have considerably less

TABLE 2.—COMPONENT MATERIAL BALANCES ON INPUT AND OUTPUT STREAMS TO FURFURAL EXTRACTIVE TOWER. ALL QUANTITIES ARE LB. MOLES/24-HR. DAY

	Input as metered			Output as metered				
Component	Hydrocarbon feed (51st tray from top)	Solvent feed (5th tray from top)	Total input to Tower	Overhead product	Stripper overhead product	Stripper bottoms product	Total output of tower	Percentage of deviation of material balance
Isobutane	8,650	0	8,650	9,030	54	0	9,084	−5.0
1-Butene	7,200	0	7,200	209	6,900	0	7,109	+1.3
n-Butane	3,659	0	3,659	2,985	585	0	3,570	+2.4
trans-2-Butene (low-boiling isomer)	2,020	0	2,020	0	1,840	0	1,840	+8.9
cis-2-Butene (high-boiling isomer)	292	0	292	0	562	0	562	−92.4
Isobutylene	656		656	0	541	0	541	+17.5
Butadiene	292	0	292	42	346	0	388	−32.9
Propanes	1,506	0	1,506	1,690	0	0	1,690	−12.2
Total hydrocarbons	24,300	0	24,300	13,950	10,810	0	24,760	−1.9
Furfural	0	283,500	283,500	0	0	284,500	284,500	−0.35
Water	0	128,000	128,000	470*	750*	133,800	135,020	−5.5
Total of all components	24,300	411,500	435,800	14,420	11,560	418,300	444,280	−1.9

*Computed values.

TABLE 3.—LOCAL OPERATING CONDITIONS WITHIN FURFURAL EXTRACTIVE TOWER

	Tray number, from top of tower								
	1	17	33	51*	67	83	95	97	99
Temp., °F.	112	133	136	145	149	153	157	158	163
Pressure, lb./sq. in. guage	86	87.4	89	91	93	95.5	97.5	97.8	98.2
Vapor rate from tray, lb. moles/24-hr. Day†									
Hydrocarbons	34,400	52,370	57,620	52,100	59,310	66,270	73,780	74,690	88,440
Water	470	1,230	1,480	1,600	2,090	2,480	3,070	3,110	4,160
Total	34,870	53,600	59,100	53,700	61,400	68,750	76,850	77,800	92,600
Total vapor rate from tray, ft./sec., based on bubbling area	0.378	0.620	0.678	0.615	0.691	0.764	0.842	0.852	1.020
Liquid rate to tray, lb. moles/24-hr. day†									
Hydrocarbons	20,600	38,570	43,820	62,830	70,040	77,000	84,510	85,420	99,170
Furfural	0	284,000	284,000	284,000	284,000	284,000	284,000	284,000	284,000
Water	0	132,260	132,510	132,630	132,120	133,510	134,100	134,140	135,190
Total	20,600	454,830	460,330	479,460‡	486,160	494,510	502,610	503,560	518,360
Total liq. rate to tray, gal./(min.) (ft. of weir), equal split of liquid flow within tower assumed	10.0	69.4	70.8	75.4	76.8	78.4	80.2	80.5	83.6

*Tray below vapor feed.
†Flow quantities of vapor and liquid were computed by enthalpy balances as described in sample calculations.
‡The metered liquid transfer from the bottom of the upper 50-tray column to the top of the lower 50-tray column was 465,000 lb. moles/24-hr. day (*see* Table 1).

solubility for the solvent than the butenes. Under the conditions of nearly constant temperature and pressure existing in the column, the solubilities are in fact about inversely proportional to the activity coefficients of the C_4 hydrocarbon components. Thus for extractive columns where the added solvent improves the relative volatility of the feed components by affecting a large difference in their activity coefficients, liquid flow rates will always vary considerably within the column. And for the usual case of constant flow rate of streams external to the column, vapor flow rates within either the rectifying or stripping section increase by the same amount as the liquid rates.

CALCULATION OF NECHES-COLUMN PLATE EFFICIENCY

Plate efficiencies were computed over most trays of the column for the key components, isobutane and 1-butene, and in some regions of the column for the *n*-butane–1-butene separation. The calculations were made on a modified McCabe-Thiele diagram. Relative volatility

TABLE 4.—LOCAL COMPOSITION VALUES FOR KEY COMPONENTS WITHIN FURFURAL EXTRACTIVE TOWER

	Liquid composition to tray, mole % Solvent and water-free basis			Vapor composition from tray, mole % Solvent and water-free basis		
Location within tower*	Isobutane	*n*-Butane	1-Butene	Isobutane	*n*-Butane	1-Butene
Distillate†	....	....	....	64.7	21.4	1.5
Tray 10	52.7	31.2	5.8	56.0	28.5	4.6
Tray 17†	46.6	34.7	10.2	51.4	31.2	7.9
Tray 22	44.9	34.9	13.9	50.0	31.4	10.7
Tray 28	41.8	34.2	18.5	47.5	31.0	14.3
Tray 33†	38.5	32.7	22.4	44.7	30.0	17.4
Tray 38	35.1	31.4	26.3	42.0	29.1	20.6
Tray 43	31.6	29.9	30.5	39.0	28.0	24.0
Feed(introduced as vapor between trays 50 and 51)	....	....	....	35.6	15.2	29.6
Tray 51†	27.8	22.5	35.8	33.4	26.0	30.0
Tray 56	23.5	27.4	39.3	28.0	31.7	34.5
Tray 59	18.2	29.4	41.6	21.6	34.0	37.4
Tray 62	12.3	30.9	44.5	14.5	35.7	40.8
Tray 64	9.4	31.4	46.3	11.0	36.3	43.0
Tray 67†	6.1	32.0	49.1	7.1	36.8	46.5
Tray 72	3.1	29.9	53.8	3.5	34.2	52.0
Tray 78	1.6	25.8	59.7	1.8	29.3	59.0
Tray 83†	1.0	21.9	63.7	1.1	24.6	63.7
Tray 95†	0.6	10.6	71.3	0.6	11.3	72.4
Tray 97†	0.5	9.4	73.0	0.5	10.0	74.3
Tray 99†	0.5	8.6	69.5	0.5	9.0	70.2
Bottoms product†	0.5	5.4	63.7			

*Trays are numbered from top of the tower.
†Composition of vapor streams from these trays obtained by sampling; other values obtained from plate number–vapor composition diagram; all liquid compositions computed by material balance, by use of flow rates from Table 3.

TABLE 5.—RELATIVE VOLATILITY VALUES WITHIN FURFURAL EXTRACTIVE TOWER

Tray No. from top of tower	Temperature, °F.	Liquid composition on tray, water-free basis, mole %: Sum of isobutane, *n*-Butane and 1-butene*	Other hydrocarbon components†	Total hydrocarbon concentration	Water concentration in solvent‡: Hydrocarbon-free basis, mole %	Relative volatility values: Isobutane to 1-butene	*n*-Butane to 1-butene
9	136	10.2	1.2	11.4	20.7	2.05	1.53
16	133	10.9	1.0	11.9	19.6	2.07	1.54
32	136	12.5	0.9	13.4	12.8	1.99	1.48
50	145	15.6	2.5	18.1	9.6	1.87	1.40
66	149	17.3	2.5	19.8	12.4	1.84	1.38
82	153	18.4	2.9	21.3	15.2	1.81	1.36
94	157	14.2	8.7	22.9	17.4	1.78	1.34

*For relative distribution of these components, *see* Table 4.
†Consists of mostly propanes above the feed, and 2-butenes, isobutylene, and butadiene below feed.
‡Computed from known solubility relationships for water in hydrocarbon-furfural mixtures.

values for C_4 hydrocarbon-furfural-water mixtures are available from references *8*, *14*, and *17* as a function of temperature and liquid composition. Special procedures were followed in employing these relative volatility data owing to the presence of many nonkey hydrocarbon components within the liquid and because of the existence of a separate water-rich liquid phase on all the trays of the column.

With regard to the latter problem, it is the composition of the solvent-rich liquid phase which determines the relative volatility; whereas the liquid compositions obtained by material and enthalpy balance calculations are those for the total liquid. Fortunately, data of Griswold and associates (*10*) are available for the conjugate liquid-phase compositions of the *n*-butane–furfural–water and 1-butene–furfural–water systems at temperatures and pressures of interest. These data show that when an excess of water is present, the water-rich liquid phase contains some furfural but essentially no C_4 hydrocarbons. Knowledge of the total liquid-phase composition along with the Griswold phase data permitted calculations to be made for the composition of the solvent-rich liquid phase for each tray considered. These values are shown in Table 5.

To obtain the proper values of relative volatility from the solvent-rich phase liquid composition and temperature, use was made of the fact that the total hydrocarbon composition and the water composition are the most important factors affecting relative volatility. The relative amounts of the various hydrocarbons present fortunately does not greatly affect the vapor-liquid equilibrium data. Thus to obtain the relative volatility of isobutane to 1-butene, data for the system isobutane – 1-butene – furfural–water were employed (*14*), with the isobutane concentration being taken as the sum of the actual isobutane concentration plus the concentrations of all other paraffin hydrocarbons (such as *n*-butane) present in the liquid. Similarly the 1-butene concentration was taken as the sum of the actual 1-butene concentration plus the concentrations of all other olefin hydrocarbons. Relative volatility data for the system *n*-butane–1-butene–furfural–water were computed from the data of references *8*, *14*, and *17*, on the same assumption as before as to the effect of other hydrocarbon components. The resulting relative volatility values are given in Table 5.

TABLE 6.—EXPERIMENTAL LOCAL PLATE EFFICIENCIES WITHIN FURFURAL EXTRACTIVE TOWER

Location within tower: Between trays	Experimental Murphree vapor efficiencies, %: Isobutane–1-butene separation	*n*-Butane–1-butene separation
10–17	25	24
17–22	21	22
22–28	20	20
28–33	19	20
33–38	19	20
38–43	21	20
43–51	21	†
51–56	21	†
56–59	33	†
59–62	44	†
62–64	40	†
64–67	40	†
67–72	35	†
72–78	25	27
78–83	*	27
83–95	*	33
95–97	*	30
Average for all trays considered	25	25
Average predicted efficiency (from Table 7)	29	32

*Values inaccurate owing to very low isobutane concentrations.
†Local composition values in doubt in this region.

The modified McCabe-Thiele diagram was drawn up for the isobutane–1-butene separation by expressing values of vapor and liquid composition on a key basis, that is, as (moles of isobutane)/(moles of isobutane + moles of 1-butene). Operating-line compositions were computed from the data of Table 4, and equilibrium compositions from the relative volatility data of Table 5. The graphical stepwise procedure of Baker and Stockhardt (*1*) was used over small tray intervals to obtain the Murphree vapor-plate efficiencies shown tabulated in Table 6. Plate-efficiency values are not reported below tray 78 for the isobutane–1-butene separation owing to the inaccuracies caused by the very small isobutane compositions in this region of the column. Similar McCabe-Thiele procedures were followed for the *n*-butane–1-butene separation. Results were not reported for this pair between trays 43 and 72, as composition values were not too consistent in this region of the column.

The experimental plate-efficiency results shown in Table 6 are consistent in spite of the widely varying conditions of relative volatility and total flow rate within the column. Further, the efficiencies for the two different separations considered are also very nearly the same in spite of large differences in relative volatility between the two. However, to determine whether the magnitude and variation of the experimental efficiencies are reasonable, plate-efficiency prediction calculations have been made by the method of Gerster, Colburn, and associates (*7*) and are presented in the next

section. Discussion of both sets of efficiency results then follows.

PREDICTION OF EFFICIENCY RESULTS FROM OXYGEN-DESORPTION DATA

As mentioned earlier, laboratory plate-efficiency measurements were made for the tray design recommended for use in the Neches extractive column. These measurements were made for a system in which the rate of mass transfer within the liquid phase is controlling: the desorption of oxygen from oxygen-rich water with air at atmospheric pressure and temperature. Plate-efficiency data were obtained under widely varying conditions of gas rate, liquid rate, outlet weir height, and slot spacing. Presentation and correlation of these results have been given elsewhere(4).

The Neches column trays considered in the predication calculations operated with a gas rate which varied from 0.61 to 0.80 ft./sec., with a liquid rate of from 70 to 80 gal./(min.) (ft. of weir), and with a depth of clear liquid on the tray computed by the Francis weir formula to be from 4.0 to 4.2 in. Under these same conditions the Murphree liquid efficiencies for the oxygen system were about 36%. The same variation in gas rate as that encountered in the Neches column caused the oxygen desorption efficiency to change as much as 1.5 efficiency %, increasing with increasing gas rate; the liquid-rate variation caused the efficiency to change as much as 5 efficiency %, increasing with decreasing liquid rate; and the effect of the small change in clear liquid depth upon efficiency was negligible.

As shown in reference 7, it is more fundamental to work with transfer units instead of efficiency values. The number of liquid film transfer units, N_L, is related to fractional efficiency expressed in liquid concentration units, E_L, for the case of no liquid mixing on the tray, as follows:

$$N_L^{cl} = -2.3 \log (1 - E_L) \quad (1)$$

The value of number of transfer units for the C_4 hydrocarbon–furfural-water system, $N_{L_{extractive}}$ may be computed from the number of transfer units for the oxygen-water system $N_{L_{O2\text{-}water}}$ by the following relationship(6):

$$N_{L_{extractive}} = N_{L_{O_2\text{-}water}} \left[\frac{(\mu/\rho D)_{O_2\text{-}water}}{(\mu/\rho D)_{extractive}} \right]^{\frac{1}{2}} \quad (2)$$

In Equation (2), μ is the viscosity of the liquid, ρ is the density of the liquid, and D is the liquid molecular-diffusion coefficient for the diffusing component. The value of $\mu/\rho D$ for the oxygen-water system is 376 dimensionless units(7). For the extractive system, the liquid viscosity is 0.68 centipoise at the top of the column, where the solvent concentration is the greatest, and the corresponding value at the bottom of the column, where the solvent concentration is the least, is 0.47 centipoise(9). The liquid density for the extractive system varies only slightly, from 65.5 lb./cu.ft. at the top of the column to 59.2 lb./cu.ft. at the bottom of the column(9). The diffusivity of C_4 hydrocarbons through the furfural solvent is estimated to vary from 1.75×10^{-5} sq. cm./sec. at the top of the column to 2.59×10^{-5} sq.cm./sec. at the bottom of the column(18). These data permit calculation of the dimensionless Schmidt group ($\mu/\rho D$) for the extractive system as 372 at the top of the column to 191 at the bottom. Variation of the liquid physical properties and the Schmidt group with tray number is shown in detail in Table 7*. Values of N_L for the oxygen-water system may now be converted by Equation (2) to the corresponding values for the extractive system. Results show that the $N_{L_{extractive}}$ values vary from 0.48 at the top of the column to 0.59 at the bottom.

As will be seen later, mass transfer resistance within the gas phase of the extractive system is quite small but not negligible. Prediction of the fractional vapor efficiency E_{OG}, including the mass transfer resistance of both the gas and liquid phases, can be made by use of the following equation(7):

$$\frac{1}{-2.3 \log (1 - E_{OG})} = \frac{1}{N_G} + \frac{mG/L}{N_L} \quad (3)$$

In this expression N_G is the number of gas-phase transfer units for the extractive system, and mG/L is the ratio of the slope of the equilibrium curve to the slope of the operating line in dimensionless units.

A value of $N_G = 2.4$ for the extractive system was used in the prediction calculations. This same value was used by Gerster and coworkers in predicting efficiencies for their C_4 hydrocarbon–furfural pilot plant column and is based upon their experimental air-humidification data(7). The value of N_G obtained for the mass transfer of water vapor through air was converted to a value of N_G for the extractive system by an equation similar to Equation (2) with the $\mu/\rho D$ groups evaluated for the gas phase. The N_G value obtained in this manner agrees closely with that which would be obtained for the extractive system if predicted from some recent University of Delaware data for the absorption of ammonia from air into water on a 2-ft. bubble plate(5). Values of mG/L were taken from the modified McCabe-Thiele diagrams. Results for each term of Equation (3), as well as for the predicted value of E_{OG}, are shown in Table 7 as a function of tray number for both the isobutane–1-butene separation and for the n-butane–1-butene separation.

Inspection of Table 7 shows that values of mG/L and N_L both increase with increasing tray number, and so the term $(mG/L)/N_L$ and thus E_{OG} do not vary widely as a function of position within the column. It is also of interest to note the relative values of $1/N_G$ and $(mG/L)/N_L$ as they represent the relative resistances to mass transfer within the gas and liquid phases respectively. For all cases considered, 80 to 85% of the mass transfer resistance lies within the liquid phase. The reasons for this will be discussed later.

The calculation of predicted efficiency is important because it shows that there should be little change in efficiency with tray number and that the liquid-phase mass transfer resistance is controlling. It is perhaps of greater interest to discuss the probable accuracy of the predicted efficiency values. This accuracy depends upon whether all the factors of operation affecting mass transfer in the extractive column are the same as those on the oxygen-desorption test tray. The same conditions of volumetric gas rate, liquid rate, weir height, and cap design were employed; it is not possible, however, to be certain that other factors such as degree of mixing on the tray, gas and liquid holdup on the operating tray, and degree of disengagement of vapor from the liquid were identical for both the furfural column and the oxygen-desorption tray. Differences in vapor density and liquid viscosity in these two systems, which may be

*Table 7 has been deposited as document 4756 with the A.D.I. Auxiliary Publications Project, Photoduplication Service, Library of Congress, Washington 25, D.C., and may be secured for $1.25 for photoprints or 35-mm. microfilm.

noted in Table 7, may affect the factors just mentioned to some degree. However, the greatest difference between the two units was in the length of the calming zone before the outlet weir. In both cases the tunnel caps were placed parallel to the direction of liquid flow and had a slotted length of 20 in.; but in the furfural column the distance from the last slot to the outlet weir was 2 in., and on the oxygen-desorption tray this distance was 12 in. Because of the high liquid rates employed, it was experimentally observed that in the latter case much of the gas was carried along into the calming zone of the oxygen-desorption tray, where additional mass transfer probably occurred. Thus the liquid on this tray could have been contacted by the gas for as much as 32 in., compared with 22 in. for the furfural-column tray. If the N_L values for the oxygen tray are reduced by a factor of 22/32 before being used in the prediction calculations, the maximum effect of this difference in tray layout can be determined. This has been done, and the resulting predicted efficiencies given in Table 7 are seen to be 7 to 9 efficiency % lower than when this difference in tray layout is ignored. If it is assumed that the actual correction for the oxygen-desorption tray calming zone is about one half the maximum correction just computed, then the average predicted efficiency for the isobutane–1-butene separation is 29%, and the average predicted efficiency for the *n*-butane–1-butene separation is 32%. These values compare well with the experimental efficiencies shown in Table 6. The predicted efficiencies assume the tray liquid to be well-mixed, but even if the tray liquid were assumed to be completely nonmixed, the predicted efficiency values would be increased by only 3 or 4 efficiency %.

DISCUSSION OF RESULTS

Both the experimental plant-performance data and efficiency values based upon laboratory measurements confirm that plate efficiencies for the furfural extractive column under examination are about 25 to 30%. It is now pertinent to examine the reasons for the low efficiency and then to determine whether anything can be done to improve it.

The prediction calculations are better suited to show the reasons for the low efficiency. They indicate that the rate of mass transfer within the liquid phase is quite low, which in turn limits and controls the efficiency of the entire mass transfer operation. The liquid-phase efficiency is low because of the adverse effect of the following variables:

1. *Low Gas Rate.* Liquid-phase efficiencies increase with increasing gas rate, because higher gas rates provide a greater interfacial area and one which is being renewed at a faster rate.

2. *Low Time of Contact of the Liquid with the Gas.* The greater the liquid contact time on the tray, the greater is the amount of mass transfer which can occur in the liquid phase. High liquid rates and a fairly small length of liquid travel are responsible for the low liquid contact time.

3. *Unfavorable Liquid Physical Properties.* Liquid phase efficiencies increase with decreasing liquid viscosity, with increasing liquid diffusivity, and with increasing liquid density. The present extractive system has a liquid viscosity about three times greater than a gasoline fraction at its boiling point.

Possibilities for overcoming these unfavorable factors which promote low plate efficiency are examined below:

1. *Increase in Gas Rate.* Very little can be done in the present column to increase the gas rate without increasing the already high liquid rate. If an extractive solvent somewhat more volatile than furfural were used, this would increase the gas rate and would be desirable from a plate-efficiency viewpoint.

2. *Increase in Liquid Contact Time.* The liquid contact time could be increased by use of a column of larger diameter; it is not likely, however, that the cost of such an increase would be less than the saving resulting from the fewer trays required. If the liquid stream were divided into only two parts instead of into four parts as in the present column, the length of liquid travel would be doubled, but because the quantity of liquid per pass would also be doubled, the liquid contact time on the tray would not be changed. The present arrangement has the advantage of a more uniform gas distribution owing to a lower hydraulic gradient of liquid. As mentioned earlier, the tunnel caps employed have a distance of 4 in. between adjacent cap faces which provides more liquid-contact time than any other type of bubble cap which could have been used. The comparatively wide cap spacing was shown in the laboratory tests not to have an adverse effect upon efficiency.

3. *Lower Solvent Viscosity.* Choice of a different solvent or use of an additive to the solvent would lower the viscosity. The additive should not affect selectivity. This latter possibility has been examined in detail in a recent publication by Baumgarten and Gerster(*2*).

The conclusion to be reached from the foregoing discussion is that with the high liquid rates and low gas rates which result from the extractive-distillation operation and with the furfural-water solvent employed, it is difficult to obtain a high plate efficiency with even the most carefully considered tray design. The present tray design appears to be highly satisfactory and represents a considerable improvement over the older Neches design in which large, closely spaced, round caps were employed on a single split-flow tray. Happel and associates(*13*) computed the tray efficiency to be 25% for this column, which has the same diameter (13 ft. I.D.) and handles the same feed components as the newer column. The hydrocarbon feed rate to the older column was only 4,300 bbl./day, however, compared with the 6,720 bbl./day fed to the tunnel-tray column. Thus the improved tray design permits considerably greater throughput without any change in plate efficiency. Neches engineers have also made performance comparisons for these two columns when operating at identical feed rates(*15*). At a feed rate below 8,500 bbl./day, purity of *n*-butylenes in the bottoms product is approximately 4.5 percentage points higher for the new column, and loss of *n*-butylenes in the overhead is 0.3 percentage point lower. At feed rates of about 9,200 bbl./day, loss of *n*-butylenes in the overhead is about 8% for the older column, but only 6% for the new. This would indicate that plate efficiencies for the new column are much more favorable than those for the old column at the higher throughput rates.

CONCLUSION

Sound procedures have been demonstrated for evaluating the performance of a commercial fractionator where vapor- and liquid-flow rates vary considerably within the column. The computed efficiencies compare favorably with those predicted by the method of Gerster, Colburn, and associates(*7*), indicating the usefulness of this procedure in showing when low efficiencies can be expected. In this case the nature of the extractive-distillation operation and the properties of the furfural-water solvent employed were shown to be responsible for the low order of

magnitude for the plate efficiency obtained. Examination of possibilities for increasing the plate efficiency has indicated that the present column could not be improved upon in design or operation and is in fact superior to the furfural extractive columns designed for Neches during World War II.

ACKNOWLEDGMENT

These calculations were carried out under the sponsorship of the Federal Facilities Corporation, Office of Synthetic Rubber, in connection with the Government's synthetic rubber program.

LITERATURE CITED

1. Baker, T., and J. S. Stockhardt, *Ind. Eng. Chem.*, **22**, 376 (1930).
2. Baumgarten, P. K., and J. A. Gerster, *loc. cit.*, **46**, 2396 (1954).
3. Colburn, A. P., *Can. Chem. Process. Inds.*, **34**, 286 (1950).
4. Feild, John, and S. A. Guerrieri, private communication to Office of Rubber Reserve.
5. Gerster, J. A., paper presented at A.I.Ch.E. meeting, St. Louis (December, 1953).
6. ———, W. E. Bonnet, and I. Hess, *Chem. Eng. Progr.*, **47**, 523, 621 (1951).
7. Gerster, J. A., A. P. Colburn, W. E. Bonnet, and T. W. Carmody, *loc. cit.*, **45**, 716 (1949).
8. Gerster, J. A., T. S. Mertes, and A. P. Colburn, *Ind. Eng. Chem.*, **39**, 797 (1947).
9. Griswold, John, W. B. Brooks, and K. K. McMillen, private communication to Office of Rubber Reserve.
10. Griswold, J., M. E. Klecka, and R. V. West, *Chem. Eng. Progr.*, **44**, 839 (1948).
11. Grohse, E. W., Ph.D. dissertation, Univ. Delaware (1948).
12. Grohse, E. W., R. F. McCartney, H. J. Hauer, J. A. Gerster, and A. P. Colburn, *Chem. Eng. Progr.*, **45**, 725 (1949).
13. Happel, J., P. W. Cornell, Dub. Eastman, M. J. Fowle, C. A. Porter, and A. H. Shutte, *Trans. Am. Inst. Chem. Engrs.*, **42**, 189 (1946).
14. Jordan, D., J. A. Gerster, A. P. Colburn, and K. Wohl, *Chem. Eng. Progr.*, **46**, 601 (1950).
15. Marks, T. N., and A. W. Catanach, private communication to Office of Rubber Reserve.
16. Mertes, T. S., and A. P. Colburn, *Ind. Eng. Chem.*, **39**, 787 (1947).
17. Welty, F., J. A. Gerster, and A. P. Colburn, *Ind. Eng. Chem.*, **43**, 162 (1951).
18. Wilke, C. R., *Chem. Eng. Progr.*, **45**, 218 (1949).

APPENDIX

Calculation of Flow Rates Within the Tower by Material and Enthalpy Balance Equations

To calculate the liquid and vapor rates at any location within an extractive distilation coumn, it is convenient to use equations requiring knowledge of the composition of only one stream and the temperatures of both streams. Grohse and associates (*12*) used such equations to analyze the performance of their extractive-distillation stripping column. Colburn (*3*) has presented the same type of extractive-distillation equations for the general case. His equations are summarized below:

ENRICHING COLUMN

Total Material Balance:

$$V_n = L_{n-1} + D - S \qquad (4)$$

where

V_n = moles of vapor leaving tray n per unit time
L_{n-1} = moles of liquid leaving tray n-1 per unit time
D = moles of overhead distillate withdrawn per unit time
S = moles of solvent added per unit time

Component Balance:

$$y_n V_n = x_{n-1} L_{n-1} + z_D D - x_s S \qquad (5)$$

where

y_n = mole fraction of component in vapor
x_{n-1} = mole fraction of component in liquid
z_D = mole fraction of component in distillate
x_s = mole fraction of component in entering solvent

Total Enthalpy Balance:

$$(\Sigma y_n H_n) V_n = (\Sigma x_{n-1} h_{n-1}) L_{n-1} + (\Sigma z_D i_D) D + Q_c - (\Sigma x_s h_s) S \qquad (6)$$

where

H_n = partial molal enthalpy of component in vapor
h_{n-1} = partial molal enthalpy of component in liquid
i_D = partial molal enthalpy of component in distillate
Q_c = enthalpy removed in condenser per unit time
h_s = partial molal enthalpy of component in entering solvent

Values of $x_{n-1} L_{n-1}$ are eliminated by substituting Equation (5) into Equation (6). The resulting equation is

$$V_n = \frac{Q_c + [\Sigma x_s (h_{n-1} - h_s)]\, S - [\Sigma z_D (h_{n-1} - i_D)]\, D}{\Sigma y_n (H_n - h_{n-1})} \qquad (7)$$

The foregoing equation is particularly useful in the present situation because it does not contain the liquid composition or flow rate for the tray considered. In the present case, where values are known for the composition, temperature, and enthalpy of the external streams and of the vapor within the column the only unknown values in the equation are the vapor rate V_n and the enthalpy of the liquid components on the tray h_{n-1}. The equation is used by assuming the liquid enthalpy values for the tray considered and then computing the resulting value of V_n. The liquid rate and composition values for tray n-1 are now readily computed by Equations (4) and (5), respectively, from which the validity of the assumed liquid enthalpy values is quickly determined.

As a sample calculation the determination of the flow rates within the tower at the seventeenth tray from the top may be considered. At this point the temperature is 133°F., the pressure is 87.4 lb./sq.in. gauge, the water content of the vapor is 2.3 mole %, the furfural composition of the vapor is negligible, and the hydrocarbon composition of the vapor is as given in Table 4. The properties of the streams external to the column are given in Tables 2 and 3.

Enthalpy charts are available for C_4 hydrocarbon–furfural mixtures (*11*), which greatly assist in the use of Equation (7). These charts include the large heat-of-solution values for C_4 hydrocarbons in furfural (*16*) and charts show that the relative amounts of the various C_4 hydrocarbons present in the solution do not greatly affect the enthalpy of the mixture. The partial enthalpy of the water present was computed separately and did not include any allowance for heats of solution of water in the mixture. This omission is justifiable, as most of the water existed on the trays as a second water-rich phase. The enthalpy and external flow-rate values used in Equation (7) are tabulated below. All enthalpy values are relative to the pure components at 32° F. in 1 atm. total pressure.

Enthalpy of Distillate $(\Sigma z_D i_D) D$:

Enthalpy of C_4 hydrocarbons 2,140 B.t.u./lb.mole
Enthalpy of water 1,190 B.t.u./lb.mole

Amount of C_4 hydrocarbons in distillate
13,800 lb. moles/day
Amount of water in distillate
470 lb. moles/day
Total enthalpy of distillate, $(\Sigma z_D i_D)D$ = (2,140) (13,800) + (1,190) (470) = 30,100,000 B.t.u./day

---

$$V_{17} = \frac{(287+1,407-1,292-57.6+30.1)\,(10^6)}{7,000} = \frac{(374)\,(10^6)}{7,000}$$

$$= 53,600 \text{ lb. moles/day}$$

Enthalpy Removed in Condenser Q_c:

Enthalpy of vapor to condenser (Table 3)
361,000,000 B.t.u./day
Enthalpy of reflux stream (Table 3)
44,000,000 B.t.u./day
Enthalpy of distillate
30,100,000 B.t.u./day

Enthalpy removed in condenser = 361,000,000 — 44,000,000 — 30,100,000 = 287,000,000 B.t.u./day

$(\Sigma z_D h_{16})D$:

Enthalpy of liquid on plate 16, h_{16}, is assumed to be 4,110 B.t.u./lb. mole for the C_4 hydrocarbon–furfural mixture, corresponding to an assumed 12 mole % C_4 hydrocarbon concentration in the water-free liquid; and 1,818 B.t.u./lb. mole is the enthalpy of the liquid water.

$(\Sigma z_D h_{16})D$ = (4,110) (13,800) + (1,818) (470) = 57,600,000 B.t.u./day

Enthalpy of Entering Solvent, $(\Sigma x_s h_s)S$:

Enthalpy of furfural
3,725 B.t.u./lb. mole
Enthalpy of water
1,780 B.t.u./lb. mole
Furfural flow rate
284,000 lb. moles/day
Water flow rate
131,500 lb. moles/day
Enthalpy of entering solvent, $(\Sigma x_s h_s)S$ = (3,725) (284,000) + (1,780) (131,500) = 1,292,000,000 B.t.u./day

$(\Sigma x_s h_{16})S$:

Using the same values as taken above, $(\Sigma x_s h_{16})S$ = (4,110) (284,000) + (1,818) (131,500) = 1,407,000,000 B.t.u./day

$\Sigma y_{17}(H_{17} - h_{16})$:

Vapor enthalpy for C_4 hydrocarbons
10,840 B.t.u./lb. mole
Vapor enthalpy for water
20,100 B.t.u./lb. mole
Vapor contains 2.3 mole % water, the remainder C_4 hydrocarbons
$\Sigma y_{17}(H_{17} - h_{16})$ = 0.977 (10,840—4,110) + 0.023 (20,100—1,818) = 7,000 B.t.u./lb. mole

Substituting the above values into Equation (7) gives

The total vapor quantity may be broken down as follows:

C_4 hydrocarbons in vapor at tray 17
(0.977) (53,600 = 52,370 lb. moles/day
Water in vapor at tray 17
(0.023) (53,600) = 1,230 lb. moles/day

The liquid quantities may be obtained by material balance:

C_4 hydrocarbons in liquid at tray 16
$L_{16} = V_{17} - D$ = 52,370 — 13,800 = 38,570 lb. moles/day
Water in liquid at tray 16
$L_{16} = V_{17} - D + S$ = 1,230 — 470 + 131,500 = 132,260 lb. moles/day
Furfural in liquid at tray 16
$L_{16} = S$ 284,000lb. moles/day
Total liquid at tray 16
454,830 lb. moles/day

C_4 hydrocarbon composition on tray 16 on a water-free basis 38,570/(38,570 + 284,000) = 0.119 mole fraction, which checks the originally assumed value used in evaluating the liquid enthalpy.

Stripping Column

The corresponding equations used in the stripping column are given below.

Total Material Balance:

$$V_m = L_{m-1} - W \qquad (8)$$

where m and m—1 refer to adjacent trays in the stripping section
W = moles of bottoms withdrawn per unit time

Component Balance:

$$y_m V_m = x_{m-1} L_{m-1} - x_w W \qquad (9)$$

where
x_w = mole fraction of component in the bottoms

Total Enthalpy Balance:

$$(\Sigma y_m H_m) V_m = (\Sigma x_{m-1} h_{m-1}) L_{m-1} - (\Sigma x_w h_w) W + Q_s \qquad (10)$$

where
h_w = partial molal enthalpy of component in bottoms
Q_s = enthalpy added to system in reboiler per unit time

To eliminate values of $x_{m-1}L_{m-1}$, Equation (9) is substituted into Equation (10) to give

$$V_m = \frac{Q_s - [\Sigma x_w\,(h_w - h_{m-1})]\,W}{\Sigma\, y_m\,(H_m - h_{m-1})} \qquad (11)$$

which is the working equation for computing local flow rates in the stripping section.

Consider as a sample calculation the determination of local flow rates and liquid compositions between trays 50 and 51 from the top of the column. The vapor feed is introduced below tray 50, but by use of the stripping equations, the vapor rate obtained will be that leaving tray 51 before joining the feed stream. At this point in the column the temperature is 145° F., the pressure is 91.0 lb./sq.in. gauge, the water content of the vapor is 3.0 mole %, the furfural composition of the vapor is negligible, and other required quantities are given in Tables 2 and 4. The calculations are made in the same manner as before, with the quantities required for Equation (11) taken as follows:

C_4 hydrocarbons and furfural — Water

$(\Sigma x_w h_w)W$ = (10,670) (294,730) + (4,680) (131,030) = 3,757,500,000 B.t.u./day
$(\Sigma x_w h_{50})W$ = (4,650) (294,730) + (2,030) (131,030) = 1,636,500,000 B.t.u./day
$\Sigma y_{51}(H_{51} - h_{50})$ = 0.97 (11,250—4,650) + 0.03 (20,240—2,030) = 6,946 B.t.u./ lb. mole
Q_s = 2,494,000,000 B.t.u./day

Substituting into Equation (11) gives

$$V_{51} = \frac{(2,494-3,758+1,637)\,(10^6)}{6,946} = \frac{(373)\,(10^6)}{6,946}$$

$$= 53,700 \text{ lb. moles/day}$$

By calculations similar to those above for the rectifying section, the C_4 hydrocarbon composition on tray 50 on a water-free basis is found to be 0.181 mole fraction.

Calculations of the same type were made for seven other tray locations within the tower. Complete results are given in Table 3.

(Presented at A.I.Ch.E. Houston meeting)

Pipe-line Design for Non-Newtonian Fluids in Streamline Flow

E. B. CHRISTIANSEN, N. W. RYAN, and W. E. STEVENS, University of Utah, Salt Lake City, Utah

A method is presented for determining the flow-rate—pressure-gradient relationship for the streamline flow of the large class of non-Newtonian, nonthixotropic fluids to which the Powell-Eyring equation applies. The general procedure and assumptions required in developing this method are the same as used in deriving the Hagen-Poiseuille equation except that the Powell-Eyring equation is used in place of Newton's equation to relate shear stress to shear rate.

The mehod can be used to predict pipe-flow pressure gradients from both precision viscometer data and pipe-flow data. Its applicability is demonstrated for three typical non-Newtonian fluids, 3% carboxymethylcellulose in water, 15% napalm in kerosene, and 33% hydrated lime in water.

When used with pipe-flow data, it resembles the method of Alves and associates, compensating for the inconvenience of an additional step in calculation procedure by providing a means of extrapolating beyond the range of the experimental data.

The relationships developed facilitate the application of shear-stress—shear-rate data in the design of conduits for non-Newtonian fluids.

The basic equation used for expressing the volumetric flow rate of a fluid in a cylindrical conduit is

$$q = \int_0^R 2\pi r u \, dr \qquad (1)$$

where the assumption is made that u is a function of r only. For Newtonian fluids in streamline flow, velocity is related to radial position by the elimination of shear stress between Newton's postulate that shear stress is directly proportional to shear rate,

$$\sigma = \mu \frac{du}{dx} \qquad (2)$$

and a force balance on a cylindrical element of fluid (radius r, length dL) coaxial with the conduit,

$$\sigma = -\frac{r}{2}\frac{dp}{dL} \qquad (3)$$

The relationship thus obtained is substituted into Equation (1), and the integration is performed to obtain the familiar Hagen-Poiseuille isothermal flow equation,

$$q = \frac{\pi R^4}{8\mu}\left(-\frac{dp}{dL}\right) \qquad (4)$$

Non-Newtonian fluids do not conform to Equations (2) and (4), as the ratio of shear stress to shear rate varies with the shear rate and in some cases is also a function of the flow history of the fluid (thixotropic fluids).

In the case of non-Newtonian flow in pipe most investigators have sought substitutes for Equation (4) by one of two general methods. In the first an empirical equation representing the experimental shear-stress–shear-rate data is used in place of Equation (2) in the derivation as outlined (reference *4*, for example). Though this method is applicable to some fluids, it is seldom that empirical equations of conveniently simple form fit the data over large ranges of shear rate with the desired accuracy. The second general method involves correlating suitable flow parameters sufficiently general in character that they may be used with laboratory tube-flow data or rotational viscometer data to predict flow in commercial piep (references *1*, *2*, and *5*, for example).

The method developed in this study embodies features of both general methods. An equation (the Powell-Eyring equation) which accurately represents the shear-stress–shear-rate data for a large number of non-Newtonian fluids over a wide shear-rate range is used in deriving a relationship between the pipe-flow variables (flow rate, pressure gradient, and pipe radius) and rheological properties of the fluid in terms of dimensionless groups. The development and application of this method follows.

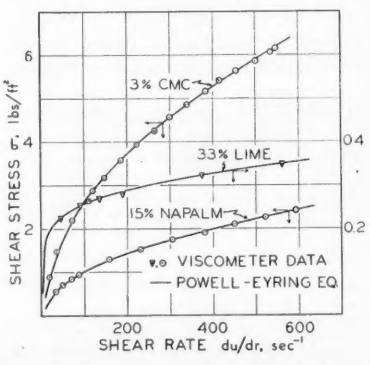

Fig. 1. Comparison of predicted shear data with experimental data.

SHEAR-STRESS—SHEAR-RATE RELATIONSHIPS

From the theory of absolute reaction rates Eyring and his associates (*3*) developed the hyperbolic sine law relating shear stress to shear rate:

$$\sigma = \frac{1}{B}\sinh^{-1}\left(\frac{1}{A}\frac{du}{dx}\right) \qquad (5)$$

Powell and Eyring (*7*) subsequently suggested a modification, called here the Powell-Eyring equation, which they and others (*9*) have applied to non-Newtonian fluids:

$$\sigma = \mu\left(\frac{du}{dx}\right) + \frac{1}{B}\sinh^{-1}\left(\frac{1}{A}\frac{du}{dx}\right) \qquad (6)$$

The constants A, B, and μ are characteristic of the fluid.

Experimental shear-stress–shear-rate data for 3% carboxymethylcellulose in water, 15% napalm in kerosene, and 33% hydrated lime in water and the corresponding curves calculated by means of the Powell-Eyring equation are compared in Figure 1. In the case of 15% napalm in kerosene, data were taken to shear rates of 2,400 sec.$^{-1}$, and the curve of Figure 1 was calculated from the Powell-Eyring equation, which fits the data to this relatively high shear rate. The agreement is within experimental error and is typical of that obtained by use of the rotational viscometer described below (*9, 10*). The constants A, B, and μ used to plot the curves in Figure 1 were determined from the smoothed experimental data, as demonstrated in Illustration 1.

The flow behavior of the lime slurry, often considered a Bingham-plastic fluid, is as well described by the equation as is the flow behavior of the typical pseudoplastic fluids. It is likely that many fluids, ordinarily regarded as Bingham plastics, are in reality extreme pseudoplastics and have flow characteristics that can be accurately represented by the Powell-Eyring equation. Although Equation (5) fits the data of this study fairly well for a limited range of

W. E. Stevens is at present with Humble Oil Company, Baytown, Texas.

variables, agreement is poor for extended ranges.

PIPE-FLOW RELATIONS

The general procedure followed in deriving the Hagen-Poiseuille Equation (4) is used in this study to derive an equivalent pipe-flow-design equation for non-Newtonian fluids. In place of Newton's Equation (2) the Powell-Eyring Equation (6) is used. The result may be represented as

$$\alpha = f(\beta, \gamma) \tag{7}$$

where α, β, and γ are dimensionless groups defined as follows:

$$\alpha = \frac{q}{AR^3} \tag{8}$$

$$\beta = -\frac{BR}{2}\frac{dp}{dL} \tag{9}$$

$$\gamma = A\,B\,\mu \tag{10}$$

These groups would be predicted by application of dimensional analysis to the pipe-flow problem, with flow rate q, pressure gradient $(-dp/dL)$, pipe radius R, and the fluid properties A, B, and μ as variables.

The complex equation obtained by the analytical solution and represented by Equation (7) was used to prepare Figure 2, the basic design chart.*

Equation (7) may be regarded as a general equation from which both Equation (4) and its analogue, derived with Equation (5) in place of Equation (2), are special forms. In either of two cases, $\gamma >> 1$ or β very large with $\gamma \neq 0$, the explicit form of Equation (7) reduces to

$$\alpha = \frac{\pi\beta}{4\gamma},$$

which is the Hagen-Poiseuille Equation (4) in terms of dimensionless groups. When $\gamma = 0$ (i.e., $\mu = 0$), the explicit form of Equation (7) becomes

$$\alpha = \frac{2\pi}{\beta^3}\left[\left(1 + \frac{\beta^2}{2}\right)\cosh\beta - \beta\sinh\beta - 1\right] \tag{11}$$

*Tabulated values of α, β, and γ have been calculated from the explicit form of Equation (7). These data, the explicit form of Equation (7), (Table 4), and shear data (Table 5) may be obtained from the American Documentation Institute, Auxiliary Publications Photo Duplications Service, Library of Congress, Washington 25, D. C., as document 4745 for $1.25 for photoprints or microfilm.

the analogue of Equation (4) based on the hyperbolic sine law (5).

Equation (6) and Figure 2 serve as the basic relationships for the design of pipe-flow systems.

DESIGN OF PIPE-FLOW SYSTEMS

The quantities that must be determined in the design of pipe-flow systems are the pipe radius R, pressure gradient $(-dp/dL)$, and flow rate q, the value of one being calculated from known or assumed values of the other two. The calculation using Figure 2 requires knowledge of the characteristic constants of the fluid, A, B, μ, just as for Newtonian flow use of Equation (4) requires that viscosity be known. In both cases the fluid characteristics may be determined in either of two ways. First, shear-stress–shear-rate data may be used with Equation (2) for Newtonian fluids or with Equation (6) for non-Newtonian fluids to which it applies. Second, tube-flow data, as obtained in capillary or larger tubes, may be used with Equation (4) for Newtonian fluids or with Figure 2 for non-Newtonian fluids.

The methods are explained in the following illustrations.

Illustration 1. Shear stress — shear-rate Data Given

PROBLEM: To calculate the pressure gradient in a 1½-in. pipe ($R = 0.0647$ ft.) when 15% napalm in kerosene flows through it at a flow rate of 0.0254 cu.ft./sec., given the rotational viscometer data of Figure 1 at the same temperature:

a. These sets of shear data are selected from Figure 1:

du/dr, sec.$^{-1}$	σ, lb. force/sq.ft.
452	2.11
104	1.05
30	0.47

b. Each of the three sets of viscometer data is substituted into Equation (6) and the three equations obtained are solved simultaneously for constants:

$A = 32.1$ sec.$^{-1}$
$B = 1.98$ sq.ft./lb. force
$\mu = 0.00093$ (lb. force) (sec.)/sq.ft.

c. From Equation (10), $\gamma = 0.059$
d. From Equation (8), $\alpha = 2.92$
e. From these values and Figure 2, $\beta = 2.5$
f. From Equation (9), $-dp/dL = 39.0$ lb. force/cu.ft.

The value obtained experimentally is 39.5 lb. force/cu.ft.

Illustration 2. Pipe-flow Data Given

PROBLEM: Same as in Illustration 1, given, in place of the viscometer data, the experimental ⅞-in. tube-flow data in Table 2.

a. For each q and the corresponding dp/dL, $A\alpha = q/R^3$ and $\beta/B = -(R/2)(dp/dL)$ are calculated by use of the ⅞-in. tube radius; $R = 0.0326$ ft. A data plot of β/B as ordinate and $A\alpha$ as abscissa is prepared on logarithmic paper having the same scale as Figure 2.

b. The data plot is placed on Figure 2 and shifted, with the two sets of coordinate axes parallel, until the best match between the lines on Figure 2 and the data plot is obtained. The value of γ is read from the line on Figure 2 matched by the data plot. In this case $\gamma = 0.075$.

c. Any convenient point is taken on Figure 2, and the values of α and β are read. From the point on the superimposed data plot, immediately above the point taken on Figure 2, the values of $A\alpha$ and β/B are read.

d. The constants A, B, and μ are calculated as follows:

$A = (A\alpha)_{\text{data}}/\alpha_{\text{Fig. 2}} = 29.5$ sec.$^{-1}$
$B = \beta_{\text{Fig. 2}}/(\beta/B)_{\text{data}} = 2.09$ sq. ft./lb. force
$\mu = \gamma/AB = 0.00122$ (lb. force) (sec.)/sq.ft.

e. The remainder of the procedure is as in Illustration 1, starting at step *c*; the constants shown above and $R = 0.0647$ ft. are used:

$\alpha = 3.18$
$\beta = 2.65$
$-dp/dL = 39.3$ lb./cu.ft., as compared to 39.5, found experimentally.

The calculation of q when $-dp/dL$ is known proceeds in a similar manner. The situation is more complicated, however, when R is desired, because R appears in both α and β. In this case the constants A, B, and γ are found as in the foregoing illustrations. For each of two assumed values of R and the given values of q and dp/dL, α and β are calculated from Equations (8) and (9). The two resulting (α, β) points are located on Figure 2. The straight line joining these points is extended until it intersects the line characterized by the known value of γ. The value of α (or β) corresponding to this intersection may be substituted into Equation (8) or (9) to yield the desired value of R.

It will be noted that the values of A, B, μ in Illustration 1 differ from those in Illustration 2, though the same fluid was considered. The two calculated values of $-dp/dL$ are, however, in good agreement. If in the case of the curve-matching method of Illustration 2, the data plot matches two adjacent γ lines of Figure 2 equally well, either γ line may be used, although the calculated constants will differ. Owing to compensating differences within the sets of constants, the resulting Powell-Eyring equations will fit the shear data about equally well. Consequently the calculated

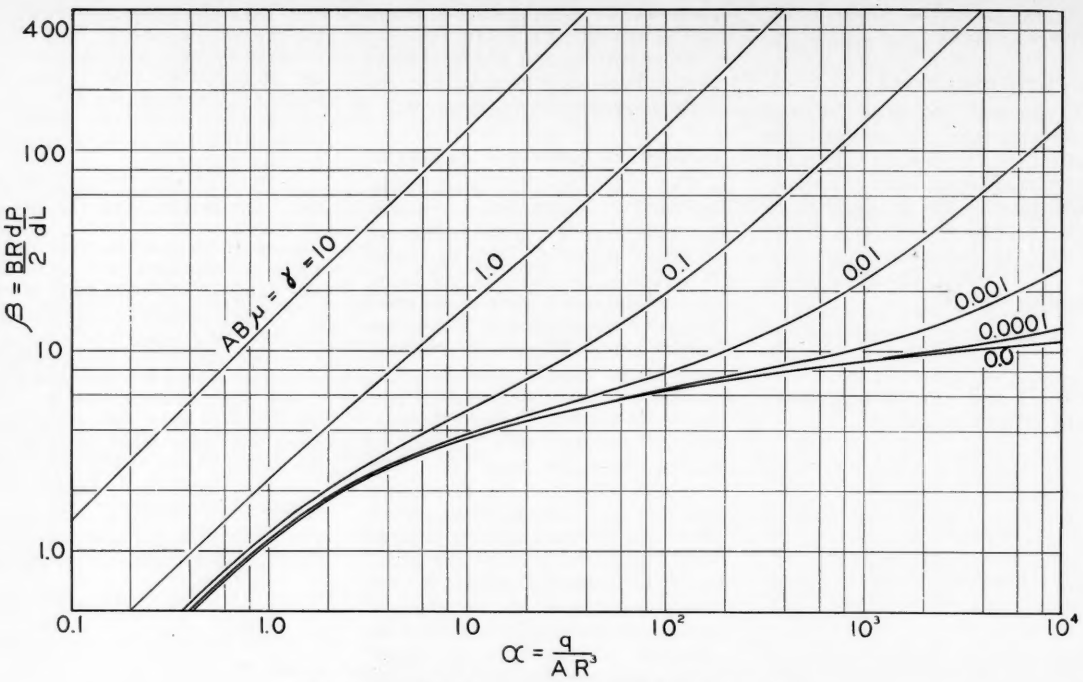

Fig. 2. Non-Newtonian pipe-flow prediction graph.

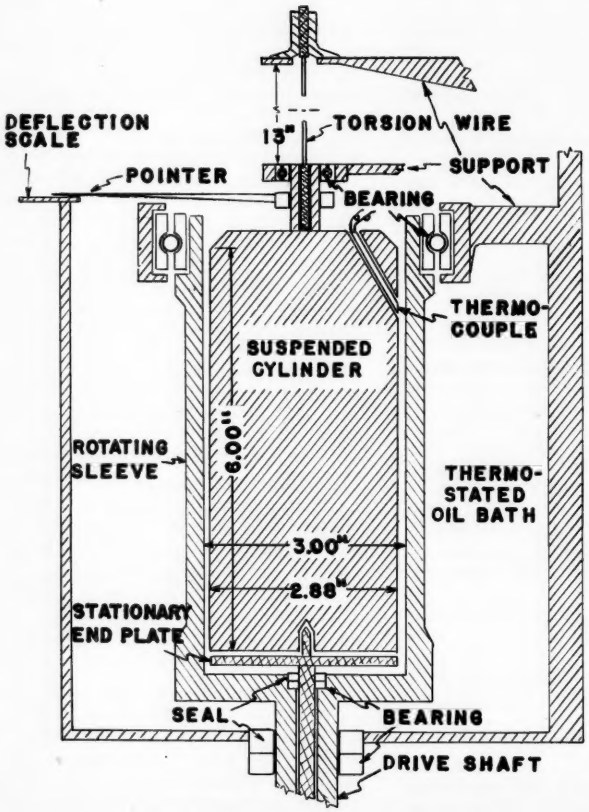

Fig. 3. Rotational viscometer.

values of q, $-dp/dL$, or R will be very nearly the same. Greater accuracy may be expected by averaging results for two adjacent, equally well-matched γ lines, particularly if the desired α and β values require extrapolation far beyond experimental pipe-flow data.

EXPERIMENTAL EQUIPMENT

Experimental measurements were taken in the rotational-type viscometer and the pipe-flow system shown in Figures 3 and 4. The equipment is described in detail in reference *10*.

Rotational Viscometer

Essential features of several rotational viscometers are discussed in the literature (*1*). The instrument used in this investigation consists of a metal cylinder suspended concentrically in a metal cylindrical sleeve by means of an interchangeable torsion wire. The clearance between the wall of the cylinder and the wall of the sleeve (0.061 in.) forms an annular space into which the fluid to be tested is placed. The instrument contains a stationary disk at the bottom of the suspended cylinder to eliminate the transmission of torque to the bottom of the suspended cylinder. The sleeve is mounted in such a manner that it can be made to rotate at controlled speeds.

The viscometer is mounted in a thermostated oil bath. The temperature of the test fluid is measured by a thermocouple mounted in the sus-

TABLE 1.—PRESSURE GRADIENT PREDICTIONS, 3% CARBOXYMETHYCELLULOSE IN WATER

⅞-in. iron tube (R=0.0322 ft.)				1½-in. pipe (R=0.0647 ft.)		
q, cu. ft./sec.	$-dp/dL$, lb force/cu. ft. Obs.	Calc.*	Calc.†	q, cu. ft./sec.	$-dp/dL$, lb. force/cu. ft. Obs.	Calc.*
0.00058	74.1	59.2	64.5	0.0089	51.1	48.9
0.00129	113.2	112.4	113	0.0159	71.1	72.8
0.00201	151	150.3	154	0.0275	97.6	100.8
				0.0304	103.8	107.5
				0.0481	132.5	137.2
				0.0501	134.6	139.6
Percentage mean deviation		(7.2)	(5.0)			(3.5)

*Calculated from viscometer data. A=26 sec.$^{-1}$, B=0.934 sq. ft./lb. force, μ=0.00399 (lb. force) (sec.)/sq. ft.
†Calculated from 1½-in. pipe-flow data. A=16.9 sec.$^{-1}$, B=1.18 sq. ft./lb. force, μ=0.00501 (lb. force) (sec.)/sq. ft.

TABLE 2.—PRESSURE GRADIENT PREDICTIONS, 15% NAPALM IN KEROSENE

⅞-in. copper tube (R=0.0326 ft.)				1½-in. pipe (R=0.0647 ft.)			
q, cu. ft./sec.	$-dp/dL$, lb. force/cu. ft. Obs.	Calc.*	Calc.‡	q, cu. ft./sec.	$-dp/dL$, lb. force/cu. ft. Obs.	Calc.*	Calc.†	Calc.‡
0.00120	40.9	39.7	46.0	0.00778	18.9	17.3	17.6	21.2
0.00197	56.8	56.3	58.7	0.01724	31.5	30.6	31.0	31.3
0.00258	65.6	66.5	67.0	0.0254	39.5	39.0	39.3	37.8
0.00584	107.6	103.7	99.7	0.0431	52.3	51.0	52.6	48.8
0.00806	127.4	122.5	116.8	0.0516	56.6	55.7	57.4	53.4
0.01007	144.6	136.2	130.0	0.0658	62.1	63.2	65.2	60.1
Percentage mean deviation		(3.1)	(7.3)			(3.1)	(2.7)	(5.4)

*Calculated from viscometer data Equation (6), and Figure 2. A=32.1 sec.$^{-1}$, B=1.98 sq. ft./lb. force, μ=0.00093 (lb. force) (sec.)/sq. ft.
†Calculated from ⅞-in. tube data and Figure 2. A=29.5 sec.$^{-1}$, B=2.09 sq. ft./lb. force, μ=0.00122 (lb. force) (sec.)/sq. ft.
‡Calculated from viscometer data and Equations (12) and (13).

TABLE 3.—PRESSURE GRADIENT PPEDICTIONS, 33% LIME SLURRY

2-in. Pipe (R=0.0865 ft.)			1½-in. Pipe (R=0.0647 ft.)			⅞-in. Copper tube (R=0.0326 ft.)		
q Cu. ft./sec.	$-dp/dL$, lb. force/cu. ft. Obs.	Calc.*	q Cu. ft./sec.	$-dp/dL$, lb. force/cu. ft. Obs.	Calc.*	q Cu. ft./sec.	$-dp/dL$, lb. force/cu. ft. Obs.	Calc.*
0.0269	6.24	6.24	0.0255	11.33	9.42	0.0136	24.5	24.6
0.0341	6.88	6.43	0.0261	10.88	9.48	0.0193	27.2	26.7
0.0457	7.45	6.75	0.0327	11.52	9.93	0.0240	29.0	28.5
0.0634	7.77	7.13	0.0385	11.71	10.31			
0.0892	7.90	7.65	0.0492	12.22	10.69			
0.1118	8.15	7.90	0.0616	13.11	11.14			
Percentage mean deviation		(5.1)			(13.8)			(1.1)

*Calculated from viscometer data. A=0.191 sec.$^{-1}$, B=27.6 sq. ft./lb. force, μ=6.16 (10^{-5}) (lb. force) (sec.)/sq. ft.

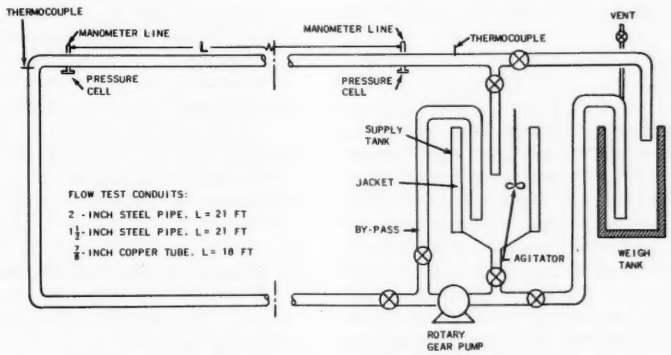

Fig. 4. Experimental pipe-flow system.

pended cylinder wall, as shown in Figure 3. The junction, flush with the cylinder surface, is insulated from the metal.

In a given test the sleeve is rotated at controlled speeds. The moment exerted by the sheared fluid on the inner cylinder causes it to rotate until the moment is balanced by the torque of the wire. Shearing stress is calculated from the angular displacement of the cylinder, the dimensions of the cylinder, and calibration data for the torsion wire. The rate of shear is calculated from the rotational speed of the sleeve and dimensions of the apparatus.

Pipe-flow System

The pipe-flow system, sketched in Figure 4, provides a 21-ft. test section preceded and followed by 8-ft. calming sections for each of the following conduits: ⅞-in. tube, 1½-in. black-iron pipe, and 2-in. galvanized-iron pipe. Temperature measurements, taken by means of thermocouples located at the ends of the pipes, are recorded by a recording potentiometer. Pressures at each end of the 21-ft. test section are determined by means of both mercury-

filled manometers and Baldwin (type EMB) fluid pressure cells. The output electromotive forces of the cells are also recorded by the potentiometer. Flow measurements are made by weighing the quantity of fluid flowing through the conduit in use during a measured time interval. The flow rates are varied by short-circuiting pumped fluid back to the feed-storage vessel. Conduit diameters were calculated from measured conduit volumes, and lengths were checked by use of Equation (4) and conduit-flow data for sucrose solutions.

DISCUSSION OF RESULTS

Experimental flow rates and pressure gradients for three non-Newtonian fluids together with pressure gradients calculated by the methods of Illustrations 1 and 2 are presented in Tables 1, 2, and 3. The shear-stress–shear-rate relationships for these fluids are shown in Figure 1. The mean deviation of predicted pressure gradients from experimental values is seen to be less than 4% for 15% napalm in kerosene. Similar accuracy can be attributed to predictions for 3% carboxymethylcellulose in water, except for very low flow-rates in the ⅞-in. tube.

Pressure-gradient predictions for the 33% lime slurry are less successful. Reproducible rotational-viscometer data were not obtained for the lime slurry, presumably because of settling of the suspended lime particles. The shear-stress–shear-rate data shown on Figure 1 were taken to be as representative of the unsettled slurry as any data taken and were used to obtain the constants A, B, and μ employed in the calculations. Under the circumstances the agreement between calculated and observed pressure gradients in the 2-in. pipe and ⅞-in. tube is much better than might be expected.

The design method presented is limited to use with fluids whose behavior does not depend on their flow history and to fluids that conform to the Powell-Eyring equation. The latter limitation is not severe, because of the versatility of the Powell-Eyring equation. As explained above, it represents very well shear data for 33% lime slurry, which is often considered to be a Bingham plastic, as well as shear data for typical pseudoplastics. Also, as demonstrated in the case of 15% napalm in kerosene, the Powell-Eyring equation fits shear-stress–shear-rate data accurately over wide ranges.

Extrapolation can be made within the range of Powell-Eyring equation applicability. For instance, the flow calculations in Table 3 for lime slurry in a ⅞-in. tube represent extrapolations beyond the experimental shearing stresses and shearing rates up to 35 and 300% respectively.

Alves and associates (*1, 2*) have recommended a design method in which tube-flow data are plotted as $q/\pi R^3$ vs. $(R/2)\,(-dp/dL)$ for the fluid of interest. This graph, which is essentially the same as the data plot described in Illustration 2, is then used to design pipe-flow systems. The advantage of using Figure 2 with the data plot is that it provides a basis for extrapolation to values of $q/\pi R^3$ and $(R/2)\,(-dp/dL)$ considerably beyond the range of the experimental data.

As previously mentioned, Eyring's hyperbolic sine law [Equation (5)] approximates the shear data of this study over small ranges of shear rate. Accordingly, for approximate results, Equations (11) and (5) with shear data or Figure 2 with $\gamma = 0$ and pipe-flow data may be used with some saving in time. When these procedures were followed with data shown in Figure 1 and Tables 1, 2, and 3, the values of dp/dL calculated were generally in error by less than 20% (*10*). For fluids conforming closely to the hyperbolic sine law in the range of shear rates of interest, these procedures should give results as accurate as the data used.

However, if approximate results will suffice and if data extrapolation is not required, the power Equations (6) (8),

$$\frac{du}{dx} = k\,\sigma^n \qquad (12)$$

and the corresponding analogue of Equations (4) (8),

$$q = \frac{\pi k}{3+n} R^{3+n} \left(\frac{-dp}{2dL}\right)^n \qquad (13)$$

together with shear data, are more convenient to use than the Eyring equation. Typical results obtained by use of Equations (12) and (13) with shear data are compared with experimental results in Table 2. Similar accuracy may also be obtained by means of Equation (13) with constants determined from pipe-flow data if appreciable shear-rate extrapolation is not involved.

ACKNOWLEDGMENT

Grateful acknowledgment is made to the University of Utah Research Fund and the Phillips Petroleum Company for fellowship grants and to the Hercules Powder Company, the Utah-Idaho Sugar Company, and the Utah General Depot, U. S. Army, for supplying materials.

NOTATION

(Units are given in the engineering system, but any consistent system may be used.)

A = constant characteristic of fluid, defined by Equation (6), sec.$^{-1}$

B = constant characteristic of fluid, defined by Equation (6), sq.ft./lb. force

f = function of

k = constant in power equation

L = distance along conduit in direction of flow, ft.

n = constant in power equation

p = static pressure of fluid, lb. force/sq. ft.

q = volumetric flow rate, cu.ft./sec.

r = radial distance from pipe axis, or from viscometer axis, ft.

R = radius of pipe or tube, ft.

u = local velocity of fluid, ft./sec.

du/dx = shearing rate, sec.$^{-1}$ *Note*: $dx = dr$ for rotating cylinder rotational viscometer, $dx = -dr$ for pipe flow

α, β, γ = dimensionless groups, defined by Equations (8), (9), and (10)

μ = constant characteristic of fluid, defined by Equation (6), or viscosity, defined by Equation (3), (lb. force/(sec.)/sq. ft.

σ = shearing stress, lb. force/sq. ft.

LITERATURE CITED

1. Alves, G. E., *Chem. Eng.*, **56**, 107 (1949).
2. Alves, G. E., D F. Boucher, and R. L. Pigford, *Chem. Eng. Progr.*, **48**, 385 (1952).
3. Glasstone, S., K. J. Laidler, and H. Eyring, "The Theory of Rate Processes," McGraw-Hill Book Company, Inc., New York (1941).
4. McMillen, E. L., *Chem. Eng. Progr.*, **44**, 537 (1948).
5. Metzner, A. B., *Chem. Eng. Progr.*, **50**, 27 (1954).
6. Porter, A. W., and P. A. M. Rao, *Trans. Faraday. Soc.*, **23**, 311 (1927).
7. Powell, R. E., and H. Eyring. *Nature*, **154**, 427 (1944).
8. Salt, D. L., M.S. thesis, Univ. Utah (1949).
9. Salt, D. L., N. W. Ryan, and E. B. Christiansen, *J. Colloid Sci.*, **6**, 146 (1951).
10. Stevens, Wayne E., Ph.D. thesis. Univ. Utah (1953).

(Presented at A.I.Ch.E. Springfield meeting)

Entrainment Removal By A Wire-mesh Separator

C. LeRoy Carpenter and Donald F. Othmer
Polytechnic Institute of Brooklyn, Brooklyn, New York

The efficiency of a wire-mesh separator as an entrainment eliminator has been experimentally determined in an evaporator employing a sodium chloride brine to trace the entrainment throughout the system. Superficial linear velocities have been tested with efficiencies ranging from less than 80% at lower velocities up to 99.9% at 17 ft./sec. Higher superficial linear velocities were explored, but the results were erratic, with reentrainment from the separator visually evident. The experimental data have been correlated by the assumption, and development, of a proposed mechanism for the capture of the entrainment particles by the wires in the separator. This mechanism is developed from a theoretical derivation by Langmuir and Blodgett used for correlating the stoppage of mist particles by the leading edges of airplanes and has been found to correlate the experimental data very well, so that predictions in unworked ranges may be made. The separator as applied in this experimental work behaved as an impingement-type, inertial entrainment eliminator.

The use of the presently developed equations permits the recommendation of specifications to be used in the fabrication of a separator for its most efficient performance if the nature of the entrainment and conditions of operation are known.

Carryover, or carry along, of liquid particles (entrainment) in gas and vapor streams has been given much attention. Some of the recent and important studies evaluating the effect of entrainment in fractionating colunms are those of Souders and Brown (*33*); Holbrook and Baker (*16*); Rhodes (*27, 28*); Sherwood and Jenny (*32*); Colburn (*4*); Rhodes and Slachman (*29*); Ashraf, Cubbage and Huntington (*1*); and Eduljee (*6*); and to evaluate the effect of entrainment in evaporators there have been the reports of Cessna and Badger (*3*) and O'Connell and Pettyjohn (*25*).

More recently, however, methods for the removal of entrainment from gas and vapor streams has been the object of most study. These studies have involved the use of standard equipment such as the settling chamber, the cyclone separator, the centrifuge, screens, baffle plates, and their modifications. Typical of such studies are those of Pollak and Work (*26*), observing the performance of various types of cyclone separators; Campbell (*2*) the design and use of a special type of scrubber for the recovery of crude-oil mist from natural gas; Lowrie-Fairs (*23*) the use of the Calder-Fox scrubber; and Houghton and Radford (*17*) the development of a new type of streamlined eliminator for removal of fine liquid droplets containing calcium chloride remaining in the air after local dissipation of natural fog by means of a spray of calcium chloride solution.

Separators consisting of targets of fine wires or fibers upon which the droplets in a stream of entrainment-laden gas or vapors are removed by filming on the filaments, have been found to be very effective. Hammond and Leary (*15*) used a separator of loosely packed Fiberglas in successfully removing the radioactive spray from the scrubbers used in washing the radioactive dusts from the waste air discharged from a laboratory in which radioactive work was being conducted. They reported that this separator showed a pressure drop of 0.67 in. of water/2-in. thickness of packing at a velocity of 150 ft./min. and showed less than 0.05% passage of the spray. York (*35*) reviews the application of the wire-mesh separator as an entrainment eliminator.

Recently Montross (*24*) has extensively reviewed proposed and used equipment and the various mechanisms suggested for entrainment removal.

The present investigation reports the results of experimental work using a knitted-wire-mesh separator as an entrainment eleminator. The theoretical effect of projecting a small water droplet, such as might be present in naturally occurring mist or fog, at a single cylinder oriented with its axis perpendicular to the motion of the droplet approaching from a great distance has been determined by Langmuir and Blodgett (*22*) under a variety of conditions. The results of their theoretical study have been modified and applied to the more complex situation presented by a great many droplets of mixed size range continuously being projected at and reaching the intricate maze of wire comprising the separator. A newly developed equation, derived later in

C. L. Carpenter is with Northern Chemical Industries, Inc., Searsport, Maine.

this paper, has provided a means for the understanding of the role of wires in the capture of entrainment in a mesh separator and has allowed the setting up of optimum design factors for such separators.

EXPERIMENTAL EQUIPMENT

The basic unit of the equipment is an evaporator having the capacity to vaporize and condense ½ ton of water/hr., which was built for experimental laboratory use by the Vulcan Copper and Supply Company, of Cincinnati, Ohio. The assembly is illustrated schematically in Figure 1. For this work a salt solution was evaporated to supply a vapor stream carrying naturally entrained droplets of salt water. Beginning at the bottom of Figure 1 and working up, section by section, the 30-in.-diam. evaporator consists of a conically shaped reservoir 30-in. high; an internal calandria 31½ in. high having thirty-six 1½-in. I.P.S. tubes in concentric arrangement surrounding a 10-in. downcomer; a disengaging chamber 60 in. high; a second disengaging chamber 33 in. high housing the separator in the orifice of an annular gutter; and, finally, a head connecting with the condenser through a gooseneck vapor-draw-off line.

All condensate streams after the separator are returned to the conical reservoir through a return line in which there are thermometers, conductivity cells, and a nutating disk type of hot-water meter. The amount of entrainment escaping the separator is determined by analysis of samples taken from the return line for salt content.

Entrainment ahead of the separator may be partially settled out in the space (approximately 60 in.) between the surface of the boiling liquid and the separator. Entrainment reaching the separator is determined by analyzing samples of the vapor-entrainment stream collected through a sampling tube extending across the diameter of the evaporator just below the separator. This sampling tube, ⅝ in. in diameter, has six ports through which the vapor-entrainment stream passes; the stream is withdrawn through an external condenser system in which there is a thermometer and a conductivity cell. The ports are small tubes 5/16 in. in diameter, brazed into holes in the underside of the sampling tube. Each port tube extends upward to the axis of the sampling tube so that all vapor entrainment entering the sampling tube will be drained into the external condensing system. All condensate except the negligible amount removed for analysis is returned to the evaporator; and thus the whole operation is carried out as a closed system.

Pressure drop across the separator is measured by a water manometer. Since thermometers are mounted in all vapor and liquid lines, temperatures may be noted at all points; and, since conductivity cells are located in all liquid lines, the approximate salt concentration at any point may be noted by switching the cell circuit through the meter. All vapor chambers and lines are connected to a surge drum in which the pressure is maintained by a rotary type of vacuum pump and controlled by a manostat.

Two wire-mesh separators were used in the experimental work. These were of the standard types available from the various suppliers of such separators specified as York .011R-24CU5-½ No. 8 crmip. One separator, 24½ in. in diameter and 4 in. thick, was mounted in the 24½-in. orifice produced by the annular gutter and was supported by six thin spokes to prevent sagging. A second separator, 5⅞ in. in diameter and 4 in. thick, was mounted in a housing which

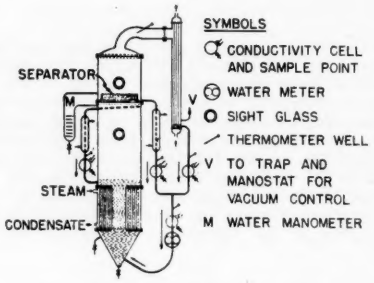

Fig. 1. Schematic flow diagram.

fitted into the 24½-in. opening and reduced the orifice through which the vapors could pass to a 5⅞-in. opening, thus correspondingly increasing the vapor velocity. The separators were made by rolling a 4-in. ribbon of knitted 0.0113-in. (287 μ)-diam. copper wire, knit to give 96 mesh by 48 needles in a tubular stocking in a knitting machine. The ribbon was flattened to a double thickness, crimped with about 0.05-in. nodes, spaced 0.2 in. apart, and rolled spirally upon itself to form a disk of uniform thickness of the desired diameter. The wire comprising the separator occupied only 2% of the space, so that there was 98% free volume.

Bypassing of the separator was minimized by purposely fabricating the separator element slightly larger in diameter than the orifice in which it was housed. Owing to the somewhat compressible nature of the separator, intimate contact was obtained between the cylindrical face of the separator and the walls of the enclosing orifice, which completely contained the separator element.

EXPERIMENTAL PROCEDURE

Four sets of experiments were performed: a series of runs with no separator in the 24½-in. orifice, a second series with the 24½-in. separator in place, a third series with no separator in the 5⅞-in. orifice, and a fourth series with the 5⅞-in. separator in place.

In each run a solution of about 5% sodium chloride with 1,000 p.p.m. of sodium chromate as corrosion inhibitor was introduced into the evaporator and the unit was then brought on stream by rapidly introducing process steam to the calandria shell to minimize the tendency of the solution to foam. [*See* the work of O'Connell and Pettyjohn (*25*) on foaming of solutions of sodium chloride in an evaporator and that of Foulk and coworkers (*7, 14*) on their study of foaming in boilers.] Operations were then adjusted to produce a definite and continuing set of recycling conditions as indicated by the steady state of thermometer, manometer, and conductivity-cell readings. While this steady state was continued, samples were taken from the condensate line, which combined to pass to the evaporator all streams after the separator; from the condensate from the sample tube ahead of the separator; and from the boiling solution. These samples were then analyzed for sodium chloride content by the Mohr titration method for chloride ion.

Special note should be made of the method of taking samples in order that they would be representative of the conditions over the period of the run. Flasks were attached to each sampling exit by means of a rubber stopper. A side arm from each flask was attached to a tube leading to the surge drum of the vacuum system and brought to the system pressure. It was then possible to open the stopcock at each sample point and to collect drop by drop during the entire run a representative composite sample. Temperatures and pressures were read. Although the conductivity meter was calibrated, the readings of the cells were noted only to guide in keeping the run on steady conditions.

The data collected in the experimental work were used in compiling the values given in Table 1 and in expressing the experimental results graphically in Figures 2, 3, 4 and 5. Entrainment, as recorded in the tables, is defined as pounds of entrained solution from the main body of the evaporator per million pounds of solvent evaporated.

One may consider any point P after the separator and arrive at the following relation:

$$p = (M \times s)/(M + z_p) \qquad (1)$$

or, by rearranging terms,

TABLE 1.—EXPERIMENTAL DATA

Run	Vapor temp., °F.	Specific vol. of sat. steam, cu. ft./lb.	Factor correcting for gas density, (31) and (34) $1/\phi\triangle_P$	Mass velocity in orifice lb./(hr.) (sq. ft.) Actual	Modified	Superficial linear vel. at flow cond., ft./sec.	Conc. of brine, wt. %	Entrainment, p. p. m. Ahead of separator	Return line	Efficiency %	Pressure drop across orifice ins.ofwater ft. of separator thickness
	T	v	$\sqrt{0.075v}$	G	$G/\phi\triangle_P$	V	s	$(\text{Ent})_Q$	$(\text{Ent})_P$	E_S‖	ΔP
1	2	3	4	5	6*	7†	8‡	9**	10¶	11	12
With 24½-in. Separator											
1	119+	208	3.95	290.9	1149	16.81	4.73	9.48×10^4	4.77×10^1	99.95	0.47
2	139.7	124.01	3.06	165.6	505	5.70	3.75	4.76×10^3	3.12×10^1	99.35	
3	168.5	64.10	2.20	173.8	381	3.09	2.77	1.62×10^3	6.75×10^1	95.84	0.71
4	198−	35.11	1.63	199.5	324	1.95	3.29	4.98×10^2	1.03×10^2	79.29	0.59
5	179.7	50.58	1.94	222.6	433	3.13	3.62	3.00×10^3	9.36×10^1	96.88	
6	181	49.20	1.92	220.3	423	3.01	4.27	9.31×10^2	5.47×10^1	94.12	0.71
7	158	80.84	2.46	208.5	513	4.68	5.59	3.76×10^3	3.98×10^1	98.94	0.71
8	153	90.57	2.60	230.7	601	5.80	5.50	4.37×10^3	4.04×10^1	99.08	0.83
9	126.5	171.91	3.59	282.1	1013	13.47	4.90	5.34×10^4	4.12×10^1	99.92	0.35
10	140	123.01	3.04	107.6	327	3.68	3.17	2.74×10^3	6.93×10^1	97.47	0.12
11	140	123.01	3.04	260.7	792	8.91	4.05	1.42×10^4	3.11×10^1	99.78	0.24
12	132	149.66	3.35	269.7	903	11.21	4.05	2.52×10^4	4.38×10^1	99.83	0.30
24½-in. Orifice without Separator											
13	110	265.4	4.46	257.6	1149	18.99	5.47	4.61×10^4	3.19×10^3	93.09	0.47
14	172.5	58.82	2.10	218.3	458	3.57	5.46	9.68×10^2	6.42×10^2	33.65	0.59
15	144	111.77	2.90	240.8	699	7.48	5.67	5.00×10^3	1.44×10^3	71.13	0.65
16	199.3	34.10	1.60	193.7	309	1.83	5.77	2.64×10^2	1.70×10^2	35.39	0.83
17	130	157.34	3.44	273.7	940	11.96	4.77	2.51×10^4	3.18×10^3	87.32	0.35
18	140	123.01	3.04	247.6	752	8.46	5.24	1.09×10^4	1.62×10^3	85.06	0.12
With 5⅞-in. Separator											
19	212−	26.80	1.42	3,166	4,500	23.6	5.92	1.46×10^3	1.78×10^1	98.78	
20	181.6	48.60	1.91	3,698	7,050	49.9	6.24	1.53×10^3	1.26×10^3	27.62	
21	170	62.06	2.16	1,686	3,640	29.1	6.29	1.26×10^3	5.39×10^1	95.72	
22	160	77.29	2.41	2,677	6,450	57.5	6.22	1.12×10^3	2.17×10^2	80.57	
23	150+	97.0	2.69	2,019	5,450	54.4	7.09	8.70×10^2	7.75×10^1	91.09	5.43
24	150−	97.2	2.70	1,804	4,880	48.7	7.09	1.01×10^3	4.62×10^1	95.41	5.67
25	130	157.34	3.43	2,922	10,000	127.7	7.33	1.32×10^4	1.43×10^3	89.14	15.35
26	146+	106.6	2.83	1,188	3,360	35.2	8.25	4.75×10^2	1.40×10^1	97.04	2.95
27	120	203.27	3.90	869	3,390	49.1	7.72	1.18×10^3	2.10×10^1	98.22	3.94
28	149−	99.4	2.73	2,717	7,420	75.0	7.54	2.13×10^3	5.93×10^2	72.21	9.09
29	130.75	154 42	3.40	2,700	9,180	115.8	7.54	5.16×10^3	6.51×10^2	87.38	13.11
30	153	90.57	2.60	2,112	5,500	53.1	2.46	1.39×10^3	1.27×10^2	90.89	4.96
31	140	123.01	3.03	1,148	3,485	39.2	3.84	1.10×10^3	3.01×10^1	97.26	3.84
32	140	123.01	3.03	1,199	3,645	41.0	3.84	9.32×10^2	3.10×10^1	96.77	1.30
33	140	123.01	3.03	1,720	5,227	58.8	3.84	1.44×10^3	5.73×10^1	96.02	6.14
34	139	126.02	3.08	2,293	7,060	80.3	4.61	1.38×10^4	4.02×10^3	70.77	9.21
35	137	132 30	3.15	2,569	8,070	94.4	4.47	8.38×10^2	1.51×10^3	81.99	11.10
36	137−	132.5	3.15	1,779	5,600	65.5	4.47	1.08×10^4	3.93×10^2	96.36	8.39
37	135	138.95	3.24	1,653	5,340	63.8	4.76	1.52×10^4	2.99×10^2	98.03	7.56
5⅞-in. Orifice without Separator											
38	120	203.27	3.91	1,939	7,580	109.5	4.76	2.54×10^4	1.51×10^4	40.75	1.42
39	130	157.34	3.44	1,649	5,670	72.1	4.66	1.03×10^4	1.88×10^2	98.17	0.94
40	124	183.25	3.71	2,700	10.000	137.4	4.66	4.82×10^3	8.54×10^2	82.28	2.16
41	139−	126.0	3.07	2.385	7.330	83.5	4.66	3.61×10^3	2.34×10^2	93.51	1.38
42	138	129.12	3.11	948	2,950	34.0	4.66	9.29×10^3	6.75×10^2	92.73	0.28
43	119	208.7	3.96	1,945	7,700	112.7	4.41	4.60×10^3	5.57×10^2	87.89	1.58

*Column 4 multiplied by Column 5.
†Product of Columns 3 and 5 divided by 3,600.
‡By Mohr's titration.
**By Mohr's titration and application of Equation (5).
¶By Mohr's tritration and application of Equation (4).
‖Application of Equation (6).

$$z_p = M\,((s/p) - 1) \qquad (2)$$

Entrainment as already defined, may be expressed as follows:

$$\text{Entrainment} = (M)/(z_p/10^6), \text{ or } (M\times10^6)/z_p \qquad (3)$$

If z_p is eliminated between Equations (2) and (3),

$$(\text{entrainment})_P = (p\times10^6)/(s-p) \qquad (4)$$

By analogy, consideration of any other point Q, just ahead of the separator, gives the expression

$$(\text{entrainment})_Q = (q\times10^6)/(s-q) \qquad (5)$$

Efficiency as recorded in the tables represents the effectiveness of removal of entrainment by the separator and is defined as the percentage of the total entrainment just ahead of the separator removed by the separator. An equation to express this definition is

$$Es = \textit{efficiency} = 100\times((\text{ent})_Q - (\text{ent})_P)/((\text{ent})_Q) \qquad (6)$$

where the subscripts Q and P represent points ahead and after the separator, respectively.

EXAMINATION AND DISCUSSION OF EXPERIMENTAL DATA

Efficiency of Separator as an Entrainment Eliminator

Figure 2, which illustrates the percentage of entrainment removed as a function of the linear velocity

in feet per second for the 24½-in. separator, shows that the efficiency is very low at the lower linear velocities and increases as the velocity increases. This can be assumed to be caused by the fact that only the smaller droplets pass upward through the settling space to reach the separator at low velocities and that many of these are carried along with the vapor around the wires; but as the velocity increases even the smaller droplets will be less likely to be carried around the wires in the vapor stream lines, owing to the inertial forces overcoming the tendency of these particles to follow the path of the vapor stream lines.

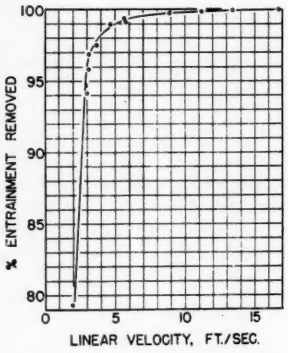

Fig. 2. Experimental efficiency of 24½-in. separator as a function of the superficial linear velocity.

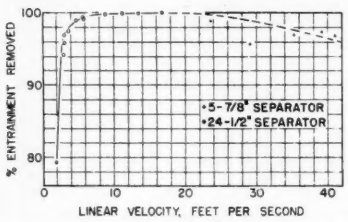

Fig. 3. Experimental efficiency of 24½- and 5⅞-in. separators as a function of the superficial linear velocity.

Then, too, the size of the droplets passing the settling space and reaching the separator will increase with increasing vapor velocity; and, since the large droplets will be less likely to be carried in the vapor stream lines, a larger proportion of them will be captured by collision with the wires. This increase in efficiency continues, reaching nearly 100% between linear velocities of 10 to 20 ft./sec. Above these velocities it was visually observed that free drainage of the separator, under the influence of gravity, is impeded by the rising vapors, and the separator begins to give evidence of liquid buildup or overload on its component wires. At sufficiently high velocities the effect of gravity and surface tension is overcome by the pressure of the rising vapors; and, at least some of the liquid film enveloping the wires comprising the separator and representing entrainment captured by the separator is swept upward to the top layer of the separator and there, when presenting a sufficiently large surface area to the rising vapors, is torn from the wires on the top surface and carried downstream from the separator as reentrainment. Thus reentrainment may be defined as entrainment that, initally removed by the separator, eventually escapes by being torn from the elements or wires of the separator in contrast to entrainment escaping the separator by virtue of its failure to make physical contact with any of these elements or wires of the separator.

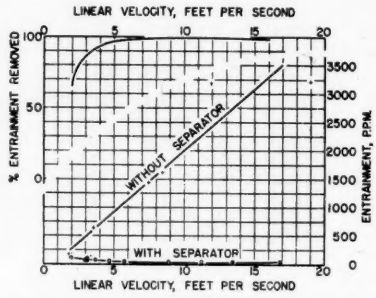

Fig. 4. Entrainment in return line after 24½-in. orifice with and without separator and calculated experimental efficiency, all as a function of the superficial linear velocity.

Reentrainment is clearly indicated in Figure 3 by the extrapolation of the line representing the performance of the 24½-in. separator through the area and into that which represents the performance of the 5⅞-in. separator. It is evident that there is a limited range of vapor velocities where the separator acts with high efficiency. It might be desirable in commercial practice to control the velocity through the separator with changing operating throughputs by partially closing the section weir of the separator with a shield to reduce its cross-sectional area and thus to increase the velocity to an optimum condition. Low separator efficiencies at the lower velocities are due largely to entrainment particles moving with the vapor stream around the wires in the separator, whereas at the higher velocities they are due to liquid build-up or overload on the wires, resulting in reentrainment. The reentrainment as shown by the experimental data was easily confirmed by the visual evidence obtained by looking through the sight glasses.

Figure 4 expresses, as a function of vapor velocity, the amounts of entrainment in the return line with and without the 24½-in. separator. The efficiency of the separator is also expressed in terms of percentage of entrainment removed as a function of the linear velocity. The efficiency of the separator at any velocity is determined by measurement of the difference in entrainment in the return line, as shown by the two lines illustrating the performance with and without the separator at that velocity divided by the entrainment without the separator at the same velocity. The data thus obtained at several

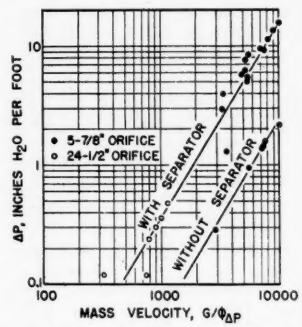

Fig. 5. Pressure drop as a function of mass velocity modified for vapor density.

velocities were then plotted with the result as shown in the curve above the two lines. This curve shows that the efficiency of the separator determined in this manner is in very good agreement with the efficiency given in Figure 2, as determined by Equation (6).

Photographic Examination of the Entrainment

Dappert (*5*) made a photographic study of the size and distribution of the entrainment particles in some of the runs. His photographs showed that sizes of the particles before the separator varied widely and that the reentrained particles above the separator were large. The formation and growth of the reentrained particles could be seen

as they collected on the top side of the separator and finally as they were torn off and projected upward into the vapor stream.

Pressure Drop

The upper line in Figure 5 represents the pressure drop in inches of water per foot of separator thickness; and the lower line shows the pressure drop between the same two points without the separator in place as a function of the mass velocity, as corrected for vapor density (*31, 34*). The actual pressure drop due to the separator at any selected velocity can be directly determined by noting the difference between the two lines at that velocity. The pressure drop caused by the separator is small and varies from about 0.1 to 13 in. of water/ft. of separator thickness as the corrected mass velocity varies from 400 to 10,000 lb. of vapor/(hr.)(sq.ft.). At the higher pressure drops shown in Figure 5 the separator was reentraining severely. However, when no visual reentrainment was observed at corrected mass velocities of 1,000 or less, the pressure drop was found to be less than 0.5 in. of water/ft. of thickness of separator. It should be noted that the pressure-drop curve is continuous, without a break, an indication that under the conditions of operation there was no tendency for the separator to "flood," in the sense of a packed column, even when reentrainment was severe.

MECHANISM OF THE CAPTURE OF ENTRAINMENT BY THE SEPARATOR

The geometry of a knitted-wire-mesh separator is very complex compared with that of a single unbent component wire. However, there is a certain degree of regularity in a knitted-wire-mesh separator resulting from the uniform and more or less parallel spacing of wires by means of equally spaced knitting needles used in the fabrication of the tubular stocking described earlier. Furthermore, the crimping also gives a regularity, if not a parallelity, to the spatial arrangement. Incidentally, others [Lapple (*21*) and Houghton and Radford (*17*)] say that the efficiency of a multiplicity of targets (wires) may be a derived function of the efficiency of single target (wire).

Langmuir and Blodgett (*22*) in their study for the Air Technical Service Command of the Army Air Forces were concerned with the formation of ice on the leading edge of the wing of an airplane; and since these leading edges are cylindrical (24 in. or more in diameter) they considered the effect of projecting water droplets at a cylinder oriented with its axis perpendicular to the motion of the droplet approaching from a great distance. With the aid of the General Electric differential analyzer, the trajectories of such droplets were traced as they approached the cylinder, and their deflection around or removal by filming on the cylinder was determined. This concept of the mechanism of the capture of a particle by a cylindrical surface of comparatively tremendous size has been considered with the necessary modifications which have been developed relating to a maze of very small cylindrical surfaces in the interpretation of the present experimental data.

The evaluation of the maximum total efficiency of deposition of particles on a cylinder was in terms of the ratio of the droplets impinging under the conditions of operation to the droplets that would impinge if the drops were to travel in straight lines without deflection by the vapor stream lines around the cylinder. This maximum total efficiency of deposition of particles, E_M, is dependent upon the vapor velocity, drop velocity, vapor viscosity, vapor density, drop density, drop radius, and cylinder radius.

It was thus desired to find whether the fundamental work of Langmuir and Blodgett on single cylindrical surfaces as targets is applicable to the performance of a separator of very small cylindrical surfaces as targets in layers and groups of layers.

The knitted-wire-mesh separator may be considered to consist of a number of more or less parallel layers of wire formed by interlocked wire loops. When a knitted-wire-mesh stocking is flattened to form a ribbon and this ribbon of double thickness is then crimped and rolled spirally upon itself to form such a separator, a considerable amount of the total wire in the separator opposes the passage of entrainment through the separator, even though only about 2% of the total volume is occupied by wire; and the space between the wires is very large compared with the size of the entrainment particles. The remaining wire in the separator, which is not particularly effective in opposing the passage of entrainment, acts as the spacer elements maintaining the layers of wire opposing the passage of entrainment a uniform distance apart. It is possible to vary the distances between layers during fabrication of a separator. By nature of the knitting process the average distance between layers in the separator used was about 0.1 in. although the actual distances between layers were alternately about 0.05, 0.15, 0.05, 0.15, etc., in., respectively. For the purpose of this analysis it has been assumed that the alternately close and wide separations between layers, averaging about 0.1 in., are relatively large by comparison with the diameters of the entrainment particles passing into the interior of the separator or through the separator without capture, so that the entrainment progressively redistributes itself uniformly among the layers of wire during its carry through the separator by the vapor itself.

Since the wires in the separator are cylindrical, it is possible to set up an expression including the conditions of the experiment and the maximum total efficiency of deposition, E_M, as previously determined for a single cylinder. From this expression the efficiency of the separator can be predicted for the conditions of (*a*) uniform particle size, (*b*) no reentrainment, (*c*) no build-up of liquid in the separator during the experiment, and (*d*) uniform redistribution of particles between layers. (These will be called hereinafter the four basic conditions.) The basis of such an expression is the assumption that each layer in the separator has the same entrainment-removal efficiency. Then the fraction of entrainment escaping a single layer may be expressed as

$$(1 - E_M/c) \qquad (7)$$

where E_M = maximum total efficiency of deposition of particles for a single filament of the separator, fraction recovered, for conditions of operation and c = modifying characteristics of the separator.

Since it has been assumed that each layer in the separator has the same entrainment removal efficiency, it follows that the fraction of entrainment escaping the separator is equal to the fraction of entrainment escaping a single layer raised to a power equivalent

to the number of parallel layers in the separator:

$$(1-E_S') = (1-E_M/c)^N \text{ or } E_S' = 1-(1-E_M/c)^N \qquad (8)^*$$

where c, the modifying characteristic of the separator, is a function of the effective area of the separator in each layer and is expressed as the fraction of the total flow cross section obstructed by wire in a single layer:

$$c = N/kF \qquad (9)$$

The modifying characteristic of the separator, c, used in this research has been evaluated from its physical properties as follows:

N = forty-eight layers in separator perpendicular to flow

F = 0.67, the fraction of the total wire in an effective position as evaluated by inspection of the separator and measurement of the length of wire in the separator perpendicular to and parallel to the superficial flow through the separator

k = 10.601 is evaluated by combining the cross-sectional area of the 24½-in. orifice of 3.2739 sq. ft. with the 0.0113-in. (9.4167×10^{-4} ft.)-diam. wire and the estimated wire length of 36,856 ft. (0.0113-in.-diam. copper wire of 556.88 lb./cu.ft. density weighing a total of 14.3 lb.) to give

$$k = \frac{36{,}856 \times 9.4167 \times 10^{-4/3}}{3.2739} = 10.601$$

then

$$c = 48/(10.601 \times 0.67) = 6.748$$

from substitution in Equation (9).

Equation (8) may be used to predict theoretically the efficiency of a separator when N, c, and E_M are known and the four basic conditions hold. It will be noted that Equation (8) predicts a straight-line correlation for a logarithmic plot of entrainment escaping a single layer of the separator vs. the entrainment escaping the entire separator. The slope of such a plot represents the number of layers in the blanket.

N and c depend upon the physical configuration of the blanket. E_M is evaluated by the wire radius, particle radius, and conditions of operation. Langmuir and Blodgett prepared tables of K, ϕ, and E_M and plotted K vs. E_M, with ϕ as the other parameter, for single cylinders (Figure 6), where

$$K = 2d_l\, Ua^2/9\eta C \qquad (10)$$

$$\varphi = 18\,(d_v)^2\, CU/\eta\, d_l \qquad (11)$$

are dimensionless ratios in which

a = radius of liquid drop, cm.

C = radius of cylinder (wire), cm.

d_l = density of liquid drop, g./cc.

d_v = density of vapor, g./cc.

η = viscosity of vapor, poises, g./cm.sec.

U = vapor velocity, cm./sec.

The theoretical efficiencies of the separator have been calculated by means of Equations (8), (9), (10), and (11) for the four basic operating conditions with 6-, 7-, and 8-μ-diam. particles, and these theoretical efficiencies have been tabulated in Table 2*, together with the experimentally determined efficiencies. These efficiencies are graphically represented in Figure 7 as a function of the linear velocities. Examination of the lines shows them to be smooth curves and demonstrates that the efficiency of the separator should increase in all cases with increase in velocity until 100% is reached.

COMPARISON OF THEORETICAL WITH EXPERIMENTALLY DETERMINED EFFICIENCY OF THE SEPARATOR

The experimentally determined efficiencies plotted against linear vapor velocities are represented in Figure 7 by small circles; a smooth line is drawn through them.

Examination of the theoretical curves in Figure 7 shows a wide divergence in efficiencies for particles of 6-, 7-, and 8-μ-diam. at low vapor velocities, but at higher vapor velocities the curves or efficiencies all merge and closely agree, irrespective of size in this range. It is also to be noted that the separator operates better for larger than for smaller particles at low vapor velocities. Comparison of the experimental curve with the theoretical curves indicates that the entrainment encountered in the experiments at low vapor velocities is made up of particles of small diameters; but as the vapor velocity increases, the average diameter of particles reaching the separator increases — finally indicating an average of more than 8 μ.

Examination of the experimental curve shows that the efficiency of the separator for removal of particles of many sizes increases as the vapor velocity increases, which is in agreement with the theoretical curves for a single particle size. The particles reaching the actual separator constantly increase in size as the vapor velocity increases, because at lower velocities the large particles settle out below the entrainment separator. This accounts for the steep slope of the curve at the low vapor velocities where not only the velocity but the size of particles is an important factor in influencing the efficiency of the separator.

Study of the curves, both theoretical and experimental, suggests that particle size is the main influence in determining the efficiency of any particular separator at low vapor velocities, while vapor velocity has a much greater influence in determining the efficiency of the separator at the higher vapor velocities. When, however, the theoretically or the experimentally determined efficiency approaches 100%, there seems to be little change in the efficiency either by change in size of particles or in vapor velocity; i.e., the spread between curves of different particle size is not great and the curves are quite flat near 100%. This high efficiency continues with increase in velocity until the separator becomes overloaded and reentrainment in significant amount takes place.

The experimental evidence is in agreement with the theoretical prediction based on the mechanism of capture of particles by a single cylinder and adapted to the performance of the complex, multiwire maze comprising the knitted-wire-mesh separator. This evidence supports the assumption that the wires of the separator furnish targets with which the particles must collide in order to be captured as a result of the envelopment of the separator wires with a thin liquid film which may then be drained free from the separator and recovered. The separator as used in this experimental work behaved as an impingement-type, inertial entrainment eliminator.

An interesting application of this type of entrainment elimination is illustrated by the work of Hough-

*This equation is in agreement with an expression given by Houghton and Radford(17).

ton and Radford in the design of their streamlined unit with staggered arrangement of the targets for removal of large particles, average 40 μ and some as large as 60 μ.

Another recent application of the staggering principle is the use of the random arrangement of small fibers of a glass-wool separator for removal of the very fine mists which fail to be trapped by other eliminators [cf. the report by Hammond and Leary (*15*)]. These glass-wool separators, like the knitted-wire-mesh separators, cause very little pressure drop. Rodebush (*30*) in speaking of filters for aerosol particles points out that when the mesh consists of "loosely aggregated fibers, and to avoid excessive resistance to the flow of air, the mesh of the filter must be large compared to the size of the particle to be removed" and that "the particles most difficult to remove by filtration are those in the range of 0.1 to 1 μ. . . . In order to obtain efficient filtration without excessive resistance the filter must contain

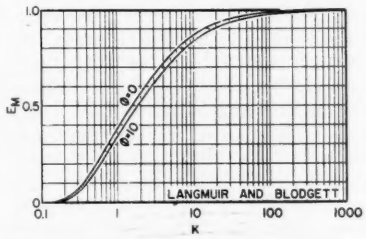

Fig. 6. Efficiency of deposition on cylinders, E_M, with ideal fluid flow (*22*).
$K = 2d_l Ua^2/9\eta C$ and $\phi = 18(d_c)^2 CU/\eta d_l$

fibers of small diameter approaching that of the particles themselves."

THEORETICAL DETERMINATION OF THE INFLUENCE OF THE EFFICIENCY OF THE SEPARATOR BY DECREASE IN WIRE DIAMETER

The evidence already presented has emphasized how vapor velocity and particle size affects the efficiency of the separator as an entrainment eliminator when the four basic conditions hold. Examination of the equations used in developing the theory of the mechanism by which particles are captured shows that there may be made mechanical modifications of the separator which would improve its efficiency. Examination of the previously used equations

$$K = 2d_l Ua^2/9\eta C \qquad (10)$$

$$\phi = 18(d_c)^2 CU/\eta d_l \qquad (11)$$

shows that any change in C, the radius of the wire, would directly change the values of both K and ϕ. For illustration, if C is divided by 2, K is doubled and ϕ is halved.

As an example, the effect on K may be considered when the diameter is divided by 2 and the length of the wire is multiplied by 2 in order to keep the target area constant. If $K = 1$ and 2, respectively, the effect upon E_M, the maximum total efficiency of deposition, for a single cylinder can be determined by reference to Figure 6 for any given value of the parameter (ϕ).

It will be noted that a change in K produces a marked change in E_M over a wide range of values for K. For the parameter $\phi = 0$ when $K = 1$, $E_M = 0.386$, and when $K = 2$, $E_M = 0.565$, there is an increase in target efficiency of 46.4%. If the values are substituted in Equation (8),

$$E_S' = 1 - (1 - (E_M/c))^N \qquad (8)$$

the expression developed to give the theoretical efficiency of the separator where c is the modifying characteristic of the separator and has been calculated as 6.748 for the separator used in this research $E'_S = 0.9408$ for $K = 1$ and $E'_S = 0.9850$ for $K = 2$ for forty-eight target layers ($N = 48$). This represents an increase in the separator efficiency of 4.7%. Inspection of Figure 6 shows a similar effect if the parameter (ϕ) selected is 10. The parameter (ϕ) for the separator is about 0.0888, the average of column 7, Table 2.*

Interpreting these values for E'_S by reference to the curves in Figure 7 shows that for the 8-μ curve an increase in efficiency from 94.08 to 98.50% would be obtained by changing the vapor velocity from 1.8 to 3.2 ft./sec., for the 7-μ curve from 2.2 to 4.0 ft./sec., for the 6-μ curve from 2.9 to 5.4 ft./sec., and for the experimental curve from 2.8 to 4.4 ft./sec.

If the same total projected area of target is maintained, there are other consequences resulting from decreasing the wire diameter with a corresponding increase in wire length or from increasing the frequency of wires:

1. In the case just considered there would be twice as many target wires in each layer; and although the total target area of the wire and the interstices for the passage of vapor remains constant, each interstice would be just half as wide as the original.

2. Since the wire is one half the original diameter and only twice as long, the total volume occupied by the wire is only one half that of the volume of the original wire and therefore requires only one half the weight of metal.

3. Since the wire is one half the diameter, the distance between the layers is slightly increased, and the total free space in the blanket would be increased from 98 to 99%.

In general, to decrease the diameter of the target wire n times and multiply its length n times, while maintaining the same total projected area of target, would increase the number of targets in each layer n times and reduce the weight of metal required to $(1/n)$th of the original conditions.

Possibility of such an improvement in the theoretical efficiency of the separator by changing the diameter of the wire depends upon the physical properties of the wire which would permit the drawing of the wire to a smaller diameter and its fabrication in a knitting machine. Separators made of stainless steel wire of much smaller diameter than was used in these experiments have been successfully fabricated and used.

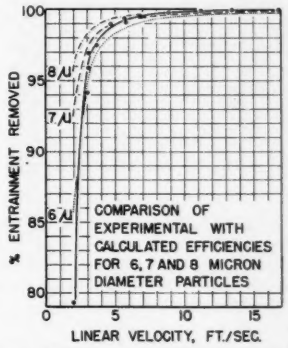

Fig. 7. Theoretical efficiency without reentrainment of 24½-in. separator as a function of the superficial linear velocity for 6-, 7-, and 8-μ diameter particles as compared with the experimental results.

THEORETICAL DETERMINATION OF THE INFLUENCE OF THE THICKNESS OF THE SEPARATOR ON ITS EFFICIENCY

Since the theoretical efficiency of the separator, based on the assumptions above, can be calculated

$$E_S' = 1 - (1 - (E_M/c))^N \qquad (8)$$

from the expression where N is the number of target layers in the

*Available as document 4733 from the Photoduplication Service, American Documentation Institute, Library of Congress, Washington 25, D. C., for $1.25 for microfilm or photoprints.

separator, the expression can be solved for separators having any chosen number of target layers by substituting for N any number desired. For example, it is possible to predict the efficiency of a wire-mesh separator for three, six, twelve, twenty-four, forty-eight, and ninety-six target layers, separator thicknesses of ¼, ½, 1, 2, 4 and 8 in., respectively, for any size of particles when the four basic conditions hold. The total projected area of wire in the separator opposing the passage of entrainment is directly proportional to the number of target layers or thickness of the separator.

E_M and E'_S have already been calculated for particles of 8-μ diam. as recorded in columns 10 and 13 of Table 2*; c is a constant, and $1/c = 0.14819$ for the separator used in these experiments. The theoretical efficiency, E'_S, of separators with three, six, twelve, twenty-four, forty-eight, and ninety-six target layers as elimi-

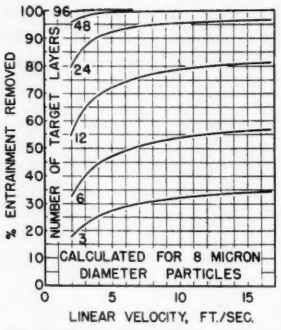

Fig. 8. Theoretical effect of number of target layers on efficiency without reentrainment of 24½-in. separator as a function of the superficial linear velocity for 8-μ diameter particles.

nators for particles 8 μ in diameter for the conditions of each of the runs have been calculated and recorded in Table 3*; and E'_S is plotted for each thickness of separator against linear velocity in Figure 8.

Examination of the curves in Figure 8 shows the effect of the number of target layers or separator thickness, or, therefore, the total projected area of the wires opposing the passage of entrainment through the separator, on the efficiency of the separator for particles having a diameter of 8 μ. The separator used in the experimental work had forty-eight target layers, and it is seen from Figure 8 that except at velocities below 4 or 5 ft./sec. there would be little advantage to be gained in doubling the number of target layers to ninety-six. It is also seen that high efficiencies could not be expected with fewer than twenty-four target layers.

*See footnote on page 555.

DESIGN FACTORS OF A KNITTED-WIRE-MESH SEPARATOR

In order best to recommend the fabrication of a knitted-wire-mesh separator of the type used in the present experimental work, as much as possible should be known about the size of the particles and the vapor velocities carrying the entrainment to be removed. For example, reference to Figure 8 shows that a forty-eight-target-layer separator has an efficiency of about 95.5% at a linear velocity of 2 ft./sec. for conditions of operation used in the experimental work. The same figure indicates that an efficiency of about 99.8% could be realized under the same conditions of operation if the number of target layers were to be doubled to ninety-six, thus requiring double the weight of metal and thereby providing twice the total projected area of wire opposing the passage of entrainment as in the forty-eight-layer separator. However, if a forty-eight-layer separator having double the length of wire of one half the diameter, were used, so that the same total projected area of the forty-eight-target-layer separator used in the experimental work might be maintained, it is calculated that an efficiency of 98.8% would be realized.

Thus almost the same improvement in efficiency may be obtained by reducing the diameter of the wire to one half and simultaneously doubling its length as can be obtained by doubling the thickness of the separator. It would therefore require four times as much wire, by weight, to fabricate the ninety-six-layer separator as to fabricate the forty-eight-layer separator from a wire one half the diameter of the wire used in the ninety-six-target-layer separator. The percentage of efficiency improvement is about the same in either case (3.5 vs. 4.5%) although doubling the separator thickness is somewhat more effective.

In general, the greatest improvement which may be made with a separator having a given total projected area of the component wires would be to reduce the diameter of the wire as much as possible and increase the vapor velocity as long as inertial effects rather than diffusional effects are controlling. The reduction in the wire diameter would be the most effective improvement for capture of small particles, but the physical properties of the material used in making the wire and fabricating it in a machine will control the extent to which a reduction in wire diameter becomes possible or practical. The particle-size range where diffusional and inertial effects are in transition is a function of the system. In the steam-brine system employed under the conditions of operation in this study it is theoretically indicated that the threshold where diffusional forces take over is in the range of particle diameters less than 1 to 3 μ. In the air-water system the threshold range would be for particle diameters somewhat larger owing primarily to the greater viscosity of air than of steam.

CONCLUSIONS

The results showed that the wire-mesh separator used in these experiments was a poor eliminator of the entrainment carried in the vapor stream above a boiling solution in an evaporator at low vapor velocities, but its effectiveness increased very rapidly as the vapor velocity increased. At linear velocities of 2, 9, and 17 ft./sec., 79, 99.8, and 99.9%, respectively, was removed. This high efficiency continued until the velocities approached 20 ft./sec. It was in this area that the separator became overloaded and reentrainment took place.

There was developed an equation

$$E_S = 1 - (1 - (E_M/c))^N \quad (8)$$

which correlated very well the actual experimental performance of the separator used for the capture of entrainment particles of mixed size in a vapor stream. The assumptions were (*a*) uniform particle size, (*b*) no reentrainment, (*c*) no modifying build up of liquid, and (*d*) constant entrainment-removal efficiency in each layer of the separator by virtue of uniform redistribution of particles after passage through each layer. This redistribution assumption is reasonable since the distances between layers in the separator were relatively large compared with the diameters of the particles not removed in the first layer of the separator which passed into the interior of the separator before capture or through the separator without capture.

The efficiency of the separator as predicted by Equation (8) agreed very favorably with the experimentally determined performance. It is therefore possible to predict the area wherein 100% removal is approached for this type of separator with the aid of Equation (8) and to recommend specifications for the fabrication of a separator for the most effective performance when the nature of the entrainment and the conditions of operation are known.

ACKNOWLEDGMENT

The authors are grateful to the Vulcan Copper and Supply Company, which furnished the separator housing-disengaging chamber, cover, and gooseneck vapor draw-off sections of Figure 1 as additions of their standard laboratory evaporator unit already installed; to Otto H. York Company, Inc., for the separators; to International Salt Co. for the salt which was used in making the brines; and to Natural Products Refining Company for the chromates used as corrosion inhibitors in the salt solutions.

NOTATION

a = radius of liquid drop, cm.

c = modifying characteristic of separator, defined by Equation (9), the fraction of the total flow cross section obstructed by wire in a single layer

C = radius of cylinder (wire), cm.

d_l = density of liquid drop, g./cc.

d_v = density of vapor, g./cc.

E_M = maximum total efficiency of deposition of particles for a single filament of the separator, fraction recovered, for conditions of operation

E'_S = theoretical efficiency of separator, fraction recovered, for the four basic conditions of operation, defined by Equation (8)

E_S = experimental efficiency of separator, defined by Equation (6)

F = fraction of total separator wire in effective position

G = mass velocity in orifice, lb./(hr.)(sq.ft.)

k = dimensionless ratio; product of diameter and length of wire in N layers of the separator divided by the area occupied by the separator perpendicular to the flow—used in evaluating c, the modifying characteristic of the separator

K = dimensionless ratio due to Langmuir and Blodgett(*22*), defined by Equation (10)

M = pounds of main body of evaporating liquid reaching point P as entrainment

n = an arbitrary number

N = number of layers in the separator perpendicular to the flow through the packing.

p = concentration of sodium chloride present in the entrained liquid together with the vapor associated with the entrained liquid at any point P after the separator in pounds sodium chloride per pound of vapor plus entrainment. (When vapor is condensed this becomes pounds sodium chloride per pound of solution.)

P = any point after the separator, i.e., evaporator recycle stream

q = concentration of sodium chloride present in the entrained liquid together with the vapor associated with the entrained liquid at any point Q just ahead of the separator in pounds sodium chloride per pound of vapor plus entrainment. (When vapor is condensed this becomes pounds sodium chloride per pound of solution)

Q = any point ahead of the separator, i.e., just preceding separator

s = concentration of sodium chloride in main body of evaporator in pounds sodium chloride per pound of solution

U = vapor velocity, cm./sec.

v = specific volume of saturated steam, cu.ft./lb.

V = superficial linear velocity at flow conditions, ft./sec.

z_p = pounds solvent reaching point P as vapor

Greek Letters

η = viscosity of vapor, poises (g./cm.sec.)

ϕ = dimensionless ratio due to Langmuir and Boldgett(*22*), defined by Equation (11)

$\phi\Delta_P = (0.075v)^{-\frac{1}{2}}$ factor correcting for gas density for pressure-drop correlation

μ = micron, 1 micron = 10^{-6} meter

Subscripts

P = after separator

Q = before separator

LITERATURE CITED

1. Ashraf, F. A., T. L. Cubbage, and R. L. Huntington, *Ind. Eng. Chem.*, **26**, 1068 (1934).
2. Campbell, J. A., *Petroleum Eng.*, **22**, C-17 (1950).
3. Cessna, O. C., and W. L. Badger, *Ind. Eng. Chem.*, **26**, 485 (1934).
4. Colburn, A. P., *Ind. Eng. Chem.*, **28**, 526 (1936).
5. Dappert, G. F., M. Ch.E. thesis, Polytech. Inst. Brooklyn (1950).
6. Eduljee, H. E., *Trans. Inst. Chem. Engrs. (London)*, **24**, 128 (1946).
7. Foulk, C. W., *Ind. Eng. Chem.*, **21**, 815 (1929).
8. ———, and N. C. Brill, *loc cit.*, **27**, 1430 (1935).
9. ———, and K. Groves, *loc. cit.*, **25**, 800 (1933).
10. ———, V. L. Hansley, *loc. cit.*, **24**, 277 (1932).
11. ———, J. M. Miller, *loc. cit.*, **23**, 1283 (1931).
12. ———, and J. W. Ryzner, *loc. cit.*, **31**, 722 (1939).
13. ———, and R. Ulmer, *loc. cit.*, **30**, 159 (1938).
14. ———, and S. F. Whirl, *loc. cit.*, **26**, 263 (1934).
15. Hammond, R. P., and J. A. Leary, in consultation with C. S. Leopold, "Air Decontamination Test with Baffle Plate Towers, Capillary Washers and Fiberglas Pads," LA-1145, Los Alamos Scientific Laboratory of the University of California (September, 1950).
16. Holbrook, G. E., and E. M. Baker, *Ind. Eng. Chem.*, **26**, 1063 (1934).
17. Houghton, H. G., and W. H. Radford, *Trans. Am. Inst. Chem. Engrs.*, **35**, 427 (1939).
18. "International Critical Tables," Vol. III., p. 79, McGraw-Hill Book Company, Inc., New York (1928).
19. Keenan, J. H., and F. G. Keyes, "Thermodynamic Properties of Steam."
20. Keyes, D. B., and A. G. Deem, "Chemical Engineers' Manual."
21. Lapple, C. E., in "Chemical Engineers' Handbook," J. H. Perry, ed., 3 ed., p. 1013 McGraw-Hill Book Company, Inc., New York.
22. Langmuir, I., and K. B. Blodgett, *U. S. Army Air Forces Tech. Rept.* No. 5418 (1946).
23. Lowrie-Fairs, G., *Trans. Inst. Chem. Engrs., (London)*, **22**, 116 (1944).
24. Montross, C., *Chem. Eng.*, **60**, No. 10, 213-236 (October, 1953).
25. O'Connell, H. E., and E. S. Petty-John, *Trans. Am. Inst. Chem. Engrs.*, **42**, 795 (1946).
26. Pollak, A., and L. T. Work, *Trans. Am. Soc. Mech. Engrs.*, **64**, 31 (1942).
27. Rhodes, F. H., *Ind. Eng. Chem.*, **26**, 1333 (1934).
28. *Ibid.*, **27**, 272 (1935).
29. ———, and P. G. Slachman, *Ind. Eng. Chem.*, **29**, 51 (1937).
30. Rodebush, W. H., "Handbook on Aerosols," U. S. Atomic Energy Commission (1950).
31. Schoenborn, E. M., and W. J. Dougherty, *Trans. Am. Inst. Chem. Engrs.*, **40**, 51 (1944).
32. Sherwood, T. K., and F. J. Jenny, *Ind. Eng. Chem.*, **27**, 265 (1935).
33. Souders, M., and G. G. Brown, *Ind. Eng. Chem.*, **26**, 98 (1934).
34. Tillson and others in "Chemical Engineers' Handbook," J. H. Perry, ed., 3 ed., p. 680 (1950).
35. York, Otto H., *Chem. Eng. Progr.*, **50**, 421 (1954).

(Presented at A.I.Ch.E. Washington meeting)

Communications

Physical Properties of Organic Acids

Morris Eisenberg, Pin Chang, Charles W. Tobias, and C. R. Wilke
University of California, Berkeley, California

Studies of rates of dissolution of organic acids are frequently used as a technique in mass transfer investigations. These substances can be readily molded and machined into various shapes of well-defined geometry. Their solubilities lie in a convenient range, and analytical procedures are simple. Further, existing evidence indicates their rate of dissolution to be mass transfer controlled with no appreciable interfacial resistance (*1, 2*).

Paucity of data on densities, viscosities, and diffusion coefficients in aqueous solutions necessitated the measurement of these properties adjunct to mass transfer studies undertaken by the authors (*1, 2, 3*). The following standard procedures were employed.

1. *Solubilities* were obtained by equilibrating the given solute with water in a 1,000-cc. flask shaken in a carefully controlled (±0.05°C.) thermostat. Twelve- to fifteen-hour periods were allowed for an equilibration at a given temperature. In special experiments, in which samples were withdrawn at various time intervals, it was found that no detectable concentration change occurred after about 3 to 4 hr. After equilibration the solution was filtered under pressure through a sintered-glass plate into another flask clamped in the same thermostat. In this manner temperature changes during filtration were avoided. Samples of 25 cc. were titrated with a standardized sodium hydroxide solution. Reproducibility was within ±2%.

2. *Viscosities* of the saturated solutions were measured with an Ubbelohde type of effusion vicosimeter. Prior to and during the determinations the solution was thermostated (±0.05°C.). Distilled water was used for calibration. The effusion times were reproducible within less than 1%.

3. *Densities* were determined by means of a 50-cc.-capacity carefully thermostated pyknometer. Distilled water was used for calibration. The density values could easily be reproduced within unity in the fourth place.

4. *Diffusion coefficients* were obtained by a McBain-Northrup type (*3*) of diaphragm cell, consisting of an approx.-3-mm.-thick, 5-cm.-diam. glass diaphragm separating two compartments of about 80 to 100 cc. volume. The cell was calibrated by use of a 0.075 *N* potassium chloride solution at 25°C. Saturated or near-saturated solutions were brought into contact through the diaphragm with pure solvent, diffusion taking place for periods of 4 to 5 days. At the conclusion both compartments were analyzed for acid content. The values presented are averages of several independent measurements, with a maximum deviation of approximately ±1.5% (*4*).

Table 1.—Physical Properties of Benzoic Acid–Saturated Aqueous Solutions

T, °C.	Solubility, g. moles/liter	Density, g./cc.	Viscosity, cps
22	.025.40	0.99836	
23	.026.05	0.99817	0.934
25	.027.46	0.99776	0.894
26	.028.33	0.99754	0.077
27	.029.36	0.99726	0.861

Table 2.—Physical Properties of Cinnamic Acid–Saturated Aqueous Solutions

T, °C.	Solubility, g. moles/liter	Density, g./cc.	Viscosity, cps
22	.003.17	0.9986	
23	.003.26	0.9983	0.935
24	.003.36	0.9980	0.915
25	.003.45	0.9978	0.895
26	.003.54	0.9975	0.876
27	.003.63	0.9973	0.857

Table 3.—Physical Properties of a 4.44-*M*. Glycerol-Water Solution Saturated with Benzoic Acid

T, °C.	Solubility, g. moles/liter	Density, g./cc.	Viscosity, cps
22	.038.0	1.1035	3.526
23	.039.6	1.1029	3.433
24	.041.1	1.1023	3.340
25	.042.7	1.1017	3.339
26	.044.3	1.1012	3.247
27	.045.8	1.1007	3.154
28	.047.3	1.1001	3,061
29	.048.9	1.0996	2.968
30	.050.5	1.0990	2.875

Table 4.—Physical Properties of a 3.65-*M*. Glycerol-Water Solution Saturated with Benzoic Acid

T, °C.	Solubility, g. moles/liter	Density, g./cc.	Viscosity, cps
20	.030.2		
21	.031.2		
22	.032.4	1.0761	2,540
23	.033.53	1.0755	2.442
24	.034.65	1.0749	2.343
25	.035.79	1.0743	2.244
26	.036.95	1.0738	2.043
27	.038.16	1.0734	2.045
28	.039.45	1.0729	1.946
29	.040.78	1.0724	1.848
30		1.0720	1.749

Table 5.—Physical Properties of Salicylic Acid–Saturated Aqueous Solutions

T, °C.	Solubility, g. moles/liter	Density, g./cc.	Viscosity, cps
22	.013.9		
23	.014.7		
24	.015.5	0.99764	0.911
25	.016.3	0.99740	0.896
26	.017.0	0.99716	0.873
27	.017.8		

Table 6.—Diffusion Coefficients

Substance	Temperature, °C.	Coefficient $D \times 10^{-5}$ sq. cm./sec.
Benzoic acid	30	1.06
Benzoic acid in 4.44-molal glycerol solution	30	0.33
Salicylic acid	30	1.24
Cinnamic acid (*5*)	25	0.91

Literature Cited

1. Wilke, C. R., M. Eisenberg, and C. W. Tobias, *Chem. Eng. Progr.*, **49**, 663 (1953).
2. ———, *Chem. Eng. Progr. Symposium Series*, **51**, No. 16, 1 (1955).
3. Gordon, A. R., *Ann. N. Y. Acad. Sci.*, **46**, 285 (1945).
4. Chang, Pin, and C. R. Wilke, *J. Phys. Chem.*, **59**, 592 (1955).
5. Chang, S., M.S. thesis, Mass. Inst. Technol., Cambridge, Mass. (1949).

Morris Eisenberg is at present with Stanford Research Institute, Stanford, California, and Pin Chang is in Taipeh, Formosa.

to the Editor

Shape Factors in Multiple-pipe Systems

Richard C. Faulkner and Robert V. Andrews
Texas Agricultural and Mechanical College System, College Station, Texas

Problems in conductive heat transfer frequently do not lend themselves to simple mathematical treatment. Except for a few geometrical configurations such as parallel plates and concentric cylinders, an exact mathematical solution is often either impossible or difficult, owing to the irregular shape of the body conducting heat and the complicated boundary conditions involved. Through the use of experimentally determined shape factors, many of these problems can be solved easily.

A simple, inexpensive means for the experimental determination of shape factors has been presented by Andrews (*1*). The method consists essentially of drawing with a silver paint on a conducting paper the figure whose shape factor is desired. The electrical resistance of this figure is then compared to the electrical resistance of a standard figure whose shape factor can be calculated mathematically. Equation (1) is then used to calculate the shape factor of the desired figure. The shape

$$\text{shape factor}_{\text{unknown}} = SF_{\text{std.}} \, R_{\text{std.}}/R_{\text{unknown}} \qquad (1)$$

where
SF = shape factor
R = resistance in ohms
factor so determined is then used in Equation (2) to calculate the heat transferred by conduction. Figure 1 shows the electrical circuit used to obtain accurate values of the resistances which are used in Equation (1).

$$q = -k\,(SF)\,(\Delta T) \qquad (2)$$

where
k = thermal conductivity, B.t.u./(hr.) (sq.ft.) (°F./ft.)
q = B.t.u./hr.
ΔT = thermal driving force, °F.

The shape factors obtained by this method are independent of the thermal conductivity of the material transferring heat or of the terminal temperatures of the heat flow path. As the units of the shape factor are length, it may be considered to be an effective area for heat transfer divided by a unit effective length of heat transfer path.

The use of buried conduits containing more than one pipe is quite common; i.e., steam tracing in connection with the transportation of substances which may solidify or become viscous if allowed to fall below a certain temperature. Shape factors for such pipe configurations are shown in Figures 2, 3 and 4. In these figures all dimensions are shown as a fraction of D_o, the diameter of the outer conduit containing the multiple pipes. Because of this, the shape factors in the

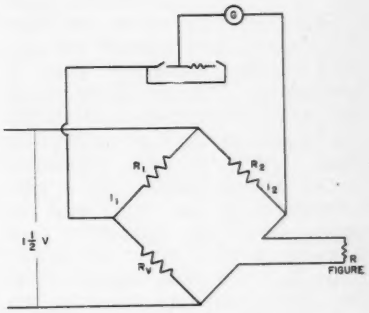

Fig. 1. Effective circuit diagram.

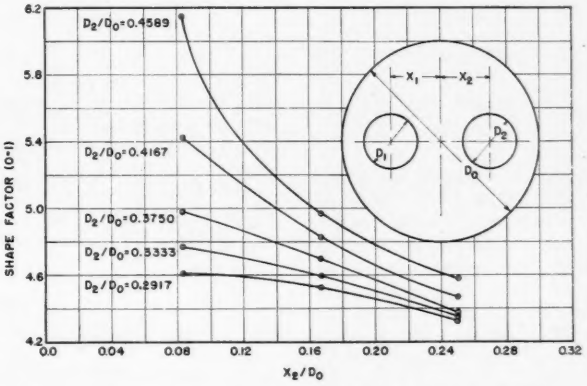

Fig. 2. Shape factor (0-1) vs. x_2/D_0 at $x_1/D_0 = 0.2500$ and $D_1/D_0 = 0.1667$.

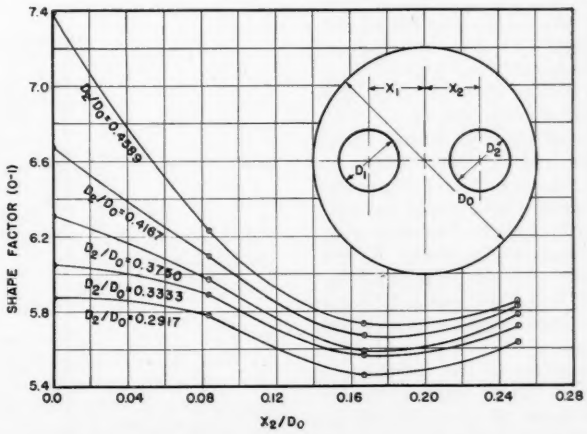

Fig. 3. Shape factor (0-1) vs. x_2/D_0 at $x_1/D_0 = 0.3333$ and $D_1/D_0 = 0.1667$.

figures are not limited to one set of dimensions, but may be applied to any geometry having the same diameter ratio. For example, if $X_2 = 3$ in. and $D_o = 12$ in. or if $X_2 = 1.5$ in. and $D_o = 6$ in., the same ratio of $X_2/D_o = 0.25$ is obtained, and the same shape factor applies. The designation of the pipes inside the conduit as pipe 1 and pipe 2 has no significance except to aid in the use of the curves.

Figures 2 and 3 give values of the shape factor between the outer conduit and either of the two pipes contained in the conduit for certain specific dimension ratios as parameters. Figure 4 gives values of the shape factor between the two pipes contained in the conduit for certain specific dimension ratios as parameters. As a generalization it was found that the shape factor for conductive heat transfer between either of the two pipes and the outer conduit could be approximated by Equation (3) to give an answer accurate within 3% of the correct value.

$$SF_{(0-1) \text{ or } (0-2)} = \frac{6.472}{\cosh^{-1}\left[\dfrac{a_1^2 + a_2^2 - d^2}{2a_1 a_2}\right]} \qquad (3)$$

Equation (3) is actually the equation for the shape factor of heat transfer between cylinders, one inside the other but not concentric. Apparently the presence of the second pipe inside the conduit has little effect on the shape factor for heat transfer between the conduit and the other pipe. Shape factors for heat transfer between the two pipes contained in the conduit did not follow an equation for heat transfer between adjacent cylinders, and no other general correlation for this case was found. Instead, graphical determination of shape factors from Figure 4 or similar curves proved the best method of determination.

For conduits containing three pipes, no general correlation for shape factors was found. Figures 5 and 6 present shape-factor data for a three-pipe conduit of common commercial design. In these figures parameters of $D_1/D_o = 0.5$ and $D_2/D_o = 0.2917$, 0.3333, and 0.3750 are used. In the ranges studied, the shape factors $(0-3)$ and $(1-3)$ are independent of the variation of D_2/D_o. It is also of interest to note that the shape of $(0-3)$ was always larger than that of $(1-3)$ or $(2-3)$. This would indicate that if pipe 3 were to be used for heating, the distance X_3 should be made as small as possible to lower the heat transfer from pipe 3 to pipe 0, and so increase the heat transfer from pipes 3 to 1 and 3 to 2; that is, the heating pipe should be as close to the center of the enclosing conduit as possible rather than merely being located as close as possible to the pipes to be heated.

The two-dimensional method of determining shape factors for multiple-pipe systems which is described here provides a rapid method of solving many of the problems commonly encountered in industry. The method is extremely simple and inexpensive and requires a minimum of equipment and skill.

Literature Cited

1. Andrews, R. V., *Chem. Eng. Progr.*, 51, 67F (1955).

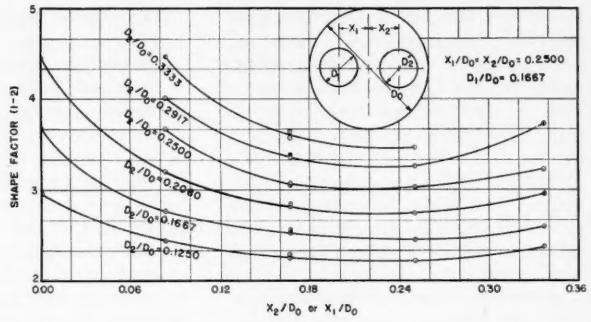

Fig. 4. Shape factor (1-2) vs. x/D_0.

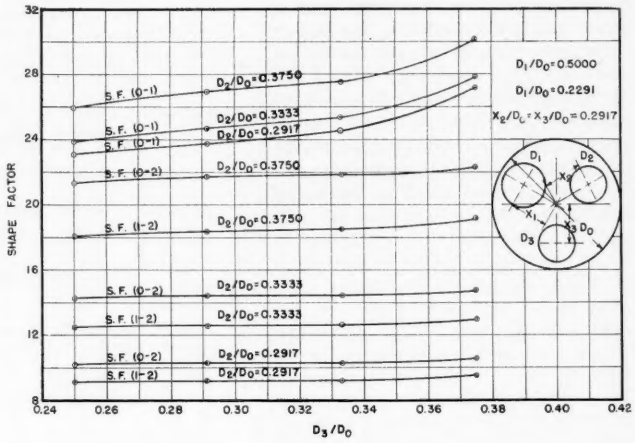

Fig. 5. Shape factor for three-pipe conduit.

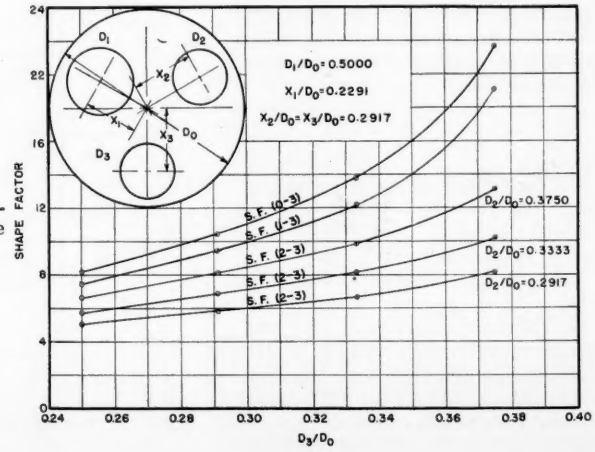

Fig. 6. Shape factor for three-pipe conduit.

Use of Computers in Kinetic Calculations

PER HALLVARD NILSEN
Aktieselskapet Borregaard, Sarpsborg, Norway

The present writer has read the paper by Gee, Linton, Maier, and Raines (*1*) with a great deal of interest. He wishes, however, to make a few comments on two of the four differential equations which the authors developed in order to describe the chemical and physical processes occurring in their tubular reactor. The writer will show that both the kinetic equation [Equation (1), Table 1] and the equation for the pressure drop through the reactor [Equation (2), Table 1] may be somewhat simplified without any loss in rigor.

In the mathematical developments which follow, the writer has adopted the nomenclature of reference *1*.

Kinetic Equation

The kinetic equation [Equation (1), Table 1 (*1*)] was developed by use of concentration units. It should be written

$$\frac{\partial z}{\partial L} = \frac{\pi K\,(1-z)}{4x_o} \cdot \frac{(r-z)}{(r+1-z)^2} \left[\frac{pD}{R\,(273+t)}\right]^2 \qquad (1)$$

Incidentally, there seems to be a typographical error in this equation in reference (*1*), as the factor π in the numerator has been omitted.

The reaction-rate constant K in Equation (1) may, according to Figure 2 in reference *1*, be written

$$K = e^{\left[a - \frac{b}{(273+t)}\right]} \qquad (2)$$

where

K has the units cu.ft./(mole) (hr.)
a and b are constants

However, if in deriving the kinetic equation one uses activities instead of concentration units, the following equation is obtained

$$\frac{\partial z}{\partial L} = \frac{\pi k\,(1-z)}{4x_o} \frac{(r-z)}{(r+1-z)^2} (pD)^2 \qquad (3)$$

where

k has the units moles/(cu.ft.) (hr.) (atm.^{2})

Equation (2) may be written in the Arrhenius form

$$K = Ae^{-\frac{E}{RT}} \qquad (4)$$

where

K = reaction-rate constant
A = a collision factor (same units as K)
E = energy of activation (cal./mole)
R = gas constant (cal./(mole) (°K.)
T = absolute temperature (°K.)

Equation (4) is, however, not rigorous, as the collision factor A is proportional to the molecular velocity, which again, according to the kinetic theory of gases, is proportional to the square root of the absolute temperature. Consequently, one may write

$$K = Z\sqrt{T}\,e^{-\frac{E}{RT}} \qquad (5)$$

where

Z = a constant

It may easily be shown that the error which is introduced by use of Equation (4) instead of Equation (5) for all practical purposes is negligible even when the temperature interval is of the order of magnitude of 300° to 400°C. As

$$k = \frac{K}{(RT)^2} = \frac{Z}{R^2\,T^{1.5}} e^{-\frac{E}{RT}} \qquad (6)$$

it is apparent that the error in this case also is negligible. Equation (6) may consequently be written in a form identical with Equation (2), or

$$k = A_1 e^{-\frac{E}{RT}} = e^{\left[a_1 - \frac{b}{(273+t)}\right]} \qquad (7)$$

where

a_1 = a constant different from a in Equation (2)
b = the same constant as b in Equation (2)

It is thus seen that one may use Equation (3) instead of Equation (1) in the reactor calculations without any loss in rigor. To what extent this simplification will reduce the time or simplify the programming in the machine computation the present author does not know.

Pressure-drop Equation

The equation for the pressure drop through the reactor [Equation (2), Table 1 (*1*)] is developed from the basic differential equation

$$-\frac{dp}{dL} = \frac{2fG^2}{g_c \rho D} \qquad (8)$$

When the following substitutions are made,

$$G = \frac{(B_o+x)\,M_{av}}{\frac{\pi}{4}D^2} \qquad (9)$$

and

$$\rho = \frac{pM_{av}}{R\,(273+t)} \qquad (10)$$

and introducing the new variables $r = B_o/x_o$ and $z = 1 - (x/x_o)$ the authors arrive at their final form of the pressure-drop equation,

$$-\frac{\partial p}{\partial L} = \frac{2f\mathrm{M}_{av}R\,(273+t)\,[x_o\,(r+1-z)]^2}{g_c\left(\frac{\pi}{4}\right)^2 D^5\,p} \qquad (11)$$

When an average molecular weight and constant feed composition are assumed the pressure drop is thus a function of feed rate, conversion, reactor diameter, temperature, and pressure; or

$$-\frac{\partial p}{\partial L} = \psi\,(x_o, z, D, t, p) \qquad (12)$$

However, if instead of Equation (9) the following substitution is made,

$$G = \frac{W}{\frac{\pi}{4}D_2} \qquad (13)$$

where

W = total weight flow rate, lb./hr.,

Equation (11) reduces to the following expression

$$-\frac{\partial d}{\partial L} = \frac{2f\,R\,(273+t)\,W^2}{g_c\left(\frac{\pi}{4}\right)^2 M_{av}\,D^5 p} \qquad (14)$$

Contrary to Equation (11), where the pressure drop is a function of five variables, Equation (14) gives the pressure drop in terms of only four variables, i.e., feed rate, reactor diameter, temperature, and pressure, or

$$-\frac{\partial p}{\partial L} = \psi(W, D, t, p) \quad (15)$$

It seems to the author that using Equation (14) instead of Equation (11) should simplify the programming of the problem and also reduce the time needed for the machine computation.

Literature Cited

1. Gee, R. E., W. H. Linton, Jr., R. E. Maier, and J. W. Raines, *Chem. Eng. Progr.*, **50**, 497 (1954).

Adiabatic-temperature Change

J. O. BALL and R. S. HUFSTEDLER
Colorado School of Mines, Golden, Colorado

The following equation may be derived from thermodynamics and is applicable to all states of matter:

$$\left(\frac{\partial T}{\partial p}\right)_s = \frac{T\alpha}{C'_p \rho} = \frac{TV\alpha}{C'_p} \quad (1)$$

where

T = temperature, °K.
p = pressure, atm.
$\alpha = 1/V(\partial V/\partial T)_p$ = cubical coefficient of expansion, °K.$^{-1}$
ρ = density, g./ml.
V = specific volume, ml./g.
C'_p = specific heat, ml. (atm.)/(g.)(°K.) = 41.3 cal./,g.)(°K.) = $41.3C_p$
S = entropy

Equation (1) may be written as

$$d \ln T = \frac{\alpha\, dp}{41.3\, C_p\, \rho} \quad (2)$$

For a liquid α, C_p, and ρ will not change greatly with pressure; therefore, integration of Equation (2) gives

$$\Delta T = T_1 \left[\left(\frac{\alpha_{avg}\, \Delta_p}{41.3\, C_{pA}\, \rho_A} \right)_{-1} \right] \quad (3)$$

where the subscripts 1 and *avg* represent initial and average values respectively, and the subscript A represents values at atmospheric pressure.

A simpler relation between ΔT and Δp may be obtained by use of the following approximate form of Equation (1):

$$\Delta T = \frac{T_1\, \alpha_{avg}\, \Delta_p}{C_{pA}\, \rho_A} \quad (4)$$

Thus it is possible to calculate the adiabatic-temperature change of a liquid produced from a given change in pressure by use of Equation (3) or (4). In most cases Equation (4) is sufficiently accurate.

This method of calculation is simple as long as α values are available as a function of pressure. Thus for water the calculated values of ΔT are in agreement with those calculated from experimental values of $(\partial T/\partial p)_s$ obtained from Dorsey (*2*). α values as a function of pressure are not available for most substances; however, values of the compressibility coefficient β as a function of pressure are known for many substances. The following discussion shows a useful relation between the cubical coefficient of expansion and the compressibility coefficient.

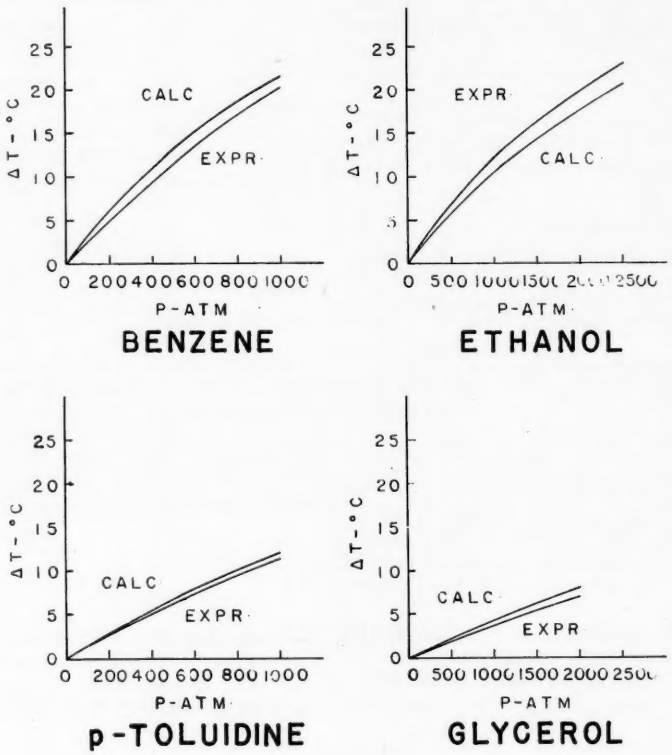

Fig. 1.

For the variables pressure, temperature, and volume, it has been shown mathematically that

$$\left(\frac{\partial p}{\partial T}\right)_V \left(\frac{\partial V}{\partial p}\right)_T \left(\frac{\partial T}{\partial V}\right)_p = -1 \quad (5)$$

Equation (5) may be written as

$$\alpha = \beta \left(\frac{\partial p}{\partial T}\right)_V \quad (6)$$

where

$\beta = -1/V(\partial V/\partial p)_T$ = compressibility coefficient, atm.$^{-1}$

When Equation (6) is differentiated, temperature constant

$$\left(\frac{\partial \alpha}{\partial p}\right)_T = \beta \frac{\partial}{\partial p}\left[\left(\frac{\partial p}{\partial T}\right)_V\right]_T + \frac{\alpha}{\beta}\left(\frac{\partial \beta}{\partial p}\right)_T \quad (7)$$

Further consideration of Equation (7) will simplify the relation between $(\partial\alpha/\partial p)_T$ and $(\partial\beta/\partial p)_T$. It will now be shown that the first term on the right side of Equation (7) is negligible compared with the second term.

Differentiation of the first term on the right side of Equation (7) may be accomplished by applying the equation of state for liquids proposed by Benson (*1*):

$$p = \frac{RT}{V - bV^{-\frac{1}{2}}} - \frac{a}{V^{5/3}T^{2/3}} \quad (8)$$

where

$a = 0.9099RT_c^{5/3}V_c^{2/3}$

$b = 0.1567V_c^{2/3}$

Differentiation of Equation (8) gives

$$\left(\frac{\partial p}{\partial T}\right)_V = \frac{R}{V - bV^{-\frac{1}{2}}} + \frac{2a}{3\,(TV)^{5/3}} \quad (9)$$

Differentiation of Equation (9) gives

$$\frac{\partial}{\partial p}\left[\left(\frac{\partial p}{\partial T}\right)_V\right]_T = -\beta\left[RV\frac{(1+0.5bV^{-3/2})}{(V-bV^{-\frac{1}{2}})^2} + 1.11\,a\,(TV)^{-5/3}\right] \quad (10)$$

Substitution of Equation (10) into Equation (7) gives

$$\left(\frac{\partial \alpha}{\partial p}\right)_T = -\beta^2\left[RV\frac{(1+0.5\,bV^{-3/2})}{(V-b\,V^{-\frac{1}{2}})^2} + 1.11\,a\,(TV)^{-5/3}\right] + \frac{\alpha}{\beta}\left(\frac{\partial \beta}{\partial p}\right)_T \quad (11)$$

It will now be shown that the first term on the right side of Equation (11) is negligible compared with the second term.

The following approximations will be made for a typical liquid:

$R = 1$/(ml.)(atm.)(g.)(°K.)

$V_c = 3$ ml./g.

$T_c = 600$°K.

$\alpha = 10^{-4}$ °K.$^{-1}$

$\beta = 10^{-6}$ atm.$^{-1}$

$(\partial\beta/\partial p)_T = -10^{-9}$ atm.$^{-2}$

$V = 1$ ml./g.

$T = 300$°K.

Therefore

$a \approx (600)^{5/3}(3)^{2/3} = 9 \times 10^4$

$b \approx 0.15\,(3)^{2/3} = 0.3$

Substitution of these approximate values into Equation (11) gives

$$\left(\frac{\partial \alpha}{\partial p}\right)_T \approx -(10^{-6})^2\left[\frac{(1+0.15)}{(1-0.30)_2} + \frac{(1.11\times 9\times 10^4)}{(300)^{5/3}}\right] - \left[\frac{10^{-4}}{10^{-6}}\times 10^{-9}\right]$$

$$\approx -10^{-13} - 10^{-7} = 10^{-7}$$

Since numbers of the order of 10^{-13} are negligible compared with numbers of the order of 10^{-7}, Equation (11) may be simplified as follows:

$$\left(\frac{\partial \alpha}{\partial p}\right)_T = \frac{\alpha}{\beta}\left(\frac{\partial \beta}{\partial p}\right)_T \quad (12)$$

Equation (12) shows a simpler relation between $(\partial\alpha/\partial p)_T$ and $(\partial\beta/\partial p)_T$ than Equation (7). Therefore α values may now be obtained for use in Equation (3) or (4).

A sample calculation will illustrate the entire procedure. It is desired to find the adiabatic temperature change produced when liquid benzene, initially at 90°C. and 1 atm., is subjected to a pressure of 1,000 atm.

$C_{pA} = 0.475$ cal./(g.)(°K.)

The specific volume vs. temperature is

T, °C.	V, ml./g.
80	1.230
90	1.245
100	1.263

From these data

$$\alpha\,(90°\text{ C., 1 atm.}) = \frac{(1.263-1.230)}{1.245\times 20}$$

$$= 1.34 \times 10^{-3}\,°\text{K.}^{-1}$$

β values at 20°C. and at various pressures are obtainable from Perry (*3*). β (20°C., 1 atm.) is 8.9×10^{-5} atm.$^{-1}$ By graphical integration

$$\beta_{mean} = \int_{\frac{p=1}{1{,}000-1}}^{p=1{,}000} \beta\,dp = 6.2 \times 10^{-5}\text{ atm.}^{-1}$$

Therefore

$$\alpha_{mean}\text{ at }90°\text{ C.} = \left(\frac{\beta_{mean}}{\beta_{(1\text{ atm.})}}\right)_{20°\text{ C.}} \times \alpha\,(90°\text{ C., 1 atm.}) = \frac{6.2\times 10^{-5}}{8.9\times 10^{-5}} \times$$

$$1.34 \times 10^{-3} = 9.33 \times 10^{-4}\,°\text{K.}^{-1}$$

From Equation (4)

$$\Delta T = \frac{363\times 9.33\times 10^{-4}\times (1{,}000-1)\times 1.245}{41.3\times 0.475}$$

$$= 21.6\,°\text{C.}$$

Graphical integration of Equation (3) of the data of Pushin (*4*) gives

$$\Delta T = \int_{p=1}^{p=1{,}000}\left(\frac{\partial T}{\partial p}\right)_s dp = 20.5\,°\text{C.}$$

Close agreement is obtained although the α and β values were not at the same temperature.

Similar calculations were made for benzene, ethanol, *p*-toluidine, and glycerol; the results were compared with those calculated from the experimental data of Pushin (*4*). β values for glycerol at high pressures were not available. It was assumed that $(\partial\beta/\partial_p)_T$ values were proportional for glycerol and glycol. The assumption proved to be valid. The results are given in Table 1 and plotted in Figure 1. It is seen that close agreement between calculated and experimental values is obtained.

TABLE 1

T, °C.	p_2, atm. (p_1 is 1 atm)	ΔT, °C. Calc.	Expr.
	Benzene		
90	500	13.1	11.5
90	750	17.9	16.1
90	1,000	21.6	20.5
	Ethanol		
30	500	6.28	6.70
30	1,000	10.6	12.0
30	1,500	14.5	16.5
30	2,500	21.0	23.7
	p-Toluidine		
80	500	6.59	6.21
80	750	9.50	8.97
80	1,000	12.2	11.7
	Glycerol		
25	500	2.28	2.14
25	1,000	4.18*	4.12
25	2,000	7.98*	7.70

*Based on extrapolated β values for glycol.

LITERATURE CITED

1. Benson, S. W., and R. A. Golding, *J. Chem. Phys.*, **17**, 1413 (1951).
2. Dorsey, "Properties of Ordinary Water — Substance," Reinhold Publishing Corporation, New York (1940).
3. Perry, J. H., "Chemical Engineers' Handbook," 3 ed. McGraw-Hill Book Company, Inc., New York (1950).
4. Pushin, N. A., and E. V. Grebenshchikov, *J. Chem. Soc.* (*London*), **123**, 2717 (1924).

INDEX TO VOLUME 1

Authors

A

Akers, W. W. 471
Alexander, L. G. 55
Alstad, C. D. 417
Amundson, N. R. 417
Andersen, L. B. 135
Andrews, R. V. 559

B

Backer, P. O. 95
Ball, J. O. 562
Baron, S. 49
Batchelor, J. D. 318
Beckmann, R. B. 426
Belck, L. H. 467
Benforado, D. M. 501
Benham, A. L. 118
Bilous, O. 480, 513
Bird, R. B. 174
Bonilla, C. F. 49
Brock, J. R. 174
Burtis, T. A. 329
Butler, R. M. 271
Byrnes, J. J. 501

C

Calvert, S. 78
Camp, D. P. 471
Carmichael, L. T. 385
Carpenter, C. L. 549
Catanach, A. W. 536
Chang, Pin 264, 558
Christiansen, E. B. 544
Clegg, J. W. 220
Coates, Jesse 241, 275, 496
Comings, E. W. 55
Cook, M. A. 391
Cullen, J. 452

D

Danckwerts, P. V. 456
Dodds, W. S. 302
Douglas, J. 505

E

Edmister, W. C. 38
Eisenberg, M. 558
Elgin, J. C. 20, 506
Ellis, S. R. M. 185

F

Fahien, R. W. 28
Fairbanks, D. F. 374
Faulkner, R. C. 559
Felix, J. R. 296
Fenske, M. R. 335
Fitch, B. 475
Flynn, A. W. 324
Foresti, R. J. 125
Forster, H. K. 531

G

Garner, F. H. 185
Gautreaux, M. F. 496
Geier, R. G. 335
Gishler, P. E. 157
Gordon, K. F. 129
Grohse, E. W. 358

H

Hagerbaumer, D. H. 152, 215
Hanson, D. N. 441
Henze, E. D. 55
Herring, W. M., Jr. 200
Hill, J. W. 185
Hinze, J. O. 289
Hirata, M. 354
Holder, C. H. 296
Hou, Yu-Chun 142, 506
Holtzlander, G. W. 312
Hu, Chengen 42
Huang, Chen-Jung 111, 412
Hnfstedler, R. S. 562
Hunt, C. d'A. 441
Hurt, D. M. 178

I

Isbin, H. S. 417

J

Jackson, M. L. 231
Johnson, A. I. 111, 412
Johnstone, H. F. ..135, 193, 318, 349

K

Kammermeyer, K. 152, 215
Keyes, J. J., Jr. 305
Kintner, R. C. 42
Kirk, R. S. 488
Kivnick, A. 55
Klassen, J. 488
Klein, J. E. 105
Kobe, K. A. 452
Kurata, F. L. 118

L

Lacey, W. N. 385
Landsbaum, E. M. 302
Lawroski, H. 335
Lebeis, E. H. 329
Leva, Max 224
Licht, W. 366
Lynch, E. J. 9

M

McCormick, B. W. 125
McCormick, R. H. 335
Malloy, J. B. 528
Marks, T. N. 536
Marshall, W. R., Jr. 200
Martin, J. J. 142, 506
Mathur, K. B. 157
Metzner, A. B. 434
Mickley, H. S. 374
Miller, P. 501
Mink, W. H. 220
Munger, H. P. 220

N

Narasimhamurty, G. S. R. 366
Naylor, R. W. 95
Nelson, L. G. 74, 506
Nilsen, P. H. 561

O

Obert, E. F. 74, 506
Olson, F. A. 391
Othmer, D. F. 549

P

Peaceman, D. W. 505
Peters, M. S. 105
Pigford, R. L. 401
Piret, E. L. 480
Plautz, D. A. 193
Proulx, A. Z. 253, 259

R

Reed, J. C. 434
Riggle, J. W. 312
Ross, C. P. 105
Rusinko, F., Jr. 125
Ryan, N. W. 544

S

Sage, B. H. 385
Sakiadis, B. C. 275
Scheibel, E. G. 410
Seelig, H. S. 528
Sesonske, A. 401
Severns, W. H. 401
Shen, C. Y. 318, 349
Sherwood, T. K. 129, 522
Shulman, H. L. 247, 253, 259
Smith, J. M. 28
Sollami, B. J. 302
Stevens, W. E. 544
Stevens, W. F. 302
Stirba, C. 178
Stutzman, L. F. 302

T

Talbot, F. D. 111
Thodos, G. 165, 168
Tobias, C. W. 558
Todd, D. B. 20, 506
Topper, L. 463
Treybal, R. E. 324
Tyner, M. 87

U

Ullrich, C. F. 247, 253, 259

V

Van Ness, H. C. 100

W

Walker, P. L., Jr. 125
Weber, J. H. 210
Wehe, W. H. 241
Wei, J. C. 522
Weisman, W. E. 342
Wells, N. 247, 259
Wicks, C. E. 426
Wilke, C. R. 9, 264, 441, 558
Williams, Brymer 78
Wilson, R. Q. 220

Z

Zimmerman, J. O. 253
Zuber, N. 531

Subjects and Titles

A

Absorption of Ethylene Oxide in a Packed Column with Various Solvents 49
Absorption, aqueous, of nitrogen oxides, controlling mechanisms in 105
in beds of rings and saddles.. 224
gas, accompanied by chemical reaction 456
and oxidation in dispersed media 135
x-ray, analysis of gas fluidized solid systems by..... 358
Acetone-methanol–carbon tetrachloride system, vapor-liquid equilibrium, estimation of 401
Acetone - methanol - chloroform system, vapor-liquid equilibrium, estimation of..... 401
Acetone–methanol–methyl acetate system, vapor-liquid equilibrium, estimation of.. 401
Activity Coefficients at Infinite Dilution 496
Activity coefficients, vapor-liquid equilibrium relations, prediction by 241
Air, thermodynamic properties of 302
upward cocurrent annular flow of, in smooth tubes and water 78
Air jet discharging into a duct, study of 55, 61, 69
Ammonia, oxidation of, in fixed and fluidized beds..... 318
Ammonia solvents, extraction of petroleum fractions by.... 335
Analysis of Gas-fluidized Solid Systems by X-ray Absorption 358
Aniline - nitrobenzene system, vapor-liquid equilibria at low absolute pressures..... 312
Approximate Equations for Time of Batch Fractionation 111
Areas, wetted and interfacial, in packed columns 253
Atomizers, vaned-disk-, performance of 200

B

Benedict Equation of State, Application to Vapor-liquid Equilibria 452
Binary aqueous mixtures of hydrazine, sodium carbonate and glycerine, enthalpy concentration diagrams for... 87
Boiling-point data, vapor-liquid equilibria from 354
1-Butene, thermodynamic properties of 210

C

Capacity Factors in the Performance of Perforated-plate Columns 441
Chemical Factors in Propellant Ignition 391
Chemical reaction, gas absorption accompanied by..... 456
Chemical Reactor Stability and Sensitivity, I..... 513
Compressibility data, calculation of thermodynamic properties from, by use of Redlich and Kwong equation of state 100
Computers, use of in kinetic calculations 561
Contacting gases with coarse solid particles 157
Continuous Reactions in Distillation Equipment 467
Continuous Stirred Tank Reactors: a New Graphical Method for Complex Reactions and Reflux Designs. 480
Controlling Mechanism in the Aqueous Absorption of Nitrogen Oxides 105
Correlation of Diffusion Coefficients in Dilute Solutions.. 264
Corresponding states, laws of.74, 506
surface tension and the principle of 174
Critical Constants of Saturated Aliphatic Hydrocarbons ... 168
Critical Constants of Unsaturated Aliphatic Hydrocarbons 165

D

Dehydration of Hydrazine by Azeotropic Distillation 220
Development of an Equation of State for Gases.....142, 506
Diffusion, gaseous, enrichment calculations in 95
ion, in mass transfer between phases 522
Diffusion coefficients in dilute solutions, correlation of... 264
Diffusion Coefficients in Hydrocarbon Systems: *n*-Hexane in the Gas Phase of the Methane–, Ethane–, and Propane– *n*-Hexane Systems 385
Diffusional Film Characteristics in Turbulent Flow, Dynamic Response Method 305
Diffusional resistances, additivity of, a note on..... 129
Dimensionless - number plots, graphical solutions on..... 475
Dispersed-phase Holdup in Packed, Countercurrent Liquid - liquid Extraction Columns 426
Dispersion processes, hydrodynamic mechanism of splitting in 289
Distillation, azeotropic, dehydration of hydrazine by..... 220
Distillation equipment, continuous reactions in..... 467
Distillation line, locus of the maximum of 271
Droplets, single liquid, rate of falling of 366
Drops, single liquid, fall through water 42
Drying conditions, effect on drying rate and physical properties of a porous solid.... 329
Ducted jet, transport of momentum and energy in.55, 61, 69
Dynamics of Vapor Bubbles and Boiling Heat Transfer..... 531

E

Effect of Drying Conditions on Drying Rate and Physical Properties of a Porous Solid 329
Effect of Fluid Properties on Mass Transfer in the Gas Phase 9
Effect of Void Volume and Prandtl Modulus on Heat Transfer in Tube Banks and Packed Beds..... 342
Efficiency and Capacity Factors in Lube Extraction..... 296
Energy transport in a ducted jet 55, 61, 69
Enrichment Calculations in Gaseous Diffusion: Large Separation Factor 95
Enthalpy - concentration Diagrams for Binary Aqueous Mixtures of Hydrazine, Sodium Carbonate, and Glycerine 87
Entrainment Removal by Wire-mesh Separator 549
Equation of state, Benedict, application to vapor-liquid equilibria 452
for gases, development of.142, 506
use of Redlich-Kwong equation in calculating thermodynamic properties of gases 100
Equations of time.....111, 410, 412
Equivalent Isothermal Temperatures for Nonisothermal Reactors 528
Errata 506
Estimation of Ternary Vapor-liquid Equilibrium: Acetone-methanol-chloroform, Acetone-methanol-carbon tetrachloride, and Acetone-methanol-methyl acetate 401
Ethanol, liquid-phase oxidation of, kinetics of..... 488

Ethylene, phase equilibria in systems with, ...20, 506
Ethylene oxide, absorption of, in packed column..... 49
Extraction, liquid-liquid, in continuous-flow agitated extractors 324
lube, efficiency and capacity factors in 296
Extraction of Petroleum Fractions by Ammonia Solvents 335
Extraction columns, liquid-liquid, dispersed-phase hold up in. 426
perforated plate, performance and wetting characteristics of 185
Extractors, continuous-flow agitated, liquid-liquid extraction in 324

F

Fall of Single Liquid Drops Through Water 42
Films, liquid, in viscous flow... 231
turbulence in 178
Fixed beds, low-temperature oxidation of ammonia in..... 318
Flow of Non-Newtonian Fluids: Correlation for the Laminar, Transition, and Turbulent Flow Regions..... 434
Fluid flow, correlation for the laminar, transition, and turbulent flow regions for flow of non-Newtonian fluids 434
flow of air and water in smoothed tubes 78
turbulent flow, diffusional film characteristics in 305
viscous flow, liquid films in... 231
Fluidized beds, gas-solid contact in 349
heat transfer to, mechanism of 374
low-temperature oxidation of ammonia in 318
Fluid properties, effect on mass transfer in gas phase..... 9
Fluids, non-Newtonian, flow of. 434
pipe-line design for..... 544
Forced-convection Heat Transfer in Cylindrical Pipes with Temperature-dependent Volume Heat Sources Within the Fluid..... 463
Fractionation, batch equations for time 111, 410, 412
Fundamentals of the Hydrodynamic Mechanism of Splitting in Dispersion Processes 289

G

Gas Absorption Accompanied by Chemical Reaction 456
Gas Absorption in Beds of Rings and Saddles 224
Gas Absorption and Oxidation in Dispersed Media..... 135
Gases, equation of state for, development of 142
Gas-solid contact, contacting gases with coarse solid particles 157
Gas-solid Contact in Fluidized Beds 349
Glycerine, hydrazine, and sodium carbonate, binary mixtures of, enthalpy - concentration diagram for 87
Graphical method for complex reactions and reflux designs 480
Graphical Solutions on Dimensionless-number Plots 475

H

Heat-flow problems, numerical solutions of two dimensional 505
Heat and Mass Transfer in Packed Beds 193
Heat of vaporization of hydrocarbon mixtures from vapor —liquid K values..... 38
Heat transfer, dynamics of vapor bubbles and boiling.... 531
to fluidized beds, mechanism of 374
forced-convection, in cylindrical pipes 463
in packed beds.....193, 342
in tube banks..... 342
to water in an annulus..... 501
Heat Transfer to Water in an Annulus 501
n-Hexane, hydrocarbon systems, diffusion coefficients in..... 385
Holdup, dispersed - phase, in packed countercurrent liquid-liquid extraction columns 426
for aqueous and nonaqueous systems in packed columns 259
total, static, and operating, in packed columns 247
Hydration of propylene oxide, kinetics of 118
Hydrazine, dehydration by azeotropic distillation 220
sodium carbonate, and glycerine, binary aqueous mixtures of, enthalpy concentration diagram 87
Hydrocarbon mixtures, isobaric integral heat of vaporization of 38
Hydrocarbons, aliphatic, saturated, critical constants of. 168
unsaturated, critical constants of 165
Hydrocarbon systems, n-hexane, diffusion coefficients in.... 385

I

Ion Diffusion in Mass Transfer Between Phases 522
Isobaric Integral Heat of Vaporization of Hydrocarbon Mixtures from Vapor-liquid K Values 38

K

Kinetic calculations, use of computers in 561
Kinetics of hydration of propylene oxide 118
of liquid-phase oxidation of ethanol 488
of methane steam reaction... 471
Kinetics of the Catalyzed and Uncatalyzed Liquid - phase Hydration of Propylene Oxide 118
Kinetics of the Liquid-phase Oxidation of Ethanol..... 488
Kinetics of the Methane-steam Reaction 471

L

Laws of Corresponding State..74, 506
Liquid Films in Viscous Flow.. 231
Liquid-liquid Extraction in Continuous-flow Agitated Extractors 324
Liquids, thermal conductivity of, studies of 275
Loop systems, single-phase natural - circulation, transient behavior of 417
Low-temperature Oxidation of Ammonia in Fixed and Fluidized Beds 318
Lube extraction, efficiency and capacity factors in..... 296

M

Mass Transfer in Packed Beds 28
Mass transfer between phases, ion diffusion in..... 522
gas- and liquid-phase, in packed columns 253
in gas phase, effect of fluid properties on 9
in packed beds.....28, 193
Mass transfer studies, selected physical properties of aqueous organic acids employed in 558
Mechanism of Heat Transfer to Fluidized Beds 374
Membranes, operating characteristics of 152
Membrane Separations in the Liquid Phase 215
Methane—steam reaction, kinetics of 471
Momentum transport in a ducted jet 55, 61, 69

N

Nitrogen oxides, aqueous absorption of, controlling mechanism in 105
Note on the Additivity of Diffusional Resistances, A.... 129
Note on Equations of Time, A.. 411
Numerical Solution of Two-dimensional Heat-flow Problems 505

O

Operating Characteristics of Membranes 152
Oxidation and gas absorption in dispersed media 135
of ethanol, liquid phase, kinetics of 488

P

Packed beds, heat and mass transfer in 193
heat transfer in, effect of void volume and Prandtl modulus on 342
mass transfer in..... 28
Packed columns, absorption of ethylene oxide in..... 49
dispersed-phase holdup in.... 426
performance of 247, 253, 259
Perforated-plate Extraction-column Performance and Wetting Characteristics 185
Perforated-plate columns, capacity factors in the performance of 441
Performance of Packed Columns 247
Performance of Small Herschel-type Venturi Tubes..... 125
Performance of Vaned-disk Atomizers 200
Petroleum fractions, extraction of, by ammonia solvents.... 335
Phase Equilibria in Systems with Ethylene Above Its Critical Temperature ...20, 506
Physical properties of a porous solid, effect of drying conditions on 329
of aqueous organic acids employed in mass transfer studies 558
Pipe-line Design for Non-Newtonian Fluids 544
Plant Performance of a 13-ft.-diameter Extractive-distillation Column 536
Prediction of Ternary Vapor-liquid Equilibria from Boiling-point Data 354
Propellant ignition, chemical factors in 391
Propylene oxide, hydration of, kinetics of 118

R

Rate of Fall of Single Liquid Droplets 366
Reactions, continuous, in distillation equipment 467
methane-steam, kinetics of... 471
Reactors, continuous stirred-tank, graphical method for complex reactions and reflux designs 480
nonisothermal, equivalent isothermal temperatures for.. 528
Redlich-Kwong equation, use in calculating the thermodynamic properties of gases. 100
Rings, gas absorption in beds of 224

S

Saddles, gas absorption in beds of 224
Separations, membrane, in liquid phase 215
Shape factors in multiple-pipe systems 559
Sodium carbonate, glycerine, and hydrazine, binary aqueous mixtures of, enthalpy-concentration diagrams for... 87
Solid, porous, drying rate and physical properties of, effect of drying conditions on... 329
Solutions, dilute, correlation of diffusion coefficients in.... 264
Splitting in dispersion processes, hydrodynamic mechanism of 289
Studies of Thermal Conductivity of Liquids 275
Surface Tension and the Principle of Corresponding States 174

T

Technique for Contacting Gases with Coarse Solid Particles, A 157
Temperature change, adiabatic, of liquids with change in pressure .....
Thermal conductivity of liquids, studies of 275
Thermodynamic Properties of Air 302
Thermodynamic properties of air 302
of 1-butene 210
of gases, calculation from experimental compressibility data 100
Thermodynamic Properties of 1-Butene 210
Time, equations for, of batch fractionation 111, 410, 412
Total Pressure Method for Vapor-liquid Equilibria at Low Absolute Pressures: Aniline-nitrobenzene System .. 312
Transient Behavior of Single-phase Natural - circulation Loop Systems 417
Transport of Momentum and Energy in a Ducted Jet... 55
Tube banks, heat transfer in, effect of void volume and Prandtl modulus on..... 342
Turbulence in Falling Liquid Films 178

U

Upward Cocurrent Annular Flow of Air and Water in Smooth Tubes 78
Use of the Redlich and Kwong Equation of State in Calculating Thermodynamic Properties of Gases from Experimental Compressibility Data 100

V

Vapor-liquid equilibria at low absolute pressures: aniline-nitrobenzene system 312
Benedict equation of state, application to 452
isobaric integral heat of vaporization of hydrocarbon mixtures from K values... 38
prediction by thermodynamic examination of activity coefficients 241
ternary, estimation of, for acetone–methanol and chloroform, carbon tetrachloride, and methylacetate systems 401
from boiling-point data..... 354
Vapor-liquid Equilibrium Relations Predicted by Thermodynamic Examination of Activity Coefficients 241
Venturi tubes, small Herschel type, performance of..... 125

W

Water, heat transfer to, in an annulus 501
air and, upward cocurrent annular flow of in smooth tubes 78

X

X-ray absorption, analysis of gas-fluidized solid systems by 358

1, 1954. The volume includes the following topics: steric effects in dyes, the structure of glyotoxin, the structure of nepetalic acid, the chemistry of flavilium salts, and some chemical studies on viruses. All the papers, as well as the opening remarks reviewing Dr. Adams's career, are presented by persons who took their Ph.D. degrees under Dr. Adams. The variety in the topics chosen for the symposium reflects the varied research activity in which Dr. Adams himself has been engaged throughout his long scientific career.

The chapters all give a good, well-written coverage of their special topics. Dr. Brode's paper gives an excellent review of current theory on dyes; his writing has a personal flavor and makes very enjoyable reading. Dr. Johnson's discussion of the structure of glyotoxin communicates some of the excitement involved in determining the structure of a very complicated natural product, and both the glyotoxin and the nepetalic acid chapter nicely illustrate the importance of infrared spectroscopy in modern structural work.

The book is a fitting tribute to an outstanding chemist and a great teacher; in addition, it should prove enjoyable reading to those interested in the application of ultraviolet absorption spectroscopy to problems in organic chemistry, in the chemistry of "ylium" salts and related colored products, and in a concise review of Stanley's classical chemical studies on viruses.

HARRY H. WASSERMAN

Production of Heavy Water. National Nuclear Energy Series. Edited by George M. Murphy. McGraw-Hill Book Company, Inc., New York (1955). -394 pages. $5.25.

The production of heavy water in tonnage quantities was one of the serious problems with which the Manhattan Project was confronted. The effort expended on the solution of this problem brought into existence a considerable amount of basic data and engineering information. The present volume of the National Nuclear Energy Series (III-4F) makes this information available to those interested in separation processes in a comprehensive and convenient form.

It would seem that Part II of this volume is the more logical as a beginning of the volume and of this review because it deals with the fundamental laboratory data, techniques for obtaining these data, and the underlying theoretical considerations of the various separation processes envisaged for the industrial production of heavy water. The six chapters of this part consider the water-distillation process, the catalytic-exchange process (with a detailed account of the development and characteristics of the various catalysts) and the dual-temperature processes (mercaptan-water, ammonia-water-hydrogen, and cyclohexane-benzene-hydrogen systems). In this part the short Chapter 8 ("Catalytic Exchange: General" by H. S. Taylor) is an outstanding example of a concise and clear presentation. The discussion of the dual-temperature processes (Chapter 12) is, in the opinion of this reviewer, somewhat lacking in an adequate treatment of the fundamental theory involved in this group of processes.

Part I of the volume is devoted almost entirely to a summary of actual engineering experience as obtained in the Trail, B.C., catalytic-exchange–electrolytic plant and the water-distillation plant at Morgantown, W. Va. The information given, though somewhat sketchy in parts, is definitely useful as a general guide for design and operational variables. Chapter 4 summarizes design considerations for the untried but promising hydrogen-distillation process.

An excellent bibliography following each chapter is a very valuable feature and, together with the subject matter treated, makes this volume a most valuable contribution to the literature of separation processes in general and isotope separation in particular.

ALLEN M. ESHAYA

DIFFUSION AND HEAT EXCHANGE IN CHEMICAL KINETICS

By D. A. Frank-Kamenetskii

Frank-Kamenetskii, a leader in Russian science, here treats mathematically the subjects of reaction ignition, quenching, and periodic processes in chemical kinetics as found in flames, combustion of solids, and other chemical reactions.

Translated from the Russian by the late N. Thon, and edited by R. Wilhelm.

388 *pages*. $6

Order from your bookstore, or

PRINCETON UNIVERSITY PRESS
Princeton, New Jersey